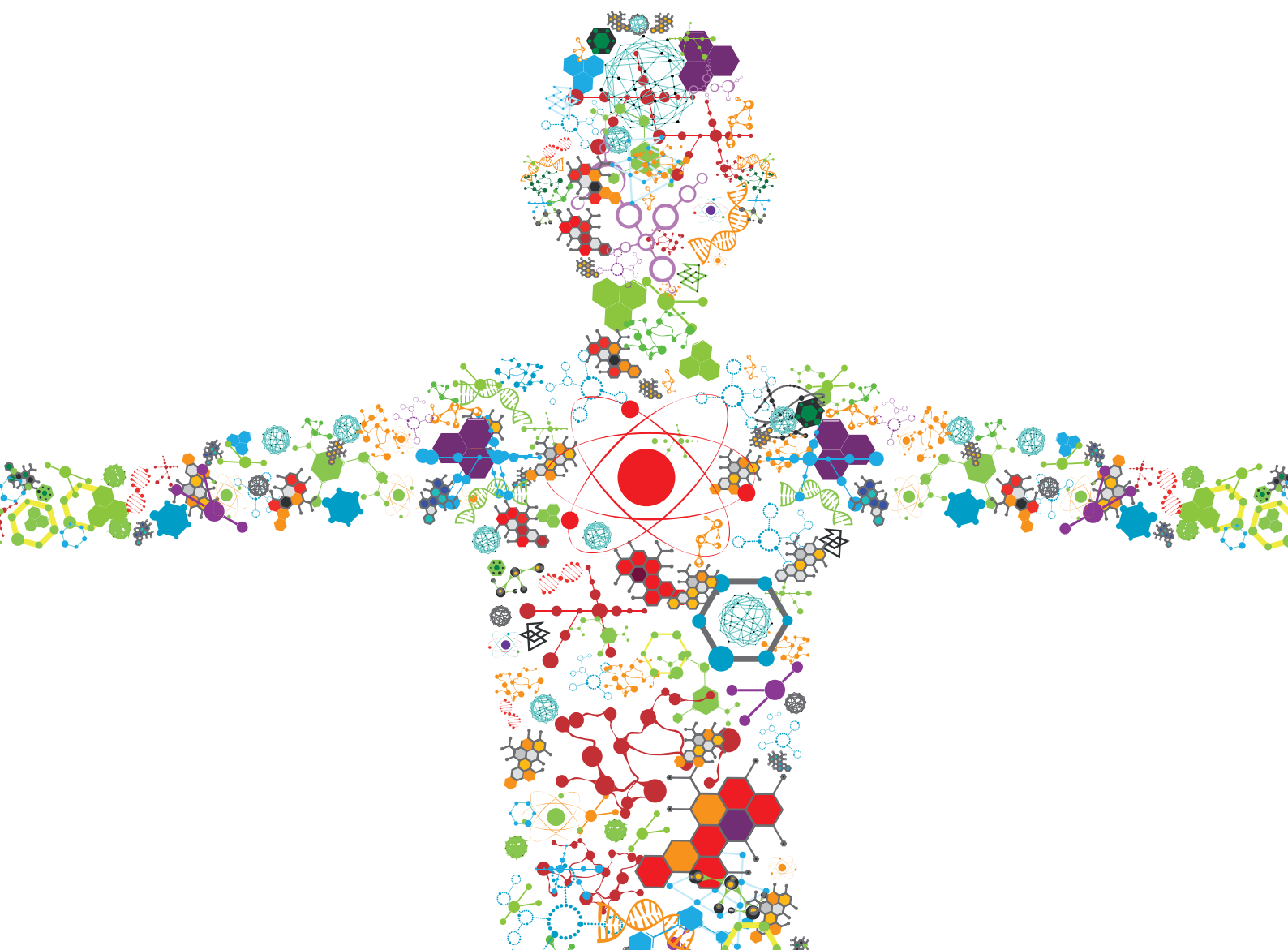


BIO-BASED COMPOUND PRODUCTION AND THEIR INNOVATIVE INDUSTRIAL APPLICATIONS

EDITED BY: Ligia R. Rodrigues, George Sakellaris and Giovanni Sannia
PUBLISHED IN: Frontiers in Bioengineering and Biotechnology





frontiers

Frontiers eBook Copyright Statement

The copyright in the text of individual articles in this eBook is the property of their respective authors or their respective institutions or funders. The copyright in graphics and images within each article may be subject to copyright of other parties. In both cases this is subject to a license granted to Frontiers.

The compilation of articles constituting this eBook is the property of Frontiers.

Each article within this eBook, and the eBook itself, are published under the most recent version of the Creative Commons CC-BY licence.

The version current at the date of publication of this eBook is CC-BY 4.0. If the CC-BY licence is updated, the licence granted by Frontiers is automatically updated to the new version.

When exercising any right under the CC-BY licence, Frontiers must be attributed as the original publisher of the article or eBook, as applicable.

Authors have the responsibility of ensuring that any graphics or other materials which are the property of others may be included in the CC-BY licence, but this should be checked before relying on the CC-BY licence to reproduce those materials. Any copyright notices relating to those materials must be complied with.

Copyright and source acknowledgement notices may not be removed and must be displayed in any copy, derivative work or partial copy which includes the elements in question.

All copyright, and all rights therein, are protected by national and international copyright laws. The above represents a summary only. For further information please read Frontiers' Conditions for Website Use and Copyright Statement, and the applicable CC-BY licence.

ISSN 1664-8714

ISBN 978-2-88974-037-6

DOI 10.3389/978-2-88974-037-6

About Frontiers

Frontiers is more than just an open-access publisher of scholarly articles: it is a pioneering approach to the world of academia, radically improving the way scholarly research is managed. The grand vision of Frontiers is a world where all people have an equal opportunity to seek, share and generate knowledge. Frontiers provides immediate and permanent online open access to all its publications, but this alone is not enough to realize our grand goals.

Frontiers Journal Series

The Frontiers Journal Series is a multi-tier and interdisciplinary set of open-access, online journals, promising a paradigm shift from the current review, selection and dissemination processes in academic publishing. All Frontiers journals are driven by researchers for researchers; therefore, they constitute a service to the scholarly community. At the same time, the Frontiers Journal Series operates on a revolutionary invention, the tiered publishing system, initially addressing specific communities of scholars, and gradually climbing up to broader public understanding, thus serving the interests of the lay society, too.

Dedication to Quality

Each Frontiers article is a landmark of the highest quality, thanks to genuinely collaborative interactions between authors and review editors, who include some of the world's best academicians. Research must be certified by peers before entering a stream of knowledge that may eventually reach the public - and shape society; therefore, Frontiers only applies the most rigorous and unbiased reviews.

Frontiers revolutionizes research publishing by freely delivering the most outstanding research, evaluated with no bias from both the academic and social point of view. By applying the most advanced information technologies, Frontiers is catapulting scholarly publishing into a new generation.

What are Frontiers Research Topics?

Frontiers Research Topics are very popular trademarks of the Frontiers Journals Series: they are collections of at least ten articles, all centered on a particular subject. With their unique mix of varied contributions from Original Research to Review Articles, Frontiers Research Topics unify the most influential researchers, the latest key findings and historical advances in a hot research area! Find out more on how to host your own Frontiers Research Topic or contribute to one as an author by contacting the Frontiers Editorial Office: frontiersin.org/about/contact

BIO-BASED COMPOUND PRODUCTION AND THEIR INNOVATIVE INDUSTRIAL APPLICATIONS

Topic Editors:

Ligia R. Rodrigues, University of Minho, Portugal

George Sakellaris, University of South Bohemia in České Budějovice, Czechia

Giovanni Sannia, University of Naples Federico II, Italy

Citation: Rodrigues, L. R., Sakellaris, G., Sannia, G., eds. (2021). Bio-Based Compound Production and Their Innovative Industrial Applications. Lausanne: Frontiers Media SA. doi: 10.3389/978-2-88974-037-6

Table of Contents

- 04 *A Broad Temperature Active Lipase Purified From a Psychrotrophic Bacterium of Sikkim Himalaya With Potential Application in Detergent Formulation***
 Anil Kumar, Srijana Mukhia, Neeraj Kumar, Vishal Acharya, Sanjay Kumar and Rakshak Kumar
- 20 *A Novel High Glucose-Tolerant β -Glucosidase: Targeted Computational Approach for Metagenomic Screening***
 Shohreh Ariaeenejad, Safura Nooshi-Nedamani, Mahdie Rahban, Kaveh Kavousi, Atefeh Ghasemi Pirbalooti, SeyedSoheil Mirghaderi, Mahsa Mohammadi, Mehdi Mirzaei and Ghasem Hosseini Salekdeh
- 34 *High-Level Production of Recombinant Snowdrop Lectin in Sugarcane and Energy Cane***
 Carmen S. Padilla, Mona B. Damaj, Zhong-Nan Yang, Joe Molina, Brian R. Berquist, Earl L. White, Nora Solís-Gracia, Jorge Da Silva and Kranthi K. Mandadi
- 50 *Applications of Microbial β -Mannanases***
 Aneesa Dawood and Kesen Ma
- 67 *High Epoxidation Yields of Vegetable Oil Hydrolyzates and Methyl Esters by Selected Fungal Peroxygenases***
 Alejandro González-Benjumea, Gisela Marques, Owik M. Herold-Majumdar, Jan Kiebitz, Katrin Scheibner, José C. del Río, Angel T. Martínez and Ana Gutiérrez
- 79 *In vivo and Post-Synthesis Strategies to Enhance the Properties of PHB-Based Materials: A Review***
 Rosa Turco, Gabriella Santagata, Iolanda Corrado, Cinzia Pezzella and Martino Di Serio
- 110 *High Quality Aspergillus aculeatus Genomes and Transcriptomes: A Platform for Cellulase Activity Optimization Toward Industrial Applications***
 Wuttichai Mhuanong, Salisa Charoensri, Aphisit Poonrisawat, Wirulda Pootakham, Sithichoke Tangphatsornruang, Chatuphon Siamphan, Surisa Suwannarangsee, Lily Eurwilaichitr, Verawat Champreda, Varodom Charoensawan and Duriya Chantasingh
- 118 *Toluene Dioxygenase-Catalyzed cis-Dihydroxylation of Quinolines: A Molecular Docking Study and Chemoenzymatic Synthesis of Quinoline Arene Oxides***
 Derek R. Boyd, Narain D. Sharma, Pui L. Loke, Jonathan G. Carroll, Paul J. Stevenson, Patrick Hoering and Christopher C. R. Allen
- 134 *Optimization of Inulin Hydrolysis by Penicillium lanosocoeruleum Inulinases and Efficient Conversion Into Polyhydroxyalkanoates***
 Iolanda Corrado, Nicoletta Cascelli, Georgia Ntasi, Leila Birolo, Giovanni Sannia and Cinzia Pezzella
- 151 *Wasteful Azo Dyes as a Source of Biologically Active Building Blocks***
 Ana Fernandes, Bruna Pinto, Lorenzo Bonardo, Beatriz Royo, M. Paula Robalo and Lúcia O. Martins



A Broad Temperature Active Lipase Purified From a Psychrotrophic Bacterium of Sikkim Himalaya With Potential Application in Detergent Formulation

Anil Kumar^{1,2†}, Srijana Mukhia^{1,3†}, Neeraj Kumar^{1,2}, Vishal Acharya¹, Sanjay Kumar¹ and Rakshak Kumar^{1*}

¹ Biotechnology Division, CSIR-Institute of Himalayan Bioresource Technology, Palampur, India, ² Academy of Scientific and Innovative Research (AcSIR), CSIR-Institute of Himalayan Bioresource Technology, Palampur, India, ³ Department of Microbiology, Guru Nanak Dev University, Amritsar, India

OPEN ACCESS

Edited by:

George Sakellaris,
University of South Bohemia in Ceské
Budějovice, Czechia

Reviewed by:

Farshad Darvishi,
University of Maragheh, Iran
Artur Ribeiro,
University of Minho, Portugal

*Correspondence:

Rakshak Kumar
rakshak@ihbt.res.in

†These authors have contributed
equally to this work

Specialty section:

This article was submitted to
Industrial Biotechnology,
a section of the journal
Frontiers in Bioengineering and
Biotechnology

Received: 24 March 2020

Accepted: 26 May 2020

Published: 25 June 2020

Citation:

Kumar A, Mukhia S, Kumar N,
Acharya V, Kumar S and Kumar R
(2020) A Broad Temperature Active
Lipase Purified From a Psychrotrophic
Bacterium of Sikkim Himalaya With
Potential Application in Detergent
Formulation.
Front. Bioeng. Biotechnol. 8:642.
doi: 10.3389/fbioe.2020.00642

Bacterial lipases with activity spanning over a broad temperature and substrate range have several industrial applications. An efficient enzyme-producing bacterium *Chryseobacterium polytrichastri* ERM1:04, previously reported from Sikkim Himalaya, was explored for purification and characterization of cold-adapted lipase. Optimum lipase production was observed in 1% (v/v) rice bran oil, pH 7 at 20°C. Size exclusion and hydrophobic interaction chromatography purified the enzyme up to 21.3-fold predicting it to be a hexameric protein of 250 kDa, with 39.8 kDa monomeric unit. MALDI-TOF-MS analysis of the purified lipase showed maximum similarity with alpha/beta hydrolase (lipase superfamily). Biochemical characterization of the purified enzyme revealed optimum pH (8.0), temperature (37°C) and activity over a temperature range of 5–65°C. The tested metals (except Cu²⁺ and Fe²⁺) enhanced the enzyme activity and it was tolerant to 5% (v/v) methanol and isopropanol. The Km and Vmax values were determined as 0.104 mM and 3.58 U/mg, respectively for *p*-nitrophenyl palmitate. Bioinformatics analysis also supported *in vitro* findings by predicting enzyme's broad temperature and substrate specificity. The compatibility of the purified lipase with regular commercial detergents, coupled with its versatile temperature and substrate range, renders the given enzyme a promising biocatalyst for potential detergent formulations.

Keywords: *Chryseobacterium polytrichastri* ERM1:04, lipase, purification, broad temperature activity, bioinformatics analysis, detergent formulation

INTRODUCTION

Lipases include an important group of biocatalysts that belong to the class of triacylglycerol hydrolases (EC: 3.1.1.3) (Gupta et al., 2004). They break down fats and are highly active against water-insoluble substrates. The lipolytic enzymes are a part of serine hydrolase superfamily whose activities depend on the catalytic triad of Ser, His, and Asp residues (Brumlik and Buckley, 1996). In addition to hydrolyzing carboxylic acid esters, they can perform esterification and transesterification reactions (Reetz, 2002). Lipases have high enantioselectivity with the ability to

perform in aqueous and non-aqueous environments which makes them highly suitable biocatalysts in many industries (Kumar et al., 2016a).

Lipases are ubiquitous as they are found in all groups of organisms from bacteria to plants and animals. Although lipases have been studied widely, not much attention has been paid to the bacterial lipases from extreme cold environments (Salwoom et al., 2019b). Lipases from high altitude bacteria are of significance due to the host of specific structural features that these enzymes have evolved as a mode of adaptation to frequent freezing and thawing conditions. They find potential industrial applications in diverse fields of detergent additives, food processing, environmental bioremediation in cold, and many more (Maiangwa et al., 2015). High-temperature active lipases are suitable biocatalysts in the synthesis of biopolymers, pharmaceutical compounds, and cosmetics owing to their thermostability and organic solvent tolerance (Ranjan et al., 2018). Due to the inactivation of enzyme components at low temperature, detergents lose their functionality. Low-temperature active lipases are greatly advantageous as detergent additives for cold washing that would diminish energy consumption as well as wear and tear of delicate fabrics (Joseph et al., 2008).

Several low-temperature, cold-adapted environments like high-altitude mountains, glaciers, and deep seas serve as sources of psychrophilic and psychrotrophic microorganisms. Psychrophilic microorganisms are cold-loving with a minimum, optimum, and maximum temperature for growth at about 0, 15, and 20°C, respectively, while psychrotrophic organisms have growth maxima above 25°C but can survive in low temperature (Junge et al., 2019). Cold-active enzymes play a major role in their physiological adaptation to low temperature and have been a focus of research at recent times owing to their potential applications in biotechnological industries (Salwoom et al., 2019b). Irrespective of their significance, cold-active lipases have some limitations like diminished activity at moderate to high temperature, limited substrate specificity, and less thermostability (Joseph et al., 2008; Kavitha, 2016). As temperature-related activity is a major characteristic for the use of enzymes in industry, lipases produced by psychrotolerant bacteria with a wider range of temperature activity can be preferable.

East Rathong glacier in Sikkim Himalaya is an unexplored region to obtain extremophilic microbial resources for bioprospection of industrial enzymes. The debris-free valley glacier experiences cold and wet climate throughout and snowfall is common even during monsoon (Luitel et al., 2012). We have reported genome-based predictions on cold-active enzymes from the psychrotrophic bacteria thriving in Sikkim Himalaya (Kumar et al., 2015a, 2016b, 2018a, 2019; Himanshu et al., 2016). In the current study, one such bacterium *Chryseobacterium polytrichastri* ERM1:04 reported as a potential candidate for various industrial enzymes has been explored (Kumar et al., 2015b). The isolate showed promising results for lipase activity in plate assay with clear halo zone indicating tributyrin hydrolysis. Considering the significance of lipase from high-altitude bacteria, we isolated, purified and characterized the enzyme in the present study. Bioinformatics verification of the

in vitro findings was carried out using amino acid sequence-based analysis for prediction of enzyme structure, and its behavior over different temperature and substrates. Finally, to determine the appropriate application of the new enzyme from Sikkim Himalaya, we tested its compatibility with a range of commercially available detergents at different temperature for its suitability as a detergent formulation.

MATERIALS AND METHODS

Chemicals

Following analytical grade chemicals were used in the current study: *p*NPP (*para*-nitrophenyl palmitate), Sephadex G-100, Octyl-Sepharose fast flow, were purchased from Sigma-Aldrich (St. Louis, MO, USA). Bradford solution, ammonium sulfate, triton X-100, SDS were purchased from Himedia Laboratories, Mumbai India.

Bacterial Strain

A previously isolated bacterial strain *Chryseobacterium polytrichastri* ERM1:04 was used in the present study (Kumar et al., 2015b).

Optimization of Culture Conditions and Production of Extracellular Lipase

Culture conditions like temperature, pH, substrate type, and substrate concentration were optimized to maximize lipase production by the bacterial isolate. The bacterium was grown in production broth containing (g/L) yeast extract (5.0), potassium chloride (0.50), sodium nitrate (3.0), ferrous sulfate heptahydrate (0.01), dipotassium hydrogen phosphate (0.10), magnesium sulfate heptahydrate (0.50) and rice bran oil (1% v/v) (Sharma et al., 2018). The seed culture was prepared in ABM broth containing (g/L) Peptone (5) and Yeast extract (2) (Shivaji et al., 2013). About 1% (v/v) of overnight grown seed culture was transferred in previously described production broth and kept at 150 rpm for 60 h. Firstly, the *C. polytrichastri* ERM1:04 was allowed to grow in different vegetable oils, i.e., olive oil, rice bran oil, sapium oil, and sunflower oil. The broth showing maximum lipase activity was selected and then bacterial isolate was grown at different temperature of 10, 15, 20, 28°C. Bacterial isolate was also grown at different pH of 6–9. The effect of different oil concentration on the production of lipase by the isolate in the culture broth was checked by growing it in 0.5, 1, 1.5, 2, and 2.5% (v/v) vegetable oil.

Lipase Activity Determination

Lipase activity was determined colourimetrically using the substrate *p*NPP by slight modification in a previous method (Zhang et al., 2018). In detail, 40 μ L of 5 mM *p*NPP substrate dissolved in isopropanol was mixed with 900 μ L of 50 mM Tris buffer pH-8 containing 0.3% (v/v) Triton X-100. The reaction was initiated by adding 60 μ L of culture supernatant and incubating the reaction tubes at 20°C for 10 min. After incubation, the reaction was stopped by placing the reaction tubes at (–20°C) for 10 min. Reaction control without enzyme was also run in parallels. The amount of *para*-nitrophenol

released after completion of the reaction was calculated by checking the absorbance at 410 nm using *para*-nitrophenol as standard. All reactions were done in triplicates. One unit of lipase activity was defined as the amount of enzyme required to release 1- μ mol of *para*-nitrophenol from substrate per minute at standard assay condition. Protein estimation was done by the method of Bradford (Bradford, 1976) with bovine serum albumin as standard.

Purification of *C. polytrichastri* ERMR1:04 Extracellular Lipase

The cell-free supernatant containing the extracellular lipase was collected by centrifuging the bacterial culture broth at $12,000 \times g$ for 10 min at 4°C. To concentrate the protein, solid ammonium sulfate was added until 70% saturation was reached. After overnight precipitation in stirring condition at 4°C, the precipitated proteins were collected by centrifuging at $15,000 \times g$ for 20 min at 4°C and dissolved in 50 mM Tris buffer pH 8. Dialysis was done at 4°C with a dialysis membrane (with a cut-off of 10 kDa) to remove the salt ions from protein samples with three changes in the buffer every 4 h. The dialyzed protein sample was then further purified using size exclusion and hydrophobic interaction chromatography. The purified lipase was stored at 4°C until further use.

Size Exclusion Chromatography

A pre-swollen Sephadex G-100 column was equilibrated with 50 mM Tris HCl buffer pH 8. Dialyzed protein sample was clarified by passing through a 0.45 μ m syringe filter before loading onto the column. Protein volume of 2 mL was loaded onto the column. Elution was done in the same buffer at a flow rate of 0.5 mL/min. The eluted fractions were checked for protein content and lipase activity and then pooled, concentrated by Amicon centrifugal filters (10 kDa cut-off), and subjected to further purification.

Hydrophobic Interaction Chromatography

An Octyl-Sepharose fast flow column was equilibrated with 50 mM Tris HCl buffer pH 8 containing 1 M ammonium sulfate. Sephadex G-100 purified protein fraction was loaded (2 mL) onto the column. The elution was done with a linear gradient of ammonium sulfate from 1 to 0 M in 50 mM Tris HCl buffer pH 8 at a flow rate of 0.5 mL/min. The fractions having the lipase activity were pooled and then dialyzed against 50 mM Tris HCl buffer pH 8 and checked for its purity and molecular weight analysis by SDS-PAGE.

Determination of Molecular Weight of Purified Lipase and Zymography

SDS-PAGE (12%) and Native PAGE (10%) analysis were done to check the purity and molecular weight of purified bacterial lipase (Laemmli, 1970). Zymogram analysis of purified lipase was performed using MUF-butyrate as substrate according to a previously described method (Prim et al., 2003).

Peptide Mass Fingerprinting by MALDI-TOF-MS

The gel bands were manually excised and then de-stained with 40 mM ammonium bicarbonate solution followed by dehydration with acetonitrile. In-gel modification of cysteine residues was done with 10 mM dithiothreitol and 55 mM iodoacetamide. The proteins in the bands were then subjected to digestion with trypsin enzyme, followed by overnight incubation at 37°C. Trypsin digested samples were then mixed with 0.1% trifluoroacetic acid and sonicated in a bath sonicator for 5–10 min. The protein solution obtained was then mixed with an equal volume of cyano-4-hydroxycinnamic acid matrix and loaded onto the MALDI plate and analyzed by Bruker Autoflex MALDI-TOF-MS (Bruker Daltonics) system. The mass profile of peptides obtained was then compared with a MASCOT database.

C. polytrichastri ERMR1:04 draft genome was then searched (from NCBI protein database) for lipase and its related amino-acid sequences. The protein sequence, alpha/beta hydrolase (topmost hit in MALDI-TOF-MS) was then aligned with the ERMR1:04 lipase and its related protein sequences (Kumar et al., 2015b) using ClustalW multiple sequence alignment tool. The phylogenetic tree was constructed using the neighbor-joining method in MEGA-X software based on 1,000 bootstrap replications (Kumar et al., 2018b). The protein sequence showing maximum similarity with the ERMR1:04 protein was then used for the bioinformatics analysis.

Biochemical Characterization of Purified Lipase

Effect of Temperature, pH, and Metal Ions

To check the effect of temperature and pH on purified lipase, activity was performed at a temperature ranging from 5 to 65°C and pH range of (7–9) using *p*NPP as substrate and 50 mM Tris buffer. To determine the effect of various metal ions (Na^+ , K^+ , Ca^{2+} , Mg^{2+} , Cu^{2+} , Mn^{2+} , Fe^{2+}) on purified lipase, the enzyme was incubated with 5 and 10 mM salts for 30 min at 37°C. After incubation, the enzyme activity was checked at 37°C using *p*NPP as substrate.

Effect of Organic Solvents, Inhibitors, and Kinetic Study of Purified Lipase

The effect of common organic solvents on purified lipase was determined by incubating lipase in 5% (v/v) solvents (Butanol, Isopropanol, Acetonitrile, and Methanol) for 30 min at 37°C. The effect of various inhibitors (EDTA, DTT, PMSF) on enzyme activity was determined by incubating the enzyme in 1, 5, and 10 mM inhibitors at 37°C for 30 min in 50 mM Tris buffer pH 8. The lipase assay was performed using *p*NPP as a substrate in 50 mM Tris buffer pH 8 at 37°C for 10 min. The kinetic parameters (K_m and V_{max}) were studied by varying *p*NPP concentration from 0.025 to 0.3 mM according to Lineweaver-Burk plots at 37°C (Lineweaver and Burk, 1934).

Detergent Compatibility Test

Detergent compatibility tests were conducted by using 1% (v/v) commercially available detergents, i.e., Tide, Surf, Aerial, and Wheel. Detergent solutions were prepared in distilled water and

hydrolytic activity was checked in pNPP. The hydrolytic activity of lipase in the presence of commercial detergents was taken as a test while lipase activity in the absence of detergent was taken as control. The assay was done at different temperature (5, 20, 37, 45, and 60°C) for 10 min.

Bioinformatics Analysis of Lipase Sequence

Protein Modeling

Protein sequences whose identity was found to be the highest with the related *C. polytrichastri* ERMRI:04 lipase sequence were considered and various physicochemical parameters (amino acid composition, molecular weight, Isoelectric point, GRAVY index etc.) were calculated for a sequence using ProtParam (<https://web.expasy.org/protparam/>) module implied in the ExPASy tools repository (<https://www.expasy.org/tools/>). The domain and motif analysis of the protein query was carried out with NCBI-CDD (Berman et al., 2000) repository.

Homology modeling is a technique deployed to predict or build a 3D structure of a protein with the help of template structures, which has good sequence similarity with the query sequence. The query protein sequence has a very low percentage similarity when subjected to Protein Data Bank (PDB) (Berman et al., 2000) database for template selection in Protein BLAST (Altschul et al., 1990). We proposed to find a better suitable template for our modeling purpose by deploying Modeler v9.20 (Webb and Sali, 2016) with multiple templates found via PSI-BLAST (Ye et al., 2006). The models built by modeler were assessed using the DOPE score and Z-score (Zhang and Skolnick, 1998) by default and then were validated employing different software viz. ProSAweb server (<https://prosa.services.came.sbg.ac.at/prosa.php>), PROCHECK (a standalone package) (Laskowski et al., 1993) and QMEAN package (Benkert et al., 2011). Further, energy minimization of the selected model was carried out using GROMACS 2018 (Abraham et al., 2015), to improve its stereochemistry. After we finally obtained a valid 3D model, we further exploited the structure with various tools like RaptorX (<http://raptorx.uchicago.edu/StructPredV2/predict/>) and COACH (a standalone package) (Yang et al., 2014) to find its binding site and evaluated its conserved domains.

Molecular Docking Simulation

Molecular docking simulation is used to predict the interaction pattern between the active site of protein and ligand. The docking process includes two steps, (a) assessment of conformation pattern of the ligand in the active site of the protein, (b) predicting binding affinity between the binding site and appropriate confirmation of ligand. For optimization of substrates for lipase production, a range of vegetable oils were tested which contain a different proportion of linoleic acid, palmitic acid, and oleic acid. These fatty acids act as inducers for lipase production. The significance of these fatty acids (linoleic acid, palmitic acid, and oleic acid) as inducers was checked by docking study. Effect of various substrates on lipolytic activity was also checked to know the nature of the enzyme through docking of various substrates viz. *para*-nitrophenyl acetate, *para*-nitrophenyl palmitate, and *para*-nitrophenylphosphoryl choline. For docking simulation

process, Autodock tools (Morris et al., 2009) and Autodock Vina (Trott and Olson, 2010) were used where it gave top eight poses as output and best pose was selected based on interaction and binding affinity. Pymol (DeLano, 2002) was further used to visualize and assess our docking results.

Molecular Dynamics Simulation (MDS)

Molecular dynamics simulation (MDS) is a computer-based graphics-intensive process used to analyze the physical movement of molecules at an atomistic level over a fixed course of the time and primarily used to understand the dynamic behavior of a biological structure. GROMACS v2018, an open-source tool, was employed to study the query protein in both ways (intact as well as in the presence of substrate). MDS was employed at various temperature to understand the broad temperature character of query lipase. Firstly, the intact protein was treated with OPLSS-AA force field, placed in the center of the cubic box, solvated and ions were added to maintain the neutrality of the overall system. The energy of the whole system was minimized with the steepest descent algorithm up to 50,000 steps. Further minimized system was followed with equilibration process using NVT and NPT ensembles for 100 picoseconds (ps) at various temperature, i.e., 268.15 K (−5°C), 278.15 K (5°C), 293.15 K (20°C), 310.15 K (37°C), 313.15 K (40°C), and 333.15 K (60°C) using Berendsen coupling. Final MDS was run for 5 nanoseconds (ns) with given temperature condition. LINC algorithm and particle mesh Ewald (PME) were employed during NVT, NPT, and final run to calculate bond constraints and long-range electrostatics treatment. The same protocol was used for MDS of lipase in complex with substrates, where GROMOS9654a7 force field was used to generate topology of the complex. PRODRG 2.5 webserver (<http://prodrgr1.dyndns.org/submit.html>) was used to retrieve ligand topology. Final MDS was carried out for 5 ns at 278.15 K (5°C). All computational calculations were carried out on Ubuntu 16.104 Tyrone workstation supported with Intel Xeon Gold6132 and Quadro P5000 graphics architecture.

RESULTS

Optimization of Culture Condition

Optimization of culture condition was done to maximize the production of the lipase. Maximum lipase activity was observed in 1% (v/v) rice bran oil followed by olive oil. Optimum lipase production was observed at pH 7 when the bacterial isolate was incubated at 20°C and 150 rpm for 55 h (Figure 1).

Purification of Extracellular Lipase

The extracellular ERMRI:04 lipase (3.4 U/mg, 0.088 mg/mL protein) secreted in 500 mL fermentation broth was subjected to ammonium sulfate precipitation up to 30–80% saturation followed by dialysis against 50 mM Tris buffer with 10 kDa dialysis membrane. The 30–80% dialyzed sample showed a maximum specific activity of 26.16 U/mg with 7-fold purification. Sephadex G-100 purified lipase showed a specific activity of 35 U/mg with 10-fold purification. The SDS-PAGE analysis of the G-100 purified fractions showed multiple bands

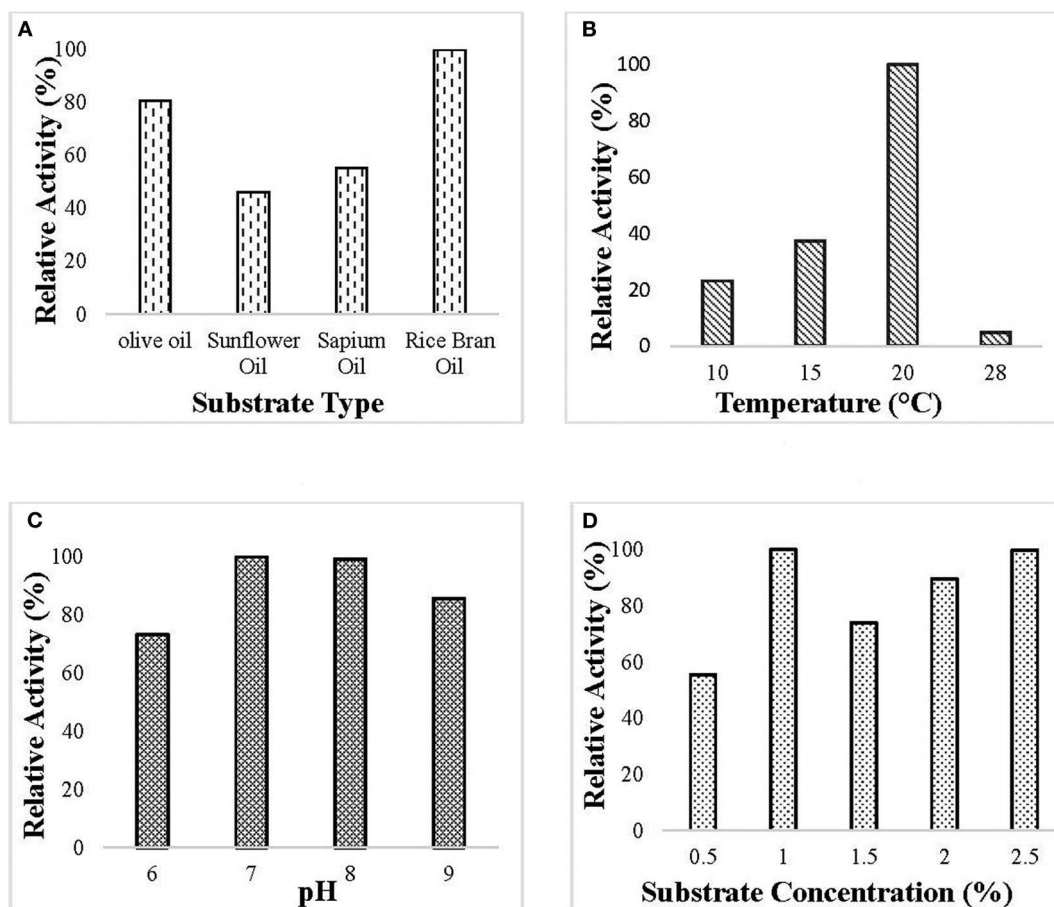


FIGURE 1 | Optimization of culture conditions for the production of ERM1:04 lipase. The bacterial isolate was grown in mineral-based production media for 60 h at 150 rpm. The optimized condition for lipase production was determined by checking the relative activity of the lipase produced at different experimental parameters, and the maximum was set to 100%. Lipase activity was determined using 50 mM tris buffer pH 8 at 37°C. Effect of **(A)** different substrate types (olive oil, sunflower oil, sapium oil, and rice bran oil) on the production of lipase. The bacterial isolate was grown at 20°C pH 7 having 1.5% (v/v) oil. Maximum lipase production was observed in rice bran oil; **(B)** different temperature (10, 15, 20, and 28°C) on lipase production in 1.5% (v/v) rice bran oil pH 7. Maximum lipase production was observed at 20°C; **(C)** different pH (6–9) on lipase production. The bacterial isolate was grown in 1.5% (v/v) rice bran oil at 20°C. Maximum lipase production was observed at pH 7; **(D)** different substrate percentage (0.5–2.5% v/v) on lipase production. The bacterial isolate was grown at 20°C pH 7 having rice bran oil as a substrate. Maximum lipase production was observed in 1% (v/v) rice bran oil.

specifying partial purification of the lipase (**Figure 2A**). Octyl-Sepharose purified fraction showed a maximum specific activity of 72 U/mg and 21-fold purification (**Table 1**) with a single protein band in SDS-PAGE (**Figure 2A**).

Determination of Molecular Weight of Purified Lipase and Zymography

The size exclusion and hydrophobic interaction chromatographic purified fractions were analyzed for its molecular weight determination by denaturing SDS-PAGE (12%) and also in non-denaturing Native-PAGE (10%). The size exclusion purified fraction showed multiple bands suggesting partial purification of the protein. The hydrophobic interaction purified protein showed a prominent single band at ~39.8 kDa in denaturing condition (**Figure 2A**) and 250 kDa in native non-denaturing condition (**Figure 2D**). The purified ERM1:04 lipase thus appeared to be hexameric with a monomer unit of 39.8 kDa.

The standard curve between log [MW] vs. R_f of proteins moved on SDS-PAGE (12%) was used to determine the exact molecular weight of purified protein (**Figure 2C**).

Zymogram of the ERM1:04 lipase showed luminescence under UV in denaturing SDS-PAGE (**Figure 2B**). This supported that the purified protein is indeed a lipase.

Peptide Mass Fingerprinting by MALDI-TOF-MS

The peptide mass pattern obtained after MALDI-TOF-MS analysis followed by MASCOT database search verified that purified protein was a lipase which showed a significant score (130) with the sequence alpha/beta hydrolase (*Solibacillus* sp. R5-41) with 34% sequence coverage (**Figure 3**). The neighbor-joining tree prepared using the amino acid sequence of alpha/beta hydrolase (topmost MALDI hit) with all the retrieved amino acid sequence of lipase and related proteins of the strain ERM1:04

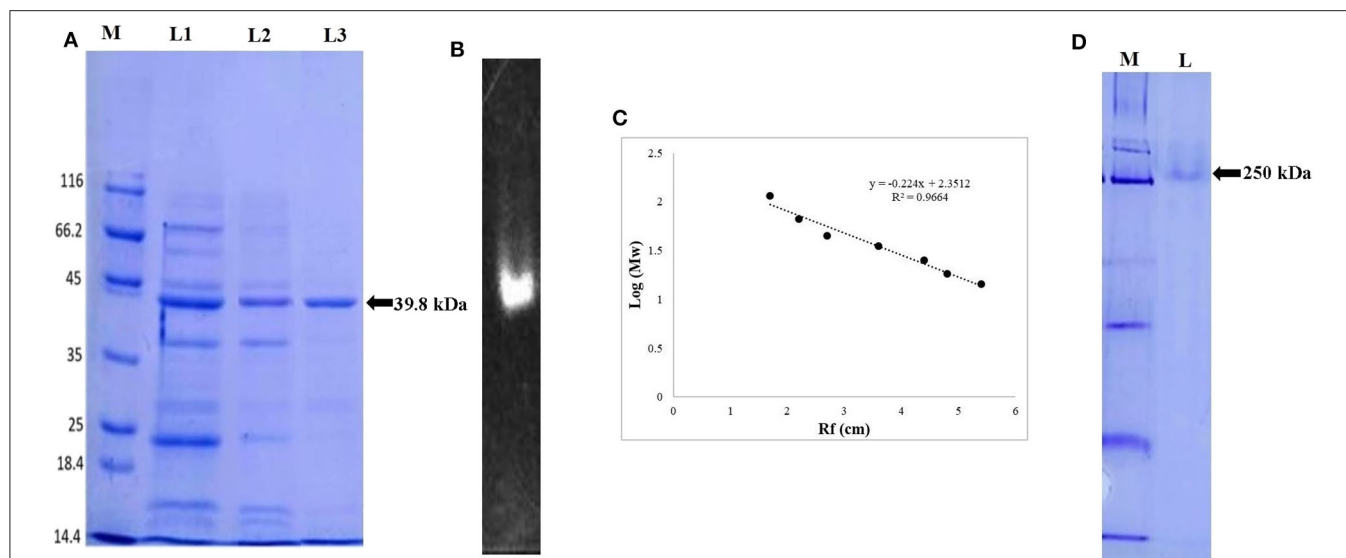


FIGURE 2 | Electrophoretic pattern of lipase, **(A)** SDS-PAGE analysis of ERM1:04 lipase at each purification step. The proteins were separated on 12% SDS-PAGE gel and then stained with Coomassie Blue R-250. M represents molecular weight marker (Pierce™ Unstained Protein MW Marker, Thermo Scientific); L1: crude cell-free extract of ERM1:04; L2: size exclusion chromatography (Sephadex G-100) purified protein fraction; L3: hydrophobic interaction chromatography (Octyl-Sepharose fast flow) purified lipase; **(B)** zymographic analysis of purified lipase in the presence of substrate MUF-butyrate in 12% SDS-PAGE; **(C)** standard curve between log [MW] vs. Rf of proteins moved on SDS-PAGE (12%). The linear relationship between protein MW markers and migration distance showed reliability in predicting MW of lipase; **(D)** native-PAGE (10%) analysis of purified lipase. M represents the molecular weight marker; L represents hydrophobic interaction chromatography (Octyl-Sepharose fast flow) purified lipase fraction.

TABLE 1 | Summary of step-wise purification of ERM1:04 lipase.

Purification stage	Total activity (U)	Total protein (mg)	Total specific activity (U/mg)	Fold purification	Yield (%)
Cell free extract	150	44.0	3.40	1	100
30–80 dialysed	92.25	3.52	26.1	7.6	61.5
Sephadex G-100	40	1.14	35.0	10.2	26.6
Octyl-Sepharose	2.4	0.03	72.7	21.3	1.6

showed clustering with GDSL lipase with bootstrap support of 57 (**Figure S1**). GDSL lipase protein sequence was then used for further *in-silico* analysis.

Biochemical Characterization of Purified Lipase

Effect of Temperature, pH, and Metal Ions

The purified lipase was active in the temperature ranging from 5 to 65°C and the optimum temperature for lipase action was observed to be 37°C (**Figure 4A**). The purified lipase was observed to be active in the pH ranging from 7 to 9 and optimum pH for lipase action was observed to be 8 (**Figure 4B**). All the tested metal ions except Cu^{2+} and Fe^{2+} enhanced the enzyme activity in both 5 and 10 mM concentration (**Figure 4C**).

Effect of Organic Solvents, Inhibitors, and Kinetic Study of Purified Lipase

The ERM1:04 lipase retained 80% of activity in isopropanol and methanol while activity was reduced considerably in the presence of butanol and acetonitrile (**Figure 5A**). All the inhibitors

decreased lipase activity. It retained more than 60% of activity in the presence of EDTA and in the presence of reducing agent, i.e., DTT, the residual activity was more than 40%. In the presence of serine protease inhibitor PMSF, the residual activity decreased linearly on increasing the inhibitor concentration in the reaction mixture. The residual activity was 50% in the presence of 1 mM PMSF (**Figure 5B**). Kinetic parameters, such as K_m and V_{max} are a good measure to study substrate affinity and reaction velocity of the purified enzyme. The observed K_m value of the purified lipase was 0.104 mM which showed its better substrate affinity. The observed V_{max} value was 3.58 U/mg (**Figure 5C**).

Detergent Compatibility Test

The compatibility of the enzyme toward different commercial detergents was checked at different temperature. The enzyme showed good hydrolytic activity in all the tested commercial detergents at different temperature. In all the tested detergents, the relative activity of the lipase was higher than the activity of the enzyme alone (**Figure 6**). This specified that the

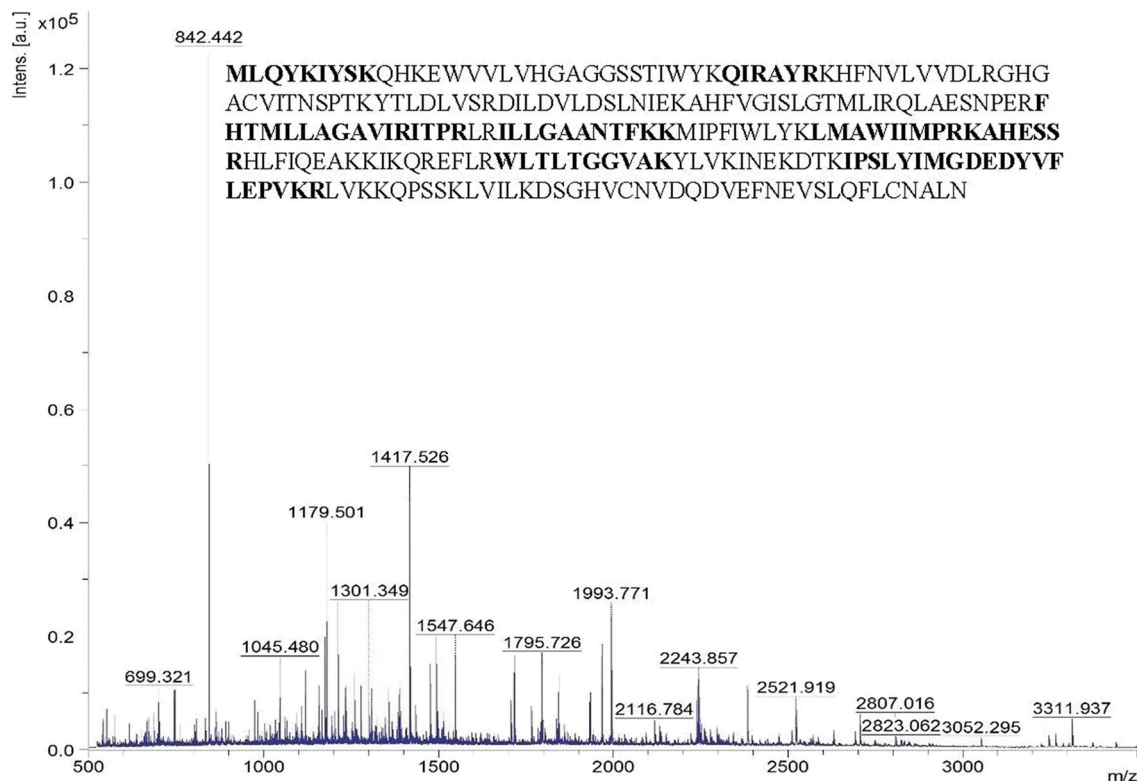


FIGURE 3 | Peptide mass spectra of purified lipase obtained from MALDI-TOF-MS. The x-axis denotes m/z ratio and the y-axis denotes intensity (a.u.) of peptides. The amino acid sequence represents the alpha/beta hydrolase of *Solibacillus* sp. to which the query sequence matched. The residues in bold are the ones identical with the query sequence.

enzyme is compatible with detergent and can be used in detergent formulations.

Bioinformatics Analysis

Prediction of Lipase Structure and Active Site Analysis

Basic physicochemical parameters calculated by ExPASy tools gave information on the protein sequence, i.e., total amino acid count (281), molecular weight (32623.30 Dalton), iso-electric point (9.39) and the GRAVY index (0.647). For finding templates against protein query, we employed PSI-BLAST rather than simple BLAST to achieve higher accuracy which was failed to achieve by simple BLAST search. From **Table S1**, 2O14 was the most favorable template based on query coverage, and still, <30% percent identity was achieved. Modeler v9.20 was employed to build a 3D model which used multiple templates instead of a single template for producing a good model prediction. Based on the DOPE score and Z-score in the modeler, the top DOPE score for the best model was -27326.658203 and Z-score was -4.28 . This model (**Figure 7A**) was then further subjected to energy minimization using the steepest descent method. Procheck tool was employed to construct the Ramachandran plot of the protein. The plot (**Figure 7B**) showed that the constructed model is of good quality as 97% region of Ramachandran plot falls in allowed quadrants. ProSA web server was also used to assess

overall model quality based on Z-score which was found to be -5.48 (**Figure S2**). This suggested a final good model for further downstream bioinformatics analysis. RaptorX web server and COACH tools were employed for exploiting binding site of the studied lipase. The active site in the studied lipase was constituted by Ile41, Ile92, Tyr130, Ile173, Pro210, Tyr211, Phe272, Val275, Thr278, Gln279, and Lys280 residues.

Molecular Docking of Lipase Using Autodock and Simulation Analysis

Lipase protein and ligand (given substrates) prepared in Autodock tools according to the protocol grid box dimensions were adjusted to $40 \times 46 \times 40$ with 0.580 \AA spacing. Effect of different inducers (linoleic acid, palmitic acid, and oleic acid) was checked to know the effect of different oils on lipase production. From the study, it was observed that linoleic acid had a maximum binding affinity (-7.4 kcal/mol) toward the enzyme, followed by palmitic acid (-6.5 kcal/mol) and oleic acid (-6.1 kcal/mol) (**Figure 8**). So, linoleic acid followed by palmitic acid acts as the best inducer for lipase production than the other tested fatty acids in ERMRI:04. To know the nature of the enzyme various substrates were used for docking study. Among three tested substrates, *p*-nitrophenyl palmitate showed the best binding affinity with the top score of -7.6 kcal/mol (**Figure 9**). Other substrates *viz.*, *p*-nitrophenylphosphoryl choline interacts with

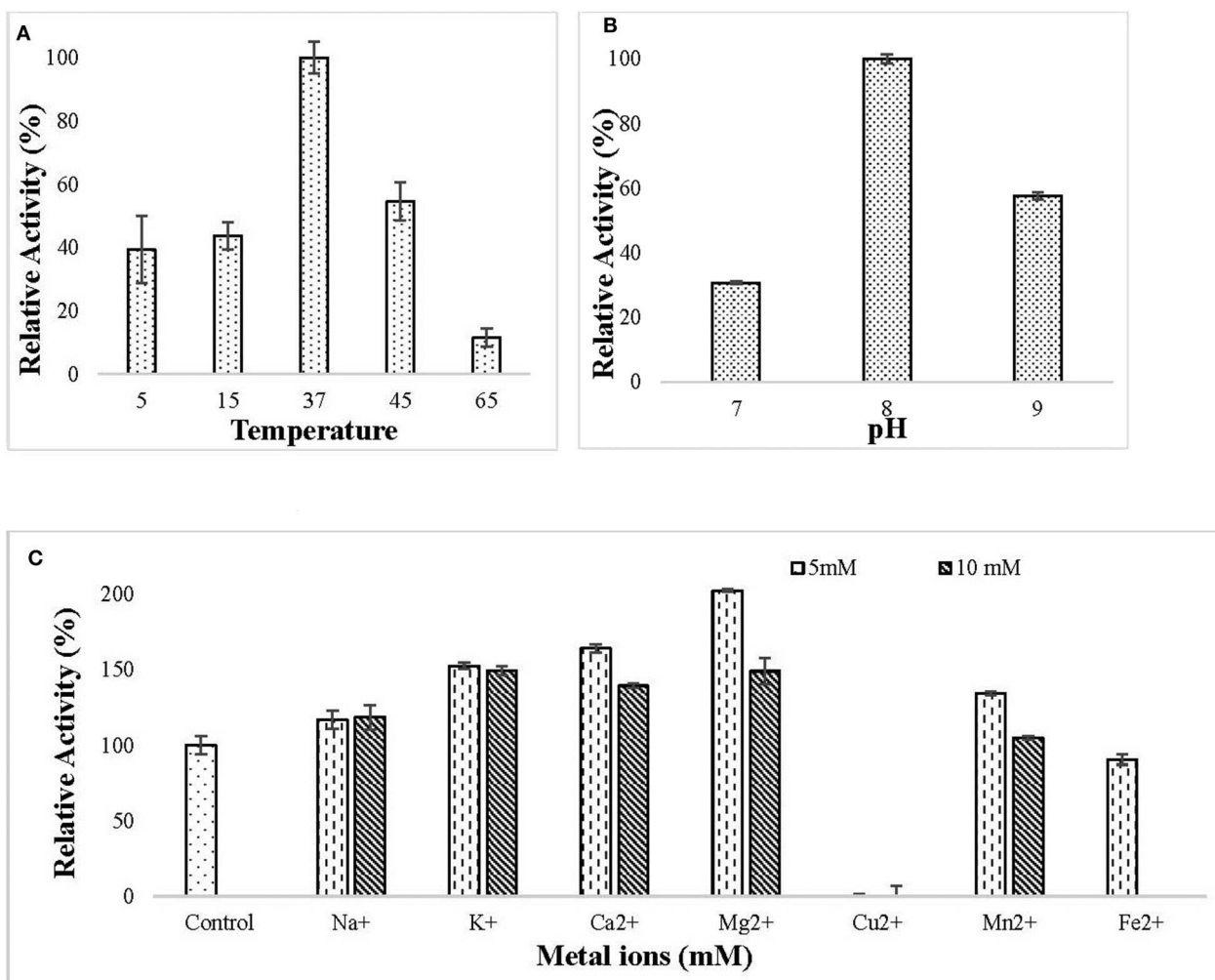


FIGURE 4 | Effect of **(A)** different temperature (5–65°C) on lipase activity. The enzyme assay was performed at a different temperature in 50 mM Tris buffer pH 8. Maximum enzyme activity was observed at 37°C and the enzyme was active in the temperature range of 5–65°C; **(B)** different pH (7–9) on lipase activity. The enzyme assay was performed at different pH in 50 mM Tris buffer. Maximum activity was observed at pH 8; **(C)** metal ions (Na⁺, K⁺, Ca²⁺, Mg²⁺, Cu²⁺, Mn²⁺, Fe²⁺) at 5 and 10 mM concentration on lipase activity. The enzyme assay was performed after pre-incubation with metal ions for 30 min at 37°C in 50 mM Tris buffer. All the metal ions except (Cu²⁺ and Fe²⁺) increased lipase activity.

–7.0 kcal/mol binding affinity and prime amino acid residues were Ile92, Pro210, Phe272, Val275, and Thr278 also shown in **Figure S3**. *p*-nitrophenyl acetate interacted with least energy of –6.3 kcal/mol depicted in **Figure S4**.

Then, Molecular dynamics studies (MDS) was carried out for lipase alone as well as for lipase in complex with substrates at various temperature to understand the broad character of the enzyme. The intact protein was simulated at 268.15 K (–5°C), 278.15 K (5°C), 293.15 K (20°C), 310.15 K (37°C), 313.15 K (40°C), and 333.15 K (60°C) temperature. Various parameters like RMSD, RMSF, and radius of gyration were considered to assess the stability of lipase protein. The overall RMSD plot (**Figure 10A**) showed that protein remains stable throughout 5 ns with insignificant fluctuation in protein backbone at 333.15 K (60°C), although the protein did not break down at all intervals across the periods. RMSF (**Figure 10B**) and

Radius of Gyration (**Figure 10C**) plots also supported a similar observation as that of RMSD results. Lipase protein reached maximum stability at 268.15 K (–5°C) and minute fluctuations at 333.15 K (60°C), showing significantly fluctuations with the increasing temperature but maintaining the overall compactness. The backbone RMSD plot in the presence of substrates showed good compactness in protein structures with mild fluctuations (**Figure S5**).

DISCUSSION

Psychrotrophic organisms possess cold-adapted proteins and enzymes which help them to maintain their metabolic function in low temperature. In the present study, an extracellular cold-adapted lipase enzyme was purified and characterized from an efficient lipase producing psychrotrophic bacterium

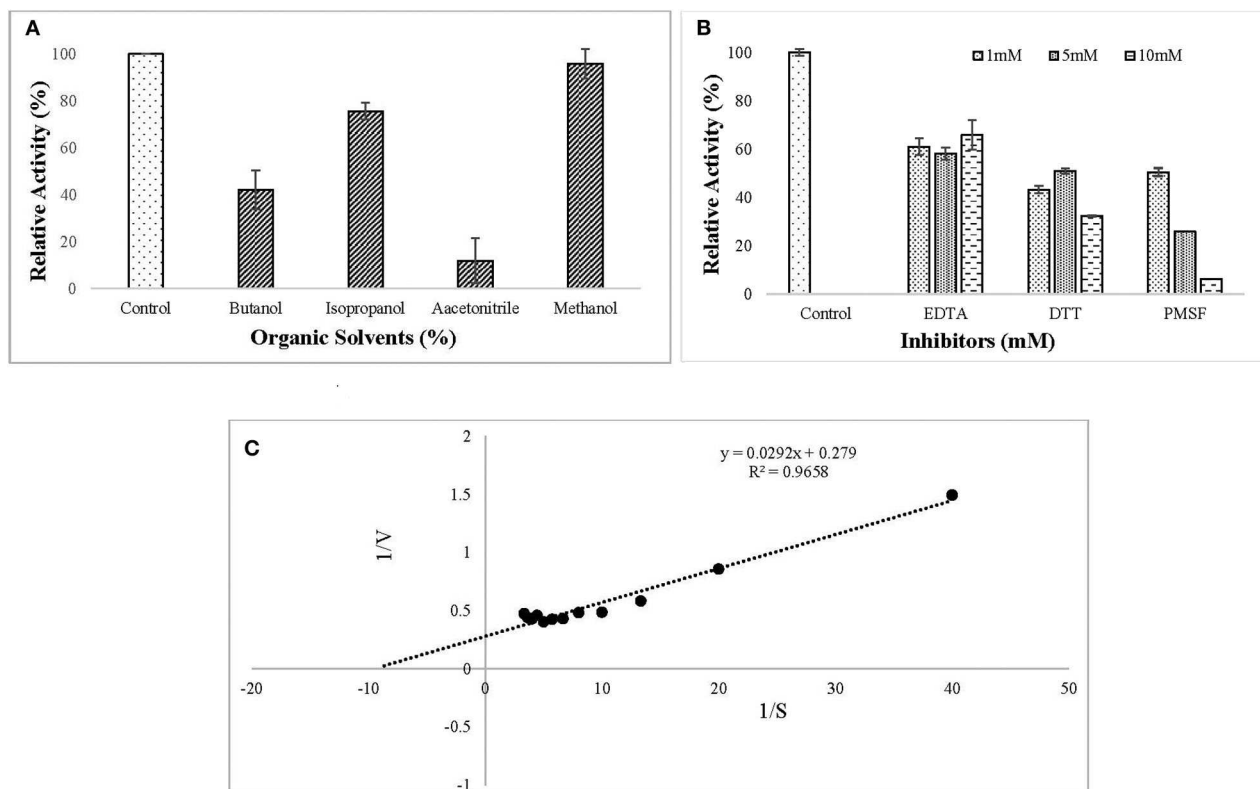


FIGURE 5 | Effect of **(A)** organic solvents (5% (v/v) Butanol, Isopropanol, Acetonitrile, and Methanol) on lipase activity. The enzyme assay was performed after pre-incubation with tested solvents for 30 min at 37°C in 50 mM tris buffer. Lipase retained 80% of activity in isopropanol and methanol while activity was reduced considerably in the presence of butanol and acetonitrile; **(B)** inhibitors (1, 5, 10 mM EDTA, DTT, PMSF) on lipase activity. The enzyme assay was performed after pre-incubation with tested solvents for 30 min at 37°C in 50 mM tris buffer. All the tested inhibitors decreased lipase activity. **(C)** Kinetic study of purified lipase was studied using the Lineweaver–Burk plot. The kinetic parameters (K_m and V_{max}) were studied by varying pNPP concentration from 0.025 to 0.3 mM. The observed K_m and V_{max} values were 0.104 mM and 3.58 U/mg, respectively.

C. polytrichastri ERM1:04 isolated from East Rathong glacier, Sikkim Himalaya.

It is known that the enzyme production is greatly dependent on the culture conditions like pH, temperature, and substrate types. In this study, maximum lipase production was observed in the pH range of 7–8, which specified that neutral to alkaline pH condition favors the lipase production by *C. polytrichastri* ERM1:04. The growth optima for the organism was also observed in the pH range of 6–10. Similar findings on lipase production in neutral to alkaline media conditions by psychrotrophic bacteria isolated from alpine regions are reported before (Barbaro et al., 2001; Gupta et al., 2004; Joseph and Ramteke, 2013; Salwoom et al., 2019b). The optimum temperature for enzyme production depends on the growth temperature of the organism. *C. polytrichastri* ERM1:04 grows well at a temperature range of 4–28°C. The enzyme production was maximum at 20°C, and a drastic decline in the production was observed with increasing temperature. Lipase is an inducible enzyme, induced by oils or fats in the culture medium (Bisht et al., 2013). In the current study, like its inherent property, lipase production was observed in all the tested lipids. The maximum production was observed in rice bran oil followed by olive oil. The

major fatty acid composition of rice bran oil includes oleic acid (18:1), linoleic acid (18:2), and palmitic acid (16:0) (Zullaikah et al., 2005). Different oils differ with the proportion of these fatty acids. To predict the reason behind the preference of rice bran oil as an inducer for lipase production in ERM1:04, binding affinities of the enzyme toward oleic acid, linoleic acid, and palmitic acid were checked by molecular docking study. The ERM1:04 lipase showed maximum affinity toward linoleic acid, followed by palmitic acid and oleic acid. Among all the tested oils, the affinity results suit the best with rice bran oil as after oleic acid, the highest percentage of composition is linoleic acid and palmitic acid. Like, in case of olive oil, the highest composition is of oleic acid but it has very low percentage of linoleic and palmitic acid (Benitez-Sánchez et al., 2003). Hence, it is hypothesized to be due to the affinity potential of the purified enzyme toward linoleic and palmitic acids, that the superior induction and production of ERM1:04 lipase is shown in the presence of rice bran oil. Earlier also, it has been reported that the fatty acid profile of oils affects lipase production by an organism (Lakshmi et al., 1999; Wang et al., 2008; Darvishi et al., 2009). Rice bran oil is low priced and readily available and the ability of the strain to produce lipase on cheap carbon source is advantageous to reduce the enzyme

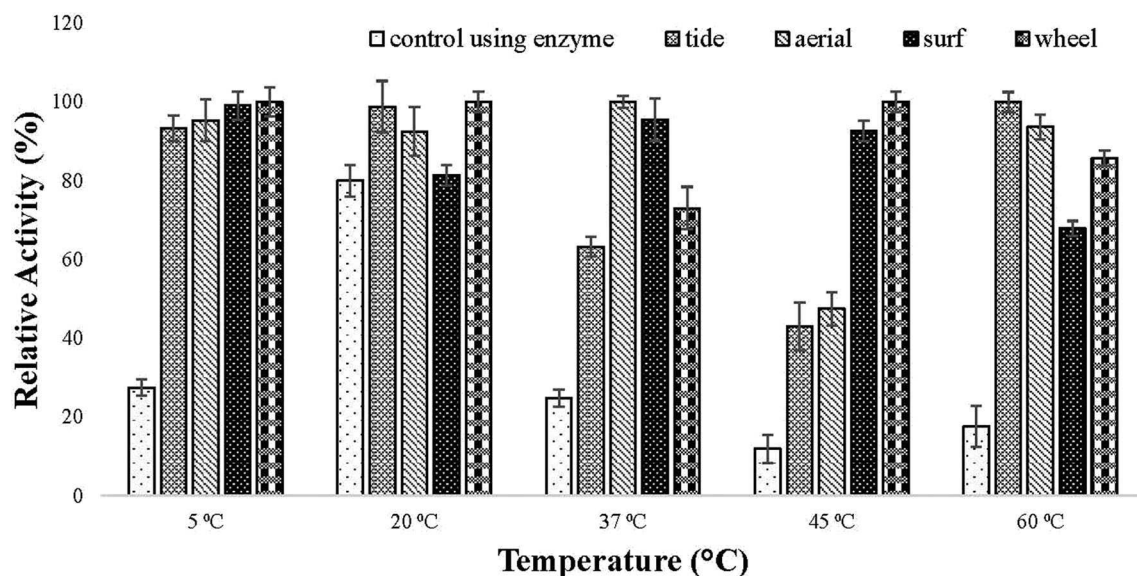


FIGURE 6 | Detergent compatibility test of purified lipase checked on commercially available detergents (1% (v/v) Tide, Surf, Aerial, and Wheel). Lipase assay was performed after incubating the enzyme in the presence of different detergents at a temperature ranging from 5 to 60°C for 30 min in tris buffer. All the detergents showed good compatibility with lipase as the activity increased in the presence of tested detergents.

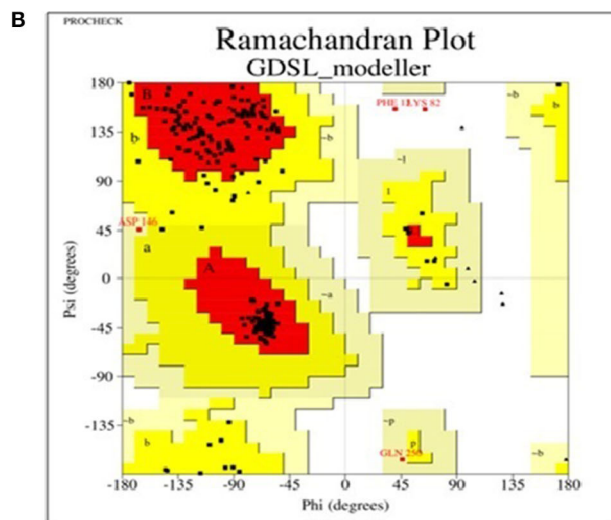
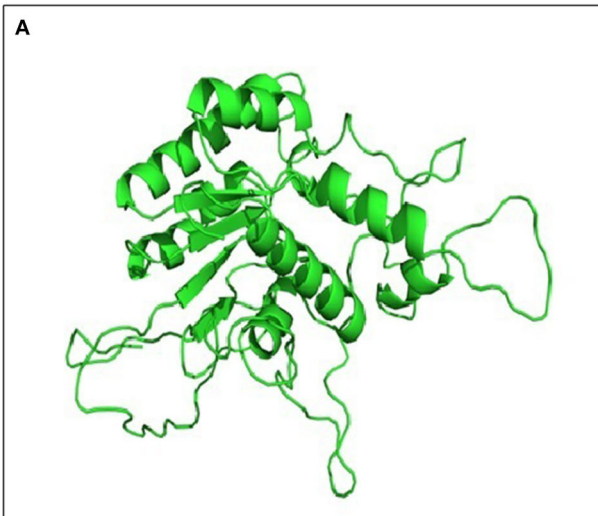


FIGURE 7 | (A) 3D model of GDSL lipase built by modeller v9.20; **(B)** model assessment by PROCHECK tool. It describes the quality of the model and shows that 97% region of Ramachandran plot falls in allowed quadrants, thereby specifying a good model quality.

production cost. In addition to the carbon source, the type of nitrogen source also affects extracellular lipase production. Generally, the organic form of nitrogen, such as peptone or yeast extract is preferred for lipase production (Ghanem et al., 2000; Sharma et al., 2002; Salwom et al., 2019b). Lipase production by ERM1:04 was done in the presence of yeast extract as a nitrogen source which is in favor of previous findings.

Purification of lipase from the culture supernatant itself is a tedious task but a certain degree of purification is necessary depending on the application of enzyme (Joseph

et al., 2008). The purification process removes contaminants and improves stability, activity and shelf life of the enzyme. Furthermore, purified protein is required for studying structure and conformation, the kinetic and thermodynamic mechanisms for substrate hydrolysis, and structure-function relationships (Javed et al., 2018). In current work, the crude enzyme was successfully purified to homogeneity in two steps, i.e., gel filtration and hydrophobic interaction chromatography with 21-fold purification and a 1.6% yield. There are numerous studies on multi-step purification of cold-active lipase from

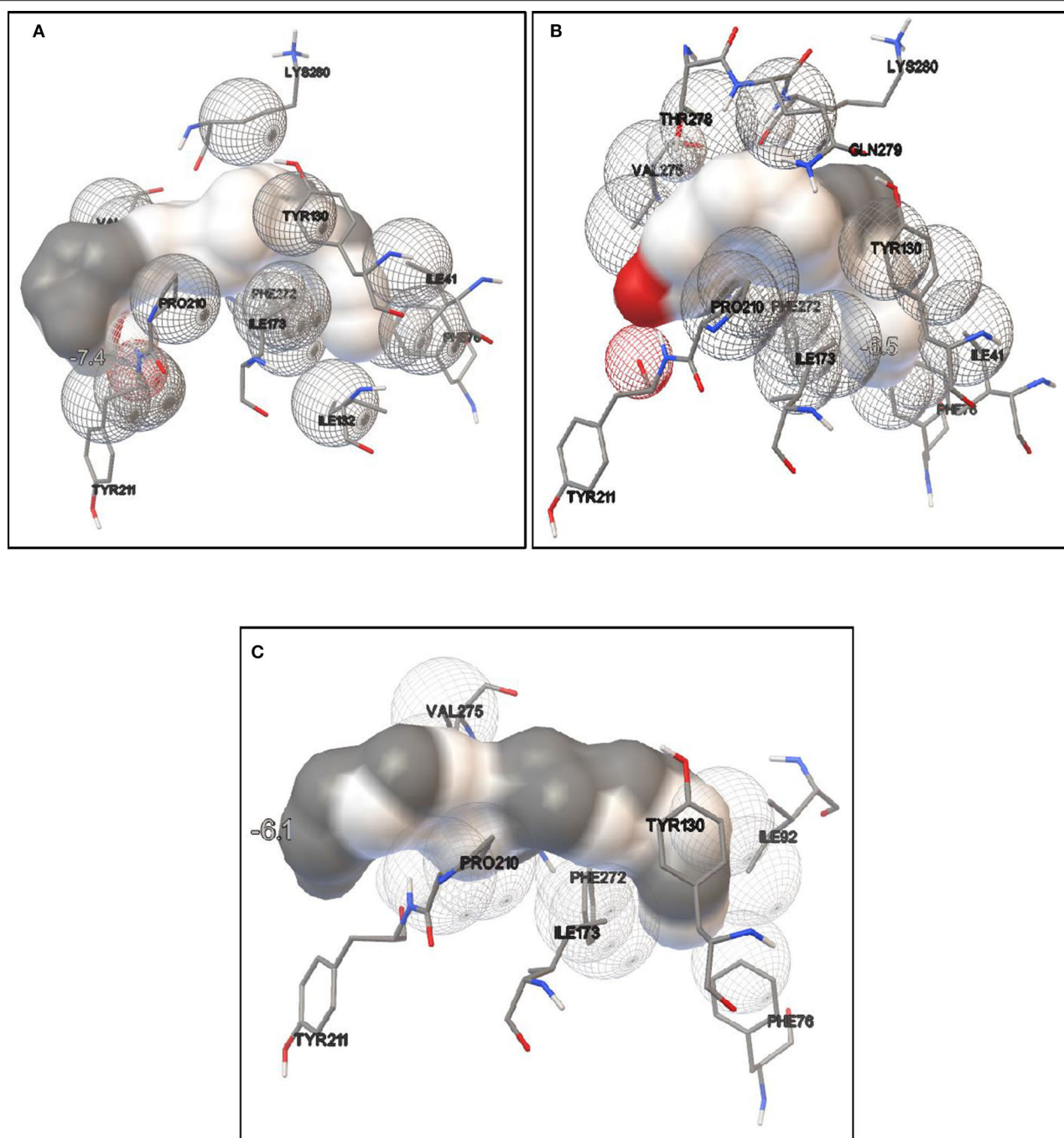


FIGURE 8 | Molecular docking simulation study of lipase with different fatty acids. It is used to predict the binding affinity of the enzyme toward different fatty acids which acts as inducers in lipase production. **(A)** Docking study in the presence of linoleic acid. The binding energy is -7.4 kcal/mol; **(B)** docking study in presence of palmitic acid, the binding energy is -6.5 kcal/mol; **(C)** docking study in presence of oleic acid, the binding energy is -6.1 kcal/mol. It is observed that maximum binding energy is observed in the presence of linoleic acid so it acts as a better inducer for ERM1:04 lipase production.

various psychrophilic and psychrotrophic bacteria, where an ammonium salt precipitation in the early stage is followed by a combination of chromatographic steps (Wang et al., 2012; Li et al., 2013; Bae et al., 2014; Ji et al., 2015). The lower yield of the enzyme might be due to the combined use of two

chromatographic steps and loss of protein during purification (Li et al., 2013; Bae et al., 2014; Ji et al., 2015). The purified lipase appeared to be a 250 kDa hexameric protein with a monomer unit of 39.8 kDa as confirmed by the Native and SDS PAGE, respectively. Zymography in the presence of substrate

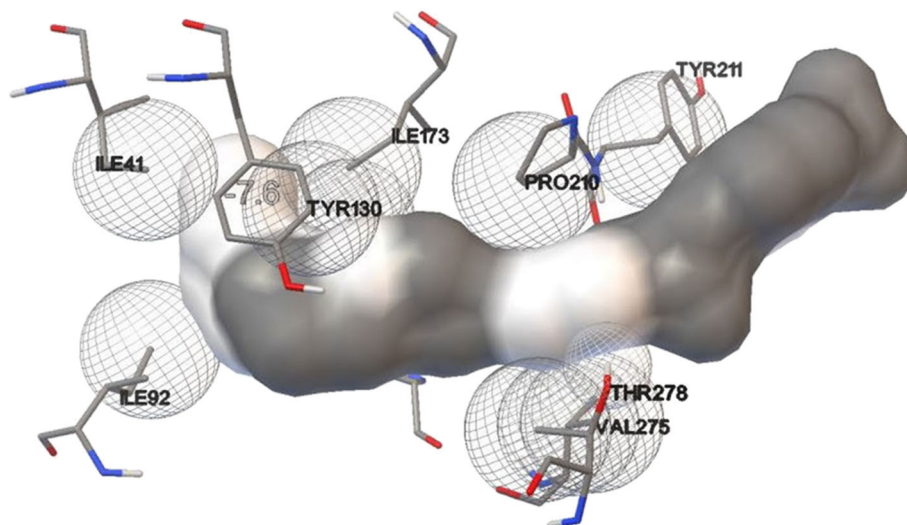


FIGURE 9 | Molecular docking simulation study of lipase with substrate *p*-nitrophenyl palmitate. It is used to predict the interaction pattern between the active site of protein and ligand. The binding affinity for *p*-nitrophenyl palmitate is (−7.6 kcal/mol), thereby specifying a good interaction with the lipase.

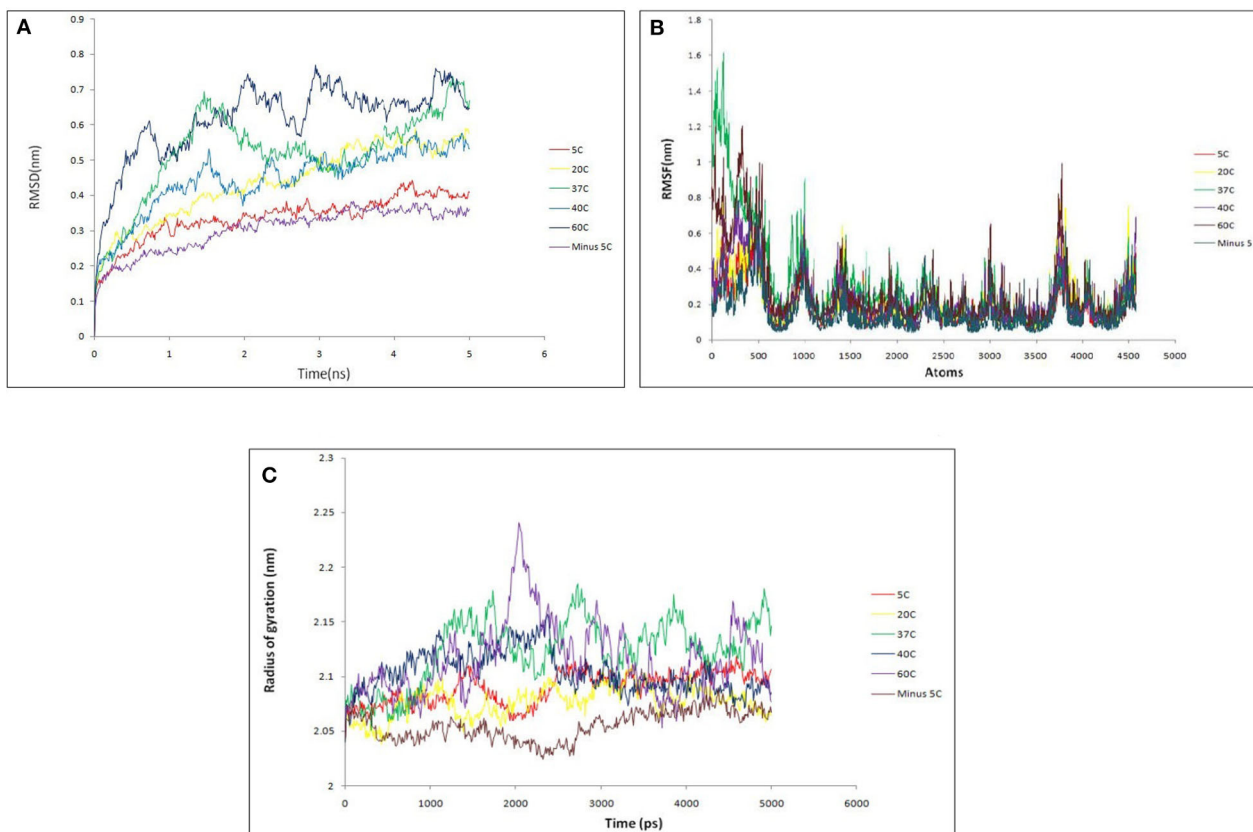


FIGURE 10 | (A) Backbone RMSD comparison of lipase protein at various temperature (−5, 5, 20, 37, 40, 60°C). It shows that protein remains stable throughout 5 ns with insignificant fluctuation in protein backbone at 60°C. The protein did not break down at any interval across the time; **(B)** RMSF comparison of lipase protein at various temperature; **(C)** radius of gyration comparison of lipase protein at various temperature. It shows the minor fluctuation in lipase structure at 60°C over 2 ns but overall protein structure remains stable.

MUF butyrate supported the identity of the purified protein as a lipase. Further, the protein sequence generated using MALDI-TOF-MS of the purified lipase showed maximum similarity with the alpha/beta hydrolase a superfamily of lipase. Afterwards, lipase and related protein sequences were retrieved from *C. polytrichastri* ERM1:04 draft genome and then a phylogenetic tree was constructed between those retrieved protein sequences and MALDI-TOF-MS topmost hit, i.e., alpha/beta hydrolase. The phylogenetic tree showed clustering of alpha/beta hydrolase with GDSL family lipase of strain ERM1:04, which was further used for structural analysis by homology modeling.

Currently, homology modeling is the most commonly used computational approach to predict and generate structural models of biological macromolecules like proteins. In the present study, an orthologous approach was used to build a 3D structure of the amino acid sequence of the purified lipase using modeler v9.20. The 3D structure was significantly valid and supported by well-known parameters like ProSA web server, Ramachandran plot and Q mean score. Previously, homology modeling approach has been used successfully to predict the 3D structure of several cold-active lipases produced by psychrotrophic bacteria (De Pascale et al., 2008; Xu et al., 2010; Kamarudin et al., 2014; Jalil et al., 2018). The final 3D model obtained was further exploited for finding the active site, docking and MD simulation studies. While analyzing ERM1:04 domain architecture, the domain length stretch expands between 39 and 271 amino acid residues according to NCBI-CDD and those active site residues were located outside of the domain length (Phe272, Val275, Thr278, Gln279, and Lys280). This finding revealed a broad substrate specificity of ERM1:04 lipase. Docking results also supported the good interaction between amino acid residues outside of the lipase domain and substrates.

Biochemical characterization of the purified lipase showed its activity in the pH ranging from 7 to 9 with an optimum activity at pH 8. This specified that the purified lipase is alkaline. Lipases with activity in a pH range of 7.6–8.6 with an optimum at 8 (Jinwal et al., 2003), pH range 8.0–10.5 with an optimum at 8.5 (Kumar et al., 2005) and pH range 7–9 with an optimum at 8.5 (Joshi et al., 2006) have been defined as alkaline in previous studies. Bioinformatics analysis performed by using the amino-acids sequence of purified lipase showed that the isoelectric point of the purified lipase is 9.39, thereby confirming the alkaline nature of the enzyme. Alkaline lipases are important in many industrial applications like leather processing, detergent formulations and sewage treatment (Salwoom et al., 2019b). The ERM1:04 lipase was active over a broad temperature range of 5–65°C, with 37°C as the optimum. This property can be valuable in many industrial processes which require low to high temperature. Most of the cold-active lipases isolated and purified till now doesn't show activity at a higher temperature (Joseph et al., 2012; Kryukova et al., 2019; Li et al., 2019; Salwoom et al., 2019a). The lipase isolated in the current study is remarkably active in a broad temperature range of 5–65°C and could be a valuable asset in many industrial processes like in detergent formulations. The lipase producing bacterium in the current study has been isolated from East Rathong Glacier, Sikkim Himalaya where temperature fluctuations are common, ranging

between –20 and 5°C (Agrawal and Tayal, 2015). Being subjected to this kind of broad temperature fluctuation, the psychrotrophic bacteria from such an environment are likely to produce versatile enzymes with broad temperature activity. In previous studies, a cold active metalloprotease enzyme isolated from a glacier bacterium (Margesin et al., 2005) and a protease isolated from a bacterium of a glacier at Lahaul and Spiti, India (Salwan et al., 2010) showed broad temperature activity. Most enzymes are metalloenzymes whose activity increases in the presence of specific metals. In this study, the lipase activity increased in Na⁺, K⁺, Ca²⁺, Mg²⁺, and Mn²⁺ ions. This showed that the enzyme is metal activated, whereby the metal ions increase the stability of the enzyme structure by changing its conformation to a stable one (Rahman et al., 2005). Other metal ions, such as Cu²⁺ and Fe²⁺ slightly inhibited the activity, indicating that these metal ions are altering the enzyme structure (Lee and Rhee, 1993; Kambourova et al., 2003; Joseph and Ramteke, 2013). Kinetic study of the purified lipase showed Km of 0.104 mM and Vmax of 3.58 U/mg for pNPP. This specified that the purified lipase has a decent substrate specificity and activity toward C-16 acyl group esters, thereby confirming the lipolytic nature of the purified enzyme as lipases show maximum activity toward long-chain esters. All the tested enzyme inhibitors reduced the lipase activity, and in the presence of serine protease inhibitor PMSE, a linear decrease in the residual activity was observed on increasing the inhibitor concentration in the reaction mixture. This indicated that the enzyme has active sites resembling the serine protease. The organic solvents (5% v/v) butanol and acetonitrile inhibited the lipase activity while isopropanol and methanol were fairly tolerated by the enzyme. This might be caused by the denaturing effect of butanol and acetonitrile on the protein.

Proteins, starch and lipids are the main components of dirt present in clothes (Olsen and Falholt, 1998). The stains present in the clothes are generally removed by beating and heating of the fabrics in presence of detergents which further shorten the life of fabrics, and is an energy-requiring process (Al-Ghanayem and Joseph, 2020). Addition of lipolytic enzymes in the detergents is becoming a common practice to improve the effectiveness of the detergent (Hasan et al., 2006). In cold environments, water used in washing should be heated for the proper functioning of enzymes as most of the mesophilic enzymes are inactive at low temperature (Al-Ghanayem and Joseph, 2020). So cold-active enzymes would be beneficial for detergents at cold regions (Joseph et al., 2008). On the other hand, at a higher temperature, most of the cold-active enzymes become inactive, so the use of a thermostable enzyme would be beneficial (Zamost et al., 1991). To address these problems, the introduction of an alkaline, cold-active enzyme with broad temperature activity as a detergent additive would be beneficial (Maharana and Ray, 2015). The lipase purified in the current study would be a better choice to use in the detergent formulation as it is active in alkaline pH ranging from 7 to 9 with optimum activity at pH 8 and temperature range of 5–65°C with an optimum at 37°C. Lipases with activity in the pH range of 7–9 with an optimum at 7 and temperature range of 0–60°C with an optimum at 15°C (Maharana and Ray, 2015), pH range of 7–11 with an optimum at 8.5 and temperature range of 5–37°C with optimum at 20°C (Li et al., 2014) were suggested as

good detergent additives in previous studies. The compatibility of the purified enzyme with common commercial detergents was checked to see its effectiveness. The activity of purified lipase increased by ~50% in the presence of all the tested commercial detergents at a temperature ranging from 5 to 60°C. In earlier studies, it has been hypothesized that enhancement of lipase activity is due to better accessibility of the substrate molecules. Binding of detergent at the active sites of the enzyme leading to its conformational change has been reported to be the possible reason for such improved substrate accessibility (Helistö and Korpela, 1998; Salameh and Wiegel, 2010). The increase in the activity of ERM1:04 lipase in presence of commercial detergents is in agreement with several earlier lipase studies (Hemachander and Puvanakrishnan, 2000; Cherif et al., 2011; Chauhan et al., 2013; Phukon et al., 2020; Sahoo et al., 2020). The studied lipase with activities in a broad temperature and alkaline pH proves to be a suitable detergent additive for enhanced washing performance at different environments ranging from colder to moderately high-temperature regions.

CONCLUSION

In the present study, a cold-adapted, broad temperature active lipase was extracted and purified to homogeneity from *C. polytrichastri* ERM1:04. The molecular weight of the monomeric unit of purified lipase was 39.8 kDa and it was a 250 kDa hexameric protein. Peptide mass fingerprinting of the purified protein confirmed it as lipase showing maximum similarity with alpha/beta hydrolase (lipase superfamily). The purified protein was broad temperature active (5–65°C) and alkalophilic. Bioinformatics predictions supported the cold-adapted and broad temperature activity of our lipase. Additionally, the *in-silico* docking studies predicted diverse substrate specificity of the purified lipase. The lipase showed promising detergent stability in presence of common commercial detergents. Owing to its versatile temperature and substrate range, and its enhanced activity with commercial detergents, the lipase qualifies as a potential candidate in detergent formulations. To the best of our knowledge, this is the first study on purification and characterization of lipase enzyme from any species of the genus *Chryseobacterium*.

REFERENCES

- Abraham, M. J., van der Spoel, D., Lindahl, E., Hess, B., and The GROMACS Development Team (2015). *GROMACS User Manual Version, 5.0.6*. Available online at: www.gromacs.org
- Agrawal, A., and Tayal, S. (2015). Mass balance reconstruction since 1963 and mass balance model for east rathong glacier, eastern himalaya, using remote sensing methods. *Geogr. Ann. Ser. A Phys. Geogr.* 97, 695–707. doi: 10.1111/geoa.12109
- Al-Ghanayem, A. A., and Joseph, B. (2020). Current prospective in using cold-active enzymes as eco-friendly detergent additive. *Appl. Microbiol. Biotechnol.* 104, 2871–2882. doi: 10.1007/s00253-020-10429-x
- Altschul, S. F., Gish, W., Miller, W., Myers, E. W., and Lipman, D. J. (1990). Basic local alignment search tool. *J. Mol. Biol.* 215, 403–410. doi: 10.1016/S0022-2836(05)80360-2

DATA AVAILABILITY STATEMENT

The datasets presented in this study can be found in online repositories. The names of the repository/repositories and accession number(s) can be found in the article/**Supplementary Material**.

AUTHOR CONTRIBUTIONS

AK: conceptualization, methodology, validation, investigation, writing—original draft, and visualization. SM: methodology, investigation, and writing—original draft. NK: software, formal analysis, investigation, and writing—original draft. VA: resources, writing—review and editing, and project administration. SK: project administration and funding acquisition. RK: conceptualization resources, writing—review and editing, supervision, project administration, and funding acquisition. All authors contributed to the article and approved the submitted version.

ACKNOWLEDGMENTS

AK acknowledges DBT, for Ph.D. studentship award from DBT, GoI (DBT/JRF/BET-17/I/2017/AL/367). RK acknowledges DST, GoI for DST INSPIRE faculty award (DST/INSPIRE/04/2014/001280). The authors acknowledge the financial support from DST, DBT, Bioinformatics Infrastructure Facility (BIF), and CSIR-IHBT in-house grant number MLP0136 and MLP0201. We are thankful to the Department of Forest, Govt. of Sikkim and Sikkim State Council of Science and Technology and for their support in sample collection. The authors duly acknowledge the support provided by Dr. Robin Joshi for MALDI-TOF-MS. This manuscript represents CSIR-IHBT communication no. 4590.

SUPPLEMENTARY MATERIAL

The Supplementary Material for this article can be found online at: <https://www.frontiersin.org/articles/10.3389/fbioe.2020.00642/full#supplementary-material>

- Bae, J. H., Kwon, M. H., Kim, I. H., Hou, C. T., and Kim, H. R. (2014). Purification and characterization of a cold-active lipase from *Pichia lynferdii* Y-7723: pH-dependant activity deviation. *Biotechnol. Bioprocess Eng.* 19, 851–857. doi: 10.1007/s12257-014-0300-5
- Barbaro, S. E., Trevors, J. T., and Inniss, W. E. (2001). Effects of low temperature, cold shock, and various carbon sources on esterase and lipase activities and exopolysaccharide production by a psychrotrophic *Acinetobacter* sp. *Can. J. Microbiol.* 47, 194–205. doi: 10.1139/w00-141
- Benitez-Sánchez, P. L., León-Camacho, M., and Aparicio, R. (2003). A comprehensive study of hazelnut oil composition with comparisons to other vegetable oils, particularly olive oil. *Eur. Food Res. Technol.* 218, 13–19. doi: 10.1007/s00217-003-0766-4
- Benkert, P., Biasini, M., and Schwede, T. (2011). Toward the estimation of the absolute quality of individual protein structure

- models. *Bioinformatics* 27, 343–350. doi: 10.1093/bioinformatics/btq662
- Berman, H. M., Westbrook, J., Feng, Z., Gilliland, G., Bhat, T. N., Weissig, H., et al. (2000). The protein data bank: nucleic acids research. *Oxford J.* 28, 235–242. doi: 10.1093/nar/28.1.235
- Bisht, D., Yadav, S. K., Gautam, P., and Darmwal, N. S. (2013). Simultaneous production of alkaline lipase and protease by antibiotic and heavy metal tolerant *Pseudomonas aeruginosa*. *J. Basic Microbiol.* 53, 715–722. doi: 10.1002/jobm.201200157
- Bradford, M. (1976). A rapid and sensitive method for the quantitation of microgram quantities of protein utilizing the principle of protein-dye binding. *Anal. Biochem.* 72, 248–254. doi: 10.1016/0003-2697(76)90527-3
- Brumlik, M. J., and Buckley, J. T. (1996). Identification of the catalytic triad of the lipase/acyltransferase from *Aeromonas hydrophila*. *J. Bacteriol.* 178, 2060–2064. doi: 10.1128/JB.178.7.2060-2064.1996
- Chauhan, M., Chauhan, S., and Garlapati, V. K. (2013). Evaluation of a new lipase from staphylococcus sp. for detergent additive capability. *Biomed Res. Int.* 2013:374967. doi: 10.1155/2013/374967
- Cherif, S., Mnif, S., Hadrich, F., Abdelkafi, S., and Sayadi, S. (2011). A newly high alkaline lipase: an ideal choice for application in detergent formulations. *Lipids Health Dis.* 10:221. doi: 10.1186/1476-511X-10-221
- Darvishi, F., Nahvi, I., Zarkesh-Esfahani, H., and Momenbeik, F. (2009). Effect of plant oils upon lipase and citric acid production in *Yarrowia lipolytica* yeast. *J. Biomed. Biotechnol.* 2009:562943. doi: 10.1155/2009/562943
- De Pascale, D., Cusano, A. M., Autore, F., Parrilli, E., Di Prisco, G., Marino, G., et al. (2008). The cold-active Lip1 lipase from the Antarctic bacterium *Pseudoalteromonas haloplanktis* TAC125 is a member of a new bacterial lipolytic enzyme family. *Extremophiles* 12, 311–323. doi: 10.1007/s00792-008-0163-9
- DeLano, W. L. (2002). *PyMOL*/pymol.org. *PyMOL Mol. Graph. Syst.* Available online at: <https://pymol.org/2/>
- Ghanem, E. H., Al-Sayed, H. A., and Saleh, K. M. (2000). An alkalophilic thermostable lipase produced by a new isolate of *Bacillus alcalophilus*. *World J. Microbiol. Biotechnol.* 16, 459–464. doi: 10.1023/A:1008947620734
- Gupta, R., Gupta, N., and Rathi, P. (2004). Bacterial lipases: an overview of production, purification and biochemical properties. *Appl. Microbiol. Biotechnol.* 64, 763–781. doi: 10.1007/s00253-004-1568-8
- Hasan, F., Shah, A. A., and Hameed, A. (2006). Industrial applications of microbial lipases. *Enzyme Microb. Technol.* 39, 235–251. doi: 10.1016/j.enzmictec.2005.10.016
- Helistö, P., and Korpela, T. (1998). Effects of detergents on activity of microbial lipases as measured by the nitrophenyl alkanoate esters method. *Enzyme Microb. Technol.* 23, 113–117. doi: 10.1016/S0141-0229(98)00024-6
- Hemachander, C., and Puvanakrishnan, R. (2000). Lipase from *Ralstonia pickettii* as an additive in laundry detergent formulations. *Process Biochem.* 35, 809–814. doi: 10.1016/S0032-9592(99)00140-5
- Himanshu, Swarnkar, M. K., Singh, D., and Kumar, R. (2016). First complete genome sequence of a species in the genus *Microterricola*, an extremophilic cold active enzyme producing bacterial strain ERGS5:02 isolated from Sikkim Himalaya. *J. Biotechnol.* 222, 17–18. doi: 10.1016/j.jbiotec.2016.02.011
- Jalil, F. N. F. A. A., Rahman, R. N. Z. R. A., Salleh, A. B., and Ali, M. S. M. (2018). Optimization and *in silico* analysis of a cold-adapted lipase from an antarctic *Pseudomonas* sp. strain ams8 reaction in triton x-100 reverse micelles. *Catalysts* 8:289. doi: 10.3390/catal8070289
- Javed, S., Azeem, F., Hussain, S., Rasul, I., Siddique, M. H., Riaz, M., et al. (2018). Bacterial lipases: a review on purification and characterization. *Prog. Biophys. Mol. Biol.* 132, 23–34. doi: 10.1016/j.pbiomolbio.2017.07.014
- Ji, X., Chen, G., Zhang, Q., Lin, L., and Wei, Y. (2015). Purification and characterization of an extracellular cold-adapted alkaline lipase produced by psychrotrophic bacterium *Yersinia enterocolitica* strain KM1. *J. Basic Microbiol.* 55, 718–728. doi: 10.1002/jobm.201400730
- Jinwal, U. K., Roy, U., Chowdhury, A. R., Bhaduri, A. P., and Roy, P. K. (2003). Purification and characterization of an alkaline lipase from a newly isolated *Pseudomonas mendocina* PK-12CS and chemoselective hydrolysis of fatty acid ester. *Bioorganic Med. Chem.* 11, 1041–1046. doi: 10.1016/S0968-0896(02)00516-3
- Joseph, B., and Ramteke, P. W. (2013). Extracellular solvent stable cold-active lipase from psychrotrophic *Bacillus sphaericus* MTCC 7526: partial purification and characterization. *Ann. Microbiol.* 63, 363–370. doi: 10.1007/s13213-012-0483-y
- Joseph, B., Ramteke, P. W., and Thomas, G. (2008). Cold active microbial lipases: Some hot issues and recent developments. *Biotechnol. Adv.* 26, 457–470. doi: 10.1016/j.biotechadv.2008.05.003
- Joseph, B., Shrivastava, N., and Ramteke, P. W. (2012). Extracellular cold-active lipase of *Microbacterium luteolum* isolated from Gangotri glacier, western Himalaya: isolation, partial purification and characterization. *J. Genet. Eng. Biotechnol.* 10, 137–144. doi: 10.1016/j.jgeb.2012.02.001
- Joshi, G. K., Kumar, S., Tripathi, B. N., and Sharma, V. (2006). Production of alkaline lipase by *Corynebacterium paurometabolum*, MTCC 6841 isolated from Lake Naukuchiatal, Uttarakhand State, India. *Curr. Microbiol.* 52, 354–358. doi: 10.1007/s00284-005-0224-6
- Junge, K., Cameron, K., and Nunn, B. (2019). “Diversity of psychrophilic bacteria in sea and glacier ice environments-insights through genomics, metagenomics, and proteomics approaches,” in *Microbial Diversity in the Genomic Era*, eds S. Das and H. R. Das (Cambridge: Academic Press), 197–216.
- Kamarudin, N. H. A., Rahman, R. N. Z. R. A., Ali, M. S. M., Leow, T. C., Basri, M., and Salleh, A. B. (2014). Unscrambling the effect of C-terminal tail deletion on the stability of a cold-adapted, organic solvent stable lipase from *Staphylococcus epidermidis* AT2. *Mol. Biotechnol.* 56, 747–757. doi: 10.1007/s12033-014-9753-1
- Kambourova, M., Kirilova, N., Mandeva, R., and Derekova, A. (2003). Purification and properties of the most stable lipase from a thermophilic *Bacillus stearothermophilus* MC 7. *J. Mol. Catal. B Enzym.* 22, 307–313. doi: 10.1016/S1381-1177(03)00045-6
- Kavitha, M. (2016). Cold active lipases—an update. *Front. Life Sci.* 9, 226–238. doi: 10.1080/21553769.2016.1209134
- Kryukova, M. V., Petrovskaya, L. E., Kryukova, E. A., Lomakina, G. Y., Yakimov, S. A., Maksimov, E. G., et al. (2019). Thermal inactivation of a cold-active esterase PMGL3 isolated from the permafrost metagenomic library. *Biomolecules* 9:880. doi: 10.3390/biom9120880
- Kumar, A., Dhar, K., Kanwar, S. S., and Arora, P. K. (2016a). Lipase catalysis in organic solvents: advantages and applications. *Biol. Proced. Online* 18:2. doi: 10.1186/s12575-016-0033-2
- Kumar, R., Acharya, V., Mukhia, S., Singh, D., and Kumar, S. (2019). Complete genome sequence of *Pseudomonas frederiksbergensis* ERDD5:01 revealed genetic bases for survivability at high altitude ecosystem and bioprospection potential. *Genomics* 111, 492–499. doi: 10.1016/j.ygeno.2018.03.008
- Kumar, R., Acharya, V., Singh, D., and Kumar, S. (2018a). Strategies for high-altitude adaptation revealed from high-quality draft genome of non-violacein producing *Janthinobacterium lividum* ERGS5:01. *Stand. Genomic Sci.* 13:11. doi: 10.1186/s40793-018-0313-3
- Kumar, R., Singh, D., Swarnkar, M. K., Singh, A. K., and Kumar, S. (2015a). Complete genome sequence of *Arthrobacter* sp. ERGS1:01, a putative novel bacterium with prospective cold active industrial enzymes, isolated from East Rathong glacier in India. *J. Biotechnol.* 214, 139–140. doi: 10.1016/j.jbiotec.2015.09.025
- Kumar, R., Singh, D., Swarnkar, M. K., Singh, A. K., and Kumar, S. (2015b). Genome assembly of *Chryseobacterium polytrichastri* ERM1:04, a psychrotolerant bacterium with cold active proteases, isolated from east rathong glacier in India. *Genome Announc.* 3, e01305–e01315. doi: 10.1128/genomeA.01305-15
- Kumar, R., Singh, D., Swarnkar, M. K., Singh, A. K., and Kumar, S. (2016b). Complete genome sequence of *Arthrobacter alpinus* ERGS4:06, a yellow pigmented bacterium tolerant to cold and radiations isolated from Sikkim Himalaya. *J. Biotechnol.* 220, 86–87. doi: 10.1016/j.jbiotec.2016.01.016
- Kumar, S., Kikon, K., Upadhyay, A., Kanwar, S. S., and Gupta, R. (2005). Production, purification, and characterization of lipase from thermophilic and alkaliphilic *Bacillus coagulans* BTS-3. *Protein Expr. Purif.* 41, 38–44. doi: 10.1016/j.pep.2004.12.010
- Kumar, S., Stecher, G., Li, M., Knyaz, C., and Tamura, K. (2018b). MEGA X: molecular evolutionary genetics analysis across computing platforms. *Mol. Biol. Evol.* 35, 1547–1549. doi: 10.1093/molbev/msy096
- Laemmli, U. K. (1970). Cleavage of structural proteins during the assembly of the head of bacteriophage T4. *Nature* 227, 680–685. doi: 10.1038/227680a0
- Lakshmi, B. S., Kanguane, P., Abraham, B., and Pennathur, G. (1999). Effect of vegetable oils in the secretion of lipase from *Candida rugosa*

- (DSM 2031). *Lett. Appl. Microbiol.* 29, 66–70. doi: 10.1046/j.1365-2672.1999.00578.x
- Laskowski, R. A., MacArthur, M. W., Moss, D. S., and Thornton, J. M. (1993). PROCHECK: a program to check the stereochemical quality of protein structures. *J. Appl. Crystallogr.* 26, 283–291. doi: 10.1107/S0021889892009944
- Lee, S. Y., and Rhee, J. S. (1993). Production and partial purification of a lipase from *Pseudomonas putida* 3SK. *Enzyme Microb. Technol.* 15, 617–623. doi: 10.1016/0141-0229(93)90026-X
- Li, M., Yang, L. R., Xu, G., and Wu, J. P. (2013). Screening, purification and characterization of a novel cold-active and organic solvent-tolerant lipase from *Stenotrophomonas maltophilia* CGMCC 4254. *Bioresour. Technol.* 148, 114–120. doi: 10.1016/j.biortech.2013.08.101
- Li, T., Zhang, W., Hao, J., Sun, M., and Lin, S. X. (2019). Cold-active extracellular lipase: expression in Sf9 insect cells, purification, and catalysis. *Biotechnol. Rep.* 21:e00295. doi: 10.1016/j.btre.2018.e00295
- Li, X. L., Zhang, W. H., Wang, Y. D., Dai, Y. J., Zhang, H. T., Wang, Y., et al. (2014). A high-detergent-performance, cold-adapted lipase from *Pseudomonas stutzeri* PS59 suitable for detergent formulation. *J. Mol. Catal. B Enzym.* 102, 16–24. doi: 10.1016/j.molcatb.2014.01.006
- Lineweaver, H., and Burk, D. (1934). The determination of enzyme dissociation constants. *J. Am. Chem. Soc.* 56, 658–666. doi: 10.1021/ja01318a036
- Luitel, K. K., Shrestha, D. G., Sharma, N. P., and Sharma, R. K. (2012). *Impact of Climate Change on East-Rathong Glacier in Rangit Basin, West Sikkim. Climate Change in Sikkim Patterns, Impacts and Initiatives*. Gangtok: Information and Public Relations Department, Government of Sikkim.
- Maharana, A., and Ray, P. (2015). A novel cold-active lipase from psychrotolerant *Pseudomonas* sp. AKM-L5 showed organic solvent resistant and suitable for detergent formulation. *J. Mol. Catal. B Enzym.* 120, 173–178. doi: 10.1016/j.molcatb.2015.07.005
- Maingwa, J., Ali, M. S. M., Salleh, A. B., Rahman, R. N. Z. R. A., Shariff, F. M., and Leow, T. C. (2015). Adaptational properties and applications of cold-active lipases from psychrophilic bacteria. *Extremophiles* 19, 235–247. doi: 10.1007/s00792-014-0710-5
- Margesin, R., Dieplinger, H., Hofmann, J., Sarg, B., and Lindner, H. (2005). A cold-active extracellular metalloprotease from *Pedobacter cryoconitii*—production and properties. *Res. Microbiol.* 156, 499–505. doi: 10.1016/j.resmic.2004.12.008
- Morris, G. M., Ruth, H., Lindstrom, W., Sanner, M. F., Belew, R. K., Goodsell, D. S., et al. (2009). Software news and updates AutoDock4 and AutoDockTools4: automated docking with selective receptor flexibility. *J. Comput. Chem.* 30, 2785–2791. doi: 10.1002/jcc.21256
- Olsen, H. S., and Falholt, P. (1998). The role of enzymes in modern detergency. *J. Surfactants Deterg.* 1, 555–567. doi: 10.1007/s11743-998-0058-7
- Phukon, L. C., Chourasia, R., Kumari, M., Godan, T. K., Sahoo, D., Parameswaran, B., et al. (2020). Production and characterisation of lipase for application in detergent industry from a novel *Pseudomonas helmanticensis* HS6. *Bioresour. Technol.* 309:123352. doi: 10.1016/j.biortech.2020.123352
- Prim, N., Sánchez, M., Ruiz, C., Pastor, F. I. J., and Diaz, P. (2003). Use of methylumbelliferyl-derivative substrates for lipase activity characterization. *J. Mol. Catal. B Enzym.* 22, 339–346. doi: 10.1016/S1381-1177(03)00048-1
- Rahman, R. N. Z. R. A., Baharum, S. N., Basri, M., and Salleh, A. B. (2005). High-yield purification of an organic solvent-tolerant lipase from *Pseudomonas* sp. strain S5. *Anal. Biochem.* 341, 267–274. doi: 10.1016/j.ab.2005.03.006
- Ranjan, R., Yadav, M. K., Suneja, G., and Sharma, R. (2018). Discovery of a diverse set of esterases from hot spring microbial mat and sea sediment metagenomes. *Int. J. Biol. Macromol.* 119, 572–581. doi: 10.1016/j.ijbiomac.2018.07.170
- Reetz, M. T. (2002). Lipases as practical biocatalysts. *Curr. Opin. Chem. Biol.* 6, 145–150. doi: 10.1016/S1367-5931(02)00297-1
- Sahoo, R. K., Das, A., Gaur, M., Sahu, A., Sahoo, S., Dey, S., et al. (2020). Parameter optimization for thermostable lipase production and performance evaluation as prospective detergent additive. *Prep. Biochem. Biotechnol.* 1–7. doi: 10.1080/10826068.2020.1719513. [Epub ahead of print].
- Salameh, M. A., and Wiegel, J. (2010). Effects of detergents on activity, thermostability and aggregation of two alkalithermophilic lipases from thermosyntrophs lipolytica. *Open Biochem. J.* 4, 22–28. doi: 10.2174/1874091X01004010022
- Salwan, R., Gulati, A., and Kasana, R. C. (2010). Phylogenetic diversity of alkaline protease-producing psychrotrophic bacteria from glacier and cold environments of Lahaul and Spiti, India. *J. Basic Microbiol.* 50, 150–159. doi: 10.1002/jobm.200800400
- Salwom, L., Rahman, R. N. Z. R. A., Salleh, A. B., Shariff, F. M., Convey, P., and Ali, M. S. M. (2019a). New recombinant cold-adapted and organic solvent tolerant lipase from psychrophilic *Pseudomonas* sp. LSK25, isolated from Signy Island Antarctica. *Int. J. Mol. Sci.* 20:1264. doi: 10.3390/ijms20061264
- Salwom, L., Rahman, R. N. Z. R. A., Salleh, A. B., Shariff, F. M., Convey, P., Pearce, D., et al. (2019b). Isolation, characterisation, and lipase production of a cold-adapted bacterial strain *Pseudomonas* sp. LSK25 isolated from Signy Island, Antarctica. *Molecules* 24:175. doi: 10.3390/molecules24040715
- Sharma, A., Meena, K. R., and Kanwar, S. S. (2018). Molecular characterization and bioinformatics studies of a lipase from *Bacillus thermoamylovorans* BHK67. *Int. J. Biol. Macromol.* 107, 2131–2140. doi: 10.1016/j.ijbiomac.2017.10.092
- Sharma, R., Soni, S. K., Vohra, R. M., Jolly, R. S., Gupta, L. K., and Gupta, J. K. (2002). Production of extracellular alkaline lipase from a *Bacillus* sp. RSJ1 and its application in ester hydrolysis. *Indian J. Microbiol.* 42, 49–54.
- Shivaji, S., Begum, Z., Shiva Nageswara Rao, S. S., Vishnu Vardhan Reddy, P. V., Manasa, P., Sailaja, B., et al. (2013). Antarctic ice core samples: culturable bacterial diversity. *Res. Microbiol.* 164, 70–82. doi: 10.1016/j.resmic.2012.09.001
- Trott, O., and Olson, A. J. (2010). Software news and update AutoDock Vina: improving the speed and accuracy of docking with a new scoring function, efficient optimization, and multithreading. *J. Comput. Chem.* 31, 455–461. doi: 10.1002/jcc.21334
- Wang, D., Xu, Y., and Shan, T. (2008). Effects of oils and oil-related substrates on the synthetic activity of membrane-bound lipase from *Rhizopus chinensis* and optimization of the lipase fermentation media. *Biochem. Eng. J.* 41, 30–37. doi: 10.1016/j.bej.2008.03.003
- Wang, Q., Hou, Y., Ding, Y., and Yan, P. (2012). Purification and biochemical characterization of a cold-active lipase from Antarctic sea ice bacteria *Pseudoalteromonas* sp. NJ 70. *Mol. Biol. Rep.* 39, 9233–9238. doi: 10.1007/s11033-012-1796-4
- Webb, B., and Sali, A. (2016). Comparative protein structure modeling using MODELLER. *Curr. Protoc. Bioinforma.* 2016, 5.6.1–5.6.37. doi: 10.1002/cpbi.3
- Xu, T., Gao, B., Zhang, L., Lin, J., Wang, X., and Wei, D. (2010). Template-based modeling of a psychrophilic lipase: conformational changes, novel structural features and its application in predicting the enantioselectivity of lipase catalyzed transesterification of secondary alcohols. *Biochim. Biophys. Acta* 1804, 2183–2190. doi: 10.1016/j.bbapap.2010.08.012
- Yang, J., Yan, R., Roy, A., Xu, D., Poisson, J., and Zhang, Y. (2014). The I-TASSER suite: protein structure and function prediction. *Nat. Methods* 12, 7–8. doi: 10.1038/nmeth.3213
- Ye, J., McGinnis, S., and Madden, T. L. (2006). BLAST: improvements for better sequence analysis. *Nucleic Acids Res.* 34, W6–W9. doi: 10.1093/nar/gkl164
- Zamost, B. L., Nielsen, H. K., and Starnes, R. L. (1991). Thermostable enzymes for industrial applications. *J. Ind. Microbiol.* 8, 71–81. doi: 10.1007/BF01578757
- Zhang, L. I., and Skolnick, J. (1998). What should the Z-score of native protein structures be? *Protein Sci.* 7, 1201–1207. doi: 10.1002/pro.5560070515
- Zhang, Y., Ji, F., Wang, J., Pu, Z., Jiang, B., and Bao, Y. (2018). Purification and characterization of a novel organic solvent-tolerant and cold-adapted lipase from *Psychrobacter* sp. ZY124. *Extremophiles* 22, 287–300. doi: 10.1007/s00792-018-0997-8
- Zullaikah, S., Lai, C. C., Vali, S. R., and Ju, Y. H. (2005). A two-step acid-catalyzed process for the production of biodiesel from rice bran oil. *Bioresour. Technol.* 96, 1889–1896. doi: 10.1016/j.biortech.2005.01.028

Conflict of Interest: The authors declare that the research was conducted in the absence of any commercial or financial relationships that could be construed as a potential conflict of interest.

Copyright © 2020 Kumar, Mukhia, Kumar, Acharya, Kumar and Kumar. This is an open-access article distributed under the terms of the Creative Commons Attribution License (CC BY). The use, distribution or reproduction in other forums is permitted, provided the original author(s) and the copyright owner(s) are credited and that the original publication in this journal is cited, in accordance with accepted academic practice. No use, distribution or reproduction is permitted which does not comply with these terms.



A Novel High Glucose-Tolerant β -Glucosidase: Targeted Computational Approach for Metagenomic Screening

Shohreh Ariaeenejad^{1*}, Safura Nooshi-Nedamani¹, Mahdie Rahban², Kaveh Kavousi², Atefeh Ghasemi Pirbalooti¹, SeyedSoheil Mirghaderi², Mahsa Mohammadi¹, Mehdi Mirzaei³ and Ghasem Hosseini Salekdeh^{1,3*}

¹ Department of Systems and Synthetic Biology, Agricultural Biotechnology Research Institute of Iran (ABRII), Agricultural Research Education and Extension Organization (AREEO), Karaj, Iran, ² Laboratory of Complex Biological Systems and Bioinformatics (CBB), Department of Bioinformatics, Institute of Biochemistry and Biophysics (IBB), University of Tehran, Tehran, Iran, ³ Department of Molecular Sciences, Macquarie University, Sydney, NSW, Australia

OPEN ACCESS

Edited by:

Giovanni Sanna,
University of Naples Federico II, Italy

Reviewed by:

Andrea Strazzulli,
University of Naples Federico II, Italy
Elisabeth Jacobsen,
Norwegian University of Science
and Technology, Norway

*Correspondence:

Shohreh Ariaeenejad
shariaee@gmail.com;
sh.ariaee@abrii.ac.ir
Ghasem Hosseini Salekdeh
h_salekdeh@abrii.ac.ir;
hsalekdeh@yahoo.com

Specialty section:

This article was submitted to
Industrial Biotechnology,
a section of the journal
Frontiers in Bioengineering and
Biotechnology

Received: 03 April 2020

Accepted: 24 June 2020

Published: 30 July 2020

Citation:

Ariaeenejad S,
Nooshi-Nedamani S, Rahban M,
Kavousi K, Pirbalooti AG,
Mirghaderi S, Mohammadi M,
Mirzaei M and Salekdeh GH (2020) A
Novel High Glucose-Tolerant
 β -Glucosidase: Targeted
Computational Approach
for Metagenomic Screening.
Front. Bioeng. Biotechnol. 8:813.
doi: 10.3389/fbioe.2020.00813

The rate-limiting component of cellulase for efficient degradation of lignocellulosic biomass through the enzymatic route depends on glucosidase's sensitivity to the end product (glucose). Therefore, there is still a keen interest in finding glucose-tolerant β -glucosidase (BGL) that is active at high glucose concentrations. The main objective of this study was to identify, isolate, and characterize novel highly glucose-tolerant and halotolerant β -glucosidase gene (PersiBGL1) from the mixed genome DNA of sheep rumen metagenome as a suitable environment for efficient cellulase by computationally guided experiments instead of costly functional screening. At first, an *in silico* screening approach was utilized to find primary candidate enzymes with superior properties. The structure-dependent mechanism of glucose tolerance was investigated for candidate enzymes. Among the computationally selected candidates, PersiBGL1 was cloned, isolated, and structurally characterized, which achieved very high activity in relatively high temperatures and alkaline pH and was successfully used for the hydrolysis of cellobiose. This enzyme exhibits a very high glucose tolerance, with the highest inhibition constant K_i (8.8 M) among BGLs reported so far and retained 75% of its initial activity in the presence of 10 M glucose. Furthermore, a group of multivalent metal, including Mg^{2+} , Mn^{2+} , and Ca^{2+} , as a cofactor, could improve the catalytic efficiency of PersiBGL1. Our results demonstrated the power of computational selected candidates to discover novel glucose tolerance BGL, effective for the bioconversion of lignocellulosic biomass.

Keywords: novel β -glucosidase, *in silico* screening, lignocellulosic biomass, high glucose tolerance, metagenome

INTRODUCTION

The term cellulosic biomass, also known as lignocellulose, refers to any constituent of plants or plant-derived biodegradable matter, namely, wood, grasses, and other feedstock across the world. Lignocellulose is mainly composed of three structural polymers (cellulose, hemicellulose, and lignin). It is the most prevalent type of raw material that exists on the earth (Guo et al., 2018).

The enormous quantity of cellulosic biomass and its renewable quality have led to a strong drive for replacing fossil fuel with more eco-friendly energy sources.

The use of fossil fuel and the problems associated with it, such as contributing to environmental pollution and the fact that nature cannot replenish fossil energy sources, have forced us to forage for an alternative and renewable source of energy (Singhania et al., 2017). In this respect, bioethanol production is receiving abundant consideration as a promising candidate for biofuel, and hence substances that participate in biofuel production are of great economic importance (Zhang et al., 2012).

Enzymatic saccharification of cellulose in biofuel production usually depends on at least three enzymes, including endoglucanases (EGs), cellobiohydrolases (CBHs), and β -glucosidases (BGLs). Together, the coordinated action of these three enzymes induces a synergistic effect on cellulose degradation. EGs hydrolyze the long-chain cellulose into celloextrin and oligosaccharides. CBHs release cellobiose units, and in the end, BGLs play a pivotal role in converting cellobiose into glucose (Cairns and Esen, 2010; Cao et al., 2015).

β -glucosidases are a set of enzymes that are typically classified in GH1 and GH3 families, with less presence in GH families (Chan et al., 2016; Cao et al., 2018) 5, 9, 16, 30, and 116 (Thongpoo et al., 2013). BGL is involved in the process of glycosidic bond cleavage that ends in glucose release. Therefore, BGLs are essential for the efficiency and completion of cellulose hydrolysis (Colabardini et al., 2016) and likewise determining the rate of forwarding reactions (Santa-Rosa et al., 2018). BGLs have been exploited in a broad range of applications such as food, animal feed, beverage, biofuel industries, and many other commercial fields (Pogorzelski and Wilkowska, 2007; Nigam et al., 2018). In the past decade, by the advent of biofuel and biomass program, BGL has drawn thorough attention for its function in the final step of lignocellulose bioconversion (Cai et al., 2019).

The catalytic efficiency of BGL is undergoing considerable interest, reasoning that its ultimate product, glucose, inhibits and limits the activity of BGL, which leads to cellobiose and oligosaccharide aggregation. Subsequently, the presence of an accumulated concentration of cellobiose and oligosaccharide operates as a barrier to repress endoglucanase and exoglucanase, which eventually hinders the whole progress of cellulose hydrolysis (Singhania et al., 2013; Teugjas and Våljamäe, 2013).

In industrial bioconversion, reaction conditions, e.g., temperature and pH stability, substrate concentration, and inhibitors are remarkable factors that can affect the hydrolyzed quality of BGLs (Limauro et al., 2018; Cai et al., 2019). Regarding the industrial utilization of enzymes that often occurs at a specific range of temperature (50°C) for an extended period and the fact that most of the BGLs with glucose resistance such as BGLs acquired from *Debaryomyces hansenii* and *Thermoanaerobacterium aotearoense* metagenome are heat-sensitive, the thermal stability of an enzyme is of great importance (Maitan-Alfenas et al., 2014; Yang et al., 2015). Thermostable enzymes offer numerous potential advantages in lignocelluloses bioconversion (Littlechild, 2015), such as increasing the reaction rate, the high solubility of the reactants,

a lower risk of contamination, lowering the solution viscosity, and decreasing the cost of energy for cooling after thermal pretreatment (Seo et al., 2015; Zeiske et al., 2016). In 2017, it was proposed that thermostability, high catalytic efficiency, and a strong tolerance for glucose of BGLs are significant features for their industrial utilization (Pang et al., 2017).

Besides the properties as mentioned above, e.g., thermostability and glucose tolerance, sometimes enzymes based on their biotechnological and commercial purposes are required to have some peculiar features, for example, salt or metal ion tolerance. To the best of our knowledge, there is a dearth of information about halophilic BGLs reported in the literature hitherto, but a BGL from a marine streptomycete and another BGL from a marine metagenomic library are some examples of enzymes with salt tolerance characteristic (Fang et al., 2010; Mai et al., 2013).

In order to assess BGL sensitivity to glucose, two kinetic values could be assessed: The half-maximal inhibitory concentration of glucose (IC_{50}) or inhibition constant (K_i). By postulating the recent research, GH1 and GH3 BGLs have revealed several fluctuations in their glucose tolerance rate (Chauve et al., 2010). Nevertheless, the BGL that belongs to the GH1 family demonstrated much higher glucose tolerance in comparison to GH3 β -glucosidases (Thongpoo et al., 2014). Although scientists have not reached a consensus about the factors responsible for high glucose tolerance of GH1 β -glucosidases, some, including Giuseppe et al., associate the high glucose-tolerant GH1 BGLs with the deeper catalytic pocket of them (De Giuseppe et al., 2014). One of the most comprehensive investigations to perceive the structural mechanism behind high glucose tolerance in BGLs has been done by Matsuzawa et al. (2016). They showed that the asparagine residue located at position 223 of a high glucose-tolerant GH1 β -glucosidase, Td2F2, has a crucial role in the glucose tolerance feature. They examined the importance of the structure at the Asn223 residue by saturation mutagenesis via replacing it with all other amino acid residues and measured their activities in the presence or absence of 500 mM glucose. This mutation drastically reduced the enzyme glucose tolerance and its substrate specificity (Matsuzawa et al., 2016).

The isolation and biochemical characterization of BGLs from a widespread class of organisms have been studied for discovering novel and industrially more productive enzyme (Tramontina et al., 2017). Up to date, there are only four BGLs with both high thermostability and glucose tolerance that are directly acquired from a hyperthermophilic microorganism (Dennett and Blamey, 2016). However, their optimum working temperature was much higher than commercially used BGLs (Akram et al., 2016). To improve the industrial operation of BGLs and combine various expedient traits, genetically manipulated enzymes are used. For instance, the Cel1A mutant (167/172) with mended glucose tolerance and resistance against extreme condition as a result of two amino acid modification developed a better enzymatic source in bioconversion of lignocellulosic materials (Guo et al., 2016). Another example of genetically enhanced BGL is Bgl1317, which appears to be the first enzyme of its kind that performs acceptable thermostability and glucose tolerance (Liu et al., 2019).

Likewise, metagenomics approaches provide a new strategy that enabled us to clone experimentally unavailable genome into culturable bacteria to detect a unique biocatalyst. A new glucose-tolerant BGL (bgl1A) was isolated from the marine metagenome that showed 50% of its activity in 1 M glucose. This result demonstrates the feasible application of bgl1A in the degradation of biomass (Fang et al., 2010).

A high glucose-tolerant GH1 β -glucosidase, Td2F2, and Ks5A7 were isolated by functional screening from the microbial metagenomic library. The recombinant β -glucosidase, Td2F2 and Ks5A7, exhibited enzymatic activity with the product inhibition by glucose and is a potent candidate for industrial applications (Uchiyama et al., 2013, 2015).

In the current study, the sheep rumen metagenomic data were computationally screened to find out proper thermostable, halotolerant, and glucose-tolerant BGL candidate enzymes, and the PersiBGL1 was cloned, expressed, purified, and biochemically characterized. In this context, the biochemical feature of the enzyme, including optimum temperature and pH, thermostability, and its activity in the presence of glucose inhibitors and metal ions, were assayed and brought in the following section. The distinctive enzymatic properties of this enzyme revealed that it is appropriate for effectively degrading lignocellulosic biomass and can be potentially utilized in bioethanol production as well as other applications in food and feed industries.

MATERIALS AND METHODS

Computational Mining of Thermostable, Halotolerant, and Glucose-Tolerant β -Glucosidase Sequences

Metagenomic data and the analysis protocol of sheep's rumen microbiota (**Supplementary File S1**) were submitted to NCBI with BioProject ID: PRJNA635543. Raw sheep rumen metagenomic data were mined for putative glucose-tolerant and preferably halotolerant and/or thermostable BGL enzymes. After quality control by FASTQC and performing assembly process using meta-velvet assembler, the MetaGeneMark software (Zhu et al., 2010) was exploited to predict the β -glucosidase genes from constructed contigs. The enzymes extracted from the metagenome were aligned against the list of 13 BGL enzymes extracted from the literature using standalone NCBI BLAST (**Supplementary File S2**). The one common property among all selected enzymes is that they all have at least one of these experimentally proven features: glucose tolerance, halotolerant, thermophilicity, or alkaliphilicity.

Based on pairwise blast, the most similar predicted metagenomic BGLs to the abovementioned known enzymes, were determined with an E-value less than $1E-50$.

To determine the evolutionary position of the chosen predicted enzyme, named PersiBGL1, the phylogenetic tree consisting of PersiBGL1 and 13 abovementioned known enzymes were inferred using the Neighbor-Joining method (Saitou and Nei, 1987).

For inferring the phylogenetic tree, the tree is drawn to scale, with branch lengths in the same units as those of the evolutionary distances used. The evolutionary distances were computed using the number of differences method (Nei and Kumar, 2000) and are in the units of the number of amino acid differences per sequence. There were a total of 321 positions in the final dataset. Evolutionary analyses were conducted in MEGA X (Kumar et al., 2018). One of the metagenomic enzymes, later called PersiBGL1, showed the most phylogenetic similarity with the known enzymes, after the following extra stages, and were selected for the lab experiments.

Additional computational steps were performed to narrow down the set of candidate metagenomics enzymes. The predicted enzymes from metagenome were compared with conserved domains using the PSSM models in the NCBI Conserved Domains Database (CDD) (Marchler-Bauer et al., 2016).

Among sequences with close similarity with known thermostable BGLs and predicted BGL CDD domain, the PersiBGL1 was chosen for further analysis. Using the Phyre2 server, the tertiary structure of this enzyme is predicted (Kelley et al., 2015). The predicted structure for PersiBGL1 was aligned against the Td2F2 as a high glucose-tolerant BGL with 3WH5 pdb code using the TM-align tools (Zhang and Skolnick, 2005).

Recombinant Expression and Purification PersiBGL1

In order to acquire BGL gene, metagenome DNA template from sheep rumen was screened. The BGL gene encoding sequence was amplified by polymerase chain reaction (PCR) using PersiBGL1 F (5'-TAATAGCATATG ATGGCAGTCAAGTATCAGTTC-3') and PersiBGL1 R (5'-TAATAG AAGCTT TCAAAATCCATGATTTCGCAATG-3') primers, which included *NdeI* and *HindIII* restriction sites, respectively. The PCR was carried out as follows: one cycle at 95°C for 5 min, 35 cycles of 94°C for 40 s, 55°C for 45 s, 72°C for 2 min, and then a cycle of 72°C for 10 min. PCR product was purified, digested with *NdeI* and *HindIII*, and ligated into pET-28a, resulting in recombinant plasmid pet28-PersiBGL1 (Ariaeenejad et al., 2019a,b).

The resulting PCR products were detected on agarose gel 1.5% (w/v) and purified using the gel extraction kit (BIORON, Germany). Purified DNA fragments were cloned and digested into the pET28an. The resulting plasmids were then transformed into the *E. coli* BLrad21 (DE3) and correct insertion was confirmed by sequencing. In the Luria-Bertani (LB) medium, the recombinant strain pET28-PersiBGL1 was cultivated at the temperature of 37°C. Adding isopropyl- β -D-thiogalactopyranoside (IPTG) to a final concentration of 0.4 mM for 20 h at 20°C, expression of enzymes was induced. By utilizing Ni-NTA Fast Start Kit (Qiagen, Hilden, Germany), N-terminal histidine-tagged recombinant protein was purified and evaluated by sodium dodecyl sulfate-polyacrylamide gel electrophoresis (SDS-PAGE).

The candidate enzyme produced from successful cloning, expression, and purification was named PersiBGL1. This BGL was subjected to further biophysical experiments. The nucleotide

sequence of the GH1 gene PersiBGL1 was submitted to GenBank Database with accession number MN016943. The nucleotide and amino acid sequences of PersiBGL1 are available in **Supplementary File S3**.

Protein concentrations were determined through the Bradford method using bovine serum albumin as the standard.

Spectroscopy Studies

Synergy HTX Multi-Mode Microplate Reader was used for UV-vis spectrophotometry. Bovine serum albumin (BSA) was used as a protein standard to matured protein concentration using the Bradford method. The β -pNPG substrate was used for enzyme activity measurement at 405 nm.

Enzymatic Activity Analysis of β -Glucosidase

PersiBGL1 activity was examined through the micro titer plate method by employing 4-nitrophenyl- β -D-glucopyranoside (β -pNPG) as a substrate (Parry et al., 2001). The reaction systems containing 30 μ l of β -pNPG (10 mM, pH 7) substrate and 30 μ l of the appropriately diluted enzyme (0.5 mg/ml) were combined at 40°C for 10 min, and the reaction was terminated by adding 120 μ l of Na_2CO_3 (1 M). By monitoring the absorbance at 405 nm, we recorded the absorbance of the developed color.

The standard curve of p-nitrophenol (pNP) has been used to measure the concentration of produced pNP. One unit of BGL was defined as the amount of enzyme required for releasing 1 μ mol of pNP per minute under the specified conditions of these assays. The kinetic parameters Michaelis constant (k_m and V_{max}) of PersiBGL1 was determined by the Lineweaver-Burk plot obtained from enzymatic hydrolysis of pNPG differing in concentration (from 0.1 to 10 mM, pH 7) (Chan et al., 2018).

Determination of Optimum Temperature and pH and Storage Stability

The enzyme's optimum temperature was identified by analyzing enzyme catalytic activity using β -pNPG (10 mM, pH 7) in temperatures varying between 20 and 90°C, during 10 min incubation of reaction mixture at each temperature and also the enzyme's optimal pH was similarly determined by investigating enzyme activity in the range of 4 to 11 at optimum temperature. The optimal reaction pH was assessed using several buffers with varying pH values at 40°C including citrate sodium buffer (50 mM, pH 4.0, 5.0), phosphate buffer (50 mM, pH 6.0–8.0), Tris-HCl buffer (50 mM, 9), and carbonate-bicarbonate buffer (pH 10, 11).

The storage stability of enzyme was determined by pre-incubation of the purified enzyme. The methods for determining storage stability was used by incubation of the purified enzymes for 11 days in elution buffer Ni-NTA Fast Start Kit (Tris-HCl 5 mM, NaCl 300 mM, and imidazole 250 mM, at pH 8.0) at 40°C, and the enzymes' activities were examined in each 24-hour interval. For reporting PersiBGL1 activity, relative activity was considered as the percentage of highest activity.

Glucose Inhibition Studies

To investigate the effect of the end product, glucose, on the catalytic activity, this reaction was performed in the presence of glucose concentration from 0 to 10 M. The concentration of the initial substrate pNPG was 10 mM. For the control, the same reaction system was used, but no glucose was added. The inhibitory influence of glucose on the initial enzymatic activity was investigated based on method proposed by Zhao et al. (2013). For this purpose, enzyme activity was assayed using the mixture including 25 μ l of enzyme (0.5 mg/ml), 25 μ l of β -pNPG (1, 5 mM), and 25 μ l of glucose (1–10 M) that is incubated at 40°C for 10 min. In the absence of glucose, the initial activity of the enzymes was considered as 100%. Glucose inhibition constant (K_i) of constructed and purified PersiBGL1 was examined utilizing the Dixon plot analysis (Zhao et al., 2018).

Effect of Metal Ions and Chemical Reagents on β -Glucosidase Activity

The β -pNPG (10 mM) was added into the reaction mixture containing each of the metal ions including MgCl_2 , CaCl_2 , NaCl , MnCl_2 , CuSO_4 , FeSO_4 , ZnCl_2 , EDTA, Urea, PMSF, NaN_3 (5 mM), and SDS, CTAB, Tween 20, and Triton X-100 at concentrations of chemical reagents (1%) with enzyme after being pre-incubated at 25°C for 30 min.

Various concentrations of NaCl (0.05, 0.1, 0.5, 1, 2, 3, 4, and 5 M) in 50 mM phosphate buffer (pH 8) were used to examine the salt tolerance of the enzyme. Meanwhile, the enzyme activity was evaluated under standard condition and the activity of control solution without the presence of metal ions and chemical reagents was assumed as 100% (Li et al., 2012).

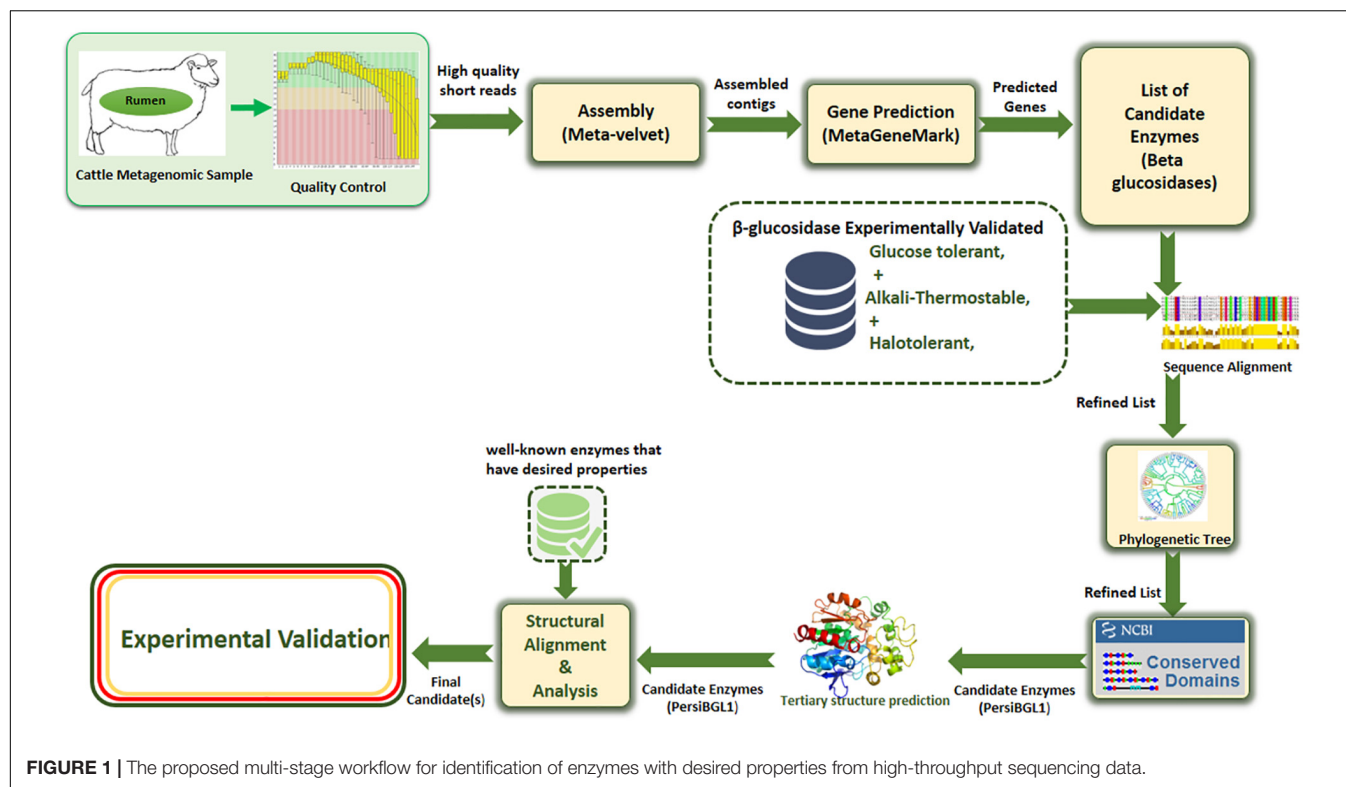
The Hydrolysis of Cellobiose by β -Glucosidase

The enzymatic hydrolysis of cellobiose (1% w/v) by PersiBGL1 was investigated by incubation of enzyme and cellobiose at 40°C in 50 mM phosphate buffer (pH 8). At different times, samples were collected and the amount of released glucose was measured in 24-h time intervals by glucose oxidase-peroxidase method using 3,3',5,5'-tetramethylbenzidine (Foerster and Lynen, 1985) until 380 h.

RESULTS AND DISCUSSION

Our applied methodology in this study greatly reduced the amount of laboratory work through a more precise multi-step computational process. Assembling and screening raw metagenome data, predicting potential BGLs, identifying the BGL enzymes having all the desired features, selecting the most appropriate candidates, 3D modeling of the selected enzymes, and investigating the molecular mechanisms behind these important features, all done before starting the laboratory phase, result in highly targeted and highly successful laboratory tasks (**Figure 1**).

By this method, we isolate a BGL from sheep rumen metagenome, which shows high stability and activity in relatively



high temperatures and alkaline pH. More importantly, it was notably insensitive to glucose as a competitive inhibitor, and even its catalytic activity soared by the addition of some ionic salt. This enzyme can substantially augment the conversion efficiency of agricultural waste to biofuel economically and industrially.

Screening of PersiBGL1 by Sequence and 3D Structure Analysis

The PersiBGL1 was one of the most similar sequences to the 13 sequences extracted from literature that its cloning and expression procedures were done successfully. The phylogenetic tree constructed using 13 BGLs with known properties besides the PersiBGL1 is demonstrated in **Figure 2A**. From the set of 13 mentioned sequences, an alkaliphilic and halotolerant BGL from *Oceanobacillus iheyensis* HTE831 (accession number BAC14719.1) with E-value $1E-173$ and Bit score 487 is the nearest neighbor of PersiBGL1 in the phylogenetic tree.

The CDD search revealed that the PersiBGL1 has a conserved 460 amino acids (AA) domain with PSSM-ID 225343 (Cdd:COG2723), Bit Score 584.60, and E-value $0e + 00$. This is a Beta-glucosidase/6-phospho-beta-glucosidase/beta-galactosidase with carbohydrate transport and metabolism functionality. The active sites and alignment of PersiBGL1 and BAC14719.1 and COG2723 are shown in **Figure 2B**. The region containing the catalytic domain in PersiBGL1, Gln18, His122, Asn167-Glu168, Trp416, and Trp424 is well conserved.

Although there is a close identity between the PersiBGL1 and a β -glucosidase from *Selenomonas bovis* (NCBI Reference Sequence WP_164175414.1), due to uncharacterized properties

of this enzyme, various experiments were performed to reveal the properties of the PersiBGL1 enzyme.

The phyre2 suggests that the double mutant (cys211ser/cys292ser) 6-2 phospho-b-d-glucosidase from *Lactobacillus plantarum* with PDB code 5NAV has the most similar tertiary structure to the PersiBGL1 with confidence score 100%.

By EzMol software (Reynolds et al., 2018), the 3D structure of PersiBGL1, including domains and the location of active sites was presented (**Figure 2B**).

The sequence and structural alignment between the predicted pdb model for PersiBGL1 and Td2F2 as a high glucose-tolerant BGL (PDB code 3WH5) were performed. **Figure 2C** illustrates the pairwise global alignment of these two BGLs. These two BGLs have only 34% sequence identity with Bit-score 253. The most prominent feature of PersiBGL1 is its ultra-high glucose tolerance. The mechanism of high glucose tolerance in BGLs was investigated by Matsuzawa et al. (2016). They identified the key role of an asparagine amino acid (Asn223) for glucose tolerance and substrate specificity in a Td2F2, a GH1 BGL with 3WH5 PDB code.

Figure 2C shows the graphical result of the structural alignment of these enzymes obtained from TM-Align. In contrast to sequence alignment, the structural alignment confirms very high similarity between the structures of PersiBGL1 and Td2F2. Among 465 residues of PersiBGL1, 93% of them aligned with Td2F2 residues with distance less than 5.0 Å. The RMSD value is 1.82 Å and the TM-score is 0.90559 and 0.94719 if normalized by length of PersiBGL1 and Td2F2, respectively. The TM-score

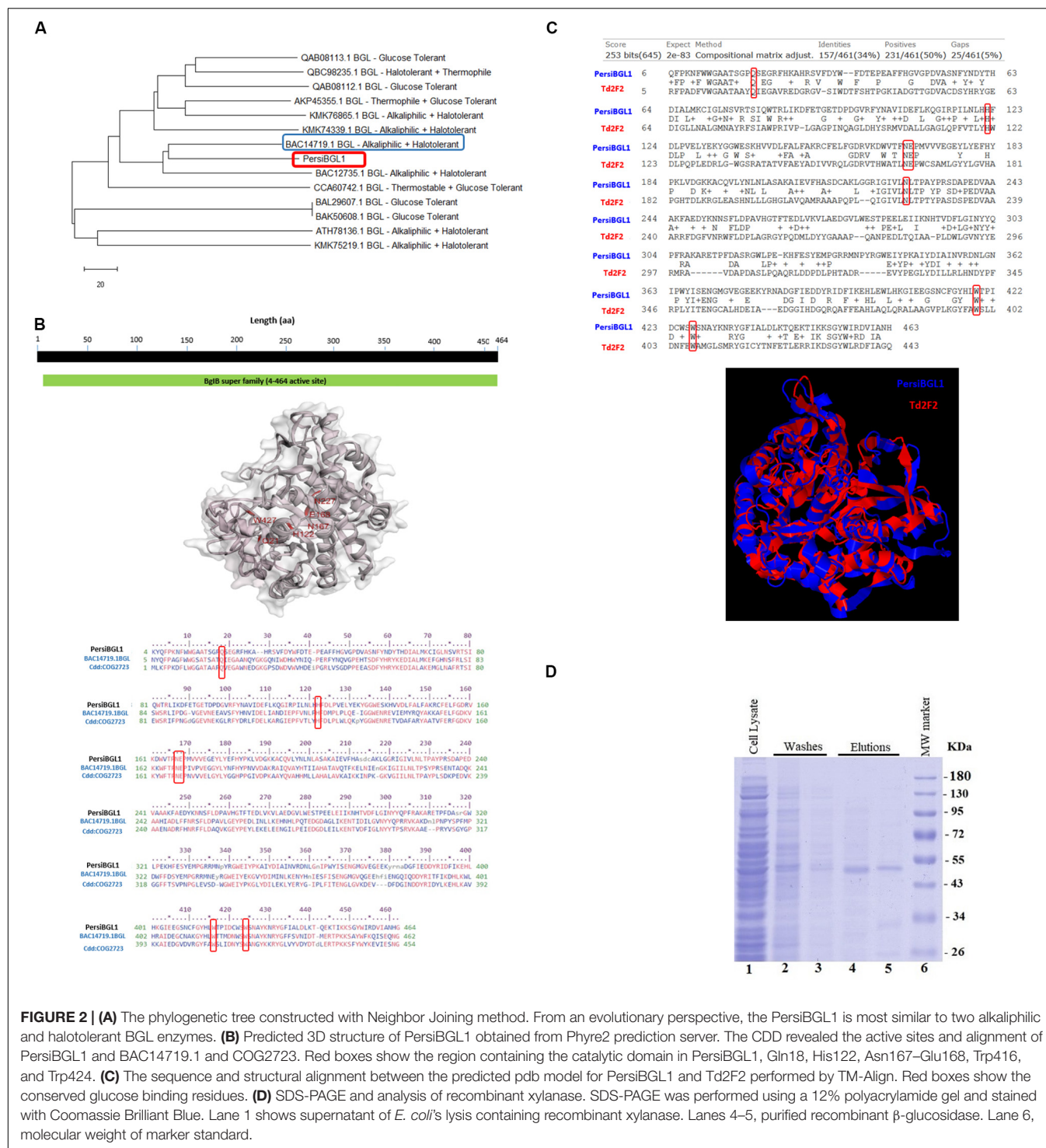


FIGURE 2 | (A) The phylogenetic tree constructed with Neighbor Joining method. From an evolutionary perspective, the PersiBGL1 is most similar to two alkaliphilic and halotolerant BGL enzymes. **(B)** Predicted 3D structure of PersiBGL1 obtained from Phyre2 prediction server. The CDD revealed the active sites and alignment of PersiBGL1 and BAC14719.1 and COG2723. Red boxes show the region containing the catalytic domain in PersiBGL1, Gln18, His122, Asn167–Glu168, Trp416, and Trp424. **(C)** The sequence and structural alignment between the predicted pdb model for PersiBGL1 and Td2F2 performed by TM-Align. Red boxes show the conserved glucose binding residues. **(D)** SDS-PAGE and analysis of recombinant xylanase. SDS-PAGE was performed using a 12% polyacrylamide gel and stained with Coomassie Brilliant Blue. Lane 1 shows supernatant of *E. coli*'s lysis containing recombinant xylanase. Lanes 2–5, purified recombinant β -glucosidase. Lane 6, molecular weight of marker standard.

near to 1 indicates that both enzymes belong to the same structural folding class and the small RMSD indicates the very high structural similarity between two BGLs. The very close structural similarity between these two enzymes suggests that they should have also similar functional properties.

As it can be seen in **Figure 2C**, the Asn223 from Td2F2 is aligned with Asn227 in the PersiBGL1. The very high

structural similarity between PersiBGL1 and a well-known glucose-tolerant enzyme besides the existence of the key asparagine amino acid in similar locations in both sequences strongly suggests that the PersiBGL1 should have high glucose tolerance features. The experiments described in the next subsections confirmed the ultra-high glucose tolerance in this novel BGL.

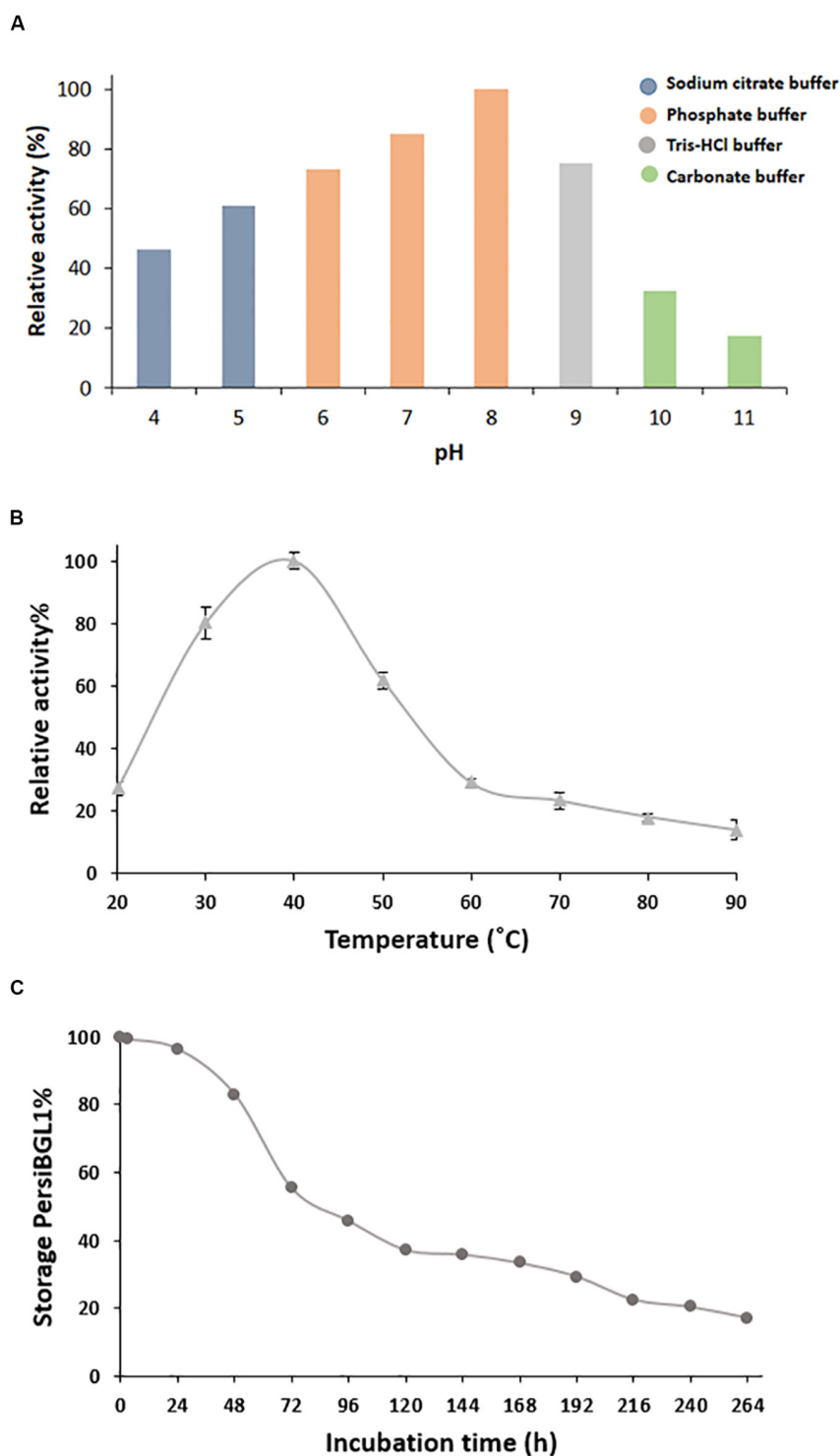
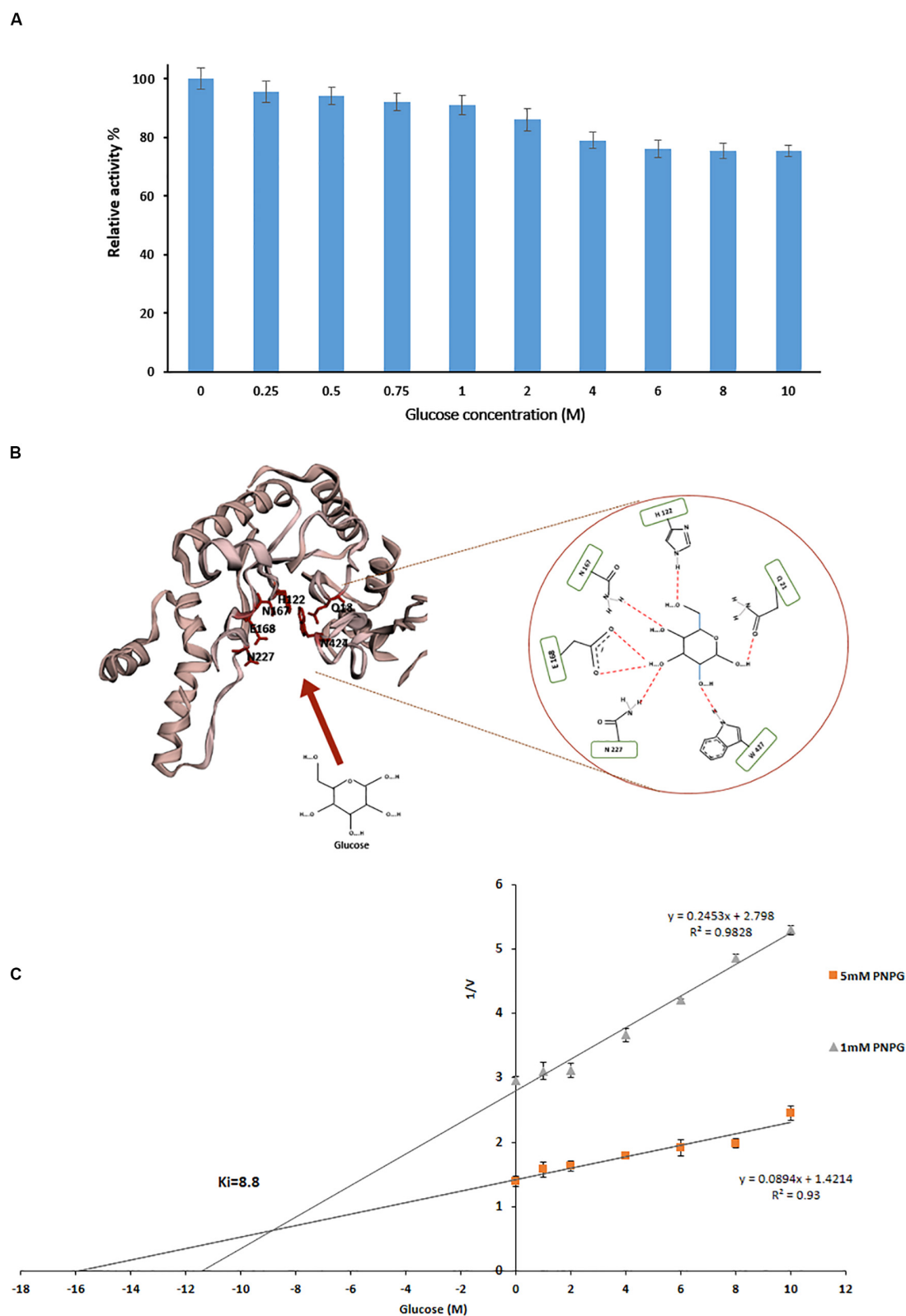


FIGURE 3 | Characterization of purified PersiBGL1. **(A)** Effect of pH on PersiBGL1 activity. **(B)** Effect of temperature on PersiBGL1 activity. **(C)** The storage stability of PersiBGL1.

Expression and Purification of PersiBGL1

The sequence of PersiBGL1 fragments was directly amplified from the metagenomic DNA of sheep rumen with degenerate

primers and overexpressed under the control of the T7 promoter of pET-28a vector in *E. coli* BL21 (DE3). The recombinant enzyme was purified as the N-terminus His-tagged protein by



using Ni-NTA Fast Start Kit and protein fractions from the purification steps were analyzed by SDS-PAGE (Maleki et al., 2020), and a single protein band was visible after the final purification step with a molecular weight to the calculated 53.92-kDa mass (Figure 2D).

Effects of pH and Temperature on the PersiBGL1 Activity

The temperature and pH are the most recognizable factors that play an instrumental role in enzyme stability. After purification of PersiBGL1, we deduced the effect of temperature and pH on catalyzing activity of the enzyme in Figure 3.

Bacterial BGLs isolated from thermophilic microorganisms depict enzyme activity mainly at pH less than 7. In contrast, PersBGL1 reached its maximum activity in pH 8 and retained more than 50% of its maximum value in the pH range between 6 and 10 (Figure 3A). All this evidence about pH feature of the PersiBGL1 substantiates its commercially valuable potential in biotechnological industries. Similarly, it has been reported that BGLs remaining active in broad range pH could ameliorate the version efficiency of cellulosic materials into glucose. Therefore, pH stability is another attribute that develops BGL productivity for marketing purposes (Jiang et al., 2011; Xia et al., 2016).

The enzymes with hydrolysis activity in the breakdown process of biomass need to be enhanced in an effort to reach higher stability at elevated temperatures (Colabardini et al., 2016).

In this case, BGLs belonging to the GH1 family are the most thermostable enzyme reported so far (Singhanian et al., 2017). In Figure 3B, PersiBGL1 activity was measured in temperature ranging from 20 to 90°C in order to determine optimal temperature, which is 40°C. According to the F.2B, the enzyme relative activity has surged approximately 100% when the temperatures increased to 40°C.

However, PersBGL1 retained 80% of its relative activity after being stored for 48 h at 40°C. The enzyme activity was diminished drastically after 264 h of storage (Figure 3C).

Kinetics Assay and Glucose Inhibition Constant

Although the mechanism of glucose inhibition effect on BGL activity is not entirely known, it is all transparent that BGL activity is frequently sensitive to glucose presence and decreases by the increased glucose concentration. Glucose inhibition limits the use of such BGs in industrial applications because an inefficient enzyme contributes toward biofuel costs. Therefore, BGLs are glucose tolerant in high demand.

Measurement of relative activity of PersiBGL1 in the presence of glucoses showed that with concentrations of less than 1 M, the enzymatic activity had no remarkable effect, and even in presence of 10 M glucose, it only had a little inhibition effect and PersiBGL1 retains 75% of its initial activity (Figure 4A).

The recombinant β -glucosidase, Td2F2 (Matsuzawa et al., 2016), which exhibited high glucose tolerance activity, was selected for further analytical studies to decipher the mechanism behind the high glucose tolerance property of PersiBGL1.

We compared the glucose binding site structure of the PersiBGL1 with the well-characterized GH1 BGL, Td2F2. The comparison reveals that almost all of the glucose binding site residues are conserved in both enzymes. Figure 4B shows the schematic view of the glucose binding mechanism to the predicted structure for PersiBGL1 and the involved residues. The important point is that, similar to Td2f2, the Asn227 residue (aligned with Asn223 in Td2f2) plays a key role in the glucose tolerance property of PersiBGL1.

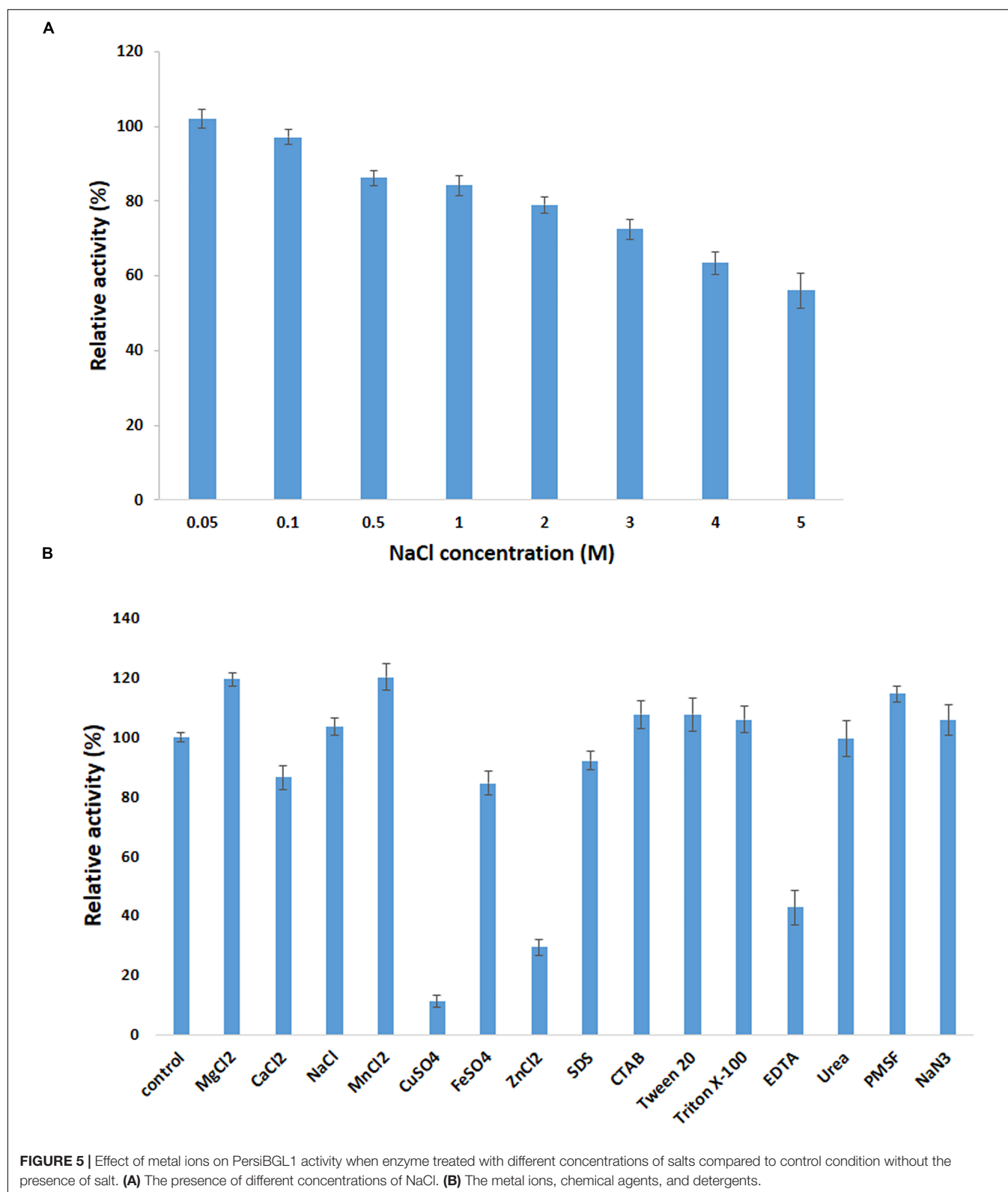
Among reported BGLs that were derived from microorganisms, a vast proportion of them (with some exceptions) showed K_i values in the range of 0.2 and 4280 mM when the enzyme was assayed with pNPG, and a nice compilation of them could be found here (Li et al., 2012; Teugjas and Våljamäe, 2013; Sinha and Datta, 2016). The highest K_i values found in the literature was 4.28 M from soil metagenomic library (Li et al., 2012). In the same manner, we tested the glucose inhibition by assessing the influence of glucose on the kinetic parameters of PersiBGL1. Then, a K_i value of 8.8 M was determined by the Dixon plot (Figure 4C).

Several glucose-tolerant BGLs have been purified and characterized. Table 1 contains a list of BGLs across the GH1 and GH3 families with K_i of glucose when the enzyme was assayed with pNPG. Aside from the microbes isolated from metagenomes, studies have identified the rest in this list of microbial sources. In Table 1, PersiBGL1 depicted an extraordinary K_i value in comparison to other known BGL representatives. Bgl1269 with a K_i value of 4.28 M was presumed

TABLE 1 | The property comparison of PersiBGL1 with some known β -glucosidase representatives.

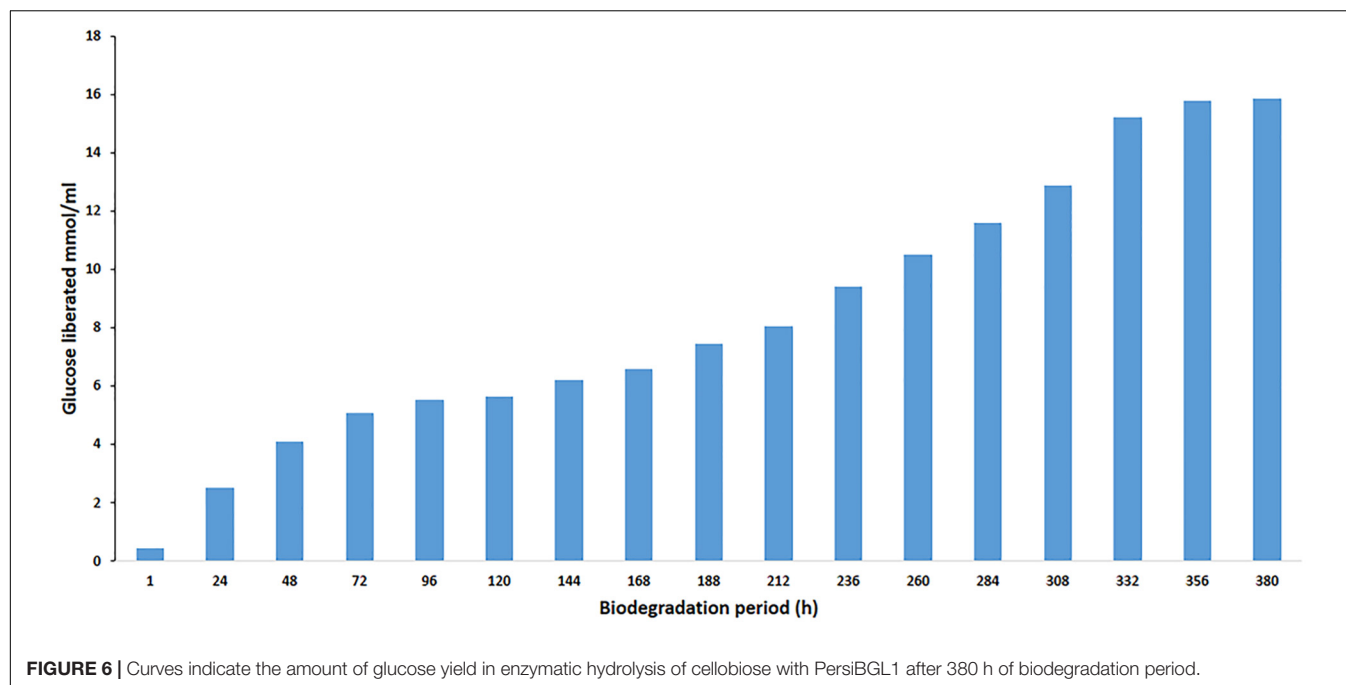
Name	Source	Optimum pH	K_i	References
Bgl6	Metagenomic library	5	3.5 M	Cao et al., 2015
Bgl1269	Soil metagenomic library	6	4.28 M	Li et al., 2012
Tt-BGL	Thermotoga thermarum DSM 5069T	4.8	1.5 M	Zhao et al., 2013
H0HC94	Agrobacterium tumefaciens	7.2	0.686 M	Sinha and Datta, 2016
TD2F2	Compost microbial metagenome	5.5	1M	Uchiyama et al., 2013
bgl1A	Marine microbial metagenome	6.5	1M	Fang et al., 2010
Unbgl1A	Soil metagenome	5	1.5 M	Lu et al., 2013
Dtur β Glu	Dictyoglomus turgidum	5.4	0.7M	Limauro et al., 2018
BglD5	Jeotgalibacillus malaysiensis	7	2.5 M	Chan et al., 2018
PersiBGL1	Rumen metagenome	8	8.8 M	This study

K_i measured for glucose with pNPG as substrate.



to have the highest tolerance to glucose compared to the BGLs discovered previously, while its K_i is less than half of the K_i measured in PersiBGL1 (8.8 M) (Li et al., 2012).

Implementing the Lineweaver–Burk map and pNPG as substrate enabled us to assess the kinetic parameters (k_m and V_{max}) corresponding to the activity of PersiBGL1. The kinetic



constants (k_m and V_{max}) corresponding to the activity of PersiBGL1 can be comprehensively determined and measured if the Lineweaver–Burk plot is used. The k_m , V_{max} , k_{cat} , and k_{cat}/k_m values of the enzyme were estimated to be 1.25 mM, 1.55 mM/min, 3.1 min^{-1} and $2.47 \text{ min}^{-1} \text{ mg}^{-1} \text{ ml}$, respectively.

Consequently, to our knowledge, PersiBGL1 displays the highest inhibitor constant (K_i) among all reported BGLs. Additionally, PersiBGL1 revealed higher V_{max} (1.55 mM/min) in comparison to some other known BGL representatives, which indicates that PersiBGL1 possesses better turnover number or catalytic rate than some enzymes brought in **Table 1**. A considerably high glucose inhibition resistance and a decent catalytic rate of PersiBGL1 clearly distinguish this enzyme from many other identified BGLs for cellulolytic production purposes.

Effect of Metal Ions and Chemical Reagents on Enzyme Activity

It has been proposed that metal ion could be responsible for impeding the catalytic activity of BGL (Chen et al., 2014). Given this fact, exploiting a BGL that is non-sensitive to salt or to some degree can tolerate the presence of metal ion in solutions is remarkably beneficial.

The influence of various metal ions and chemicals on the activity of PersiBGL1 was investigated by using pNPG as a substrate and standard assay procedure (**Figure 5**). The control reaction was carried out under the same conditions only without the presence of metal ions and chemical reagents.

It can be readily observed that the enzyme could maintain its activity in the presence of all the metal ions except Cu^{2+} and Fe^{2+} , which inhibited the activity of PersiBGL1 to 11.13 and 29.27%, respectively. On the other hand, the maximum

relative activities among the metal ions were obtained by MnCl_2 (120.07%) followed by MgCl_2 (119.30%) and NaCl (103.36%).

The addition of the different surfactants and detergents showed no observable change in the activity of the enzyme. Among the surfactants, only the presence of the EDTA showed a negative effect on the action of PersiBGL1 (42.74%). Reduction of the enzymatic activity by the metal-chelating EDTA could represent the fact that PersiBGL1 could be a metal-dependent enzyme.

The salt tolerance of the PersiBGL1 was tested by measuring the activity in the presence of various concentrations of NaCl (**Figure 5**). Results indicated that the enzyme could maintain its activity at high and low concentrations of NaCl . The relative activities slightly decreased by the increment of salt concentration. At the highest concentration of NaCl (5 M), the PersiBGL1 demonstrated near 60% of activity, which confirmed the salt tolerance of the β -glucosidase. Thus, in addition to thermostability and glucose tolerance significance in biofuel, this feature is another notable characteristic of PersiBGL1 that is worth mentioning.

Effect of BGLs on Enzymatic Saccharification of Cellobiose Hydrolysis

Cellulose, a naturally occurring linear polysaccharide, is a substantial structural component of the primary cell wall in green plants. Cellulose, as a renewable feedstock, is ranked first among all bio-polymers, and its potential for conversion to ethanol and other chemicals has made it one of the main promising green alternatives to fossil fuels. However, the efficient bioconversion of lignocellulosic biomass into biofuels in general and the saccharification of cellobiose as the most critical stage of this conversion in particular remain a major challenge in

cellulose degradation. The cellobiose, a disaccharide reducing sugar, needs a BGL to be converted to glucose in the final step of cellulose hydrolysis and had important applications in the feed, food, biofuel, and other fields (Pogorzelski and Wilkowska, 2007; Song et al., 2011; Sun et al., 2014). One of the efficient strategies to circumvent this challenge is to search for a BGL with high glucose tolerance, thermostability, and high catalytic efficiency in harsh environments. The rumen environment is a good example of such environments, and we applied a metagenomic approach to screen this BGL.

The effect of BGL on the liberation of glucose during the degradation of cellobiose was studied. To evaluate enzyme efficiency in cellobiose hydrolysis, cellobiose (1% w/v) was hydrolyzed at 40°C in phosphate buffer (50 mM, pH 8). The enzyme/substrate ratio was 1 mg/g cellobiose (1:1000). In the hydrolysis process, the amount of used PersiBGL1 was 0.1 μ g. The final liberated concentration of glucose is 15.85 mM and the rate of conversion reaches to zero after 380 min, while 25% of cellulose was hydrolyzed at this point (Figure 6).

Similarly, spontaneous increases in the concentration of glucose liberated during the degradation period from 1 h (0.44 μ mol/ml) to 380 h were observed, yielding maximum release of glucose (15.85 μ mol/ml). Glucose production did not decrease significantly after 300 h. Hence, this result suggests that this novel BGL could be a suitable enzyme in the saccharification of lignocellulosic biomass.

CONCLUSION

In this study, the sheep rumen metagenome was explored using computational screening for finding a novel stable BGL with a significantly very high tolerance to glucose. The main advantage of applying our proposed computational method is that instead of simple alignment-based screening, a multi-step procedure is employed to refine a vast amount of potential BGLs and narrow down the list of candidates to a very limited number of enzymes with required properties. In this approach, the relatively heavy cost of functional screening is replaced by computational costs. This approach uses an eight-stage procedure including quality control, assembly of metagenomic short reads, gene prediction, filtering enzymes based on sequence similarity with known enzymes mined from literature, determining phylogenetic position of candidates, finding conserved domain related to the desired enzymatic activity, prediction of tertiary structure of candidate enzymes, and performing structural alignment with the best-known enzymes to find an appropriate candidate from metagenomic data and ensure that the final candidates have

desirable properties. Applying this approach is not limited to BGLs and certainly can be used in a wide domain of enzymatic applications in order to identify novel natural enzymes, suitable for specific industrial applications.

After identification, cloning, expression, purification, and characterization of PersiBGL1, the accuracy of computational prediction was experimentally confirmed. The PersiBGL1 is a halotolerant stable enzyme with distinguished resistance to high concentration of glucose. It was successfully utilized for the saccharification of cellobiose.

DATA AVAILABILITY STATEMENT

The datasets presented in this study can be found in online repositories. The names of the repository/repositories and accession number(s) can be found in the article/Supplementary Material.

AUTHOR CONTRIBUTIONS

SA: conceptualization, methodology, supervision, investigation, writing - original draft, resources, and project administration. SN-N, MR, and MeM: biochemical characterization and analyzed and interpreted the data. KK: conceptualization, methodology, contributed to the computational and bioinformatics data analysis, writing - review and editing. AP and MaM: performed the gene cloning, expression, and purification. SM: investigation, resources, and writing - original draft. GS: supervision, resources, writing - review and editing, project administration, funding acquisition, and conceptualization. All authors contributed to the article and approved the submitted version.

FUNDING

This research was supported by a grant from the Agricultural Biotechnology Research Institute of Iran (ABRII), the Institute of Biochemistry and Biophysics (IBB), and the Iran National Science Foundation (INSF).

SUPPLEMENTARY MATERIAL

The Supplementary Material for this article can be found online at: <https://www.frontiersin.org/articles/10.3389/fbioe.2020.00813/full#supplementary-material>

REFERENCES

- Akram, F., Haq, I. U., Khan, M. A., Hussain, Z., Mukhtar, H., and Iqbal, K. (2016). Cloning with kinetic and thermodynamic insight of a novel hyperthermostable β -glucosidase from *Thermotoga naphthophila* RKU-10 T with excellent glucose tolerance. *J. Mol. Catal. B Enzym.* 124, 92–104. doi: 10.1016/j.molcatb.2015.12.005

- Ariaeenejad, S., Hosseini, E., Maleki, M., Kavousi, K., Moosavi-Movahedi, A. A., and Salekdeh, G. H. (2019a). Identification and characterization of a novel thermostable xylanase from camel rumen metagenome. *Int. J. Biol. Macromol.* 126, 1295–1302. doi: 10.1016/j.ijbiomac.2018.12.041
- Ariaeenejad, S., Maleki, M., Hosseini, E., Kavousi, K., Moosavi-Movahedi, A. A., and Salekdeh, G. H. (2019b). Mining of camel rumen metagenome to identify novel alkali-thermostable xylanase capable of enhancing the recalcitrant

- lignocellulosic biomass conversion. *Bioresour. Technol.* 281, 343–350. doi: 10.1016/j.biortech.2019.02.059
- Cai, L. N., Xu, S. N., Lu, T., Lin, D. Q., and Yao, S. J. (2019). Directed expression of halophilic and acidophilic β -glucosidases by introducing homologous constitutive expression cassettes in marine *Aspergillus niger*. *J. Biotechnol.* 292, 12–22. doi: 10.1016/j.jbiotec.2018.12.015
- Cairns, J. R. K., and Esen, A. (2010). β -Glucosidases. *Cell. Mol. Life Sci.* 67, 3389–3405. doi: 10.1007/s00018-010-0399-2
- Cao, L., Li, S., Huang, X., Qin, Z., Kong, W., Xie, W., et al. (2018). Enhancing the thermostability of highly active and glucose-tolerant β -Glucosidase Ks5A7 by directed evolution for good performance of three properties. *J. Agric. Food Chem.* 66, 13228–13235. doi: 10.1021/acs.jafc.8b05662
- Cao, L. C., Wang, Z. J., Ren, G. H., Kong, W., Li, L., Xie, W., et al. (2015). Engineering a novel glucose-tolerant β -glucosidase as supplementation to enhance the hydrolysis of sugarcane bagasse at high glucose concentration. *Biotechnol. Biofuels* 8, 1–12. doi: 10.1186/s13068-015-0383-z
- Chan, C. S., Sin, L. L., Chan, K. G., Shamsir, M. S., Manan, F. A., Sani, R. K., et al. (2016). Characterization of a glucose-tolerant β -glucosidase from *Anoxybacillus* sp. DT3-1. *Biotechnol. Biofuels* 9:174. doi: 10.1186/s13068-016-0587-x
- Chan, K.-G., Woo, H. Y., Goh, K. M., Liew, K. J., Lim, L., and Shamsir, M. S. (2018). Purification and characterization of a novel GH1 beta-glucosidase from *Jeotgallibacillus malaysiensis*. *Int. J. Biol. Macromol.* 115, 1094–1102. doi: 10.1016/j.jbiomac.2018.04.156
- Chauve, M., Mathis, H., Huc, D., Casanave, D., Monot, F., and Ferreira, N. L. (2010). Comparative kinetic analysis of two fungal β -glucosidases. *Biotechnol. Biofuels* 3:3. doi: 10.1186/1754-6834-3-3
- Chen, T., Yang, W., Guo, Y., Yuan, R., Xu, L., and Yan, Y. (2014). Enhancing catalytic performance of β -glucosidase via immobilization on metal ions chelated magnetic nanoparticles. *Enzyme Microb. Technol.* 63, 50–57. doi: 10.1016/j.enzmictec.2014.05.008
- Colabardini, A. C., Valkonen, M., Huuskonen, A., Siika-aho, M., Koivula, A., Goldman, G. H., et al. (2016). Expression of two novel β -glucosidases from *Chaetomium atrobrunneum* in trichoderma reesei and characterization of the heterologous protein products. *Mol. Biotechnol.* 58, 821–831. doi: 10.1007/s12033-016-9981-7
- De Giuseppe, P. O., Souza, T. D. A. C. B., Souza, F. H. M., Zanphorlin, L. M., Machado, C. B., Ward, R. J., et al. (2014). Structural basis for glucose tolerance in GH1 β -glucosidases. *Acta Crystallogr. Sect. D Biol. Crystallogr.* 70(Pt 6), 1631–1639. doi: 10.1107/S1399004714006920
- Dennett, G. V., and Blamey, J. M. (2016). A new thermophilic nitrilase from an antarctic hyperthermophilic microorganism. *Front. Bioeng. Biotechnol.* 4:5. doi: 10.3389/fbioe.2016.00005
- Fang, Z., Fang, W., Liu, J., Hong, Y., Peng, H., Zhang, X., et al. (2010). Cloning and characterization of a β -glucosidase from marine microbial metagenome with excellent glucose tolerance. *J. Microbiol. Biotechnol.* 20, 1351–1358. doi: 10.4014/jmb.1003.03011
- Foerster, E. C., and Lynen, F. (1985). Malonyl coenzyme A. Radiometric method. *Methods Enzym. Anal.* 7, 231–240.
- Guo, B., Amano, Y., and Nozaki, K. (2016). Improvements in glucose sensitivity and stability of trichoderma reesei β -glucosidase using site-directed mutagenesis. *PLoS One* 11:e0147301. doi: 10.1371/journal.pone.0147301
- Guo, H., Chang, Y., and Lee, D. J. (2018). Enzymatic saccharification of lignocellulosic biorefinery: research focuses. *Bioresour. Technol.* 252, 198–215. doi: 10.1016/j.biortech.2017.12.062
- Jiang, C., Li, S.-X., Luo, F.-F., Jin, K., Wang, Q., Hao, Z.-Y., et al. (2011). Biochemical characterization of two novel β -glucosidase genes by metagenome expression cloning. *Bioresour. Technol.* 102, 3272–3278. doi: 10.1016/j.biortech.2010.09.114
- Kelley, L. A., Mezulis, S., Yates, C. M., Wass, M. N., and Sternberg, M. J. E. (2015). The Phyre2 web portal for protein modeling, prediction and analysis. *Nat. Protoc.* 10:845. doi: 10.1038/nprot.2015.053
- Kumar, S., Stecher, G., Li, M., Nkayaz, C., and Tamura, K. (2018). MEGA X: molecular evolutionary genetics analysis across computing platforms. *Mol. Biol. Evol.* 35, 1547–1549. doi: 10.1093/molbev/msy096
- Li, G., Jiang, Y., Fan, X. J., and Liu, Y. H. (2012). Molecular cloning and characterization of a novel β -glucosidase with high hydrolyzing ability for soybean isoflavone glycosides and glucose-tolerance from soil metagenomic library. *Bioresour. Technol.* 123, 15–22. doi: 10.1016/j.biortech.2012.07.083
- Limauro, D., Bartolucci, S., Pedone, E., Fusco, F. A., Contursi, P., and Fiorentino, G. (2018). Biochemical characterization of a novel thermostable β -glucosidase from *Dictyoglomus turgidum*. *Int. J. Biol. Macromol.* 113, 783–791. doi: 10.1016/j.jbiomac.2018.03.018
- Littlechild, J. A. (2015). Enzymes from extreme environments and their industrial applications. *Front. Bioeng. Biotechnol.* 3:161. doi: 10.3389/fbioe.2015.00161
- Liu, X., Cao, L., Zeng, J., Liu, Y., and Xie, W. (2019). Improving the cellobiose-hydrolysis activity and glucose-tolerance of a thermostable β -glucosidase through rational design. *Int. J. Biol. Macromol.* 136, 1052–1059. doi: 10.1016/j.jbiomac.2019.06.029
- Lu, J., Du, L., Wei, Y., Hu, Y., and Huang, R. (2013). Expression and characterization of a novel highly glucose-tolerant β -glucosidase from a soil metagenome. *Acta Biochim. Biophys. Sin.* 45, 664–673. doi: 10.1093/abbs/gmt061
- Mai, Z., Yang, J., Tian, X., Li, J., and Zhang, S. (2013). Gene cloning and characterization of a novel salt-tolerant and glucose-enhanced β -glucosidase from a marine streptomycete. *Appl. Biochem. Biotechnol.* 169, 1512–1522. doi: 10.1007/s12010-012-0080-3
- Maitan-Alfenas, G. P., Lorena, L. G., De Almeida, M. N., Visser, E. M., De Rezende, S. T., and Guimarães, V. M. (2014). Hydrolysis of soybean isoflavones by *Debaryomyces hansenii* UFV-1 immobilised cells and free β -glucosidase. *Food Chem.* 146, 429–436. doi: 10.1016/j.foodchem.2013.09.099
- Maleki, M., Shahraki, M. F., Kavousi, K., Ariaeenejad, S., and Salekdeh, G. H. (2020). A novel thermostable cellulase cocktail enhances lignocellulosic bioconversion and biorefining in a broad range of pH. *Int. J. Biol. Macromol.* 154, 349–360. doi: 10.1016/j.jbiomac.2020.03.100
- Marchler-Bauer, A., Bo, Y., Han, L., He, J., Lanczycki, C. J., Lu, S., et al. (2016). CDD/SPARCLE: functional classification of proteins via subfamily domain architectures. *Nucleic Acids Res.* 45, D200–D203.
- Matsuzawa, T., Jo, T., Uchiyama, T., Manninen, J. A., Arakawa, T., Miyazaki, K., et al. (2016). Crystal structure and identification of a key amino acid for glucose tolerance, substrate specificity, and transglycosylation activity of metagenomic β -glucosidase Td2F2. *FEBS J.* 238, 2340–2353. doi: 10.1111/febs.13743
- Nei, M., and Kumar, S. (2000). *Molecular Evolution and Phylogenetics*. Oxford: Oxford university press.
- Nigam, D., Asthana, M., and Kumar, A. (2018). “Penicillium: a Fungus in the Wine and Beer Industries,” in *New Futur. Dev. Microb. Biotechnol. Bioeng*, eds V. K. Gupta and S. Rodriguez-Couto (Amsterdam: Elsevier).
- Pang, P., Cao, L. C., Liu, Y. H., Xie, W., and Wang, Z. (2017). Structures of a glucose-tolerant β -glucosidase provide insights into its mechanism. *J. Struct. Biol.* 198, 154–162. doi: 10.1016/j.jsb.2017.02.001
- Parry, N. J., Beever, D. E., Owen, E., Vandenbergh, I., Van Beeumen, J., and Bhat, M. K. (2001). Biochemical characterization and mechanism of action of a thermostable β -glucosidase purified from *Thermoascus aurantiacus*. *Biochem. J.* 353, 117–127. doi: 10.1042/bj3530117
- Pogorzelski, E., and Wilkowska, A. (2007). Flavour enhancement through the enzymatic hydrolysis of glycosidic aroma precursors in juices and wine beverages: a review. *Flavour Fragr. J.* 22, 251–254. doi: 10.1002/ffj.1784
- Reynolds, C. R., Islam, S. A., and Sternberg, M. J. E. (2018). EzMol: a web server wizard for the rapid visualization and image production of protein and nucleic acid structures. *J. Mol. Biol.* 430, 2244–2248. doi: 10.1016/j.jmb.2018.01.013
- Saitou, N., and Nei, M. (1987). The neighbor-joining method: a new method for reconstructing phylogenetic trees. *Mol. Biol. Evol.* 4, 406–425.
- Santa-Rosa, P. S., Souza, A. L., Roque, R. A., Andrade, E. V., Astolfi-Filho, S., Mota, A. J., et al. (2018). Production of thermostable β -glucosidase and CMCase by *Penicillium* sp. LMI01 isolated from the Amazon region. *Electron. J. Biotechnol.* 31, 84–92. doi: 10.1016/j.ejbt.2017.11.005
- Seo, J.-W., Park, H.-S., Choi, M.-S., Nguyen, C. L., Loc, N. H., Park, S.-M., et al. (2015). Characterization of a novel manganese dependent endoglucanase belongs in GH family 5 from *Phanerochaete chrysosporium*. *J. Biosci. Bioeng.* 121, 154–159. doi: 10.1016/j.jbiosc.2015.06.009
- Singhania, R. R., Patel, A. K., Pandey, A., and Ganansounou, E. (2017). Genetic modification: a tool for enhancing beta-glucosidase production for biofuel application. *Bioresour. Technol.* 245, 1352–1361. doi: 10.1016/j.biortech.2017.05.126
- Singhania, R. R., Patel, A. K., Sukumaran, R. K., Larroche, C., and Pandey, A. (2013). Role and significance of beta-glucosidases in the hydrolysis of cellulose

- for bioethanol production. *Bioresour. Technol.* 127, 500–507. doi: 10.1016/j.biortech.2012.09.012
- Sinha, S. K., and Datta, S. (2016). β -Glucosidase from the hyperthermophilic archaeon *Thermococcus* sp. is a salt-tolerant enzyme that is stabilized by its reaction product glucose. *Appl. Microbiol. Biotechnol.* 100, 8399–8409. doi: 10.1007/s00253-016-7601-x
- Song, X., Xue, Y., Wang, Q., and Wu, X. (2011). Comparison of three thermostable β -glucosidases for application in the hydrolysis of soybean isoflavone glycosides. *J. Agric. Food Chem.* 59, 1954–1961. doi: 10.1021/jf1046915
- Sun, H., Xue, Y., and Lin, Y. (2014). Enhanced catalytic efficiency in quercetin-4'-glucoside hydrolysis of *thermotoga maritima* β -glucosidase by site-directed mutagenesis. *J. Agric. Food Chem.* 62, 6763–6770. doi: 10.1021/jf501932v
- Teugjas, H., and Våljamäe, P. (2013). Selecting β -glucosidases to support cellulases in cellulose saccharification. *Biotechnol. Biofuels* 6, 1–13. doi: 10.1186/1754-6834-6-105
- Thongpoo, P., McKee, L. S., Araújo, A. C., Kongsaree, P. T., and Brumer, H. (2013). Identification of the acid/base catalyst of a glycoside hydrolase family 3 (GH3) β -glucosidase from *Aspergillus niger* ASKU28. *Biochim. Biophys. Acta Gen. Subj.* 1830, 2739–2749. doi: 10.1016/j.bbagen.2012.11.014
- Thongpoo, P., Srisomsap, C., Chokchaichamnankit, D., Kitpreechavanich, V., Svasti, J., and Kongsaree, P. T. (2014). Purification and characterization of three β -glycosidases exhibiting high glucose tolerance from *Aspergillus niger* ASKU28. *Biosci. Biotechnol. Biochem.* 78, 1167–1176. doi: 10.1080/09168451.2014.915727
- Tramontina, R., de Oliveira Neto, M., Ematsu, G. C. G., Alvarez, T. M., Gandin, C. A., Mandelli, F., et al. (2017). Biochemical and biophysical properties of a metagenome-derived GH5 endoglucanase displaying an unconventional domain architecture. *Int. J. Biol. Macromol.* 99, 384–393. doi: 10.1016/j.ijbiomac.2017.02.075
- Uchiyama, T., Miyazaki, K., and Yaoi, K. (2013). Characterization of a novel β -Glucosidase from a compost microbial metagenome with strong transglycosylation activity. *J. Biol. Chem.* 288, 18325–18334. doi: 10.1074/jbc.M113.471342
- Uchiyama, T., Yaoi, K., and Miyazaki, K. (2015). Glucose-tolerant β -glucosidase retrieved from a Kusaya gravity metagenome. *Front. Microbiol.* 6:548. doi: 10.3389/fmicb.2015.00548
- Xia, W., Xu, X., Qian, L., Shi, P., Bai, Y., Luo, H., et al. (2016). Engineering a highly active thermophilic β -glucosidase to enhance its pH stability and saccharification performance. *Biotechnol. Biofuels* 9:147. doi: 10.1186/s13068-016-0560-8
- Yang, F., Yang, X., Li, Z., Du, C., Wang, J., and Li, S. (2015). Overexpression and characterization of a glucose-tolerant β -glucosidase from *T. aotearoense* with high specific activity for cellobiose. *Appl. Microbiol. Biotechnol.* 99, 8903–8915. doi: 10.1007/s00253-015-6619-9
- Zeiske, T., Stafford, K. A., and Palmer, A. G. (2016). Thermostability of enzymes from molecular dynamics simulations. *J. Chem. Theory Comput.* 12, 2489–2492. doi: 10.1021/acs.jctc.6b00120
- Zhang, Y., and Skolnick, J. (2005). TM-align: a protein structure alignment algorithm based on the TM-score. *Nucleic Acids Res.* 33, 2302–2309. doi: 10.1093/nar/gki524
- Zhang, Z., Zhang, R., Song, S., Shen, Q., Liu, D., Yang, X., et al. (2012). Characterization of a thermostable β -glucosidase from *Aspergillus fumigatus* Z5, and its functional expression in *Pichia pastoris* X33. *Microb. Cell Fact.* 11:25. doi: 10.1186/1475-2859-11-25
- Zhao, L., Xie, J., Zhang, X., Cao, F., and Pei, J. (2013). Overexpression and characterization of a glucose-tolerant β -glucosidase from *Thermotoga thermarum* DSM 5069T with high catalytic efficiency of ginsenoside Rb1 to Rd. *J. Mol. Catal. B Enzym.* 95, 62–69. doi: 10.1016/j.molcatb.2013.05.027
- Zhao, X., Jiang, L., Luo, H., Zhao, X., Zhu, C., Wang, Z., et al. (2018). Purification and characterization of a glucose-tolerant β -glucosidase from black plum seed and its structural changes in ionic liquids. *Food Chem.* 274, 422–428. doi: 10.1016/j.foodchem.2018.09.007
- Zhu, W., Lomsadze, A., and Borodovsky, M. (2010). Ab initio gene identification in metagenomic sequences. *Nucleic Acids Res.* 38:e132. doi: 10.1093/nar/gkq275

Conflict of Interest: The authors declare that the research was conducted in the absence of any commercial or financial relationships that could be construed as a potential conflict of interest.

Copyright © 2020 Ariaeenejad, Nooshi-Nedamani, Rahban, Kavousi, Pirbalooti, Mirghaderi, Mohammadi, Mirzaei and Salekdeh. This is an open-access article distributed under the terms of the Creative Commons Attribution License (CC BY). The use, distribution or reproduction in other forums is permitted, provided the original author(s) and the copyright owner(s) are credited and that the original publication in this journal is cited, in accordance with accepted academic practice. No use, distribution or reproduction is permitted which does not comply with these terms.



High-Level Production of Recombinant Snowdrop Lectin in Sugarcane and Energy Cane

Carmen S. Padilla^{1†}, Mona B. Damaj^{1†}, Zhong-Nan Yang², Joe Molina¹, Brian R. Berquist^{3†}, Earl L. White^{4†}, Nora Solís-Gracia¹, Jorge Da Silva^{1,5} and Kranthi K. Mandadi^{1,6*}

¹ Texas A&M AgriLife Research and Extension Center, Weslaco, TX, United States, ² Institute for Plant Gene Function, Department of Biology, Shanghai Normal University, Shanghai, China, ³ iBio, Bryan, TX, United States, ⁴ MDx BioAnalytical Laboratory, Inc., College Station, TX, United States, ⁵ Department of Soil and Crop Sciences, Texas A&M University, College Station, TX, United States, ⁶ Department of Plant Pathology and Microbiology, Texas A&M University, College Station, TX, United States

OPEN ACCESS

Edited by:

Ligia R. Rodrigues,
University of Minho, Portugal

Reviewed by:

Yongjun Wei,
Zhengzhou University, China
Getu Beyene,
Donald Danforth Plant Science
Center, United States

*Correspondence:

Kranthi K. Mandadi
kkmandadi@tamu.edu

[†]These authors have contributed
equally to this work

Specialty section:

This article was submitted to
Industrial Biotechnology,
a section of the journal
Frontiers in Bioengineering and
Biotechnology

Received: 02 June 2020

Accepted: 27 July 2020

Published: 18 August 2020

Citation:

Padilla CS, Damaj MB, Yang Z-N,
Molina J, Berquist BR, White EL,
Solís-Gracia N, Da Silva J and
Mandadi KK (2020) High-Level
Production of Recombinant
Snowdrop Lectin in Sugarcane
and Energy Cane.
Front. Bioeng. Biotechnol. 8:977.
doi: 10.3389/fbioe.2020.00977

Sugarcane and energy cane (*Saccharum* spp. hybrids) are ideal for plant-based production of recombinant proteins because their high resource-use efficiency, rapid growth and efficient photosynthesis enable extensive biomass production and protein accumulation at a cost-effective scale. Here, we aimed to develop these species as efficient platforms to produce recombinant *Galanthus nivalis* L. (snowdrop) agglutinin (GNA), a monocot-bulb mannose-specific lectin with potent antiviral, antifungal and antitumor activities. Initially, GNA levels of 0.04% and 0.3% total soluble protein (TSP) (0.3 and 3.8 mg kg⁻¹ tissue) were recovered from the culms and leaves, respectively, of sugarcane lines expressing recombinant GNA under the control of the constitutive maize *ubiquitin 1* (*Ubi*) promoter. Co-expression of recombinant GNA from stacked multiple promoters (*pUbi* and culm-regulated promoters from sugarcane *dirigent5-1* and *Sugarcane bacilliform virus*) on separate expression vectors increased GNA yields up to 42.3-fold (1.8% TSP or 12.7 mg kg⁻¹ tissue) and 7.7-fold (2.3% TSP or 29.3 mg kg⁻¹ tissue) in sugarcane and energy cane lines, respectively. Moreover, inducing promoter activity in the leaves of GNA transgenic lines with stress-regulated hormones increased GNA accumulation to 2.7% TSP (37.2 mg kg⁻¹ tissue). Purification by mannose-agarose affinity chromatography yielded a functional sugarcane recombinant GNA with binding substrate specificity similar to that of native snowdrop-bulb GNA, as shown by enzyme-linked lectin and mannose-binding inhibition assays. The size and molecular weight of recombinant GNA were identical to those of native GNA, as determined by size-exclusion chromatography and MALDI-TOF mass spectrometry. This work demonstrates the feasibility of producing recombinant GNA at high levels in *Saccharum* species, with the long-term goal of using it as a broad-spectrum antiviral carrier molecule for hemopurifiers and in related therapeutic applications.

Keywords: therapeutic protein, recombinant protein, snowdrop-bulb lectin, *Galanthus nivalis* agglutinin, promoter stacking, biofactory, *Saccharum* species

INTRODUCTION

The production of recombinant therapeutic proteins on a large scale is a fast-growing sector of biopharmaceutical research and industry. Many proteins are currently produced using conventional cell culture-based systems, including those using mammals and microbes (Alqazlan, 2014). However, the need for a platform that offers low production costs, safety and high scalability has led to the use of plants as biofactories (Williams et al., 2014; Chen and Davis, 2016).

Sugarcane and energy cane (*Saccharum* spp. hybrids) are ideal platforms for the production of native and recombinant protein-based therapeutics at commercial levels, due to their high resource-use efficiencies, rapid growth, efficient photosynthesis and high biomass production capacity, with potential yields of up to 49 tons of dry biomass per hectare per annum (Ando et al., 2011; Matsuoka et al., 2014). In general, sugarcane offers a high level of transgene containment (Altpeter and Oraby, 2010). Sugarcane/energy cane are primarily propagated by vegetative means and natural reproductive propagation is rare in many temperate and subtropical regions due to its photoperiod sensitivity, thus limiting transgene flow by pollen. Furthermore, many of the commercial sugarcane or energy cane varieties do not produce viable pollen or seeds under typical field conditions. Sugarcane has been tested as a potential biofactory for the production of recombinant proteins such as the human cytokine granulocyte-macrophage colony-stimulating factor GM-CSF (Wang M.L. et al., 2005), canecystatins (cysteine protease inhibitors) (Gianotti et al., 2006; Ribeiro et al., 2008; Henrique-Silva and Soares-Costa, 2012) and the cellulolytic enzymes endoglucanase and cellobiohydrolases I and II (Harrison et al., 2011; Harrison et al., 2014). The accumulation level of these recombinant proteins ranged from 0.02% to 2.0% of the total soluble protein (TSP) in leaves. By contrast, energy cane has not been studied for its use as a biofactory for recombinant therapeutic proteins.

Lectins related to *Galanthus nivalis* L. (snowdrop) agglutinin (GNA), which is tetrameric, represent a superfamily of strictly 2-D-mannose-binding-specific lectins from bulbs that is widespread among monocots. The subunits of all GNA-related lectins share a similar three-dimensional structure with GNA, despite differences in their amino-acid sequences (Barre et al., 1996). The clinical application of GNA-related plant-bulb lectins is an ongoing area of research due to their important antitumor, antifungal and antiviral activities (Damodaran et al., 2008; Li et al., 2009; Liu et al., 2009; Beyene et al., 2011; Wu and Bao, 2013; Akkouch et al., 2015). The first GNA-related lectin, termed GNA, was isolated from snowdrop bulbs and is composed of four identical subunits of about 12.0 kDa (Van Damme et al., 1987). The GNA lectin has exclusive binding specificity for mannose and has been characterized in particular for its potent inhibition of retroviruses (Akkouch et al., 2015). GNA inhibits hepatitis C virus infection of serum in a dose-dependent manner by binding N-linked glycans located at the top of the viral envelope (Ashfaq et al., 2011). Additionally, GNA selectively inhibits several varieties of

immunodeficiency type 1 and 2 viruses in different cell types (Balzarini et al., 2004) and prevents cell-cell fusion in cells expressing HIV viral envelope glycoproteins and T cells (CD4⁺) (Yee et al., 2011).

GNAs and other plant lectins have been produced as recombinant and heterologous proteins as an alternative to the native sources. The main expression systems were using bacteria (*Escherichia coli*) and yeast (*Pichia pastoris*) and to some extent plant and mammalian cells (Oliveira et al., 2013; Martínez-Alarcón et al., 2018). Production in microbes results in good yields, however the recombinant lectins are often insoluble or not properly processed, requiring further downstream processing like refolding, extraction from inclusion bodies and post-translational modifications such as glycosylation. In this context, plant-based systems are relatively closer to native snowdrop lily conditions when compared to other prokaryotic or yeast systems. Among the plant-based systems, GNA was produced in transgenic rice, maize and sugarcane, mainly in leaves with yields reaching approximately 0.1–0.5% TSP, 0.28% TSP and 0.89% TSP, respectively (Rao et al., 1998; Tinjuangjun et al., 2000; Tang et al., 2001; Setamou et al., 2002; Nagadhara et al., 2003; Wang Z. et al., 2005).

In this work, we demonstrate the feasibility of sugarcane and energy cane as platforms for the efficient production of recombinant snowdrop GNA protein at high levels. In transgenic sugarcane, GNA yields using a constitutive single promoter (maize *ubiquitin 1*) reached 0.04% TSP and 0.3% TSP in culms and leaves, respectively. GNA accumulation was increased further to 1.8% TSP and 2.3% TSP in culms and leaves, respectively, of sugarcane and energy cane by co-expressing recombinant GNA using a stack of three different constitutive and culm-regulated promoters and combinatorial plant transformation. The highest GNA level of up to 2.7% TSP was achieved by inducing the promoter activity of GNA transgenic lines with stress-regulated hormones. Mannose-agarose affinity chromatography purification allowed the recovery of a functional GNA that retained binding specificity to anti-GNA antibody and the mannose substrate in a manner similar to the native snowdrop-bulb GNA.

MATERIALS AND METHODS

Expression Vectors

A series of GNA expression vectors was constructed using the full-length cDNA (570 bp) that encodes *G. nivalis* L. (snowdrop) lectin, LECGNA2 (GenBank Accession Number M55556, Protein Data Bank accession number AAA33346). The full-length GNA cDNA was obtained from Van Damme et al. (1991) in the pT7T3-18U vector (Addgene, Watertown, MA, United States).

A recombinant GNA, GNA₁₀₉ (*G. nivalis* lectin LECGNA2 with four additional amino acids, Thr₁₀₆ His₁₀₇ Thr₁₀₈ Gly₁₀₉, at the C-terminus of the mature protein), was synthesized (GenScript United States, Inc., Piscataway, NJ, United States) and used as a control due to its known binding affinity to mannan (Raemaekers, 2000).

Single-Terminator Vectors

The GNA expression vector *pUbi-GNA-NOST/pUC18*, which contains the constitutive maize *ubiquitin 1* promoter (*pUbi*), was generated (Christensen et al., 1992; Christensen and Quail, 1996). The GNA full-length cDNA (570 bp) was excised from *GNA/pT7T3-18U* with *EcoRI*, filled in and cloned into *Sall*-digested/filled-in *pUNos_C1* (a gift from Jane Glazebrook and Fumi Katagiri; Addgene plasmid # 33297), which is *pUC18* with *pUbi* and the terminator from the *Agrobacterium tumefaciens* nopaline synthase gene (*NOST*).

Double-Terminator Vectors

Four GNA expression vectors with a double terminator were generated. The first vector, *pUbi-GNA-35STNOST/pZero2*, was constructed with *pUbi* (1,977 bp) and the double terminators *NOST* (253 bp) and the 197-bp *Cauliflower mosaic virus* 35S polyadenylation signal (35S) (Beyene et al., 2011). The GNA fragment (570 bp) was amplified from *pUbi-GNA-NOST/pUC18*, *BamHI* restriction sites were added using the primers GNA-1F 5'-GGATCCCACTACAAGTTACAAAATGGCTA-3' and GNA-570R 5'-GGATCCCGCGACGAGGTTCGATTATCTCAAA-3' and the fragment was fused to the *BamHI*-digested *pUbi-BvLz_m-35STNOST/pZero2* vector (Damaj and Mirkov, 2019), to replace the *BvLz_m* fragment. The second vector, *pSHEF1α-GNA-35STNOST/pNEB193*, was assembled as follows: the *XbaI/BbsI*-digested/filled-in *pUbi-GNA-35STNOST/pZero2* GNA-35STNOST fragment was fused to *BamHI*-digested/filled-in *pNEB193* (New England BioLabs, Ipswich, MA). The *pSHEF1α* fragment (1,959 bp), excised from *pSHEF1α/pSK⁺* (Yang et al., 2003) with *EcoRI* and filled in, was fused to GNA in *GNA-35STNOST/pNEB193* following *AscI* digestion and filling in.

The two remaining GNA expression vectors containing a double terminator were generated to include the culm-regulated promoters from *Sugarcane bacilliform virus* (*pSCBV21*) (Gao et al., 2017) and from the *Saccharum* spp. hybrid *dirigent5-1* gene (*pSHDIR5-1*) (Damaj et al., 2010; Damaj and Mirkov, 2017). The *pSCBV21-GNA-35STNOST/pGEMT-T* Easy vector was created by cloning the GNA fragment (570 bp), amplified from *pUbi-GNA-NOST/pUC18* with added *BamHI* restriction sites (using the primers GNA-1F and GNA-570R), into the *BamHI*-digested *pSCBV21* (1,816 bp)-*BvLz_m-35STNOST/pGEM-T* Easy vector (Damaj and Mirkov, 2019), thereby replacing the *BvLz_m* fragment. To construct the *pSHDIR5-1-GNA-35STNOST/pGEM-T* Easy vector, the *pSHDIR5-1* fragment (4,710 bp), excised from *pSHDIR5-1-GUS-NOST/pUC19* (Damaj and Mirkov, 2017) with *HindIII/SpeI* and filled in, was fused to GNA in *SacII/SpeI*-digested and filled-in *pSCBV21-GNA-35STNOST/pGEMT-T* Easy vector, thereby replacing *pSCBV21*.

All DNA cloning steps were carried out as previously described (Sambrook et al., 1989). The filling in of ends of digested DNA fragments and the dephosphorylation of vectors were performed using T4 DNA polymerase (New England BioLabs, Ipswich, MA, United States) and Antarctic Phosphatase (New England BioLabs), respectively. The PCR

amplification was performed using Platinum™ PCR SuperMix High Fidelity (Invitrogen, ThermoFisher Scientific, Waltham, MA, United States).

Plant Transformation

The tops of field-grown sugarcane (*Saccharum* spp. hybrids) commercial varieties CP72-1210, CP89-2143, TCP87-3388, TCP89-3505 and TCP98-4454, and energy cane varieties TCP10-4928 and Ho02-113 were collected during the growing season, and leaf-roll discs were prepared for stable transformation mainly as previously described (Ramasamy et al., 2018). Briefly, leaf blades and sheaths were removed down to leaf 1 (the topmost visible dewlap leaf), and the upper 20–30 cm portion of the shoot (leaf-roll culm) was surface-sterilized in 70% (v/v) ethanol for 20 min. Immature leaf rolls close to the apical meristem were sliced transversely into 1-mm thick sections and cultured on MS3 medium (Murashige and Skoog medium [MS] with 3 mg L⁻¹ 2,4-dichlorophenoxyacetic acid [2,4-D]) for 30–35 days (for the generation of embryogenic calli) (Murashige and Skoog, 1962) or on MS0.6 medium (MS with 0.6 mg L⁻¹ 2,4-D) for 7–10 days (for the generation of embryogenic leaf-roll discs) (Snyman et al., 2006). Embryogenic calli and leaf-roll discs were preconditioned on MS3- and MS0.6-osmoticum supplemented with 0.2 M D-mannitol and 0.2 M D-sorbitol, respectively, for 4 h before and after DNA particle bombardment. The DNA bombardment was performed according to Ramasamy et al. (2018). Briefly, gold particles (0.3 μm, Crescent Chemical Company, Islandia, NY, United States) (1 mg) were coated separately with 1.0 μg plasmid DNA of different constructs in equimolar ratios together with the *pUbi:BAR/pUC8* selectable marker plasmid, using 1 M calcium chloride and 14 mM spermidine. The DNA particle suspension (containing the selectable marker plasmid with one or more GNA plasmids) (4 μL, 0.5 μg DNA per bombardment) was placed at the center of a syringe filter and delivered into tissue by a particle inflow gun using a 26-inch Hg vacuum and 7-cm target distance. Bombarded embryogenic calli were maintained on MS3 for 10 days in the dark at 28°C for recovery. Shoot regeneration and root initiation were performed under bialaphos selection (3 mg L⁻¹ for sugarcane and 1.5 mg L⁻¹ for energy cane) as described previously (Gao et al., 2013; Ramasamy et al., 2018). Rooted plantlets were transferred to potting soil (Metro-Mix, Scotts, Hope, AR, United States) in pots and maintained in the greenhouse at 25–30°C during the day and 15–24°C at night with a light intensity of 1,200–1,600 μmol m⁻² s⁻¹ at midday.

Transgenic Plant Screening

Integration and size of each GNA expression cassette in the single and multiple stacked promoter:GNA sugarcane lines were determined by Southern blotting and PCR analyses, respectively. Controls included vector-transformed lines and non-transformed plants (tissue culture-derived). Genomic DNA was isolated by grinding leaf tissues (3 g) collected from 3- to 4-month-old transgenic sugarcane plants in liquid nitrogen as previously reported (Tai and Tanksley, 1990; Chiong et al., 2017).

For Southern blot analysis, genomic DNA (15 μg per reaction) was digested overnight with *Sall*, electrophoresed on 0.8% (w/v) agarose gels and transferred to nylon membranes (Amersham

Hybond-XL, GE Healthcare Bio-Sciences Corp., Piscataway, NJ, United States) in 0.4 M sodium hydroxide (Sambrook and Russell, 2001). Pre-hybridization, hybridization, washing and detection of DNA gel blots were performed as described by Mangwende et al. (2009), using Church's buffer. The GNA-specific probe (570 bp) was released from *pUbi:GNA/pUC18* with *Pst*I. Probes were labeled with [α - 32 P]dCTP using the Random Primers DNA Labeling kit (Invitrogen, ThermoFisher Scientific) (Mangwende et al., 2009).

PCR was performed on a C1000 TouchTM thermal cycler (Bio-Rad Laboratories, Inc., Hercules, CA) in a total reaction volume of 25.0 μ L using 300.0 ng of DNA and AccuStartTM II PCR ToughMix[®] (Quantabio, Beverly, MA, United States) according to the manufacturer's instructions with the following conditions: 94°C for 3 min, 35 cycles each at 94°C for 30 s, 55–60°C for 30 s, and 72°C for 3–6 min. Primers encompassing the entire promoter:GNA-terminator cassette (**Supplementary Table S1**) were designed with Primer 3.0. All PCR amplicons were separated by electrophoresis on 0.7% agarose (w/v) gels stained with ethidium bromide. A “no DNA template” was included as a negative control and the transformation plasmid as a positive control for PCR.

Plant Growth and Treatment Conditions

For experiments involving hormone induction, treatments were conducted by spraying 1-year-old transgenic plants of three single-promoter *pUbi-pSCBV21-pSHDIR5-1:GNA* lines and 12 triple-promoter *pUBD5:GNA* lines with 5 mM salicylic acid (SA) (S3007-500G; Sigma-Aldrich, St. Louis, MO) (in 0.05% [v/v] Tween-20 aqueous solution) in the greenhouse (28°C with 14 h-light/10 h-dark). Control plants were sprayed only with 0.05% Tween-20. Leaf samples were collected at 0 and 48 h following treatment. The plants were distributed randomly, with two plants per line grown in a 16-L pot, and four pots per line were selected for each time point.

Bench-Scale Extraction of Recombinant GNA

For the bench-scale extraction of total soluble protein (TSP) from GNA transgenic sugarcane leaves, 200 mg of tissue was homogenized in 0.2 M sodium acetate and 0.2 M acetic acid (pH 5.2) buffer (600 μ L) (1:3 tissue to buffer ratio) in 2-mL screw-cap microcentrifuge tubes for 30 s at 5,000 rpm with a Precellys 24 homogenizer (MO BIO Laboratories, Carlsbad, CA, United States) in the presence of a ceramic spherical bead (0.64 cm-diameter). The TSP supernatants were collected by centrifugation at 10,600 g twice for 10 min at 4°C and were stored at –80°C for analysis.

For the bench-scale extraction of TSP from GNA transgenic sugarcane culms, tissue was harvested, shredded with a garden shredder (MTD1400K, Yard machines, Home Depot, Weslaco, TX, United States) and frozen at –80°C. Frozen tissue (25 g) was ground with a IKA[®]-WERKE M20 Universal Mill (Breisgau, Germany), mixed with 50 mL extraction buffer (0.1 M citric acid/0.2 M sodium acetate buffer, pH 4.0 or 0.1 M sodium acetate/0.2 M acetic acid with 1 mM EDTA and 0.05%

[v/v] Tween 20, pH 5.2) (1:2 tissue to buffer ratio) in a WARING[®] commercial blender (Model 7011HS) for 5 min and heated at 65°C for 15 min with occasional shaking. The TSP supernatants were collected by centrifugation at 12,000 g for 20 min and clarified by being passed through four layers of Miracloth (475855-1R, Millipore Sigma, Darmstadt, Germany). Clarified TSPs were precipitated with acetone and 0.1% [v/v] β -mercaptoethanol (1:5) at –20°C for 1 h. The TSP pellets were collected by centrifugation at 12,000 g for 20 min at 4°C and resuspended in 50 μ L of 6 \times sample buffer (0.38 M Tris–HCl, pH 6.8, 10% SDS, 30% [v/v] glycerol, 30% [v/v] β -mercaptoethanol and 0.2% [w/v] bromophenol blue). The GNA standard was prepared from pure *Galanthus nivalis* snowdrop-bulb lectin (L-7401-5; EY Laboratories, Inc., San Mateo, CA, United States).

Semi-Quantitative Immunoblot Analysis

The TSPs extracted from GNA transgenic sugarcane leaves and culms were boiled for 5 min in 12 μ L of 6 \times sample buffer and were analyzed by SDS-PAGE in Novex[®] NuPAGE 4–12% Bis-Tris gels (Invitrogen, ThermoFisher Scientific). The TSP content of leaf and culm extracts was determined using the Qubit fluorometer (ThermoFisher Scientific) and the Lowry method together with the DC Protein Assay kit (Bio-Rad Laboratories Ltd., Hercules, CA, United States), respectively.

The TSPs were transferred onto NitroBind nitrocellulose membranes (0.22 μ) (GE Water and Process Technologies, Boulder, CO, United States) using a Mini Trans-Blot Electrophoretic Transfer Cell (Bio-Rad Laboratories Ltd.). Blocking of non-specific sites was performed with 5% [w/v] skim milk in 1 \times Tris buffered saline (TBS)–Tween solution (TBST) (25 mM Tris–HCl, pH 7.8, 190 mM sodium chloride (NaCl) and 0.1% [v/v] Tween-20) for 1 h. Incubation with the polyclonal anti-GNA antibody (produced in rabbits; Research Genetics Inc., Huntsville, AL, United States) was performed for 1 h at a concentration of 1:1,000 in blocking solution (3% [w/v] skim milk, 1 \times TBS), followed by three washes with 1 \times TBST (1 \times TBS with 0.05% [v/v] Tween 20). Samples were incubated with the peroxidase-linked goat anti-mouse secondary antibody (A6154, Sigma-Aldrich) (1:2,000 in 3% [w/v] skim milk, 1 \times TBS blocking solution) for 2 h and then washed three times with 1 \times TBST. Signals were detected by incubation with 4-chloro-1-naphthol (Sigma-Aldrich) and hydrogen peroxide in 1 \times TBS. Immunoblots were quantified using ImageJ software (<https://imagej.nih.gov/ij/download.html>) by comparing sample band intensity with that of the GNA standard (pure GNA protein) present on the same membrane.

Affinity Chromatography Purification

A pool of leaves (892.0 g) from three representative single-promoter *pUbi:GNA* lines and four triple-promoter:GNA lines was mixed with extraction buffer (50 mM sodium phosphate, 150 mM NaCl, 5 mM EDTA, pH 8.0, 60 mM freshly prepared ascorbic acid and 1 mM phenylmethylsulfonyl fluoride) and was mechanically homogenized in batches. A final ratio of buffer to biomass of 6:1 (v/w) was used. The homogenate was clarified by centrifugation, gravity filtration and depth filtration. The clarified extract was concentrated 20-fold by tangential flow filtration

(TFF) using a 5.0 kDa MWCO TFF cassette (Millipore Sigma, Danvers, MA, United States). Because the aim was to generate only sufficient material for analytical characterization, mannose-agarose affinity chromatography was employed to capture GNA (mannose agarose has a 45 mg mL⁻¹ binding capacity for GNA). A 10 mL (5 cm) mannose agarose (M6400-10ML; Millipore Sigma) column (with the capacity to bind approximately 90 mg GNA) column was equilibrated with five column volumes (CVs) of 1 × phosphate buffered saline (PBS). The clarified extract was loaded at a flow velocity of 75 cm h⁻¹ (a 4-min residence time). The column was washed with 20 CVs of 1 × PBS, and elution was performed with 10 CVs of 1 × PBS and 0.5 M mannose. The mannose-bound elution fractions, monitored by absorbance at 280 nm, were pooled, concentrated by TFF using a 5.0-kDa-MWCO membrane (Millipore Sigma) and diafiltered with 10 volumes of 1 × PBS to remove mannose.

Size-Exclusion Chromatography

The mannose-agarose purified and concentrated sugarcane recombinant GNA was subjected to size-exclusion (SE) chromatography using a TSKgel G3000SW xL (Tosoh Bioscience, King of Prussia, PA, United States), 7.8 mm × 30 cm, 5 μm column and an HP 1100 Series HPLC system with a diode array detector (Agilent Technologies, Inc., Santa Clara, CA, United States). The mobile phase for SEC consisted of 50 mM sodium phosphate (monobasic, monohydrate)/sodium phosphate (dibasic, anhydrate) and 0.3 M NaCl, pH 7.0. An SE chromatography protein mix standard consisting of thyroglobulin (0.5 mg mL⁻¹), bovine serum albumin (1 mg mL⁻¹), ovalbumin (1 mg mL⁻¹), α-lactalbumin (1 mg mL⁻¹) and aprotinin (0.4 mg mL⁻¹) with molecular weights of 675, 66.5, 45, 14.2 and 6.5 kDa, respectively, was used to determine the molecular weight of the sample chromatographic peaks. The protein mix molecular weight standard was prepared prior to sample analysis and 20 μL was injected into the column. Mobile phase buffer was used for blank injections. The column was equilibrated with the mobile phase before sample analysis. The GNA samples were separated on the column at a flow rate of 1.0 mL min⁻¹ for a total run time of 15 min.

Data were analyzed using ChemStation Data Analysis software (Agilent Technologies, A.01.04 025) (Agilent, Santa Clara, CA, United States). Data were recorded at 220 nm and 280 nm, the UV signal of each GNA sample was integrated, and the relative percentage of each peak detected was determined. All peaks with a percent relative abundance ≥ 0.1% were considered for quantification.

MALDI-TOF Mass Spectrometry

Following mannose-agarose purification and concentration, the molecular weight of the sugarcane recombinant GNA was analyzed under non-reducing conditions using matrix-assisted laser desorption ionization time-of-flight mass spectrometry (MALDI-TOF MS). The sinapinic acid (SiA) matrix was prepared at 10 mg mL⁻¹ in 30:70 acetonitrile:0.1% trifluoroacetic acid:water (TFA:H₂O). GNA samples were mixed 1:9 in a 0.5 mL Eppendorf® centrifuge tube, and 1.5 μL of each mixture was spotted onto a MALDI plate.

The samples were co-crystallized with the matrix under a gentle flow of air prior to analysis (about 2–3 min). The plate was then loaded into the MALDI-TOF mass spectrometer (Applied Biosystems, Waltham, MA, United States) and acquisitions were performed manually. The instrument was operated in linear delayed positive ion mode with an accelerating voltage of 25 kV, the grid set to 66–74% and a delay time of 200 ns. The Shots/Spectrum was set to 200 with a mass range of 4,500–50,000 Da and a low mass gate of 4,000 Da. The SiA matrix was selected to acquire the calibration and data file spectra. The initial laser power was set to 1800 for calibration and was adjusted as necessary during spectrum acquisition. A one-point calibration curve was generated using the mean mass peak of myoglobin (16,952.5 Da) in the standard test mix and was used to analyze the samples. The calibration file was opened and entered in Voyager with Data Explorer™ software for subsequent data acquisition and processing.

Enzyme-Linked Lectin Assay

The binding efficiency of GNA to mannose was determined using the enzyme-linked lectin assay (ELLA), which allows lectin-mannose interactions to be analyzed in a standard microtiter plate format. The ELLA requires the immobilization of mannan onto the surface of an ELISA plate. Mannan derived from *Saccharomyces cerevisiae* was used, which has a short peptide tail and binds well to the plate.

As a coating substrate, mannan was immobilized onto an ELISA plate (96-well plate; ThermoFisher 62409-024) at 1 μg per well (using 100 μL per well of a pre-prepared stock solution of 10 μg mL⁻¹ in 1 × PBS) with incubation overnight at 4°C. Mannan-coated plates were washed twice with PBST (1 × PBS, 0.2% [v/v] Tween 20) and were blocked with 150 μL of 1 × carbo-free blocker solution (Vector Laboratories, Inc. [Vector Labs]; Burlingame, CA, United States) for 2 h at 28°C. All subsequent steps were performed at 28°C. The wells were washed twice with 1 × PBST. Snowdrop-bulb native GNA (Vector Labs) was used to create a standard curve starting from 25 ng mL⁻¹, with seven two-fold serial dilutions. Different dilutions of the purified GNA sample prepared in 0.1% carbo-free blocker solution were added to the ELISA plate and incubated for 1 h. Unbound lectin was removed by washing each well twice with PBST. The plates were then incubated with goat anti-GNA polyclonal antibody (100 μL per well) (1:1,000 in 0.1 × blocking solution) for 1 h at 28°C. After two washes with PBST, the plates were incubated for 1 h at 28°C with anti-goat IgG (whole molecule)-alkaline phosphatase antibody produced in rabbit (100 μL per well) (1:1,000 in 0.1 × blocking solution). Plates were subsequently washed twice with PBST and then once with 1 × PBS. Plates containing alkaline phosphatase yellow substrate (100 μL per well) were incubated in the dark at 28°C for 15 min. The reaction was stopped with 3 N sodium hydroxide (25 μL per well), and absorbance was measured at 405 nm using the 96-well Synergy H1 5.1 Hybrid Multi-Mode plate reader (BioTeck, Winnoski, VT, United States).

Inhibition assays were performed with a constant concentration (100 ng mL⁻¹) of recombinant GNA samples

pre-incubated for 1 h with two-fold serial dilutions (3.9, 7.8, 15.6, 31.3, 62.5, 125 and 250 mM) of methyl α -D-mannoside (Sigma-Aldrich) (100 mg mL⁻¹ stock; MW 194), a competitive inhibitor of mannan binding. Samples were added to the plate that was pre-blocked with carbo-free blocker, and the ELLA protocol was performed as described above. The recombinant GNA concentration was estimated based on a standard curve of different concentrations of snowdrop-bulb native GNA (Vector Labs).

RESULTS AND DISCUSSION

Recombinant Snowdrop-Bulb GNA Is Synthesized in Transgenic Sugarcane

We generated several independent transgenic sugarcane lines that expressed *GNA* from the single *Ubi* promoter and 35STNOST double terminator (*pUbi:GNA-35STNOST*) (Figure 1A) and confirmed their identity by Southern blot analysis. These

consisted of eight lines (20 plants) for TCP87-3388, nine lines (12 plants) for TCP89-3505, three lines (60 plants) for TCP98-4454 and seven lines (23 plants) for CP72-1210. Southern blot analysis revealed that the majority of the *pUbi:GNA* lines exhibited a simple integration pattern (two to five integration events) (Figure 1B; representative *pUbi:GNA* line 1D; Supplementary Figure S1). Several lines, such as 1G-1 and 30A, displayed a more complex integration pattern (Figure 1B; Supplementary Figure S1).

We analyzed the accumulation of GNA in all lines by semi-quantitative immunoblot analysis of TSP from clarified extract of culms and leaves. The yield of GNA from the single-promoter *pUbi:GNA* lines varied in culms from low (< 0.1 mg kg⁻¹ culm weight or < 0.01% TSP; 54.0% of 115 recovered plants), to moderate (≥ 0.1 mg kg⁻¹ culm weight or $\geq 0.01\%$ TSP; 22.7% of 115 recovered plants) and high (0.3 mg kg⁻¹ culm weight or 0.04% TSP; 23.3% of 115 recovered plants) (Table 1). The GNA yield range was 0.07–0.30 mg kg⁻¹ culm weight (0.01–0.04% TSP) (Table 1).

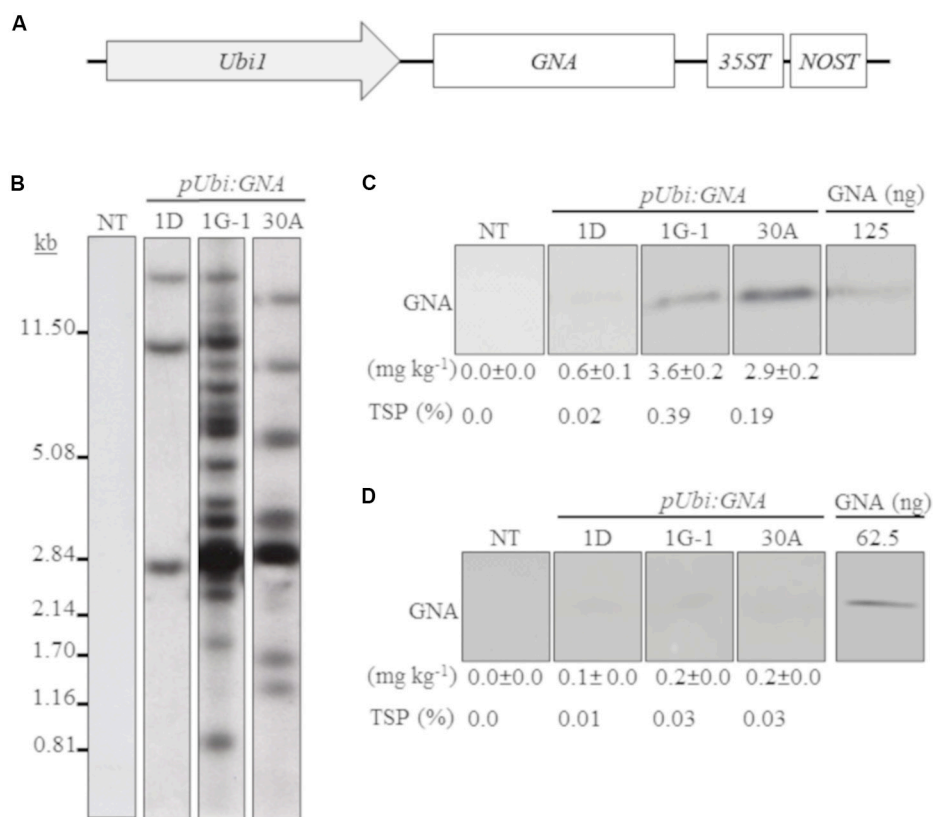


FIGURE 1 | Molecular characterization of single-promoter:GNA-expressing lines. **(A)** Design of the expression vector with the constitutive maize *ubiquitin 1* promoter (*Ubi1*; *pUbi*), *GNA* and double-terminator 35ST (from *Cauliflower mosaic virus 35S* RNA) and NOST (from *Agrobacterium tumefaciens* nopaline synthase). Vector assembly and cloning sites are described under 'MATERIALS AND METHODS.' **(B)** Stable integration of recombinant *GNA* in three representative sugarcane *pUbi:GNA* lines as detected by Southern blot analysis. DNA gel blots were hybridized to a probe corresponding to the *GNA* coding region. GNA accumulation in sugarcane leaves **(C)** and culms **(D)** of three representative sugarcane *pUbi:GNA* lines as assessed by semi-quantitative immunoblot analysis of total soluble proteins (TSP), using a polyclonal anti-GNA antibody. Molecular weight of GNA is ~12 kDa. All immunoblots were loaded with an equal amount of TSP (60 μ g) per lane, and 62.5 or 125 ng of snowdrop-bulb native GNA as a standard. The GNA yield (mg kg⁻¹ of tissue) in clarified juice extract is indicated. Yield values represent two biological replicates and are reported with the standard error. NT: non-transformed (tissue culture derived) plant. The full-length uncropped DNA autoradiograms and TSP immunoblots are displayed in **Supplementary Figures S1–S4**, respectively.

TABLE 1 | Recombinant GNA yield in transgenic sugarcane and energy cane culms.

GNA-expressing line and percentage of plants analyzed	GNA yield as determined by semi-quantitative immunoblot analysis	
	GNA (mg kg ⁻¹ culm weight)	TSP (%)
Sugarcane		
Single-promoter:GNA lines		
<i>pU</i> :GNA double-terminator (35STNOST) lines (27 lines; 115 plants)	0.07–0.3 (range)	0.01–0.04 (range)
54.0%	< 0.1	< 0.01
22.7%	≥ 0.1	≥ 0.01
23.3%	≥ 0.3	≥ 0.04
Triple-promoter:GNA lines		
<i>pUBD5-1</i> :GNA double-terminator (35STNOST) (11 lines; 49 plants)	0.34–12.7 (range)	0.05–1.8 (range)
51.0%	1.2–12.7	0.2–1.8
49.0%	0.34–1.1	0.05–0.1
Energy cane		
Quadruple-promoter:GNA lines		
<i>pUBED5-1</i> :GNA double-terminator (35STNOST) (3 lines; 9 plants)	0.9–8.3 (range)	0.12–1.2 (range)
40.0%	2.7–8.3	0.37–1.2
20.0%	1.6–1.7	0.22–0.24
40.0%	0.9–1.4	0.12–0.19

The percentage (%) of plants carrying the single or stacked promoter:GNA is presented under each line category. U, maize ubiquitin 1 promoter; B, promoter for Sugarcane bacilliform virus; E, promoter for sugarcane elongation factor 1α; D5-1, promoter for sugarcane dirigent5-1; 35ST, Cauliflower mosaic virus 35S terminator; NOST, *Agrobacterium tumefaciens* nopaline synthase terminator; TSP, Total soluble protein.

The yield of GNA from the single-promoter *pUbi*:GNA lines was higher in leaves than in culms (Tables 1, 2). The yield range of GNA was 1.60–3.82 mg/kg⁻¹ of leaf material (0.1–0.3% TSP), with 70% of plants producing GNA in the range 1.60–2.48 mg kg⁻¹ of tissue (0.10–0.19% TSP) and 30% in the range 2.60–3.82 mg/kg⁻¹ of tissue (0.2–0.3% TSP) (Table 2). Therefore, a 7.5–10 fold increase in GNA yield was achieved in the leaves of the single-promoter *pUbi*:GNA lines.

The Accumulation of Recombinant GNA in Transgenic Sugarcane and Energy Cane Is Enhanced by Promoter Stacking

We previously developed and successfully used a combinatorial stacking gene-promoter expression system to significantly enhance the accumulation of recombinant bovine lysozyme (BvLz) in sugarcane culms (Damaj and Mirkov, 2019). The system consists of co-expressing the gene from multiple constitutive or culm-regulated promoters on separate expression vectors via combinatorial plant transformation. Culm tissue constitutes the largest fraction of harvestable biomass and represents a suitable tissue for the large-scale production of bulk proteins. To test whether the

TABLE 2 | Recombinant GNA yield in transgenic sugarcane leaves.

GNA-expressing line and percentage of plants analyzed	GNA yield as determined by semi-quantitative immunoblot analysis	
	GNA (mg kg ⁻¹ leaf weight)	TSP (%)
Single-promoter:GNA lines		
<i>pU</i> :GNA double-terminator (35STNOST) lines (27 lines; 115 plants)	1.6–3.82 (range)	0.1–0.3 (range)
70.0%	1.6–2.48	0.1–0.19
30.0%	2.6–3.82	0.2–0.3
Triple-promoter:GNA lines		
<i>pUBD5-1</i> :GNA double-terminator (35STNOST) (11 lines; 49 plants)	3.96–29.3 (range)	0.31–2.3 (range)
85.0%	3.96–7.0	0.31–1.0
15.0%	7.7–29.3	1.1–2.3

The percentage (%) of plants carrying the single or stacked promoter:GNA is presented under each line category. U, maize ubiquitin 1 promoter; B, promoter for Sugarcane bacilliform virus; E, promoter for sugarcane elongation factor 1α; D5-1, promoter for sugarcane dirigent5-1; 35ST, Cauliflower mosaic virus 35S terminator; NOST, *Agrobacterium tumefaciens* nopaline synthase terminator; TSP, Total soluble protein.

recombinant GNA levels recovered from the culms of the single-promoter *pUbi*:GNA lines was enhanced by using multiple promoter:GNA sequences, we co-transformed 2-month-old embryogenic calli of sugarcane (CP72-1210, TCP87-3388 and CP89-2143) and energy cane (CP10-4928 and Ho02-113) with the multiple promoter:GNA expression vectors (Figure 2A), using the *bar* gene (phosphinothricin acetyl transferase) as a selectable marker. In total, 11 independent transgenic GNA lines (49 plants) generated from the combinatorial transformation of sugarcane with the triple-promoter:GNA expression vectors were identified by Southern blot analysis (Figure 2B). The size of each respective GNA expression vector (promoter, GNA and double terminator) in the stacked triple-promoter:GNA lines was confirmed by PCR using primers encompassing each of the different promoter:GNA-terminator cassettes (Figure 2C and Supplementary Figure 3).

Most of the sugarcane triple-promoter:GNA lines exhibited a complex integration pattern (> 8 integration events) by Southern blotting (Figure 2B; representative *pUBD5-1*:GNA lines 1-2T, 5-1G and 5-3C; Supplementary Figure S1). No phenotypic differences were observed between the transgenic sugarcane GNA lines and non-transformed plants (Supplementary Figure S2), as previously observed with transgenic sugarcane *BvLz* plants (Damaj and Mirkov, 2019).

We analyzed the accumulation of GNA in all lines by semi-quantitative immunoblot analysis of TSP from clarified extract of culms and leaves. The GNA yield of transgenic sugarcane lines from the stacked triple-promoter *pUbi*-*pSCBV21*-*pSHDIR5-1*(*pUBD5-1*):GNA increased in culms by up to about 42.3-fold (up to 12.7 mg kg⁻¹ of tissue or 1.8% TSP) compared to the yield in single-promoter *pUbi*:GNA lines (*pU*:GNA; 0.3 mg kg⁻¹ of tissue or 0.04% TSP), with 49% of plants containing 0.34–1.1 mg kg⁻¹ tissue (0.05–0.100% TSP)

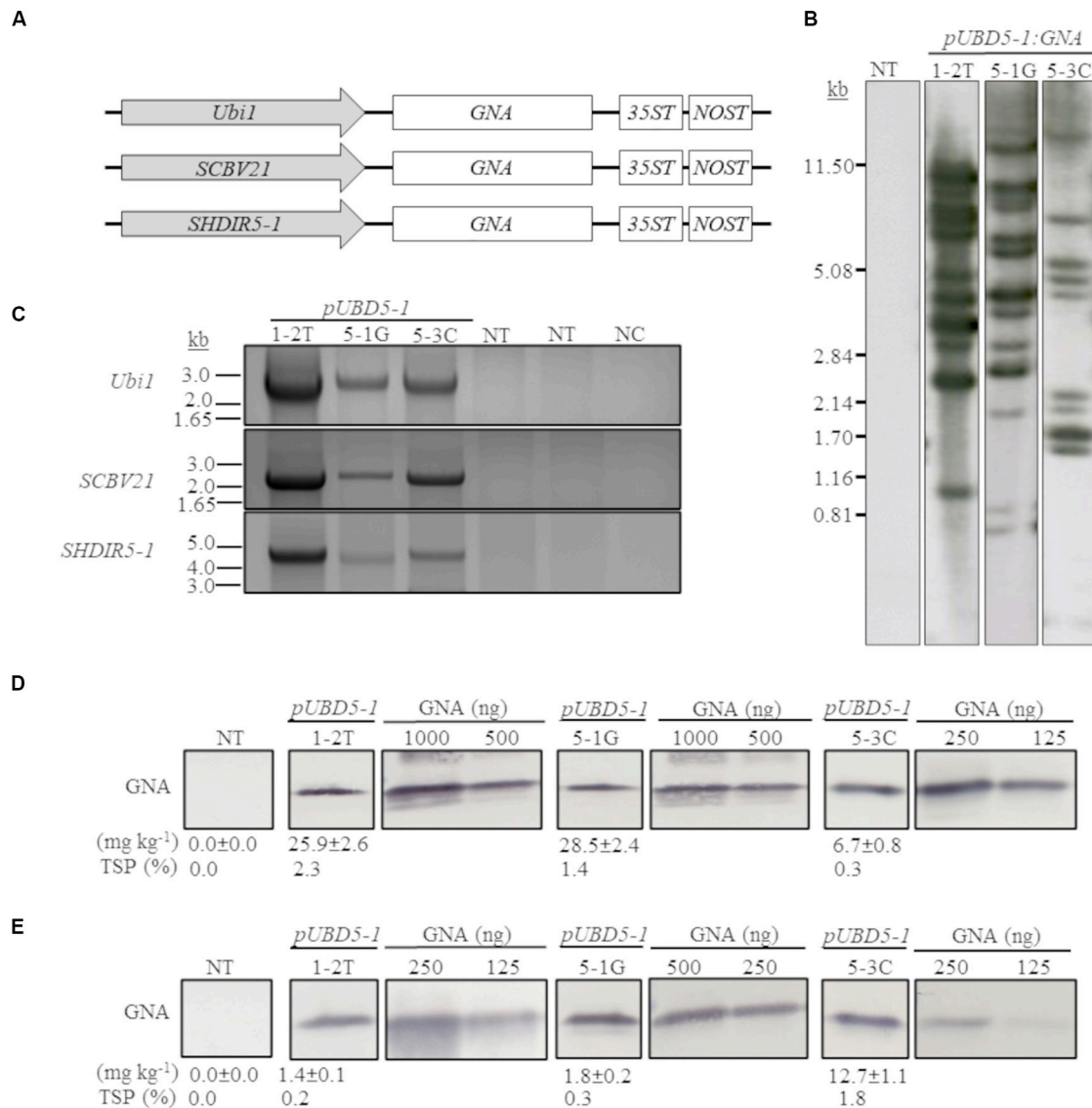


FIGURE 2 | Molecular characterization of the stacked promoter:GNA-expressing lines. **(A)** Design of a representative stacked promoter:recombinant GNA expression system developed for sugarcane. Promoters used include the constitutive maize *ubiquitin 1* (*Ubi1*; *pU*) or the culm-regulated promoters from *Sugarcane bacilliform virus* (*SCBV21*; *B*) and sugarcane *dirigent5-1* (*SHDIR5-1*; *D5-1*). 35SST: terminator derived from *Cauliflower mosaic virus* 35S RNA; NOST: *Agrobacterium tumefaciens* nopaline synthase terminator. Vector assembly and cloning sites are described under 'MATERIALS AND METHODS.' **(B)** Stable integration of recombinant GNA in three representative sugarcane triple-promoter *pUBD5-1:GNA* lines as detected by Southern blot analysis. DNA gel blots were hybridized to a probe corresponding to the GNA coding region. **(C)** Integration of the multiple expression cassettes for the triple promoter:GNA stacked lines was confirmed by polymerase chain reaction using primers specific to each promoter. Detection of *Ubi1* promoter with primer set *pUbi-FI/35ST-R* (2.5 Kb fragment), detection of *SCBV21* promoter with primer set *pSCBV21-F/35ST-R* (2.179 Kb fragment) and detection of *pSHDIR5-1* with primer set *pSHDIR5-1-F/GNA127-R* (4.88 Kb fragment). GNA accumulation in sugarcane leaves **(D)** and culms **(E)** of three representative sugarcane *pUBD5-1:GNA* lines (shown as *pUBD5-1* in Figure) as assessed by quantitative immunoblot analysis of total soluble proteins (TSP), using a polyclonal anti-GNA antibody. Molecular weight of GNA is ~12 kDa. All immunoblots were loaded with an equal amount of TSP (60 μ g) per lane and 25, 62.5, 125, 250, 500 or 1000 ng of snowdrop-bulb native GNA as a standard. The GNA yield (mg kg^{-1} of tissue) in clarified juice extract is indicated. Yield values represent two biological replicates and are reported with the standard error. NT: non-transformed (tissue culture derived) plant; NC: no DNA template. The full-length uncropped DNA autoradiograms are displayed in **Supplementary Figure S1**, and the TSP immunoblots in **Supplementary Figures S5, S6**.

and 51% containing 1.2–12.7 mg kg^{-1} of tissue (0.20–1.8% TSP) (Table 1).

The GNA yield of transgenic lines containing the stacked triple-promoter *pUBD5-1:GNA* was also enhanced in leaves,

by about 7.7-fold (up to 29.3 mg kg^{-1} of tissue or 2.3% TSP) more than that of the single-promoter *pUbi:GNA* lines, with 85% of plants containing 3.96–7.00 mg GNA kg^{-1} of tissue (0.31–1.00% of TSP) and 15% containing

between 7.7–29.3 mg GNA kg⁻¹ of tissue (1.1–2.3% of TSP) (Table 2).

We also generated transgenic sugarcane lines containing stacked quadruple-promoter:GNA expression vectors, but the maximum yield of GNA obtained was 9.4 mg kg⁻¹ of tissue (1.3% TSP). Therefore, stacking more than three promoter:GNA vectors did not further enhance GNA yield. Furthermore, the yield of GNA from energy cane transformed with GNA driven from four stacked promoters (*pUbi-pSHEF1α-pSCVB21-pSHDIR5-1:GNA*) was comparable to that obtained from quadruple-stacked promoter:GNA sugarcane. Three lines (nine plants) were generated that accumulated GNA to levels ranging from low at 0.9–1.4 mg kg⁻¹ (0.10–0.19% TSP) (40% of plants), to moderate at 1.6–1.7 mg kg⁻¹ (0.22–0.24% TSP) (20% of plants), and high at 2.7–8.3 mg kg⁻¹ of culm (0.37–1.20% TSP) (40% of plants) (Table 1).

A comparison of the GNA yield in the sugarcane single-promoter *pUbi:GNA* line 1G-1 (3.6 mg kg⁻¹ of leaf and 0.20 mg kg⁻¹ of culm) (Figures 1C,D; Supplementary Figure S4) with that of the triple-promoter *pUBD5-1:GNA* line 1-2T (25.9 mg kg⁻¹ leaf tissue and 1.4 mg kg⁻¹ culm tissue) (Figures 2D,E; Supplementary Figures S5, S6), which contained about 14 GNA insertions (Figures 1B, 2B; Supplementary Figure S1), showed that there was a clear increase in GNA yield irrespective of the number of transgenic insertions. This suggests that the increase in GNA yield is primarily correlated with the number of combinatorial stacked promoters and is not dependent on the number of GNA insertions alone, which was reported for combinatorial promoter:*BvLz* stacking in sugarcane (Damaj and Mirkov, 2019).

Our results show that levels of GNA can be enhanced by stacking or co-expressing the gene under the control of multiple different promoters. We speculate that the observed additive increase is mainly due to increased transcriptional output from the different transgene units stably integrated into the plant genomes. However, often multiple copies do not result in greater expression. It has been noted that integration of multiple transgenes, often in tandem, using same promoter can lead to homology-dependent gene silencing (HDGS) via DNA methylation events (Matzke et al., 1989, 1994; Tu et al., 2000; Bock, 2013; Rajeevkumar et al., 2015). This can lower the net expression (Assaad et al., 1993; Kumpatla and Hall, 1998; Pawlowski and Somers, 1998; Kanno et al., 2000; Khaitová et al., 2011). In our system, HDGS may not be an issue mainly due to the use of different promoter sequences and separate vectors that would avoid tandem integration of transgenes.

Thus, increasing the expression level of stably transformed recombinant GNA sequences through combinatorial promoter-gene stacking proved to be an efficient approach to increase protein accumulation and resulted in high GNA levels that typically approached 1.8% and 2.3% of the TSP from transgenic culms (12.7 mg kg⁻¹ of tissue) (Table 1) and leaves (29.3 mg kg⁻¹ of tissue) (Table 2), respectively.

The Accumulation of Recombinant GNA Is Responsive to Stress-Regulated Hormones

Another approach to increase the level of recombinant GNA is to induce promoter activity in transgenic plants by applying stress-regulated hormones. The *Ubi* and *SHDIR16* promoters can be induced by stress-signaling hormones such as salicylic acid (SA) (Damaj et al., 2010). To test whether SA can further induce GNA expression, we sprayed and irrigated several representative single-promoter *pUbi:GNA* and triple-promoter *pUBD5-1:GNA* sugarcane lines with SA for 48 h in the greenhouse. The level of GNA accumulation in leaves increased by 5.4-fold (from 3.0 to 16.1 mg kg⁻¹ of tissue) following SA application in the single-promoter *pUbi:GNA* 1G-1 line and by 1.3-fold (from 29.3 to 37.2 mg kg⁻¹ of tissue) in the triple-promoter *pUBD5-1:GNA* line 1-2T (Figure 3; Supplementary Figure S7). These results corroborate those of previous studies (Damaj and Mirkov, 2019), and the patterns of SA induction of recombinant GNA are consistent with the kinetics of promoter activation by SA (Damaj et al., 2010). The use of promoters such as *pUbi*, *pSHDIRs* and *pSCBV21* that can be turned on and off by stress-regulated hormones such as SA holds great potential for the bioengineering industry, as a means to increase the production of GNA and other recombinant therapeutic proteins.

Optimization of the Bench-Scale Extraction of Recombinant GNA From Transgenic Sugarcane and Energy Cane

Because no previous attempts have been made to extract GNA from sugarcane culms, we first evaluated a bench-scale extraction of recombinant GNA from transgenic culms of sugarcane and energy cane. We tested two different buffers to extract recombinant GNA from the culms of sugarcane and energy cane that expressed the triple-promoter *pUBD5-1:GNA*, with GNA expression driven by *pUbi* (U), *pSCBV21* (B) and *pSHDIR5-1* (D5-1), sodium acetate buffer (pH 5.2) and citric acid (pH 4.0), as outlined in Supplementary Figure S8 (described in section “MATERIALS AND METHODS”). The GNA yield of representative *pUbi-pSCBV21-pSHDIR5-1(pUBD5-1):GNA* lines 1-2T and 5-1G was 0.4 and 0.5 mg kg⁻¹, respectively (0.06% TSP for both), using sodium acetate (pH 5.2), and 0.2 and 0.2 mg kg⁻¹, respectively (0.03% of TSP for both lines), with citric acid (Figure 4; Supplementary Figure S9); this represented a 2.0- to 2.5-fold increase in GNA yield with sodium acetate compared to that with citric acid.

We then further optimized the extraction of recombinant GNA from culm tissue by using sodium acetate buffer (pH 5.2) supplemented with 0.05 mM Tween 20 (v/v) (a mild surfactant) and 1 mM EDTA. This increased the yield of GNA from 0.4 mg kg⁻¹ (0.06% TSP) to 1.4 mg kg⁻¹ (0.2% TSP) for *pUBD5-1:GNA* line 1-2T and from 0.5 mg kg⁻¹ (0.06% TSP) to 1.0 mg kg⁻¹ (0.14% TSP) for *pUBD5-1:GNA* line 5-1G (Figure 4; Supplementary Figure S9). This represented at least a 2.0- to 3.5-fold increase following the addition of Tween 20 and EDTA.

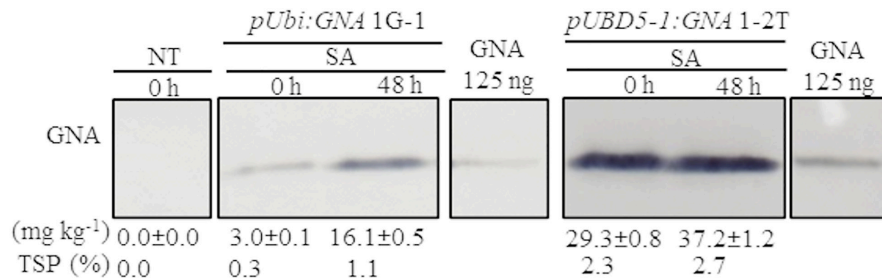


FIGURE 3 | Accumulation of recombinant GNA is enhanced by the stress-signaling hormone salicylic acid (SA) in single and triple-promoter:GNA-expressing sugarcane lines. GNA accumulation was determined by quantitative immunoblot analysis in total soluble protein (TSP) extracted from leaf tissue of representative *pUbi:GNA* and *pUBD5-1:GNA* lines at 0 and 48 h of SA treatment (5 mM), using a polyclonal anti-GNA antibody. Molecular weight of GNA is ~12 kDa. All immunoblots were loaded with an equal amount of TSP (60 µg) per lane and 125 ng of snowdrop-bulb native GNA as a standard. The GNA yield (mg kg⁻¹ of tissue) in clarified juice extract is indicated. Yield values represent two biological replicates and are reported with the standard error. Molecular weight of GNA is ~12 kDa. *pUbi* and *pU*: maize *ubiquitin 1* promoter; *B*: promoter for *Sugarcane bacilliform virus*; *D5-1*: promoter for sugarcane *dirigent5-1*. NT: non-transformed (tissue culture derived) plant. The full-length uncropped TSP immunoblots are displayed in **Supplementary Figure S7**.

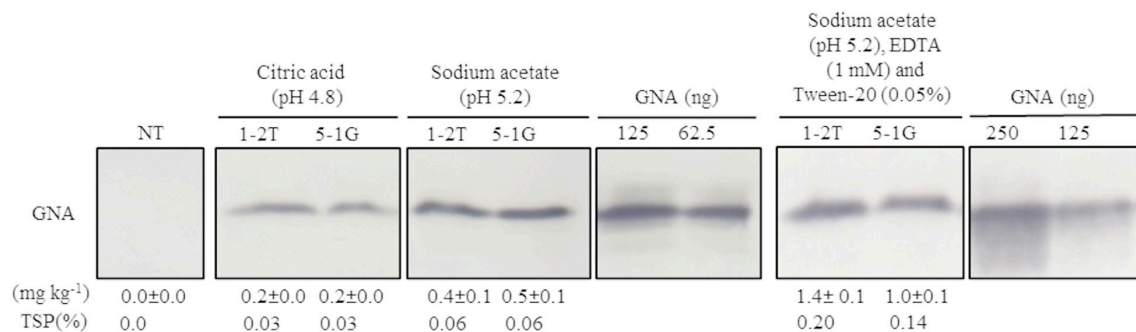


FIGURE 4 | Optimization of recombinant GNA extraction in sugarcane transgenic culms. Accumulation of recombinant GNA was assessed by semi-quantitative immunoblot analysis of representative lines expressing GNA from the three promoters, maize *ubiquitin 1*, *Sugarcane bacilliform virus* and sugarcane *dirigent5-1*, using a polyclonal anti-GNA antibody. All immunoblots were loaded with an equal amount of TSP (60 µg) per lane and 62.5, 125 or 250 ng of snowdrop-bulb native GNA as a standard. Molecular weight of GNA is ~12 kDa. The GNA yield (mg kg⁻¹ of tissue) in clarified juice extract is indicated. Yield values represent two biological replicates and are reported with the standard error. NT: non-transformed (tissue culture derived) plant. The full-length uncropped TSP immunoblots are displayed in **Supplementary Figure S9**.

Surfactants are commonly added to protein extraction buffers to increase cell wall and membrane breakage and thus potentially increase the amount of extracted protein. To our knowledge, this is the first attempt to extract recombinant GNA from culms and to recover high amounts of protein.

We also optimized the extraction of recombinant GNA from transgenic sugarcane leaves. Under our experimental conditions, Tris-HCl (pH 6.8), which is a common buffer for the extraction of GNA from leaves, did not yield detectable GNA (data not shown). However, using an optimized 0.2 M sodium acetate/0.2 M acetic acid buffer (pH 5.2), we could recover GNA from transgenic sugarcane leaves at a level up to 29.3 mg kg⁻¹ of tissue (2.3% TSP). This yield is higher than that previously reported for sugarcane and other monocot crops. Accumulation levels of recombinant GNA of 0.01–0.25% and 0.13–0.28% TSP have been obtained from rice leaves using Tris-HCl (pH 9.0) (Rao et al., 1998) and from maize leaves using phosphate buffer (with 1% [v/v] β-mercaptoethanol and 10% [v/v] glycerol). A higher recombinant GNA yield of 0.89% TSP has been achieved from lyophilized sugarcane leaves using Tris-HCl (pH 6.8) with 2%

(w/v) SDS, 10% (v/v) glycerol (Wang Z. et al., 2005) and 5% (v/v) β-mercaptoethanol as an extraction buffer (Setamou et al., 2002).

Recombinant GNA Accumulates Differentially in Transgenic Culms and Leaves

In the expression system here, recombinant GNA differentially accumulated in the leaves and culms of transgenic sugarcane plants. For example, the GNA yield from the representative single-promoter *pUbi:GNA* lines 1D, 1G-1 and 30A was 6.0–18-, and 14.5-fold higher in leaves (0.60, 3.6 and 2.9 mg kg⁻¹ of tissue) than in culms (0.10, 0.20 and 0.2 mg kg⁻¹ of tissue) (Figures 1C,D; **Supplementary Figure S4**).

The GNA yield from representative sugarcane triple-promoter *pUBD5-1:GNA* lines 1-2T, 5-1G and 5-3C was 2.3, 1.4 and 0.30% TSP (25.9, 28.5 and 6.7 mg kg⁻¹, respectively) in leaf tissue (Figure 2D; **Supplementary Figure S5**), and 0.20, 0.3 and 1.8% TSP (1.4, 1.8 and 12.7 mg kg⁻¹, respectively) in culm tissue (Figure 2E; **Supplementary Figure S6**). This represented

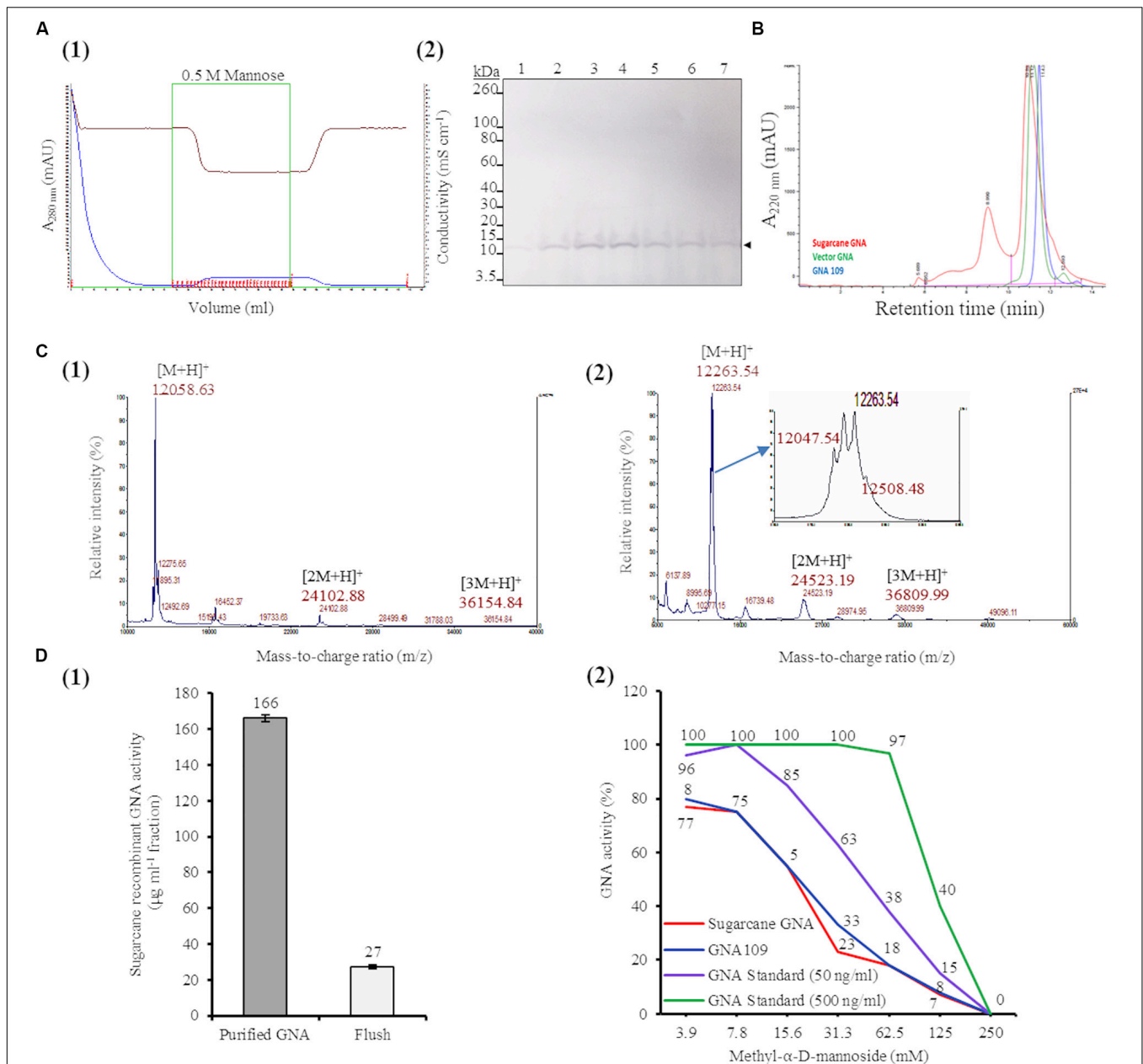


FIGURE 5 | Characterization of sugarcane recombinant GNA. **(A)** Purification of GNA from transgenic sugarcane leaves by mannose-agarose affinity chromatography. (1) Chromatogram of eluted mannose-bound fractions. Blue line: chromatogram of UV absorbance at 280 nm ($A_{280\text{ nm}}$; mAU) to monitor eluted fractions; brown line: chromatogram of conductivity (mS cm^{-1}), which reflects the ionic strength of the buffer; green line: chromatogram of concentrated fractions. Eluted fractions are marked in red. (2) Immunoblot analysis of eluted fractions, using a polyclonal anti-GNA antibody. Lanes 1 to 7 represent elution fractions 1.A.7, 1.A.8, 1.A.9, 1.A.10, 1.A.11, 1.A.12 and 1.B.1, respectively, as shown in the chromatogram. The GNA protein band is indicated by an arrow. The full-length uncropped immunoblot is displayed in **Supplementary Figure S10**. **(B)** Analysis of purified sugarcane recombinant GNA under non-reduced conditions by size-exclusion chromatography at absorbance of 220 nm over time. The chromatogram of sugarcane recombinant GNA is overlaid with those of GNA₁₀₉ and the snowdrop-bulb native GNA standard (Vector GNA). **(C)** Analysis of purified sugarcane recombinant GNA under non-reduced conditions using Matrix-Assisted Laser Desorption Ionization Time-of-Flight Mass Spectrometry (MALDI-TOF MS). (1) The MS spectra of sugarcane GNA displaying molecular weights of m/z 12,058.63 $[M+H]^+$, m/z 24,102.88 $[2M+H]^+$ and m/z 36,154.84 $[3M+H]^+$, which represent monomer, dimer and trimer sugarcane GNA, respectively. (2) The MS spectrum of snowdrop-bulb native GNA standard displaying three additional peaks along with actual m/z of 12,048.63 $[M+H]^+$ (monomer) (enlarged spectrum area). **(D)** Competitive binding assay of recombinant GNA with mannan-binding inhibitor, methyl- α -D-mannoside. (1) Estimation of activity of purified sugarcane recombinant GNA with enzyme-linked lectin assay. Sugarcane recombinant GNA activity is expressed in $\mu\text{g mL}^{-1}$ of pooled pure enriched GNA fractions from **Figure 5A**. (2) GraphPad prism analysis of inhibition assay with purified sugarcane recombinant GNA, GNA₁₀₉ and GNA standard (500 ng mL^{-1} and 50 ng mL^{-1}), using two-fold serial dilutions of the inhibitor (3.9, 7.8, 15.6, 31.3, 62.5, 125 and 250 mM). GraphPad prism data conversion of absorbance at 450 nm into percentage of activity is recorded.

an 18.5- and 15.8-fold higher GNA accumulation for lines 1-2T and 5-1G, respectively, in leaf than in culm tissue, and 1.9-fold more GNA for line 5-3C in culms than in leaves (Figures 2D,E; Supplementary Figures S5, S6). These results suggest that the accumulation of GNA is differentially regulated between sugarcane leaves and culms. We speculate the differences could be attributed to the contrasting biochemical compositions of the two tissue types. Sugarcane culms are mainly composed of soluble sugars and lignocellulosic fiber, with low levels of native protein (Palaniswamy et al., 2016). While leaves have lower fiber content and proportionally more biochemically active cells, which could lead to greater transcriptional output. One could technically combine either tissue types (leaves or culms) for GNA extraction, and as such are not mutually exclusive. However, extraction of proteins from culm tissue may be practical since most of the harvesting and processing equipment used for sugarcane and extracting sugar can be readily extended for purification of recombinant proteins from culms.

Purification and MALDI-TOF Characterization of Sugarcane Recombinant GNA

We purified sugarcane recombinant GNA from TSP extracts from a pool of leaves (0.89 kg of tissue; GNA yield of 7.71 mg kg⁻¹ tissue weight) from seven representative single- and triple-promoter GNA lines in parallel with recombinant GNA₁₀₉ and the snowdrop-bulb native GNA (Vector Labs) using immobilized mannose. Following enrichment of mannose-binding proteins in the sugarcane recombinant GNA sample by mannose-agarose affinity chromatography (Figure 5A1), we detected a polypeptide band corresponding to mature GNA (about 12.0 kDa) by immunoblot analysis of SDS-PAGE of mannose-bound elution fractions (Figure 5A2; Supplementary Figure S10). We performed analytical characterization of GNA after concentration of the enriched elution GNA fractions using a 5.0-kDa-MWCO tangential flow filtration device (about 20-fold). The analysis of purified sugarcane recombinant GNA by size-exclusion (SE) chromatography under non-reducing conditions showed one major peak at 10.89 min and a small peak at 8.9 min (Figure 5B). The purities of the recombinant GNA monomer and tetramer were 65.5% and 24%, respectively, at 8.9 min. We compared the sugarcane GNA SEC chromatogram with that of the snowdrop-bulb native GNA (*G. nivalis* agglutinin; 1NIV, Protein Data Bank accession number 1NIV_A) and recombinant GNA₁₀₉ (*G. nivalis* lectin, LECGNA2 with four additional amino acids, Thr₁₀₆ His₁₀₇ Thr₁₀₈ Gly₁₀₉, at its C-terminus; high mannose-binding activity; (Raemaekers, 2000). Snowdrop-bulb GNA and GNA₁₀₉ displayed a major peak at 11.12 and 11.43 min, respectively (Figure 5B), close to the major peak observed for sugarcane recombinant GNA.

To determine the molecular weight of sugarcane recombinant GNA protein, we performed MALDI-TOF MS analysis under non-reducing conditions. The MS spectra of sugarcane recombinant GNA displayed one peak with a mass-to-charge ratio (m/z) of 12,058.63 $[M + H]^+$, representing the GNA monomer (Figure 5C1). We also detected peaks of m/z 24,102.88

$[2M + H]^+$ and m/z 36,154.84 $[3M + H]^+$, which represented the GNA dimer and trimer, respectively (Figure 5C1). For comparison, the recombinant GNA₁₀₉ MS spectrum also showed a single peak, similar to sugarcane recombinant GNA, with an m/z of 12,052.08 $[M + H]^+$ representing the GNA₁₀₉ monomer (Supplementary Figure S11). The theoretical amino-acid sequence molecular weight for GNA₁₀₉ is 12,051.42 Da. The snowdrop-bulb native GNA (Vector Labs) spectrum revealed three additional peaks (12,263.54 and 12,508.48), as well as the peak corresponding to the actual m/z of 12,047.54 $[M + H]^+$ (monomer) (Figure 5C2, enlarged peak area). The theoretical molecular weight of snowdrop-bulb native GNA is 12,054.41 Da. These results demonstrate that sugarcane recombinant GNA has very similar molecular weight MS peak characteristics and functionality in comparison to the native snowdrop-bulb GNA protein.

Recombinant GNA Retains Binding Specificity to Mannan

The binding efficiency of purified sugarcane recombinant GNA protein to immobilized mannan was determined by ELLA. This assay allows specific lectin-mannose interactions to be analyzed and forms the basis for a functional assay that quantitatively estimates the amount of GNA (Gornik and Lauc, 2007; Couzens et al., 2014). Sugarcane recombinant GNA in the purified sample bound to mannan with an estimated specific activity of 166 $\mu\text{g mL}^{-1}$ based on a standard curve with snowdrop-bulb native GNA (Figure 5D1).

Most lectins synthesized in plants were initially characterized using inhibition assays, in which monosaccharides or their derivatives were used to block lectin binding sites; the lectins were then grouped by their specificity for the monosaccharide(s) that inhibited their binding at millimolar concentrations (Cummings et al., 2017). Therefore, we confirmed the specificity of the interaction between recombinant sugarcane GNA and mannan through an inhibition assay with methyl- α -D-mannoside, a competitive inhibitor of mannan binding (Raemaekers, 2000; Sommer et al., 2018). Equal concentrations of sugarcane recombinant GNA, GNA₁₀₉ and snowdrop-bulb native GNA were incubated with two-fold serial dilutions (3.9, 7.8, 15.6, 31.3, 62.5, 125.0 and 250.0 mM) of methyl- α -D-mannoside (Figure 5D2). The inhibition assay revealed that the mannan-binding activity of all three GNAs decreased with an increase in mannoside concentration, as expected, with binding being reduced to a minimum at a limiting concentration of 250 mM mannoside. Sugarcane recombinant GNA and GNA₁₀₉ showed a similar rapid reduction in binding activity with an increase in the inhibitor, compared to the delayed reduction in the level of the snowdrop-bulb native GNA (Figure 5D2). At a low (3.9 mM) inhibitor concentration, the activities of all three GNAs were only slightly affected; the sugarcane recombinant GNA and GNA₁₀₉ activities decreased by about 20% (from 100% to 80%) compared to that of the snowdrop-bulb native GNA, which remained at 100%. However, the inhibitor concentration required to reduce mannan-binding activity to about 55% was much lower for sugarcane recombinant GNA and GNA₁₀₉ (15.6 mM

of inhibitor) than for the native GNA standard at 50 ng mL⁻¹ (31.3 mM inhibitor) (**Figure 5D2**). The mannan-binding activity for all three GNAs decreased to 0% at an inhibitor concentration of 250 mM.

The ELLA and mannan inhibition assay indicated that sugarcane recombinant GNA, GNA₁₀₉ and snowdrop-bulb native GNA were all able to selectively bind to the anti-GNA antibody and the mannan substrate. However, sugarcane recombinant GNA and GNA₁₀₉ possessed similar mannan-binding activities and were more sensitive to mannan inhibition than snowdrop-bulb native GNA.

To check whether any sequence differences existed that might affect the binding selectivity and affinity of the sugarcane recombinant GNA to the anti-GNA antibody or the mannan substrate, we compared the translated peptide sequence used to transform sugarcane (*G. nivalis* lectin; LECGNA2, Protein Bank accession number AAA33346) with that of the mature snowdrop-bulb native GNA (*G. nivalis* agglutinin; 1NIV, Protein Data Bank accession number 1NIV_A). The amino-acid alignment of the two proteins (**Supplementary Figure S12**) showed that the sequences of the mature GNA protein region were identical in both GNA proteins, with LECGNA2 N and C terminal signal sequences that are presumably cleaved in sugarcane and snowdrop. Both GNA proteins contain the consensus sequence motif QXDXNXVXY (QEDCNLVLY) (**Supplementary Figure S12**), which is involved in recognition of the α -D-mannose substrate.

The MALDI-TOF MS data showed that the spectrum of the snowdrop-bulb native GNA displayed three additional peaks in addition to that of the actual molecular weight of m/z 12,047.54 [M + H]⁺ (**Figure 5C2**), compared to the spectra of sugarcane recombinant GNA and GNA₁₀₉. This suggests that the snowdrop-bulb native GNA is composed of more than one isoform. This is consistent with reports about the presence of multiple isoforms or isolectins in the snowdrop-bulb native GNA (Van Damme et al., 1991), which reflect sequence variability in the C-terminal amino-acid region. Although these isolectins have a similar overall specificity and share a high sequence similarity, it is unclear whether they possess identical biological activities (Peumans and Van Damme, 1995). This is an important consideration when expressing these isolectins in transgenic plants, and individual lectins should be tested to identify individual activity. In our study, only one GNA isolectin was synthesized and characterized in sugarcane. Further assessment of the qualities of the other native snowdrop-bulb GNA isoforms would be useful to select the most potent one and compare it with sugarcane recombinant GNA.

CONCLUSION

Sugarcane and energy cane represent promising candidates as biofactories for the production of recombinant therapeutic snowdrop GNA. In this work, a gene-promoter stacking approach resulted in levels of GNA that were 1.8% and 2.3% of TSP in transgenic culms and leaves, respectively. Our approach consisted of stacking multiple promoters to co-express

recombinant GNA from separate expression vectors, using combinatorial transformation. High TSP levels of 2.7% were also achieved by inducing promoter activity in GNA transgenic lines with stress-regulated hormones such as SA. Sugarcane recombinant GNA purified by mannose-agarose affinity chromatography and native snowdrop-bulb GNA exhibited a similar binding specificity to the anti-GNA antibody and mannan substrate. Our results suggest that high levels of GNA (up to 2.7% TSP) can be successfully isolated from transgenic sugarcane and energy cane tissues.

DATA AVAILABILITY STATEMENT

All datasets presented in this study are included in the article/Supplementary Material.

AUTHOR CONTRIBUTIONS

CP, MD, Z-NY, JM, JD, and KM designed the experiments. MD, CP, and Z-NY generated the GNA constructs. CP, MD, NS-G, and JM conducted plant transformation. CP, MD, and JM screened transgenic plants. CP and MD performed hormone experiments. CP, MD, JM, and NS-G conducted small-scale protein extraction and western blot analyses. BB and EW performed the large-scale purification and characterization of the sugarcane recombinant protein. CP and MD prepared the manuscript. JD and KM supervised the study and reviewed the manuscript. All authors contributed to the article and approved the submitted version.

FUNDING

The authors declare that this study received funding from BioCane Inc. The funder was not involved in the study design, collection, analysis, interpretation of data, the writing of this article or the decision to submit it for publication. This research was also supported by Texas A&M AgriLife Research grants (124190–96210) to KM.

ACKNOWLEDGMENTS

We would like to dedicate this manuscript to the late Professor T. Erik Mirkov (1959–2018), a pioneer of sugarcane biotechnology. We gratefully acknowledge Sonia Irigoyen (Texas A&M AgriLife Research) for critical review of the manuscript; Carmen M. Avila, Victoria Garza, Denise Rossi, Chris Lukaszewski, Abigail Cruz, Aditya Kamesh, Denis Odokonyero, and Rolando Mireles (Texas A&M AgriLife Research) for technical assistance.

SUPPLEMENTARY MATERIAL

The Supplementary Material for this article can be found online at: <https://www.frontiersin.org/articles/10.3389/fbioe.2020.00977/full#supplementary-material>

FIGURE S1 | (A,B) Full-length uncropped DNA gel blot autoradiograms used to prepare Southern blots in **Figures 1B, 2B**, respectively. **(A)** Single-promoter *pUbi:GNA* lines 1G-1: lane 8, 1D: lane 5, and 30A: lane 18. **(B)** Triple-promoter *pUBD5-1:GNA* lines 1-2T: lane 3, 5-1G: lane 7, and 5-3C: lane 4. Non-transformed control plant: lane 1 in both blots. **(A,B)** Full-length uncropped DNA gel blot autoradiograms used to prepare Southern blots in **Figures 1B, 2B**, respectively.

FIGURE S2 | Qualitative phenotype of the triple-promoter:*GNA*-expressing sugarcane lines. One-year-old mature plants are shown. *GNA*, *GNA* transgenic plants; WT, wild type plants.

FIGURE S3 | (A–C) Uncropped agarose gel used to prepare **Figure 2C**. **(A)** Integration of *pUbi:GNA* expression cassettes: lane 1, 1 kb DNA plus ladder; lane 2, *pUBD5-1:GNA* line 1-2T; lane 3, *pUBD5-1:GNA* line 5-1G; lane 4, *pUBD5-1:GNA* line 5-3C; lanes 5 and 6: Non-transformed (NT) CP72-1210 and CP89-2143, respectively; lane 7, NC-no DNA template and lane 8, *pUbi:GNA* plasmid. **(B)** Integration of *SCBV21:GNA* expression cassettes: lane 1, 1 kb DNA plus ladder; lane 2, *pUBD5-1:GNA* line 1-2T; lane 3 *pUBD5-1:GNA* line 5-1G; lane 4, *pUBD5-1:GNA* line 5-3C; lanes 5 and 6: NT CP72-1210 and CP89-2143, respectively; lane 7, NC-no DNA template and lane 8, *pSCBV21:GNA* plasmid. **(C)** Integration of *pSHDIR5-1:GNA* expression cassettes: lane 1, 1 kb DNA plus ladder; lane 2, *pUBD5-1:GNA* line 1-2T; lane 3 *pUBD5-1:GNA* line 5-1G; lane 4, *pUBD5-1:GNA* line 5-3C (full and truncated amplicons); lanes 5 and 6: NT CP72-1210 and CP89-2143, respectively; lane 7, NC-no DNA template; and lane 8, *pSHDIR5-1:GNA* plasmid.

FIGURE S4 | (A,B) Full-length uncropped immunoblot membranes used to prepare **Figures 1C,D**. **(A)** Uncropped immunoblot used to prepare **Figure 1C** (leaves) single-promoter *pUbi:GNA* lines 1G-1: lane 3 and 30A: lane 5 and *GNA* standard 125 ng: lane 13. **(B)** Uncropped immunoblot used to prepare **Figure 1D** (culms) single-promoter *pUbi:GNA* lines 1G-1: lane 3, 1D: lane 4 and 30A: lane 5 and non-transformed (NT): lane 11.

FIGURE S5 | (A–C) Full-length uncropped immunoblot membranes used to prepare **Figure 2D** (Immunoblot for leaf samples). **(A)** *GNA* standard 1000 ng and 500 ng: lanes 2 and 3, respectively, and triple-promoter *pUBD5-1:GNA* line 1-2T: lane 10. **(B)** *GNA* standard 1000 ng and 500 ng: lanes 2 and 3, respectively, and triple-promoter *pUBD5-1:GNA* line 5-1G: lane 10. **(C)** *GNA* standard 250 ng and 125 ng: lanes 4 and 5, respectively, and *pUBD5-1:GNA* line 5-3C: lane 11.

FIGURE S6 | (A–C) Full-length uncropped immunoblot membranes used to prepare **Figure 2E** (Immunoblot for culm samples). **(A)** *GNA* standard 250 ng and 125 ng: lanes 4 and 5, respectively, and triple-promoter *pUBD5-1:GNA* line 1-2T:

lane 7. **(B)** *GNA* standard 500 ng and 250 ng: lanes 2 and 3; respectively, triple-promoter *pUBD5-1:GNA* line 5-1G: lane 10. **(C)** *GNA* standard 250 ng and 125 ng: lanes 2 and 3; respectively, and triple-promoter *pUBD5-1:GNA* line 5-3C: lane 10.

FIGURE S7 | Full-length uncropped immunoblot membrane used to prepare **Figure 3**. Lanes 2 and 3 show single-promoter *pUbi:GNA* line 1G-1 before and after salicylic acid treatment, respectively; lanes 10 and 12 show triple-promoter *pUBD5-1:GNA* line 1-2T before and after salicylic acid treatment, respectively; lane 13 shows 125 ng of *GNA* standard.

FIGURE S8 | Flowchart of the bench-scale extraction of recombinant *GNA* from transgenic sugarcane and energy cane culms.

FIGURE S9 | (A,B) Full-length uncropped immunoblot membrane used to prepare **Figure 4**. **(A)** The following: *GNA* standard 125 ng and 62.5 ng: lanes 5 and 6, respectively; triple-promoter *pUBD5-1:GNA* lines 1-2T and 5-1G total soluble protein (TSP) extraction with citric acid pH 4.8: lane 8 and 9, respectively; TSP extraction of the same lines with sodium acetate pH 5.2: lanes 12 and 13, respectively. **(B)** *GNA* standard 250 ng and 125 ng: lanes 4 and 5, respectively, and triple promoter *pUBD5-1:GNA* lines 1-2T and 5-1G TSP extractions with sodium acetate (pH5.2)/EDTA/Tween-20: lanes 7 and 8.

FIGURE S10 | Full-length uncropped immunoblot membrane used to prepare **Figure 5A2**. Lanes 1 to 7 represent elution fractions 1.A.7, 1.A.8, 1.A.9, 1.A.10., 1.A.11, 1.A.12, and 1.B.1, respectively.

FIGURE S11 | Analysis of recombinant *GNA*₁₀₉ under non-reduced conditions using Matrix-Assisted Laser Desorption Ionization Mass Spectrometry (MALDI-TOF MS). The MS spectra of *GNA*₁₀₉ display the molecular weights of *m/z* 12,052.08 [*M* + *H*]⁺, *m/z* 24,103.60 [*2M* + *H*]⁺ and *m/z* 36,159.76 [*3M* + *H*]⁺, representing the monomer, dimer and trimer of *GNA*₁₀₉, respectively.

FIGURE S12 | Multiple alignment of amino-acid sequences of the translated *GNA* peptide transformed into sugarcane (*Galanthus nivalis* lectin; LECGNA2, Protein Bank accession number AAA33346) and the mature snowdrop-bulb native *GNA* (Vector Labs) (*Galanthus nivalis* agglutinin; 1NIV, Protein Data Bank accession number 1NIV_A). The consensus sequence motif QXDXNXVXY (QEDCNLVLY), involved in recognition of the α-D-mannose substrate, is boxed in red. Multiple amino-acid sequence alignment was performed using ClustalW 2.0 program (www.ebi.ac.uk/clustalw).

TABLE S1 | Primers used for determination of promoter:*GNA* cassette integration in staked triple promoter:*GNA* sugarcane lines.

REFERENCES

- Akkouh, O., Ng, T. B., Singh, S. S., Yin, C., Dan, X., Chan, Y. S., et al. (2015). Lectins with anti-HIV activity: a review. *Molecules* 20, 648–668. doi: 10.3390/molecules20010648
- Alqazlan, N. (2014). *Transgenic Plants as Novel Bioreactors to Produce Human Protein*. Ontario: The University of Western Ontario.
- Altpeter, F., and Oraby, H. (2010). “Sugarcane,” in *Genetic Modification of Plants: Agriculture, Horticulture and Forestry*, eds F. Kempken and C. Jung (Berlin: Springer), 453–472.
- Ando, S., Sugiura, M., Yamada, T., Katsuta, M., Ishikawa, S., Terajima, Y., et al. (2011). Overwintering ability and dry matter production of sugarcane hybrids and relatives in the kanto region of Japan. *Jpn. Agric. Res. Q. JARQ* 45, 259–267. doi: 10.6090/jarq.45.259
- Ashfaq, U., Masoud, M., Khaliq, S., Nawaz, Z., and Riazuddin, S. (2011). Inhibition of Hepatitis C Virus 3a genotype entry through Glanthus Nivalis Agglutinin. *Virol. J.* 8:248. doi: 10.1186/1743-422X-8-248
- Assaad, F. F., Tucker, K. L., and Signer, E. R. (1993). Epigenetic repeat-induced gene silencing (RIGS) in *Arabidopsis*. *Plant Mol. Biol.* 22, 1067–1085. doi: 10.1007/BF00028978
- Balzarini, J., Hatse, S., Vermeire, K., Princen, K., Aquaro, S., Perno, C.-F., et al. (2004). Mannose-specific plant lectins from the Amaryllidaceae family qualify as efficient microbicides for prevention of human immunodeficiency virus infection. *Antimicrob. Agents Chemother.* 48:3858. doi: 10.1128/AAC.48.10.3858-3870.2004
- Barre, A., Van Damme, E. J. M., Peumans, W. J., and Rouge, P. (1996). Structure-function relationship of monocot mannose-binding lectins. *Plant Physiol.* 112:1531. doi: 10.1104/pp.112.4.1531
- Beyene, G., Buenrostro-Nava, M. T., Damaj, M. B., Gao, S.-J., Molina, J., and Mirkov, T. E. (2011). Unprecedented enhancement of transient gene expression from minimal cassettes using a double terminator. *Plant Cell Rep.* 30, 13–25. doi: 10.1007/s00299-010-0936-3
- Bock, R. (2013). Strategies for metabolic pathway engineering with multiple transgenes. *Plant Mol. Biol.* 83, 21–31. doi: 10.1007/s11103-013-0045-0
- Chen, Q., and Davis, K. R. (2016). The potential of plants as a system for the development and production of human biologics. *F1000Research* 5:F1000FacultyRev-1912. doi: 10.12688/f1000research.8010.1
- Chiong, K., Damaj, M., Padilla, C., Avila, C., Panta, S., Mandadi, K., et al. (2017). Reproducible genomic DNA preparation from diverse crop species for molecular genetic applications. *Plant Methods* 13:106. doi: 10.1186/s13007-017-0255-6
- Christensen, A. H., and Quail, P. H. (1996). Ubiquitin promoter-based vectors for high-level expression of selectable and/or screenable marker genes in monocotyledonous plants. *Transgenic Res.* 5, 213–218. doi: 10.1007/bf01969712

- Christensen, A. H., Sharrock, R. A., and Quail, P. H. (1992). Maize polyubiquitin genes: structure, thermal perturbation of expression and transcript splicing, and promoter activity following transfer to protoplasts by electroporation. *Plant Mol. Biol.* 18, 675–689. doi: 10.1007/BF00020010
- Couzens, L., Gao, J., Westgeest, K., Sandbulte, M., Lugovtsev, V., Fouchier, R., et al. (2014). An optimized enzyme-linked lectin assay to measure influenza A virus neuraminidase inhibition antibody titers in human sera. *J. Virol. Methods* 210, 7–14. doi: 10.1016/j.jviromet.2014.09.003
- Cummings, R. D., Darvill, A. G., Etzler, M. E., and Hahn, M. G. (2017). “Glycan-recognizing probes as tools,” in *Essentials of Glycobiology*, Third Edn, eds V. Ajit, D. C. Richard, and E. Jeffrey (Cold Spring Harbor, NY: Cold Spring Harbor Laboratory Press), 611–625.
- Damaj, M., Kumpatla, S., Emani, C., Beremand, P., Reddy, A., Rathore, K., et al. (2010). Sugarcane DIRIGENT and O-methyltransferase promoters confer stem-regulated gene expression in diverse monocots. *Planta* 231, 1439–1458. doi: 10.1007/s00425-010-1138-5
- Damaj, M. B., and Mirkov, T. E. (2017). *Stem-Specific Promoter From Sugarcane Dirigent Gene*. U.S. patent application. College Station, TX: Texas A&M University System.
- Damaj, M. B., and Mirkov, T. E. (2019). *Compositions, Organisms, Systems, and Methods For Expressing A Gene Product in Plants*. U.S. patent application. College Station, TX: Texas A&M University System.
- Damodaran, D., Jeyakani, J., Chauhan, A., Kumar, N., Chandra, N., and Surolia, A. (2008). CancerLectinDB: a database of lectins relevant to cancer. *Glycoconjugate J.* 25, 191–198. doi: 10.1007/s10719-007-9085-5
- Gao, S.-J., Damaj, M., Park, J.-W., Beyene, G., Buenrostro-Nava, M., Molina, J., et al. (2013). Enhanced transgene expression in sugarcane by co-expression of virus-encoded RNA silencing suppressors. *PLoS One* 8:e66046. doi: 10.1371/journal.pone.0066046
- Gao, S.-J., Damaj, M., Park, J.-W., Wu, X., Sun, S.-R., Chen, R.-K., et al. (2017). A novel Sugarcane bacilliform virus promoter confers gene expression preferentially in the vascular bundle and storage parenchyma of the sugarcane culm. *Biotechnol. Biofuels* 10:172. doi: 10.1186/s13068-017-0850-9
- Gianotti, A., Rios, W. M., Soares-Costa, A., Nogaroto, V., Carmona, A. K., Oliva, M. L. V., et al. (2006). Recombinant expression, purification, and functional analysis of two novel cystatins from sugarcane (*Saccharum officinarum*). *Protein Express. Purif.* 47, 483–489. doi: 10.1016/j.pep.2005.10.026
- Gornik, O., and Lauc, G. (2007). Enzyme linked lectin assay (ELLA) for direct analysis of transferrin sialylation in serum samples. *Clin. Biochem.* 40, 718–723. doi: 10.1016/j.clinbiochem.2007.01.010
- Harrison, M., Geijskes, R., Lloyd, R., Miles, S., Palupe, A., Sainz, M., et al. (2014). Recombinant cellulase accumulation in the leaves of mature, vegetatively propagated transgenic sugarcane. *Mol. Biotechnol.* 56, 795–802. doi: 10.1007/s12033-014-9758-9
- Harrison, M. D., Geijskes, J., Coleman, H. D., Shand, K., Kinkema, M., Palupe, A., et al. (2011). Accumulation of recombinant cellobiohydrolase and endoglucanase in the leaves of mature transgenic sugar cane. *Plant Biotechnol. J.* 9, 884–896. doi: 10.1111/j.1467-7652.2011.00597.x
- Henrique-Silva, F., and Soares-Costa, A. (2012). Production of a his-tagged canecystatin in transgenic sugarcane. *Methods Mol. Biol.* 847, 437–450. doi: 10.1007/978-1-61779-558-9_34
- Kanno, T., Naito, S., and Shimamoto, K. (2000). Post-transcriptional gene silencing in cultured rice cells. *Plant Cell Physiol.* 41, 321–326. doi: 10.1093/pcp/41.3.321
- Khaitová, L. C., Fojtová, M., Křížová, K., Lunerová, J., Fulneček, J., Depicker, A., et al. (2011). Paramutation of tobacco transgenes by small RNA-mediated transcriptional gene silencing. *Epigenetics* 6, 650–660. doi: 10.4161/epi.6.5.15764
- Kumpatla, S. P., and Hall, T. C. (1998). Recurrent onset of epigenetic silencing in rice harboring a multi-copy transgene. *Plant J.* 14, 129–135. doi: 10.1046/j.1365-3113.1998.00097.x
- Li, C.-Y., Meng, L., Liu, B., and Bao, J.-K. (2009). *Galanthus nivalis* agglutinin (GNA)-related lectins: traditional proteins, burgeoning drugs? *Curr. Chem. Biol.* 3, 324–333. doi: 10.2174/187231309789054913
- Liu, B., Cheng, Y., Bian, H.-J., and Bao, J.-K. (2009). Molecular mechanisms of *Polygonatum cyrtoneura* lectin-induced apoptosis and autophagy in cancer cells. *Autophagy* 5, 253–255. doi: 10.4161/auto.5.2.7561
- Mangwende, T., Wang, M.-L., Borth, W., Hu, J., Moore, P., Mirkov, T., et al. (2009). The P0 gene of Sugarcane yellow leaf virus encodes an RNA silencing suppressor with unique activities. *Virology* 384, 38–50. doi: 10.1016/j.virol.2008.10.034
- Martínez-Alarcón, D., Blanco-Labra, A., and García-Gasca, T. (2018). Expression of lectins in heterologous systems. *Int. J. Mol. Sci.* 19:616. doi: 10.3390/ijms19020616
- Matsuoka, S., Kennedy, A. J., Santos, E. G. D., Tomazela, A. L., and Rubio, L. C. S. (2014). Energy cane: its concept, development, characteristics, and prospects. *Adv. Bot.* 20, 1–13. doi: 10.1155/2014/597275
- Matzke, A. J., Neuhuber, F., Park, Y. D., Ambros, P. F., and Matzke, M. A. (1994). Homology-dependent gene silencing in transgenic plants: epistatic silencing loci contain multiple copies of methylated transgenes. *Mol. Gen. Genet. MGG* 244, 219–229. doi: 10.1007/BF00285449
- Matzke, M. A., Primig, M., Trnovsky, J., and Matzke, A. J. M. (1989). Reversible methylation and inactivation of marker genes in sequentially transformed tobacco plants. *EMBO J.* 8, 643–649. doi: 10.1002/j.1460-2075.1989.tb03421.x
- Murashige, T., and Skoog, F. (1962). A revised medium for rapid growth and bioassays with tobacco tissue cultures. *Physiol. Plant.* 15, 473–497. doi: 10.1111/j.1399-3054.1962.tb08052.x
- Nagadhara, D., Ramesh, S., Pasalu, I. C., Rao, Y. K., Krishnaiah, N. V., Sarma, N. P., et al. (2003). Transgenic indica rice resistant to sap-sucking insects. *Plant Biotechnol. J.* 1, 231–240. doi: 10.1046/j.1467-7652.2003.00022.x
- Oliveira, C., Teixeira, J. A., and Domingues, L. (2013). Recombinant lectins: an array of tailor-made glycan-interaction biosynthetic tools. *Critic. Rev. Biotechnol.* 33, 66–80. doi: 10.3109/07388551.2012.670614
- Palaniswamy, H., Syamaladevi, D., Mohan, C., Philip, A., Petchiyappan, A., and Narayanan, S. (2016). Vacuolar targeting of r-proteins in sugarcane leads to higher levels of purifiable commercially equivalent recombinant proteins in cane juice. *Plant Biotechnol. J.* 14, 791–807. doi: 10.1111/pbi.12430
- Pawlowski, W. P., and Somers, D. A. (1998). Transgenic DNA integrated into the oat genome is frequently interspersed by host DNA. *Proc. Natl. Acad. Sci. U.S.A.* 95, 12106–12110. doi: 10.1073/pnas.95.21.12106
- Peumans, W. J., and Van Damme, E. J. M. (1995). Lectins as plant defense proteins. *Plant Physiol.* 109:347. doi: 10.1104/pp.109.2.347
- Raemaekers, R. J. M. (2000). *Expression of Functional Plant Lectins in Heterologous Systems*. Durham: Durham University.
- Rajeevkumar, S., Anunanthini, P., and Ramalingam, S. (2015). Epigenetic silencing in transgenic plants. *Front. Plant Sci.* 6:693. doi: 10.3389/fpls.2015.00693
- Ramasamy, M., Mora, V., Damaj, M. B., Padilla, C. S., Ramos, N., Rossi, D., et al. (2018). A biolistic-based genetic transformation system applicable to a broad-range of sugarcane and energycane varieties. *GM Crops Food* 9, 211–227. doi: 10.1080/21645698.2018.1553836
- Rao, K. V., Rathore, K. S., Hodges, T. K., Fu, X., Stoger, E., Sudhakar, D., et al. (1998). Expression of snowdrop lectin (GNA) in transgenic rice plants confers resistance to rice brown planthopper. *Plant J.* 15, 469–477. doi: 10.1046/j.1365-3113.1998.00226.x
- Ribeiro, C., Soares-Costa, A., Falco, M., Chabregas, S., Ulian, E., Cotrin, S., et al. (2008). Production of a his-tagged canecystatin in transgenic sugarcane and subsequent purification. *Biotechnol. Prog.* 24, 1060–1066. doi: 10.1002/btpr.45
- Sambrook, J., Fritsch, E. F., and Maniatis, T. (1989). *Molecular Cloning: A Laboratory Manual*. Cold Spring Harbor, NY: Cold Spring Harbor Laboratory Press.
- Sambrook, J., and Russell, D. W. (2001). *Molecular Cloning: A Laboratory Manual*. Cold Spring Harbor, NY: Cold Spring Harbor Laboratory Press.
- Setamou, M., Bernal, J., Legaspi, J., Mirkov, T., and Legaspi, B. (2002). Evaluation of lectin-expressing transgenic sugarcane against stalkborers (Lepidoptera: Pyralidae): effects on life history parameters. *J. Econ. Entomol.* 95, 469–477. doi: 10.1603/0022-0493-95.2.469
- Snyman, S., Meyer, G., Richards, J., Haricharan, N., Ramgareeb, S., and Hockett, B. (2006). Refining the application of direct embryogenesis in sugarcane: effect of the developmental phase of leaf disc explants and the timing of DNA transfer on transformation efficiency. *Plant Cell Rep.* 25, 1016–1023. doi: 10.1007/s00299-006-0148-z
- Sommer, R., Wagner, S., Rox, K., Varrot, A., Hauck, D., Wamhoff, E.-C., et al. (2018). Glycomimetic, orally bioavailable lecB inhibitors block biofilm formation of *Pseudomonas aeruginosa*. *J. Am. Chem. Soc.* 140, 2537–2545. doi: 10.1021/jacs.7b11133

- Tai, T. H., and Tanksley, S. D. (1990). A rapid and inexpensive method for isolation of total DNA from dehydrated plant tissue. *Plant Mol. Biol. Rep.* 8, 297–303. doi: 10.1007/BF02668766
- Tang, K., Zhao, E., Sun, X., Wan, B., Qi, H., and Lu, X. (2001). Production of transgenic rice homozygous lines with enhanced resistance to the rice brown planthopper. *Acta Biotechnol.* 21, 117–128. doi: 10.1002/1521-3846(200105)21:2<117::aid-abio117>3.0.co;2-y
- Tinjuangjun, P., Loc, N. T., Gatehouse, A. M. R., Gatehouse, J. A., and Christou, P. (2000). Enhanced insect resistance in Thai rice varieties generated by particle bombardment. *Mol. Breed.* 6, 391–399. doi: 10.1023/A:1009633703157
- Tu, J., Zhang, G., Datta, K., Xu, C., He, Y., Zhang, Q., et al. (2000). Field performance of transgenic elite commercial hybrid rice expressing bacillus thuringiensis delta-endotoxin. *Nat. Biotechnol.* 18, 1101–1104. doi: 10.1038/80310
- Van Damme, E. J. M., Allen, A. K., and Peumans, W. J. (1987). Isolation and characterization of a lectin with exclusive specificity towards mannose from snowdrop (*Galanthus nivalis*) bulbs. *FEBS Lett.* 215, 140–144. doi: 10.1016/0014-5793(87)80129-1
- Van Damme, E. J. M., Kaku, H., Perini, F., Goldstein, I. J., Peeters, B., Yagi, F., et al. (1991). Biosynthesis, primary structure and molecular cloning of snowdrop (*Galanthus nivalis* L.) lectin. *Eur. J. Biochem.* 202, 23–30. doi: 10.1111/j.1432-1033.1991.tb16339.x
- Wang, M.-L., Goldstein, C., Su, W., Moore, P. H., and Albert, H. H. (2005). Production of biologically active GM-CSF in sugarcane: a secure biofactory. *Transgenic Res.* 14, 167–178. doi: 10.1007/s11248-004-5415-6
- Wang, Z., Zhang, K., Sun, X., Tang, K., and Zhang, J. (2005). Enhancement of resistance to aphids by introducing the snowdrop lectin gene gna into maize plants. *J. Biosci.* 30, 627–638. doi: 10.1007/BF02703563
- Williams, L., Deana, A., Romero, A., Molina, A., and Lunello, P. (2014). High-level production of active human TFPI-2 Kunitz domain in plant. *Protein Exp. Purif.* 96, 14–19. doi: 10.1016/j.pep.2014.01.011
- Wu, L., and Bao, J. K. (2013). Anti-tumor and anti-viral activities of *Galanthus nivalis* agglutinin (GNA)-related lectins. *Glycoconj. J.* 30, 269–279. doi: 10.1007/s10719-012-9440-z
- Yang, M., Bower, R., Burow, M., Paterson, A., and Mirkov, T. (2003). A rapid and direct approach to identify promoters that confer high levels of gene expression in monocots. *Crop Sci.* 43, 805–1813. doi: 10.2135/cropsci2003.1805
- Yee, M., Konopka, K., Balzarini, J., and Düzgüneş, N. (2011). Inhibition of HIV-1 Env-mediated cell-cell fusion by lectins, peptide T-20, and neutralizing antibodies. *Open Virol. J.* 5, 44–51. doi: 10.2174/1874357901105010044

Conflict of Interest: BB and EW were employed by the companies iBio (Bryan, TX) and MDx BioAnalytical Laboratory (College Station, TX) respectively.

The remaining authors declare that the research was conducted in the absence of any commercial or financial relationships that could be construed as a potential conflict of interest.

Copyright © 2020 Padilla, Damaj, Yang, Molina, Berquist, White, Solis-Gracia, Da Silva and Mandadi. This is an open-access article distributed under the terms of the Creative Commons Attribution License (CC BY). The use, distribution or reproduction in other forums is permitted, provided the original author(s) and the copyright owner(s) are credited and that the original publication in this journal is cited, in accordance with accepted academic practice. No use, distribution or reproduction is permitted which does not comply with these terms.



Applications of Microbial β -Mannanases

Aneesa Dawood^{1,2*} and Kesen Ma³

¹ Department of Microbiology, Quaid-I-Azam University, Islamabad, Pakistan, ² Department of Radiology and Medical Imaging, University of Virginia, Charlottesville, VA, United States, ³ Department of Biology, University of Waterloo, Waterloo, ON, Canada

OPEN ACCESS

Edited by:

Giovanni Sanna,
University of Naples Federico II, Italy

Reviewed by:

Evangelia Chronopoulou,
Agricultural University of Athens,
Greece
Vicente Gotor-Fernández,
Universidad de Oviedo, Mieres, Spain

*Correspondence:

Aneesa Dawood
aneesadawood.qau@gmail.com

Specialty section:

This article was submitted to
Industrial Biotechnology,
a section of the journal
Frontiers in Bioengineering and
Biotechnology

Received: 25 August 2020

Accepted: 28 October 2020

Published: 15 December 2020

Citation:

Dawood A and Ma K (2020)
Applications of Microbial
 β -Mannanases.
Front. Bioeng. Biotechnol. 8:598630.
doi: 10.3389/fbioe.2020.598630

Keywords: hemicellulose, microbial β -mannanase, industrial applications, bioengineering, heterologous production

INTRODUCTION

Hemicellulose is the second most abundant polymer found in nature. It is usually present together with lignin and cellulose in the plant cell walls (Harris and Stone, 2009). It is estimated that hemicellulose is a third of the total components in plants, for example, hemicellulose makes up 25–30% of the total weight of dry wood. Hetero-1,4- β -D-mannans and hetero-1,4- β -D-xylans are two most significant types of hemicelluloses (Chauhan et al., 2012).

In grasses and hardwoods, xylan is the major hemicellulose component, while in softwoods, plant fruits and seeds the hemicellulose is mainly present in the form of mannan (Scheller and Ulvskov, 2010). Mannan mainly appears in four different forms: linear mannan, galactomannan, glucomannan, and galactoglucomannan. β -mannanase is a major mannan degrading enzyme (Figure 1). However, due to heterogenous nature of mannan, its biodegradation may require a close association and synergy among β -mannanase (EC 3.2.1.78), β -mannosidase (EC 3.2.1.25), acetyl mannan esterase (EC 3.1.1.6), β -glucosidase (EC 3.2.1.21), and α -galactosidase (EC 3.2.1.22) to break the main and the side chains of mannan (Chauhan et al., 2012; Malgas et al., 2015).

Mannan-degrading enzymes are classified into different glycosyl hydrolase families (like GH 1, GH 2, GH 3, GH 5, GH 26, GH 27, GH 113, etc.) catalyzing the production of oligosaccharides and monosaccharides that can be used for microbial metabolism. These enzymes can also enhance plant metabolism, such as ripening and maturation by metabolizing mannan present in cell wall (Morreira, 2008).

The primary structure of mannanases in different GH families is different but they are similar in their spatial arrangement, (β/α)8-barrel protein folds and are assembled into clan GH-A (Srivastava and Kapoor, 2017). Mannanases often exhibit modular structure consisting of carbohydrate binding

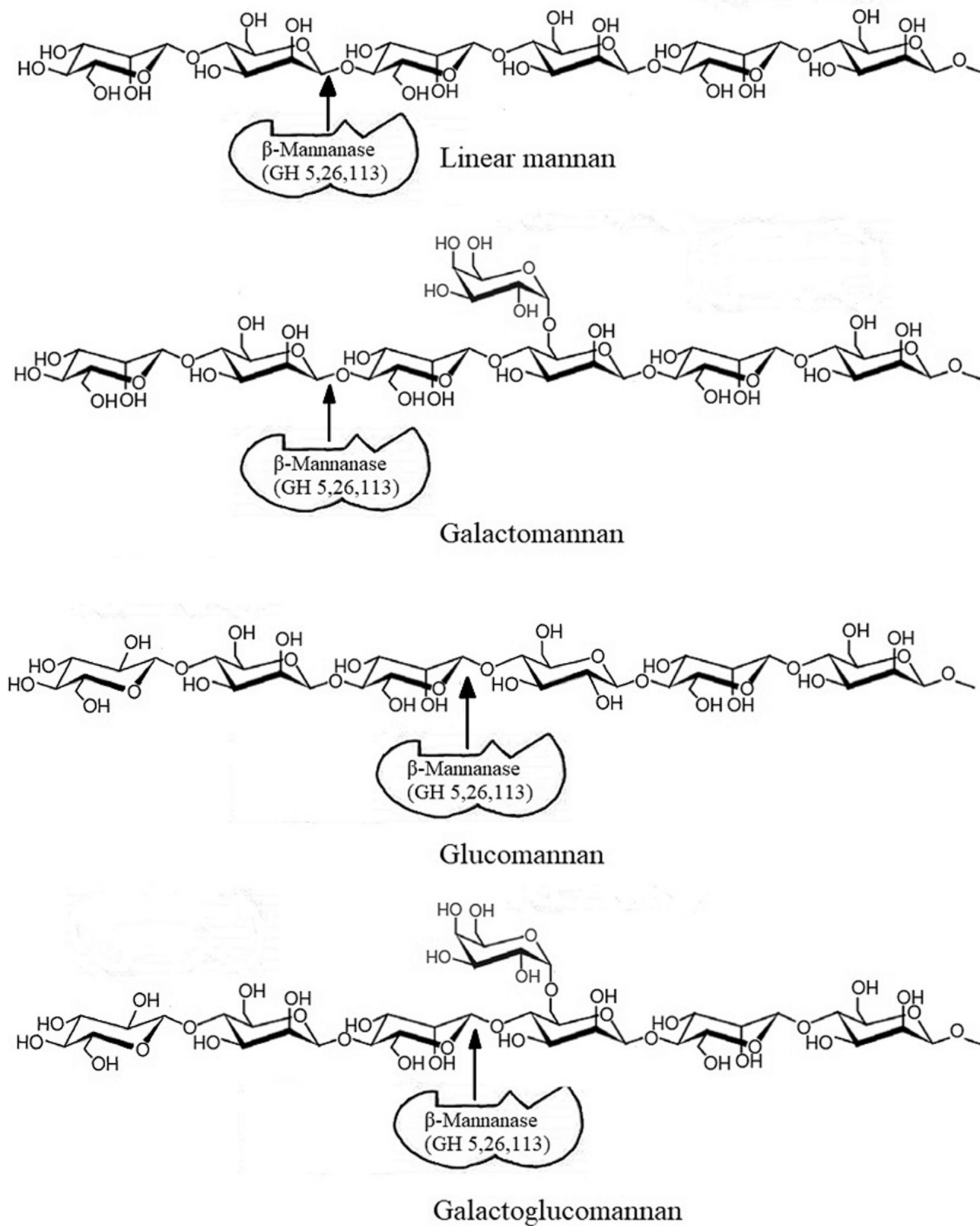


FIGURE 1 | Action of β -mannanase on different types of mannan. Modified from Yeoman et al. (2010).

module(s) (CBM), catalytic domain(s), and additional functional domain(s) (**Figure 2**; Sunna, 2010).

Site-directed mutagenesis and X-ray crystallographic studies in a broad variety of species have showed that β -mannanase needs a minimum of five substrate binding sites and a cleft shaped active site with nucleophile catalyst and a well conserved acid/base catalyst which are at a distance of 5.5 Å from each other for efficient hydrolysis of substrates (**Figure 3**; Hogg et al., 2003; Yan et al., 2008; Tailford et al., 2009; Songsiririthigul et al., 2011).

Recently β -mannanases have attracted significant attention from both industry as well as academia because of their potential applications in many important sectors of industry including oil drilling, detergents, textile, food, animal feed, and production of bioethanol. This paper presents an in-depth review of potential applications of β -mannanase in light of recently reported studies (2015–2020). Engineering of β -mannanases to efficiently meet industrial needs is also discussed along with a brief but comprehensive discussion of β -mannanase occurrence, purification, and yield improvement.

However, the present review does not discuss in detail the structure, reaction mechanism, assay methods, and biochemical characteristics of β -mannanases. For this the readers are directed to earlier reviews (Dhawan and Kaur, 2007; Chauhan et al., 2012; Srivastava and Kapoor, 2017).

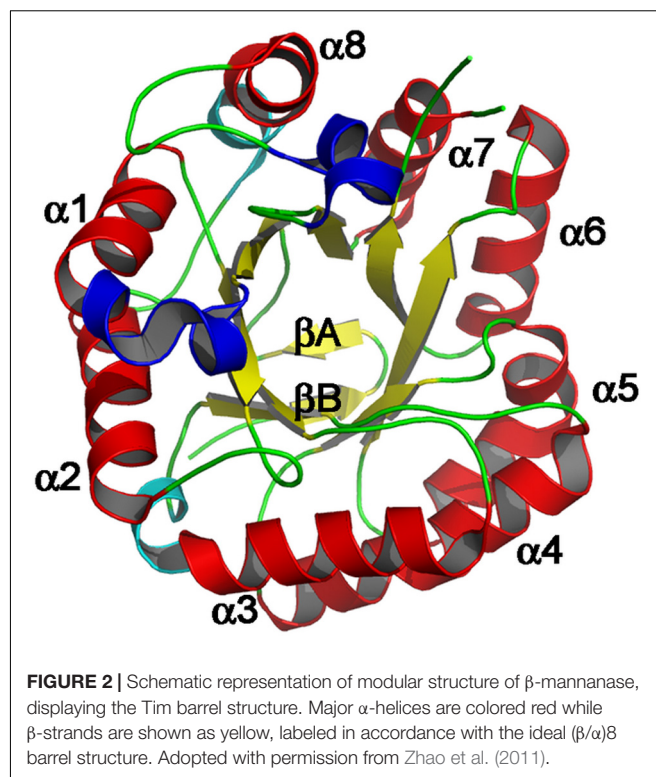
MICROBIAL β -MANNANASES

Mannanases have been isolated from plants, animals and microorganisms (Kim et al., 2013; Wang et al., 2015; Jana et al., 2018). Most of the commercial β -mannanases have been produced from microbes due to their higher stability, production within limited time and space, cost effectiveness and ease of genetic manipulation (**Table 1**). This increases their market value and makes them suitable candidates for applications in industry.

In the microbial world, numerous microbes possess the ability to degrade mannan efficiently (**Table 2**). Among bacteria, most of the mannan degraders are gram positive bacteria such as *Bacillus* species (David et al., 2018). But there also some gram-negative bacteria like *Klebsiella Oxytoca* that also efficiently degrade mannan (Tuntrakool and Keawsompong, 2018). Competent mannan degraders among fungi are the members of genus *Aspergillus* while β -mannanases have also been isolated from *Trichoderma* sp. and *Penicillium* sp. (Agrawal et al., 2011; Blibech et al., 2011; Liu et al., 2020). Among actinomycetes *Streptomyces* sp. and *Nocardioopsis* sp. have shown appreciable mannan degrading ability (Gohel and Singh, 2015; Pradeep et al., 2016).

PRODUCTION, YIELD IMPROVEMENT AND PURIFICATION OF β -MANNANASES

β -mannanases are mostly produced by using submerged fermentation. However, in a few studies β -mannanases have been produced in solid state fermentation. A number of nutritional and physico-chemical factors like temperature, incubation



time, pH, carbon source, and nitrogen content affect the production of β -mannanase. These factors are different for different microorganisms. For example, the incubation time for β -mannanase production in *Acinetobacter* sp. ST 1 is 24 h (Titapoka et al., 2008) while in *Bacillus nealsonii* PN-11 is 96 h (Chauhan et al., 2014). In contrast, the incubation time in fungi usually ranges from 6 days in case of *Penicillium occitanis* (Blibech et al., 2011) to 11 days by *Aspergillus* ATCC 20114 (Mohamad et al., 2011). In majority of the cases the optimum temperature for β -mannanase production lies in mesophilic range, which is closely related to the growth temperature required for that microorganism. In general, for growth and β -mannanase production, fungi usually prefer acidic pH while bacteria prefer neutral to alkaline conditions (Chantorn et al., 2013; Yopi et al., 2017). Several studies have shown enhanced production of β -mannanase through process optimization. Approaches such as one factor at a time have been employed to improve production (Olaniyi et al., 2013; Khattab et al., 2020). Statistical methods like central composite design, Box Behnken and placket Burman or their combination have also been used to enhance the production of β -mannanase (Abd Rashid et al., 2012; Yatmaz et al., 2016; Jana et al., 2018; Blibech et al., 2020).

In addition, in a number of cases, β -mannanase production have also been increased through heterologous expression systems to meet certain industrial needs and ensure economic feasibility of the process.

An engineered acidophilic and thermophilic β -mannanase (ManAK) derived from *Aspergillus kawachii* strain IFO4308 is overexpressed in *Pichia pastoris* (Liu et al., 2020). By

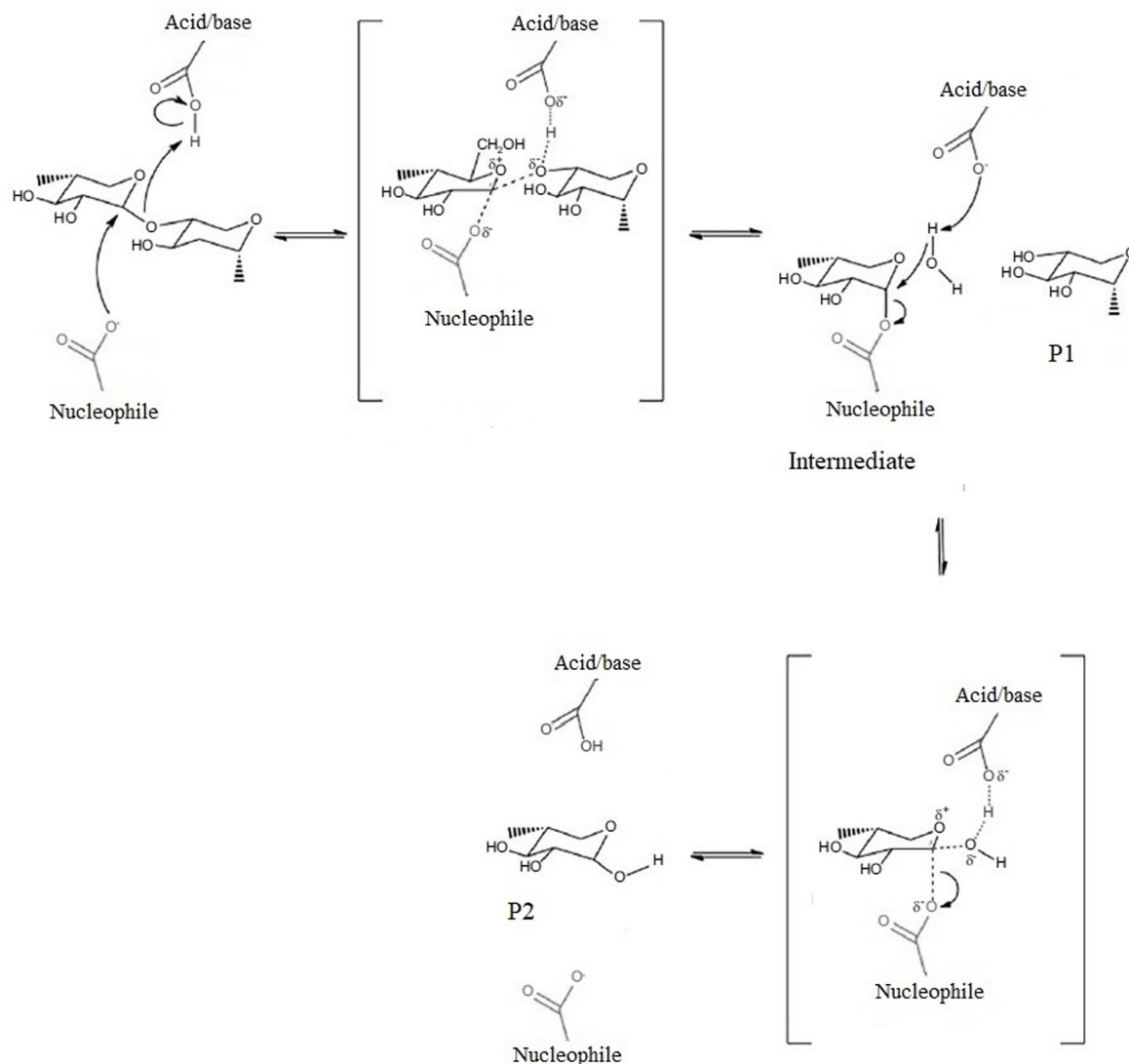


FIGURE 3 | Reaction mechanism of β -mannanase. Modified from Sharma et al. (2018). The brackets indicate transition state. P1 is product 1, P2 is product 2.

means of high cell density fermentation, a maximum yield of 11,600 U/mL and 15.5 g/L are obtained, which is greater than majority of β -mannanases. However, the highest titers of β -mannanase have been reported from *Rhizomucor miehei* (79,680 U mL^{-1}) and *Chaetomium* sp. CQ31 (50,030 U/ml) following cloning and expression of their β -mannanase enzyme gene in *Pichia pastoris* (Katrolia et al., 2012; Li et al., 2018).

Heterologous expression of β -mannanase in *Pichia Pastoris* has been used widely, however, *Saccharomyces cerevisiae* expression system has also been reported to be safe and effective. A β -mannanase gene derived from *Aspergillus sulphureus* is optimized and expressed in five different *S. cerevisiae* strains and the properties of the strains are evaluated (Liu et al., 2018). Haploid strain BY4741 integrated with β -mannanase gene

under constitutive promoter TEF1 shows the highest efficiency expression. After 36 h the enzyme activity reaches ~ 24 U/ml and production efficiency 16 U/mL/day.

Depending on properties of β -mannanases, different protocols related to purification of mannanase often involve the use of 2–4 chromatographic steps (Table 3).

INDUSTRIAL APPLICATIONS OF β -MANNANASES

There is a wide range of industrial applications of β -mannanases in various areas. The following will describe some examples including use in food, pulp, energy production, textile, detergent, animal feed, and pharmaceuticals.

TABLE 1 | Commercial production information of β -mannanases.

Company	Country	Mannanase source	Trademark
ChemGen	United States	<i>Paenibacillus lentus</i>	Hemicell®
CTC Bio Inc	Seoul, South Korea	<i>Bacillus lentus</i>	CTCzyme®
Sunson	China	<i>Bacillus lentus</i>	Nutrizyme®
Novo Nordisk	Denmark	<i>Aspergillus niger</i>	Gamanase®
Advanced Enzymes	India	N. A	DigeGrain M
Novozymes	Denmark	<i>Talaromyces leycettanus</i>	Mannaway
Aumgene Biosciences	India	N. A	Mannazyme XP®
PhylloZyme	United States	<i>Trichoderma reesei</i>	Cp-mannanase
Genencor International	United States	N.A	MannaStar™
Megazyme	Ireland	<i>Aspergillus niger</i>	E-BMANN
Genencor International	United States	Fungal β -mannanase	Purabrite
Diversa Corp.	United States	<i>Thermotoga</i> sp.	Pyrolase160
Diversa Corp.	United States	<i>Thermotoga</i> sp.	Pyrolase200

Use in Oil Drilling

Due to an ever-widening gap between global demand and supply of energy, well fracturing is frequently carried out for the recovery of oil and gas. Following fracturing of well formations, controlled breakage of fluid is required to facilitate enhanced recovery of the trapped gas or oil.

In drilling operations β -mannanase application can be useful. To maximize product flow, now a days, guar gum along with sand particles is used to flood the well followed by pressurizing of the bedrock until it breaks open (Thombare et al., 2016). In order to ease the flow of the product from the well, the polymer solution must be thinned out and β -mannanases that can bring about hydrolysis of guar gum at high temperature ($>80^{\circ}\text{C}$) can be useful for this purpose.

β -mannanases with high temperature optima are particularly suited for oil drilling operations because of the presence of geothermal gradients in deep oil wells. The use of such enzymes prevents the hydrolysis of guar gum at the earth's surface while only the environmental temperature at the depth of the well are suitable for the enzyme activity. Considerable research efforts have been directed toward the isolation and characterization of such β -mannanases. A novel β -mannanase (DtManB) from *Dictyoglomus thermophilum* has been reported to be a suitable candidate for oil drilling operations because it shows excellent activity and stability at high temperature (80°C) and low activity at low temperature (Hu et al., 2014). DtManB effectively reduces the viscosity of hydroxypropyl guar solution, even in the presence of different additives. In addition, DtManB could adequately break cross linked fracturing fluid. However, the increase in optimum temperature of DtManB to even higher degree ($>90^{\circ}\text{C}$) through enzyme engineering could make it an even more desirable candidate.

Similarly, another β -mannanase suitable for oil drilling operations has been discovered in a hydrothermal vent sample that can prevent rehealing of gel by effectively breaking linear and

TABLE 2 | Sources of β -mannanases*.

Sources	References
Bacteria	
<i>Bacillus</i> sp. SWU60	Seesom et al., 2017
<i>Bacillus subtilis</i> subsp. <i>inaquosorum</i> CSB31	Regmi et al., 2017
<i>Gloeophyllum trabeum</i> CBS900.73	Wang et al., 2016
<i>Lactobacillus casei</i> HDS-01	Zhao et al., 2020
<i>Klebsiella pneumonia</i> SS11	Singh et al., 2019
<i>Bacillus pumilus</i> GBSW19	Zang et al., 2015
<i>Bacillus nealsonii</i> PN-11	David et al., 2018
<i>Bacillus subtilis</i> YH12	Liu et al., 2015
<i>Bacillus</i> sp. MK-2	Zhang et al., 2019
<i>Bacillus</i> sp. R2AL2A	Kim et al., 2018
<i>Klebsiella oxytoca</i> KUB-CW2-3	Tuntrakool and Keawsompong, 2018
<i>Bacillus subtilis</i> P2-5	Pangsri and Pangsri, 2017
<i>Bacillus clausii</i> strain S10	Zhou et al., 2018
Fungi	
<i>Talaromyces trachyspermus</i> B168	Ichinose et al., 2017
<i>Lichtheimia ramosa</i>	Xie et al., 2019
<i>Aspergillus kawachii</i> IFO 4308	Liu et al., 2020
<i>Trichoderma longibrachiatum</i> RS1	Ismail et al., 2019
<i>Rhizopus microsporus</i>	Li et al., 2020
<i>Aspergillus nidulans</i>	von Freiesleben et al., 2016
<i>Aspergillus terreus</i> FBCC 1369	Soni et al., 2016
<i>Aspergillus niger</i> CBS 513.88	Tang et al., 2019
<i>Aspergillus oryzae</i> RIB40	Tang et al., 2016
Other	
<i>Streptomyces</i> Sp. CS147	Yoo et al., 2015
<i>Streptomyces</i> Sp. CS428	Pradeep et al., 2016
<i>Nocardioopsis xinjiangensis</i> strain OM-6	Gohel and Singh, 2015

*Only representative references published after 2015 are included. For more information, the readers are advised to refer to Dhawan and Kaur (2007), Chauhan et al. (2012), Srivastava and Kapoor (2017).

borate cross linked guar polymers into small soluble fragments (Zhang et al., 2013). The enzyme shows excellent activity between 60 and 80°C . During fracturing operations, the enzymatic reaction can be activated by a change in temperature and pH of the environment. A good dose response has also been displayed by this β -mannanase which may enable the user to adjust the dosage of the enzyme to achieve a desired viscosity/time profile. In addition, it has been reported that this superior β -mannanase effectively reduces viscosity even in the presence of different additives such as salts, buffers, cross linkers and stabilizers. Thus, making this β -mannanase very suitable for effective viscosity reduction in oil drilling operations.

The selection of the enzyme for breaking the guar gel should be made on the basis of well temperature so as to maximize the performance of the enzyme. Some oil wells have low temperature and for those low temperature active β -mannanase can be effective.

A halotolerant, low temperature active β -mannanase isolated from a novel strain of *Enterobacter* sp. N18 is purified and tested for its potential in hydrolyzing fracturing fluid based on guar gum (You et al., 2016). Within 10 min, the viscosity of the

TABLE 3 | Protocols used to purify β -mannanases from various microorganisms.

Organism	Purification protocol	No. of steps	Yield (%)	Purification fold	Specific activity (U/mg)	References
<i>Weissella viridescens</i> LB37	(NH ₄) ₂ SO ₄ , DEAE-Sephadex, Sephacryl S-200	3	20.5	188.07	63.94	Adiguzel et al., 2016
<i>Bacillus</i> sp. CFR1601	(NH ₄) ₂ SO ₄ (50–80%), DEAE-Cellulose, DEAE-Sepharose and Phenyl-Sepharose	4	21.3	50.7	10,461.5	Srivastava and Kapoor, 2016
<i>Bacillus nealsonii</i> PN11	(NH ₄) ₂ SO ₄ (60–80%), Sephadex G-150, and DEAE-Cellulose	3	8.92	38.96	2280.9	Chauhan et al., 2014
<i>Klebsiella pneumoniae</i> SS11	(NH ₄) ₂ SO ₄ (50–80%) Sephacryl S-200	2	9.6%	5.50	7573.57 IU/mg	Singh et al., 2019
<i>Bacillus</i> sp.CSB39	Sepharose CL-6B, DEAE Sepharose Fast Flow	2	25.47	19.32	1063.91	Regmi et al., 2016
<i>Enterobacter ludwigii</i>	(NH ₄) ₂ SO ₄ (30–60%), Sephadex G-25, DEAE cellulose, Sephadex G-100	4	15.16	11.71	4510.37	Yang et al., 2017
<i>Lactobacillus plantarum</i> (M24)	(NH ₄) ₂ SO ₄ (60–80%), DEAE-Sephadex, Sephacryl S-200	3	14.7	2619.05	82.5	Adiguzel et al., 2015
<i>Pholiota adiposa</i> SKU0714	MWCO 10 kDa, Gel filtration chromatography	2	9.99	57.2	1,870	Ramachandran et al., 2014

fracturing agent was reduced by more than 95%. The enzyme has a temperature optimum of 50°C and at 20°C it retains 50% of its activity, showing that β -mannanase from strain N18 could be very effective in oil wells where the temperature is low and chemical gel breaking agents are inactive.

As the temperature of most oil wells can be higher than 80°C, many fungal mannan-degrading enzymes do not find use in oil drilling operations. However, TtMan5A, a thermostable β -mannanase derived from fungus *Talaromyces trachyspermus* has an optimal temperature of 85°C and good catalytic activity in a wide range of pH (Ichinose et al., 2017). TtMan5A could be an excellent candidate for use in drilling operations.

A few β -mannanases with high thermostability have appeared on the market showing potential for enhanced viscosity reduction, leading to increased production as well as revenue per well. Mannanases marketed by Diversa (San Diego, CA, United States) under the trade name Pyrolase are the typical examples. Isolated from the nature and screened for their high thermostability, Pyrolase160 and Pyrolase 200 have shown excellent performance in drilling operations.

Fruit Juice Clarification

In recent years, the preference for natural fruit juice consumption has increased in health-conscious consumers. Raw fruit juice, however, is viscous and turbid and typically settles during storage (Nagar et al., 2012). To market it, it must be clarified first. The viscosity and turbidity of natural fruit juice is mainly due to pectin, starch, cellulosic and hemicellulosic compounds (Dey and Banerjee, 2014; Sharma et al., 2014). For processing of these polysaccharides, microbial enzymes are used which hydrolyze these compounds and this results in a juice that is more suitable for the consumers taste, in addition to having good storage stability. The amount and composition of these polysaccharides varies in different fruits so different enzymes are needed for their processing. Compared to the use of chemicals the enzymatic process is advantageous because it has higher specificity, requires

mild reaction conditions and produces less waste (Sharma et al., 2014). The addition of β -mannanase has shown improvement in fruit juice clarification and increased yield. Different studies have investigated the effect of β -mannanase to reduce the viscosity and turbidity of different juices like apples, grape, kiwi, peach, pomegranate, and orange.

β -mannanase hydrolyzes the mannan fraction of the hemicellulose present in fruit juice thus reducing its viscosity and releasing the water trapped within it. Thus, β -mannanase hydrolysis also increases the amount of fruit juice. A β -mannanase isolated from *Weissella viridescens* LB37 was effective in juice clarification from different fruits, with a ratio of 112.7%, 108.97%, 107.8%, 110.0%, 117.21%, 109.2% in grape, peach, orange, pomegranate, kiwi, and apple, respectively, as compared to control (Adiguzel et al., 2016). In another study, a thermo-alkaline β -mannanase from *Bacillus pumilus* (M27) was isolated from a sausage sample (Adiguzel et al., 2015). This β -mannanase is highly stable at a range of temperature (30–80°C) and pH (3–11). Among different fruit juices tested, the highest yield at the rate of 154% was obtained when β -mannanase enzyme was used to clarify apple juice.

Filtration and centrifugation can also be employed in fruit juice clarification, but enzymatic process is superior because it has high efficiency. In a study reported by Zhao et al. (2019) β -mannanase is isolated from *Lactobacillus casei* HDS-01 with high biosafety level and its potential in fruit juice clarification is tested. β -mannanase treatment of fruit juice results in a significant increase in clarity and yield of different fruit juices. Pear juice clarified from 54.32 to 65.28%, orange juice from 39.50 to 46.30%, and apple juice from 57.20 to 69.25%. In terms of juice yields represented by volumes, *L. casei* HDS-01 crude β -mannanase treatment produces apple, orange and pear juice with a yield ratio of 132.5%, 156.00%, and 151.04%, respectively compared to control.

Further purification of crude β -mannanase in this study is not considered necessary because of the high biosafety level

of *Lactobacillus casei* HDS-01 strain. Thus, β -mannanase is not separated from bacterial cells to clarify juices. The use of crude β -mannanase can be more advantageous because enzyme purification requires time and cost. However, when purified enzyme is used the yield and clarity of juice increases further (Zhao et al., 2020). For orange juice clarification, the application of the purified *L. casei* HDS-01 β -mannanase when compared with control results in a clarity of $47.55 \pm 0.02\%$ and yield of $188.20 \pm 0.40\%$. For apple juice clarification, treatment with HDS-01 β -mannanase achieves the clarity of $72.30 \pm 0.04\%$ and yield of $150.96 \pm 0.40\%$.

Bio-Bleaching of Pulp

Bleaching is the treatment of cellulosic fiber with chemicals to increase brightness which can be achieved through lignin removal or lignin decolorization (bleaching). This may require the use of a lot of chemicals which are hazardous to environment. However, the process can be made more environmentally friendly by using hemicellulases that open up the fiber structure, preparing the lignin to be removed away rather easily and thus reduce the amount of chemicals used in the subsequent steps.

Majority of pulp is derived from softwood which contains about 15–20% hemicellulose present as galactomannan (Chauhan et al., 2012). β -mannanase enzymes that are highly specific for galactomannan substrate thus can make good candidates for use in pulp and paper industry.

Patel and Dudhagara (2020) report that rice straw pulp can be effectively bleached by first treating it with an enzyme cocktail (xylanase, β -mannanase, pectinase) and then with diluted chemicals (DC) instead of a sole application of either the enzymatic mixture or DC. Treatment of rice straw pulp with both DC (0.25% EDTA and 0.5% H_2O_2) and enzyme cocktail leads to an increase in the release of phenolic compounds, reducing sugars and hydrophobic compounds and reduction in Kappa number. Based on these observations, it is concluded that pretreatment of pulp with an enzymatic mixture derived from *Isoptericola variabilis* UD-6 can decrease the quantity of chemicals employed in the process, thus making the process cost effective and environmentally friendly.

Enzymes that have high thermostability and are active at a broad range of pH are of special interest in pulp and paper industry because of the high pH and temperature conditions applied. This is why research efforts have been directed toward discovering β -mannanases that are remarkably alkali tolerant and thermostable. In Kraft pulping an additional important feature is required which is that the enzyme should be resistant to both alkaline and neutral proteases. A good example is Man5A that has been reported to retain its catalytic efficiency more than 97% following treatment with chymotrypsin, trypsin, collagenase, proteinase K, and subtilisin A for 30 or 60 min (Luo et al., 2012). Similarly, in another study, a multi-tolerant thermostable β -mannanase (MnCSB39) from *Bacillus sp.* CSB3 is isolated and characterized (Regmi et al., 2016). In addition to being active at a wide pH and temperature range the enzyme is also urea, NaCl, surfactant, and protease tolerant. The increased halotolerance of MnCSB39 makes it very suitable for bio-bleaching of pulp,

where the concentration of Na^+ and Cl^- can be very high. Worth mentioning are a few other multi-stress tolerant enzymes such as Man5p1 isolated from *Neosartorya fischeri* P1 and rMan5HJ14 isolated from *Bacillus sp.* HJ14 and MnB31 from *Bacillus inaquosorum* CSB31 which are resistant to urea, NaCl, Ag^+ ions, SDS as well as the action of proteases (Yang et al., 2015; Zhang et al., 2016; Regmi et al., 2017).

The combination of β -mannanase with other hemicellulases may augment the positive effects of β -mannanase application. Yang et al. (2017) observes that significant improvement occurs in brightness of kraft pulp when β -mannanase is coupled with xylanase.

Hydrolysis of Coffee Extract

Instant coffee provides its consumers with combined advantages of convenience and high added value. The main residue produced during instant coffee production is spent coffee ground (SCG) which consists mainly of polysaccharides like galactomannan and cellulose (Jooste et al., 2013). These polysaccharides do not get solubilized during the extraction process and therefore are left as insoluble solids (Figure 4).

In this backdrop, application of β -mannanase is seen as a favorable strategy for solubilizing/hydrolyzing remaining solids, thereby increasing yields of soluble solids of instant coffee. Jooste et al. (2013) applied different carbohydrase enzymes to enhance solubilization of remaining solids produced during coffee production. Among the enzymes tested for the hydrolysis of SCG, the highest increase in soluble solids yield is obtained by use of β -mannanase (Man 1). Combining β -mannanase (Man1) with other enzymes shows an additive effect instead of a synergistic one which indicates that β -mannanase is mainly responsible for the highest soluble solids yield. Similarly, Favaro et al. (2020) also demonstrate that a large amount of carbohydrates in the SCG can be hydrolyzed by β -mannanase. The hydrolysis yield increases even more (56%) when a commercial cellulase cocktail is added to β -mannanase, demonstrating the promise to increase soluble coffee processing. In a study reported by Baraldi et al. (2016) enzymatic and thermal processes are compared during the production of instant coffee. Roasted coffee is first extracted with water at 125°C and the spent coffee is then processed by either enzymatic hydrolysis at 50°C (with the aid of a cocktail of enzymes containing β -mannanase) or thermal hydrolysis at 180°C . Enzymatic hydrolysis yield (18%) is lower than thermal hydrolysis yield (28%). But instant coffee produced through enzymatic hydrolysis not only has low amount of unwanted compounds like furfural, acetaldehyde and 5-HMF but also less energy is consumed in the process. These findings demonstrate that the enzymatic procedure is a viable substitute to thermal hydrolysis for the production of instant coffee.

Bioethanol Production

Ethanol production can be divided into first generation and second-generation processing. Fermenting food-biomass into ethanol in a process similar to wine and beer making produces first generation ethanol. Second generation ethanol is produced by fermentation of lignocellulosic materials by microorganisms,

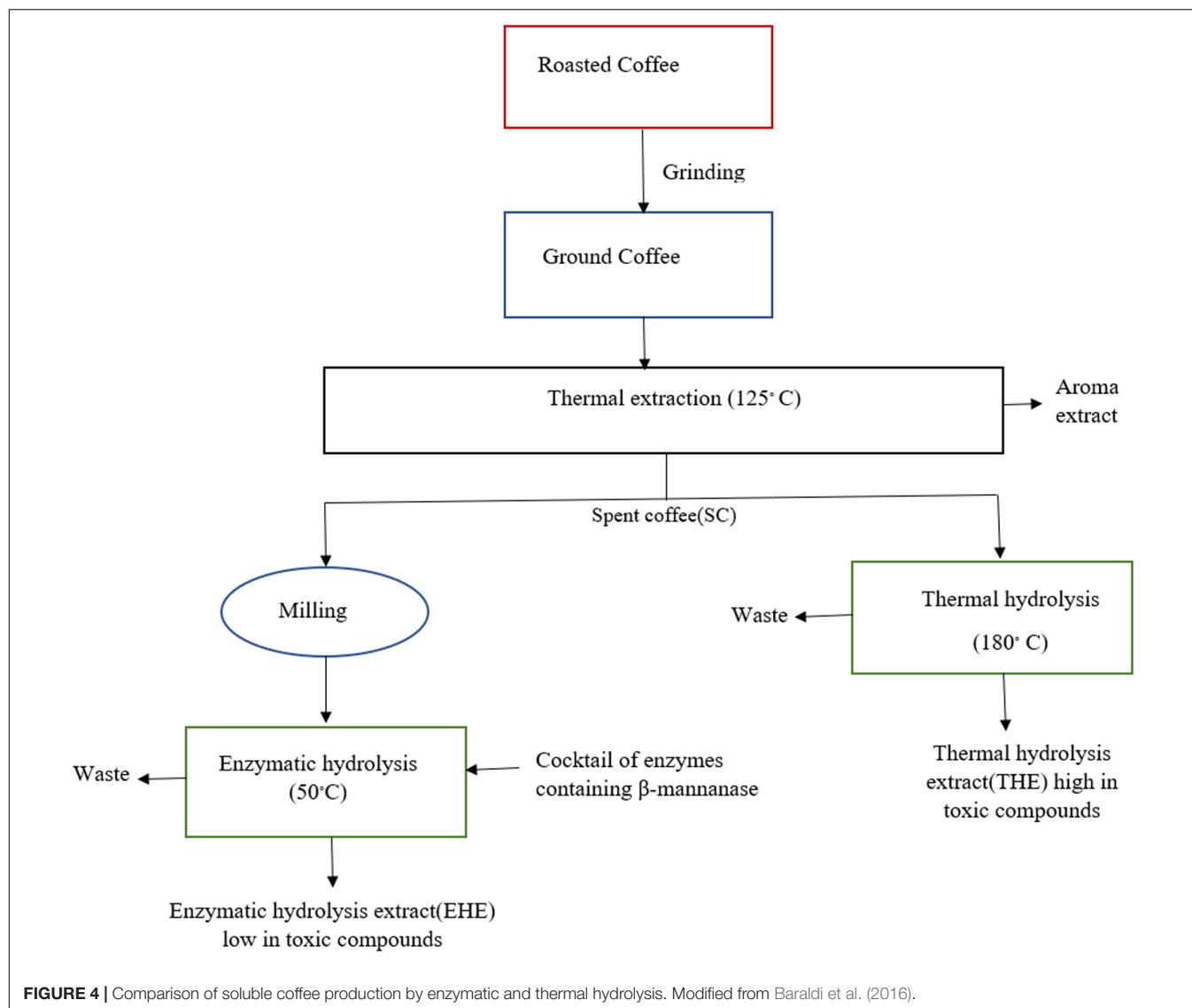


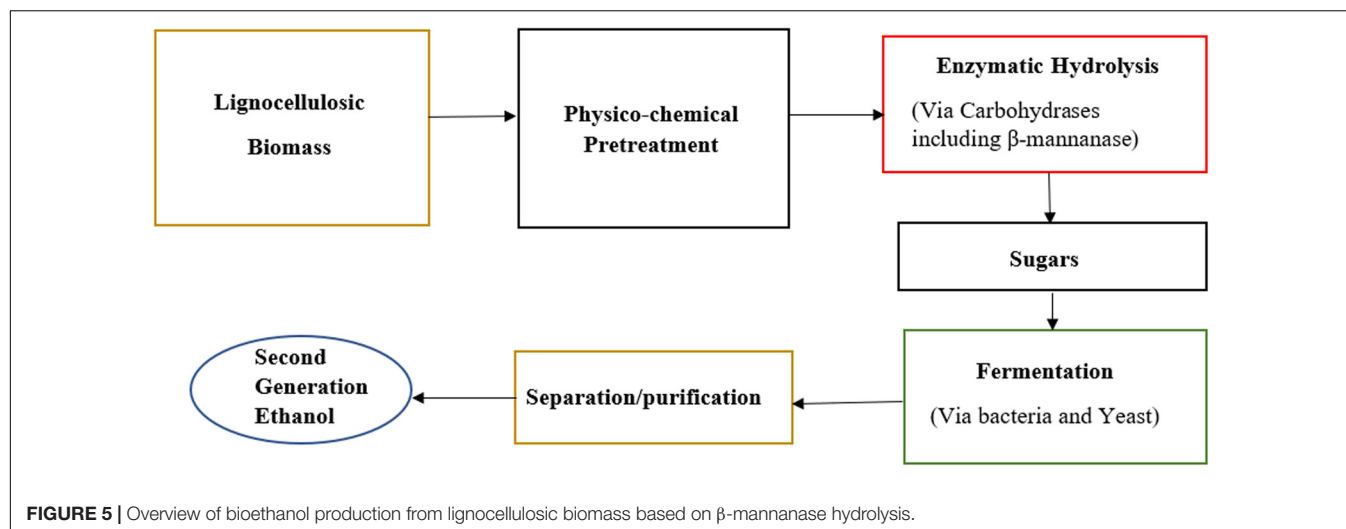
FIGURE 4 | Comparison of soluble coffee production by enzymatic and thermal hydrolysis. Modified from Baraldi et al. (2016).

however, this requires pretreatment because of the recalcitrance of plant cell wall (Zhang, 2019). Once the recalcitrance of plant cell wall is reduced through pretreatment, the hydrolytic enzymes of the microorganisms can act on cell wall polysaccharides and hydrolyze them to sugars monomers. As mannan is a component of lignocellulosic materials, supplementation of mannan-degrading enzymes can be beneficial in the production of mannose sugar which is then fermented by yeast into second generation ethanol (Figure 5).

A promising mannan rich bioresource is palm kernel cake (PKC) that can be used for fermentable sugar extraction. Hydrolysis of PKC by β -mannanase is increased under optimum conditions where β -mannanase loading, time, pH, temperature, and PKC concentration are optimized (Shukor et al., 2016). A total of 71.54 ± 2.54 g/L of fermentable sugars are produced under optimized conditions. This sugar hydrolysate is fermented by *Clostridium saccharoperbutylacetonicum* N1-4, producing a total of 3.27 ± 1.003 g/L of biobutanol.

In another study a bio-engineered mannanase (mRmMan5A) derived from *R. miehei* is successfully used for mannoooligosaccharides production from steam explosion pretreated PKC (Li et al., 2018). More than 80% of PKC mannan is converted into mannoooligosaccharides by the hydrolytic action of mRmMan5A. In addition, to ascertain the feasibility of mass production, kilogram scale of mannoooligosaccharide production is also carried out and a yield of 26.1% is obtained, proving mRmMan5A is an efficient β -mannanase for the bioconversion of mannan rich biomass.

β -mannanase is an important enzyme for hydrolysis of mannan. When it degrades mannan it mainly produces oligomers along with a small amount of mannose. These oligomers or mannoooligosaccharides (MOS) need to be degraded further by mannosidases to produce monomers which can then be utilized by ethanologens. In a study reported by Raita et al. (2016) a thermophilic bio-engineered ethanologen *Geobacillus thermoglucosidasius* TM242 is used to produce



ethanol directly from MOS rich sugar hydrolysate of PKC. Without needing mannosidase, *G. thermoglucosidasius* TM242 produces a maximum concentration of ethanol of 9.9 ± 0.4 g/L, which is equivalent to $92 \pm 2\%$ of theoretical yield based on the total convertible sugars present in PKC. This yield of ethanol is much greater than when *S. cerevisiae* is used under the same conditions to hydrolyze PKC. For the production of ethanol from mannan rich waste, use of ethanologens like *G. thermoglucosidasius* TM242 seems highly attractive as mild pre-treatment conditions are required and all sugars and oligosaccharides present in the substrate can be utilized without the need of β -mannosidase supplementation in hydrolysis step.

Effectiveness of β -mannanase for bioconversion of lignocellulosic biomass increases when used in combination with other carbohydrase enzymes. Addition of β -mannanase (MtMan26A) from thermophilic fungus *Myceliophthora thermophila*, to commercial enzyme mixture (Novozymes® 188 and Celluclast® 1.5 L) effectively hydrolyzes pretreated beechwood sawdust, increasing the release of total sugars by 13% and glucose by 12% (Katsimpouras et al., 2016). Similarly Cerveró et al. (2010) report that the conversion of lignocellulosic biomass into monosaccharides could be increased by using a binary mixture of commercial enzymes in the ratio of 1:1. Combining commercial enzymes, i.e., Mannaway (mannanase) and Gammanase (mannanase and galactosidase) shows an excellent synergistic effect that releases 30% more mannose than when those enzymes are used individually. Zhang and Sang (2015) also demonstrate that it is more effective to use a cocktail of enzymes to produce fermentable sugars from lignocellulosic biomass.

Textile Industry

β -mannanases in combination with detergents can be used for cleaning or preparation of fibers in textile and cellulosic processing industries. To prepare the material that is ready for garment manufacture the cellulosic material is processed through several steps: singeing, desizing, scouring, bleaching, dyeing, and finishing (Mojsov, 2011). Application of β -mannanase can be

useful in the bio-scouring and desizing of cellulosic fibers, thus preparing the material for good response in subsequent dyeing operations.

Bio-scouring is the process in which the fabric is cleaned through enzymatic action from impurities like pectin, hemicelluloses, wax, and mineral salts (Bristi et al., 2019). These impurities make the raw cotton hydrophobic and thus interfere with aqueous chemical process like dyeing and finishing. Therefore, removal of these impurities is essential before the fabric can be dyed.

Detergent Additives

Application of microbial enzymes in the detergent industry is well known. Among them, the most frequently used enzymes are proteinases, lipases, amylases, and cellulases (Srivastava and Kapoor, 2014). Lately, alkaline β -mannanases which show stability toward detergent components are increasingly being used as stain removal boosters in certain laundry segments. β -mannanase hydrolyzes different mannan based materials such as guar gum, glucomannan, galactomannans and others (Liao et al., 2014). Present as thickeners and for their gel textures, guar gums are found in an increasing number of consumer products, including barbecue sauce, ice cream, salad dressing, makeup, and hairstyling (Mudgil et al., 2014). These gums act like glue and stick to soil particles, thus making it difficult to remove dirt. β -mannanases effectively hydrolyze these gums, removing it from the fabric and thus preventing the dirt from sticking to the fabric.

ManSS11, a β -mannanase enzyme isolated from a novel *Klebsiella pneumoniae* strain SS11 was used to conduct wash performance experiments (Singh et al., 2019). Analysis of the hydrolyzed products, done at the end of washing process, shows that β -mannanase had $80.5 \pm 1.07\%$ better detergency (cleansing power) in removing locust bean gum + dust fixed strain than when detergent is used alone which shows only $30.6 \pm 0.86\%$ detergency. Similarly, in another study, cleaning power of β -mannanase derived from *Bacillus* sp. CFR1601 is tested against a cotton cloth stained with chocolate-ice cream and tomato sauce (Srivastava and Kapoor, 2014). Detergent

combined with β -mannanase shows enhanced stain removal than sole application of detergent. In addition, the stability and compatibility of the isolated β -mannanase with different laundry detergents available in the market, has also been checked. The enzyme reserves 89.0–100% of its original activity at 37°C for up to 1 h in the presence of different detergents in the sequence: Wheel > Surf > excel > Ariel > Tide > Rin. This shows that performance of the enzyme is influenced by the ingredients present in the detergent, as enzyme stability varied with different detergents tested. In a study reported by David et al. (2018) optimization of co-production of protease and β -mannanase from a *Bacillus nealsonii* strain PN-11 is investigated along with the potential of both of these enzymes as additives to detergents. The enzymes show good compatibility with detergents and the detergent performance is improved on different kinds of stains, when either β -mannanase or protease is used. However, the destaining is much more efficient when both β -mannanase and protease are used in combination.

For application in detergent industry, the enzyme should be highly thermostable and active in broad range of pH like the case of β -mannanase isolated from *Bacillus halodurans* PPKS-2. This enzyme is reported to be extremely alkaliophilic, halotolerant, detergent, and thermostable (Vijayalaxmi et al., 2013). It has an optimum temperature of 70°C and retains 100% of its original activity at 70°C for up to 3 h. Its optimum pH is 11 and the enzyme is active in a wide range of NaCl concentrations (0–16%). These properties make it a suitable candidate for the detergent industry. Another extremely alkaline, thermostable β -mannanase is isolated from *Streptomyces* sp. CS428 which effectively hydrolyzes galactomannan and thus can be effective in removing guar gum stains (Pradeep et al., 2016). Similarly, RmMan5A is especially suitable for use in detergent industry, due to its excellent stability in a wide range of pH (4.0–10.0) and thermostability up to 55°C (Katrolia et al., 2013). In addition, it displays remarkable tolerance toward sodium dodecyl sulfate (SDS), which has been reported to impede the activity of several other β -mannanases.

There are opportunities for geographical and numerical extension of β -mannanase use in detergents. In developing countries β -mannanases have not found a wide spread use, even though these countries are dusty and hot and thus frequent washing of clothes is often needed. In west, particularly in United States, β -mannanase has found its way in commercial household detergents preparations. Novozymes, a Danish company, markets Mannaway which is a washing detergent containing β -mannanase. This can effectively be used for removal of mannan based stains. The inclusion of β -mannanase in detergents not only improves the stain removal ability of detergent but also prevents other particles from sticking to the fabric during washing process.

Purabrite is another commercial β -mannanase marketed by another United States company Genencor. For decades, detergent formulators have faced the main challenge of developing products with superior cleaning performance at competitive prices. Genencor claims that Purabrite meets these requirements. Purabrite is available in both liquid and granular form. The

granular shape including a patented Enzoguard® coating is a proprietary technology of Genencor. These granules are safer to handle than poly powders and have enhanced properties for easy mixing and storage.

In Animal Feed Industry

β -mannanase supplementation in diet especially in high fiber diets or low energy diet has been reported to benefits the animals in many different ways.

β -Mannanase enhances growth performance and ileal digestible energy (IDE) and decreases intestinal viscosity in broilers fed diets with varying levels of galactomannan (Latham et al., 2018). The observed beneficial effects of β -mannanase are considered to be contingent upon concentration of dietary galactomannan. In a study carried out on turkeys β -mannanase supplementation had a beneficial effect on jejunum mucosal morphology (Ayoola et al., 2015). The villus tip width increased by 36%, villus height/crypt depth by 32%, villus surface area by 34%, and base width by 22.5%. Besides improving gut morphology Ayoola et al. (2015) observed that β -mannanase supplementation also causes thinning of ileal mucin layer. Increased mucin secretions have been linked to proliferation of intestinal pathogens. Thus, a reduction in mucin secretions may reduce the risk of pathogen proliferation in the gut and help establish symbiotic enteric ecosystem. β -mannanase supplemented with a cocktail of enzymes has also shown to be beneficial. Govil et al. (2017) observes that β -mannanase supplementation in combination with other carbohydrase enzymes shows significant improvement in feed conversion efficiency, weight gain and performance index in broilers.

Copra meal is easily available in many parts of the world and can be a cheap alternative to commonly used feed ingredients like SBM and corn. But its reduced amino acid (AA) digestibility and low energy content can be a barrier to its frequent use. Kim et al. (2017) demonstrate that copra meal if supplemented with β -mannanase (800 IU) can replace corn and SBM up to 25% without negatively affecting the growth performance and pork quality in growing finishing pigs. El-Masry et al. (2017) observes that addition of 5% guar meal (GM) in broiler diet has deleterious effect on growth performance. But with supplemental β -mannanase GM can be used at 5% without adversely affecting blood biochemistry and growth.

Very few studies have been conducted on β -mannanase supplementation in aquaculture. Chen et al. (2016) observes that β -mannanase supplementation (0.5 and 1.0 g/kg) in a plant based diet to tilapia significantly improved weight gain, FCR and specific growth rate indicating that β -mannanase is beneficial for tilapia.

Production of Mannooligosaccharides (MOS) as Immune Modulators, Anti-Tumor and Weight Loss Agents

Mannan is degraded into MOS by β -Mannanase. MOS are a kind of prebiotics and have been reported to boost the growth of beneficial gut microbiota like *Lactobacilli* and *Bifidobacteria*.

These bacteria or probiotics have many beneficial functions. Actually, most of the positive effects of MOS are due to propagation of these beneficial bacteria. Various researchers have studied MOS production by hydrolytic action of β -mannanases from different microorganisms (Pradeep et al., 2016; Rahmani et al., 2017; Yopi et al., 2017; Bååth et al., 2018).

Mannooligosaccharides can function as immune modulators. Atopic allergies have recently increased as dietary habits and environment have changed. Allergic reactions are characterized by an increase in serum IgE antibody, cytokine production (IL-8 and TNF- α) and infiltration of acidophil cells (Galli and Tsai, 2012). Prebiotics can be used to suppress allergic reactions (Brosseau et al., 2019). *In vitro* studies of MOS on ovalbumin-sensitized mice showed a decrease of 56.2 to 36.2 in serum IgE titer. There was also a significant decrease in TNF- α and IL-8 from Peyer's Patch suggesting that MOS have anti-allergic properties and can be used as anti-allergic agents (Ozaki et al., 2007).

Mannooligosaccharides can be used as anti-tumor agents. Colon cancer in western countries is the second-most common type of cancer (Fernández et al., 2015). The use of prebiotics could lead to more positive effects on the health compared to commercial anti-cancer agents. Prebiotics have been reported to possess anti-cancer properties and detoxify gastrointestinal genotoxins. Recent studies have shown that prebiotics such as MOS have powerful anti-tumor properties. *In vitro* cytotoxicity assay of MOS (500 μ g/mL) on human epithelial colorectal adenocarcinoma cell line (HT-29) shows after 48 h, a 60% decrease in the viability of cells (Ghosh et al., 2015). Thus, for colon cancer treatment, MOS can be good therapeutic agents.

Mannooligosaccharides can be used as weight loss agents. Clinical studies have shown that MOS consumption may reduce body weight and thus can be used as an aid to a weight loss regimen. Salinardi et al. (2010) report that in overweight men, consumption of MOS containing drink as part of a weight maintaining diet reduces total body volume and body weight compared to placebo. Similarly, St-Onge et al. (2012) have also observed that adding MOS to a weight loss diet can expedite adipose tissue and weight loss in men suggesting a potential functional usage of MOS in adipose tissue distribution and weight management. However, more research is necessary to further understand the mechanism by which MOS improves the composition of the body and to clarify the influence of gender.

BIOENGINEERING OF β -MANNANASES FOR IMPROVING THEIR INDUSTRIAL APPLICATIONS

To meet industrial needs, an ideal β -mannanase should exhibit certain properties that include high specific activity, good thermostability, activity over a wide range of pH and strong resistance to chemical products and metal cations. As most of the native β -mannanases do not possess optimal properties required by the industry, research efforts have been

directed toward bioengineering β -mannanases to enhance their stability and activity.

Increasing Activity of β -Mannanases

Using crystal structure as basis Huang et al. (2014) apply rational design to an *Aspergillus niger* β -mannanase (ManBK) for increasing its enzyme activity. The most promising mutant (Y216W) produced out of the 23 mutants examined shows an $18 \pm 2.7\%$ increase in specific activity compared to the wild type enzyme. The heat tolerance profile and the optimal temperature of both Y216W and the wild type enzyme are similar but the K_{cat} values on konjac and guar gum are higher for Y216W, as revealed by the kinetic studies. The enhanced catalytic activity of Y216W is ascribed to the faster dissociation of cleaved sugars which may be due to extended aromatic ring of Trp that changed interaction with bound polysaccharides. By restricting the enzyme from holding the substrate in the binding site the substrate conversion rate is increased.

Suitable substitution of amino acids can facilitate the access of substrate to the substrate binding groove and maintain it therein, thus improving the substrate affinity and catalytic efficiency of the enzyme. In a study by Li et al. (2014) the substrate affinity of AuMan5A is improved by rational modification, which is predicted by *in silico* design, including molecular docking simulations and calculations of binding free energies. Based on this design, the mutant genes *Auman5AY111F* and *Auman5AY115F* are created by site-directed mutagenesis. The Auman5A and its mutant genes are expressed in *Pichia pastoris* and characterized. The pH and temperature profile of the expressed mutants is similar to the parental enzyme. However, the K_m values of reAuMan5AY115F and reAuMan5AY111F for guar gum decrease about 47% and 34%, respectively, and their catalytic efficiencies increase 0.7 and 0.5-fold correspondingly as compared with those of parental enzyme, making them excellent candidates for different industrial processes.

Li et al. (2017b) report that the catalytic efficiencies of a *Rhizomucor miehei* β -mannanase (RmMan5A) under acidic and thermophilic conditions is enhanced. By using error prone PCR and DNA shuffling a mutant library having 0.72% mutation frequency is created. Following two rounds of screening a variant (mRmMan5A) with superior catalytic activity in high temperature and acidic conditions is obtained and characterized. The mutant shows an increase of 10°C in optimum temperature and a 2.5 unit acidic shift in optimum pH compared to the wild type enzyme. Moreover, the catalytic efficiencies (K_{cat}/K_m) of mRmMan5A toward different mannan based substrates increase more than threefold in thermophilic and acidic conditions, making it a highly desirable candidate for application in biorefinery industry.

Molecular engineering of Bman26 (a recombinant β -mannanase from *Bacillus* sp. MK-2) is carried out using random mutagenesis in *Bacillus subtilis* WB800, to obtain an enzyme with higher specific activity (Zhang et al., 2019). With the help of error prone PCR, mutant libraries are constructed and three positive mutants with considerably

enhanced specific activities are selected and characterized. Among them K291E is the best, in which a single amino acid substitution caused a 3.5-fold increase in K_{cat}/K_m . The catalytic efficiency for Konjac glucomannan also increases approximately 80% and 200% for the L211I and Q112R mutants, respectively. Structural and functional analysis of these three positive mutants shows that a small conformational alteration like loss of hydrogen bond between Gln112 and Thr75 in case of mutant Q112R may cause a significant change in substrate binding and certain enzyme characteristics.

A random mutagenesis strategy is used by Couturier et al. (2013) to produce 10,800 mutants of GH5 (PaMan5A) and GH26 (PaMan26A) β -mannanases isolated from the fungus *Podospira anserina*. Further characterization is done of five mutants (PaMan26A-P140L/D416G, PaMan5A-V256L/G276V/Q316H, PaMan5A-36R/I195T/V256A, PaMan5A-K139R/Y223H, and PaMan5A-G311S). Circular dichroism, temperature and pH profiles are like those of their respective parental enzymes. However, compared to the wild type enzymes, all the chosen variants display a significantly enhanced activity. The double mutant PaMan26A-P140L/D416G having mutations at the entry of the active site (D416G) and the linker region (P140L) display an increase of 30% in K_{cat}/K_m , compared to parental enzyme. The increase in K_{cat}/K_m is partially explained by an increase in the flexibility of the linker produced due to P140L mutation, while D416G mutation promotes the entry of the substrate into active site. The Triple mutant PaMan5A-W36R/I195T/V256A displays higher catalytic efficiency with an increase of 1.8-fold and enhanced hydrolysis of galactomannan. With an almost unaltered structure except a slight change in the beta-strand 8, the single mutant PaMan5A-G311S shows an increase in K_{cat}/K_m of 8.2-fold, possibly due to a reduction in K_m because of the positioning of the residue W315 at the surface of the enzyme. These results show that variants with improved catalytic activity can be produced to efficiently hydrolyze softwood biomass to produce MOS and sugar.

To improve the hydrolysis of hemicellulosic biomass, Guo et al. (2013) have created chimeras of β -mannanase and xylanases. The characteristics of β -mannanase and xylanase in chimera and their synergistic abilities to hydrolyze *Luffa cylindrica* fiber efficiently is shown to be affected by the length of linker, the type of linker, and their order of integration.

Enhancing Thermostability of β -Mannanases

Rational design method is employed to enhance thermostability of β -mannanase (ManTJ102) leading to a mutant with enhanced performance (Wang et al., 2018). With the help of a molecular dynamics simulation, flexible area surrounding residues 330–340 in ManTJ102 is first identified. Then by virtual mutation the critical amino acid residue (Ala336Pro) having the lowest resulting free energy is determined. The mutant produced is named Mutant336. A range of high temperature (50–80°C)

is used to experimentally verify the thermostability of both the Mutant336 and the wild type enzyme. Compared to ManTJ102, Mutant 336 shows better thermostability with a half-life at 60°C being 24-fold higher than ManTJ102 and the irreversible thermal denaturation constant is about 2/5 of ManTJ102, making it a highly attractive candidate for MOS production in industry.

Mutations that enhance the thermostability of the enzyme usually lead to reduction in catalytic activity. Therefore, enzyme activity needs to be preserved while improving its thermostability. Zhu et al. (2019) report that directed evolution based on iterative saturation mutagenesis applied to Man25 (a *Thermoanaerobacterium aotearoense* SCUT27 derived β -mannanase) at the five potential Ca^{2+} binding sites lead to improvements in thermostability of the enzyme without decreasing its activity. Out of 7000 clones produced, the best mutant ManM3-3 (D143A) shows enhanced thermostability and satisfactory catalytic activity. Compared to the wild type, its half-life increased 3.6 fold at 55°C.

To enhance the thermostability and catalytic efficiency of a glycoside hydrolase family 5 β -mannanase), a family 27 carbohydrate-binding module of a *Thermotoga maritima* β -mannanase (TmCBM27) is fused to its C-terminus linked with a flexible peptide F (GGGGS)₃ and rigid peptide R (EAAAK)₃ (Li et al., 2017a). Thus two fusion β -mannanases, AuMan5A-R-M and AuMan5A-F-M are designed and their encoding genes are constructed, and expressed along with the parental enzyme in *Pichia pastoris* GS115. Among the three recombinant β -mannanases (reAuMan5A, reAuMan5A-R-M, and reAuMan5A-FM), the optimum temperature of reAuMan5A-R-M is similar to the parental enzyme reAuMan5A but its melting temperature (T_m) and thermostability are 8.4 and 8.0°C higher than the wild type enzyme. Moreover, the K_m values of reAuMan5A-R-M toward Konjac gum, guar gum and Locust bean gum increase significantly and its catalytic efficiency values (K_{cat}/K_m) decrease significantly in comparison to reAuMan5A. The superior thermostability and substrate affinity of reAuMan5A-R-M make it a suitable candidate for many industrial processes.

Numerous studies have shown that the alteration of the loop structures in proximity to the active centers of the glycoside hydrolases may enhance their catalytic efficiency and/or thermostability. Dong et al. (2016) have sought to improve the characteristics of an *Aspergillus usamii* derived β -mannanase (AuMan5A) by substitution of its loop structure. Based on enzymatic characteristics and structural analysis of various GH 5 β -mannanases, three mutants (AuMan5A, AuMAN5A-An, AuMAN5A-AF) are designed by substituting a piece of loop structure with seven amino acids in the substrate binding groove of AuMan5A with the corresponding sequences of three other family 5 β -mannanases, respectively. AuMan5A and its mutants are expressed in *Pichia pastoris* and characterized. The expressed recombinant AuMan5A-Af (re-AuMan5A-Af) is the best performing mutant. It shows a T_m value of 76.6°C, temperature optimum of 75°C

and a half-life of 480 min at 70°C which are 12.1 and 10°C higher and 48-fold longer than those of the parental enzymes, respectively.

A β -mannanase (MAN) derived from *B. subtilis* B10-02 and over expressed in *B. subtilis* 168 is unstable under acidic conditions, thus restricting its use in food and feed industry (Xu et al., 2013). To enhance the acid stability of BsMAN6H several surface exposed basic amino acid residues are altered to neutral or acidic ones by site-directed mutagenesis. Among the variants produced, the variant H54D shows a decrease in the pH optima from 6.5 to 5.5 and an increased acid stability in the pH range of 4.0–5.5. In addition, the mutant H54D shows an enhanced enzyme activity (of 3207.82 U/ml) compared to parental enzyme. The enhanced enzymatic activity in H54D is attributed to, greater number of hydrogen bonds set up between the Asp54 and the neighboring amino acid residues, and negative potential around the mutated site which significantly altered the modeled electrostatic potential on the protein surface.

Higher Protease Resistance of β -Mannanase

Modification through artificial glycosylation is a technology that can improve the characteristics of a protein by changing its structure with a carbohydrate chain. Hu et al. (2017) employ rationally designed N-glycosylation to enhance the protease resistance and stability of a recombinant β -mannanase (MAN 47) from *Armillariella tabescens*. To facilitate N-glycosylation an enhanced aromatic sequon sequence was introduced into specific MAN47 loop regions. The mutant MAN47 enzymes (g-123 and g-347) are expressed in yeast, glycosylated as expected and characterized. The pH stability, thermostability and protease resistance improved significantly when compared to the wild type enzyme. It is speculated that the carbohydrate chain protects protease target sites, interacts with amino acid residues and enhances the hydrophilicity of β -mannanase. Thus, as a result the molecular rigidity of β -mannanase is increased. Thereby, mutants of β -mannanase MAN47 with improved stability are obtained. An enzyme with multiple improved stability characteristics has broad applications in different industrial fields especially in the detergent and animal feed industries.

Similarly, in another study protease resistance of β -mannanase is improved to make it suitable for the feed industry which is necessary because of the presence of secretory proteases in the digestive tract. Li et al. (2013) employ rational method for improvement in trypsin resistance of β -mannanase. By using computational design via H-bond analysis and molecular dynamics simulations, optimal mutations of K280N, K371Q, and K280N/K107H/R102N are predicted. The trypsin resistance of mutants produced (K371Q, K280N/K107H/R102N, K280N) and the wild type β -mannanase is determined. There is a significant increase in trypsin resistance of triple mutant compared to wild type showing that molecular rational evolution can be used to increase the trypsin resistance of an enzyme.

FUTURE PROSPECTS

The application of β -mannanases in commercial sector has been steadily increasing over the past few decades. The cut-throat competition forces the enzyme industry to continuously look for better and newer enzymes. Researchers and engineers are looking for novel microbial β -mannanases that fulfill the requirements of industry. In general, conventional methods for β -mannanase discovery are expensive, have low success rate and time consuming. Metagenomics is an excellent alternative approach to these methods and can help in discovering novel β -mannanases from mother nature. However, β -mannanases from natural sources are sometimes not suitable for rigorous industrial biocatalytic processes because either the lower yield of the enzyme or other important catalytic properties. Thus, tailoring or bioengineering of the enzyme is required.

Advances in protein engineering has brought forth new opportunities to introduce predesigned changes to create customized β -mannanases having the desirable properties. However, in engineering of β -mannanases a few challenges lie ahead: (1) It must be considered that enhancing the thermostability of an enzyme often decreases its overall flexibility, therefore the produced enzyme will likely have lower catalytic efficiency; (2) Before the engineered β -mannanases can be used in food and feed sector, there's need to investigate how these designed proteins interact with biological systems; (3) The paucity of general rules in prioritization of enzymatic properties must be improved while selection of appropriate methods is also a difficult issue in bioengineering of β -mannanase. Collection of successful studies in β -mannanase engineering should provide suitable guidelines; (4) The quest for an ideal β -mannanase is ongoing even after many research efforts, while the *de novo* design of highly optimized industrial β -mannanase remains still elusive. There is need to enhance the mechanistic knowledge of the structure-function and dynamics relationships, so as to improve the algorithm for computational enzyme design. Once these advanced technologies are developed, designed β -mannanases will be easier to manufacture and industrialize.

Finally, a principal obstacle in the marketing of enzymatic processes is the cheap, large scale production of β -mannanase enzyme. To realize this goal, strategies need to be discovered which help facilitate the cheap production of bulk β -mannanase. It is hoped that in the near future, newer methods for simple and affordable production of β -mannanase, which can effectively meet the requirements of different industries will be discovered.

Conclusion

β -mannanases have been used in a wide range of industries such as feed, detergent, biorefinery and textile. The production and use of β -mannanases are on the rise due to increased awareness of their utility and the incorporation of enzyme engineering and gene manipulation techniques. Now, there is an urgent need to create β -mannanases better suited to demands of the industrial sector at cheap costs, so that the use of noxious chemicals in the industrial sector is replaced by eco-friendly biocatalysts. The state and the higherups should take

charge of encouraging this change so that industrial products are produced more cleanly and the risk of eco-pollution is reduced.

AUTHOR CONTRIBUTIONS

AD wrote the manuscript. KM reviewed the manuscript and made the necessary corrections. Both authors

contributed to the article and approved the submitted version.

ACKNOWLEDGMENTS

We would like to express our thanks to Dr. David Wood, The Ohio State University, United States for his useful critique of a part (β -mannanase bioengineering) of this review article.

REFERENCES

- Abd Rashid, J. I., Samat, N., and Yusoff, W. M. W. (2012). Screening and optimization of medium composition for mannanase production by *Aspergillus terreus* SUK-1 in solid state fermentation using statistical experimental methods. *Res. J. Microbiol.* 7:242. doi: 10.3923/jm.2012.242.255
- Adiguzel, A., Nadaroglu, H., and Adiguzel, G. (2015). Purification and characterization of β -mannanase from *Bacillus pumilus* (M27) and its applications in some fruit juices. *J. Food Sci. Technol.* 52, 5292–5298. doi: 10.1007/s13197-014-1609-y
- Adiguzel, G., Sonmez, Z., Adiguzel, A., and Nadaroglu, H. (2016). Purification and characterization of a thermostable endo- β -1, 4 mannanase from *Weissella viridescens* LB37 and its application in fruit juice clarification. *Eur. Food Res. Technol.* 242, 769–776. doi: 10.1007/s00217-015-2584-x
- Agrawal, P., Verma, D., and Daniell, H. (2011). Expression of *Trichoderma reesei* β -mannanase in tobacco chloroplasts and its utilization in lignocellulosic woody biomass hydrolysis. *PLoS One* 6:e29302. doi: 10.1371/journal.pone.0029302
- Ayoola, A. A., Malheiros, R. D., Grimes, J. L., and Ferket, P. R. (2015). Effect of dietary exogenous enzyme supplementation on enteric mucosal morphological development and adherent mucin thickness in Turkeys. *Front. Vet. Sci.* 2:45. doi: 10.3389/fvets.2015.00045
- Bååth, J. A., Martínez-Abad, A., Berglund, J., Larsbrink, J., Vilaplana, F., and Olsson, L. (2018). Mannanase hydrolysis of spruce galactoglucomannan focusing on the influence of acetylation on enzymatic mannan degradation. *Biotechnol. Biofuels* 11, 1–15.
- Baraldi, I., Giordano, R., and Zangirolami, T. (2016). Enzymatic hydrolysis as an environmentally friendly process compared to thermal hydrolysis for instant coffee production. *Braz. J. Chem. Eng.* 33, 763–771. doi: 10.1590/0104-6632.20160334s20140028
- Blibech, M., Ellouz Ghorbel, R., Chaari, F., Dammak, I., Bhiri, F., Neifar, M., et al. (2011). Improved mannanase production from *Penicillium occitanis* by fed-batch fermentation using acacia seeds. *ISRN Microbiol.* 2011 2011:938347.
- Blibech, M., Farhat-Khemakhem, A., Kriaa, M., Asloul, R., Boukhris, I., Alghamdi, O. A., et al. (2020). Optimization of β -mannanase production by *Bacillus subtilis* US191 using economical agricultural substrates. *Biotechnol. Prog.* 36:e2989.
- Bristi, U., Pias, A., and Lavlu, F. (2019). A Sustainable process by bio-scouring for cotton knitted fabric suitable for next generation. *J. Text. Eng. Fashion Technol.* 5, 41–48.
- Brosseau, C., Selle, A., Palmer, D. J., Prescott, S. L., Barbarot, S., and Bodinier, M. (2019). Prebiotics: mechanisms and preventive effects in allergy. *Nutrients* 11:1841. doi: 10.3390/nu11081841
- Cerveró, J. M., Skovgaard, P. A., Felby, C., Sørensen, H. R., and Jørgensen, H. (2010). Enzymatic hydrolysis and fermentation of palm kernel press cake for production of bioethanol. *Enzyme Microb. Technol.* 46, 177–184. doi: 10.1016/j.enzmictec.2009.10.012
- Chantorn, S. T., Buengrisawat, K., Pokaseam, A., Sombat, T., Dangpram, P., Jantawon, K., et al. (2013). Optimization of extracellular mannanase production from *Penicillium oxalicum* KUB-SN2-1 and application for hydrolysis property. *Songklanakarin J. Sci. Technol.* 35, 17–22.
- Chauhan, P. S., Bharadwaj, A., Puri, N., and Gupta, N. (2014). Optimization of medium composition for alkali-thermostable mannanase production by *Bacillus nealsonii* PN-11 in submerged fermentation. *Int. J. Curr. Microbiol. Appl. Sci.* 3, 1033–1045.
- Chauhan, P. S., Puri, N., Sharma, P., and Gupta, N. (2012). Mannanases: microbial sources, production, properties and potential biotechnological applications. *Appl. Microbiol. Biotechnol.* 93, 1817–1830. doi: 10.1007/s00253-012-3887-5
- Chen, W., Lin, S., Li, F., and Mao, S. (2016). Effects of dietary mannanase on growth, metabolism and non-specific immunity of *Tilapia* (*Oreochromis niloticus*). *Aquacult. Res.* 47, 2835–2843. doi: 10.1111/are.12733
- Couturier, M., Feliu, J., Bozonnet, S., Roussel, A., and Berrin, J.-G. (2013). Molecular engineering of fungal GH5 and GH26 β -(1, 4)-mannanases toward improvement of enzyme activity. *PLoS One* 8:e79800. doi: 10.1371/journal.pone.0079800
- David, A., Chauhan, P. S., Kumar, A., Angural, S., Kumar, D., Puri, N., et al. (2018). Coproduction of protease and mannanase from *Bacillus nealsonii* PN-11 in solid state fermentation and their combined application as detergent additives. *Int. J. Biol. Macromol.* 108, 1176–1184. doi: 10.1016/j.ijbiomac.2017.09.037
- Dey, T. B., and Banerjee, R. (2014). Application of decolourized and partially purified polygalacturonase and α -amylase in apple juice clarification. *Braz. J. Microbiol.* 45, 97–104. doi: 10.1590/s1517-83822014000100014
- Dhawan, S., and Kaur, J. (2007). Microbial mannanases: an overview of production and applications. *Crit. Rev. Biotechnol.* 27, 197–216. doi: 10.1080/07388550701775919
- Dong, Y. H., Li, J. F., Hu, D., Yin, X., Wang, C. J., Tang, S. H., et al. (2016). Replacing a piece of loop-structure in the substrate-binding groove of *Aspergillus usamii* β -mannanase, AuMan5A, to improve its enzymatic properties by rational design. *Appl. Microbiol. Biotechnol.* 100, 3989–3998. doi: 10.1007/s00253-015-7224-7
- El-Masry, K. N., Ragaa, N. M., Tony, M. A., and El-Banna, R. (2017). Research article effect of dietary inclusion of guar meal with or without β -mannanase supplementation on broiler performance and immunity. *Pakistan J. Nutrition* 16, 341–350. doi: 10.3923/pjn.2017.341.350
- Favaro, C. P., Baraldi, I. J., Casciatori, F. P., and Farinas, C. S. (2020). β -Mannanase production using coffee industry waste for application in soluble coffee processing. *Biomolecules* 10:227. doi: 10.3390/biom10020227
- Fernández, J., Redondo-Blanco, S., Miguélez, E. M., Villar, C. J., Clemente, A., and Lombó, F. (2015). Healthy effects of prebiotics and their metabolites against intestinal diseases and colorectal cancer. *AIMS Microbiol.* 1:48. doi: 10.3934/microbiol.2015.1.48
- Galli, S. J., and Tsai, M. (2012). IgE and mast cells in allergic disease. *Nat. Med.* 18, 693–704. doi: 10.1038/nm.2755
- Ghosh, A., Verma, A. K., Tingirikari, J. R., Shukla, R., and Goyal, A. (2015). Recovery and purification of oligosaccharides from copra meal by recombinant endo- β -mannanase and deciphering molecular mechanism involved and its role as potent therapeutic agent. *Mol. Biotechnol.* 57, 111–127. doi: 10.1007/s12033-014-9807-4
- Gohel, S., and Singh, S. (2015). Thermodynamics of a Ca^{2+} -dependent highly thermostable alkaline protease from a haloalkaliphilic actinomycete. *Int. J. Biol. Macromol.* 72, 421–429. doi: 10.1016/j.ijbiomac.2014.08.008
- Govil, K., Nayak, S., Baghel, R., Patil, A., Malapure, C., and Thakur, D. (2017). Performance of broiler chicken fed multicarbohydrases supplemented low energy diet. *Vet. World* 10:727. doi: 10.14202/vetworld.2017.727-731
- Guo, N., Zheng, J., Wu, L.-S., Tian, J., and Zhou, H.-B. (2013). Engineered bifunctional enzymes of endo-1, 4- β -xylanase/endo-1, 4- β -mannanase were constructed for synergistically hydrolyzing hemicellulose. *J. Mol. Catal. B: Enzymatic* 97, 311–318. doi: 10.1016/j.molcatb.2013.06.019
- Harris, P. J., and Stone, B. A. (2009). “Chemistry and molecular organization of plant cell walls,” in *Biomass Recalcitrance: Deconstructing the Plant Cell Wall for Bioenergy*, ed. M. E. Himmel, (Hoboken, NJ: Wiley Online Library), 61–93. doi: 10.1002/9781444305418.ch4
- Hogg, D., Pell, G., Dupree, P., Goubet, F., Martin-Orue, S. M., Armand, S., et al. (2003). The modular architecture of *Cellvibrio japonicus* mannanases in glycoside hydrolase families 5 and 26 points to differences in their role in mannan degradation. *Biochem. J.* 371, 1027–1043. doi: 10.1042/bj20021860

- Hu, K., Li, C.-X., Pan, J., Ni, Y., Zhang, X.-Y., and Xu, J.-H. (2014). Performance of a new thermostable mannanase in breaking guar-based fracturing fluids at high temperatures with little premature degradation. *Appl. Biochem. Biotechnol.* 172, 1215–1226. doi: 10.1007/s12010-013-0484-8
- Hu, W., Liu, X., Li, Y., Liu, D., Kuang, Z., Qian, C., et al. (2017). Rational design for the stability improvement of *Armillariella tabescens* β -mannanase MAN47 based on N-glycosylation modification. *Enzyme Microb. Technol.* 97, 82–89. doi: 10.1016/j.enzmictec.2016.11.005
- Huang, J.-W., Chen, C.-C., Huang, C.-H., Huang, T.-Y., Wu, T.-H., Cheng, Y.-S., et al. (2014). Improving the specific activity of β -mannanase from *Aspergillus niger* BK01 by structure-based rational design. *Biochimica et Biophysica Acta (BBA)-Proteins Proteomics* 1844, 663–669. doi: 10.1016/j.bbapap.2014.01.011
- Ichinose, H., Suzuki, K., Michikawa, M., Sato, H., Yuki, M., Kamino, K., et al. (2017). Purification, cloning, functional expression, structure, and characterization of a thermostable β -mannanase from *Talaromyces trachyspermus* B168 and its efficiency in production of mannoooligosaccharides from coffee wastes. *J. Appl. Glycosci. JAG-2017_2018* 65, 13–21. doi: 10.5458/jag.jag.2017_018
- Ismail, S. A., Hassan, A. A., and Emran, M. A. (2019). Economic production of thermo-active endo β -mannanase for the removal of food stain and production of antioxidant manno-oligosaccharides. *Biocatal. Agric. Biotechnol.* 22:101387. doi: 10.1016/j.bcab.2019.101387
- Jana, U. K., Suryawanshi, R. K., Prajapati, B. P., Soni, H., and Kango, N. (2018). Production optimization and characterization of mannoooligosaccharide generating β -mannanase from *Aspergillus oryzae*. *Bioresour. Technol.* 268, 308–314. doi: 10.1016/j.biortech.2018.07.143
- Jooste, T., García-Aparicio, M., Brienzo, M., Van Zyl, W., and Görgens, J. (2013). Enzymatic hydrolysis of spent coffee ground. *Appl. Biochem. Biotechnol.* 169, 2248–2262. doi: 10.1007/s12010-013-0134-1
- Katrolia, P., Yan, Q., Zhang, P., Zhou, P., Yang, S., and Jiang, Z. (2013). Gene cloning and enzymatic characterization of an alkali-tolerant endo-1, 4- β -mannanase from *Rhizomucor miehei*. *J. Agric. Food Chem.* 61, 394–401. doi: 10.1021/jf303319h
- Katrolia, P., Zhou, P., Zhang, P., Yan, Q., Li, Y., Jiang, Z., et al. (2012). High level expression of a novel β -mannanase from *Chaetomium* sp. exhibiting efficient mannan hydrolysis. *Carbohydrate Pol.* 87, 480–490. doi: 10.1016/j.carbpol.2011.08.008
- Katsimpouras, C., Dimarogona, M., Petropoulos, P., Christakopoulos, P., and Topakas, E. (2016). A thermostable GH26 endo- β -mannanase from *Myceliophthora thermophila* capable of enhancing lignocellulose degradation. *Appl. Microbiol. Biotechnol.* 100, 8385–8397. doi: 10.1007/s00253-016-7609-2
- Khattab, O. K., Ismail, S. A., Abosereh, N. A., Abo-Elnasr, A. A., Nour, S. A., and Hashem, A. M. (2020). Optimization and comparative studies on activities of β -mannanase from newly isolated fungal and its mutant. *Egypt. Pharmaceut. J.* 19:29. doi: 10.4103/epj.epj_48_19
- Kim, H., Nam, S., Jeong, J., Fang, L., Yoo, H., Yoo, S., et al. (2017). Various levels of copra meal supplementation with β -Mannanase on growth performance, blood profile, nutrient digestibility, pork quality and economical analysis in growing-finishing pigs. *J. Animal Sci. Technol.* 59:19.
- Kim, M.-K., An, Y. J., Jeong, C.-S., Song, J. M., Kang, M. H., Lee, Y.-H., et al. (2013). Expression at 279 K, purification, crystallization and preliminary X-ray crystallographic analysis of a novel cold-active β -1, 4-d-mannanase from the Antarctic springtail *Cryptopygus antarcticus*. *Acta Crystallogr. Sec F Struct. Biol. Cryst. Commun.* 69, 1007–1010. doi: 10.1107/s1744309113020538
- Kim, S., Lee, M.-H., Lee, E.-S., Nam, Y.-D., and Seo, D.-H. (2018). Characterization of mannanase from *Bacillus* sp., a novel *Codium fragile* cell wall-degrading bacterium. *Food sci. Biotechnol.* 27, 115–122. doi: 10.1007/s10068-017-0210-3
- Latham, R., Williams, M., Walters, H., Carter, B., and Lee, J. (2018). Efficacy of β -mannanase on broiler growth performance and energy utilization in the presence of increasing dietary galactomannan. *Poult. Sci.* 97, 549–556. doi: 10.3382/ps/pex309
- Li, J., Wang, C., Hu, D., Yuan, F., Li, X., Tang, S., et al. (2017a). Engineering a family 27 carbohydrate-binding module into an *Aspergillus usamii* β -mannanase to perfect its enzymatic properties. *J. Biosci. Bioeng.* 123, 294–299. doi: 10.1016/j.jbiosc.2016.09.009
- Li, J., Wei, X., Tang, C., Wang, J., Zhao, M., Pang, Q., et al. (2014). Directed modification of the *Aspergillus usamii* β -mannanase to improve its substrate affinity by in silico design and site-directed mutagenesis. *J. Ind. Microbiol. Biotechnol.* 41, 693–700. doi: 10.1007/s10295-014-1406-7
- Li, Y.-x., Liu, H.-j., Shi, Y.-q., Yan, Q.-j., You, X., and Jiang, Z.-q. (2020). Preparation, characterization, and prebiotic activity of manno-oligosaccharides produced from cassia gum by a glycoside hydrolase family 134 β -mannanase. *Food Chem.* 309:125709. doi: 10.1016/j.foodchem.2019.125709
- Li, Y.-X., Yi, P., Yan, Q.-J., Qin, Z., Liu, X.-Q., and Jiang, Z.-Q. (2017b). Directed evolution of a β -mannanase from *Rhizomucor miehei* to improve catalytic activity in acidic and thermophilic conditions. *Biotechnol. Biofuels* 10, 1–12.
- Li, Y., Hu, F., Wang, X., Cao, H., Liu, D., and Yao, D. (2013). A rational design for trypsin-resistant improvement of *Armillariella tabescens* β -mannanase MAN47 based on molecular structure evaluation. *J. Biotechnol.* 163, 401–407. doi: 10.1016/j.jbiotec.2012.12.018
- Li, Y.-X., Yi, P., Liu, J., Yan, Q.-J., and Jiang, Z.-Q. (2018). High-level expression of an engineered β -mannanase (mRmMan5A) in *Pichia pastoris* for manno-oligosaccharide production using steam explosion pretreated palm kernel cake. *Bioresour. Technol.* 256, 30–37. doi: 10.1016/j.biortech.2018.01.138
- Liao, H., Li, S., Zheng, H., Wei, Z., Liu, D., Raza, W., et al. (2014). A new acidophilic thermostable endo-1, 4- β -mannanase from *Penicillium oxalicum* GZ-2: cloning, characterization and functional expression in *Pichia pastoris*. *BMC Biotechnol.* 14:90. doi: 10.1186/s12896-014-0090-z
- Liu, H.-X., Gong, J.-S., Li, H., Lu, Z.-M., Li, H., Qian, J.-Y., et al. (2015). Biochemical characterization and cloning of an endo-1, 4- β -mannanase from *Bacillus subtilis* YH12 with unusually broad substrate profile. *Process Biochem.* 50, 712–721. doi: 10.1016/j.procbio.2015.02.011
- Liu, J., Basit, A., Miao, T., Zheng, F., Yu, H., Wang, Y., et al. (2018). Secretory expression of β -mannanase in *Saccharomyces cerevisiae* and its high efficiency for hydrolysis of mannans to mannoooligosaccharides. *Appl. Microbiol. Biotechnol.* 102, 10027–10041. doi: 10.1007/s00253-018-9355-0
- Liu, Z., Ning, C., Yuan, M., Yang, S., Wei, X., Xiao, M., et al. (2020). High-level expression of a thermophilic and acidophilic β -mannanase from *Aspergillus kawachii* IFO 4308 with significant potential in mannoooligosaccharide preparation. *Bioresour. Technol.* 295:122257. doi: 10.1016/j.biortech.2019.122257
- Luo, H., Wang, K., Huang, H., Shi, P., Yang, P., and Yao, B. (2012). Gene cloning, expression, and biochemical characterization of an alkali-tolerant β -mannanase from *Humicola insolens* Y1. *J. Ind. Microbiol. Biotechnol.* 39, 547–555. doi: 10.1007/s10295-011-1067-8
- Malgas, S., van Dyk, J. S., and Pletschke, B. I. (2015). A review of the enzymatic hydrolysis of mannans and synergistic interactions between β -mannanase, β -mannosidase and α -galactosidase. *World J. Microbiol. Biotechnol.* 31, 1167–1175. doi: 10.1007/s11274-015-1878-2
- Mohamad, S. N., Ramanan, R. N., Mohamad, R., and Ariff, A. B. (2011). Improved mannan-degrading enzymes' production by *Aspergillus niger* through medium optimization. *New Biotechnol.* 28, 146–152. doi: 10.1016/j.nbt.2010.10.008
- Mojsov, K. (2011). "Application of enzymes in the textile industry: a review," in *Proceedings of the II International Congress "Engineering, Ecology and Materials in the Processing Industry"*, (Jahorina), 230–239.
- Morreira, L. (2008). An overview of mannan structure and mannan-degrading enzyme systems. *Appl. Microbiol. Biotechnol.* 79, 165–178. doi: 10.1007/s00253-008-1423-4
- Mudgil, D., Barak, S., and Khatkar, B. S. (2014). Guar gum: processing, properties and food applications—a review. *J. Food Sci. Technol.* 51, 409–418. doi: 10.1007/s13197-011-0522-x
- Nagar, S., Mittal, A., and Gupta, V. K. (2012). Enzymatic clarification of fruit juices (apple, pineapple, and tomato) using purified *Bacillus pumilus* SV-85S xylanase. *Biotechnol. Bioprocess Eng.* 17, 1165–1175. doi: 10.1007/s12257-012-0375-9
- Olaniyi, O. O., Igbe, F. O., and Ekundayo, T. C. (2013). Optimization studies on mannanase production by *Trichosporonoides oedocephalis* in submerged state fermentation. *J. Biotechnol. Pharmaceutical Res.* 4, 110–116.
- Ozaki, K., Fujii, S., and Hayashi, M. (2007). Effect of dietary mannoooligosaccharides on the immune system of ovalbumin-sensitized mice. *J. Health Sci.* 53, 766–770. doi: 10.1248/jhs.53.766
- Pangsri, P., and Pangsri, P. (2017). Mannanase enzyme from *Bacillus subtilis* P2-5 with waste management. *Energy Procedia* 138, 343–347. doi: 10.1016/j.egypro.2017.10.136

- Patel, K., and Dudhagara, P. (2020). Compatibility testing and enhancing the pulp bleaching process by hydrolases of the newly isolated thermophilic *Isotericola variabilis* strain UD-6. *Biocatalysis Biotransf.* 38, 144–160. doi: 10.1080/10242422.2019.1711067
- Pradeep, G., Cho, S. S., Choi, Y. H., Choi, Y. S., Jee, J.-P., Seong, C. N., et al. (2016). An extremely alkaline mannanase from *Streptomyces* sp. CS428 hydrolyzes galactomannan producing series of mannooligosaccharides. *World J. Microbiol. Biotechnol.* 32:84.
- Rahmani, N., Kashiwagi, N., Lee, J., Niimi-Nakamura, S., Matsumoto, H., Kahar, P., et al. (2017). Mannan endo-1, 4- β -mannosidase from *Kitasatospora* sp. isolated in Indonesia and its potential for production of mannooligosaccharides from mannan polymers. *AMB Exp.* 7, 1–11.
- Raita, M., Ibenegbu, C., Champreda, V., and Leak, D. J. (2016). Production of ethanol by thermophilic oligosaccharide utilising *Geobacillus thermoglucosidarius* TM242 using palm kernel cake as a renewable feedstock. *Biomass Bio.* 95, 45–54.
- Ramachandran, P., Zhao, Z., Singh, R., Dhiman, S. S., Choi, J.-H., Kim, D., et al. (2014). Characterization of a β -1, 4-mannanase from a newly isolated strain of *Pholiota adiposa* and its application for biomass pretreatment. *Bioproc. Biosyst. Eng.* 37, 1817–1824. doi: 10.1007/s00449-014-1156-y
- Regmi, S., Pradeep, G., Choi, Y. H., Choi, Y. S., Choi, J. E., Cho, S. S., et al. (2016). A multi-tolerant low molecular weight mannanase from *Bacillus* sp. CSB39 and its compatibility as an industrial biocatalyst. *Enzyme Microb. Technol.* 92, 76–85. doi: 10.1016/j.enzmictec.2016.06.018
- Regmi, S., Yoo, H. Y., Choi, Y. H., Choi, Y. S., Yoo, J. C., and Kim, S. W. (2017). Prospects for bio-industrial application of an extremely alkaline mannanase from *Bacillus subtilis* subsp. inaquosorum CSB31. *Biotechnol. J.* 12:1700113. doi: 10.1002/biot.201700113
- Salinardi, T. C., Rubin, K. H., Black, R. M., and St-Onge, M.-P. (2010). Coffee mannooligosaccharides, consumed as part of a free-living, weight-maintaining diet, increase the proportional reduction in body volume in overweight men. *J. Nutr.* 140, 1943–1948. doi: 10.3945/jn.110.128207
- Scheller, H. V., and Ulvskov, P. (2010). Hemicelluloses. *Annu. Rev. Plant Biol.* 61, 263–289.
- Seesom, W., Thongket, P., Yamamoto, T., Takenaka, S., Sakamoto, T., and Sukhumsirichart, W. (2017). Purification, characterization, and overexpression of an endo-1, 4- β -mannanase from thermotolerant *Bacillus* sp. SWU60. *World J. Microbiol. Biotechnol.* 33:53. doi: 10.1007/s11274-017-2224-7
- Sharma, H. P., Patel, H., and Sharma, S. (2014). Enzymatic extraction and clarification of juice from various fruits—a review. *Trends Post Harvest Technol.* 2:56.
- Sharma, K., Dhillon, A., and Goyal, A. (2018). Insights into structure and reaction mechanism of β -mannanases. *Curr. Protein Pept. Sci.* 19, 34–47.
- Shukor, H., Abdeslahian, P., Al-Shorgani, N. K. N., Hamid, A. A., Rahman, N. A., and Kalil, M. S. (2016). Enhanced mannan-derived fermentable sugars of palm kernel cake by mannanase-catalyzed hydrolysis for production of biobutanol. *Bioresour. Technol.* 218, 257–264. doi: 10.1016/j.biortech.2016.06.084
- Singh, S., Singh, G., Khatri, M., Kaur, A., and Arya, S. K. (2019). Thermo and alkali stable β -mannanase: characterization and application for removal of food (mannans based) stain. *Int. J. Biol. Macromol.* 134, 536–546. doi: 10.1016/j.ijbiomac.2019.05.067
- Songsiririthigul, C., Lapboonrueng, S., Roytrakul, S., Haltrich, D., and Yamabhai, M. (2011). Crystallization and preliminary crystallographic analysis of β -mannanase from *Bacillus licheniformis*. *Acta Cryst. Sec. F Struct. Biol. Cryst. Commun.* 67, 217–220. doi: 10.1107/s1744309110049067
- Soni, H., Rawat, H. K., Pletschke, B. I., and Kango, N. (2016). Purification and characterization of β -mannanase from *Aspergillus terreus* and its applicability in depolymerization of mannans and saccharification of lignocellulosic biomass. *3 Biotech* 6:136. doi: 10.1007/s13205-016-0454-2
- Srivastava, P. K., and Kapoor, M. (2014). Cost-effective endo-mannanase from *Bacillus* sp. CFR1601 and its application in generation of oligosaccharides from guar gum and as detergent additive. *Preparat. Biochem. Biotechnol.* 44, 392–417. doi: 10.1080/10826068.2013.833108
- Srivastava, P. K., and Kapoor, M. (2016). Metal-dependent thermal stability of recombinant endo-mannanase (ManB-1601) belonging to family GH 26 from *Bacillus* sp. CFR1601. *Enzyme Microb. Technol.* 84, 41–49. doi: 10.1016/j.enzmictec.2015.12.010
- Srivastava, P. K., and Kapoor, M. (2017). Production, properties, and applications of endo- β -mannanases. *Biotechnol. Adv.* 35, 1–19. doi: 10.1016/j.biotechadv.2016.11.001
- St-Onge, M. P., Salinardi, T., Herron-Rubin, K., and Black, R. M. (2012). A weight-loss diet including coffee-derived mannooligosaccharides enhances adipose tissue loss in overweight men but not women. *Obesity* 20, 343–348. doi: 10.1038/oby.2011.289
- Sunna, A. (2010). Modular organisation and functional analysis of dissected modular β -mannanase CsMan26 from *Caldicellulosiruptor* Rt8B. *4. Appl. Microbiol. Biotechnol.* 86, 189–200. doi: 10.1007/s00253-009-2242-y
- Tailford, L. E., Ducros, V. M.-A., Flint, J. E., Roberts, S. M., Morland, C., Zechel, D. L., et al. (2009). Understanding how diverse β -mannanases recognize heterogeneous substrates. *Biochemistry* 48, 7009–7018. doi: 10.1021/bi900515d
- Tang, C.-D., Shi, H.-L., Tang, Q.-H., Zhou, J.-S., Yao, L.-G., Jiao, Z.-J., et al. (2016). Genome mining and motif truncation of glycoside hydrolase family 5 endo- β -1, 4-mannanase encoded by *Aspergillus oryzae* RIB40 for potential konjac flour hydrolysis or feed additive. *Enzyme Microb. Technol.* 93, 99–104. doi: 10.1016/j.enzmictec.2016.08.003
- Tang, S.-z., Lin, F.-l., Zheng, J., and Zhou, H.-b. (2019). Effect of gene dosage and incubation temperature on production of β -mannanase by recombinant *Pichia pastoris*. *J. Cent. South Univ.* 26, 184–195. doi: 10.1007/s21771-019-3992-z
- Thombare, N., Jha, U., Mishra, S., and Siddiqui, M. (2016). Guar gum as a promising starting material for diverse applications: a review. *Int. J. Biol. Macromol.* 88, 361–372. doi: 10.1016/j.ijbiomac.2016.04.001
- Titapoka, S., Keawsompong, S., Haltrich, D., and Nitisinprasert, S. (2008). Selection and characterization of mannanase-producing bacteria useful for the formation of prebiotic manno-oligosaccharides from copra meal. *World J. Microbiol. Biotechnol.* 24, 1425–1433. doi: 10.1007/s11274-007-9627-9
- Tuntrakool, P., and Keawsompong, S. (2018). Kinetic properties analysis of beta-mannanase from *Klebsiella oxytoca* KUB-CW2-3 expressed in *Escherichia coli*. *Pro. Exp. Purif.* 146, 23–26. doi: 10.1016/j.pep.2018.01.009
- Vijayalaxmi, S., Prakash, P., Jayalakshmi, S., Mulimani, V., and Sreeramulu, K. (2013). Production of extremely alkaliphilic, halotolerant, detergent, and thermostable mannanase by the free and immobilized cells of *Bacillus halodurans* PPKS-2. purification and characterization. *Appl. Biochem. Biotechnol.* 171, 382–395. doi: 10.1007/s12010-013-0333-9
- von Freiesleben, P., Spodsborg, N., Blicher, T. H., Anderson, L., Jørgensen, H., Ståhlbrand, H., et al. (2016). An *Aspergillus nidulans* GH26 endo- β -mannanase with a novel degradation pattern on highly substituted galactomannans. *Enzyme Microb. Technol.* 83, 68–77. doi: 10.1016/j.enzmictec.2015.10.011
- Wang, C., Zhang, J., Wang, Y., Niu, C., Ma, R., Wang, Y., et al. (2016). Biochemical characterization of an acidophilic β -mannanase from *Gloeophyllum trabeum* CBS900.73 with significant transglycosylation activity and feed digesting ability. *Food chem.* 197, 474–481. doi: 10.1016/j.foodchem.2015.10.115
- Wang, X.-C., You, S.-P., Zhang, J.-X., Dai, Y.-M., Zhang, C.-Y., Qi, W., et al. (2018). Rational design of a thermophilic β -mannanase from *Bacillus subtilis* TJ-102 to improve its thermostability. *Enzyme Microb. Technol.* 118, 50–56. doi: 10.1016/j.enzmictec.2018.07.005
- Wang, Y., Azhar, S., Gandini, R., Divne, C., Ezcurra, I., and Aspeborg, H. (2015). Biochemical characterization of the novel endo- β -mannanase AtMan5-2 from *Arabidopsis thaliana*. *Plant Sci.* 241, 151–163. doi: 10.1016/j.plantsci.2015.10.002
- Xie, J., He, Z., Wang, Z., Wang, B., and Pan, L. (2019). Efficient expression of a novel thermophilic fungal β -mannosidase from *Lichtheimia ramosa* with broad-range pH stability and its synergistic hydrolysis of locust bean gum. *J. Biosci. Bioeng.* 128, 416–423. doi: 10.1016/j.jbiosc.2019.04.007
- Xu, M., Zhang, R., Liu, X., Shi, J., Xu, Z., and Rao, Z. (2013). Improving the acidic stability of a β -mannanase from *Bacillus subtilis* by site-directed mutagenesis. *Process Biochem.* 48, 1166–1173. doi: 10.1016/j.procbio.2013.06.014
- Yan, X.-X., An, X.-M., Gui, L.-L., and Liang, D.-C. (2008). From structure to function: insights into the catalytic substrate specificity and thermostability displayed by *Bacillus subtilis* mannanase BCman. *J. Mol. Biol.* 379, 535–544. doi: 10.1016/j.jmb.2008.03.068
- Yang, H., Shi, P., Lu, H., Wang, H., Luo, H., Huang, H., et al. (2015). A thermophilic β -mannanase from *Neosartorya fischeri* P1 with broad pH stability and significant hydrolysis ability of various mannan polymers. *Food Chem.* 173, 283–289. doi: 10.1016/j.foodchem.2014.10.022

- Yang, M., Cai, J., Wang, C., Du, X., and Lin, J. (2017). Characterization of endo- β -mannanase from *Enterobacter ludwigii* MY271 and application in pulp industry. *Bioprocess Biosyst. Eng.* 40, 35–43. doi: 10.1007/s00449-016-1672-z
- Yatmaz, E., Karahalil, E., Germec, M., Oziyici, H., Karhan, M., Duruksu, G., et al. (2016). Enhanced β -mannanase production from alternative sources by recombinant *Aspergillus sojae*. *Acta Alimentaria* 45, 371–379. doi: 10.1556/066.2016.45.3.8
- Yeoman, C. J., Han, Y., Dodd, D., Schroeder, C. M., Mackie, R. I., and Cann, I. K. (2010). Thermostable enzymes as biocatalysts in the biofuel industry. *Adv. Appl. Microbiol.* 70, 1–55. doi: 10.1016/s0065-2164(10)70001-0
- Yoo, H. Y., Pradeep, G., Lee, S. K., Park, D. H., Cho, S. S., Choi, Y. H., et al. (2015). Understanding β -mannanase from *Streptomyces* sp. CS147 and its potential application in lignocellulose based biorefining. *Biotechnol. J.* 10, 1894–1902. doi: 10.1002/biot.201500150
- Yopi, Rahmani, N., Jannah, A. M., Nugraha, I. P., and Ramadana, R. M. (2017). “Production of mannanase from *Bacillus Subtilis* LBF-005 and its potential for manno-oligosaccharides production,” in *Proceedings of the AIP Conference Proceedings*, (College Park, MD: AIP Publishing LLC), 020022.
- You, J., Liu, J.-F., Yang, S.-Z., and Mu, B.-Z. (2016). Low-temperature-active and salt-tolerant β -mannanase from a newly isolated *Enterobacter* sp. strain N18. *J. Biosci. Bioeng.* 121, 140–146. doi: 10.1016/j.jbiosc.2015.06.001
- Zang, H., Xie, S., Wu, H., Wang, W., Shao, X., Wu, L., et al. (2015). A novel thermostable GH5_7 β -mannanase from *Bacillus pumilus* GBSW19 and its application in manno-oligosaccharides (MOS) production. *Enzyme Microb. Technol.* 78, 1–9. doi: 10.1016/j.enzmictec.2015.06.007
- Zhang, B., Davenport, A. H., Whipple, L., Urbina, H., Barrett, K., Wall, M., et al. (2013). A Superior, high-performance enzyme for breaking borate crosslinked fracturing fluids under extreme well conditions. *SPE Production Operations* 28, 210–216. doi: 10.2118/160033-pa
- Zhang, C. (2019). *Lignocellulosic Ethanol: Technology and Economics, Alcohol Fuels-Current Technologies and Future Prospect*. London: IntechOpen.
- Zhang, H., and Sang, Q. (2015). Production and extraction optimization of xylanase and β -mannanase by *Penicillium chrysogenum* QML-2 and primary application in saccharification of corn cob. *Biochem. Eng. J.* 97, 101–110. doi: 10.1016/j.bej.2015.02.014
- Zhang, R., Song, Z., Wu, Q., Zhou, J., Li, J., Mu, Y., et al. (2016). A novel surfactant-, NaCl-, and protease-tolerant β -mannanase from *Bacillus* sp. HJ14. *Folia Microbiol.* 61, 233–242. doi: 10.1007/s12223-015-0430-y
- Zhang, W., Liu, Z., Zhou, S., Mou, H., and Zhang, R. (2019). Cloning and expression of a β -mannanase gene from *Bacillus* sp. MK-2 and its directed evolution by random mutagenesis. *Enzyme Microb. Technol.* 124, 70–78. doi: 10.1016/j.enzmictec.2019.02.003
- Zhao, D., Wang, Y., Na, J., Ping, W., and Ge, J. (2019). The response surface optimization of β -mannanase produced by *Lactobacillus casei* HDS-01 and its potential in juice clarification. *Preparat. Biochem. Biotechnol.* 49, 202–207. doi: 10.1080/10826068.2019.1566151
- Zhao, D., Zhang, X., Wang, Y., Na, J., Ping, W., and Ge, J. (2020). Purification, biochemical and secondary structural characterisation of β -mannanase from *Lactobacillus casei* HDS-01 and juice clarification potential. *Int. J. Biol. Macromol.* 154, 826–834. doi: 10.1016/j.ijbiomac.2020.03.157
- Zhao, Y., Zhang, Y., Cao, Y., Qi, J., Mao, L., Xue, Y., et al. (2011). Structural analysis of alkaline β -mannanase from alkaliphilic *Bacillus* sp. N16-5: implications for adaptation to alkaline conditions. *PLoS One* 6:e14608. doi: 10.1371/journal.pone.0014608
- Zhou, C., Xue, Y., and Ma, Y. (2018). Characterization and high-efficiency secreted expression in *Bacillus subtilis* of a thermo-alkaline β -mannanase from an alkaliphilic *Bacillus clausii* strain S10. *Microb. Cell Fact.* 17:124. doi: 10.1186/s12934-018-0973-0
- Zhu, M., Zhang, L., Yang, F., Cha, Y., Li, S., Zhuo, M., et al. (2019). A Recombinant β -Mannanase from *Thermoanaerobacterium aotearoense* SCUT27: biochemical characterization and its thermostability improvement. *J. Agric. Food Chem.* 68, 818–825. doi: 10.1021/acs.jafc.9b06246

Conflict of Interest: The authors declare that the research was conducted in the absence of any commercial or financial relationships that could be construed as a potential conflict of interest.

Copyright © 2020 Dawood and Ma. This is an open-access article distributed under the terms of the Creative Commons Attribution License (CC BY). The use, distribution or reproduction in other forums is permitted, provided the original author(s) and the copyright owner(s) are credited and that the original publication in this journal is cited, in accordance with accepted academic practice. No use, distribution or reproduction is permitted which does not comply with these terms.



High Epoxidation Yields of Vegetable Oil Hydrolyzates and Methyl Esters by Selected Fungal Peroxygenases

Alejandro González-Benjumea¹, Gisela Marques¹, Owik M. Herold-Majumdar², Jan Kiebig³, Katrin Scheibner³, José C. del Río¹, Angel T. Martínez⁴ and Ana Gutiérrez^{1*}

¹ Instituto de Recursos Naturales y Agrobiología de Sevilla (IRNAS), CSIC, Seville, Spain, ² Novozymes A/S, Bagsvaerd, Denmark, ³ JenaBios GmbH, Jena, Germany, ⁴ Centro de Investigaciones Biológicas Margarita Salas (CIB), CSIC, Madrid, Spain

OPEN ACCESS

Edited by:

Giovanni Sanna,
University of Naples Federico II, Italy

Reviewed by:

Rosa Turco,
University of Naples Federico II, Italy
Chris Allen,
Queen's University Belfast,
United Kingdom

*Correspondence:

Ana Gutiérrez
anagu@irnase.csic.es

Specialty section:

This article was submitted to
Industrial Biotechnology,
a section of the journal
Frontiers in Bioengineering and
Biotechnology

Received: 13 September 2020

Accepted: 01 December 2020

Published: 05 January 2021

Citation:

González-Benjumea A,
Marques G, Herold-Majumdar OM,
Kiebig J, Scheibner K, del Río JC,
Martínez AT and Gutiérrez A (2021)
High Epoxidation Yields of Vegetable
Oil Hydrolyzates and Methyl Esters by
Selected Fungal Peroxygenases.
Front. Bioeng. Biotechnol. 8:605854.
doi: 10.3389/fbioe.2020.605854

Epoxides of vegetable oils and free and methylated fatty acids are of interest for several industrial applications. In the present work, refined rapeseed, sunflower, soybean, and linseed oils, with very different profiles of mono- and poly-unsaturated fatty acids, were saponified and transesterified, and the products treated with wild unspecific peroxygenases (UPOs, EC 1.11.2.1) from the ascomycete *Chaetomium globosum* (Cg/UPO) and the basidiomycete *Marasmius rotula* (MroUPO), as well as with recombinant UPO of the ascomycete *Humicola insolens* (rHinUPO), as an alternative to chemical epoxidation that is non-selective and requires strongly acidic conditions. The three enzymes were able of converting the free fatty acids and the methyl esters from the oils into epoxide derivatives, although significant differences in the oxygenation selectivities were observed between them. While Cg/UPO selectively produced “pure” epoxides (monoepoxides and/or diepoxides), MroUPO formed also hydroxylated derivatives of these epoxides, especially in the case of the oil hydrolyzates. Hydroxylated derivatives of non-epoxidized unsaturated fatty acids were practically absent in all cases, due to the preference of the three UPOs selected for this study to form the epoxides. Moreover, rHinUPO, in addition to forming monoepoxides and diepoxides of oleic and linoleic acid (and their methyl esters), respectively, like the other two UPOs, was capable of yielding the triepoxides of α -linolenic acid and its methyl ester. These enzymes appear as promising biocatalysts for the environmentally friendly production of reactive fatty-acid epoxides given their self-sufficient monooxygenase activity with selectivity toward epoxidation, and the ability to epoxidize, not only isolated pure fatty acids, but also complex mixtures from oil hydrolysis or transesterification containing different combinations of unsaturated (and saturated) fatty acids.

Keywords: epoxidation, vegetable oils, enzymes, peroxygenases, polyunsaturated fatty acids, fatty acid methyl esters, complex lipid mixtures, biocatalysis

INTRODUCTION

In the search for sustainable chemistry, considerable attention is being paid to renewable feedstocks and, among these, vegetable oils represent a great proportion of the current consumption by the chemical industry. However, the chemical possibilities of renewable oils and fats are still very far from being fully exploited. Indeed, most of oleochemical reactions have been those occurring at the

fatty acid carboxy group, while only a very minor proportion of them have involved transformations of the alkyl chain. Nevertheless, the latter reactions have great potential for extending the range of compounds available from oils and fats.

In this context, the epoxidation of vegetable oils is being studied due to the current and potential commercial applications of the products obtained. Oil epoxides are used as stabilizers and plasticizers (Kandula et al., 2014; Jia et al., 2016), and are also promising intermediates for the production of polyols (Zhang et al., 2014a), polyurethanes (Zhang et al., 2014b), biolubricants (Borugadda and Goud, 2014), and epoxy resins (Xia and Larock, 2010), among other uses. Moreover, by simple industrial procedures, fatty acids are available from vegetable oils in such purity that they may be used for further chemical transformations. Their conversion to fatty-acid methyl esters (FAMES) is a well-known application, largely investigated for biodiesel production. Moreover, unsaturated fatty acids and FAMES can be further epoxidized, and used in industrial syntheses of chemicals and intermediates.

Industrial epoxidation of unsaturated fatty-acid compounds is generally performed by the Prileschajew (1909) reaction via percarboxylic acids. However, this method, which includes strong mineral acids as catalysts for the “*in situ*” generation of peracids, suffers from several drawbacks such as the low selectivity for epoxide formation, due to the oxirane ring opening in acidic medium, the corrosive nature of acids, and the unstable character of peracids (Danov et al., 2017). New methods have been investigated aimed at searching an alternative, such as the chemo-enzymatic synthesis with lipases catalyzing carboxylic acid reaction with H₂O₂ yielding the reactive peracids (Björkling et al., 1992; Tiran et al., 2008). On the other hand, direct enzymatic processes emerge as a solution for more selective and environmentally friendly epoxidation of unsaturated lipids. Several enzymes are known to catalyze epoxidation directly, such as some cytochrome P450 monooxygenases (P450), diiron-center oxygenases, and plant peroxygenases (Ruettinger and Fulco, 1981; Oliw, 1994; Piazza et al., 2003). However, they often present some drawbacks, such as their intracellular nature and frequent association to membranes (in the case of plant peroxygenases and some P450s), and the requirement for costly cosubstrates or FAD-containing auxiliary enzymes or domains (in the case of P450s and diiron oxygenases).

Phylogenetically distant fungal unspecific peroxygenases (UPOs, EC 1.11.2.1) are related to P450s in the sense that they also contain a heme prosthetic group coordinated by a cysteine ligand, but they do not depend on the reductive activation of molecular oxygen but catalyze the transfer of an oxygen atom from peroxides to reducing substrates (Hofrichter et al., 2015). The first UPO was described in the basidiomycete *Agrocybe aegerita* (AaeUPO) (Ullrich et al., 2004) and since then, UPO enzymes have been purified from other Basidiomycota and Ascomycota species such as *Coprinellus radians* (CraUPO) (Anh et al., 2007), *Marasmius rotula* (MroUPO) (Gröbe et al., 2011), and *Chaetomium globosum* (CglUPO) (Kiehist et al., 2017), which is indicative for their widespread occurrence in the fungal kingdom. In addition to these wild (i.e., non-recombinant) enzymes, there are other UPOs, e.g., from

Coprinopsis cinerea (rCciUPO) (Babot et al., 2013) and *Humicola insolens* (rHinUPO) (Kiehist et al., 2017), that are only known as recombinant proteins heterologously expressed by Novozymes A/S (Bagsvaerd, Denmark) in the mold *Aspergillus oryzae* (Landvick et al., 2016), and very recently additional UPOs heterologously expressed in *Escherichia coli* (Linde et al., 2020). Initially, UPO enzymes were shown to catalyze oxygenation reactions on aromatic compounds (Hofrichter et al., 2010), and their action on aliphatic compounds was demonstrated later (Gutiérrez et al., 2011; Peter et al., 2011).

Here, we demonstrate a promising enzymatic technology to epoxidize, under mild and environmentally friendly conditions, complex mixtures of free and methylated fatty acids from representative vegetable oils, which had been previously applied on isolated pure fatty acids (Aranda et al., 2018), for its industrial application in the production of biobased binder ingredients, in collaboration with interested companies. This includes the use of two wild UPOs, namely MroUPO and CglUPO, and recombinant rHinUPO, all of them with preferential epoxidation (vs. hydroxylation) oxygenation patterns. These and related fungal peroxygenases elude some of the limitations of other monooxygenases since they are secreted proteins, therefore far more stable, and only require H₂O₂ for activation (Wang et al., 2017; Hofrichter et al., 2020). Moreover, their recent expression as soluble and active enzymes in *Escherichia coli* is expanding the number of UPO enzymes available from related genes in sequenced genomes (Linde et al., 2020) and, simultaneously, enabling the rational design of the available UPOs as *ad hoc* biocatalysts of industrial interest, using the protein engineering tools (Carro et al., 2019; González-Benjumea et al., 2020; Municoy et al., 2020).

MATERIALS AND METHODS

Oils

Four refined vegetable oils—namely rapeseed, soybean, sunflower, and linseed oils—were provided by the Cargill company and stored at 4°C, before their saponification, transesterification and use as UPO substrates. For characterization of the whole lipid profiles (“intact” lipids), aliquots were directly treated with BSTFA [N,O-bis-(trimethylsilyl)trifluoroacetamide] at 80°C for 1 h, and analyzed by GC-MS.

Enzymes

MroUPO and CglUPO are wild enzymes isolated at JenaBios (Jena, Germany) from pure cultures of *M. rotula* DSM 25031 and *C. globosum* DSM 62110 from the German Collection of Microorganisms and Cell Cultures (Braunschweig, Germany). rHinUPO is a recombinant enzyme obtained at Novozymes A/S (Bagsvaerd, Denmark) (Kiehist et al., 2017), by heterologous expression of the cloned gene in the *A. oryzae* industrial host, using proprietary technology (Landvick et al., 2016). In all cases, the secreted enzyme was recovered after eliminating the fungal mycelium by filtration of liquid cultures, concentrated by ultrafiltration or ammonium sulfate precipitation, and purified

by successive steps of fast protein liquid chromatography (FPLC) using Äkta systems (GE Healthcare) and different ion-exchange and size-exclusion columns till apparent homogeneity. This was confirmed by sodium dodecylsulfate-polyacrylamide gel electrophoresis under denaturing conditions, and presence of the Soret band characteristic of heme-thiolate proteins at 418 nm of their UV-visible spectra. In the case of *Mro*UPO, Q-Sepharose FF, Source 15Q, and Superdex-75 columns were used, and the purified enzyme presented a molecular mass of 32 kDa (Gröbe et al., 2011). Purified *Cgl*UPO showed a molecular mass of 36 kDa (Kiebiest et al., 2017), while *rHin*UPO presents a theoretical molecular mass of 29 kDa according to its reported amino-acid sequence (Lund et al., 2013). In all cases, the enzyme concentrations were estimated from the characteristic spectrum of peroxxygenase complex with carbon monoxide (Otey, 2003).

Chemicals

All chemicals and substrates were purchased from Merck except the following *cis*-epoxide standards: 9,10-epoxyoctadecanoic acid and its methyl ester and 9,10-epoxyoctadec-12(*Z*)-enoic acid from Santa Cruz Biotechnology; 12,13-epoxyoctadec-9(*Z*)-enoic acid from Cayman; and 9,10–12,13-diepoxyoctadecanoic acid from Larodan.

Mono, di, and triepoxides from α -linolenic acid were synthesized with *meta*-chloroperbenzoic acid (in 1.3, 2.7, and 4.5 molar excess for mono-, di-, and tri-epoxides, respectively), in CHCl_3 at room temperature for 1 h. The reaction was quenched with saturated NaHCO_3 and the organic layer was recovered and dried with MgSO_4 before GC-MS analysis. Methyl esters of the above epoxy-fatty acids were synthesized using trimethylsilyldiazomethane (2 equiv) in MeOH-ether (2:3) at room temperature for 30 min. The solution was dried under N_2 and dissolved in CHCl_3 for GC-MS analysis.

Hydrolysis and Transesterification of Vegetable Oils

For achieving an accurate quantification of triglyceride fatty acids in the vegetable oils, saponification, and transesterification reactions were performed as described below, and the resulting free fatty-acid and FAMES were analyzed by GC-MS.

Saponification was carried out by preparing a suspension of the vegetable oils (100 mg) in a freshly prepared solution (1.5 mL) of 0.5 M KOH in absolute EtOH, and refluxing for 30 min. The solution was acidified to pH 3 with HCl, and extracted three times with *n*-hexane in a separation funnel. The mixture was stored at 4°C, and trimethylsilyl (TMS) derivatives were prepared by BSTFA treatment before analysis by GC-MS.

Lipid conversion into FAMES was done by preparing a suspension of the vegetable oils (100 mg) in a freshly prepared solution (4 mL) of 0.5 M NaOMe in anhydrous MeOH, and heating to 50°C for 30 min, with vigorous shaking (each 5 min). Then, the reaction was quenched with glacial AcOH (200 μL) and diluted with H_2O (8 mL). Finally, FAMES were extracted three times with *n*-hexane. The mixture was stored at 4°C, and analyzed without further derivatization. From the FAME yields obtained, and average purity (triglyceride

content) of the different vegetable oils analyzed near 99% could be estimated.

Enzymatic Reactions

For UPO reactions (1 mL) with saponified oils (0.1 mM), the saponified sample (0.1 μmol) was solved in acetone and diluted with sodium phosphate buffer, pH 5.5 (*Mro*UPO) or 7.0 (*Cgl*UPO and *rHin*UPO). After addition of the enzyme (0.1 nmol) the solution was heated to 30°C, and the reaction was triggered by adding aqueous H_2O_2 (1.25 μmol) in pulses for 30 min. Taking advantage from previous studies on fatty-acid oxygenation by UPOs (Gutiérrez et al., 2011; Babot et al., 2013; Aranda et al., 2018; Carro et al., 2019; González-Benjumea et al., 2020; Municoy et al., 2020), acetone at a concentration of 20% (v/v) was used as cosolvent. The reactions with transesterified oils were carried out following a similar procedure for 2 h. The enzyme (0.5 or 1 nmol) was added in a split dose (at the beginning and after 1 h) to maximize the conversion, and the solution was heated to 40°C. H_2O_2 (1.25–5 μmol) was added in pulses, although a syringe pump was also tested. The acetone concentration was 40% (v/v). Control experiments in which saponified and transesterified oil samples were treated under the same conditions (including H_2O_2), but without enzyme, were also performed. In all cases, the products were extracted with methyl *tert*-butyl ether (MTBE) and dried under N_2 . BSTFA was used to prepare TMS derivatives that were analyzed by GC-MS.

In scaling-up experiments of enzymatic epoxidation of saponified sunflower oil, the substrate concentration could be increased up to 30 mM (buffer pH 7.0 and 40% acetone) and the enzyme dose was 30 μM , which means the same substrate/enzyme ratio previously used. The concentration of H_2O_2 was 234.0 mM (5.5 equiv) for *Cgl*UPO and 93.5 mM (2.1 equiv) for *Mro*UPO and *rHin*UPO. In all cases, the oxidant was slowly added with a syringe pump and the reaction was heated to 30°C. The reaction time was 2.5 h with *Mro*UPO and 1 h with *Cgl*UPO and *rHin*UPO. The products were recovered with MTBE and dried in a rotary evaporator. Reaction volumes up to 100 mL were tested with *Mro*UPO. Because of the optimum pH for *Mro*UPO, the scale-up was also performed at pH 5.5. In this case, the maximal substrate loading was 4 mM (55% acetone), the enzyme dose was 4 μM and the oxidant was 12.5 mM (2.1 equiv) with identical reaction time.

All the enzymatic reactions were performed in duplicate, or triplicate if required, and the dispersion of the results after the GC-MS analysis described below, was always below 10% of the corresponding mean values. Fatty-acid conversions were calculated by comparing the remaining (unreacted) substrate in the UPO reactions with the same substrate in the control experiments. Epoxidation yields were calculated taking into account the products obtained for each substrate and their epoxidation degree. Then, the result were corrected according to the conversion (see above) calculated for each substrate. Selectivities (between family products or diastereomers) were calculated taking into account the product/s of interest, with respect to all the products formed from one initial substrate.

GC-MS Analyses

The GC-MS analyses of “intact” lipids were performed on a Star 3400 gas chromatograph (Varian, Walnut Creek, CA, United States) equipped with a capillary column (DB-5HT, 12 m \times 0.25 mm internal diameter, 0.1 μ m film thickness; J&W Scientific, Santa Clara, CA, United States), and coupled with an ion-trap detector (Varian Saturn 400). Helium was used as carrier gas at a rate of 2.0 mL min⁻¹. The injector was set to 120°C during the injection and, 0.1 min after it was programmed to 380°C at a rate of 200°C min⁻¹ and held for 10 min. The oven was heated from 120°C (1 min) to 380°C (5 min) at 10°C min⁻¹, and the transfer line was set to 300°C. Compounds were identified by mass fragmentography and by mass spectra comparison with those of the Wiley and NIST libraries, and with authentic standards. Quantification was accomplished from total-ion (or characteristic-ion) peak areas, using molar response factors of the same or similar compounds. For quantification of triglyceride conversion, trilinolein was used in a concentration range between 0.01 and 0.8 mg·mL⁻¹ to elaborate calibration curves.

The GC-MS analyses of fatty acids were performed with a Shimadzu GC-MS QP2010 Ultra equipment, using the same capillary column mentioned above but with longer length (30 m). Helium was used at a rate of 0.83 mL min⁻¹. The injection was performed at 300°C, the oven was heated from 120°C (1 min) to 300°C (15 min) at 5°C min⁻¹, and the transfer line was kept at 300°C. Compounds were identified and quantified as described above. Methyl palmitate, methyl stearate, methyl oleate, methyl linoleate, and methyl α -linolenate were used in a concentration range between 0.004 and 0.05 mg mL⁻¹ to obtain calibration curves.

RESULTS AND DISCUSSION

Chemical Characterization of Whole Oils, Oil Hydrolyzates, and Methyl Esters

Samples of rapeseed, soybean, sunflower, and linseed vegetable oils provided by Cargill were first analyzed by GC-MS as whole oils (i.e., without prior hydrolysis or transesterification). As shown under the chromatographic conditions used (12 m columns and high temperature programs), the refined oils consisted exclusively of triglycerides. The composition of each of them, determined by mass fragmentography using characteristic single ions (profiles not shown), revealed the presence of triglycerides containing one (T1), two (T2), and three unsaturated (T3) fatty acids (**Supplementary Figure S1**). However, quantification of the different triglycerides that coelute in the same peak is not possible under these conditions.

With the aim of achieving an accurate quantification of fatty acids in triglycerides, saponification and transesterification of vegetable oils were performed, and the fatty-acid and FAME patterns were analyzed by GC-MS. To ensure that oils were completely hydrolyzed/transesterified, all reactions were first analyzed under the chromatographic conditions

for analysis of “intact” lipids (using 12 m short columns) (**Supplementary Figure S2**). After checking complete reactions, quantification of individual acids and esters was performed under the corresponding chromatographic conditions (using 30 m columns).

The GC-MS analyses (**Table 1**) revealed that all oils analyzed are composed of C16 and C18 fatty acids—namely palmitic, stearic, oleic, linoleic, and α -linolenic acids—and present high purities (estimated triglyceride content near 99%) as expected for refined oils. Soybean oil has the highest abundance of saturated fatty acids and a good concentration of polyunsaturated fatty acids (PUFAs), almost exclusively linoleic acid. In contrast, rapeseed oil has a relatively low content of saturated fatty acids but also a low content on PUFAs, due to the high proportion of oleic acid. On the other hand, sunflower and linseed oils combine a moderated or low profile of saturated fatty acids and a high concentration in PUFAs. In principle, this makes them good candidates for epoxidation reactions, especially linseed oil, with high content of triunsaturated α -linolenic acid. The samples containing free fatty acids and FAMES were used as substrates for the enzymatic epoxidation reactions.

UPO Epoxidation of Fatty Acids From Hydrolysis of Different Vegetable Oils

To study the feasibility of enzymatic epoxidation, firstly, hydrolyzates from the four vegetable oils were treated with *CglUPO*, *MroUPO*, and *rHinUPO*. The conversion degree (which is generally near complete) and the percentages of the different reaction products (**Supplementary Figures S3–S5**) as well as the epoxidation yields (based on the number of unsaturations of each substrate) were evaluated (**Table 2**).

In the reactions with rapeseed oil hydrolyzate (**Supplementary Figure S6**), *CglUPO* and *MroUPO* yielded the epoxidized derivatives as main products, including monoepoxide from oleic acid and diepoxides from linoleic and α -linolenic acids. While *CglUPO* was remarkably selective toward epoxidation, and yielded the “pure” fatty-acid epoxides, *MroUPO* formed oxygenated (hydroxy, keto, and carboxy) derivatives of fatty-acid epoxides to a high extent, mainly at

TABLE 1 | Fatty acid (as methyl esters) profile (mg/100 mg oil) of refined rapeseed, sunflower, soybean, and linseed oils, and saturated (SFA), and polyunsaturated (PUFA) totals.

Fatty acids*	Vegetable oils			
	Rapeseed	Sunflower	Soybean	Linseed
C16:0	4.0	7.1	12.7	5.4
C18:0	3.2	4.1	2.1	2.1
C18:1	59.8	31.8	26.6	20.1
C18:2	22.5	56.4	56.3	16.5
C18:3	10.5	0.6	2.2	55.9
SFA	7.2	11.2	14.8	7.5
PUFA	33.0	57.0	58.5	72.4

*C16:0, palmitic acid; C18:0, stearic acid; C18:1, oleic acid; C18:2, linoleic acid; C18:3, α -linolenic acid.

TABLE 2 | Conversion (C, percentage of substrate transformed) of unsaturated fatty acids from oil hydrolyzates (0.1 mM total fatty-acid concentration) by UPOs (100 nM) and relative percentage of products, including monoepoxides, diepoxides, and triepoxides (1E, 2E, and 3E, respectively), and other oxygenated (hydroxy, keto, and carboxy) derivatives (O), and calculated epoxidation yield (EY).

Enzymes	Oils	Products (%)						EY	C
		1E	O-1E	2E	O-2E	3E	O	(%)	(%)
Rapeseed									
CglUPO	C18:1	90	9	–	–	–	1	99	> 99
	C18:2	13	–	87	–	–	–	93	> 99
	C18:3	27	–	73	–	–	–	58	> 99
MroUPO	C18:1	12	88 ^a	–	–	–	–	95	94
	C18:2	–	54	35	11	–	–	72	98
	C18:3	–	36	64	–	–	–	55	> 99
rHinUPO	C18:1	30	69	–	–	–	1	99	> 99
	C18:2	14	4	80	–	–	2	88	99
	C18:3	–	–	> 99	–	–	–	67	> 99
Sunflower									
CglUPO	C18:1	89	9	–	–	–	2	97	99
	C18:2	16	< 1	83	–	–	< 1	91	> 99
	C18:3	–	–	> 99	–	–	–	67	> 99
MroUPO	C18:1	63	32	–	–	–	5	87	92
	C18:2	8	59	22	11	–	–	60	95
	C18:3	–	–	> 99	–	–	–	67	> 99
rHinUPO	C18:1	17	83	–	–	–	–	97	97
	C18:2	2	5	91	–	–	2 ^b	94	99
	C18:3	–	–	> 99	–	–	–	67	> 99
Soybean									
CglUPO	C18:1	84	15	–	–	–	1	98	99
	C18:2	9	–	91	–	–	< 1	95	99
	C18:3	–	–	> 99	–	–	–	67	> 99
MroUPO	C18:1	46	50	–	–	–	4	90	94
	C18:2	6	57	23	14	–	–	67	98
	C18:3	–	–	> 99	–	–	–	67	> 99
rHinUPO	C18:1	13	87	–	–	–	–	< 95	95
	C18:2	< 1	4	95	–	–	1	95	98
	C18:3	8	–	92	–	–	–	64	> 99
Linseed									
CglUPO	C18:1	88 (49)	12 (51)	–	–	–	–	> 99 (97)	> 99 (97)
	C18:2	8	–	92 (> 99)	–	–	–	96 (66)	> 99 (99)
	C18:3	6	–	94 (91)	–	(9)	–	65 (70)	> 99 (> 99)
MroUPO	C18:1	57 (42)	37 (58) ^c	–	–	–	6	71 (76)	76 (76)
	C18:2	10 (1)	46 (45)	34 (41)	10 (13)	–	–	70 (75)	97 (98)
	C18:3	8 (< 1)	21 (20)	71 (80)	–	–	–	56 (58)	99 (97)
rHinUPO	C18:1	7	93 (> 99)	–	–	–	–	86 (93)	86 (93)
	C18:2	< 1	3	95 (86)	–	–	2 (14)	92 (85)	95 (99)
	C18:3	< 1	(9)	92 (32)	2 (7)	6 (52)	–	68 (81)	> 99 (> 99)

See chromatographic profiles in **Supplementary Figures S6–S9**, and chemical structures in **Supplementary Figures S3–S5**.

^aIncluding OH-1E (43%), keto-1E (34%), and COOH-1E (11%).

^bIncluding OH (1%) and keto (1%).

^cIncluding OH-1E (42%) and keto-1E (16%).

Results at 200 nM enzyme in parentheses.

the terminal (ω), subterminal ($\omega-1$), and allylic ($\omega-7$) positions of the carbon chain. The higher selectivity of CglUPO had already been shown with standards of oleic and linoleic acids (Aranda et al., 2018). On the other hand, the unique ability of MroUPO, amongst known UPOs, for oxygenating the terminal position of aliphatic compounds forming carboxylic acids

was previously reported (Olmedo et al., 2016). Curiously, the terminal oxygenation of fatty acids was only observed with oleic acid, yielding the dicarboxylic acid epoxide, and not with linoleic and α -linolenic acids. The reaction of rHinUPO with fatty acids is reported here for the first time. Its reactivity toward rapeseed oil hydrolyzate was intermediate between CglUPO

and *MroUPO*, with the proportion of epoxide and epoxidized derivatives from oleic acid being similar to those found with *MroUPO*. However, an epoxidation pattern closer to *CglUPO* was observed with linoleic and α -linolenic acids except for the diastereoselectivity of linoleic acid diepoxides where the *anti*

isomer was predominantly formed, as in the *MroUPO* reaction. Moreover, predominant hydroxylation of oleic acid in ω -6 (instead of allylic or subterminal positions) was observed. The high selectivity of the above UPOs epoxidizing oleic acid (up to 100%) differs from that of P450 (BM3) where hydroxylation

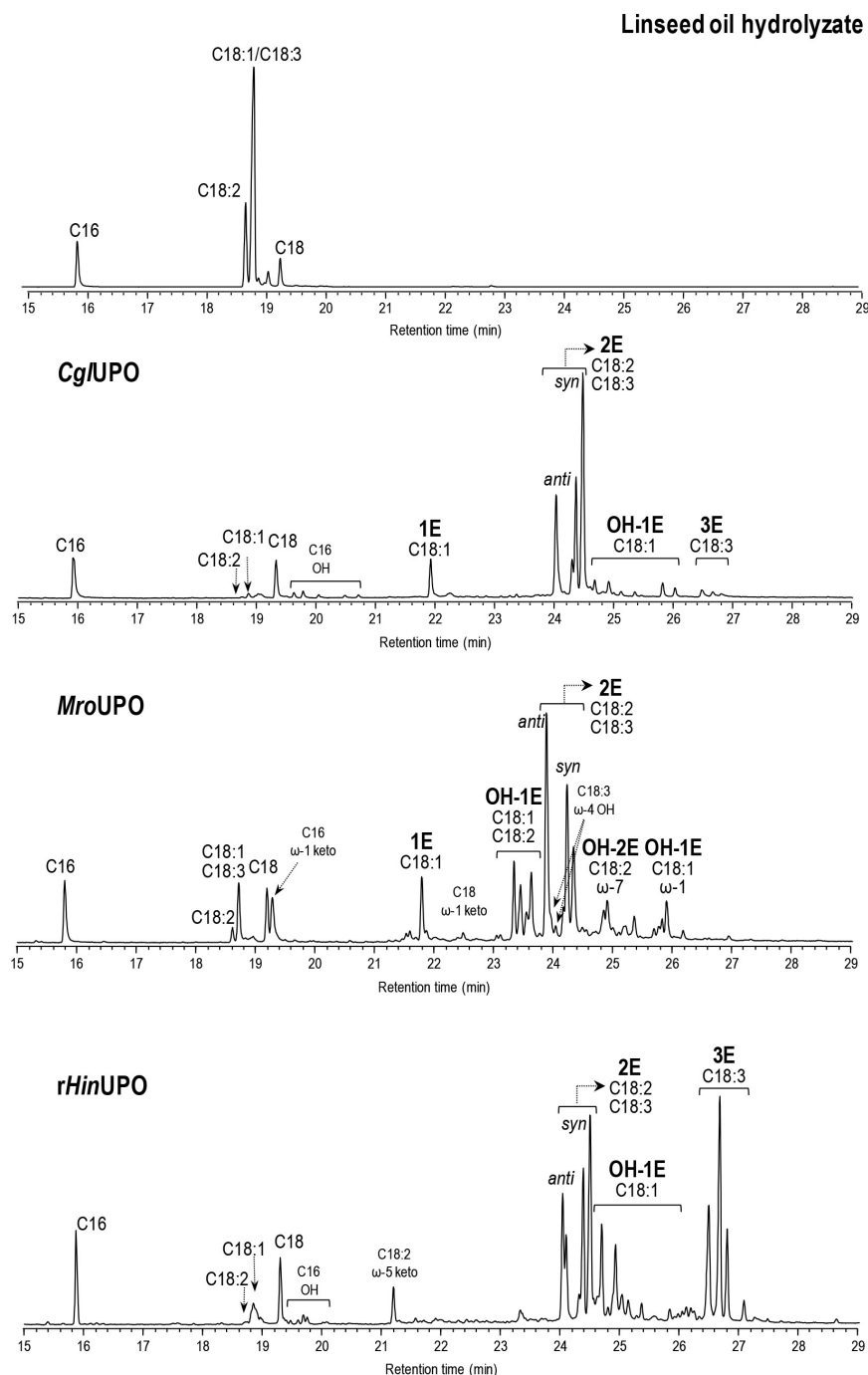


FIGURE 1 | GC-MS analysis of linseed oil hydrolyzate (0.1 mM total fatty-acid concentration) reactions with *CglUPO*, *MroUPO*, and *rHinUPO* (200 nM), showing monoepoxides, diepoxides (including *syn* and *anti* isomers from linoleic acid), and triepoxides (1E, 2E, and 3E, respectively), and other oxygenated (hydroxy, OH, and keto) derivatives. Control chromatogram is also shown (in the top). The oleic and α -linolenic peaks partially overlap under the optimized conditions for analysis of their oxygenated products, and quantitation was done using specific ions.

TABLE 3 | Conversion (C, percentage of substrate transformed) of unsaturated FAME (0.1 mM total concentration) from transesterified oils by UPO (0.5 μ M) and relative percentage of products (methyl esters), including mono-, di-, and tri-epoxides (1E, 2E, and 3E, respectively), and other oxygenated (hydroxy and keto) derivatives (O), and calculated epoxidation yield (EY).

Enzyme	Oils	Products (%)						EY	C
		1E	O-1E	2E	O-2E	3E	O	(%)	(%)
Rapeseed									
CglUPO	C18:1	91	9	–	–	–	< 1	92	92
	C18:2	–	7	93	–	–	–	95	98
	C18:3	–	–	> 99	–	–	–	67	> 99
MroUPO	C18:1	61	38	–	–	–	< 1	91	91
	C18:2	12	33	32	23	–	–	77	99
	C18:3	–	–	> 99	–	–	–	67	> 99
rHinUPO	C18:1	54	46	–	–	–	–	91	91
	C18:2	–	10	90	–	–	–	92	97
	C18:3	–	–	66	10	24	–	71	95
Sunflower									
CglUPO	C18:1	97	–	–	–	–	3	95	99
	C18:2	40	2	58	–	–	–	79	> 99
	C18:3	–	–	> 99	–	–	–	67	> 99
MroUPO	C18:1	79	21	–	–	–	–	82	82
	C18:2	15	21	50	14	–	–	70	85
	C18:3	–	–	> 99	–	–	–	67	> 99
rHinUPO	C18:1	54	46 ^a	–	–	–	–	> 99	> 99
	C18:2	–	14	86	–	–	–	93	> 99
	C18:3	–	–	> 99	–	–	–	67	> 99
Soybean									
CglUPO	C18:1	94	3	–	–	–	3	94	97
	C18:2	22	3	75	–	–	–	87	99
	C18:3	–	–	> 99	–	–	–	67	> 99
MroUPO	C18:1	91	7	–	–	–	2	78	80
	C18:2	8	24	62	6	–	–	77	89
	C18:3	–	–	> 99	–	–	–	67	> 99
rHinUPO	C18:1	64	36 ^b	–	–	–	–	> 99	> 99
	C18:2	–	8	89	3	–	–	96	> 99
	C18:3	–	–	73	–	28	–	76	> 99
Linseed									
CglUPO	C18:1	94 (68)	5 (32)	–	–	–	1 (< 1)	94 (91)	95 (91)
	C18:2	–	6 (4)	91 (96)	–	–	3	90 (95)	96 (97)
	C18:3	3 (< 1)	6 (6)	85 (64)	–	6 (30)	< 1	65 (73)	98 (98)
MroUPO	C18:1	87 (80)	13 (20)	–	–	–	–	95 (91)	95 (91)
	C18:2	19	42 (31)	26 (24)	13 (45)	–	–	67 (82)	98 (97)
	C18:3	–	18 (6)	78 (83)	1 (2)	3 (9)	–	61 (66)	98 (97)
rHinUPO	C18:1	46 (44)	54 ^c (56) ^d	–	–	–	–	> 99 (> 99)	> 99 (> 99)
	C18:2	–	6 (7)	94 (93)	–	–	–	< 97 (97)	> 99 (> 99)
	C18:3	–	10 (10)	52 (51)	13 (11)	26 (28)	–	72 (73)	> 99 (> 99)

See chromatographic profiles in **Supplementary Figures S10–S13**, and chemical structures in **Supplementary Figures S3–S5**.

^aIncluding OH-1E (38%) and keto-1E (8%).

^bIncluding OH-1E (35%) and keto-1E (1%).

^cIncluding OH-1E (41%) and keto-1E (13%).

^dIncluding OH-1E (46%) and keto-1E (10%).

Results at 1 μ M enzyme in parentheses.

(> 97%) predominates over epoxidation (< 3%), with a substrate conversion around 80%.

In reactions with sunflower and soybean oil hydrolyzates (Table 2 and Supplementary Figures S7, S8), both with

a predominance of linoleic acid, CglUPO, and MroUPO yielded monoepoxides of oleic and linoleic acids, and diepoxides of linoleic and α -linolenic acids. Similar to the reactions with rapeseed oil hydrolyzate, CglUPO was more

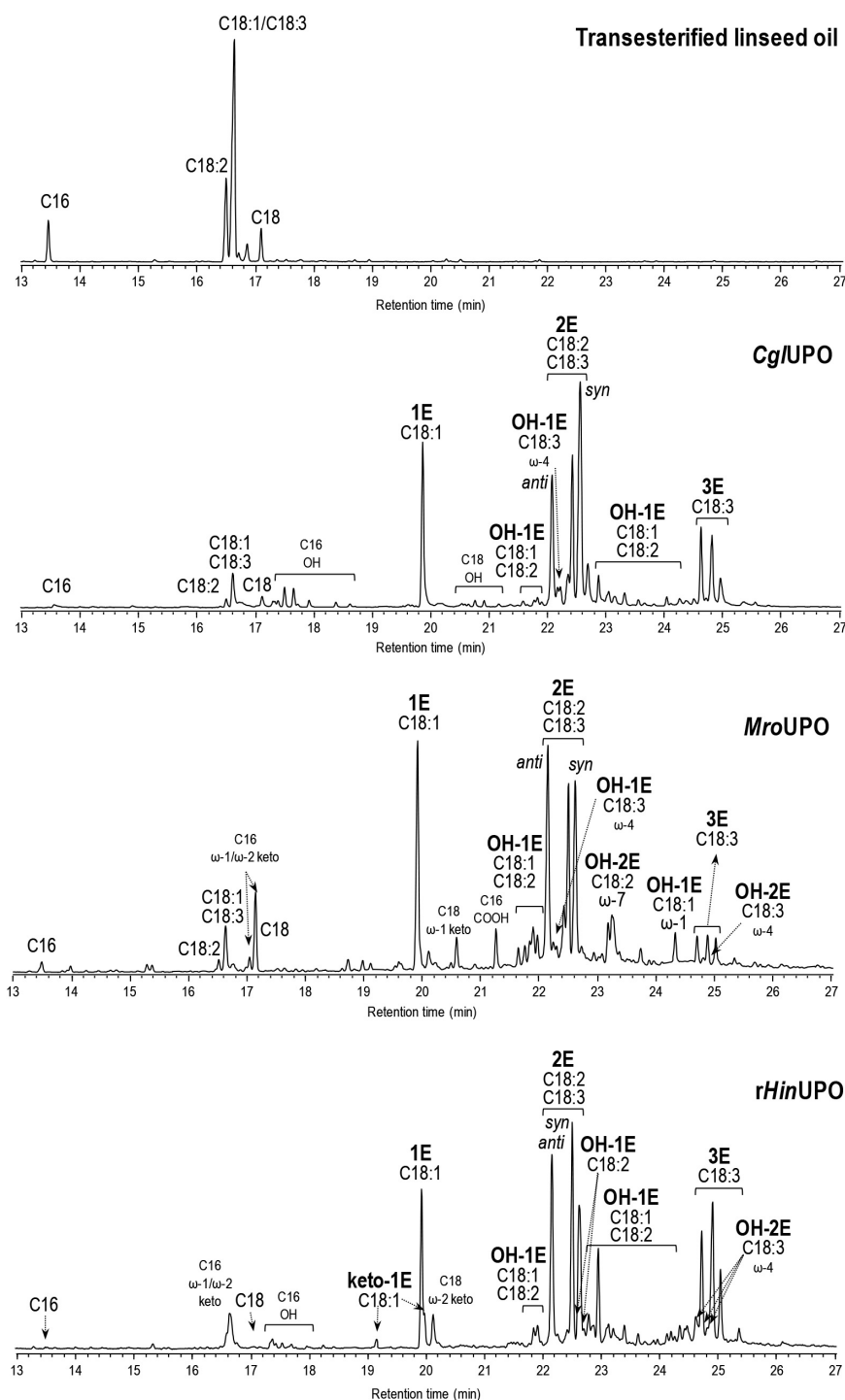


FIGURE 2 | GC-MS analysis of transesterified linseed oil (0.1 mM total fatty-acid concentration) reactions with *CglUPO*, *MroUPO*, and *rHinUPO* (1 μ M), showing monoepoxides, diepoxides (including *syn* and *anti* isomers from linoleic acid) and triepoxides (1E, 2E, and 3E, respectively), and other oxygenated (hydroxy, OH, and keto) derivatives. Control chromatogram is also shown (in the top).

selective toward “pure” epoxidation than *MroUPO*, and formed mainly the oleic acid epoxide and the linoleic acid diepoxides (with the *syn* diastereoisomer predominating). *MroUPO*, in addition to pure epoxides, formed their further

oxygenated derivatives, mainly at the allylic (ω -7) position. Respecting stereoselectivity of linoleic acid diepoxides, the *anti*-isomer was preferably formed by *MroUPO*. The *rHinUPO* reaction pattern followed that of rapeseed oil, since

oleic acid was almost fully epoxidized, and high amounts of hydroxy epoxides (especially at ω -6) were observed. Likewise, diepoxides from linoleic and α -linolenic acids predominated over monoepoxides. Moreover, with both *Mro*UPO and *rHin*UPO, the *anti*-isomer of linoleic acid diepoxides was preferably formed.

The reactions of linseed oil hydrolyzate are particularly interesting due to the high α -linolenic acid content (56%) in this oil, and the subsequent possibility of obtaining triepoxides, which are promising building blocks and cross-linking agents difficult to be synthesized (Çelik et al., 2005; Sauveplane et al., 2009). The three enzymes revealed an oxygenation pattern (Table 2 and Supplementary Figure S9) similar to that obtained with sunflower and soybean oils, including monoepoxides (preferably from oleic acid) and diepoxides (from linoleic and α -linolenic acids). Additionally, hydroxylated derivatives at ω -7 and ω -6 (by *Mro*UPO and *rHin*UPO, respectively), of epoxidized oleic acid, and hydroxylated derivatives at ω -7 of mono- and di-epoxidized linoleic acid at (by *Mro*UPO) were formed. Interestingly, some triepoxides (6% of total products) were produced by *rHin*UPO under the reaction conditions used (including 100 nM enzyme). Moreover, increasing the *rHin*UPO loading (to 200 nM) allowed to increase the triepoxide yield up to 52% (Figure 1 and Table 2), an interesting result for the industrial use of these biocatalysts that is further explored in the upscaling section included below. The formation of fatty-acid triepoxides by UPOs is reported here for the first time.

In summary, although the three UPOs showed similar epoxidation yields toward oleic acid, *Cgl*UPO yielded more epoxides from linoleic acid, and *rHin*UPO from α -linolenic acid (Table 2). Concerning saturated fatty acids, which represent a minor fraction of compounds in vegetable oils (7–15% in Table 1), they were poorly transformed by these UPOs (only up to 56%) (Supplementary Figures S6–S9). Focusing on products, partially regioselective oxygenation (at ω -1) was only observed

with *Mro*UPO, especially with palmitic acid, while unspecific hydroxylation occurred with the other two UPOs.

UPO Epoxidation of FAMES From Transesterification of Different Vegetable Oils

In addition to the hydrolyzates, the transesterified oils were also tested as substrates of the three UPOs to evaluate their epoxidation feasibility. The conversion degrees of the different FAMES and the different reaction products (Supplementary Figures S3–S5), as well as the epoxidation yields were evaluated (Table 3) revealing first that higher enzyme doses (of all UPOs) were needed to achieve similar conversion degrees to those obtained with the oil hydrolyzates.

The *Cgl*UPO behavior was similar to that observed with the oil hydrolyzates, that is, a remarkable selectivity toward “pure” epoxidation, producing the monoepoxidation of oleic acid and the diepoxidation of linoleic and α -linolenic methyl esters (Supplementary Figures S10–S13). Moreover, *Mro*UPO showed improved selectivity toward pure epoxidation of methyl oleate and linoleate (particularly in diepoxides) compared with their saponified counterparts. This led to lower amounts of hydroxylated derivatives of mono- and diepoxides, although a new hydroxylated epoxide from methyl oleate (at ω -10) was formed by *Mro*UPO. Furthermore, unlike in hydrolyzate reactions, terminal hydroxylation was not observed with FAMES. Likewise, the improved pure epoxidation of methyl oleate (compared with oleic acid) was also observed in the *rHin*UPO reactions.

Triepoxides were formed in the *rHin*UPO reactions with linseed oil FAME in higher amount (up to 26%) than with the linseed oil hydrolyzate. Interestingly, triepoxides were also observed in the *Cgl*UPO (6%) and *Mro*UPO (3%) reactions with transesterified linseed oil, and in the *rHin*UPO reactions with

TABLE 4 | Conversion (C, percentage of substrate transformed) of unsaturated fatty acids from upscaled treatment of sunflower oil hydrolyzate (30 mM total fatty-acid concentration, and pH 7 unless otherwise stated by several UPO (30 μ M), at different reaction times 1 h for *Cgl*UPO and *rHin*UPO and 2.5 h for *Mro*UPO) and relative percentage of reaction products, including mono-, di-, and tri-epoxides (1E, 2E, and 3E, respectively), and other oxygenated (hydroxyl and keto) derivatives (O), and calculated epoxidation yield (EY).

Enzymes	Fatty acids	Products (%)					EY	C
		1E	O-1E	2E	O-2E	O	(%)	(%)
<i>Cgl</i> UPO	C18:1	77	22	–	–	1	99	> 99
	C18:2	–	17 ^a	84	–	–	93	> 99
	C18:3	–	–	> 99	–	–	67	> 99
<i>Mro</i> UPO	C18:1	72 (71)	5 (16)	–	–	23 (13)	59 (87)	77 (> 99)
	C18:2	69 (35)	21 (33)	4 (22)	(3)	6 (8)	48 (59)	98 (> 99)
	C18:3	> 99	–	(> 99)	–	–	33 (67)	> 99 (> 99)
<i>rHin</i> UPO	C18:1	68	32	–	–	–	99	99
	C18:2	–	6 ^b	94	–	–	97	> 99
	C18:3	–	–	> 99	–	–	67	> 99

See chromatographic profiles in Supplementary Figure S14, and chemical structures in Supplementary Figures S3–S5.

^aIncluding OH-1E (4%) and keto-1E (13%).

^bIncluding OH-1E (3%) and keto-1E (3%).

Results with 4 mM substrate and pH 5.5, are shown in parentheses.

transesterified rapeseed and soybean oils up to 76% epoxidation yield (**Supplementary Figure S13**). With the aim of increasing the production of FAME triepoxides, reactions with twofold enzyme dose (1 μ M) were conducted with the three enzymes (**Figure 2**) and higher amounts of triepoxides were obtained with *CglUPO* (up to 30%) and *MroUPO* (up to 9%) improving their epoxidation yields (from 65 to 73%, and from 61 to 66%, respectively) (**Table 3**).

Finally, the enzyme behavior with the saturated FAMES was dissimilar (**Figure 2** and **Supplementary Figures S10–S13**). *CglUPO* and *MroUPO* reached moderate to good conversions, while *rHinUPO* achieved quantitative conversions. Regarding the reaction products, *CglUPO* gave a series of hydroxylated compounds (from ω -8 to ω -3 positions) while terminal and/or subterminal oxygenation was observed with *rHinUPO* and *MroUPO*. In the latter case, the carboxylic acid and the (ω -1) ketone predominated. With *rHinUPO*, the (ω -2/ ω -1) ketones were obtained with very high regioselectivity.

Upscaling Epoxidation of Oil Fatty Acids by UPO

Aimed to scaling-up the production of epoxidized fatty acids for industrial applicability, an attempt of increasing the substrate loading of the enzymatic reactions was performed. With this purpose, sunflower oil was selected considering economical, technical suitability, and sustainability aspects. For comparative purposes, the substrate/enzyme ratio of the previous reactions (S/E 1000) was fixed, remaining as reaction variables the substrate loading, the reaction time and the H_2O_2 dose. Besides, taking into account the pH effect on fatty-acid solubility and enzyme activity, the reactions were performed at pH 7.0, which enabled to increase the substrate concentration up to 300-fold (30 mM substrate) using 40% (v/v) of acetone. Moreover, different reaction times (1–20 h) and H_2O_2 doses (1–8 equiv per unsaturation) were assayed to attain the best conversion and epoxidation degrees.

With *MroUPO*, conversions over 98% of linoleic and α -linolenic acids, and 77% of oleic acid were reached (**Table 4** and **Supplementary Figure S14**) within 2.5 h, using of 93.5 mM H_2O_2 (i.e., 2.1 equiv per unsaturation). Under these conditions, a decrease in the epoxidation yield was observed compared with the initial reactions, together with higher amounts of hydroxylated derivatives (23 and 6% from oleic and linoleic acids, respectively), and a reduction of diepoxides. These differences are explained by the lower activity of *MroUPO* at pH 7.0 (compared with optimal pH 5.5). To check the effect of pH, we also performed the *MroUPO* reaction at pH 5.5, maintaining the other conditions. At this pH (and 4 mM substrate loading) the conversion rates were higher and close to quantitative (**Table 4**). In particular, a general increment in the epoxidation was observed for all compounds, with higher amounts of diepoxides from linoleic and α -linolenic acids.

Interestingly, in the *CglUPO* and *rHinUPO* reactions with 30 mM substrate loading (**Table 4** and **Supplementary Figure S14**), conversions over 99% of all unsaturated fatty acids were produced after 1 h with 240.0 mM (5.5 equiv) and 93.5 mM (2.1 equiv) H_2O_2 concentration, respectively (while

longer reaction times were required with *MroUPO*). The H_2O_2 concentration in these reactions was over-stoichiometric (2.1–5.5 equiv) to overcome the “catalase-like” activity produced by the reaction of peroxide-activated UPO with H_2O_2 (Karich et al., 2016). Although more hydroxy/keto epoxides were found with *CglUPO*, compared with initial conditions, the opposite happened in the *rHinUPO* reactions, in which a strong increase of the desired pure epoxide of oleic acid (from 17 to 68%) was produced.

CONCLUSION

A series of oil-producing plants of world-wide significance are available for the production of renewable lipid epoxides and other oxygenated derivatives. Commercially exploited oil seeds, such as rapeseed, soybean, sunflower, or linseed, exhibit a considerable variation in their fatty acid profiles, which makes them interesting raw materials for production of different lipid compounds. The hydrolyzated and transesterified products of the above vegetable oils were treated with three fungal UPOs to obtain epoxides. The three enzymes were capable of transforming the fatty acids and FAMES from the oils into the corresponding epoxide derivatives, although some significant differences in selectivity toward epoxidation were observed, with *CglUPO* being generally more selective. Noteworthy is the ability of these UPOs, particularly *rHinUPO*, to produce triepoxides from these samples. Therefore, UPOs appear as promising biocatalysts for the environmentally friendly production of reactive fatty-acid epoxides given their self-sufficient monooxygenase activity with high epoxidation selectivity, including recently reported enantioselectivity (in addition to strict regioselectivity) of some of their reactions (Municoy et al., 2020). However, in spite of all recent progresses in our understanding of UPO catalysis and application (Wang et al., 2017; Hofrichter et al., 2020), some difficulties are still to be solved, such as the inactivation by H_2O_2 that affects enzyme reuse. The latter could be overcome by continuous feeding low H_2O_2 concentration, or its *in situ* generation by enzymatic or chemical systems, enabling to further increase the concentration of FA substrates and final epoxide products.

DATA AVAILABILITY STATEMENT

The original contributions presented in the study are included in the article/**Supplementary Material**, further inquiries can be directed to the corresponding author/s.

AUTHOR CONTRIBUTIONS

AG-B: methodology development, oil saponification, transesterification, enzymatic treatments, product analysis, and first draft writing. GM: contribution to chemical characterization of the oils. OH-M: production of *rHinUPO*. JK and KS: production of *MroUPO* and *CglUPO*. JdR: contribution to

mass-spectrometry analyses. AM: advise in enzymatic treatment and contribution to final draft writing. AG: work design and supervision, funding acquisition, and contribution to first and final draft writing. All authors contributed to the article and approved the version submitted.

FUNDING

This work was received funding from the Bio Based Industries Joint Undertaking under the European Union's Horizon 2020 Research and Innovation Programme Under Grant Agreement No. 792063 (SusBind project, <https://susbind.eu>) and the Consejo Superior de Investigaciones Científicas projects PIE201740E071 and PIE-202040E185.

REFERENCES

- Anh, D. H., Ullrich, R., Benndorf, D., Svatos, A., Muck, A., and Hofrichter, M. (2007). The coprophilous mushroom *Coprinus radians* secretes a haloperoxidase that catalyzes aromatic peroxygenation. *Appl. Environ. Microbiol.* 73, 5477–5485. doi: 10.1128/aem.00026-07
- Aranda, C., Olmedo, A., Kiebitz, J., Scheibner, K., del Río, J. C., Martínez, A. T., et al. (2018). Selective epoxidation of fatty acids and fatty acid methyl esters by fungal peroxygenases. *ChemCatChem* 10, 3964–3968. doi: 10.1002/cctc.201800849
- Babot, E. D., del Río, J. C., Kalum, L., Martínez, A. T., and Gutiérrez, A. (2013). Oxyfunctionalization of aliphatic compounds by a recombinant peroxygenase from *Coprinopsis cinerea*. *Biotechnol. Bioeng.* 110:2332.
- Björklund, F., Frykman, H., Godtfredsen, S. E., and Kirk, O. (1992). Lipase catalyzed synthesis of peroxycarboxylic acids and lipase mediated oxidations. *Tetrahedron* 48, 4587–4592. doi: 10.1016/s0040-4020(01)81232-1
- Borugadda, V. B., and Goud, V. V. (2014). Epoxidation of castor oil fatty acid methyl esters (COFAME) as a lubricant base stock using heterogeneous ion-exchange resin (IR-120) as a catalyst. *Energy Proc.* 54, 75–84. doi: 10.1016/j.egypro.2014.07.249
- Carro, J., González-Benjumea, A., Fernández-Fueyo, E., Aranda, C., Guallar, V., Gutiérrez, A., et al. (2019). Modulating fatty acid epoxidation vs hydroxylation in a fungal peroxygenase. *ACS Catal.* 9, 6234–6242. doi: 10.1021/acscatal.9b01454
- Çelik, A., Sperandio, D., Speight, R. E., and Turner, N. J. (2005). Enantioselective epoxidation of linolenic acid catalysed by cytochrome P450BM3 from *Bacillus megaterium*. *Org. Biomol. Chem.* 3, 2688–2690. doi: 10.1039/b506155e
- Danov, S. M., Kazantsev, O. A., Esipovich, A. L., Belousov, A. S., Rogozhin, A. E., and Kanakov, E. A. (2017). Recent advances in the field of selective epoxidation of vegetable oils and their derivatives: a review and perspective. *Catal. Sci. Technol.* 7, 3659–3675. doi: 10.1039/c7cy00988g
- González-Benjumea, A., Carro, J., Renau, C., Linde, D., Fernández-Fueyo, E., Gutiérrez, A., et al. (2020). Fatty acid epoxidation by the new *Collariella virescens* peroxygenase and heme-channel variants. *Catal. Sci. Technol.* 10, 717–725. doi: 10.1039/c9cy02332a
- Gröbe, G., Ullrich, M., Pecyna, M., Kapturska, D., Friedrich, S., Hofrichter, M., et al. (2011). High-yield production of aromatic peroxygenase by the agaric fungus *Marasmius rotula*. *AMB Exp.* 1, 31–42. doi: 10.1186/2191-0855-1-31
- Gutiérrez, A., Babot, E. D., Ullrich, R., Hofrichter, M., Martínez, A. T., and del Río, J. C. (2011). Regioselective oxygenation of fatty acids, fatty alcohols and other aliphatic compounds by a basidiomycete heme-thiolate peroxidase. *Arch. Biochem. Biophys.* 514, 33–43. doi: 10.1016/j.abb.2011.08.001
- Hofrichter, M., Kellner, H., Herzog, R., Karich, A., Liers, C., Scheibner, K., et al. (2020). “Fungal peroxygenases: A phylogenetically old superfamily of heme enzymes with promiscuity for oxygen transfer reactions,” in *Grand Challenges in Fungal Biotechnology*, ed. H. Nevalainen (Cham: Springer), 369–403. doi: 10.1007/978-3-030-29541-7_14
- Hofrichter, M., Kellner, H., Pecyna, M. J., and Ullrich, R. (2015). Fungal unspecific peroxygenases: Heme-thiolate proteins that combine peroxidase and

ACKNOWLEDGMENTS

We thank Cargill for supplying the vegetable oils.

SUPPLEMENTARY MATERIAL

The Supplementary Material for this article can be found online at: <https://www.frontiersin.org/articles/10.3389/fbioe.2020.605854/full#supplementary-material>

Supplementary figures show: (i–ii) GC-MS analyses of intact oils and different linseed-oil samples; (iii–v) chemical structures of oleic, linoleic, and α -linolenic acids, and their oxygenated derivatives; (vi–ix) GC-MS analyses of oil-hydrolyzate reactions; (x–xiii) GC-MS analysis of transesterified-oil reactions; and (xiv) GC-MS analysis of upscaled reactions of sunflower-oil hydrolyzate.

- cytochrome P450 properties. *Adv. Exp. Med. Biol.* 851, 341–368. doi: 10.1007/978-3-319-16009-2_13
- Hofrichter, M., Ullrich, R., Pecyna, M. J., Liers, C., and Lundell, T. (2010). New and classic families of secreted fungal heme peroxidases. *Appl. Microbiol. Biotechnol.* 87, 871–897. doi: 10.1007/s00253-010-2633-0
- Jia, P., Zhang, M., Hu, L., and Zhou, Y. (2016). Green plasticizers derived from soybean oil for poly(vinyl chloride) as a renewable resource material. *Korean J. Chem. Eng.* 33, 1080–1087. doi: 10.1007/s11814-015-0213-9
- Kandula, S., Stolp, L., Grass, M., Woldt, B., and Kodali, D. (2014). Synthesis and functional evaluation of soy fatty acid methyl ester ketals as bioplasticizers. *Journal of the American Oil Chemists' Society* 91, 1967–1974. doi: 10.1007/s11746-014-2529-8
- Karich, A., Scheibner, K., Ullrich, R., and Hofrichter, M. (2016). Exploring the catalase activity of unspecific peroxygenases and the mechanism of peroxide-dependent heme destruction. *J. Mol. Catal. B Enzym.* 134, 238–246. doi: 10.1016/j.molcatb.2016.10.014
- Kiebitz, J., Schmidtke, K. U., Zimmermann, J., Kellner, H., Jehmlich, N., Ullrich, R., et al. (2017). A peroxygenase from *Chaetomium globosum* catalyzes the selective oxygenation of testosterone. *ChemBioChem* 18, 563–569. doi: 10.1002/cbic.201600677
- Landvick, S., Ostergaard, L. H., and Kalum, L. (2016). *P*olypeptides Having Peroxygenase Activity*. U.S. Patent No. Washington, DC: U.S. Patent and Trademark Office.
- Linde, D., Olmedo, A., González-Benjumea, A., Renau, C., Estévez, M., Carro, J., et al. (2020). Two new unspecific peroxygenases from heterologous expression of fungal genes in *Escherichia coli*. *Appl. Environ. Microbiol.* 86, e2899–e2819. doi: 10.1128/AEM.02899-19
- Lund, H., Kalum, L., Hofrichter, M., and Peter, S. (2013). *Epoxidation Using Peroxygenase*. U.S. Patent No WO2013144105A1. Washington, DC: U.S. Patent and Trademark Office.
- Municoy, M., González-Benjumea, A., Carro, J., Aranda, C., Linde, D., Renau-Mínguez, C., et al. (2020). Fatty-acid oxygenation by fungal peroxygenases: From computational simulations to preparative regio- and stereo-selective epoxidation. *ACS Catal.* 10, 13584–13595. doi: 10.1021/acscatal.0c03165
- Oliw, E. H. (1994). Oxygenation of polyunsaturated fatty acids by cytochrome P450 monooxygenases. *Progr. Lipid Res.* 33, 329–354. doi: 10.1016/0163-7827(94)90029-9
- Olmedo, A., Aranda, C., del Río, J. C., Kiebitz, J., Scheibner, K., Martínez, A. T., et al. (2016). From alkanes to carboxylic acids: Terminal oxygenation by a fungal peroxygenase. *Angew. Chem. Int. Ed.* 55, 12248–12251. doi: 10.1002/anie.201605430
- Otey, C. R. (2003). High-throughput carbon monoxide binding assay for cytochromes P450. *Methods Mol. Biol.* 230, 137–139. doi: 10.1385/1-59259-396-8:137
- Peter, S., Kinne, M., Wang, X., Ulrich, R., Kayser, G., Groves, J. T., et al. (2011). Selective hydroxylation of alkanes by an extracellular fungal peroxygenase. *FEBS J.* 278, 3667–3675. doi: 10.1111/j.1742-4658.2011.08285.x

- Piazza, G. J., Nuñez, A., and Foglia, T. A. (2003). Epoxidation of fatty acids, fatty methyl esters, and alkenes by immobilized oat seed peroxygenase. *J. Mol. Catal. B Enzym.* 21, 143–151. doi: 10.1016/s1381-1177(02)00122-4
- Prileschajew, N. (1909). Oxydation ungesättigter Verbindungen mittels organischer Superoxyde. *Ber. Dtsch. Chem. Ges.* 42, 4811–4815. doi: 10.1002/cber.190904204100
- Ruettinger, R. T., and Fulco, A. J. (1981). Epoxidation of unsaturated fatty-acids by a soluble cytochrome P-450-dependent system from *Bacillus megaterium*. *J. Biol. Chem.* 256, 5728–5734.
- Sauveplane, V., Kandel, S., Kastner, P. E., Ehlting, J., Compagnon, V., Werck-Reichhart, D., et al. (2009). *Arabidopsis thaliana* CYP77A4 is the first cytochrome P450 able to catalyze the epoxidation of free fatty acids in plants. *FEBS J.* 276, 719–735. doi: 10.1111/j.1742-4658.2008.06819.x
- Tiran, C., Lecomte, J., Dubreucq, E., and Villeneuve, P. (2008). Chemo-enzymatic epoxidation of fatty compounds- Focus on processes involving a lipase-catalyzed perhydrolysis step. *OCL* 15, 179–183. doi: 10.1051/ocl.2008.0191
- Ullrich, R., Nuske, J., Scheibner, K., Spantzel, J., and Hofrichter, M. (2004). Novel haloperoxidase from the agaric basidiomycete *Agrocybe aegerita* oxidizes aryl alcohols and aldehydes. *Appl. Environ. Microbiol.* 70, 4575–4581. doi: 10.1128/aem.70.8.4575-4581.2004
- Wang, Y., Lan, D., Durrani, R., and Hollmann, F. (2017). Peroxygenases en route to becoming dream catalysts. What are the opportunities and challenges? *Curr. Opin. Chem. Biol.* 37, 1–9. doi: 10.1016/j.cbpa.2016.10.007
- Xia, Y., and Larock, R. C. (2010). Vegetable oil-based polymeric materials: synthesis, properties, and applications. *Green Chem.* 12, 1893–1909. doi: 10.1039/c0gc00264j
- Zhang, C., Ding, R., and Kessler, M. R. (2014a). Reduction of epoxidized vegetable oils: A novel method to prepare bio-based polyols for polyurethanes. *Macromol. Rapid Commun.* 35, 1068–1074. doi: 10.1002/marc.201400039
- Zhang, C., Li, Y., Chen, R., and Kessler, M. R. (2014b). Polyurethanes from solvent-free vegetable oil-based polyols. *ACS Sustain. Chem. Eng.* 2, 2465–2476. doi: 10.1021/sc500509h

Conflict of Interest: JK and KS were employed by the company JenaBios GmbH, and OH-M by Novozymes A/S.

The remaining authors declare that the research was conducted in the absence of any commercial or financial relationships that could be construed as a potential conflict of interest.

Copyright © 2021 González-Benjumea, Marques, Herold-Majumdar, Kiebitz, Scheibner, del Río, Martínez and Gutiérrez. This is an open-access article distributed under the terms of the Creative Commons Attribution License (CC BY). The use, distribution or reproduction in other forums is permitted, provided the original author(s) and the copyright owner(s) are credited and that the original publication in this journal is cited, in accordance with accepted academic practice. No use, distribution or reproduction is permitted which does not comply with these terms.



In vivo and *Post-synthesis* Strategies to Enhance the Properties of PHB-Based Materials: A Review

Rosa Turco¹, Gabriella Santagata², Iolanda Corrado¹, Cinzia Pezzella^{3*} and Martino Di Serio¹

¹ Department of Chemical Sciences, University of Naples Federico II, Complesso Universitario di Monte Sant'Angelo, Naples, Italy; ² Institute for Polymers, Composites and Biomaterials, National Council of Research, Pozzuoli, Italy; ³ Department of Agricultural Sciences, University of Naples Federico II, Portici, Italy

OPEN ACCESS

Edited by:

Ligia R. Rodrigues,
University of Minho, Portugal

Reviewed by:

Anouk Duque,
NOVA University of Lisbon, Portugal
Mualla Öner,
Yildiz Technical University, Turkey

*Correspondence:

Cinzia Pezzella
cpezzella@unina.it

Specialty section:

This article was submitted to
Industrial Biotechnology,
a section of the journal
Frontiers in Bioengineering and
Biotechnology

Received: 19 October 2020

Accepted: 30 November 2020

Published: 14 January 2021

Citation:

Turco R, Santagata G, Corrado I,
Pezzella C and Di Serio M (2021) *In
vivo* and *Post-synthesis* Strategies to
Enhance the Properties of PHB-Based
Materials: A Review.
Front. Bioeng. Biotechnol. 8:619266.
doi: 10.3389/fbioe.2020.619266

The transition toward “green” alternatives to petroleum-based plastics is driven by the need for “drop-in” replacement materials able to combine characteristics of existing plastics with biodegradability and renewability features. Promising alternatives are the polyhydroxyalkanoates (PHAs), microbial biodegradable polyesters produced by a wide range of microorganisms as carbon, energy, and redox storage material, displaying properties very close to fossil-fuel-derived polyolefins. Among PHAs, polyhydroxybutyrate (PHB) is by far the most well-studied polymer. PHB is a thermoplastic polyester, with very narrow processability window, due to very low resistance to thermal degradation. Since the melting temperature of PHB is around 170–180°C, the processing temperature should be at least 180–190°C. The thermal degradation of PHB at these temperatures proceeds very quickly, causing a rapid decrease in its molecular weight. Moreover, due to its high crystallinity, PHB is stiff and brittle resulting in very poor mechanical properties with low extension at break, which limits its range of application. A further limit to the effective exploitation of these polymers is related to their production costs, which is mostly affected by the costs of the starting feedstocks. Since the first identification of PHB, researchers have faced these issues, and several strategies to improve the processability and reduce brittleness of this polymer have been developed. These approaches range from the *in vivo* synthesis of PHA copolymers, to the enhancement of *post-synthesis* PHB-based material performances, thus the addition of additives and plasticizers, acting on the crystallization process as well as on polymer glass transition temperature. In addition, reactive polymer blending with other bio-based polymers represents a versatile approach to modulate polymer properties while preserving its biodegradability. This review examines the state of the art of PHA processing, shedding light on the green and cost-effective tailored strategies aimed at modulating and optimizing polymer performances. Pioneering examples in this field will be examined, and prospects and challenges for their exploitation will be presented.

Furthermore, since the establishment of a PHA-based industry passes through the designing of cost-competitive production processes, this review will inspect reported examples assessing this economic aspect, examining the most recent progresses toward process sustainability.

Keywords: polyhydroxybutyrate, plasticizer, reactive processing, biopolymer, bio-based network

INTRODUCTION

The exploitation of fossil resources to satisfy the current demand for plastic materials is a serious threat for the environment, with consequences in terms of global warming, human health risks, and ecosystem toxicity (Harding et al., 2007). The superior chemical and physical properties of petro-plastics, which are responsible for their wide applicability, turn out into very low degradation rate in the environment, determining their accumulation as serious pollutants. European policies in relation to waste management, emission reduction, and sustainable development strongly encourage the search for new green solutions to the plastic issue (Directive 2008/98/EC on waste).

Polyhydroxyalkanoates (PHAs) are biodegradable and naturally synthesized polyesters, accumulated by various microorganisms as carbon, energy, and redox storage material, in response to stressful/unbalanced growth conditions. The discovery of polyhydroxybutyrate (PHB) accumulation in *Bacillus megaterium* dates back to 1926 by Lemoigne. Since then, several steps ahead have been done in the field, from the identification of other hydroxyalkanoic acid monomers (1974), to the cloning and characterization of the genes involved in PHA biosynthesis (1988) (Choi et al., 2020). In 1995, the occurrence of more than 91 PHA monomers had been reported, with this number increasing to up to 150 (R)-hydroxyalkanoic acids at present (Muneer et al., 2020). Other important milestones in this field, including the characterization of the first copolymers and the description of the PHA biosynthetic pathways (1990s), up to the elucidation of the first crystal structure of the main PHA biosynthetic enzymes (2017) (Kim et al., 2017), have contributed to progresses in PHA production process as well as

in modulation of polymer composition (Sudesh et al., 2000; Choi et al., 2020).

According to their monomer chain length, PHAs have been classified into three main categories: short chain length (scl)-PHA (C4 and C5), medium chain length (mcl)-PHA ($C \geq 6$), and long chain length (lcl)-PHA ($C > 14$). Since their discovery and characterization, PHAs and particularly PHB gained intensive attention from the scientific community, being the first example of bio-based and biodegradable polyesters synthesized *in vivo* by microorganisms for the intracellular storage. Hence, differently from the other bio-based polymers, PHAs are polymerized by several bacterial strains, and being natural polyesters, they are considered the most easily biodegradable polymers in aerobic (soil, compost, and marine) and anaerobic (sewage sludge, digesters, and landfills) environments, thanks to the biotic degradative action of several bacterial and fungal enzymes. Furthermore, PHA degradation products are easily assimilated into usable products for microbial growth. As a matter of fact, also PLA is a bio-based polymer produced through fermentation of lactic acid, but it is chemically polymerized and, most noteworthy, it is a compostable polymer, making it unsuitable to reduce the plastic waste pollution (Meereboer et al., 2020).

Among the PHAs, polyhydroxybutyrate (PHB), a scl-PHA, is by far the most well-studied PHA polymer, accumulated to up to 80% of cell dry weight by native as well as recombinant microorganisms (Aldor and Keasling, 2003). Being thermoplastic, it can develop bio-plastics by exploiting the common processing methodologies widely used for the oil-derived polymers and biodegradable polyesters, i.e., film casting and blowing, injection molding, extrusion, thermoforming, etc. (Raza et al., 2018). Due to its mechanical and barrier properties, which are similar to those of oil-based polymers such as polypropylene, this material can be proposed as an excellent candidate to substitute petroleum-derived plastics increasingly drawing the commercial attention. Indeed, PHB high melting temperature and high tensile strength are similar to that of polypropylene, whereas its gas barrier properties result in its being even better and more promising than those of polypropylene and polyethylene terephthalate; in light of the above, PHB deserves many attention for its great potential in several applications such as in food packaging. As an assessment, in **Table 1**, the main properties of PHB compared with that of PP are detailed (Masood, 2017; Markl, 2018). In particular, the molar mass of the polymers, representing the measure of the distribution of the individual molar masses around an average value, is reported. For the PHB, this value is measured to be very high and depends on the type of microorganism used and the conditions adopted for the fermentation process, the growth

Abbreviations: 3H9D, 3-hydroxy-9-decenoate; 9DEO, 9-decenol; ATBC, acetyl tributyl citrate; AVF, aloe vera fibers; BDO, 1,4-butanediol; BIB, di-(2-tert-butylperoxyisopropyl)-benzene; CT, chain transfer; DBS, dibutyl sebacate; DCP, dicumyl peroxide; DDA, dodecanoic acid; DHBA, 2,3-dihydroxybutyrate; DOS, dioctyl sebacate; EB, elongation at break; FC, cellulose fibers; FDA, federation; G, geraniol; GA, geraniol acetate; HB, hydroxybutyrate; HD, hydroxydecanoate; HDD, hydroxydodecanoate; HHx, hydroxyhexanoate; HP, hydroxypropionate; HPhV, hydroxy-3-phenylvalerate; HTD, hydroxytetradecanoate; HV, hydroxyvalerate; IRR, internal rate of return; L, linalool; L503, Lapro1503; LA, levulinic acid; MA, maleic anhydride; NA, nucleating agents; NCS, neural stem cells; PCL, polycaprolactone; PCT, poprianyl CoA transferase; PDLLA, poly(DL-lactide); PDO, 1,3-propanediol; PE, polyethylene; PEG, polyethylene glycol; PhaP, PHA binding protein; PLA, polylactic acid; PP, Polypropylene; PVA, 5-phenylvaleric acid; RBS, ribosome-binding site; RGD, arginyl-glycyl-aspartic acid peptide; TBC, tributyl citrate; Tc, crystallization temperature; TC, triethyl citrate; Tcc, cold crystallization temperature; Tg, glass transition temperature; Tm, melting temperature; YM, Young's modulus; δ , solubility parameter.

TABLE 1 | Range of typical properties of PHB (Bucci et al., 2005; Bugnicourt et al., 2014; dos Santos et al., 2017; Keskin et al., 2017; Rajan et al., 2017).

Property	Value	PP
Density, ρ (g/cm ³)	1.23	0.095
Glass transition temperature, T_g (°C)	4–7	–10
Melting temperature, T_m (°C)	175–180	176
Crystallinity, Xcr (%)	50–90	50–70
Young's modulus, YM (GPa)	1–2	1.5–1.7
Tensile strength, TS (MPa)	15–40	38
Elongation at break, EB (%)	1–15	4
Water vapor transmission rate, WVTR (g·mm/m ² ·day MPa)	1–5	0.2–0.4
Oxygen transmission rate, OTR (cc·mm/m ² ·day)	2	67.7

rate of the polymer, and the final purification procedures. This parameter is very important, since it significantly influences molecular, processing, and final properties of the polymer, in particular its mechanical performance (dos Santos et al., 2018).

In addition, PHB is biocompatible, and its degradation inside the body occurs slowly. For this reason, PHB can be used both as a polymer drug carrier in case of gradual and controlled releasing kinetics and as scaffold in the field of tissue engineering (Degli Esposti et al., 2019; Babos et al., 2020). Anyway, despite the comparable features with synthetic polymers, PHB exploitation is strongly limited due to its high stiffness, brittleness, and narrow processability window.

Although this phenomenon is not clearly elucidated, it is assumed that the interlamellar amorphous chains are progressively tightened up resulting in an increase in the amorphous rigid fraction (Crétois et al., 2016). This outcome could be explained by two plausible hypothesis. The first one is related to a secondary crystallization slowly occurring during the storage at room temperature: small crystallites not only can bridge crystalline lamellae but also freeze the remaining amorphous PHB chains, leading to the embrittlement of the material (Di Lorenzo and Righetti, 2013). The second assumption is based on the physical aging of the amorphous phase strictly linked to the non-equilibrium character of the glassy state. Actually, based on this theory, two types of amorphous phase coexist: a mobile amorphous fraction (MAF) far from the crystalline lamellae and a rigid amorphous fraction (RAF), which, due to the interaction with the crystals, evidences restricted mobility; in this last case, the boundary T_g associated is disturbed by the presence of crystals, and the physical aging process occurs below this T_g (Esposito et al., 2016).

Actually, both phenomena have strong consequences on the physical properties of PHB such as crystallinity, impact strength, Young's modulus, toughness, and elongation at break that undergo continuous worsening even to several days above its processing (dos Santos et al., 2017).

From the structural point of view, crystallinity is strongly related to its regular structure, which in turn depends on the type of synthesis adopted to obtain it. The isotactic PHB is characterized by the only presence of a chiral carbon in absolute

configuration R (Michel and Billington, 2012) and is produced by bacterial fermentation (Vroman and Tighzert, 2009), while the syndiotactic PHB is synthesized starting from the monomers with R and S configuration (Barham et al., 1984). In this way, the fermentation route allows to obtain the highest crystallinity. Depending on the several approaches used to synthesize and process PHB, it is possible to affirm that they shoot in a high range between 40 and 80% (dos Santos et al., 2017).

In addition to its marked brittleness, with very low deformability, PHB has a very strong susceptibility to rapid thermal degradation, posing serious problems to processing using conventional technologies for thermoplastics (Erceg et al., 2005). Indeed, the polyester undergoes thermal degradation and depolymerization at temperatures close to its melting point at around 180°C, so that the acceptable residence time in the processing equipment is severely limited to only few minutes (Erceg et al., 2005).

The thermal degradation is believed to happen almost exclusively via a random chain cleavage mechanism. The degradative reaction, occurring with the elimination of cis β -CH and a six-membered ring transition (Gras et al., 1984; Doi et al., 1994), leads to a rapid decrease in molecular weight (Bugnicourt et al., 2014); however, some kinetically favorable cleavages occur near the ends of macromolecules (Erceg et al., 2005). Thus, several degraded products such as olefinic compounds, carboxylic acids, crotonic acid, and oligomers form (Figure 1).

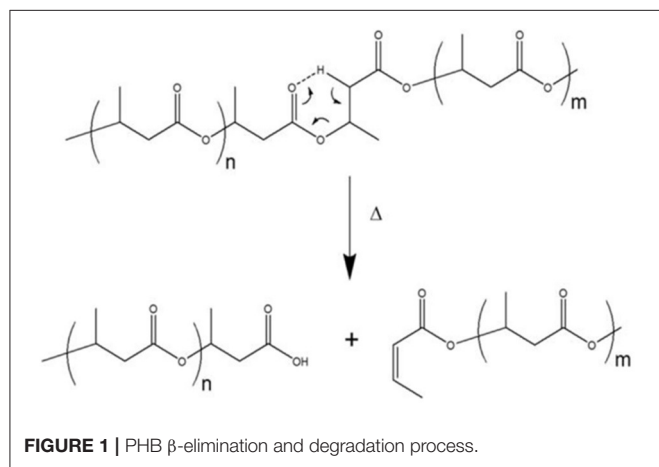
Most of the bio-based polymers suffer from these shortcomings to such an extent that their diffusion as commodity materials has been confined to niche applications. As a result of the above flaws and to curb the previous drawbacks, several investigations reported in the literature have been performed aimed at producing PHB-based materials with improved properties.

In this review, the most promising strategies finalized to obtain PHB-based materials with suitable and performing properties have been outlined (Figure 2). In particular, green and cost-effective approaches aimed to modulate and optimize the polymer technological performances have been discussed, as well as pioneering examples, prospects, and challenges for their effective exploitation have been detailed, too.

Specifically, in this review, two different approaches have been followed. The first one concerned the modification of the monomeric composition of PHA polymers; different kinds of PHAs have been *in vivo* biosynthesized by incorporating additional units into the PHB backbone, thus providing the possibility to fine tune the polymer properties: a general decrease in the glass transition and melting temperatures are observed with a consequent decreasing material brittleness and broadening processing window. In addition, *in vivo* biosynthetic methodologies aimed to modulate polymer molecular weight and cost competitiveness of the overall process have been also reviewed.

The second overture concerned the fine tuning of the properties of *post-synthesis* PHB-based polymers. To this aim, several studies related to PHB processing with compatible organic or inorganic materials, in order to obtain polymer physical blends, chemical reactive modifications, and

bionanocomposites, have been recently reported, and a short account of them will be detailed in the following sections, together with the description of the main chemical–physical and mechanical properties. In particular, since the toughness and processability of PHB can be improved by incorporating natural additives, like plasticizers, a closer analysis on PHB, their main function, and of course, their most suitable plasticizers will be provided.



In this work, the literature data of the past 20 years, focusing specifically on the past decade, has been reviewed.

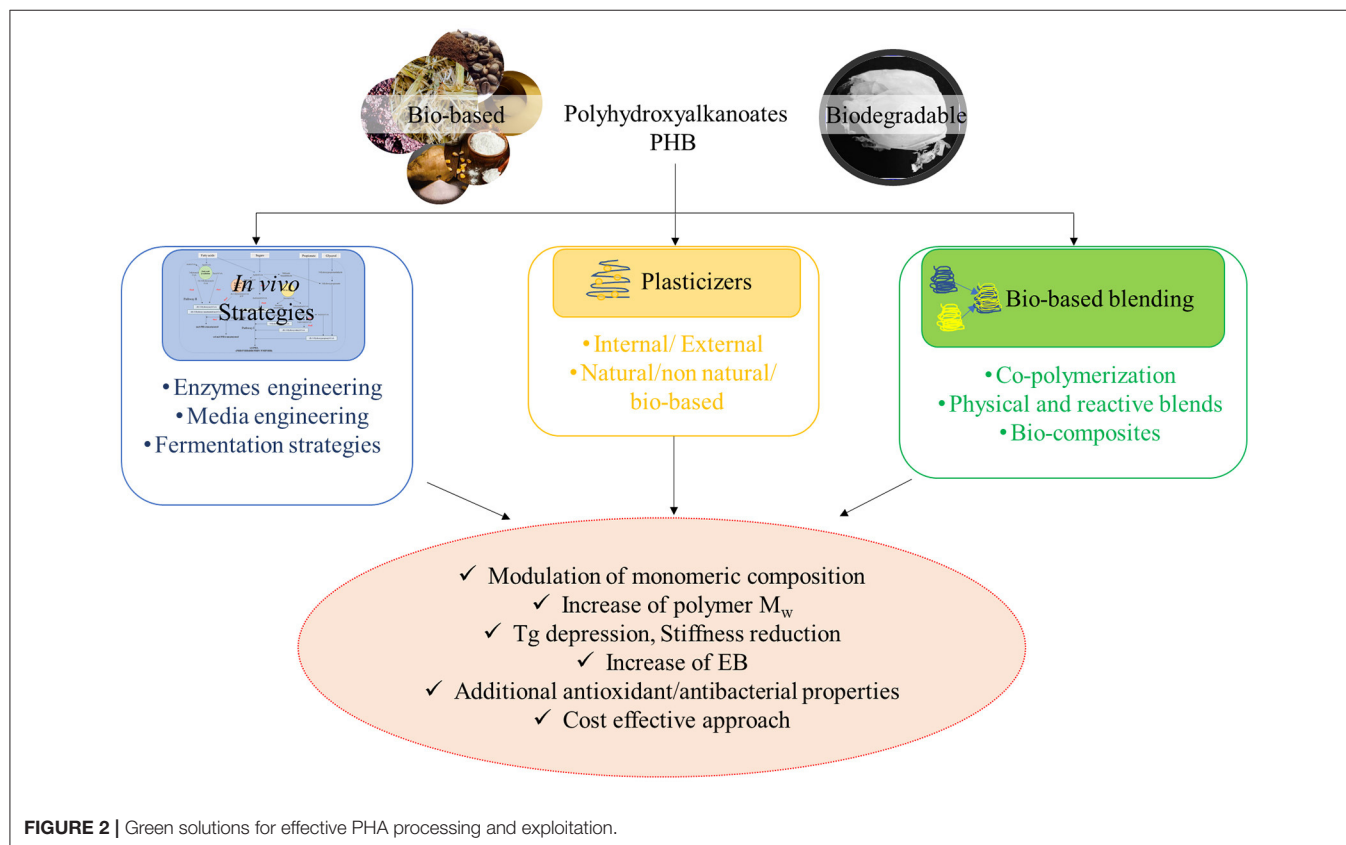
IN VIVO STRATEGIES TO MODULATE PHB PROPERTIES: SYNTHESIS AND APPLICATIONS

Copolymer Synthesis

The synthesis of copolymers of various molecular weights, compositions, and architectures has led to the ability to broaden the knowledge and the exploitation of new materials with unique properties. In addition to the control of the stereochemical microstructure, the copolymerization represents a way to opportunely modulate the physical properties of the polymeric materials. By varying the composition, monomer sequencing, and molecular weight, the polymer microstructure can be tailored for specific applications, mostly if a proper balance between the mechanical and thermal properties, together with degradation rate, is needed.

The introduction of other monomeric units in the PHB backbone has been reported to change polymer properties in favor of a reduced stiffness, higher elongation to break, and lower melting point.

Copolymerization is obtained by the activation of different pathways for PHA biosynthesis in the microbial cell. Depending on the available carbon source, three main pathways regulate PHA biosynthesis *in vivo* (Figure 3), although up to 13 different



routes allowing channeling specific precursors into PHA have been described (Tan et al., 2014b). If sugars are supplied, pathways I and III can be followed, yielding short chain length PHA (scl-PHA) and medium chain length PHA (mcl-PHA), respectively. These carbon sources are unrelated since their structure is different from that of PHA. If related carbon sources, such as fatty acids, are supplied, pathway II is followed, yielding mcl-PHA. Both pathways II and III can also produce PHA copolymers (Verlinden et al., 2007). It follows that the polymer composition is strictly related to the supplied C-source and to the activated pathway within the cell.

In vivo approaches for tailored copolymer synthesis are based on the use of both pure cultures and mixed microbial cultures (MMCs), in which the supplying of precursor compounds, structurally related to the monomer of interest, determines the activation of the metabolic pathway/s required for its synthesis. In the case of MMC, a raw complex organic substrate is first fermented to obtain volatile fatty acids (VFAs) by anaerobic acidogenic fermentation; then, the VFA-rich stream is used to select for PHA-producing microorganisms against the non-producing ones. Finally, the enriched microbial population is fed with the VFA under optimal conditions to maximize PHA production (Mannina et al., 2020). The type of starting feedstock, the operating conditions for VFA production, and their relative proportions, as well as the applied enrichment strategies directly affect the yield, productivity, and monomeric composition of the produced polymer (Kourmentza et al., 2017). Being based on natural principles of selection and competition among the microorganisms, MMC-based processes display an economic advantage since they are carried in unsterile conditions. Moreover, they allow to broaden the choice of possible feedstocks as the microbial consortium naturally adapts itself to the provided C-source (Mannina et al., 2020).

On the other hand, the use of pure cultures, although requiring sterile and thus costly conditions, is widely applied for PHA production (Anjum et al., 2016; Kourmentza et al., 2017). Both naturally occurring microorganisms as well as engineered strains have been used for copolymer synthesis, taking advantage of their heterogeneous metabolic pathways or finely manipulating them. Protein engineering, applied to the key enzymes of the biosynthetic pathway (Figure 3), also allowed to tailor their substrate specificity, favoring the incorporation of monomer of interests and, more recently, also of non-natural ones (Choi et al., 2020).

This section will cover the most significant examples in the field of copolymer synthesis. The mechanical and thermal properties of the most relevant examples of PHA copolymers have been collected in Table 2.

Poly (3-Hydroxybutyrate-co-Hydroxyvalerate)

Poly (3-hydroxybutyrate-co-hydroxyvalerate) is one of the most studied copolymers, has been developed on an industrial scale (Chang et al., 2014), and has recently attracted the attention of both industry and researchers as a promising material due to its biotechnological potentiality and its applicability in the medical, agricultural, and packaging fields (Rivera-Briso and Serrano-Aroca, 2018). PHBV has gained attention due to its better

flexibility, strength, reduced chain packaging, and toughness compared to PHB (Tebaldi et al., 2019). The higher is the amount of the HV fraction, the lower is the melting point of the resulting PHBV copolymer, which broadens the processing window of the material (Ishida et al., 2005; Wang et al., 2013b). In addition, due to the longer side chain of HV, the segmental mobility in the amorphous phase of this copolymer increases, thus reducing the Tg (Ishida et al., 2005). Ultimately, PHBV copolymers show improvement in flexibility and ductility in comparison to PHB (Wang et al., 2013b).

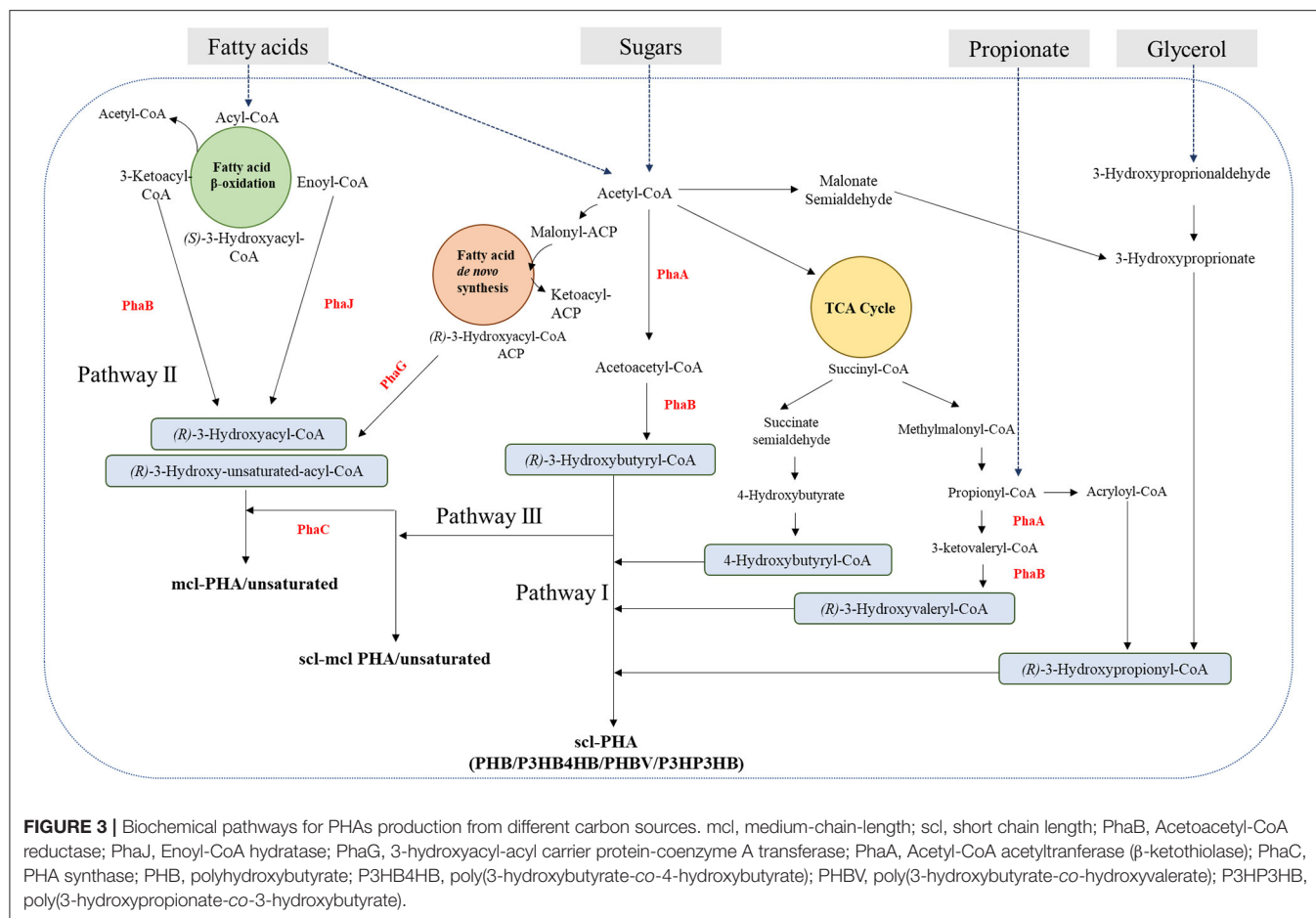
PHBV thermomechanical properties vary widely depending on the mol% of 3-hydroxyvalerate (3HV). Although the incorporation of 3HV moieties in the PHB polymer is expected to reduce its crystallinity, this reduction is limited by the occurrence of the isodimorphism phenomenon, by which 3HB and 3HV are able to co-crystallize (Yeo et al., 2018). As a fact, PHBV still exhibits a high degree of crystallinity throughout a wide range of compositions from 0 to 95 mol% HV (Cai and Qiu, 2009).

Different cultivation strategies have been designed for the incorporation of 3HV monomers in the forming polymeric chain, using organic acid precursors, such as propionic and valeric acid (Zinn et al., 2003; Masood et al., 2012; Follonier et al., 2014; Hilliou et al., 2016; Martla et al., 2018).

In one of the first examples Madden et al. (1998) applied an alternate feeding strategy of glucose and propionic acid to *Ralstonia eutropha* cultures, to produce mixtures of PHB and smaller amount of 3HV-rich (7–18 mol% HV) random copolymer, PHBV. The process of chain termination resulted in the synthesis of polymer mixtures rather than block copolymers.

The demand for cost-competitive PHA production processes has translated into an increasing number of examples reporting the production of PHBV from waste materials and/or less costly, renewable precursors of HV moieties. Gahlawat and Soni (2017) tested the feeding with different acids to *Cupriavidus necator* cultures growing on waste glycerol from jatropha oil as the main carbon source. A multiple-pulse feeding strategy was applied to prevent growth inhibition caused by high acid concentration. In the best conditions, up to 25% HV content was achieved in the copolymer, reaching around 5 g/L polymer accumulation. The polymers produced in these conditions display a low molecular weight, consistently with the role of glycerol as chain termination agents. Similar production levels, although with a lower HV content (2.8–8%) were obtained by García et al. (2013) using all crude by-products (waste glycerol and rapeseed hydrolysates) as C-sources. A different approach to improve PHBV productivity as well as HV content (up to 36.7%) was applied by de Paula et al. (2017), through the selection of a *Pandoraea* sp. MA03 mutant strain with the highest performances on crude glycerol supplemented with propionic and valeric acids. In all the cases, the copolymers composition was found to be affected by the specific precursor feed rate, resulting into PHBV with different 3HV mol%. Saturated fatty acids from the animal processing industry were used as main C-source for the synthesis of PHBV copolymer from *C. necator* (Koller et al., 2014).

In view of process sustainability, the use of levulinic acid (LA) as 3HV precursor has been suggested by several authors. LA



can be produced from a wide range of renewable biomaterials, such as cellulose-containing agricultural and forest wastes, in a cost-effective manner. Although *R. eutropha* could grow in the presence of LA as the sole carbon source, accumulation of PHBV occurred in significant amount only in the presence of glucose as cosubstrate and was strongly affected by the type of added nitrogen source (Wang et al., 2013b). More recently, the fine engineering of LA catabolic pathway in *Pseudomonas putida* EM42 allowed the production of various type of scl-PHA, containing 3HV and 4-hydroxyvalerate (4HV) with different monomer compositions and proportions, depending on the expression of different PHA reductases and synthases endowed with different substrate specificities (Cha et al., 2020). The incorporation of 4HV in place of 3HV into PHBV has been reported to further decrease the melting point of the final copolymer (Schmack et al., 1998) and improve toughness without affecting the degradation temperature (Sheu et al., 2018).

Hydrolysates of residual spent coffee ground after oil extraction are also interesting source of LA, promoting the accumulation of PHBV copolymer (up to 11.6 mol% HV) by *Burkholderia cepacia* (Obrucá et al., 2014). Another original example of waste valorization has been described by Pramanik et al. (2014), who reported the production of PHBV (13.8 mol% 3HV) from an alkaliphilic microbe, *Alkaliphilus oremlandii*

OhILAs strain, through the biodegradation of linseed oil-based elastomeric film.

To overcome the need for acid cosubstrates, which cannot only inhibit cell growth but also increase production costs, PHBV copolymer synthesis has been also approached using glucose as C-source. To this aim, fine engineering strategies, focused on the pathways responsible for propionyl-CoA synthesis in *Haloferax mediterranei*, have been applied (Chen et al., 2011; Tan et al., 2014a; Yang et al., 2014). In one of the most recent examples, the CRISP/cas9 approach was used to simultaneously target different genes of the tricarboxylic acid cycle without compromising cell growth, resulting in up to 25 mol% 3HV in the synthesized polymer (Chen et al., 2019).

PHBV copolymers have also been produced in MMC-based processes, starting from a various range of complex organic substrates, such as food waste (Gouveia et al., 2017), municipal wastewater sludge (Wijeyekoon et al., 2018), the liquid fraction resulting from pyrolysis processes (Bio-oil) (Moita Fidalgo et al., 2014), and brewery wastewaters (Tamang et al., 2019). In an interesting example, the modulation of pH in the range of 4.5–7 during the acidogenic reactor operating conditions led to different monomer precursor profiles, which resulted in PHBV copolymers with different compositions starting from cheese whey as model feedstock (Gouveia et al., 2017). By increasing the

TABLE 2 | Main properties of PHA copolymers.

Copolymer	Strain, bioprocess	Properties		References
		Thermal	Mechanical	
P(3HB-co-10.2 mol% 3HV)	<i>Ralstonia eutropha</i> , alternate feeding with glucose or propionate	M_w (g mol ⁻¹) 6.7×10^{-5} T_m (°C) 169 T_g (°C) -1 T_c (°C) 75	TS (MPa) 29.0 EB (%) 17.4 YM (MPa) 472	Madden et al., 1998
P(3HB-co-18.1 mol% 3HV)		M_w (g mol ⁻¹) 5.6×10^{-5} T_m (°C) 161 T_g (°C) -3 T_c (°C) 80	TS (MPa) 28.7 EB (%) 121.1 YM (MPa) 286	
P(3HB-co-7.5 mol% 3HV)		M_w (g mol ⁻¹) 6.9×10^{-5} T_m (°C) 174 T_g (°C) -3 T_c (°C) 70	TS (MPa) 19.0 EB (%) 13.6 YM (MPa) 272	
P(3HB-co-7.3 mol% 3HV)		M_w (g mol ⁻¹) 7.1×10^{-5} T_m (°C) 172 T_g (°C) n.d. T_c (°C) 60	n.d.	
P(3HB-co-5 mol% 3HV)	<i>A. hydrophila</i> 4AK4, grown on lauric acid and/or valerate	M_w (g mol ⁻¹) n.d. T_m (°C) 170 T_g (°C) 2.2	TS (MPa) 18.1 EB (%) 2.3 YM (MPa) 1465	Zhang et al., 2009
P(3HB-co-6 mol% 3HV)	<i>Cupriavidus necator</i> , odd-numbered carboxylic acid mix (FAM) as carbon source for large scale production of copolymers	M_w (g mol ⁻¹) 4.4×10^5 T_m (°C) 159 T_g (°C) 2.2 T_c (°C) 50.9	n.d.	Koller et al., 2014
P(3HB-co-9 mol% 3HV)		M_w (g mol ⁻¹) 4.5×10^5 T_m (°C) 159 T_g (°C) 3.3 T_c (°C) 56	n.d.	
P(3HB-co-12 mol% 3HV)	<i>C. necator</i> , grown on waste glycerol and rapeseed hydrolysates	T_m (°C) 155 T_g (°C) -1.9 T_c (°C) n.d.	n.d.	García et al., 2013
P(3HB-co-13.5 mol% 3HV)	<i>A. oremlandii</i> , biodegradation of linseed oil-based elastomeric film	M_w (g mol ⁻¹) 2.3×10^5 T_m (°C) 152 T_g (°C) -3.8 T_c (°C) n.d.	n.d.	Pramanik et al., 2014
P(3HB-co-26 mol% 3HV)	<i>C. necator</i> DSM 545, multiple-pulse feeding with valeric acid	M_w (g mol ⁻¹) 1.1×10^5 T_m^1 (°C) 142 T_m^2 (°C) 156	n.d.	Gahlawat and Soni, 2017
P(3HB-co-59 mol% 3HV)	Recombinant <i>Escherichia coli</i> , functionalization of copolymer PHBV with ascorbic acid	T_m (°C) 135	n.d.	Bhatia et al., 2019a
P(3HB-co-2.35 mol% 3HV)	<i>H. bluephagenesis</i> ; engineering of TCA cycle by CRISP/cas9 approach for copolymer production from glucose	T_m (°C) 166 T_g (°C) -0.4	n.d.	Chen et al., 2019
P(3HB-co-4.01 mol% 3HV)		T_m (°C) 163 T_g (°C) -0.5	n.d.	
P(3HB-co-8.6 mol% 3HV)		T_m (°C) 158 T_g (°C) 3.1	n.d.	
P(3HB-co-11.7 mol% 3HV)		T_m (°C) 156 T_g (°C) 2.3	n.d.	
P(3HB-co-15.2 mol% 3HV)		T_m (°C) 158 T_g (°C) 2.8	n.d.	
P(3HB-co-19.6 mol% 3HV)		T_m (°C) 137 T_g (°C) 0.5	n.d.	
P(3HB-co-11 mol% 4HB)	Recombinant <i>E. coli</i> , unrelated carbon sources	T_m (°C) 131 T_g (°C) -4.4	TS (MPa) 20 EB (%) 698	Li et al., 2010
P(3HB-co-18 mol% 4HB)		T_m (°C) 130 T_g (°C) -9.2	TS(MPa) 9.9 EB (%) 729	

(Continued)

TABLE 2 | Continued

Copolymer	Strain, bioprocess	Properties		References
		Thermal	Mechanical	
P(3HB-co-38 mol% 4HB)	<i>C. necator</i> strain A-04, different ratios of fructose and 1,4-butanediol	M_w (g mol ⁻¹) 1.0×10^5 T_m (°C) 152 T_g (°C) -10 T_c (°C) 55	TS (MPa) 2.9 EB (%) 48 YM (MPa) 0.6×10^3	Chanprateep et al., 2010
P(3HB-co-5 mol% 4HB)		M_w (g mol ⁻¹) 1.4×10^5 T_m (°C) 161 T_g (°C) -5 T_c (°C) 83	TS (MPa) 0.9 EB (%) 22 YM (MPa) 0.8×10^3	
P(3HB-co-24 mol% 4HB)		M_w (g mol ⁻¹) 1.0×10^5 T_m (°C) 168 T_g (°C) -2 T_c (°C) 104	TS (MPa) 1.4 EB (%) 11 YM (MPa) 1.4×10^3	
P(3HB-co-95 mol% 4HB)	<i>C. malaysiensis</i> , batch	M_w (g mol ⁻¹) 4.4×10^5	TS (MPa) 23 EB (%) 463 YM (MPa) 187	Norhafini et al., 2017
P(3HB-co-97 mol% 4HB)	<i>C. malaysiensis</i> ; pulse feed of C and N sources	M_w (g mol ⁻¹) 3.4×10^5	TS (MPa) 31 EB (%) 473 YM (MPa) 272	
P(3HB-co-95 mol% 4HB)	<i>C. malaysiensis</i> ; mixed feeding strategy	M_w (g mol ⁻¹) 1.7×10^5	TS (MPa) 24 EB (%) 471 YM (MPa) 214	
P(3HB-co-97 mol% 4HB)	<i>C. malaysiensis</i> ; constant feeding strategy	M_w (g mol ⁻¹) 3.2×10^5	TS (MPa) 31 EB (%) 515 YM (MPa) 256	
P(3HB-co-99 mol% 4HB)	<i>C. malaysiensis</i> ; twice pulse feed of C and N sources	M_w (g mol ⁻¹) 3.3×10^5	TS (MPa) 25 EB (%) 368 YM (MPa) 184	
P(3HB-co-20 mol% 4HB)	Recombinant, <i>Cupriavidus</i> sp. USMAA1020	M_w (g mol ⁻¹) 391×10^3 T_m (°C) 129 T_g (°C) -16	TS (MPa) 12 EB (%) 353 YM 72	Syafiq et al., 2017
P(3HB-co-85 mol% 4HB)		M_w (g mol ⁻¹) 87×10^3 T_m (°C) 63 T_g (°C) -41	TS (MPa) 11 EB (%) 380 YM (MPa) 103	
P(3HB-co-91 mol% 4HB)		M_w (g mol ⁻¹) 60×10^3 T_m (°C) 53 T_g (°C) -53	TS (MPa) 14 EB (%) 402 YM (MPa) 93	
P(3HB-co-10 mol% 4HB)	<i>C. necator</i> B10646, valeric acid, hexanoic acid, and γ -butyrolactone as precursor for copolymer production	M_w (g mol ⁻¹) 5.7×10^5 T_m (°C) 150 T_g (°C) 3.4 T_c (°C) 66	TS (MPa) 14.8 EB (%) 5.7 YM (MPa) 957	Zhila and Shishatskaya, 2018
P(3HB-co-29 mol% 4HB)		M_w (g mol ⁻¹) 8.3×10^5 T_m (°C) 162 T_g (°C) n.d. T_c (°C) 96	TS (MPa) 7.8 EB (%) 31 YM (MPa) 243	
P(3HB-co-75 mol% 4HB)		M_w (g mol ⁻¹) 7.0×10^5 T_m (°C) 158 T_g (°C) n.d. T_c (°C) 88	TS (MPa) 15.4 EB (%) 323 YM (MPa) 425	
P3HP	Recombinant <i>E. coli</i> , grown on mixtures of 1,3- propanediol (PDO) and 1,4-butanediol (BDO)	M_w (g mol ⁻¹) 1.6×10^5 T_m (°C) 78 T_g (°C) -18	TS (MPa) 22 EB (%) 498 YM (MPa) 2889	Meng et al., 2012
P(3HP-co-38 mol% 4HB)		M_w (g mol ⁻¹) 2.8×10^5 T_m (°C) 63 T_g (°C) -36	TS (MPa) 0.5 EB (%) 1611 YM (MPa) 4.4	
P(3HP-co-82 mol% 4HB)		M_w (g mol ⁻¹) 3.0×10^5 T_m (°C) 36 T_g (°C) -29	TS (MPa) 6.3 EB (%) 595 YM (MPa) 18.5	

(Continued)

TABLE 2 | Continued

Copolymer	Strain, bioprocess	Properties		References
		Thermal	Mechanical	
P3HP	Recombinant <i>E. coli</i> for the synthesis of a block copolymer consisting of highly elastic P4HB portion with a P3HP block, PDO-BDO alternate feeding	M_w (g mol ⁻¹) 1.6×10^5 T_m (°C) 78 T_g (°C) -18	TS (MPa) 21 EB (%) 498 YM (MPa) 2889	Tripathi et al., 2013b
P4HB		M_w (g mol ⁻¹) 3.9×10^5 T_m (°C) 61 T_g (°C) -47	TS (MPa) 35 EB (%) 697 YM (MPa) 181	
P(3HP-co-25 mol% 4HB)		M_w (g mol ⁻¹) 2.6×10^5 T_m (°C) 63 T_g (°C) -31	TS (MPa) 6.4 EB (%) 963 YM (MPa) 15.5	
P(3HP-co-38 mol% 4HB)		M_w (g mol ⁻¹) 2.8×10^5 T_m (°C) 63 T_g (°C) -36	TS (MPa) 0.6 EB (%) 1611 YM (MPa) 4.4	
P3HP-b-29 mol% P4HB		M_w (g mol ⁻¹) 5.5×10^5 T_m (°C) 55;68 T_g (°C) -20; -46	TS (MPa) 45 EB (%) 877 YM (MPa) 177	
P3HP-b-37 mol% P4HB	Wild-type <i>A. hydrophila</i> , using lauric acid as carbon source	M_w (g mol ⁻¹) 5.5×10^5 T_m (°C) 53;67 T_g (°C) -22; -45	TS (MPa) 25.3 EB (%) 1031 YM (MPa) 113	Noda et al., 2005
P(3HB-co-8 mol% 3HV)		T_m (°C) 170 T_g (°C) 2	n.d.	
P(3HB-co-12 mol% 3HHx)		T_m (°C) 110 T_g (°C) -2.5	n.d.	
P(3HB-co-8 mol% 3HHx)		T_m (°C) 140 T_g (°C) 0	n.d.	
P(3HB-co-2.7 mol% 3HHx)		T_m (°C) 151 T_g (°C) -2.3 T_c (°C) 50	n.d.	
P(3HB-co-5.9 mol% 3HHx)	<i>C. necator</i> , regulation of 3HHx mol% by expression of R-specific enoyl-CoA hydratases	T_m (°C) 139 T_g (°C) -2.4 T_c (°C) -	n.d.	Arikawa et al., 2016
P(3HB-co-7.9 mol% 3HHx)		T_m (°C) 131 T_g (°C) -2.2 T_c (°C) -	n.d.	
P(3HB-co-10.8 mol% 3HHx)		T_m (°C) 113 T_g (°C) -4.7 T_c (°C) -	n.d.	
P(3HB-co-7 mol% 3HHx)		M_w (g mol ⁻¹) 2.3×10^5 T_m (°C) 122; 141 T_g (°C) 2.3 T_{cc} (°C) 62	n.d.	
P(3HB-co-10 mol% 3HHx)		M_w (g mol ⁻¹) 4.5×10^5 T_m (°C) 121;139 T_g (°C) 2.9 T_{cc} (°C) 58	n.d.	
P(3HB-co-18 mol% 3HHx)	Crystallization study on commercial PHBPHHx (Kaneka corporation) containing different mol% HHx monomer	M_w (g mol ⁻¹) 2.6×10^5 T_m (°C) n.d. T_g (°C) 1.3 T_{cc} (°C) n.d.	n.d.	Cai and Qiu, 2009
P(3HB-co-22 mol% 3HHx)		M_w (g mol ⁻¹) 2.9×10^5	n.d.	
P(3HB-co-3HO)		M_w (g mol ⁻¹) 49×10^4 T_m (°C) 150; 163 T_g (°C) 0.4	n.d.	
P(3HB-co-3HO)				
P(3HB-co-3HO)				

(Continued)

TABLE 2 | Continued

Copolymer	Strain, bioprocess	Properties		References
		Thermal	Mechanical	
mcl copolymer from heptadecanoic acid	<i>P. aeruginosa</i> ATCC 27853, odd-chain fatty acids from C17 to C21 under nitrogen starvation	M_w (g mol ⁻¹) 77×10^{-3} T_m (°C) 52 T_g (°C) -45	n.d.	Impallomeni et al., 2018
mcl copolymer from non-adeanoic acid		M_w (g mol ⁻¹) 97×10^{-3} T_m (°C) 48 T_g (°C) -43	n.d.	
mcl copolymer from heneicosanoic acid		M_w (g mol ⁻¹) 188×10^{-3} T_m (°C) 49 T_g (°C) -39	n.d.	
P(16 mol%3HD-co-3HDD)	<i>P. putida</i> mutant, grown on dodecanoate	M_w (g mol ⁻¹) 15.5×10^4 T_m (°C) 78 T_g (°C) -32	TS (MPa) 5.2 EB (%) 88 YM (MPa) 103	Liu et al., 2011b
100% 3HD		M_w (g mol ⁻¹) 36.1×10^4 T_m (°C) 72 T_g (°C) -37	TS (MPa) 12 EB (%) 313 YM (MPa) 20	
P(15 mol% 3HHx-co-40 mol% 3HO-co-30 mol% 3HD-co-15 mol% 3HDD)	<i>P. putida</i> mutant, sequential supplementation of hexanoate and dodecanoic acid	M_w (g mol ⁻¹) 10×10^4 T_m (°C) 53 T_g (°C) -44	TS (MPa) 8.7 EB (%) 189 YM (MPa) 3.6	Tripathi et al., 2013a
P(15.86 mol% 3HD-co-35.25 mol% 3HDD).		M_w (g mol ⁻¹) 16×10^4 T_m (°C) 33;66 T_g (°C) -43	TS (MPa) 16 EB (%) 369 YM (MPa) 38	
P(3HDD-co-10 mol%3H9D)	<i>P. entomophila</i> with deficient β -oxidation pathway	M_w (g mol ⁻¹) 9.5×10^4 T_m (°C) 69 T_g (°C) -48	TS (MPa) 4.0 EB (%) 221 YM (MPa) 51	Li et al., 2014
P(3HDD-co-40 mol%3H9D)		M_w (g mol ⁻¹) 8.8×10^4 T_m (°C) 52 T_g (°C) -54	TS (MPa) 3.5 EB (%) 206 YM (MPa) 20	
P(3HDD-co-52 mol%3H9D)		M_w (g mol ⁻¹) 1.0×10^5 T_m (°C) 45 T_g (°C) -55	TS (MPa) 2.2 EB (%) 124 YM (MPa) 3	
P(3HDD-co-77 mol%3H9D)		M_w (g mol ⁻¹) 9.9×10^4 T_m (°C) 43 T_g (°C) -55	TS (MPa) 3.6 EB (%) 173 YM (MPa) 3	
P(3HDD-co-81 mol%3H9D)		M_w (g mol ⁻¹) 9.4×10^4 T_m (°C) 43 T_g (°C) -56	TS (MPa) 3.7 EB (%) 105 YM (MPa) 4.7	
P3HDD-b-70 mol%P3H9D		M_w (g mol ⁻¹) 13×10^4 T_m (°C) 46 T_g (°C) -55	TS (MPa) 3 EB (%) 138 YM (MPa) 8	
P(3HDD-co-29 mol% 3HD-co-12 mol% 3HTD-co-10 mol%3HO-co-6 mol%3HHx)	<i>Ps. chlororaphis</i> subsp. <i>aurantiaca</i> , using crude glycerol from biodiesel production as the sole carbon source	M_w (g mol ⁻¹) 1.1×10^5 T_m (°C) 43 T_g (°C) -47	TS (MPa) 3.9 EB (%) 273 YM (MPa) 8	Pereira et al., 2019
mcl-PHA (75 mol% 3HD)	Mixed culture of <i>Pseudomonas aeruginosa</i> , <i>Pseudomonas</i> sp., and <i>Ralstonia</i> sp.	T_m (°C) 50; 82 T_g (°C) -38 T_c (°C) 20	n.d.	Sangkharkar et al., 2020
mcl-PHA (75 mol% 3HD)/TGCN		T_m (°C) 50; 82 T_g (°C) -37 T_c (°C) 12	n.d.	
P(3HDD-co-12 mol% 3HTD-co-10 mol% 3HO-co-6 mol% 3HHx)	mcl-PHA by <i>Pseudomonas mendocina</i> CH50 from waste oils; plasticising effect of the oligomeric mcl-PHA on P(3HB)	M_w (g mol ⁻¹) 21×10^4	n.d.	Lukasiewicz et al., 2018

(Continued)

TABLE 2 | Continued

Copolymer	Strain, bioprocess	Properties		References
		Thermal	Mechanical	
OligoHA: hydrolyzed P(3HHx-3HO-3HD-3HDD) P3HB-OligoHA blend (95/5)		M_w (g mol ⁻¹) 10×10^3 T_m (°C) 172	n.d. TS (MPa) 12.5 EB (%) 4 YM (MPa) 1000	
P3HB-OligoHA blend (90/10)		T_m (°C) 175	TS (MPa) 15 EB (%) 6 YM (MPa) 1200	
P3HB-OligoHA blend (80/20)		T_m (°C) 173	TS (MPa) 6 EB (%) 16 YM (MPa) 480	
P3HB		T_m (°C) 177	TS (MPa) 20 EB (%) 5 YM (MPa) 1440	
P(3HDD-co-3HPhV)	<i>P. entomophila</i> grown on 5-phenylvaleric acid (PVA) and dodecanoic acid for synthesis of controllable composition of 3HDD and phenyl group on the side chain	M_w (g mol ⁻¹) 10×10^4 T_m (°C) 82 T_g (°C) -49	TS (MPa) 5.5 EB (%) 60 YM (MPa) 61	Shen et al., 2014
P(3HDD-co-2.9 mol% 3HPhV)		M_w (g mol ⁻¹) 6.6×10^4 T_m (°C) 81 T_g (°C) -33	TS (MPa) 2.0 EB (%) 37 YM (MPa) 94	
P(3HDD-co-18.7 mol% 3HPhV)		M_w (g mol ⁻¹) 7.3×10^4 T_m (°C) 80 T_g (°C) -36	TS (MPa) 4.4 EB (%) 86 YM (MPa) 95	
P(3HDD-co-32 mol% 3HPhV)		M_w (g mol ⁻¹) 6.1×10^4 T_m (°C) 76 T_g (°C) -35	TS (MPa) 3.1 EB (%) 32 YM (MPa) 49	
P(3HPhV)		M_w (g mol ⁻¹) 4.41×10^4 T_m (°C) 50 T_g (°C) 6	TS (MPa) n.d. EB (%) n.d. YM (MPa) n.d.	
P(3HB-co-11 mol% 3HV-co-10 mol% 3HHx)	Recombinant <i>A. hydrophila</i> 4AK4, grown on lauric acid, and sodium valerate	n.d.	TS (MPa) 8.4 EB (%) 341 YM (MPa) 235	Zhang et al., 2009
P(3HB-co-17 mol% 3HV-co-10 mol% 3HHx)		n.d.	TS (MPa) 14 EB (%) 740 YM (MPa) 97	
P(3HB-co-13 mol% 3HV-co-15 mol% 3HHx)		n.d.	TS (MPa) 13 EB (%) 833 YM (MPa) 66	
P(3HB-co-10 mol% 3HV-co-38 mol% 4HB)	<i>Cupriavidus eutrophus</i> B10646, valeric acid, hexanoic acid, and γ -butyrolactone as precursor for copolymer production	M_w (g mol ⁻¹) 4.9×10^5 T_m (°C) 164 T_g (°C) -5 T_c (°C) 61	TS (MPa) 5.3 EB (%) 130 YM (MPa) 48	Zhila and Shishatskaya, 2018
P(3HB-co-17 mol% 3HV-co-55 mol% 4HB)		M_w (g mol ⁻¹) 5.4×10^5 T_m (°C) 166 T_g (°C) n.d. T_c (°C) 25	TS (MPa) 8.8 EB (%) 365 YM (MPa) 34	
P(3HB-co-21 mol% 3HV-co-13 mol% 4HB-co-2 mol% 3HHx)		M_w (g mol ⁻¹) 7.9×10^5 T_m (°C) 169 T_g (°C) -0.7 T_c (°C) 51	TS (MPa) 7.3 EB (%) 94 YM (MPa) 128	
P(3HB-co-6 mol% 3HV-co-9 mol% 4HB-co-1 mol% 3HHx)		M_w (g mol ⁻¹) 7.6×10^5 T_m (°C) 161 T_g (°C) -4.4 T_c (°C) 63	TS (MPa) 12 EB (%) 49 YM (MPa) 419	

operating pH of the acidogenic reactor, up to 30 mol% HV could be achieved, while at low pH (<6), the HV content significantly reduced to 5 mol%. Similarly, Huang et al. investigated the effect of pH of β -cyclodextrin and glycerol on the profile of odd C-number VFA in the anaerobic digestion of waste-activated sludge. The glycerol amount was found to be the predominant factor in regulating the odd VFA proportion, being the latter positively correlated to the mol% HV of the synthesized copolymers (Huang et al., 2018).

In another recent report, a valerate-dominant sludge hydrolysate was fed to enrich a PHA culture under feast-famine conditions. The valerate uptake was shown to correlate with the production of 3HV and 3-hydroxy-2-methylvalerate (3H2MV) precursors, resulting in a P(3HB-co-23.7% 3HV-co-7.9% 3H2MV) mmol C % copolymer. Microbial analysis revealed that such valerate-rich feedstock caused *Delftia* to be the prevailing group over other PHA-producing bacteria (Hao et al., 2017).

Furthermore, the use of phototrophic mixed cultures (PMCs) for PHBHV production has also been proposed to decrease operational costs, as these microorganisms are able to draw energy from sunlight and not require oxygen to produce ATP. Fradinho et al. (2019) applied an anaerobic permanent feast strategy to select for a PMC consortium able to regulate internal reducing power via PHA production. When the selected PMC was applied to fermented cheese whey, a PHBHV copolymer with 12 mol% HV was obtained, using light intensities corresponding to those of direct sunlight illumination and without any aeration requirement.

The PHBV properties as a function of HV content (Table 2) indicate a gradual decrease in the T_m together with an improvement in EB, resulting in a range of polymers with enlarged processability, useful to make films and fibers with different elasticities (Anjum et al., 2016; Keskin et al., 2017). Biopol is the trade name of a PHBV copolymer, currently produced by Metabolix, having a range of uses such as packaging, disposable cutlery, razors, cups, shampoo bottles, as well as surgical stitches, pins, and medical patches (Anjum et al., 2016). Evidencing good gas barrier properties, this polymer can be a good candidate for the production of biodegradable food packaging material, able to both extend the shelf life of food products and delay the foods' spoilage. The physical-chemical and structural stability of PHBHV (3 mol% HV) films under food contact conditions was evaluated by Chea et al. (2016). It was concluded that mechanical properties and water vapor permeability of PHBHV films were preserved after contact at 40°C for 10 days with different food simulating liquids tested (water, acetic acid 3% w/v, ethanol 20% w/v, iso-octane) except with ethanol 95% (v/v).

Processing of PHBHV material via traditional melt spinning is hampered by the transition from viscoelasticity to brittleness that occurs with increase in storage time (Wang et al., 2016). The obtainment of PLA/PHBHV fibers via conventional melt-spinning and hot-drawing processes represented a solution to overcome this problem (Li et al., 2015a). Mechanical properties of PHBHV fibers were also improved through the application of drawing and heat setting processes after the formation of the fibers (Hufenus et al., 2015).

The use of PHBHV electrospun fibers to develop active multilayer materials for food packaging application was also investigated (Castro-Mayorga et al., 2017a; Figueroa-Lopez et al., 2020). An active PHBHV-based multilayer, loaded with silver nanoparticles, was found effective against *Salmonella enterica*. The mechanical performance of the PHBHV was not altered by the incorporation of the electrospun PHBHV coating, and the presence of AgNPs did not affect the properties of the coated system as well (Castro-Mayorga et al., 2017a). In a more recent example, a novel multilayer system based on PHBHV (2–3 mol% HV) with antimicrobial properties was developed. Electrospun mats of PHBHV fibers containing eugenol were used as an active interlayer between a food contact layer of PHBHV and a cast-extruded PHB sheet. After the annealing at mild temperature, the novel multilayer active packaging material exhibited, besides antimicrobial activity, high hydrophobicity, strong mechanical resistance, and improved barrier properties against water vapor and limonene vapors (Figueroa-Lopez et al., 2020).

Additional updated examples of PHBV bioactive nanocomposites will be detailed in section *PHB-Based Bionanocomposites*.

The uses of PHBHV copolymers have been also investigated in biomedical sectors, where they have been shown to provide a positive effect on cellular growth and adhesion (Keen et al., 2007; Ahmed et al., 2010). Furthermore, the more amorphous structure displayed by PHBV copolymer has favored its exploitation in drug delivery applications due to easy diffusion of active molecules. Despite the improved polymer properties, copolymers often exhibit slow degradability and resorbability due to their intrinsic hydrophobicity, which limits cell colonization. Bhatia et al. (2019b) addressed this issue through the functionalization of PHBV copolymer (59% HV) with ascorbic acid, mediated by *Candida antarctica* lipase B. The modified polymer displayed antioxidant activity as well as a 1.6-fold increase in biodegradability as compared to the neat copolymer. In addition, the functionalization also resulted into a lower degree of crystallinity (due to imperfection of crystals) and higher thermal degradation temperature and hydrophilicity degree.

Poly (3-Hydroxybutyrate-co-Hexanoate)

Poly (3-hydroxybutyrate-co-hexanoate) (PHBHHx) is a promising copolymer based on 3HB with minor contents of 3HHx comonomer. Differently from PHBV, the presence of short chain branches of three carbon atoms in PHBHHx has a marked effect on reducing the regularity of the polymer chain, thus lowering both crystallinity and T_m (Noda et al., 2010). Actually, although the crystallization mechanism and the crystal cell structure do not change, the overall isothermal crystallization rate of PHBHHx copolymers reduces with HHx content and occurs at lower crystallization temperature from the melt (Cai and Qiu, 2009). Indeed, due to their steric hindrance, the 3HHx does not co-crystallize with 3HB units; thus, PHBHHx displays slower crystallization rate than PHB homopolymers, which can be a challenge for its efficient processing (Vandewijngaarden et al., 2016). The fact is that due to reduced crystallinity, when PHBHHx copolymers with different mol% HHx are subjected to

anaerobic biodegradation, the higher is the HHx, the faster is the rate of weight loss (Morse et al., 2011).

The synthesis of PHBHHx copolymer has been mainly obtained through strain engineering approaches, focusing on the specificity of the key PHA biosynthetic enzymes toward HHx precursors. The mol% HHx in PHBHHx copolymer was finely regulated (from 2.7 to 10.8%) by acting on the expression level of the *phaJs* in a *C. necator* strain harboring the PHA synthase gene from *Aeromonas caviae*. The same gene target was also overexpressed in *R. eutropha* Re2133, together with a PhaC2 synthase from *Rhodococcus aetherivorans* endowed with a broad specificity for mcl-monomer, as well as with the deletion of *phaB* genes. This strategy was effective in promoting up to 22% HHx using coffee waste oil as the substrate (Bhatia et al., 2018).

Escherichia coli has been used as chassis for the production of PHBHHx by introducing synthase genes specific for mcl-precursors and/or acting on the pathways channeling specific precursors (Taguchi et al., 1999; Lu et al., 2003). A high mol% HHx (50 mol%) has been achieved in *E. coli* strain engineered with the PHA biosynthetic operon from *Bacillus cereus*, using fatty acids as well as complex C-sources such as waste frying oils as substrates (Vastano et al., 2017, 2019).

Most of the engineering approaches have been focused on *Aeromonas hydrophila*, this strain being naturally able to produce PHBHHx from dodecanoate. First attempts of strain engineering reveal the synergic effect of the overexpression of phasins—proteins associated to PHA granules in the cells—and PhaJ coding genes in increasing 3HHx fraction (Han et al., 2004). An increase in 3HHx content is also obtained by deleting acetic acid pathway-related genes (Liu et al., 2011a). Interestingly, the overexpression of phasin coding genes in the engineered *A. hydrophila* strain not only determines an increase in 3HHx content but also causes a reduction in polymer molecular weight due to the formation of more PHA granules with reduced size (Tian et al., 2005).

To address PHBHHx production from glucose or gluconate instead of fatty acids, *A. hydrophila* and *P. putida* have been engineered with different combinations of target genes, with *tesA* thioesterase and *phaG* being the key targets in the two strains, respectively (Qiu et al., 2005).

In terms of thermomechanical properties, PHBHHx combines those of polyethylene (PE) (i.e., strength, flexibility, toughness, and elasticity), with printability and dyeability features (Anjum et al., 2016). Compared to conventional polymers used in packaging, PHBHHx films obtained by compression molding display relatively low oxygen permeability and a water vapor permeability slightly higher than those of PE, PP, and PS. CO₂ permeability is rather high if compared to known barrier materials (PET, PA, and EVOH) but also lower than those for packaging materials such as PP and PE (Vandewijngaarden et al., 2014). Despite its potential in food packaging application, the slow crystallization that characterizes this copolymer has represented an obstacle for its industrial processing. In fact, the addition of different additives acting as nucleating agents has been proposed. Ultrafine talc was reported to drastically improve PHBHHx crystallization, causing also an increase in the YM (Vandewijngaarden et al., 2016) without modification of the

material barrier properties, thus opening the way to its use as a protection layer for moisture-sensitive O₂ barrier layers. The use of zinc oxide as filler, on the other hand, also improved PHBHHx crystallization but strongly affected its opacity, although resulting in a successful UV-blocking property.

The exploitation of PHBHHx copolymers in combination with reinforcing materials (Dehouche et al., 2020) as well as in blending with other polyesters, mainly polylactic acid (PLA), can provide final materials with improved properties. Bio-composites based on PHBHHx and aloe vera fibers (AVFs) have been prepared by testing different surface treatment methods of AVF in order to improve the interfacial adhesion between the fiber and the polymer matrix (Dehouche et al., 2020). Blending of PHBHHx (11% HHx) with poly(DL-lactide) (PDLA) from solvent casting, at ratios of 2:1 and 1:2, exhibit a lower YM and a higher EB compared to unblended PDLA, whereas melt compounding of PLA and PHBHHx in different ratios inhibits PLA crystallization, resulting in enhanced elongation and toughness with respect to neat PLA (Lim et al., 2013).

Due to its biocompatibility and higher elasticity compared with PHB and PHBV, PHBHHx has been widely applied as scaffold matrix in tissue engineering and cell transplantation (Gao et al., 2006).

3HHx content affects *in vitro* growth and differentiation of smooth muscle cells (Qu et al., 2006a). When compared to PHB, PHBHHx reveals a higher degradation rate in subcutaneous implants in rabbits, and, most importantly, the copolymer elicits a very mild tissue response during implantation (Qu et al., 2006b). In one of the most recent examples, PHBHHx supports the residence, survival, and stemness of the transplanted neural stem cells (NSCs) cells in rat brain (Wang et al., 2019).

Surface modification of PHBHHx films under alkaline conditions has been found effective in promoting osteoblast cell response for application in bone-tissue engineering (Li et al., 2005). In a pioneering approach, Li et al. (2015b) have coated PHBHHx scaffolds with PHA binding protein (PhaP) fused with the arginyl-glycyl-aspartic acid peptide (PhaP-RGD) to promote proliferation and differentiation of mesenchymal stem cells seeded on them. Due to their reliable safety profile and strong hydrophobicity, PHBHHx is suitable for prolonged release delivery systems. Implantable sandwich PHBHHx films have been designed to address long time release of drugs, reducing the burst release effect (Peng et al., 2018). In addition, PHBHHx nanoparticles have been applied to this aim (Peng et al., 2013; Heathman et al., 2014). Interestingly, a hybrid copolymer, such as PEG200-end capped PHBHHx, has been synthesized by *A. hydrophila* in microbial fermentation and the derived nanoparticle tested as intracellular delivery nanocarriers for sustained drug release (Lu et al., 2004). Noteworthy, besides drug delivery, incorporation of PHBHHx nanoparticle in whey protein-based films, improves the mechanical properties of the derived bio-plastics producing more extensible materials preserving their mechanical resistance (Corrado et al., 2021).

Poly (3-Hydroxybutyrate-co-4-Hydroxybutyrate)

Several studies have been focused on the synthesis of poly (3-hydroxybutyrate-co-4-hydroxybutyrate) (P3HB4HB)

copolymers, using wild-type strains under feeding of 4HB precursors such as 4-hydroxybutyric acid, γ -butyrolactone, 1,4-butanediol, etc. (Choi et al., 1999; Lee et al., 2004).

Copolymers with different mol% 4HB (from 5 to 64%) have been produced in *C. necator* strain A-04 by tuning the ratios of fructose to 1,4-butanediol. The characterization of the copolymers reveals an increase in both elongation at break and tensile strength, as well as a reduction in polymer toughness, with increasing 4HB content (Chanprateep et al., 2010).

Co-feeding of soybean oil and γ -butyrolactone produces high yield of copolymer accumulation, although higher supplementation of the precursor has been shown to increase the 4HB fraction while inhibiting cell growth (Park and Kim, 2011). High PHA density fed-batch cultivation strategies employing mixed precursors (5:1 ratios 1,4-butanediol and 1,6-hexanediol) have been developed to boost the 4HB content up to 99 mol% in *Cupriavidus malaysiensis* transformed with additional copies of PHA synthase gene (PhaC) (Norhafini et al., 2017, 2019; Syafiq et al., 2017).

Waste materials such as saccharose from sugarcane industry (de Sousa Dias et al., 2017) and waste frying oils (Rao et al., 2010) have been also used in combination with 4HB precursors in processes employing *Burkholderia sacchari* and *C. necator*, respectively. Accumulation of P3HB4HB from slaughterhouse residues was achieved by using *Delftia acidovorans* DSM39 expressing and heterologous lipase (Romanelli et al., 2014).

The high cost of the 4HB precursors supplied to the growth media has encouraged the construction of engineered strains able to produce P3HB4HB copolymer from unrelated C-sources. An engineered *E. coli* strain has been designed to produce up to 65.5% P3HB4HB (11.1 mol% 4HB) accumulation using glucose as C-source. To enhance the carbon flux to 4HB biosynthesis, genes involved in succinate formation from succinate semi-aldehyde (succinate semi-aldehyde dehydrogenase) have been deleted (Li et al., 2010). A significant increase in copolymer accumulation has been achieved by the “enlarged cell strategy,” based on the alteration of the genes involved in cell division, in order to get filamentary *E. coli* with larger internal space. As an additional advantage, this filamentary recombinant *E. coli* also allows easier downstream separation from the fermentation broth (Wang et al., 2014). A P4HB homopolymer (PHA4400) is currently commercialized by Tepha Inc. (Cambridge, MA), which uses a proprietary transgenic fermentation process based on *E. coli*. The polymer is characterized by remarkable flexibility and good absorbability behavior *in vivo*, being well-suited for implantable medical applications. Noteworthy, the first products approved by the Food and Drug Administration (FDA) for clinical uses were P3HB4HB-based devices produced by Tepha (US) (Zhila and Shishatskaya, 2018).

A low-cost platform for non-sterile and continuous production of P3HB4HB from glucose has been designed using the halophilic *Halomonas bluephagenesis* as chassis. In this example, combinatorial deletions of multiple orthologs of succinate semi-aldehyde dehydrogenases has allowed to increase the 4HB molar fraction up to 24-fold (Ye et al., 2018).

Finally, a complex engineering strategy has been applied to *E. coli* to get co-polyesters of 3-hydroxypropionate (3HP)

and 4HB by redesigning the pathways for the synthesis of the corresponding monomers from 1,3-propanediol (PDO) and 1,4-butanediol (BDO). P(3HP-co-4HB) with adjustable monomer ratios have been produced and characterized (Meng et al., 2012). Interestingly, the same recombinant *E. coli* strain has been used for the synthesis of a block copolymer consisting of highly elastic P4HB portion together with a P3HP block endowed with enormous tensile strength, by applying an alternate PDO-BDO feeding. In comparison to the homopolymers P3HP and P4HB, the block microstructure displays reduced Tm as well as increased YM and TS (Tripathi et al., 2013b).

Medium Chain Length PHA Copolymers

The incorporation of longer monomers ($C \geq 6$) within the PHA polymeric chain determines the shift toward a more elastomeric behavior of the resulting polymer. These properties suit well with applications in tissue engineering and drug delivery, justifying the great interest in this research area.

Most of mcl-PHA are produced from *Pseudomonas* sp., which possess the specific metabolic pathways necessary for the synthesis of mcl-precursors from fatty acids. Mcl-copolymers with monomer composition ranging from C5 to C17 are synthesized by *P. aeruginosa* ATCC 27853 grown on odd-chain fatty acids from C17 to C21 under nitrogen starvation. The highest yield is obtained for heptadecanoic acid, probably because of limitation in the uptake of longer fatty acids. The characterized polymers are soft, sticky, rubber-like materials (Impallomeni et al., 2018). Previously, mcl-PHA production has been achieved by supplying even-chain n-alkanoic acids from C8 to C22 (Ballistreri et al., 2001). The use of complex oily sources, including waste frying oils, has been also explored for the synthesis of mcl-PHA from different *Pseudomonas* strains (Haba et al., 2007; Gamal et al., 2013; Follonier et al., 2014; Vastano et al., 2019).

The comonomer composition can be finely regulated by using β -oxidation weakened mutants of *P. putida* (Wang et al., 2011), so that the monomer composition is strictly related to the nature of the supplied fatty acid (Liu et al., 2011b). In an interesting example, a β -oxidation *P. putida* mutant has been exploited for the production of a novel diblock copolymer P3HHx-b-P(3HD-co-3HDD) by sequential supplementation of hexanoate and dodecanoic acid (Tripathi et al., 2013a). The incorporation of block microstructure determines an increase in TS, YM, and EB if compared to corresponding random copolymers. Thus, the blocky feature helps to capture the amorphous nature of the mcl-polymers, as well as to gain crystallinity, improving the overall polymer properties (Tripathi et al., 2013a). The incorporation of unsaturated PHA side chains represents a useful strategy to obtain functional and easily modifiable PHAs. By using a *Pseudomonas entomophila* strain with deficient β -oxidation pathway, the incorporation of 3-hydroxydodecanoate (3HDD) and 3-hydroxy-9-decenoate (3H9D) moieties in different ratios has been obtained from feeding with mixture of dodecanoic acid (DDA) and 9-decenol (9DEO). Due to the presence of unsaturated bonds, the copolymers can be cross-linked under UV radiation. Moreover, a diblock polymer P3HDD-b-P3H9D has been synthesized under specific feeding strategies. This polymer

displays a 2-fold increase in YM compared with the random copolymer with similar 3HDD/3H9D ratios (Li et al., 2014).

A rather unique copolymer composed of 3HB and 3HO units was obtained using an enriched culture of *Pseudomonas* sp. as initial inoculum for the production of PHA from acidified oil mill wastewater. The weight average molecular mass of polymer was characterized by a wide polydispersion index, as a consequence of the high complexity of the final microbial consortium (Ntaikou et al., 2014).

When the so-called glycogen-accumulating organisms (GAOs) from mixed culture anaerobic-aerobic wastewater treatment processes were used to produce PHAs from acetate, the applied operational conditions were found to affect polymer microstructure. As a fact, a mixture of true copolymers consisting of monomers HB, HV, 3H2MV, and 3-hydroxy-2-methylbutyrate (HMB) was produced under anaerobic conditions, while the aerobic process primarily produced the HB monomer, most likely forming separate homopolymer blocks (Dai et al., 2008).

Despite their potential, the widespread use of mcl-PHA is limited by the difficulty in their processing, which is due to low viscosity, poor melt strength, adhesive-sticky nature, and very slow crystallization. Gopi et al. (2018) have proposed a chemical modification strategy involving the reaction with dicumylperoxide and triallylotrimethacrylate co-agent to introduce branching and thus enhancing the crystallization kinetics of poly(3-hydroxydecanoate) (P3HD). The authors pointed out a possible application of these improved polymers in 3D printing of biomedical products.

The adhesive properties of an mcl-PHA (43 mol% HDD, 12 mol% HTD, 10 mol% HO, 6 mol% HHx) produced by *Pseudomonas chlororaphis* subsp. *aurantiaca* when grown on crude glycerol were investigated by Pereira et al. (2019). The films displayed good adhesion properties toward porcine and human skins, together with high tension and shear bond strength, suggesting the potential use of this material as novel natural adhesive for wound dressing. A different applicative scenario for this class of polymers has been recently reported (Sangkharak et al., 2020). The authors designed a novel biocomposite of an mcl-PHA (75 mol% HD) incorporating torch ginger cellulose nanowhiskers (TGNCs) as a filtering material for wastewater treatment.

Finally, an mcl-PHA (7.6 mol% HHx, 45.4 mol% HO, 41.8 mol% HD, 5.2 mol% HDD) produced by *Pseudomonas mendocina* CH50 from waste oils was transformed into an oligomeric derivative by acid hydrolysis and efficiently used as a plasticizer for PHB, resulting in softer and more flexible materials. The obtained materials, entirely based on PHA, were found applicable in soft tissue engineering, thanks to their improved properties as well as the demonstrated *in vitro* biocompatibility (Lukasiewicz et al., 2018).

Other Copolymers

Manipulation of synthetic pathways for PHA production has allowed to design new engineered strains able to incorporate unnatural monomers within the polymer backbone (Choi et al., 2020). Whatever is the unnatural monomer to be introduced in the bio-polyester, the designing of new evolved PHA synthases

endowed with proper specificity in recognizing uncommon substrates is a *sine qua non*-condition for effective *in vivo* synthesis (Park et al., 2012). The introduction of a phenyl group on the side chain has been obtained in *P. entomophila* β -oxidation weakened mutant, in the presence of 5-phenylvaleric acid (PVA) as precursor (Shen et al., 2014). A microbial cell factory for the production of P(LA-co-3HB) copolymer has been designed through fine *E. coli* engineering (Taguchi et al., 2008). Besides the PhaA and PhaB from *R. eutropha*, the recombinant strain expresses a propionyl-CoA transferase (PCT) from *Megasphaera elsdenii*, able to catalyze coenzyme A addition to lactic acid, and a mutated PHA synthase from *Pseudomonas* sp. 61-3, endowed with the ability to polymerize lactoyl-CoA precursor. Interestingly, the same strain was exploited for the production of P(LA-co-3HB) from on a lignocellulosic feedstock, taking advantage of the *E. coli* abilities to metabolize both xylose and galactose derived from woody-extract hemicellulosic hydrolysate (Takisawa et al., 2017).

A similar approach allows to incorporate 2,3-dihydroxybutyrate (DHBA) in engineered *E. coli* using glycolate as the sole C-source (Insomphun et al., 2016).

Properly designed feeding strategies, combined with a set of PHA synthetic genes with suitable specificities, have been developed to obtain complex ter- or quarter-polymers. Terpolyesters composed of HB, HV, and HHx monomers have been produced by providing *Aeromonas hydrophila* 4AK4 strain with a set of PHA synthesis genes, allowing to supply the corresponding monomer precursors from lauric acid and/or valerate. Among the different synthesized polyesters, P(3HB-co-11% 3HV-co-10% 3HHx; PHBV11HHx10), and P(3HB-co-17% 3HV-co-10% 3HHx; PHBV17HHx10) have the suitable combination of YM, EB, and TS ranging from 97 to 235 MPa, 341 to 740%, and 8.4 to 14.3 MPa, respectively (Zhang et al., 2009).

In a similar approach, *R. eutropha* has been engineered with *A. hydrophila* PHA biosynthetic operon to produce PHBV7HHx11 and PHBV18HHx11 when fed with increasing amount of propionic acid. Compared with PHBHHx with 12 mol% HHx (PHBHHx12), the terpolymer has higher crystallization rate and degree of crystallinity. Crystallization studies have revealed that the simultaneous introduction of 3HHx and 3HV monomers in PHB improves the mobility of chain stems along the chain direction, leading to easier intralamellar slip during heating or drawing, finally resulting in improvement of mechanical properties (Ye et al., 2010). Furthermore, different P3HB4HB biopolymers, P3HBHV4HB terpolymers, and P3HBHV4HBHHx quarter-polymers with varying 4HB amount have been synthesized by *C. necator* strains under specific feeding strategies. The effect of 4H monomer unit into all the synthesized copolymers is in lowering the melting and the crystallization temperatures, thus improving processing-related properties of these materials. All the copolymers also display enhanced EB compared to PHB (Zhila and Shishatskaya, 2018).

Tuning Polymer Molecular Weight

The average molecular weight of PHB synthesized by bacteria is usually in the range of $0.1\text{--}2.0 \times 10^6 \text{ g mol}^{-1}$ in *R. eutropha* (Tsuge, 2016). However, ultrahigh molecular weight

PHB (UHMW-PHB) with defined M_w $43.0 \times 10^6 \text{ g mol}^{-1}$ display high mechanical strength (TS, 1,320 MPa; EB, 35%; YM, 18.1 GPa) and are preferred in applications requiring high mechanical strength, such as in developing high-strength fibers and films (Iwata, 2005).

Several factors have been shown to increase molecular weight during *in vivo* synthesis of PHA polymers: the concentration and the activity of the PHA synthase, the occurrence of chain transfer (CT) reactions, and the simultaneous degradation of PHA during biosynthesis (Tsuge, 2016). The molecular weight has been shown to decrease with increasing PHA synthase concentration and to increase proportionally with its catalytic activity. A CRISPRi-based approach to modulate PhaC expression level in *E. coli* has come to the same correlation: the higher the PhaC activity, the more the PHA accumulation, yet the less the molecular weight and the wider the polydispersity (Li et al., 2017).

The CT reaction is caused by the presence of molecules (CT agent) that promote the transesterification reaction between their hydroxy group and the carboxy group of the growing polymer chain-PHA synthase complex. Commonly occurring CT agents include water, 3HB, and ethanol. Thus, high-molecular-weight PHA can be synthesized, for example, by ensuring sufficient culture aeration to facilitate cell growth while preventing ethanol production. Furthermore, deletion of PHA depolymerase genes promotes the production of high-molecular weight PHA by turning off the polymer degradation within the cell (Tsuge, 2016).

CHEMICAL AND PHYSICAL STRATEGIES TO IMPROVE POST-SYNTHESIS PHB-BASED MATERIALS

Use of Plasticizers

In general, in the field of polymers, it is possible to identify two types of plasticizers: internal and external (Vidéki et al., 2007). The internal plasticizers are part of the polymer molecules, as they are chemically bound to the polymer chains, grafted or reacted with the original polymer, thus making the polymer chains more difficult to adapt and compact together closely. Their main role is to soften the polymers by lowering their glass transition temperature (T_g) and reducing their elastic modulus (Vieira et al., 2011). External plasticizers, instead, are low volatility molecules added to interact with polymers, widening the polymer chains without chemical reaction. In this case, the internal molecular forces between plasticizer molecules and between a plasticizer and a polymer play a fundamental role, such as dispersion forces, induction forces, dipole-dipole interaction, and hydrogen bonds (Mekonnen et al., 2013). Several theories have been proposed to explain the mechanism and role of plasticizers in polymers. The most important are (a) the lubricity theory, (b) the gel theory, and (c) the free volume theory (Vieira et al., 2014).

Although these theories are widely accepted and used in plasticizer selection for polymers, Shtarkman and Razinskaya (1983) have emphasized the limitation of current theories on the mechanism of plasticization. Indeed, according to these authors, it is not possible to establish a plasticization mechanism because

of the huge versatility of the investigated polymer and plasticizer systems; hence, instead of trusting on the above theories, it would be much more useful to consider the direct correlation between compatibility-efficiency-property of each investigated polymer-plasticizer blend. As an example, since the behavior of a single polymer highly depends on its thermal history, different film processing can provide substantial diverse crystalline pattern, and the effect of the same plasticizer on these polymer substrate will, therefore, be quite different.

Therefore, the choice of a plasticizer involves several important criteria, including a high degree of compatibility with the polymer matrix, responsible of its easy solubility and inclusion in both crystalline (toughening) and amorphous (softening) regions. The compatibility should be consistent with the whole temperature range of applications; hence, plasticizer molecular mass and chemical structure, including polarity, shape, and size, must be considered to assure a suitable plasticizing effect. Generally, plasticizers are responsible for T_g lowering and elastic modulus decreasing, as reported above. Hence, the efficiency may be expressed in terms of T_g depression and stiffness reduction. With the lowering of T_g, elongation at break and flexibility of the polymer increases. In fact, elongation and impact resistance strongly depend on polymer T_g and molecular structural organization. In addition, the plasticizers should remain inside the polymer matrix. The larger the plasticizer, the lower its vapor pressure, and thus, the greater its permanence inside the polymer; on the other hand, bigger molecules are slowly diffused inside the macromolecular chains, since the highest diffusion rate is associated to small molecules that, on contrary, show higher vapor pressures (Vieira et al., 2011).

As noted above, the blending with the plasticizers is considered to be one of the simplest route to overcome the limitations of PHB, allowing for a broader application window. Generally, the use of natural or non-natural plasticizers would allow to lower the glass transition and melting temperature, through the enhanced macromolecular movement. In this way, it would be possible to process the polymer at lower temperatures without inducing its thermal degradation (Baltieri et al., 2003; Erceg et al., 2005). Furthermore, plasticizers could improve both the toughness and softness of the polymer by decreasing its crystallinity, weakening the intramolecular bond, and facilitating conformational changes.

For these reasons, many efforts have focused on the industrial formulation of PHB with external plasticizers able to improve their thermal and mechanical properties (Mangeon et al., 2018). The relevant literature is rich in number and type of plasticizers for PHB. They vary from those of natural origin to synthetic one from those with low to high molecular weight, from linear to branched structures. **Table 3** summarizes some of the best known plasticizers in the literature, together with the main properties investigated, when used in mixing with PHB with a molecular weight in the range of 100,000–300,000 g mol^{-1} .

From **Table 3**, it emerges that blending with plasticizers induce a general lowering of the glass transition temperature and an improvement in elongation at break for almost all the additives used, with few exceptions. The difference can be

TABLE 3 | Main plasticizers for PHB.

Plasticizers	Acronyms	M _w (g mol ⁻¹)	% w/w	T _g (°C)	T _m (°C)	EB (%)	TS (MPa)	YM (MPa)	References
Glycerol	G	92	13		170	0.9	24.8	2835	Jost and Langowski, 2015
Triacetyl glycerol	TAG	218	20	-16.7	161	10.3	14.1	238.4	Baltieri et al., 2003
Dioctyl phthalate	DOP		20	-9.4	164.5	10.5	18.0	448	Baltieri et al., 2003; Wang et al., 2008
Dioctyl adipate	DOA		30	-6.9	165.3	6.2	16.1	576	
Dioctyl sebacate	DOS		30	-3.6	163.5	4.3	6.0	374	
Propylene glycol	PG	76	17		171	0.9	24.9	3,360	Râpe et al., 2015
Triethyl acetate	TEC	276	20	-30	164	2.3	15.8	1,135	Choi and Park, 2004; Râpe et al., 2015
Soybean oil	SO	920	20	-3.4	161		15		Choi and Park, 2004
Epoxidized soybean oil	ESO	975	13–20	-19	160	1.0	30	2,729	Choi and Park, 2004; Jost and Langowski, 2015; Panaitescu et al., 2017
Castor oil	CO	933	13		171	0.9	27.1	3,089	Jost and Langowski, 2015
Triethyl citrate	TC	276	30	-24	–	21	18.6	960	Râpe et al., 2015
Tributyl citrate	BTC	515	30	-23	–	32	9.4	800	Râpe et al., 2015
Acetylbutyryltriheptyl citrate	ABTC	558	30	-30.7	156.8	9.7	6.1	192.7	Erceg et al., 2005; Râpe et al., 2015; Chaos et al., 2019
Salicylic acid decylester	–	–	30	-28	–	104	11.8	850	Kunze et al., 2002
Salicylic acid 2-butyloctyl ester	–	–	30	-28	–	22	13.5	810	Kunze et al., 2002
Acetylsalicylic acid hexylester	–	–	30	-14	–	126	11.8	680	Kunze et al., 2002
Ketoprofenethylester	–	–	30	-14	–	58	11.8	600	Kunze et al., 2002
polyhydroxy-butyrate-hexanoate	PHHBX	1760	PHB–1/6	-10	102	9.8	25		Wang et al., 2008
Polyethylene glycol	PEG 1000	950–1050	50	–	170	1.0	23	2,700	Bibe et al., 1999
Linalool	L	154	20	-11.0	174	5.2	20	560	Mangeon et al., 2018
Geraniol	G	154	20	-9.0	179	5.9	21	760	Mangeon et al., 2018
Geranyl acetate	GA	196	20	-13.0	170	13.8	15	395	Mangeon et al., 2018
Dodecanol		186	10	7	155				Yoshie et al., 2000
Lauric acid	–	200	10	4	171				Yoshie et al., 2000
Tributylin	–	302	10	1	172				Yoshie et al., 2000
Trilaurin	–	639	10	-4	173				Yoshie et al., 2000

ascribed to the variation in combining the chemical structure of the plasticizer, the molecular weight, the solubility, and compatibility with the polymer, as above discussed. Therefore, the summarized plasticizers can be discussed after their subdivision based on building block molecule: (i) glycerol, (ii) oil, (iii) citric acid, and (iv) salicylic acid. Besides these, we must also add the category of plasticizers that have structures similar to some phthalates, common plasticizers of PVC, and those of smaller natural molecules such as those of terpenes.

Yoshie et al. (2000) compared the effect of tributyrin, trilaurine, lauric acid, and dodecanol on the physical properties of PHB. All the molecules used act to reduce the T_g and the cold crystallization temperature, T_{cc}. In this trend, the best seems to be tributyrin, given its good miscibility with the polymer chains. Although there is this advantage, all additives, even in small amounts (1% by weight), promote the enzymatic degradation of the polymer.

Recently, bio-based compounds such as the terpenes have also been studied as additives for PHB, thanks to their additional beneficial properties such as antioxidant and antibacterial activities (Persico et al., 2012). Terpenes are interesting components of essential oils extracted from plants, with a chemical structure of repeating units of isoprene (C₅H₈). Among these, the oxygenated monoterpenes that contain alcohol have been described as having greater biological activity. Mangeon et al. (2018) studied linalool (L), geraniol (G), and geraniol acetate (GA) as PHB plasticizers. In this study, the use of terpenes led to a decrease in T_g and an increase in elongation at break over 650% combined with a decrease in Young's modulus compared to pure PHB. The effect is more pronounced with GA due to the presence of the segment bearing an ester group, which increases free volume and molecular mobility. The fact that terpenes are already widely used in the chemical industry gives them real potential as a PHB plasticizer with antibacterial properties.

Salicylic acid esters and ibuprofen ketones have also been reported as suitable plasticizers of PHB. Their use, given their properties, is recommended for medical packaging (Kunze et al., 2002).

Dibutyl sebacate (DBS), dioctyl sebacate (DOS), polyethylene glycol (PEG), and Lapro1503 (L503), have also been reported in the literature as biodegradable lower molecular weight plasticizers to improve the properties of PHB. All the additives proved to be compatible with the polymer, forming monophasic mixtures up to a concentration of 15–20% by weight. For all, a decrease in T_g and an improvement and a decrease in the crystallization temperature were found (Baltieri et al., 2003; Wang et al., 2008).

Citric acid ester plasticizers are among the most important plasticizers and environment friendly because of their safety and non-toxicity. They have been approved in the United States, the European Union, and other developed countries for use in plastic products in close contact with the human body and meet high hygiene requirements (Chabrat et al., 2012). Acetyl tributyl citrate (ATBC) and tributyl citrate (TBC) are among the most studied in detail, thanks to their excellent performance. In addition, TBC has antibacterial and flame-retardant properties, which further expand its applicability (Chaos et al., 2019).

Many of these have been described as good plasticizers for PHB, improving its processability, in particular ATBC, TBC, and triethyl citrate (TC). The incorporation of plasticizers into PHB decreased TS and YM but increased the elongation at break. TBC and ATBC were the most compatible and efficient plasticizers on improving the thermal, mechanical, and barrier properties of PHB. The optimum concentration could be up to 20% depending on the desired properties of the final products (Erceg et al., 2005; Râpe et al., 2015; Chaos et al., 2019). From the study of Choi and Park (2004), triethyl citrate was the most effective plasticizer in terms of reduction in the glass transition temperature as well as in terms of improvement in the impact strength and elongation.

This result can be explained by the decrease in crystallinity and the crystalline size and in the formation of small spherulites, due to the easier penetration of the additive molecules between the polymer chains, which reduce the hydrogen bond. These data were correlated with the increase in elongation at break of the initial degradation temperature of the PHB.

Suárez Palacios et al. (2014) postponed the use of glycerol-based plasticizers and as an alternative to phthalates in the medical field. When mixed with PHB, glycerol and its derivatives showed good results due to their polarity (Jost and Langowski, 2015).

Many works in the literature point out that the use of high molecular weight plasticizers has a more pronounced effect in improving the mechanical properties. This is the case with PEG and epoxidized oils (Bibe et al., 1999). Epoxidized oils are among the most studied plasticizers of PVC, obtained by epoxidation with peracids with various oils (Turco et al., 2019b). The behavior in mixture with PHB can be explained by the higher reactivity of the epoxide group and the possibility of hydrogen bond formation (Choi and Park, 2004; Jost and Langowski, 2015; Panaitescu et al., 2017).

The main drawback in the use of plasticizers mainly concerns the external plasticization with the migration of the plasticizer from the plasticized material. This process can occur by diffusion of the plasticizer from the bulk material to the surface (exudation) or by interface phenomena and absorption or by evaporation in the surrounding medium. This phenomenon causes a decrease in the plasticizer amount in the polymer, with loss of elasticity and ductility of the material. Additionally, the leaking plasticizer from the material can contaminate the surrounding medium (medical application problems). Several factors influence the migration of the plasticizer, the main ones with regard to the type and concentration of the plasticizer, its molecular weight, branching, and polarity. Low-molecular-weight plasticizers are more prone to migrate from the polymeric material. The more linear the plasticizer structure, the faster the extraction and migration rate will be compared to more branched plasticizers. The migration of the plasticizer is also influenced by the type of polymer, its molecular weight, and its compatibility with the plasticizer, and from the plasticization process and the homogeneity of the product.

PHB Physical Blends and Reactive Blends

For a sustainable processing strategy, the blending with other polymers or additives represents a much more easy and cost-effective approach and, as a result, is the more frequently used technique in the industrial sector (Anna and Arrigo, 2019). In fact, following this procedure, polymeric materials with enhanced and tailored chemico-physical and mechanical properties can be obtained by opportunely regulating the weight ratio between the selected polymers. Actually, the blending of two polymeric matrices is strictly correlated to their miscibility, i.e., to their respective solubility parameters (δ). If they are quite similar, a good miscibility should be expected. Anyway, the miscibility between two or more polymers also depends on the processing temperature, weight ratio in the blend compositions, as well as polymer respective molecular weights and crystallinity (Arrieta et al., 2017). Among bio-based polymers, poly(lactic acid) (PLA) is the most used mainly in food packaging area because of its easy processability, high transparency, and relatively low costs. PLA is produced through fermentation of lactic acid, followed by chemical polymerization; differently from PHB, it is a compostable material mainly commercialized for single-use disposal packaging items, such as bottles, cold food cups, and trays, as well as for flexible films (Auras et al., 2004; Jamshidian et al., 2010). Blending PHB with PLA could gain mutual advantages; indeed, PLA shows low crystallinity, scarce barrier properties, low heat distortion temperature (softening above 60°C), and difficult biodegradation at ambient conditions. These drawbacks, limiting its industrial exploitation, could be improved by its melt blending with another highly crystalline biopolymer matrix with similar melting temperature, lower T_g , and suitable barrier properties and biodegradability, as in PHB (González-Ausejo et al., 2017). Hence, PHB/PLA blends have gained a great interest, since their combination allows to obtain new biopolymer based systems with enhanced properties as compared to the single components while preserving their ecosustainability (Modi et al., 2013). Nevertheless, generally, PHB and PLA do

not evidence fine miscibility although they have similar solubility parameters, ranging between 19.5 and 20.5 ($\text{MPa}^{1/2}$) for PLA and between 18.5 and 20.1 ($\text{MPa}^{1/2}$) for PHB. Actually, in polymer blending, several parameters should be taken in consideration. The first one is the polymer molecular weight. In their paper, Blümm and Owen found that low-molecular-weight (LMW) PLA and high-molecular-weight (HMW) PHB were melting miscible over the whole composition range, whereas a blend of HMW-PLA with LMW-PHB evidenced phase separation above PHB content of 25% (Blümm and Owen, 1995).

Similarly, Zhang and Thomas (2011) reported the formulation of PLA/PHB blends with different weight ratios (100:0, 80:20, 60:40, 40:60, and 0:100), showing that some interactions between the two polymers were established, notwithstanding their immiscibility. In particular, the blend containing 25 wt% of PHB evidenced outstandingly improved tensile properties compared with pure PLA because of the homogeneous dispersion of PHB crystals, which acted as a filler and nucleating agent in PLA. Anyway, the processing temperature can play a decisive role on PHB-PLA miscibility by providing, in some case, to melt reactive compatibilized blends. Indeed, while LMW-PLA and HMW-PHB blends obtained by solvent casting at room temperatures evidence phase separation in all compositions, the same blend melt blended at 200°C showed higher miscibility, evidenced by the lowering of both PHB melting temperature and PLA glass transition temperature. The better miscibility was ascribed to transesterification reactions occurring between PLA and PHB chains during heating, leading to the formation *in situ* of low-molecular-weight PLA-PHB block copolymers acting in the interfacial region between the two phases as enhancer of their compatibility (Zhang et al., 2012). In addition, PHB/PLA interfacial compatibilization can be improved by melt-reactive extrusion in the presence of an external compatibilizer agent. For instance, Jandas et al. (2014) used maleic anhydride (MA) as reactive compatibilizer for PLA and PHB matrices to increase their miscibility. Actually, MA chemically grafted the α -carbon atom of the carbonyl group of PHB and PLA. Moreover, the presence of the reactive dicumyl peroxide was responsible of the formation of cross-linked and branched structures at their interfaces. In addition, the compatibilized blends evidenced substantial improvement of mechanical flexibility as a function of MA concentration. Passing from 1 to 9 wt%, PLA-PHB 70:30 blend changed from a brittle to a ductile material, reaching the best flexibility of more than 500% by grafting 7 wt% of MA (Jandas et al., 2014).

In order to improve PHB-PLA blends flexibility, by both increasing the polymer chain mobility and improving their processing for film manufacturing, plasticizers are frequently added to the blend. In this sense, PLA-PHB plasticization has been proven to be an effective way to enhance mechanical performance as well as to improve the compatibility between PLA and PHB biopolymers. Nowadays, the traditional plasticizers give way to natural ones due to the migration phenomenon, which could result in potential human health and environmental hazards (Harmon and Otter, 2018). Several plasticizers have been used mainly at concentrations between 10 and 30 wt% for film applications, such as glycerol (Martin and Avérous, 2001),

poly(adipates) (Martino et al., 2011), PEG (Wang et al., 2008), citrate esters (Fenollar et al., 2013), and low-molecular-weight additives such as aroma compounds including D-limonene, carvacrol, and thymol (Arrieta et al., 2014). Most of them were able to decrease PLA Tg and increase polymer blend tensile strain (Arrieta et al., 2017), as previously detailed.

The blending with another natural polymers, such as thermoplastic starch (TPS), could represent a valid support to both obtain cost-effective biopolymer-based systems and enhance PHB properties without compromising environmental and carbon management benefits. Starch, a biodegradable polysaccharide produced by numerous plants, is one of the most abundant renewable feedstock resources known to man. Thanks to its biodegradability, renewability, and easy availability, starch has been extensively studied as a low-cost component of biodegradable plastic materials (Zhang et al., 2014). It is mostly composed of linear amylose and highly branched amylopectin organized in granular state due to the inherent hydrogen bonding between molecules. This native structure, providing a high crystalline material, severely hinders the dispersion of starch into a polymer matrix at a fine scale. When mixed with some water and/or plasticizers such as glycerol and following subjection to heat and shearing action, starch undergoes spontaneous destructure, provoking the breaking down of intermolecular hydrogen bonds in favor of the polymer gelatinization. A homogeneous melt known as thermoplastic starch (TPS), evidencing typical thermoplastic behavior, is thus formed (Pyshpadass et al., 2008). Hence, TPS can be obtained and formulated by means of standard equipment commonly used in industrial manufacturing of synthetic polymers (Liminana et al., 2019). However, the high hydrophilicity and hygroscopicity, the quick physical aging effect due to the retrogradation process, and the poor mechanical properties strongly affect the industrial application of neat TPS (Ortega-Toro et al., 2017). This is why blending with more hydrophobic polymers, such as PHB, could enhance its functional properties (Turco et al., 2019a).

Hence, the mixing of PHB and TPS would combine the advantages of the two polymers by synergizing their properties while preserving the complete biodegradability of the blend. In their work, Godbole et al. (2003) blended PHB and TPS at different weight ratio compositions and studied the thermal and mechanical properties of the obtained films. They found that the blends PHB/TPS with a w/w percentage ratio of 70:30 showed a consistent improvement of mechanical performances with respect to neat PHB; as an example, the blending of only 30% w/w of TPS to PHB could double and quadruple the stress and strain at break values of the polyester, respectively. Although no shifting of PHB melting temperature could be observed, thus indicating that there were no interactions at molecular level, a strong delay of PHB decomposition temperature could be highlighted passing from about 220 to 260°C; TPS could act as a thermal stabilizer of PHB.

Vice versa, by investigating the influence of PHB on TPS properties, Lai et al. (2006) studied the mechanical properties of films based on TPS doped with different amounts of PHB (1, 3, 5, and 7 wt%). They found that the mechanical properties of films increased by increasing PHB content, whereas the values of water

absorption, one of the main issues of hygroscopic TPS, decreased because of the higher PHB hydrophobicity. Actually, it is worthy to underline that, for PHB/TPS blends, there is an optimized ratio between glycerol (used to thermoplasticize starch) and PHB concentration finalized to reach a suitable compatibility between the polymers. The same authors found that, when TPS contains 25% of glycerol, the tensile strength of the blend TPS/PHB significantly increased by increasing PHB content, whereas when 33% of glycerol is used, only slight changing could be observed. This outcome could be probably due to the higher gelatinization degree, resulting in a structure more prone to water diffusion. Similar results were found by Thiré et al. (2006). In their work, the authors investigated compression-molded PHB/starch blends with starch content varying between 0 and 50%. They found that, above 30% in weight of TPS blended with PHB, higher starch contents led to the worsening of mechanical properties due to the lack of interfacial adhesion between starch and PHB, also evidenced by morphological analysis.

In order to improve the interfacial adhesion between the polymers, Zhang and Thomas (2010) prepared PHB/starch blends by melt process and investigated the properties in terms of interfacial adhesion between the polymers. Two types of maize starch, starch 1 (containing 70% amylose) and starch 2 (containing 72% amylopectin), were melt blended with PHB. The spectroscopic and morphological analyses evidenced that starch particles acted as nucleating agent for PHB crystallite formation by significantly reducing the spherulites size; moreover, the starch fillers physically interacted with PHB by means of intermolecular hydrogen bonds. This effect was particularly highlighted when the more linear and tighter structure of amylose-rich starch was used. Hydrogen bonding between the polar residues of starch (hydroxyl groups) and carbonyl residues of PHB could inhibit the chain scission degradation in PHB, thus improving its thermal stability. As a consequence, higher melt shear viscosity and better mechanical properties were observed when starch 1 was used.

PHB Reactive Blends

Blending different polymers opens up a range of possibility for the development of novel materials with interesting properties. As previously underscored, melt compounding is one of the most effective methods to tune the polymer blending properties. This method allows preparation of new bio-based polymer blends or composites with pleasing properties. Anyway, most of the blends consist of thermodynamically immiscible polymers, and the simple physical mixing in the melt state usually leads to phase separation on the micrometer scale resulting in unfulfilling properties of the final products. To overcome the problems related to incompatibility, bio-based polymer blends and composites require a reduction in interfacial tension between the components leading to improved final properties of the materials (Muthuraj et al., 2018). Among various strategies for compatibilization, reactive blending seems to be one of the most promising and environment-friendly approaches (Raquez et al., 2008). It is a fast, solvent-free, low-cost, and environment-friendly method by which designed chemical reactions between the components in suitable processing conditions occur. Reactive blending is really versatile since it can be successfully

applied during “*in situ* polymerization” of biodegradable polymers, functionalization of natural fibers/fillers, or chemical modification of the polymer structure. Moreover, the reactive blending occurring by using the “dynamic curing” of bio-based polymers and composites is worthy of consideration in this research field. The method consists on using reactive species as organic peroxides in the melt chamber resulting in the formulation of copolymers, which act as interface compatibilizers between two (or more) polymer matrices. In the literature data, the dynamic curing of biodegradable aliphatic polyesters blends (Ma et al., 2014), aliphatic polyester/natural rubber blends (Wang et al., 2015), and, more recently, bio-composites (Luo et al., 2016) indicated that the high temperature necessary to decompose organic peroxides also induces transesterification reactions of aliphatic polyesters, responsible of polymer chain rearrangements toward soluble copolymers. This confirms that dynamic curing of bio-based polymer blends and composites can lead to the development of semi-interpenetrating networks connecting two (or more) phases, which significantly enhances their physicomechanical properties.

In their paper, Przybysz et al. (2018) used two different organic peroxides, dicumyl peroxide (DCP) and di-(2-tert-butylperoxyisopropyl)-benzene (BIB), to compatibilize polycaprolactone (PCL)/PHB blend. Polycaprolactone is a synthetic semi-crystalline linear aliphatic polyester that is biocompatible and biodegradable. It is ductile and has a significantly lower melting point than PHB at about 60°C. Blends of PCL and PHB have attracted much attention due to their inherent biodegradability and biocompatibility, although they are immiscible on the molecular scale as proven by Antunes and Felisberti (2005).

It was observed that the addition of free radical initiators to PCL/PHB blends resulted in the significant enhancement of mechanical and thermal properties in comparison to uncompatibilized blend obtained by only physical mixing. The severe improvement of PCL/PHB properties was due to the partial cross-linking and/or branching of the covalently linked blends, as evidenced by the melt flowrate. Moreover, the better efficiency of BIB due to its higher number of free radicals was responsible for a tightened final compatibilized structure (Przybysz et al., 2018).

PHB-Based Bionanocomposites

One of the main drawbacks of PHB is the high costs correlated to the fermentation and extraction processes. As a result, several studies investigated on the preparation of PHB bio-composites by blending it with natural fibers and fillers, aiming at producing more cost-effective materials with improved properties (Delmas et al., 2011; Garcia-Garcia et al., 2016). Inspired by these considerations and in the frame of an eco-sustainable approach, Angelini et al. (2014) prepared compression-molded bio-composites employing a lignin-containing filler obtained as a by-product of the bioethanol fermentative production process, using *Arundo donax* as a biomass (Vishtal and Kraslawski, 2011). When blended with biodegradable aromatic and aliphatic polyesters, an increase in thermal stability and elastic moduli of the resulting composites was observed, not neglecting the

valid opportunity for converting an agro-food by-product into a bio-resource, aimed to improve the properties of PHB in an environment-friendly and cost-effective way (Mousavioun et al., 2010). Therefore, in order to reduce the costs of filler processing, hence the bio-composite overall cost, no pretreatments other than milling were performed on the crude lignin-containing residue filler prior to use. The biodegradation behavior of the composites, qualitatively assessed by analyzing the surface of soil buried films, evidenced a significant surface degradation of PHB-based bio-composites. The authors demonstrated that lignin positively affected the rheological behavior of the polymer melt and acted as a PHB nucleating agent (Angelini et al., 2014). In mixtures, the nucleation rate and size of the spherulite depend on the cooling rate and the nucleation density. Nucleating agents (NAs) provide polymers with homogeneous nuclei and allow more rapid crystallization during the cool-down period after the polymer melts. Indeed, it is very important to both accelerate the crystallization rate of PHB-based materials and provide the formation of small and more homogeneous spherulite sizes in order to enhance its mechanical properties. In general, adding NAs results in an increase in melt crystallization temperature and narrowing of the crystallization peak during non-isothermal melt crystallization; in other words, in the presence of NA, less degree of supercooling and shorter crystallization time occur (Shi et al., 2015).

Recently, natural fibers are increasingly being utilized as environment-friendly materials to improve polymer properties. The natural fibers can represent a valid alternative to synthetic oil-fossil-derived fibers, such as glass and carbon fibers, commonly used as reinforcements in bio-plastics due to their strong mechanical properties. The cellulose-based fibers are eco-sustainable and cost effective (Tan et al., 2015) due to their biodegradability, renewability, and availability; moreover, they have low density, competitive specific mechanical properties, and a relatively low cost (Ching et al., 2016). Generally, along with a number of benefits as reinforcements, there are some drawbacks associated with the exploitation of these natural lignocellulosic fibers. Indeed, the hydrophilicity and strong cross-linking of lignocellulosic fibers prevent the compatibility with biopolymer matrices, leading to poor interfacial adhesion and mechanical properties (Sanchez-Garcia et al., 2008). In their paper, Tănase et al. (2015), prepared new bio-composite materials based on PHB and different percentages of cellulose fibers (from 2 to 10%) in order to improve PHB physical and mechanical behavior. By increasing the cellulose fiber content, the authors evidenced a decrease in melt viscosity and melting temperature, making the composites easy to process.

The crystallinity of PHB/FC composites decreased for all samples compared to neat PHB. The decrease in the crystallinity of the tested samples could be attributed to the hindered motion of the polymer segments due to the presence of cellulose fibers in the polymer matrix. The composite showed a blocking effect in the UV light spectra region while maintaining high transparency, resulting in a suitable property for a packaging material. On the other side, the water vapor barrier was poor due to the hydrophilicity of cellulose fibers (Tănase et al., 2015).

Driven by the necessity to overcome these issues, attempts to improve bio-composite performances have been carried out by the development of bionanocomposites. Polymer nanocomposites, obtained by incorporation of nanosized particles into polymer matrices, evidenced clear improvements of PHB properties, mostly if mechanical performances are concerned. For example, studies on the effect of organoclay minerals on mechanical properties of PHAs have been performed (Ozkoc and Kemalolu, 2009). As a matter of fact, polymer nanocomposites exhibited markedly improved properties when compared to the pure polymer. Mineral clays are the most used silicates in bionanocomposites manufacturing. Indeed, they can modify the polymer characteristics and improve their processability. As clays are naturally hydrophilic, in order to make them more compatible with hydrophobic polymer like PHB, the cations between the layers can be changed by cationic surfactants like the alkyl ammonium (Alexandre and Dubois, 2000). The modified clay becomes organophilic, its surface energy decreases, and the interbasal distance increases. The modified organo-nanosilicates are more compatible with the hydrophobic PHB nature due to the improvement of the interfacial adhesion. Furthermore, it makes possible the polymer molecules intercalating inside clay galleries, thus strongly modifying the mechanical, thermal, and barrier properties of the polymer (Bordes et al., 2009a).

Among the traditional composites, bentonite is one of the lamellar silicates most used as inorganic filler. Indeed, it is environment friendly and available in large quantities at a relatively low cost. Thus, it provides for the manufacture of bionanocomposites, preserving the biodegradability of the whole system (Bordes et al., 2009b). In their paper, Júnior et al. evaluated the thermal behavior of PHB/PEG/clay bionanocomposites. It was observed that the initial temperature of degradation of bionanocomposites increased with organobentonite content. It was also verified that clay addition to most of the systems led to an increase in crystallinity compared to the PHB matrix, which was attributed to clay nucleating action able to reduce the size of the spherulitic crystals by both decreasing the free energy barrier required for crystal growth and increasing the number of nucleation sites available for crystal growth. This effect was due to the organic modification of the bentonite able to provide suitable different interlayer structures for the bionanocomposites (Júnior et al., 2019). Actually, from the application point of view, PHBV is widely investigated in the preparation of high-performing nanocomposites to be exploited in food packaging. However, the main drawbacks needed to be overcome are its slow crystallization rate and low crystallinity responsible for the dropping down of mechanical and barrier properties. According to Zhang et al. (2017), the addition of cellulose nanocrystals (CNCs) substantially modulates the crystallization profile of the polymer, thus enhancing its mechanical property and thermal stability. In addition, finalized to bestow antibacterial properties, thus obtaining a bioactive food packaging material, the authors included bifunctional nanohybrids composed of CNCs and antibacterial agents, such as silver nanoparticles, AgNPs, in the biopolymeric matrix and found that they acted as suitable nucleating agent able to

strongly improve PHBV crystallization temperature and rate and whole crystallinity. As a consequence, also thermal stability, mechanical, barrier, and antibacterial properties of the ternary bionanocomposite significantly enhanced.

In their paper, Yu et al. (2010) performed a pioneering research about the structural and optical properties of PHBV/ZnO nanofibers fabricated by the electrospinning technique. ZnO nanoparticles (NPs), doped in the PHBV fibers, resulted in well-dispersion due to the hydrogen bonding occurring between the polar groups of ZnO and PHBV. The crystallinity and crystallization rate were lowered by adding ZnONPs.

Based on the previous research, recently, Castro-Mayorga et al. (2017b) investigated the effect of zinc oxide size, morphology, and crystalline structure on their antimicrobial activity against the foodborne pathogens *Salmonella enterica* and *Listeria monocytogenes* of PHBV for active food packaging and food contact applications. They found that ZnO particles were significantly effective when their specific surface area increased, i.e., when the hexagonal-pyramid nanoparticles (PZnO) were used. In addition, they evidence that the antibacterial properties were preserved even when they were incorporated in coating PHBV structures. Moreover, ZnO nanoparticles positively influenced the thermal stability and optical properties of PHBV active films, avoiding their browning after the thermal processing, even if they worsened the polymer mechanical and oxygen barrier properties due to the high concentration required to obtain suitable bactericide effect against *L. monocytogenes*.

In order to improve PHBV gas barrier properties, which is useful for food and electronic packaging materials, and its sensitivity to oxygen, many efforts have been performed. The introduction of nanosized fillers inside polymeric matrix attracted a great interest since their fine and homogeneous distribution inside the polymer hinders gas permeability. In their paper, Öner et al. (2016) used boron nitride crystals in hexagonal nanoplate and nanoflake due to their structural similarities to graphene. BN nanoparticles included in the PHBV matrix during the extrusion process improved the gas barrier of the polymer. Anyway, in order to enhance the physical interaction occurring between PHBV and BNPs, thus assuring a stable dispersion of BNPs, the same authors used a silane coupling agent, octyltriethoxysilane (OTES), to modify the surface of boron nitride. In their research, Öner et al. (2019) included different amounts of BNPs with different crystalline silane surfaces in PHBV, via melt compounding, and investigated their effects on the barrier properties of PHBV nanocomposites. For all the nanocomposites, the oxygen permeability decreased in comparison to the neat PHBV due to the presence of both BN nanoparticles and silane coupling agent. In particular, the physical interaction occurring between PHBV and BN were strongly enhanced in the presence of OTES, furthermore improving the barrier properties.

Similarly, Öner and İlhan (2016) investigated the chemical-physical properties of bio-composites based on PHBV and hydroxyapatite (HAP), obtained by extrusion processing. HAP is one of the bioactive and biocompatible calcium phosphates fillers widely used for polymer nanocomposites. Since both synthetic

and natural HAPs have the same chemical composition and crystallographic properties of bone joint, it is widely used as osteoconductive filler for bone regeneration (Basile et al., 2015).

The bio-composites, produced by melt extrusion of PHBV with untreated HAP and silane surface-treated HAP crystals, were investigated by structural, morphological, and thermal analyses. At high loading of unmodified HAP nanoparticles, physical agglomeration occurred, and mechanical properties dropped down, as the lack of proper adhesion between the matrix and the HAP results in insufficient stress transfer. The silane coupling agent induced a better dispersion of HAP NPs inside PHBV, as evidenced by SEM analysis; as a consequence, a good stress transfer from the matrix to the dispersed phase could be observed. Thus, surface treatment by silanization proved to be necessary to avoid a decrease in the mechanical properties of the filled biopolymer matrix (Öner and İlhan, 2016).

Finally, Ambrosio-Martín et al. (2015a,b) prepared novel nanocomposites based on PHBV and functionalized graphene nanosheets (FGS) by means of mechano-physic ball milling method. Morphological characterization evidenced proper nanofiller dispersion into the matrix, whereas DSC analysis evidenced an increased crystallinity of the polymer. Thermal stability tests revealed that FGS affected the mechanism of oxidative thermal degradation while they did not influence the thermal degradation by pyrolysis. The authors highlighted the positive influence of the homogeneous dispersion of FGS nanofiller within the polymeric matrix, for both the mechanical reinforcing effect of FGS and also gas barrier enhancement (Ambrosio-Martín et al., 2015a,b).

CHALLENGES AND PERSPECTIVES FOR EFFECTIVE PHA EXPLOITATION

The main challenge for exploitation of PHA polymers is related to their high production costs. The costs of the raw materials and recovery process are ~10 times higher than those of conventional polymers, with the carbon sources used to feed the fermentation process accounting for more than the 50% of the total (Wang et al., 2013a; Koller et al., 2017). An estimation of the biopolymer costs is ~\$6–15/kg, almost two orders of magnitude higher than those of PE and PP (\$0.23–0.48/kg) (Reddy et al., 2003).

An important aspect related to the cost competitiveness of PHA production is the final process productivity, which in turn depends on production yield as well as on the efficiency of downstream procedure. Genome-editing and synthetic biology approaches have emerged as powerful and innovative tools to address both these aspects (Zhang et al., 2020). Ribosome-binding site (RBS) optimization, promoter engineering, and, more importantly, CRISPR-cas9-based approaches have been effective in model organisms, such as *E. coli* and non-model ones, such as *Halomonas* spp. and *Pseudomonas* spp., to boost process competitiveness (Zhang et al., 2020). Cell sizes and growth behavior are crucial targets for increasing polymer accumulation. Engineering cell size/shape or cell walls is an effective way to boost PHA accumulation within the intracellular space. CRISPR/cas9 and CRISPi methods have

been used to manipulate genes related to cell division. The deletion of fission-related genes, together with overexpression of the genes involved in the division process in *E. coli*, allows to significantly increase PHB accumulation by inducing a multiple division pattern and, consequently, the formation of a cell with increased volume (Jiang et al., 2015; Elhadi et al., 2016; Wu et al., 2016a,b). Cell shape is also an important factor influencing further cell separation from the culture broth. A convenient downstream process has been designed in engineered *Halomonas campaniensis* LS21, by deleting an *etf* operon encoding two subunits of an electron transferring flavoprotein, causing self-flocculation and an easy and rapid recovery at the bottom of the bioreactor (Ling et al., 2019; Shen et al., 2019).

Biomass feedstocks and waste materials have emerged as promising substrates for cost-effective PHA production, and their different kinds have been explored, including lignocellulosic materials and agroindustrial and food wastes (El-malek et al., 2020; Sirohi et al., 2020). Progresses in this field have been achieved through the application of *in vivo* engineering approaches. Microbial cell factories able to convert different wastes into PHA have been designed, focusing on different approaches: (i) introducing the catabolic genes required for the metabolization of waste C-sources in native PHA producers; (ii) conferring PHA-producing abilities to non-native producers endowed with advantageous metabolic/physiological features, i.e., halophilic bacteria and/or microorganisms naturally able to metabolize complex C-sources; (iii) modulating PHA composition acting on precursor-supplying pathways (Favaro et al., 2019).

Although PHA at industrial scale is currently produced by pure culture systems (wild-type or engineered microorganisms), the use of MMC is emerging as a promising strategy to reduce the intensive costs related to aeration and media and equipment sterilization (Fradinho et al., 2019; Mannina et al., 2020). A further advantage of MMC-based processes is the possibility to integrate PHA production in waste treatment plants (Kourmentza et al., 2017). In one of the most promising examples, up to 75 wt% of PHA content has been reported by MMC from fermented molasses (Albuquerque et al., 2010). It has been estimated that, by optimizing the acidogenic fermentation to get a large amount of organic acids from organic fraction of municipal solid waste (OFMSW) to be further transformed into PHA, a total gross revenue of \$7.6–16.9 billion might be achieved (Colombo et al., 2017). The feasibility of the MMC-based processes on waste substrates has been demonstrated at pilot scale, and several European projects aim at demonstrating PHA production at pilot scale have been funded (Mannina et al., 2020). Future improvements for the exploitation of MMC-based processes should address the increase in cell densities and polymer productivities (Argiz et al., 2020) as well as the improvements in the extraction technologies due to their higher resistance to cell hydrolysis with respect to pure cultures (Samorì et al., 2015; Mannina et al., 2020).

Most of the reported studies focus on the successful design and optimization of the processes for PHA production from

wastes on lab-scale; however, an estimation of process costs has been reported only in few cases. In an interesting example, PHB process economics using cheese whey as the low-cost substrate was simulated on scenarios with different plant capacity. The bioprocess was found efficient at 1,000 ton/h whey feed with an estimated cost of US\$10.2/kg (Peña-Jurado et al., 2019).

Although the use of waste materials certainly allows to reduce the costs of raw material supply, the PHA production process is still not economically competitive. Exploiting microbial cell factories to obtain multiple products from the same process would enhance process competitiveness. Several examples of coproduction of PHA with other value-added products (amino acids, proteins, alcohols, hydrogen, biosurfactants, exopolysaccharides, and lipids) have been described in the recent literature (Kumar and Kim, 2018; de Jesus Assis et al., 2019). From an economical and technical point of view, the most advantageous processes are those that couple an optimized accumulation of intracellular PHA together with the recovery of extracellular products (Kumar and Kim, 2018). A further breakthrough in the same direction is represented by the implementation of “waste bio-refineries,” wherein the PHA production is integrated in an ensemble of processes aimed at the complete valorization of raw materials. A techno-economic and environmental analysis of a sugar cane bagasse biorefinery for the production of fuel ethanol, PHB, and electricity was performed by Moncada et al. (2013). An optimization procedure was applied to select the most promising process pathways for each product and to define the criteria for the selection of technologies and raw material distribution. It was demonstrated that, if considered in the frame of a multiproduct biorefinery, where all the products contribute in incomes and also share costs, instead of a separate process, the PHA production becomes a feasible process.

A similar approach was applied to evaluate the economic viability of a biorefinery for the coproduction of succinic acid, PHB, and electricity from sugarcane bagasse and trash lignocelluloses (Nieder-Heitmann et al., 2019). Different scenarios were simulated, and the most favorable configuration (where PHB was produced from 25% of the fermentable glucose stream and succinic acid from the remaining glucose together plus the hemicellulose hydrolysate) resulted in an internal rate of return (IRR) of 24.1% with a net present value of US\$477.2 million.

Although the above-described strategies of PHB production from renewable, eco-sustainable, and cost-effective bioresources are ever more biotechnologically advanced and promising approaches to drastically reduce the high production cost of PHB, its commercialization is still in its early stages, even if its global production capacity is one of the fastest growing among biopolymers (Aeschelmann and Carus, 2017). This is due to the restricted areas of PHB application unavoidably associated to the lost challenge in up-front competition with the petroleum-based plastics produced on a very large scale. A valid attempt to obtain a cost-competitive material is to strongly broaden its industrial production and diffusion in bioplastics industry. A lot of progress has been recently made through the formulation of PHB with tailored additives (plasticizers, nucleating agents, organic, and inorganic fillers),

polymers (physical blending and/or melt reactive blending), copolymers, and bio-composites, leading to greatly improved mechanical profiles, wider processability windows, and improved post-processed thermal stability, without neglecting that PHB compounding requires lower amounts of the neat polymer with a consequent reduction in the final material costs. These advances will improve PHB capacity to match with the practical needs in several application fields, ranging from surgical sutures, tissue engineering (Misra et al., 2010), agricultural foils, and packaging materials for the storage of food products (Bucci et al., 2005).

In this way, PHB could both shed lights on its commercial applications and enhance its penetration in wider market sectors, with a consequent reduction of its high production cost.

Nevertheless, it is expected that the PHA production will almost quadruple by 2021 with regard to 2016, as a result of a ramp-up of capacities in Asia and the USA (www.europanbioplastics.org/market), and thus, it seems that the costs of PHAs will decrease. This upcoming perspective is the result of an important trend, driven by the changing of consumer demands to make plastic products more efficient, eco-friendly,

and cost effective and to reduce greenhouse gas emissions and dependency on fossil-derived plastics.

AUTHOR CONTRIBUTIONS

RT: conceptualization, writing (review and editing), and special focus on plasticizers. GS: conceptualization, writing (review and editing), special focus on blending, and bio-composites. IC: investigation and visualization. CP: conceptualization, writing (review and editing), special focus on copolymer synthesis and *in vivo* approaches, and supervision. MD: funding acquisition. All authors contributed to the article and approved the submitted version.

FUNDING

This work was supported by grants from PRIN: PROGETTI DI RICERCA DI RILEVANTE INTERESSE NAZIONALE—Bando 2017. CARDoon valorisation by InteGrAted biorefiNery (CARDIGAN). IC acknowledges Università degli Studi di Napoli Federico II for doctoral fellowships.

REFERENCES

- Aeschelmann, F., and Carus, M. (2017). *Bio-Based Building Blocks and Polymers. Global Capacities*. nova-Institut GmbH. Available online at: <http://www.bio-based.eu/reports/>
- Ahmed, T., Marçal, H., Lawless, M., Wanandy, N. S., Chiu, A., and Foster, L. J. R. (2010). Polyhydroxybutyrate and its copolymer with polyhydroxyvalerate as biomaterials: influence on progression of stem cell cycle. *Biomacromolecules* 11, 2707–2715. doi: 10.1021/bm1007579
- Albuquerque, M. G. E., Concas, S., Bengtsson, S., and Reis, M. A. M. (2010). Mixed culture polyhydroxyalkanoates production from sugar molasses: the use of a 2-stage CSTR system for culture selection. *Bioresour. Technol.* 101, 7112–7122. doi: 10.1016/j.biortech.2010.04.019
- Aldor, I. S., and Keasling, J. D. (2003). Process design for microbial plastic factories: Metabolic engineering of polyhydroxyalkanoates. *Curr. Opin. Biotechnol.* 14, 475–483. doi: 10.1016/j.copbio.2003.09.002
- Alexandre, M., and Dubois, P. (2000). Polymer-layered silicate nanocomposites: preparation, properties and uses of a new class of materials. *Mater. Sci. Eng. R Rep.* 28, 1–63. doi: 10.1016/S0927-796X(00)00012-7
- Ambrosio-Martin, J., Gorrasi, G., Lopez-Rubio, A., Fabra, M. J., Mas, L. C., López-Manchado, M. A., et al. (2015a). On the use of ball milling to develop PHBV-graphene nanocomposites (I)—morphology, thermal properties, and thermal stability. *J. Appl. Polym. Sci.* 132:42101. doi: 10.1002/app.42101
- Ambrosio-Martin, J., Gorrasi, G., Lopez-Rubio, A., Fabra, M. J., Mas, L. C., López-Manchado, M. A., et al. (2015b). On the use of ball milling to develop poly(3-hydroxybutyrate-co-3-hydroxyvalerate)-graphene nanocomposites (II)—mechanical, barrier, and electrical properties. *J. Appl. Polym. Sci.* 132:42217. doi: 10.1002/app.42217
- Angelini, S., Cerruti, P., Immirzi, B., Santagata, G., Scarinzi, G., and Malinconico, M. (2014). From biowaste to bioresource: effect of a lignocellulosic filler on the properties of poly(3-hydroxybutyrate). *Int. J. Biol. Macromol.* 71, 163–173. doi: 10.1016/j.ijbiomac.2014.07.038
- Anjum, A., Zuber, M., Zia, K. M., Noreen, A., Anjum, M. N., and Tabasum, S. (2016). Microbial production of polyhydroxyalkanoates (PHAs) and its copolymers: a review of recent advancements. *Int. J. Biol. Macromol.* 89, 161–174. doi: 10.1016/j.ijbiomac.2016.04.069
- Anna, A. D., and Arrigo, R. (2019). PLA/PHB blends: biocompatibilizer effects. *Polymers* 11:1416. doi: 10.3390/polym11091416
- Antunes, M. C. M., and Felisberti, M. I. (2005). Blends of poly(hydroxybutyrate) and poly(ϵ -caprolactone) obtained from melting mixture maria. *Polimeros Cienc. e Tecnol.* 15, 134–138. doi: 10.1590/S0104-14282005000200014
- Argiz, L., Fra-Vázquez, A., del Río, Á. V., and Mosquera-Corral, A. (2020). Optimization of an enriched mixed culture to increase PHA accumulation using industrial saline complex wastewater as a substrate. *Chemosphere* 247:125873. doi: 10.1016/j.chemosphere.2020.125873
- Arikawa, H., Sato, S., Fujiki, T., and Matsumoto, K. (2016). A study on the relation between poly(3-hydroxybutyrate) depolymerases or oligomer hydrolases and molecular weight of polyhydroxyalkanoates accumulating in *Cupriavidus necator* H16. *J. Biotechnol.* 227, 94–102. doi: 10.1016/j.jbiotec.2016.04.004
- Arrieta, M. P., López, J., Hernández, A., and Rayón, E. (2014). “The potential of D(+)-limonene to improve PLA-PHB blends properties,” in *Citrus: Molecular Phylogeny, Antioxidant Properties and Medicinal Uses* (New York, NY: Nova Science Publishers), 185–197.
- Arrieta, M. P., Samper, M. D., Aldas, M., and López, J. (2017). On the use of PLA-PHB blends for sustainable food packaging applications. *Materials* 10:1008. doi: 10.3390/ma10091008
- Auras, R., Harte, B., and Selke, S. (2004). An overview of polylactides as packaging materials. *Macromol. Biosci.* 4, 835–864. doi: 10.1002/mabi.200400043
- Babos, G., Rydz, J., Kawalec, M., Klim, M., Fodor-Kardos, A., Trif, L., et al. (2020). Poly(3-Hydroxybutyrate)-based nanoparticles for sorafenib and doxorubicin anticancer drug delivery. *Int. J. Mol. Sci.* 21:7312. doi: 10.3390/ijms21197312
- Ballistreri, A., Giuffrida, M., Guglielmino, S. P. P., Carnazza, S., Ferreri, A., and Impallomeni, G. (2001). Biosynthesis and structural characterization of medium-chain-length poly(3-hydroxyalkanoates) produced by *Pseudomonas aeruginosa* from fatty acids. *Int. J. Biol. Macromol.* 29, 107–114. doi: 10.1016/S0141-8130(01)00154-4
- Baltieri, R. C., Mei, L. H. I., and Bartoli, J. (2003). Study of the influence of plasticizers on the thermal and mechanical properties of poly(3-hydroxybutyrate) compounds. *Macromol. Symp.* 197, 33–44. doi: 10.1002/masy.200350704
- Barham, P. J., Keller, A., Otun, E. L., and Holmes, P. A. (1984). Crystallization and morphology of a bacterial thermoplastic: poly-3-hydroxybutyrate. *J. Mater. Sci.* 19, 2781–2794. doi: 10.1007/BF01026954
- Basile, M. A., d'Ayala, G. G., Malinconico, M., Laurienzo, P., Coudane, J., Nottelet, B., et al. (2015). Functionalized PCL/HA nanocomposites as microporous membranes for bone regeneration. *Mater. Sci. Eng. C* 48, 457–468. doi: 10.1016/j.msec.2014.12.019

- Bhatia, S. K., Gurav, R., Choi, T. R., Jung, H. R., Yang, S. Y., Moon, Y. M., et al. (2019a). Bioconversion of plant biomass hydrolysate into bioplastic (polyhydroxyalkanoates) using *Ralstonia eutropha* 5119. *Bioresour. Technol.* 271, 306–315. doi: 10.1016/j.biortech.2018.09.122
- Bhatia, S. K., Kim, J. H., Kim, M. S., Kim, J., Hong, J. W., Hong, Y. G., et al. (2018). Production of (3-hydroxybutyrate-co-3-hydroxyhexanoate) copolymer from coffee waste oil using engineered *Ralstonia eutropha*. *Bioprocess Biosyst. Eng.* 41, 229–235. doi: 10.1007/s00449-017-1861-4
- Bhatia, S. K., Wadhwa, P., Hong, J. W., Hong, Y. G., Jeon, J. M., Lee, E. S., et al. (2019b). Lipase mediated functionalization of poly(3-hydroxybutyrate-co-3-hydroxyvalerate) with ascorbic acid into an antioxidant active biomaterial. *Int. J. Biol. Macromol.* 123, 117–123. doi: 10.1016/j.ijbiomac.2018.11.052
- Bibe, I., Tupure, V., Dz, A., and Ka, M. (1999). Improvement of the deformative characteristics of poly-β-hydroxybutyrate by plasticization. *Mech. Comp. Mater.* 35, 357–364. doi: 10.1007/BF02259726
- Blümm, E., and Owen, A. J. (1995). Miscibility, crystallization and melting of poly(3-hydroxybutyrate)/ poly(l-lactide) blends. *Polymer* 36, 4077–4081. doi: 10.1016/0032-3861(95)90987-D
- Bordes, P., Hablot, E., Pollet, E., and Avérous, L. (2009a). Effect of clay organomodifiers on degradation of polyhydroxyalkanoates. *Polym. Degrad. Stab.* 94, 789–796. doi: 10.1016/j.polymdegradstab.2009.01.027
- Bordes, P., Pollet, E., and Avérous, L. (2009b). Nano-biocomposites: biodegradable polyester/nanoclay systems. *Prog. Polym. Sci.* 34, 125–155. doi: 10.1016/j.progpolymsci.2008.10.002
- Bucci, D. Z., Tavares, L. B. B., and Sell, I. (2005). PHB packaging for the storage of food products. *Polym. Test.* 24, 564–571. doi: 10.1016/j.polymertesting.2005.02.008
- Bugnicourt, E., Cinelli, P., Lazzeri, A., and Alvarez, V. (2014). Polyhydroxyalkanoate (PHA): Review of synthesis, characteristics, processing and potential applications in packaging. *Express Polym. Lett.* 8, 791–808. doi: 10.3144/expresspolymlett.2014.82
- Cai, H., and Qiu, Z. (2009). Effect of comonomer content on the crystallization kinetics and morphology of biodegradable poly(3-hydroxybutyrate-co-3-hydroxyhexanoate). *Phys. Chem. Chem. Phys.* 11, 9569–9577. doi: 10.1039/b907677h
- Castro-Mayorga, J. L., Fabra, M. J., Cabedo, L., and Lagaron, J. M. (2017a). On the use of the electrospinning coating technique to produce antimicrobial polyhydroxyalkanoate materials containing in situ-stabilized silver nanoparticles. *Nanomaterials* 7:4. doi: 10.3390/nano7010004
- Castro-Mayorga, J. L., Fabra, M. J., Pourrahimi, A. M., Olsson, R. T., and Lagaron, J. M. (2017b). The impact of zinc oxide particle morphology as an antimicrobial and when incorporated in poly(3-hydroxybutyrate-co-3-hydroxyvalerate) films for food packaging and food contact surfaces applications. *Food Bioprod. Process* 101, 32–44. doi: 10.1016/j.fbp.2016.10.007
- Cha, D., Ha, H. S., and Lee, S. K. (2020). Metabolic engineering of *Pseudomonas putida* for the production of various types of short-chain-length polyhydroxyalkanoates from levulinic acid. *Bioresour. Technol.* 309:123332. doi: 10.1016/j.biortech.2020.123332
- Chabrat, E., Abdillahi, H., Rouilly, A., and Rigal, L. (2012). Influence of citric acid and water on thermoplastic wheat flour/poly(lactic acid) blends. I: thermal, mechanical and morphological properties. *Ind. Crops Prod.* 37, 238–246. doi: 10.1016/j.indcrop.2011.11.034
- Chang, H. M., Wang, Z. H., Luo, H. N., Xu, M., Ren, X. Y., Zheng, G. X., et al. (2014). Poly(3-hydroxybutyrate-co-3-hydroxyhexanoate)-based scaffolds for tissue engineering. *Braz. J. Med. Biol. Res.* 47, 533–539. doi: 10.1590/1414-431X20143930
- Chanprateep, S., Buasri, K., Muangwong, A., and Utiswannakul, P. (2010). Biosynthesis and biocompatibility of biodegradable poly(3-hydroxybutyrate-co-4-hydroxybutyrate). *Polym. Degrad. Stab.* 95, 2003–2012. doi: 10.1016/j.polymdegradstab.2010.07.014
- Chaos, A., Sangroniz, A., Gonzalez, A., Iriarte, M., Sarasua, J. R., del Río, J., et al. (2019). Tributyl citrate as an effective plasticizer for biodegradable polymers: effect of plasticizer on free volume and transport and mechanical properties. *Polym. Int.* 68, 125–133. doi: 10.1002/pi.5705
- Chen, V., Angellier-Coussy, H., Peyron, S., Kemmer, D., and Gontard, N. (2016). Poly(3-hydroxybutyrate-co-3-hydroxyvalerate) films for food packaging: physical-chemical and structural stability under food contact conditions. *J. Appl. Polym. Sci.* 133:41850. doi: 10.1002/app.41850
- Chen, Q., Wang, Q., Wei, G., Liang, Q., and Qi, Q. (2011). Production in *Escherichia coli* of poly(3-hydroxybutyrate-co-3-hydroxyvalerate) with differing monomer compositions from unrelated carbon sources. *Appl. Environ. Microbiol.* 77, 4886–4893. doi: 10.1128/AEM.00091-11
- Chen, Y., Chen, X. Y., Du, H. T., Zhang, X., Ma, Y. M., Chen, J. C., et al. (2019). Chromosome engineering of the TCA cycle in *Halomonas bluephagenesis* for production of copolymers of 3-hydroxybutyrate and 3-hydroxyvalerate (PHBV). *Metab. Eng.* 54, 69–82. doi: 10.1016/j.ymben.2019.03.006
- Ching, Y. C., Ershad Ali, M., Abdullah, L. C., Choo, K. W., Kuan, Y. C., Julaihi, S. J., et al. (2016). Rheological properties of cellulose nanocrystal-embedded polymer composites: a review. *Cellulose* 23, 1011–1030. doi: 10.1007/s10570-016-0868-3
- Choi, J. S., and Park, W. H. (2004). Effect of biodegradable plasticizers on thermal and mechanical properties of poly(3-hydroxybutyrate). *Polym. Test.* 23, 455–460. doi: 10.1016/j.polymertesting.2003.09.005
- Choi, M. U. N. H., Yoon, S. C., and Lenz, R. W. (1999). Production of poly(3-hydroxybutyric acid-co-4-hydroxybutyric acid) and poly(4-hydroxybutyric acid) without subsequent degradation by *Hydrogenophaga pseudoflava*. *Appl. Environ. Microbiol.* 65, 1570–1577. doi: 10.1128/AEM.65.4.1570-1577.1999
- Choi, S. Y., Rhie, M. N., Kim, H. T., Joo, J. C., Cho, I. J., Son, J., et al. (2020). Metabolic engineering for the synthesis of polyesters: a 100-year journey from polyhydroxyalkanoates to non-natural microbial polyesters. *Metab. Eng.* 58, 47–81. doi: 10.1016/j.ymben.2019.05.009
- Colombo, B., Favini, F., Scaglia, B., Sciarria, T. P., D'Imporzano, G., Pognani, M., et al. (2017). Enhanced polyhydroxyalkanoate (PHA) production from the organic fraction of municipal solid waste by using mixed microbial culture. *Biotechnol. Biofuels* 10:201. doi: 10.1186/s13068-017-0888-8
- Corrado, I., Abdalrazeq, M., Pezzella, C., Di Girolamo, R., Porta, R., Sannia, G., et al. (2021). Design and characterization of poly(3-hydroxybutyrate-co-hydroxyhexanoate) nanoparticles and their grafting in whey protein-based nanocomposites. *Food Hydrocoll.* 110:160167. doi: 10.1016/j.foodhyd.2020.106167
- Crétois, R., Chenal, J.-M., Sheibat-Othman, N., Monnier, A., Martin, C., Astruz, O., et al. (2016). Physical explanations about the improvement of polyhydroxybutyrate ductility: hidden effect of plasticizer on physical ageing. *Polymer* 102, 176–182. doi: 10.1016/j.polymer.2016.09.017
- Dai, Y., Lambert, L., Yuan, Z., and Keller, J. (2008). Microstructure of copolymers of polyhydroxyalkanoates produced by glycogen accumulating organisms with acetate as the sole carbon source. *Process Biochem.* 43, 968–977. doi: 10.1016/j.procbio.2008.04.023
- de Jesus Assis, D., Santos, J., de Jesus, C. S., de Souza, C. O., Costa, S. S., Miranda, A. L., et al. (2019). Valorization of crude glycerol based on biological processes for accumulation of lipophilic compounds. *Int. J. Biol. Macromol.* 129, 728–736. doi: 10.1016/j.ijbiomac.2019.02.077
- de Paula, F. C., de Paula, C. B. C., Gomez, J. G. C., Steinbüchel, A., and Contiero, J. (2017). Poly(3-hydroxybutyrate-co-3-hydroxyvalerate) production from biodiesel by-product and propionic acid by mutant strains of *Pandora* sp. *Biotechnol. Prog.* 33, 1077–1084. doi: 10.1002/btpr.2481
- de Sousa Dias, M. M., Koller, M., Puppi, D., Morelli, A., Chiellini, F., and Brauneegg, G. (2017). Fed-batch synthesis of poly(3-hydroxybutyrate) and poly(3-hydroxybutyrate-co-4-hydroxybutyrate) from sucrose and 4-hydroxybutyrate precursors by *Burkholderia sacchari* strain DSM 17165. *Bioengineering* 4:36. doi: 10.3390/bioengineering4020036
- Degli Esposti, M., Chiellini, F., Bondioli, F., Morselli, D., and Fabbri, P. (2019). Highly porous PHB-based bioactive scaffolds for bone tissue engineering by *in situ* synthesis of hydroxyapatite. *Mater. Sci. Eng. C* 100, 286–296. doi: 10.1016/j.msec.2019.03.014
- Dehouche, N., Idres, C., Kaci, M., Zembouai, I., and Bruzard, S. (2020). Effects of various surface treatments on Aloe Vera fibers used as reinforcement in poly(3-hydroxybutyrate-co-3-hydroxyhexanoate) (PHBHHx) biocomposites. *Polym. Degrad. Stab.* 175:109131. doi: 10.1016/j.polymdegradstab.2020.109131
- Delmas, G.-H., Benjelloun-Mlayah, B., Le Bigot, Y., and Delmas, M. (2011). Functionality of wheat straw lignin extracted in organic acid media. *J. Appl. Polym. Sci.* 121, 491–501. doi: 10.1002/app.33592
- Di Lorenzo, M. L., and Righetti, M. C. (2013). Effect of thermal history on the evolution of crystal and amorphous fractions of poly[(R)-3-hydroxybutyrate] upon storage at ambient temperature. *Eur. Polym. J.* 49, 510–517. doi: 10.1016/j.eurpolymj.2012.11.004

- Doi, Y., Mukai, K., Kasuya, K., and Yamada, K. (1994). Biodegradation of biosynthetic and chemosynthetic polyhydroxyalkanoates. *Stud. Polym. Sci.* 12, 39–51. doi: 10.1016/B978-0-444-81708-2.50010-5
- dos Santos, A. J., Oliveira Dalla Valentina, L. V., Hidalgo Schulz, A. A., and Tomaz Duarte, M. A. (2017). From Obtaining to Degradation of PHB: Material Properties. Part I. *Ing. y Cienc.* 13, 269–298. doi: 10.17230/ingciencia.13.26.10
- dos Santos, A. J., Oliveira Dalla Valentina, L. V., Hidalgo Schulz, A. A., and Tomaz Duarte, M. A. (2018). From obtaining to degradation of PHB: a literature review. Part II. *Ing. y Cienc.* 14, 207–228. doi: 10.17230/ingciencia.14.27.9
- Elhadi, D., Lv, L., Jiang, X. R., Wu, H., and Chen, G. Q. (2016). CRISPRi engineering *E. coli* for morphology diversification. *Metab. Eng.* 38, 358–369. doi: 10.1016/j.ymben.2016.09.001
- El-malek, F. A., Khairy, H., Farag, A., and Omar, S. (2020). The sustainability of microbial bioplastics, production and applications. *Int. J. Biol. Macromol.* 157, 319–328. doi: 10.1016/j.ijbiomac.2020.04.076
- Erceg, M., Kovačić, T., and Klarić, I. (2005). Thermal degradation of poly(3-hydroxybutyrate) plasticized with acetyl tributyl citrate. *Polym. Degrad. Stab.* 90, 313–318. doi: 10.1016/j.polymdegradstab.2005.04.048
- Esposito, A., Delpouve, N., Causin, V., Dhotel, A., Delbreilh, L., and Dargent, E. (2016). From a three-phase model to a continuous description of molecular mobility in semicrystalline poly(hydroxybutyrate-co-hydroxyvalerate). *Macromolecules* 49, 4850–4861. doi: 10.1021/acs.macromol.6b00384
- Favaro, L., Basaglia, M., and Casella, S. (2019). Improving polyhydroxyalkanoate production from inexpensive carbon sources by genetic approaches: a review. *Biofuels Bioprod. Biorefining* 13, 208–227. doi: 10.1002/bbb.1944
- Fenollar, O., Garcia-Sanoguera, D., Sanchez-Nacher, L., Boronat, T., López, J., and Balart, R. (2013). Mechanical and thermal properties of polyvinyl chloride plasticized with natural fatty acid esters. *Polym. Plast. Technol. Eng.* 52, 761–767. doi: 10.1080/03602559.2013.763352
- Figuerola-Lopez, K. J., Cabedo, L., Lagaron, J. M., and Torres-Giner, S. (2020). Development of electrospun poly(3-hydroxybutyrate-co-3-hydroxyvalerate) monolayers containing eugenol and their application in multilayer antimicrobial food packaging. *Front. Nutr.* 7:140. doi: 10.3389/fnut.2020.00140
- Follonier, S., Goyder, M. S., Silvestri, A. C., Crelieu, S., Kalman, F., Riesen, R., et al. (2014). Fruit pomace and waste frying oil as sustainable resources for the bioproduction of medium-chain-length polyhydroxyalkanoates. *Int. J. Biol. Macromol.* 71, 42–52. doi: 10.1016/j.ijbiomac.2014.05.061
- Fradinho, J. C., Oehmen, A., and Reis, M. A. M. (2019). Improving polyhydroxyalkanoates production in phototrophic mixed cultures by optimizing accumulator reactor operating conditions. *Int. J. Biol. Macromol.* 126, 1085–1092. doi: 10.1016/j.ijbiomac.2018.12.270
- Gahlawat, G., and Soni, S. K. (2017). Valorization of waste glycerol for the production of poly (3-hydroxybutyrate) and poly (3-hydroxybutyrate-co-3-hydroxyvalerate) copolymer by *Cupriavidus necator* and extraction in a sustainable manner. *Bioresour. Technol.* 243, 492–501. doi: 10.1016/j.biortech.2017.06.139
- Gamal, R. F., Abdelhady, H. M., Khodair, T. A., El-Tayeb, T. S., Hassan, E. A., and Aboutaleb, K. A. (2013). Semi-scale production of PHAs from waste frying oil by *Pseudomonas fluorescens* S48. *Brazilian J. Microbiol.* 44, 539–549. doi: 10.1590/S1517-83822013000200034
- Gao, Y., Kong, L., Zhang, L., Gong, Y., Chen, G., Zhao, N., et al. (2006). Improvement of mechanical properties of poly(dl-lactide) films by blending of poly(3-hydroxybutyrate-co-3-hydroxyhexanoate). *Eur. Polym. J.* 42, 764–775. doi: 10.1016/j.eurpolymj.2005.09.028
- García, I. L., López, J. A., Dorado, M. P., Kopsahelis, N., Alexandri, M., Papanikolaou, S., et al. (2013). Evaluation of by-products from the biodiesel industry as fermentation feedstock for poly(3-hydroxybutyrate-co-3-hydroxyvalerate) production by *Cupriavidus necator*. *Bioresour. Technol.* 130, 16–22. doi: 10.1016/j.biortech.2012.11.088
- García-García, D., Ferri, J. M., Montanes, N., Lopez-Martinez, J., and Balart, R. (2016). Plasticization effects of epoxidized vegetable oils on mechanical properties of poly(3-hydroxybutyrate). *Polym. Int.* 65, 1157–1164. doi: 10.1002/pi.5164
- Godbole, S., Gote, S., Latkar, M., and Chakrabarti, T. (2003). Preparation and characterization of biodegradable poly-3-hydroxybutyrate-starch blend films. *Bioresour. Technol.* 86, 33–37. doi: 10.1016/S0960-8524(02)00110-4
- González-Ausejo, J., Sánchez-Safont, E., Lagarón, J. M., Balart, R., Cabedo, L., and Gámez-Pérez, J. (2017). Compatibilization of poly(3-hydroxybutyrate-co-3-hydroxyvalerate)–poly(lactic acid) blends with diisocyanates. *J. Appl. Polym. Sci.* 134, 1–11. doi: 10.1002/app.44806
- Gopi, S., Kontopoulou, M., Ramsay, B. A., and Ramsay, J. A. (2018). Manipulating the structure of medium-chain-length polyhydroxyalkanoate (MCL-PHA) to enhance thermal properties and crystallization kinetics. *Int. J. Biol. Macromol.* 119, 1248–1255. doi: 10.1016/j.ijbiomac.2018.08.016
- Gouveia, A. R., Freitas, E. B., Galinha, C. F., Carvalho, G., Duque, A. F., and Reis, M. A. M. (2017). Dynamic change of pH in acidogenic fermentation of cheese whey towards polyhydroxyalkanoates production: impact on performance and microbial population. *N. Biotechnol.* 37, 108–116. doi: 10.1016/j.nbt.2016.07.001
- Gras, N., Murray, E. J., and Holme, P. A. (1984). The thermal degradation of poly(-d)-β-hydroxybutyric acid): Part 1—identification and quantitative analysis of products. *Polym. Degrad. Stud.* 6, 47–61. doi: 10.1016/0141-3910(84)90016-8
- Haba, E., Vidal-Mas, J., Bassas, M., Espuny, M. J., Llorens, J., and Manresa, A. (2007). Poly 3-(hydroxyalkanoates) produced from oily substrates by *Pseudomonas aeruginosa* 47T2 (NCBIM 40044): effect of nutrients and incubation temperature on polymer composition. *Biochem. Eng. J.* 35, 99–106. doi: 10.1016/j.bej.2006.11.021
- Han, J., Qiu, Y. Z., Liu, D. C., and Chen, G. Q. (2004). Engineered *Aeromonas hydrophila* for enhanced production of poly(3-hydroxybutyrate-co-3-hydroxyhexanoate) with alterable monomers composition. *FEMS Microbiol. Lett.* 239, 195–201. doi: 10.1016/j.femsle.2004.08.044
- Hao, J., Wang, X., and Wang, H. (2017). Overall process of using a valerate-dominant sludge hydrolysate to produce high-quality polyhydroxyalkanoates (PHA) in a mixed culture. *Sci. Rep.* 7:6939. doi: 10.1038/s41598-017-07154-3
- Harding, K. G., Dennis, J. S., von Blottnitz, H., and Harrison, S. T. L. (2007). Environmental analysis of plastic production processes: comparing petroleum-based polypropylene and polyethylene with biologically-based poly-β-hydroxybutyric acid using life cycle analysis. *J. Biotechnol.* 130, 57–66. doi: 10.1016/j.jbiotec.2007.02.012
- Harmon, J. P., and Otter, R. (2018). Green chemistry and the search for new plasticizers. *ACS Sustain. Chem. Eng.* 6, 2078–2085. doi: 10.1021/acsschemeng.7b03508
- Heathman, T. R. J., Webb, W. R., Han, J., Dan, Z., Chen, G. Q., Forsyth, N. R., et al. (2014). Controlled production of poly (3-hydroxybutyrate-co-3-hydroxyhexanoate) (PHBHHx) nanoparticles for targeted and sustained drug delivery. *J. Pharm. Sci.* 103, 2498–2508. doi: 10.1002/jps.24035
- Hilliou, L., Teixeira, P. F., Machado, D., Covas, J. A., Oliveira, C. S. S., Duque, A. F., et al. (2016). Effects of fermentation residues on the melt processability and thermomechanical degradation of PHBV produced from cheese whey using mixed microbial cultures. *Polym. Degrad. Stab.* 128, 269–277. doi: 10.1016/j.polymdegradstab.2016.03.031
- Huang, L., Chen, Z., Xiong, D., Wen, Q., and Ji, Y. (2018). Oriented acidification of wasted activated sludge (WAS) focused on odd-carbon volatile fatty acid (VFA): regulation strategy and microbial community dynamics. *Water Res.* 142, 256–266. doi: 10.1016/j.watres.2018.05.062
- Hufenus, R., Reifler, F. A., Fernández-Ronco, M. P., and Heuberger, M. (2015). Molecular orientation in melt-spun poly(3-hydroxybutyrate) fibers: effect of additives, drawing and stress-annealing. *Eur. Polym. J.* 71, 12–26. doi: 10.1016/j.eurpolymj.2015.07.039
- Impallomeni, G., Ballistreri, A., Carnemolla, G. M., Rizzo, M. G., Nicolò, M. S., and Guglielmino, S. P. P. (2018). Biosynthesis and structural characterization of polyhydroxyalkanoates produced by *Pseudomonas aeruginosa* ATCC 27853 from long odd-chain fatty acids. *Int. J. Biol. Macromol.* 108, 608–614. doi: 10.1016/j.ijbiomac.2017.12.037
- Insomphun, C., Kobayashi, S., Fujiki, T., and Numata, K. (2016). Biosynthesis of polyhydroxyalkanoates containing hydroxyl group from glycolate in *Escherichia coli*. *AMB Expr.* 6:29. doi: 10.1186/s13568-016-0200-5
- Ishida, K., Asakawa, N., and Inoue, Y. (2005). Structure, properties and biodegradation of some bacterial copoly(hydroxyalkanoate)s. *Macromol. Symp.* 224, 47–58. doi: 10.1002/masy.200550605
- Iwata, T. (2005). Strong fibers and films of microbial polyesters. *Macromol. Biosci.* 5, 689–701. doi: 10.1002/mabi.200500066
- Jamshidian, M., Tehrani, E. A., Imran, M., Jacquot, M., and Desobry, S. (2010). Poly-lactic acid: production, applications, nanocomposites,

- and release studies. *Compr. Rev. Food Sci. Food Saf.* 9, 552–571. doi: 10.1111/j.1541-4337.2010.00126.x
- Jandas, P. J., Mohanty, S., and Nayak, S. K. (2014). Morphology and thermal properties of renewable resource-based polymer blend nanocomposites influenced by a reactive compatibilizer. *ACS Sustain. Chem. Eng.* 2, 377–386. doi: 10.1021/sc400395s
- Jiang, X. R., Wang, H., Shen, R., and Chen, G. Q. (2015). Engineering the bacterial shapes for enhanced inclusion bodies accumulation. *Metab. Eng.* 29, 227–237. doi: 10.1016/j.ymben.2015.03.017
- Jost, V., and Langowski, H. C. (2015). Effect of different plasticisers on the mechanical and barrier properties of extruded cast PHBV films. *Eur. Polym. J.* 68, 302–312. doi: 10.1016/j.eurpolymj.2015.04.012
- Júnior, R. M. S., de Oliveira, T. A., Araque, L. M., Alves, T. S., De Carvalho, L. H., and Barbosa, R. (2019). Thermal behavior of biodegradable bionanocomposites: influence of bentonite and vermiculite clays. *J. Mater. Res. Technol.* 8, 3234–3243. doi: 10.1016/j.jmrt.2019.05.011
- Keen, I., Raggatt, L. J., Cool, S. M., Nurcombe, V., Fredericks, P., Trau, M., et al. (2007). Investigations into poly(3-hydroxybutyrate-co-3-hydroxyvalerate) surface properties causing delayed osteoblast growth. *J. Biomater. Sci. Polym. Ed.* 18, 1101–1123. doi: 10.1163/156856207781554046
- Keskin, G., Kizil, G., Bechelany, M., Pochat-Bohatier, C., and Öner, M. (2017). Potential of polyhydroxyalkanoate (PHA) polymers family as substitutes of petroleum based polymers for packaging applications and solutions brought by their composites to form barrier materials. *Pure Appl. Chem.* 89, 1841–1848. doi: 10.1515/pac-2017-0401
- Kim, J., Kim, Y.-J., Choi, S. Y., Lee, S. Y., and Kim, K.-J. (2017). Crystal structure of *Ralstonia eutropha* polyhydroxyalkanoate synthase C-terminal domain and reaction mechanisms. *Biotechnol. J.* 12:1600648. doi: 10.1002/biot.201600648
- Koller, M., Maršálek, L., de Sousa Dias, M. M., and Braunegg, G. (2017). Producing microbial polyhydroxyalkanoate (PHA) biopolyesters in a sustainable manner. *N. Biotechnol.* 37, 24–38. doi: 10.1016/j.nbt.2016.05.001
- Koller, M., Salerno, A., Strohmeier, K., Schober, S., Mittelbach, M., Illieva, V., et al. (2014). Novel precursors for production of 3-hydroxyvalerate-containing poly[(R)-hydroxyalkanoate]s. *Biotransformation* 32, 161–167. doi: 10.3109/10242422.2014.913580
- Kourmentza, C., Plácido, J., Venetsaneas, N., Burniol-Figols, A., Varrone, C., Gavala, H. N., et al. (2017). Recent advances and challenges towards sustainable polyhydroxyalkanoate (PHA) production. *Bioengineering* 4:55. doi: 10.3390/bioengineering4020055
- Kumar, P., and Kim, B. S. (2018). Valorization of polyhydroxyalkanoates production process by co-synthesis of value-added products. *Bioresour. Technol.* 269, 544–556. doi: 10.1016/j.biortech.2018.08.120
- Kunze, C., Freier, T., Kramer, S., and Schmitz, K. P. (2002). Anti-inflammatory prodrugs as plasticizers for biodegradable implant materials based on poly(3-hydroxybutyrate). *J. Mater. Sci. Mater. Med.* 13, 1051–1055. doi: 10.1023/A:1020392606225
- Lai, S. M., Don, T. M., and Huang, Y. C. (2006). Preparation and properties of biodegradable thermoplastic starch/poly(hydroxy butyrate) blends. *J. Appl. Polym. Sci.* 100, 2371–2379. doi: 10.1002/app.23085
- Lee, W. H., Azizan, M. N. M., and Sudesh, K. (2004). Effects of culture conditions on the composition of poly(3-hydroxybutyrate-co-4-hydroxybutyrate) synthesized by *Comamonas acidovorans*. *Polym. Degrad. Stab.* 84, 129–134. doi: 10.1016/j.polymdegradstab.2003.10.003
- Li, D., Lv, L., Chen, J. C., and Chen, G. Q. (2017). Controlling microbial PHB synthesis via CRISPRi. *Appl. Microbiol. Biotechnol.* 101, 5861–5867. doi: 10.1007/s00253-017-8374-6
- Li, J., Yun, H., Gong, Y., Zhao, N., and Zhang, X. (2005). Effects of surface modification of poly(3-hydroxybutyrate-co-3-hydroxyhexanoate) (PHBHHx) on physicochemical properties and on interactions with MC3T3-E1 cells. *J. Biomed. Mater. Res. Part A* 75, 985–998. doi: 10.1002/jbm.a.30504
- Li, L., Huang, W., Wang, B., Wei, W., Gu, Q., and Chen, P. (2015a). Properties and structure of polylactide/poly(3-hydroxybutyrate-co-3-hydroxyvalerate) (PLA/PHBV) blend fibers. *Polymer* 68, 183–194. doi: 10.1016/j.polymer.2015.05.024
- Li, S., Cai, L., Wu, L., Zeng, G., Chen, J., Wu, Q., et al. (2014). Microbial synthesis of functional homo-, random, and block polyhydroxyalkanoates by β -oxidation deleted *Pseudomonas entomophila*. *Biomacromolecules* 15, 2310–2319. doi: 10.1021/bm500669s
- Li, X., Chang, H., Luo, H., Wang, Z., Zheng, G., Lu, X., et al. (2015b). Poly(3-hydroxybutyrate-co-3-hydroxyhexanoate) scaffolds coated with PhaP-RGD fusion protein promotes the proliferation and chondrogenic differentiation of human umbilical cord mesenchymal stem cells *in vitro*. *J. Biomed. Mater. Res. Part A* 103, 1169–1175. doi: 10.1002/jbm.a.35265
- Li, Z. J., Shi, Z. Y., Jian, J., Guo, Y. Y., Wu, Q., and Chen, G. Q. (2010). Production of poly(3-hydroxybutyrate-co-4-hydroxybutyrate) from unrelated carbon sources by metabolically engineered *Escherichia coli*. *Metab. Eng.* 12, 352–359. doi: 10.1016/j.ymben.2010.03.003
- Lim, J. S., Park, K., Il, C., G. S., and Kim, J. H. (2013). Effect of composition ratio on the thermal and physical properties of semicrystalline PLA/PHB-HHx composites. *Mater. Sci. Eng. C* 33, 2131–2137. doi: 10.1016/j.msec.2013.01.030
- Liminana, P., Garcia-Sanoguera, D., Quiles-Carrillo, L., Balart, R., and Montanes, N. (2019). Optimization of maleinized linseed oil loading as a bio-based compatibilizer in poly(Butylene Succinate) composites with almond shell flour. *Materials* 12:685. doi: 10.3390/ma12050685
- Ling, C., Qiao, G. Q., Shuai, B. W., Song, K. N., Yao, W. X., Jiang, X. R., et al. (2019). Engineering self-flocculating *Halomonas campaniensis* for wastewaterless open and continuous fermentation. *Biotechnol. Bioeng.* 116, 805–815. doi: 10.1002/bit.26897
- Liu, F., Jian, J., Shen, X., Chung, A., Chen, J., and Chen, G. Q. (2011a). Metabolic engineering of *Aeromonas hydrophila* 4AK4 for production of copolymers of 3-hydroxybutyrate and medium-chain-length 3-hydroxyalkanoate. *Bioresour. Technol.* 102, 8123–8129. doi: 10.1016/j.biortech.2011.05.074
- Liu, Q., Luo, G., Zhou, X. R., and Chen, G. Q. (2011b). Biosynthesis of poly(3-hydroxydecanoate) and 3-hydroxydodecanoate dominating polyhydroxyalkanoates by β -oxidation pathway inhibited *Pseudomonas putida*. *Metab. Eng.* 13, 11–17. doi: 10.1016/j.ymben.2010.10.004
- Lu, X., Zhang, J., Wu, Q., and Chen, G. Q. (2003). Enhanced production of poly(3-hydroxybutyrate-co-3-hydroxyhexanoate) via manipulating the fatty acid β -oxidation pathway in *E. coli*. *FEMS Microbiol. Lett.* 221, 97–101. doi: 10.1016/S0378-1097(03)00173-3
- Lu, X. Y., Wu, Q., and Chen, G. Q. (2004). Production of poly(3-hydroxybutyrate-co-3-hydroxyhexanoate) with flexible 3-hydroxyhexanoate content in *Aeromonas hydrophila* CGMCC 0911. *Appl. Microbiol. Biotechnol.* 64, 41–45. doi: 10.1007/s00253-003-1417-1
- Lukasiewicz, B., Basnett, P., Nigmatullin, R., Matharu, R., Knowles, J. C., and Roy, I. (2018). Binary polyhydroxyalkanoate systems for soft tissue engineering. *Acta Biomater.* 71, 225–234. doi: 10.1016/j.actbio.2018.02.027
- Luo, S., Cao, J., and McDonald, A. G. (2016). Interfacial improvements in a green biopolymer alloy of poly(3-hydroxybutyrate-co-3-hydroxyvalerate) and lignin via *in situ* reactive extrusion. *ACS Sustain. Chem. Eng.* 4, 3465–3476. doi: 10.1021/acssuschemeng.6b00495
- Ma, P., Cai, X., Zhang, Y., Wang, S., Dong, W., Chen, M., et al. (2014). *In-situ* compatibilization of poly(lactic acid) and poly(butylene adipate-co-terephthalate) blends by using dicumyl peroxide as a free-radical initiator. *Polym. Degrad. Stab.* 102, 145–151. doi: 10.1016/j.polymdegradstab.2014.01.025
- Madden, L. A., Anderson, A. J., and Asrar, J. (1998). Synthesis and characterization of poly(3-hydroxybutyrate) and poly(3-hydroxybutyrate-co-3-hydroxyvalerate) polymer mixtures produced in high-density fed-batch cultures of *Ralstonia eutropha* (*Alcaligenes eutrophus*). *Macromolecules* 31, 5660–5667. doi: 10.1021/ma980606w
- Mangeon, C., Michely, L., Rios De Anda, A., Thevenieau, F., Renard, E., and Langlois, V. (2018). Natural terpenes used as plasticizers for Poly(3-hydroxybutyrate). *ACS Sustain. Chem. Eng.* 6, 16160–16168. doi: 10.1021/acssuschemeng.8b02896
- Mannina, G., Presti, D., Montiel-Jarillo, G., Carrera, J., and Suárez-Ojeda, M. E. (2020). Recovery of polyhydroxyalkanoates (PHAs) from wastewater: a review. *Bioresour. Technol.* 297:122478. doi: 10.1016/j.biortech.2019.122478
- Markl, E. (2018). PHB - bio based and biodegradable replacement for PP: a review. *Nov. Tech. Nutr. Food Sci.* 2, 206–209. doi: 10.31031/NTNF.2018.02.000546
- Martin, O., and Avérous, L. (2001). Poly(lactic acid): plasticization and properties of biodegradable multiphase systems. *Polymer* 42, 6209–6219. doi: 10.1016/S0032-3861(01)00086-6
- Martino, V. P., Jiménez, A., Ruseckaite, R. A., and Avérous, L. (2011). Structure and properties of clay nano-biocomposites based on poly(lactic acid) plasticized with polyadipates. *Polym. Adv. Technol.* 22, 2206–2213. doi: 10.1002/pat.1747

- Martla, M., Umsakul, K., and Sudesh, K. (2018). Production and recovery of poly(3-hydroxybutyrate-co-3-hydroxyvalerate) from biodiesel liquid waste (BLW). *J. Basic Microbiol.* 58, 977–986. doi: 10.1002/jobm.201800279
- Masood, F. (2017). *Polyhydroxyalkanoates in the Food Packaging Industry*. Elsevier Inc. doi: 10.1016/B978-0-12-811942-6.00008-X
- Masood, F., Hasan, F., Ahmed, S., and Hameed, A. (2012). Biosynthesis and characterization of poly(3-hydroxybutyrate-co-3-hydroxyvalerate) from *Bacillus cereus* FA11 isolated from TNT-contaminated soil. *Ann. Microbiol.* 62, 1377–1384. doi: 10.1007/s13213-011-0386-3
- Meereboer, K. W., Misra, M., and Mohanty, A. K. (2020). Review of recent advances in the biodegradability of polyhydroxyalkanoate (PHA) bioplastics and their composites. *Green Chem.* 22, 5519–5558. doi: 10.1039/D0GC01647K
- Mekonnen, T., Mussone, P., Khalil, H., and Bressler, D. (2013). Progress in bio-based plastics and plasticizing modifications. *J. Mater. Chem. A* 1, 13379–13398. doi: 10.1039/c3ta12555f
- Meng, D. C., Shi, Z. Y., Wu, L. P., Zhou, Q., Wu, Q., Chen, J. C., et al. (2012). Production and characterization of poly(3-hydroxypropionate-co-4-hydroxybutyrate) with fully controllable structures by recombinant *Escherichia coli* containing an engineered pathway. *Metab. Eng.* 14, 317–324. doi: 10.1016/j.ymben.2012.04.003
- Michel, A. T., and Billington, S. L. (2012). Characterization of polyhydroxybutyrate films and hemp fiber reinforced composites exposed to accelerated weathering. *Polym. Degrad. Stab.* 97, 870–878. doi: 10.1016/j.polymdegradstab.2012.03.040
- Misra, S. K., Ohashi, F., Valappil, S. P., Knowles, J. C., Roy, I., Silva, S. R. P., et al. (2010). Characterization of carbon nanotube (MWCNT) containing P(3HB)/bioactive glass composites for tissue engineering applications. *Acta Biomater.* 6, 735–742. doi: 10.1016/j.actbio.2009.09.023
- Modi, S., Koelling, K., and Vodovotz, Y. (2013). Assessing the mechanical, phase inversion, and rheological properties of poly-[(R)-3-hydroxybutyrate-co-(R)-3-hydroxyvalerate] (PHBV) blended with poly-(l-lactic acid) (PLA). *Eur. Polym. J.* 49, 3681–3690. doi: 10.1016/j.eurpolymj.2013.07.036
- Moita Fidalgo, R., Ortigueira, J., Freches, A., Pelica, J., Gonçalves, M., Mendes, B., et al. (2014). Bio-oil upgrading strategies to improve PHA production from selected aerobic mixed cultures. *N. Biotechnol.* 31, 297–307. doi: 10.1016/j.nbt.2013.10.009
- Moncada, J., Matallana, L. G., and Cardona, C. A. (2013). Selection of process pathways for biorefinery design using optimization tools: a colombian case for conversion of sugarcane bagasse to ethanol, poly-3-hydroxybutyrate (PHB), and energy. *Ind. Eng. Chem. Res.* 52, 4132–4145. doi: 10.1021/ie3019214
- Morse, M. C., Liao, Q., Criddle, C. S., and Frank, C. W. (2011). Anaerobic biodegradation of the microbial copolymer poly(3-hydroxybutyrate-co-3-hydroxyhexanoate): effects of comonomer content, processing history, and semi-crystalline morphology. *Polymer* 52, 547–556. doi: 10.1016/j.polymer.2010.11.024
- Mousavioun, P., Doherty, W. O. S., and George, G. (2010). Thermal stability and miscibility of poly(hydroxybutyrate) and soda lignin blends. *Ind. Crops Prod.* 32, 656–661. doi: 10.1016/j.indcrop.2010.08.001
- Muneer, F., Rasul, I., Azeem, F., Siddique, M. H., Zubair, M., and Nadeem, H. (2020). Microbial polyhydroxyalkanoates (PHAs): efficient replacement of synthetic polymers. *J. Polym. Environ.* 28, 2301–2323. doi: 10.1007/s10924-020-01772-1
- Muthuraj, R., Misra, M., and Mohanty, A. K. (2018). Biodegradable compatibilized polymer blends for packaging applications: a literature review. *J. Appl. Polym. Sci.* 135:45726. doi: 10.1002/app.45726
- Nieder-Heitmann, M., Haigh, K., and Görgens, J. F. (2019). Process design and economic evaluation of integrated, multi-product biorefineries for the co-production of bio-energy, succinic acid, and polyhydroxybutyrate (PHB) from sugarcane bagasse and trash lignocelluloses. *Biofuels Bioprod. Biorefining* 13, 599–617. doi: 10.1002/bbb.1972
- Noda, I., Lindsey, S. B., and Caraway, D. (2010). “Nodax™ class PHA copolymers: their properties and applications,” in *Plastics From Bacteria. Microbiology Monographs*, Vol. 14 (Berlin; Heidelberg: Springer). doi: 10.1007/978-3-642-03287-5_10
- Noda, I., Green, P. R., Satkowski, M. M., and Schechtman, L. A. (2005). Preparation and properties of a novel class of polyhydroxyalkanoate copolymers. *Biomacromolecules* 6, 580–586. doi: 10.1021/bm049472m
- Norhafini, H., Huong, K. H., and Amirul, A. A. (2019). High PHA density fed-batch cultivation strategies for 4HB-rich P(3HB-co-4HB) copolymer production by transformant *Cupriavidus malaysiensis* USMAA1020. *Int. J. Biol. Macromol.* 125, 1024–1032. doi: 10.1016/j.ijbiomac.2018.12.121
- Norhafini, H., Thinagaran, L., Shantini, K., Huong, K. H., Syafiq, I. M., Bhubalan, K., et al. (2017). Synthesis of poly(3-hydroxybutyrate-co-4-hydroxybutyrate) with high 4HB composition and PHA content using 1,4-butanediol and 1,6-hexanediol for medical application. *J. Polym. Res.* 24:189. doi: 10.1007/s10965-017-1345-x
- Ntaikou, I., Valencia Peroni, C., Kourmentza, C., Ilieva, V. I., Morelli, A., Chiellini, E., et al. (2014). Microbial bio-based plastics from olive-mill wastewater: generation and properties of polyhydroxyalkanoates from mixed cultures in a two-stage pilot scale system. *J. Biotechnol.* 188, 138–147. doi: 10.1016/j.jbiotec.2014.08.015
- Obruca, S., Benesova, P., Petrik, S., Oborna, J., Prikrýl, R., and Marova, I. (2014). Production of polyhydroxyalkanoates using hydrolysate of spent coffee grounds. *Process Biochem.* 49, 1409–1414. doi: 10.1016/j.procbio.2014.05.013
- Öner, M., Çöl, A. A., Pochat-Bohatier, C., and Bechelany, M. (2016). Effect of incorporation of boron nitride nanoparticles on the oxygen barrier and thermal properties of poly(3-hydroxybutyrate-co-hydroxyvalerate). *RSC Adv.* 6, 90973–90981. doi: 10.1039/C6RA19198C
- Öner, M., and İlhan, B. (2016). Fabrication of poly(3-hydroxybutyrate-co-3-hydroxyvalerate) biocomposites with reinforcement by hydroxyapatite using extrusion processing. *Mater. Sci. Eng. C* 65, 19–26. doi: 10.1016/j.msec.2016.04.024
- Öner, M., Keskin, G., Kizil, G., Pochat-Bohatier, C., and Bechelany, M. (2019). Development of poly(3-hydroxybutyrate-co-3-hydroxyvalerate)/boron nitride bionanocomposites with enhanced barrier properties. *Polym. Compos.* 40, 78–90. doi: 10.1002/pc.24603
- Ortega-Toro, R., Bonilla, J., Talens, P., and Chiralt, A. (2017). *Future of Starch-Based Materials in Food Packaging*. Elsevier Inc. doi: 10.1016/B978-0-12-809439-6.00009-1
- Ozkoc, G., and Kemaloglu, S. (2009). Morphology, biodegradability, mechanical, and thermal properties of nanocomposite films based on PLA and plasticized PLA. *J. Appl. Polym. Sci.* 114, 2481–2487. doi: 10.1002/app.30772
- Panaiteanu, D. M., Nicolae, C. A., Frone, A. N., Chiulan, I., Stanescu, P. O., Draghici, C., et al. (2017). Plasticized poly(3-hydroxybutyrate) with improved melt processing and balanced properties. *J. Appl. Polym. Sci.* 134, 1–14. doi: 10.1002/app.44810
- Park, D. H., and Kim, B. S. (2011). Production of poly(3-hydroxybutyrate) and poly(3-hydroxybutyrate-co-4-hydroxybutyrate) by *Ralstonia eutropha* from soybean oil. *N. Biotechnol.* 28, 719–724. doi: 10.1016/j.nbt.2011.01.007
- Park, S. J., Kim, T. W., Kim, M. K., Lee, S. Y., and Lim, S. C. (2012). Advanced bacterial polyhydroxyalkanoates: towards a versatile and sustainable platform for unnatural tailor-made polyesters. *Biotechnol. Adv.* 30, 1196–1206. doi: 10.1016/j.biotechadv.2011.11.007
- Peña-Jurado, E., Pérez-Vega, S., Zavala-Díaz de la Serna, F. J., Pérez-Reyes, I., Gutiérrez-Méndez, N., Vázquez-Castillo, J., et al. (2019). Production of poly(3-hydroxybutyrate) from a dairy industry wastewater using *Bacillus subtilis* EPAH18: bioprocess development and simulation. *Biochem. Eng. J.* 151:107324. doi: 10.1016/j.bej.2019.107324
- Peng, K., Wu, C., Wei, G., Jiang, J., Zhang, Z., and Sun, X. (2018). Implantable sandwich PHBHHx film for burst-free controlled delivery of thymopentin peptide. *Acta Pharm. Sin. B* 8, 432–439. doi: 10.1016/j.apsb.2018.03.003
- Peng, Q., Sun, X., Gong, T., Wu, C. Y., Zhang, T., Tan, J., et al. (2013). Injectable and biodegradable thermosensitive hydrogels loaded with PHBHHx nanoparticles for the sustained and controlled release of insulin. *Acta Biomater.* 9, 5063–5069. doi: 10.1016/j.actbio.2012.09.034
- Pereira, J. R., Araújo, D., Marques, A. C., Neves, L. A., Grandfils, C., Sevrin, C., et al. (2019). Demonstration of the adhesive properties of the medium-chain-length polyhydroxyalkanoate produced by *Pseudomonas chlororaphis* subsp. *aurantiaca* from glycerol. *Int. J. Biol. Macromol.* 122, 1144–1151. doi: 10.1016/j.ijbiomac.2018.09.064
- Persico, P., Ambrogio, V., Baroni, A., Santagata, G., Carfagna, C., Malinconico, M., et al. (2012). Enhancement of poly(3-hydroxybutyrate) thermal and processing stability using a bio-waste derived additive. *Int. J. Biol. Macromol.* 51, 1151–1158. doi: 10.1016/j.ijbiomac.2012.08.036

- Pramanik, N., Das, R., Rath, T., and Kundu, P. P. (2014). Microbial degradation of linseed oil-based elastomer and subsequent accumulation of poly(3-hydroxybutyrate-co-3-hydroxyvalerate) copolymer. *Appl. Biochem. Biotechnol.* 174, 1613–1630. doi: 10.1007/s12010-014-1061-5
- Przybylski, M., Marć, M., Klein, M., Saeb, M. R., and Formela, K. (2018). Structural, mechanical and thermal behavior assessments of PCL/PHB blends reactively compatibilized with organic peroxides. *Polym. Test.* 67, 513–521. doi: 10.1016/j.polymertesting.2018.03.014
- Pyshpadass, H. A., Marx, D. B., and Hanna, M. A. (2008). Effects of extrusion temperature and plasticizers on the physical and functional properties of starch films. *Starch* 60, 527–538. doi: 10.1002/star.200800713
- Qiu, Y. Z., Han, J., Guo, J. J., and Chen, G. Q. (2005). Production of poly(3-hydroxybutyrate-co-3-hydroxyhexanoate) from gluconate and glucose by recombinant *Aeromonas hydrophila* and *Pseudomonas putida*. *Biotechnol. Lett.* 27, 1381–1386. doi: 10.1007/s10529-005-3685-6
- Qu, X. H., Wu, Q., Liang, J., Zou, B., and Chen, G. Q. (2006a). Effect of 3-hydroxyhexanoate content in poly(3-hydroxybutyrate-co-3-hydroxyhexanoate) on *in vitro* growth and differentiation of smooth muscle cells. *Biomaterials* 27, 2944–2950. doi: 10.1016/j.biomaterials.2006.01.013
- Qu, X. H., Wu, Q., Zhang, K. Y., and Chen, G. Q. (2006b). *In vivo* studies of poly(3-hydroxybutyrate-co-3-hydroxyhexanoate) based polymers: biodegradation and tissue reactions. *Biomaterials* 27, 3540–3548. doi: 10.1016/j.biomaterials.2006.02.015
- Räpe, M., Darie-Nit, E. R. N., Grosu, E., Tenase, E. E., Trifoi, A. R., Pap, T., et al. (2015). Effect of plasticizers on melt processability and properties of PHB. *J. Optoelectron. Adv. Mater.* 17, 1778–1784.
- Rajan, K. P., Thomas, S. P., Gopanna, A., and Chavali, M. (2017). “Polyhydroxybutyrate (PHB): a standout biopolymer for environmental sustainability,” in *Handbook of Ecomaterials*, eds L. M. T. Martinez, O. V. Kharissova, and B. I. Kharisov (Cham: Springer International Publishing), 1–23. doi: 10.1007/978-3-319-48281-1_92-1
- Rao, U., Sridhar, R., and Sehgal, P. K. (2010). Biosynthesis and biocompatibility of poly(3-hydroxybutyrate-co-4-hydroxybutyrate) produced by *Cupriavidus necator* from spent palm oil. *Biochem. Eng. J.* 49, 13–20. doi: 10.1016/j.bej.2009.11.005
- Raquez, J. M., Narayan, R., and Dubois, P. (2008). Recent advances in reactive extrusion processing of biodegradable polymer-based compositions. *Macromol. Mater. Eng.* 293, 447–470. doi: 10.1002/mame.200700395
- Raza, Z. A., Abid, S., and Banat, I. M. (2018). Polyhydroxyalkanoates: characteristics, production, recent developments and applications. *Int. Biodeterior. Biodegrad.* 126, 45–56. doi: 10.1016/j.ibiod.2017.10.001
- Reddy, C. S. K., Ghai, R., and Kalia, V. C. (2003). Polyhydroxyalkanoates: an overview. *Bioresour. Technol.* 87, 137–146. doi: 10.1016/S0960-8524(02)00212-2
- Rivera-Briso, A. L., and Serrano-Aroca, Á. (2018). Poly(3-hydroxybutyrate-co-3-hydroxyvalerate): enhancement strategies for advanced applications. *Polymers* 10:732. doi: 10.3390/polym10070732
- Romanelli, M. G., Povo, S., Favaro, L., Fontana, F., Basaglia, M., and Casella, S. (2014). Engineering *Delftia acidovorans* DSM39 to produce polyhydroxyalkanoates from slaughterhouse waste. *Int. J. Biol. Macromol.* 71, 21–27. doi: 10.1016/j.ijbiomac.2014.03.049
- Samori, C., Basaglia, M., Casella, S., Favaro, L., Galletti, P., Giorgini, L., et al. (2015). Dimethyl carbonate and switchable anionic surfactants: two effective tools for the extraction of polyhydroxyalkanoates from microbial biomass. *Green Chem.* 17, 1047–1056. doi: 10.1039/C4GC01821D
- Sanchez-Garcia, M. D., Gimenez, E., and Lagaron, J. M. (2008). Morphology and barrier properties of solvent cast composites of thermoplastic biopolymers and purified cellulose fibers. *Carbohydr. Polym.* 71, 235–244. doi: 10.1016/j.carbpol.2007.05.041
- Sangkhak, K., Paichid, N., Yunu, T., and Prasertsan, P. (2020). Novel polyhydroxyalkanoate-based biocomposites obtained by solution casting and their application for bacteria removal and domestic wastewater purification. *J. Polym. Environ.* 28, 1893–1900. doi: 10.1007/s10924-020-01738-3
- Schmack, G., Gorenflo, V., and Steinbuechel, A. (1998). Biotechnological production and characterization of polyesters containing 4-hydroxyvaleric acid and medium-chain-length hydroxyalkanoic acids. *Macromolecules* 31, 644–649. doi: 10.1021/ma970864d
- Shen, R., Cai, L. W., Meng, D. C., Wu, L. P., Guo, K., Dong, G. X., et al. (2014). Benzene containing polyhydroxyalkanoates homo- and copolymers synthesized by genome edited *Pseudomonas entomophila*. *Sci. China Life Sci.* 57, 4–10. doi: 10.1007/s11427-013-4596-8
- Shen, R., Ning, Z. Y., Lan, Y. X., Chen, J. C., and Chen, G. Q. (2019). Manipulation of polyhydroxyalkanoate granular sizes in *Halomonas bluephagenesis*. *Metab. Eng.* 54, 117–126. doi: 10.1016/j.ymben.2019.03.011
- Sheu, D. S., Chen, Y. L. L., Jhuang, W. J., Chen, H. Y., and Jane, W. N. (2018). Cultivation temperature modulated the monomer composition and polymer properties of polyhydroxyalkanoate synthesized by *Cupriavidus* sp. L7L from levulinate as sole carbon source. *Int. J. Biol. Macromol.* 118, 1558–1564. doi: 10.1016/j.ijbiomac.2018.06.193
- Shi, X., Zhang, G., Phuong, T. V., and Lazzeri, A. (2015). Synergistic effects of nucleating agents and plasticizers on the crystallization behavior of Poly(lactic acid). *Molecules* 20, 1579–1593. doi: 10.3390/molecules20011579
- Shtarkman, B. P., and Razinskaya, I. N. (1983). Plasticization mechanism and structure of polymers. *Acta Polym.* 34, 514–520. doi: 10.1002/actp.1983.010340812
- Sirohi, R., Prakash Pandey, J., Kumar Gaur, V., Gnansounou, E., and Sindhu, R. (2020). Critical overview of biomass feedstocks as sustainable substrates for the production of polyhydroxybutyrate (PHB). *Bioresour. Technol.* 311:123536. doi: 10.1016/j.biortech.2020.123536
- Suárez Palacios, O. Y., Narváez Rincón, P. C., Corriou, J. P., Camargo Pardo, M., and Fonteix, C. (2014). Low-molecular-weight glycerol esters as plasticizers for poly(vinyl chloride). *J. Vinyl Addit. Technol.* 20, 65–71. doi: 10.1002/vnl.21351
- Sudesh, K., Abe, H., and Doi, Y. (2000). Synthesis, structure and properties of polyhydroxyalkanoates: Biological polyesters. *Prog. Polym. Sci.* 25, 1503–1555. doi: 10.1016/S0079-6700(00)00035-6
- Syafiq, I. M., Huong, K. H., Shantini, K., Vigneswari, S., Aziz, N. A., Amirul, A. A. A., et al. (2017). Synthesis of high 4-hydroxybutyrate copolymer by *Cupriavidus* sp. transformants using one-stage cultivation and mixed precursor substrates strategy. *Enzyme Microb. Technol.* 98, 1–8. doi: 10.1016/j.enzmictec.2016.11.011
- Taguchi, K., Aoyagi, Y., Matsusaki, H., Fukui, T., and Doi, Y. (1999). Co-expression of 3-ketoacyl-ACP reductase and polyhydroxyalkanoate synthase genes induces PHA production in *Escherichia coli* HB101 strain. *FEMS Microbiol. Lett.* 176, 183–190. doi: 10.1111/j.1574-6968.1999.tb13660.x
- Taguchi, S., Yamada, M., Matsumoto, K., Tajima, K., Satoh, Y., Munekata, M., et al. (2008). A microbial factory for lactate-based polyesters using a lactate-polymerizing enzyme. *Proc. Natl. Acad. Sci. U.S.A.* 105, 17323–17327. doi: 10.1073/pnas.0805653105
- Takisawa, K., Ooi, T., Matsumoto, K., Kadota, R., and Taguchi, S. (2017). Xylose-based hydrolysate from eucalyptus extract as feedstock for poly(lactate-co-3-hydroxybutyrate) production in engineered *Escherichia coli*. *Process Biochem.* 54, 102–105. doi: 10.1016/j.procbio.2016.12.019
- Tamang, P., Banerjee, R., Köster, S., and Nogueira, R. (2019). Comparative study of polyhydroxyalkanoates production from acidified and anaerobically treated brewery wastewater using enriched mixed microbial culture. *J. Environ. Sci.* 78, 137–146. doi: 10.1016/j.jes.2018.09.001
- Tan, B. K., Ching, Y. C., Poh, S. C., Abdullah, L. C., and Gan, S. N. (2015). A review of natural fiber reinforced poly(vinyl alcohol) based composites: application and opportunity. *Polymers* 7, 2205–2222. doi: 10.3390/polym7111509
- Tan, D., Wu, Q., Chen, J. C., and Chen, G. Q. (2014a). Engineering *Halomonas* TD01 for the low-cost production of polyhydroxyalkanoates. *Metab. Eng.* 26, 34–47. doi: 10.1016/j.ymben.2014.09.001
- Tan, G. Y. A., Chen, C. L., Li, L., Ge, L., Wang, L., Razaad, I. M. N., et al. (2014b). Start a research on biopolymer polyhydroxyalkanoate (PHA): a review. *Polymers* 6, 706–754. doi: 10.3390/polym6030706
- Tănase, E. E., Popa, M. E., Răpă, M., and Popa, O. (2015). PHB/cellulose fibers based materials: physical, mechanical and barrier properties. *Agric. Agric. Sci. Procedia* 6, 608–615. doi: 10.1016/j.aaspro.2015.08.099
- Tebaldi, M. L., Maia, A. L. C., Poletto, F., de Andrade, F. V., and Soares, D. C. F. (2019). Poly(3-hydroxybutyrate-co-3-hydroxyvalerate) (PHBV): current advances in synthesis methodologies, antitumor applications and biocompatibility. *J. Drug Deliv. Sci. Technol.* 51, 115–126. doi: 10.1016/j.jddst.2019.02.007

- Thiré, R. M. S. M., Ribeiro, T. A. A., and Andrade, C. T. (2006). Effect of starch addition on compression-molded poly(3-hydroxybutyrate)/ starch blends. *J. Appl. Polym. Sci.* 100, 4338–4347. doi: 10.1002/app.23215
- Tian, S. J., Lai, W. J., Zheng, Z., Wang, H. X., and Chen, G. Q. (2005). Effect of over-expression of phasin gene from *Aeromonas hydrophila* on biosynthesis of copolyesters of 3-hydroxybutyrate and 3-hydroxyhexanoate. *FEMS Microbiol. Lett.* 244, 19–25. doi: 10.1016/j.femsle.2005.01.020
- Tripathi, L., Wu, L. P., Dechuan, M., Chen, J., Wu, Q., and Chen, G. Q. (2013a). *Pseudomonas putida* KT2442 as a platform for the biosynthesis of polyhydroxyalkanoates with adjustable monomer contents and compositions. *Bioresour. Technol.* 142, 225–231. doi: 10.1016/j.biortech.2013.05.027
- Tripathi, L., Wu, L. P., Meng, D., Chen, J., and Chen, G. Q. (2013b). Biosynthesis and characterization of diblock copolymer of P(3-hydroxypropionate)-block-P(4-hydroxybutyrate) from recombinant *Escherichia coli*. *Biomacromolecules* 14, 862–870. doi: 10.1021/bm3019517
- Tsuge, T. (2016). Fundamental factors determining the molecular weight of polyhydroxyalkanoate during biosynthesis. *Polym. J.* 48, 1051–1057. doi: 10.1038/pj.2016.78
- Turco, R., Ortega-Toro, R., Tesser, R., Mallardo, S., Collazo-Bigliardi, S., Boix, A. C., et al. (2019a). Poly (lactic acid)/thermoplastic starch films: effect of cardoon seed epoxidized oil on their chemico-physical, mechanical, and barrier properties. *Coatings* 9:574. doi: 10.3390/coatings9090574
- Turco, R., Tesser, R., Cucciolito, M. E., Fagnano, M., Ottiano, L., Mallardo, S., et al. (2019b). *Cynara cardunculus* biomass recovery: an eco-sustainable, nonedible resource of vegetable oil for the production of poly(lactic acid) bioplasticizers. *ACS Sustain. Chem. Eng.* 7, 4069–4077. doi: 10.1021/acssuschemeng.8b05519
- Vandewijngaarden, J., Murariu, M., Dubois, P., Carleer, R., Yperman, J., D'Haen, J., et al. (2016). Effect of ultrafine talc on crystallization and end-use properties of poly(3-hydroxybutyrate-co-3-hydroxyhexanoate). *J. Appl. Polym. Sci.* 133:43808. doi: 10.1002/app.43808
- Vandewijngaarden, J., Murariu, M., Dubois, P., Carleer, R., Yperman, J., Adriaenssens, P., et al. (2014). Gas permeability properties of poly(3-hydroxybutyrate-co-3-hydroxyhexanoate). *J. Polym. Environ.* 22, 501–507. doi: 10.1007/s10924-014-0688-1
- Vastano, M., Corrado, I., Sannia, G., Solaiman, D. K. Y., and Pezzella, C. (2019). Conversion of no/low value waste frying oils into biodiesel and polyhydroxyalkanoates. *Sci. Rep.* 9:13751. doi: 10.1038/s41598-019-50278-x
- Vastano, M., Pellis, A., Immirzi, B., Dal Poggetto, G., Malinconico, M., Sannia, G., et al. (2017). Enzymatic production of clickable and PEGylated recombinant polyhydroxyalkanoates. *Green Chem.* 19, 5494–5504. doi: 10.1039/C7GC01872J
- Verlinden, R. A. J., Hill, D. J., Kenward, M. A., Williams, C. D., and Radecka, I. (2007). Bacterial synthesis of biodegradable polyhydroxyalkanoates. *J. Appl. Microbiol.* 102, 1437–1449. doi: 10.1111/j.1365-2672.2007.03335.x
- Vidéki, B., Klébert, S., and Pukánszky, B. (2007). External and internal plasticization of cellulose acetate with caprolactone: structure and properties. *J. Polym. Sci. Part B Polym. Phys.* 45, 873–883. doi: 10.1002/polb.21121
- Vieira, M. G. A., Da Silva, M. A., Dos Santos, L. O., and Beppu, M. M. (2011). Natural-based plasticizers and biopolymer films: a review. *Eur. Polym. J.* 47, 254–263. doi: 10.1016/j.eurpolymj.2010.12.011
- Vieira, M. G. A., Da Silva, M. A., Maçumoto, A. C. G., Dos Santos, L. O., and Beppu, M. M. (2014). Synthesis and application of natural polymeric plasticizer obtained through polyesterification of rice fatty acid. *Mater. Res.* 17, 386–391. doi: 10.1590/S1516-14392014005000017
- Vishtal, A., and Kraslawski, A. (2011). Challenges in industrial applications of technical lignins. *BioResources* 6, 3547–3568. doi: 10.15376/biores.6.3.3547-3568
- Vroman, I., and Tighzert, L. (2009). Biodegradable polymers. *Materials* 2, 307–344. doi: 10.3390/ma2020307
- Wang, B., Sharma-Shivappa, R. R., Olson, J. W., and Khan, S. A. (2013a). Production of polyhydroxybutyrate (PHB) by *Alcaligenes latus* using sugarbeet juice. *Ind. Crops Prod.* 43, 802–811. doi: 10.1016/j.indcrop.2012.08.011
- Wang, H. H., Zhou, X. R., Liu, Q., and Chen, G. Q. (2011). Biosynthesis of polyhydroxyalkanoate homopolymers by *Pseudomonas putida*. *Appl. Microbiol. Biotechnol.* 89, 1497–1507. doi: 10.1007/s00253-010-2964-x
- Wang, L., Yang, Z., Fan, F., Sun, S., Wu, X., Lu, H., et al. (2019). PHBHHx facilitated the residence, survival and stemness maintain of transplanted neural stem cells in traumatic brain injury rats. *Biomacromolecules* 20, 3294–3302. doi: 10.1021/acs.biomac.9b00408
- Wang, L., Zhu, W., Wang, X., Chen, X., Chen, G.-Q., and Xu, K. (2008). Processability modifications of poly(3-hydroxybutyrate) by plasticizing, blending, and stabilizing. *J. Appl. Polym. Sci.* 107, 166–173. doi: 10.1002/app.27004
- Wang, S., Chen, W., Xiang, H., Yang, J., Zhou, Z., and Zhu, M. (2016). Modification and potential application of short-chain-length polyhydroxyalkanoate (SCL-PHA). *Polymers* 8:273. doi: 10.3390/polym8080273
- Wang, Y., Chen, K., Xu, C., and Chen, Y. (2015). Supertoughened biobased poly(lactic acid)-epoxidized natural rubber thermoplastic vulcanizates: fabrication, co-continuous phase structure, interfacial *in situ* compatibilization, and toughening mechanism. *J. Phys. Chem. B* 119, 12138–12146. doi: 10.1021/acs.jpcc.5b06244
- Wang, Y., Chen, R., Cai, J. Y., Liu, Z., Zheng, Y., Wang, H., et al. (2013b). Biosynthesis and thermal properties of PHBV produced from levulinic acid by *Ralstonia eutropha*. *PLoS ONE* 8:e0060318. doi: 10.1371/journal.pone.0060318
- Wang, Y., Wu, H., Jiang, X., and Chen, G. Q. (2014). Engineering *Escherichia coli* for enhanced production of poly(3-hydroxybutyrate-co-4-hydroxybutyrate) in larger cellular space. *Metab. Eng.* 25, 183–193. doi: 10.1016/j.ymben.2014.07.010
- Wijeyekoon, S., Carere, C. R., West, M., Nath, S., and Gapes, D. (2018). Mixed culture polyhydroxyalkanoate (PHA) synthesis from nutrient rich wet oxidation liquors. *Water Res.* 140, 1–11. doi: 10.1016/j.watres.2018.04.017
- Wu, H., Chen, J., and Chen, G. Q. (2016a). Engineering the growth pattern and cell morphology for enhanced PHB production by *Escherichia coli*. *Appl. Microbiol. Biotechnol.* 100, 9907–9916. doi: 10.1007/s00253-016-7715-1
- Wu, H., Fan, Z., Jiang, X., Chen, J., and Chen, G. Q. (2016b). Enhanced production of polyhydroxybutyrate by multiple dividing *E. coli*. *Microb. Cell Fact.* 15:128. doi: 10.1186/s12934-016-0531-6
- Yang, J. E., Choi, Y. J., Lee, S. J., Kang, K. H., Lee, H., Oh, Y. H., et al. (2014). Metabolic engineering of *Escherichia coli* for biosynthesis of poly(3-hydroxybutyrate-co-3-hydroxyvalerate) from glucose. *Appl. Microbiol. Biotechnol.* 98, 95–104. doi: 10.1007/s00253-013-5285-z
- Ye, H. M., Wang, Z., Wang, H. H., Chen, G. Q., and Xu, J. (2010). Different thermal behaviors of microbial polyesters poly(3-hydroxybutyrate-co-3-hydroxyvalerate-co-3-hydroxyhexanoate) and poly(3-hydroxybutyrate-co-3-hydroxyhexanoate). *Polymer* 51, 6037–6046. doi: 10.1016/j.polymer.2010.10.030
- Ye, J., Hu, D., Che, X., Jiang, X., Li, T., Chen, J., et al. (2018). Engineering of *Halomonas bluephagenesis* for low cost production of poly(3-hydroxybutyrate-co-4-hydroxybutyrate) from glucose. *Metab. Eng.* 47, 143–152. doi: 10.1016/j.ymben.2018.03.013
- Yeo, J. C. C., Muiruri, J. K., Thitsartarn, W., Li, Z., and He, C. (2018). Recent advances in the development of biodegradable PHB-based toughening materials: approaches, advantages and applications. *Mater. Sci. Eng. C* 92, 1092–1116. doi: 10.1016/j.msec.2017.11.006
- Yoshie, N., Nakasato, K., Fujiwara, M., Kasuya, K., Abe, H., Doi, Y., et al. (2000). Effect of low molecular weight additives on enzymatic degradation of poly(3-hydroxybutyrate). *Polymer* 41, 3227–3234. doi: 10.1016/S0032-3861(99)00547-9
- Yu, W., Lan, C.-H., Wang, S.-J., Fang, P.-F., and Sun, Y.-M. (2010). Influence of zinc oxide nanoparticles on the crystallization behavior of electrospun poly(3-hydroxybutyrate-co-3-hydroxyvalerate) nanofibers. *Polymer* 51, 2403–2409. doi: 10.1016/j.polymer.2010.03.024
- Zhang, H., Yu, H.-Y., Wang, C., and Yao, J. (2017). Effect of silver contents in cellulose nanocrystal/silver nanohybrids on PHBV crystallization and property improvements. *Carbohydr. Polym.* 173, 7–16. doi: 10.1016/j.carbpol.2017.05.064
- Zhang, H. F., Ma, L., Wang, Z. H., and Chen, G. Q. (2009). Biosynthesis and characterization of 3-hydroxyalkanoate terpolyesters with adjustable properties by *Aeromonas hydrophila*. *Biotechnol. Bioeng.* 104, 582–589. doi: 10.1002/bit.22409
- Zhang, K., Mohanty, A. K., and Misra, M. (2012). Fully biodegradable and biorenewable ternary blends from polylactide, poly(3-hydroxybutyrate-co-hydroxyvalerate) and poly(butylene succinate) with balanced properties. *ACS Appl. Mater. Interfaces* 4, 3091–3101. doi: 10.1021/am3004522
- Zhang, M., and Thomas, N. L. (2010). Preparation and properties of polyhydroxybutyrate blended with different types of starch. *J. Appl. Polym. Sci.* 116, 688–694. doi: 10.1002/app.30991

- Zhang, M., and Thomas, N. L. (2011). Blending polylactic acid with polyhydroxybutyrate: the effect on thermal, mechanical, and biodegradation properties. *Adv. Polym. Technol.* 30, 67–79. doi: 10.1002/adv.20235
- Zhang, X., Lin, Y., Wu, Q., Wang, Y., and Chen, G. Q. (2020). Synthetic biology and genome-editing tools for improving PHA metabolic engineering. *Trends Biotechnol.* 38, 689–700. doi: 10.1016/j.tibtech.2019.10.006
- Zhang, Y., Rempel, C., and Liu, Q. (2014). Thermoplastic starch processing and characteristics-a review. *Crit. Rev. Food Sci. Nutr.* 54, 1353–1370. doi: 10.1080/10408398.2011.636156
- Zhila, N., and Shishatskaya, E. (2018). Properties of PHA bi-, ter-, and quarter-polymers containing 4-hydroxybutyrate monomer units. *Int. J. Biol. Macromol.* 111, 1019–1026. doi: 10.1016/j.ijbiomac.2018.01.130
- Zinn, M., Weilenmann, H.-U., Hany, R., Schmid, M., and Egli, T. (2003). Tailored synthesis of Poly([R]-3-hydroxybutyrate-co-3-hydroxyvalerate) (PHB/HV) in *Ralstonia eutropha* DSM 428. *Acta Biotechnol.* 23, 309–316. doi: 10.1002/abio.200390039
- Conflict of Interest:** The authors declare that the research was conducted in the absence of any commercial or financial relationships that could be construed as a potential conflict of interest.

Copyright © 2021 Turco, Santagata, Corrado, Pezzella and Di Serio. This is an open-access article distributed under the terms of the Creative Commons Attribution License (CC BY). The use, distribution or reproduction in other forums is permitted, provided the original author(s) and the copyright owner(s) are credited and that the original publication in this journal is cited, in accordance with accepted academic practice. No use, distribution or reproduction is permitted which does not comply with these terms.



High Quality *Aspergillus aculeatus* Genomes and Transcriptomes: A Platform for Cellulase Activity Optimization Toward Industrial Applications

Wuttichai Mhuantong^{1†}, Salisa Charoensri^{1†}, Aphisit Poonsrisawat¹, Wirulda Pootakham², Sithichoke Tangphatsornruang², Chatuphon Siamphan¹, Surisa Suwannarangsee¹, Lily Eurwilaichitr¹, Verawat Champreda¹, Varodom Charoensawan^{3,4,5*} and Duriya Chantasingh^{1*}

OPEN ACCESS

Edited by:

Ligia R. Rodrigues,
University of Minho, Portugal

Reviewed by:

Artur Ribeiro,
University of Minho, Portugal
Carla Silva,
University of Minho, Portugal

*Correspondence:

Varodom Charoensawan
varodom.cha@mahidol.ac.th
Duriya Chantasingh
duriya@biotec.or.th

[†]These authors have contributed
equally to this work

Specialty section:

This article was submitted to
Industrial Biotechnology,
a section of the journal
Frontiers in Bioengineering and
Biotechnology

Received: 14 October 2020

Accepted: 31 December 2020

Published: 27 January 2021

Citation:

Mhuantong W, Charoensri S, Poonsrisawat A, Pootakham W, Tangphatsornruang S, Siamphan C, Suwannarangsee S, Eurwilaichitr L, Champreda V, Charoensawan V and Chantasingh D (2021) High Quality *Aspergillus aculeatus* Genomes and Transcriptomes: A Platform for Cellulase Activity Optimization Toward Industrial Applications. *Front. Bioeng. Biotechnol.* 8:607176. doi: 10.3389/fbioe.2020.607176

¹ National Center for Genetic Engineering and Biotechnology, Thailand Science Park, Pathum Thani, Thailand, ² National Omics Center, National Science and Technology Development Agency, Thailand Science Park, Pathum Thani, Thailand, ³ Department of Biochemistry, Faculty of Science, Mahidol University, Bangkok, Thailand, ⁴ Integrative Computational Bioscience Center, Mahidol University, Nakhon Pathom, Thailand, ⁵ Systems Biology of Diseases Research Unit, Faculty of Science, Mahidol University, Bangkok, Thailand

Keywords: plant biomass degradation, cellulolytic enzyme activities, genome sequencing, transcriptome sequencing, *de novo* assembly

INTRODUCTION

Plant biomass is an important feedstock for the production of biofuel and other value-added chemicals in biorefinery industry (Rosales-Calderon and Arantes, 2019). In theory, a ton of cellulose could be converted to ~170 gallons of bioethanol, and thus the global cellulosic biomasses (including corn stover, rice straw and wood residues) can potentially be used to produce over 167 billion gallons of bioethanol annually (Murdock et al., 2019). Despite its great potential, the challenges of biomass utilization lie in the current uncompetitive production cost when compared to that of fossil fuel. Feedstock prices, raw material transportation, and production process, especially pretreatment, saccharification, and fermentation, are major factors of the high capital costs in the production of biofuels (Lynd et al., 2008; Mithra and Padmaja, 2017; Zoghalmi and Paës, 2019). Unlike other bottlenecks, the pretreatment and saccharification processes can be biologically catalyzed by enzymes, especially from microorganisms, providing one of the most environmentally and economically sustainable solutions (Wang and Sun, 2010; Wang et al., 2012). Evidently, it has already been shown that genetic modification of a cellulase producing microbe, *Trichoderma reesei*, could provide a low-cost on-site enzyme production in Brazil (Zhuang et al., 2007), where the genetically engineered *T. reesei* could efficiently utilize local biomasses such as soybean hulls and molasse.

Cellulolytic enzymes from filamentous fungi such as *Aspergillus* (de Vries et al., 2000, 2017), *Neurospora* (Campos Antonieto et al., 2017), *Penicillium* (Gusakov and Sinitsyn, 2012), and *Trichoderma* (Novy et al., 2019) have been screened for cellulose-, hemicellulose-, and other polysaccharide-degrading enzyme activities, and successfully applied in lignocellulose conversion. Among the cellulase-producing fungi, *Aspergillus aculeatus* is one of the most important models for optimization of cellulolytic enzymes due to its versatile metabolism and ability to grow on a wide range of substrates and under various conditions (Jayani et al., 2005; Poonsrisawat et al., 2014; Kunitake et al., 2015; Zhao et al., 2020). Different types of enzymes from *A. aculeatus* have already been used effectively by us and others, in the productions of animal feed

(Saxena et al., 2019), paper (Jayani et al., 2005), cotton fabric (Abdulrachman et al., 2017), and bioethanol (Poonsrisawat et al., 2014). To explore new microorganisms for industrial applications, we have previously screened over 1,300 isolates from our institutional depository known as “Thailand Bioresource Research Center (TBRC, www.tbrcnetwork.org),” and the fungus *A. aculeatus* strain “BCC199” (also known as TBRC277 in our repository) came out as one of the most promising cellulolytic enzyme producers in our collection, based on its cellulolytic enzyme activity on saccharification of different types of biomass (Suwannarangsee et al., 2012, 2014). Random mutagenesis had already been applied for further industrial development (Champreda et al., 2019), leading to an increment of cellulolytic activity up to 2-folds. However, such strategies are time-consuming and not yet able to sufficiently ameliorate the enzyme activity to the level that is economically feasible for industrial production and utilization.

Here, we have sequenced and comprehensively analyzed the genomes and transcriptomes of *A. aculeatus* strain “BCC199” (TBRC277) and two additional strains representing different levels of cellulase activities. The three genomes were sequenced and assembled at higher coverages, as compared to the *A. aculeatus* genomes publicly available. Transcriptome of each strain were also constructed to facilitate transcript annotation. Both types of omic data sets not only provide the highest quality reference genomes and annotations of the cellulolytic enzyme-producing fungus *A. aculeatus*, which can be used to investigate distinct genomic features of the fungus that may play the role in cellulolytic activity.

DATA

The genomes of three *A. aculeatus* strains with different cellulase enzyme activities (see **Table 1**—Enzymatic activities, and Methods), including BCC56535 (the strain representing “low” cellulase activity), BCC199 (representing “moderate” activity), and HUT2365 (representing “high” activity), were completely sequenced in-house using the PacBio RS II platform (Pacific Biosciences, USA), giving the total circular consensus sequences of 345.3–463.3 Mb, equivalent to the genome coverages of 9.3X–12.1X (**Table 1**—Genome sequencing and analyses, see **Supplementary Figure 1** for the analytical process). The final genome sizes after assembly were between 36.0 and 37.7 Mb, similar to the size of the most closely-related publicly available genome *A. aculeatus* ATCC16872 (36.01 Mb) (<https://mycocosm.jgi.doe.gov/Aspac1/Aspac1.home.html>), and with consistent GC contents of 49.4–50.8%.

To improve the annotation and functional analyses of the newly sequenced *A. aculeatus* genomes, we constructed multiple reference transcriptomes of each strain using RNA-seq, and obtained the averages of 47.69, 47.31, and 71.61 M clean reads from BCC56535, BCC199, and HUT2365, respectively (**Table 1** - Transcriptome sequencing and **Supplementary Table 3**). *De novo* transcriptome assembly followed by integrating the gene models with those from genome annotation (see Methods and **Supplementary Figure 1**), yielded comparable genomic features

among the three *A. aculeatus* genomes, including number of genes (11,000–12,000 genes), GC contents, as well as genomic and functional contents, when compared against publicly available databases such as NCBI’s non-redundant database (Coordinators, 2014), enzyme commission (Webb, 1990), and Gene Ontology (Carbon et al., 2009) (**Supplementary Table 2**). Two of the newly sequenced genomes, BCC199 and HUT2365, are of higher quality than the closely-related reference genomes publicly available, *A. aculeatus* ATCC16872 and *A. niger* CBS513.88, in terms of the largest contig sizes and N50 (**Supplementary Figure 2**).

We identified 14,618 orthologs and singletons and the vast majority (~97% in each strain) could be assigned with at least one known function based on the Uniport Blast hit (**Supplementary Figure 3**). Among these predicted genes, 9,294 (64%) have orthologs in all three strains (**Figure 1A**). Between 417–429 predicted genes (3.5–4%) of each strain were classified into one of the carbohydrate-active enzyme families (CAZy; Cantarel et al., 2009) (**Supplementary Table 2**); whereas the total of 280 genes were assigned as Glycosyl Hydrolase (GH) genes and 195 (~70%) of these are common in our three strains (**Figure 1B**). Focusing on the cellulase-relating genes (comprising GH5, 6, 7, and AA9 families), the vast majority (18 out of 22 genes with these GH or AA9 functions, ~82%) are commonly found in the three strains (**Figure 1C**). Importantly, none of these families is uniquely present or absent in any particular strain (**Supplementary Table 4**). However, we noted that one cellulose-degrading gene, endo-1,4-glucanase gene (Acu12065_1: GH5), was exclusively found in the *A. aculeatus* HUT2365 (**Figure 1C**) and potentially be one of the candidate genes contributing to the higher cellulase activity in *A. aculeatus* HUT2365. The Acu12065_1 gene contains a signal peptide (1–17 amino acids), GH5 protein domain (58–245 amino acids), and conserved catalytic domain (157–166 amino acids) with one active site, E164 (**Supplementary Figure 4**).

We further investigated the phylogenetic relationships of the cellulose-degrading enzyme sequences (GH5, 6, 7, and AA9, **Figure 1E**), compared to those of selected housekeeping genes (**Figure 1D**). All three *A. aculeatus* strains and the publicly available ATCC16872 are closely related based on the housekeeping references, although BCC199 and HUT2365 appeared slightly closer to one another (**Figure 1D**). However, based on the cellulose-degrading protein sequences, our moderate-cellulase-activity BCC199 strain diverges the most among the three, and thus there is no clear evidence that the high cellulase activity seen in HUT2365 can be accounted for by the overall divergence of the protein sequences (**Figure 1E**). On the contrary, we observed several single nucleotide polymorphisms (SNPs) within the protein domains and some are in proximity to the active sites (**Figure 1F**, **Supplementary Figures 5, 6**), suggesting that small genomic variations such as point mutations in the cellulolytic genes between the strains might also play a role in their different cellulase activities.

In addition to the genomic data, our transcriptomics of the three *A. aculeatus* strains cultivated on plant biomass as the sole carbon source, can be used to investigate the expression of cellulolytic genes and their facilitating genes, that

TABLE 1 | Key features of three *A. aculeatus* strains, their genomes, and transcriptomes.

Enzyme activities (unit/mg of protein)	BCC56535	BCC199	HUT2365
FPase	0.009 ^c ± 0.003	0.039 ^b ± 0.007	0.327 ^a ± 0.040
CMCase	0.563 ^c ± 0.045	2.879 ^b ± 0.496	10.573 ^a ± 0.619
Genome sequencing and analyses	BCC56535	BCC199	HUT2365
Sequence base (CCS)	345,347,605	463,390,377	423,885,346
Estimated genome coverage*	9.3X	12.1X	11.4X
Assembled genome size (bp)	37,193,364	37,670,955	36,004,422
No. contigs (>=50 kb)	34	11	14
N50	1,914,919	4,861,851	3,415,456
L50	7	4	4
GC (%)	49.4	49.5	50.8
Transcriptome sequencing and analyses	BCC56535	BCC199	HUT2365
Average no. of raw reads (reads)	47.69 M	47.31 M	71.61 M
Average no. of clean reads (reads)	46.97 M	45.71 M	70.18 M
Sequence depth	119.79	116.75	136.78
Q20 (%)	97.21	96.26	97.08
GC (%)	55.70	55.66	54.67
No. predicted gene	12,005	11,442	11,489

Enzymatic assays were performed in triplicate, and the data were shown as means ± standard deviations. The data were compared by ANOVA test. Means in a row followed by different letters (a–c) are significant at $p < 0.05$. Data were analyzed separately for each enzymatic activity. HUT, Hiroshima University Culture Collection; BCC, BIOTEC Culture Collection; CCS, Circular Consensus Sequence with corrections.

*Sequenced base (bp)/estimated genome size (*A. aculeatus* ATCC16872, 36.01 Mb, <https://mycocosm.jgi.doe.gov/Aspac1/Aspac1.home.html>).

may contribute to the cellulose-degrading activities. **Figure 1G** provides an example of a highly expressed putative sugar transporter (Acu07785_1), which is unique to HUT2365. Indeed, we observed this and other Major Facilitator Superfamily (MFS) genes (Nogueira et al., 2020) being transcribed at higher levels in the high-cellulase-activity HUT2365 than in the other strains. As shown in *Neurospora crassa* (Wang et al., 2017) and *T. reesei* (Zhang et al., 2013), modifications of genes encoding glucose transporters greatly affected the cellulase production. These newly constructed transcriptomic data, together with the genomes and gene models described above, not only provide an important resource for genetic engineering of the fungal strains for industrial applications, but also serve as high-quality references for future characterization of the fungi and other related species and their genomic evolution.

MATERIALS AND METHODS

Experimental Plan and Sample Preparation

The three *A. aculeatus* strains of interest: BCC199, BCC56535, and HUT2365, were cultivated on potato dextrose agar (PDA; Difco Laboratories, USA) at 25°C for 4 days, before spore collection. The spores were harvested by washing PDA plate with 10 ml of sterile water containing 1% Triton X-100 (Fischer Scientific, USA). In order to express cellulases (endoglucanases, exoglucanases, and β-D-glucosidases), the fungi have to be cultivated in a medium containing cellulose fiber, such as wheat bran and soybean. Therefore, fungal spores were then cultivated

into 50 ml of wheat bran (3% w/v) and soybean (2% w/v) medium, to the final concentration of 10^7 per ml. The fungal strains were cultured for 72 h in an aerobic cultivation condition at 30°C with 150 rpm in Innova 44R (Eppendorf AG, Germany). To collect cells and crude enzymes in the broth, fungal cells were separated from the whole broth by centrifugation (12,000 × g). The resulting supernatant was used in enzymatic assay. The cells were kept at –80°C for further genomic DNA and RNA isolations.

Total cellulase activity was measured with No. 1 Whatman filter paper (FPase activity) (Miller et al., 1960). For the major cellulose polymer degradation, endoglucanase activity was measured with carboxymethylcellulose (CMCase activity) (Miller et al., 1960). Briefly, the reaction mixture contained 20 μL of crude supernatant, 30 μL of 100 mM (pH 5.5) sodium acetate buffer and 50 μL of substrate to the 0.5% (w/v) final concentration in the final volume of 1 ml. The reaction was incubated for 60 min (for FPase assay) and for 10 min (for CMCase assay). The reaction was stopped by adding 100 μL of DNS. The enzymatic activities were calculated based on a corresponding standard containing glucose. One unit (U) of enzyme activity was defined as the amount of enzyme needed to liberate 1 μmol of reducing sugars per minute. All samples were analyzed in triplicates and the mean values were calculated and reported.

Genome Sequencing and Assembly

Genomic DNA (gDNA) samples of the three fungal strains grown in potato dextrose broth (PDB) were extracted using

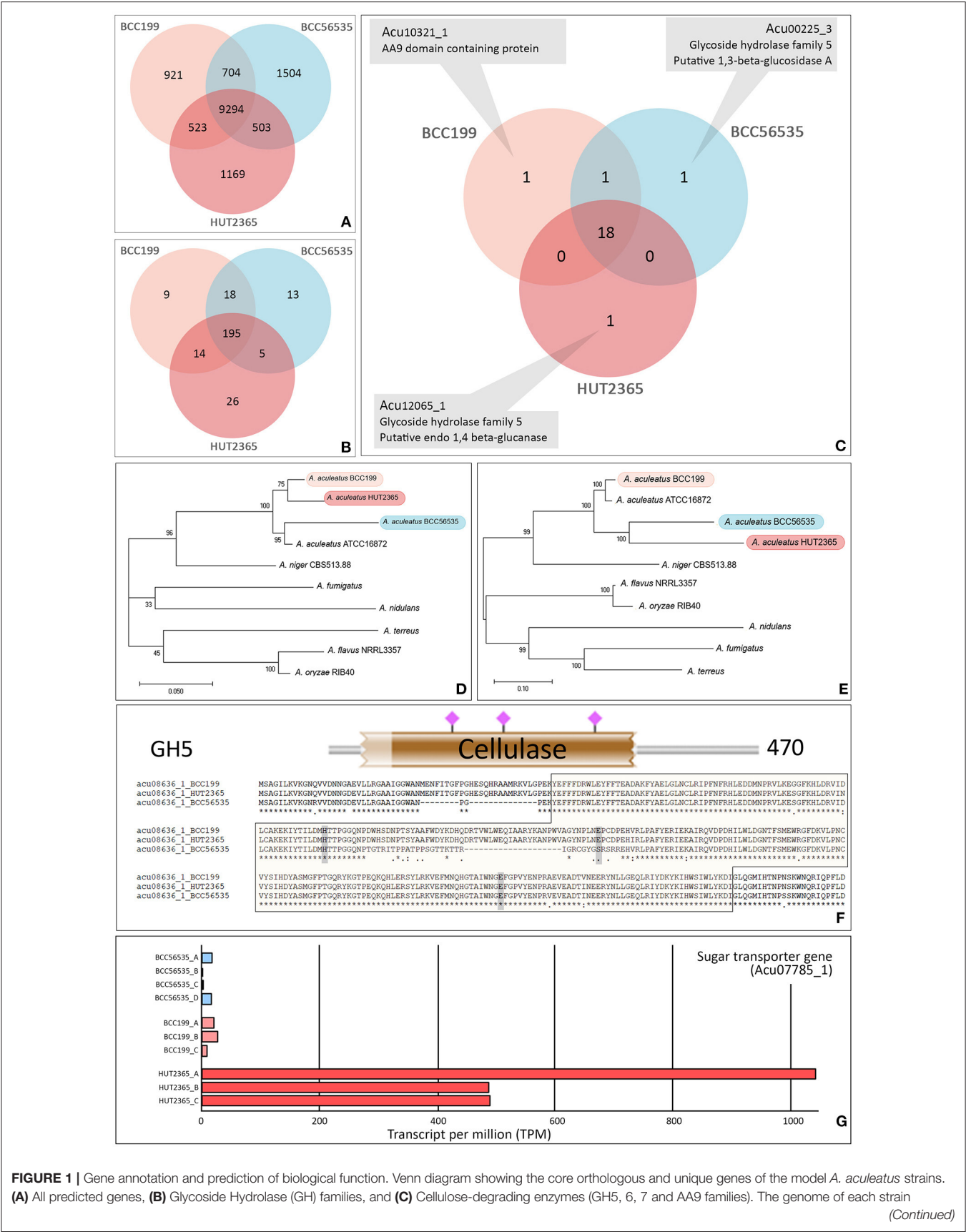


FIGURE 1 | Gene annotation and prediction of biological function. Venn diagram showing the core orthologous and unique genes of the model *A. aculeatus* strains. (A) All predicted genes, (B) Glycoside Hydrolase (GH) families, and (C) Cellulose-degrading enzymes (GH5, 6, 7 and AA9 families). The genome of each strain (Continued)

FIGURE 1 | possesses a unique putative gene: endo-1,4- glucanase gene (Acu12065_1) in HUT2365, 1,3-beta-glucosidase gene (Acu00225_3) in BCC56535, and AA9 domain-containing gene (Acu10321_1) in BCC199. **(D,E)** Phylogenetic relationships between studied *A. aculeatus* strains and other seven *Aspergilli*. Maximum likelihood phylogeny was constructed by using **(D)** the concatenation of housekeeping genes, translation elongation factor 1 alpha, ubiquitin-conjugating enzyme, and beta-tubulin, and **(E)** the concatenation of cellulose-degrading enzymes, GH5, 6, 7, and AA9. The percentages of reproducible trees in which the associated taxa clustered together in the bootstrap test (from 1,000 replicates) are shown next to the branches. **(F)** Sequence variations between the strains—e.g., multiple alignments, SNP positions in relation to functional genomic positions of glycoside hydrolase protein domain (in brown block), and active sites (shown by pink), predicted by HMMER 3.0 (Potter et al., 2018). **(G)** Example of a differentially expressed gene, a putative sugar transporter (Acu07785_1), which was uniquely over-expressed in all three replicates of HUT2365 transcriptomes.

Wizard[®] genomic DNA purification kit (Promega, USA). The extracted gDNA was quality-checked using NanoDrop spectrophotometer (Thermo Scientific, USA) and agarose gel electrophoresis (Al Samarrai and Schmid, 2000). Purified gDNA was used to construct the DNA sequencing libraries, according to the PacBio RSII protocol (Pacific Bioscience, USA). Genome assembly was done using the SMRT Analysis Software version 2.3.0 (<http://www.pacb.com/productsand-services/analytical-software/smrt-analysis/>) with the following steps (**Supplementary Figure 1**): extracting subreads by bash5tools (<https://github.com/PacificBiosciences/pbh5tools>) with the default parameters [min read length = 500 bp, minimum polymerase read quality (QV) = 0.8]; correcting subreads by HGAP3 (Chin et al., 2013) with seed coverage = 30X; performing *de novo* assembly using HGAP3, with assembly target coverage = 40X. The assembled genomes were further polished by Quiver (<https://github.com/PacificBiosciences/GenomicConsensus>), using the default parameters (max divergence percentage = 30, minimum anchor size = 12). The contiguity of assembled sequences was evaluated by comparing the newly assembled genomes to those of publicly available *A. niger* CBS513.88 and *A. aculeatus* ATCC16872, using QUAST (Gurevich et al., 2013). The completeness of genome assembly and annotation was also assessed using the Benchmarking Universal Single-Copy Orthologs (BUSCO, version 4.1.2) pipeline (Simão et al., 2015), using the “Fungal set” (odb10) in the OrthoDB database (Zdobnov et al., 2017) as a reference. AUGUSTUS (Stanke et al., 2006), a Hidden Markov Model (HMM)-based gene prediction program, was employed to predict and locate the positions of genes (including start-stop codons, exons, and introns) in the three fungal genomes sequenced. *A. terreus* was used as the pre-trained model, as it was the most closely related reference genome available in the database.

RNA-seq Library Preparation and Transcriptome Assembly

In addition to genome sequencing, we also analyzed the transcriptomes of the three *A. aculeatus* strains to improve the gene annotation. Fungal mycelium, cultured for 72 h in an aerobic cultivation condition at 30°C, was used to extract RNA following the Tri Reagent[®] protocol (MRC, USA). On-column DNase digestion kit (Qiagen, Germany) was used to further remove DNA traces. Then, the RNA was subjected to quantity and quality assessments by Advances Analyzer[™] automated CS system (Advanced Analytical Technologies Inc., USA).

RNA-seq library preparation and sequencing were performed by Novogene (Beijing, China). In short, ribosomal RNA was

degraded from 10 µg of total RNA using the Ribominus[™] Eukaryotic kit (Life Technologies, USA). The RNA was enriched using the Absolutely mRNA Purification kit (Agilent Technologies, USA) and further quantified by BioAnalyzer 2100 (Agilent Technologies, USA) before cDNA library construction. The cDNA libraries were constructed using the NEBNext Ultra RNA Library Prep Kit for Illumina (NEB, USA). Illumina paired-end adapters and barcode sequences were ligated onto the cDNA fragments. The quality and quantity of the libraries were then assessed, before being sequenced using the Illumina HiSeq2000 platform (Illumina, USA). Quality control (QC) of raw reads were done using FastQC (<http://www.bioinformatics.babraham.ac.uk/projects/fastqc/>) and the adapters were trimmed using FastP (Chen et al., 2018) (see also **Supplementary Figure 1**). Reads after QC were assembled using Trinity (version 2014-07-17) (Grabherr et al., 2011). The assembled RNA-seq reads were then used as inputs for gene prediction, which were done using BRAKER (Hoff et al., 2015) and MAKER (Cantarel et al., 2008).

Gene Prediction and Functional Annotation

EvidenceModeler (Haas et al., 2008) was used to combine the set of gene predictions from AUGUSTUS, BRAKER, and MAKER, where the gene models from the three programs were equally weighted. OrthoFinder (Emms and Kelly, 2019) was used to identify and cluster orthologous genes of the three fungal strains, and their putative functions were assessed using UniProt (The UniProt Consortium, 2019), InterProScan (Jones et al., 2014), and CAZy databases (Cantarel et al., 2009). We also performed additional manual reciprocal BLAST to find the best hits between the strains, to refine the orthologous genes, especially within the multi-copy gene clusters. We set stringent criteria for assigning a gene function to an orthologous group as follows: 1) when the genes from at least 2 out of 3 strains were assigned to the same function; 2) when none of the hits from the 3 strains agreed, we took the one with the highest BLAST score as the representative function of the orthologous group with (**Supplementary Table 5**).

For the predicted proteins, BLASTP (Wheeler et al., 2006) was used to align the protein sequences against the UniProtKB database Release 2019_08, using E-value cut off = 1e-6. Putative protein functions were also obtained using InterProScan (Jones et al., 2014), by matching amino acid sequences against Pfam (Finn et al., 2014), TIGRFAMs (Haft et al., 2012), SMART (Letunic et al., 2015), Prosite (Sigrist et al., 2012), and Gene3D (Lewis et al., 2018). CAZymes Analysis Toolkit (CAT) (Cantarel et al., 2009) was employed to assess the enzymatic activities based on the similarity of amino acid sequences and or protein

domain structures. Identification of enzyme active sites and protein domain was performed using HMMER 3.0 (Potter et al., 2018) (<http://hmmer.org>). To further assess the functional genes in biological pathways, KOALA (KEGG Orthology And Links Annotation, Kanehisa et al., 2016) was also used. Transcription levels were computed separately for each strain based on the newly assembled genomes and gene annotations. HISAT2 (Kim et al., 2019) and StringTie (Pertea et al., 2016) were used to estimate the transcript per million (TPM) values, as previously described (Cortijo et al., 2017).

Phylogenetic Tree Reconstruction

To investigate the phylogenetic relationship of the *Aspergillus* strains based on their housekeeping (translation elongation factor 1 alpha, ubiquitin conjugating enzyme and beta-tubulin) and cellulolytic genes (AA9, GH5, 6, and 7), we constructed phylogenetic trees using the MEGA X software (Kumar et al., 2018). The evolutionary history of the genes was inferred using the maximum likelihood method with a bootstrapping test of 1,000 replicates.

DATA AVAILABILITY STATEMENT

The datasets presented in this study can be found in online repositories. The names of the repository/repositories and accession number(s) can be found at: <https://www.ncbi.nlm.nih.gov/sra>, PRJNA659152; <https://www.ncbi.nlm.nih.gov/geo/>, GSE157700.

PRJNA659152; <https://www.ncbi.nlm.nih.gov/geo/>, GSE157700.

AUTHOR CONTRIBUTIONS

LE, VCham, VChar, and DC conceived the overall study. AP, WP, ST, CS, and SS performed the experiments. WM and SC analyzed the data. VChar and DC wrote the manuscript with input from all authors. All authors read and approved the final manuscript.

FUNDING

This work was supported by the National Science and Technology Development Agency (NSTDA), National Center for Genetic Engineering and Biotechnology (BIOTEC), Thailand, under the Grant P-18-52106 to DC and VChar; and the Thailand Research Fund (TRF) Grant for New Researcher (MRG6080235) and Faculty of Science, Mahidol University to VChar.

SUPPLEMENTARY MATERIAL

The Supplementary Material for this article can be found online at: <https://www.frontiersin.org/articles/10.3389/fbioe.2020.607176/full#supplementary-material>

REFERENCES

- Abdulrachman, D., Thongkred, P., Kocharin, K., Nakpathom, M., Somboon, B., Narumol, N., et al. (2017). Heterologous expression of *Aspergillus aculeatus* endo-polygalacturonase in *Pichia pastoris* by high cell density fermentation and its application in textile scouring. *BMC Biotechnol.* 17:15. doi: 10.1186/s12896-017-0334-9
- Al Samarrai, T., and Schmid, J. (2000). A simple method for extraction of fungal genomic DNA. *Lett. Appl. Microbiol.* 30, 53–56. doi: 10.1046/j.1472-765x.2000.00664.x
- Campos Antoniôto, A. C., Ramos Pedersoli, W., dos Santos Castro, L., da Silva Santos, R., da Silva Cruz, A. H., Nogueira, K. M. V., et al. (2017). Deletion of pH regulator pac-3 affects cellulase and xylanase activity during sugarcane bagasse degradation by *Neurospora crassa*. *PLoS ONE* 12:e0169796. doi: 10.1371/journal.pone.0169796
- Cantarel, B. L., Coutinho, P. M., Rancurel, C., Bernard, T., Lombard, V., and Henrissat, B. (2009). The Carbohydrate-Active EnZymes database (CAZy): an expert resource for glycogenomics. *Nucleic Acids Res.* 37(Suppl. 1), D233–D238. doi: 10.1093/nar/gkn663
- Cantarel, B. L., Korf, I., Robb, S. M., Parra, G., Ross, E., Moore, B., et al. (2008). MAKER: an easy-to-use annotation pipeline designed for emerging model organism genomes. *Genome Res.* 18, 188–196. doi: 10.1101/gr.6743907
- Carbon, S., Ireland, A., Mungall, C. J., Shu, S., Marshall, B., Lewis, S., et al. (2009). AmiGO: online access to ontology and annotation data. *Bioinformatics* 25, 288–289. doi: 10.1093/bioinformatics/btn615
- Champrada, V., Suwannarangsri, S., Arnthong, J., Siamphan, C., Poonsrisawat, A., Ketsub, N., et al. (2019). *Mutant Strain Aspergillus aculeatus for Producing Cellulase and Xylanase and Preparation Method Thereof*. World Patent WO2018226171A3, filed May 30, 2018 and issued March 3, 2019. Bangkok. Available online at: <https://patentimages.storage.googleapis.com/a0/ab/ba/010f019f291ba8/WO2018226171A3.pdf>
- Chen, S., Zhou, Y., Chen, Y., and Gu, J. (2018). fastp: an ultra-fast all-in-one FASTQ preprocessor. *Bioinformatics* 34, i884–i890. doi: 10.1093/bioinformatics/bty560
- Chin, C.-S., Alexander, D. H., Marks, P., Klammer, A. A., Drake, J., Heiner, C., et al. (2013). Nonhybrid, finished microbial genome assemblies from long-read SMRT sequencing data. *Nat. Methods* 10:563. doi: 10.1038/nmeth.2474
- Coordinators, N. R. (2014). Database resources of the national center for biotechnology information. *Nucleic Acids Res.* 42, D7–D17. doi: 10.1093/nar/gkt1146
- Cortijo, S., Charoensawan, V., Brestovitsky, A., Buning, R., Ravarani, C., Rhodes, D., et al. (2017). Transcriptional regulation of the ambient temperature response by H2A.Z nucleosomes and HSF1 transcription factors in arabidopsis. *Mol. Plant* 10, 1258–1273. doi: 10.1016/j.molp.2017.08.014
- de Vries, R. P., Kester, H. C., Poulsen, C. H., Benen, J. A., and Visser, J. (2000). Synergy between enzymes from *Aspergillus* involved in the degradation of plant cell wall polysaccharides. *Carbohydr. Res.* 327, 401–410. doi: 10.1016/S0008-6215(00)00066-5
- de Vries, R. P., Riley, R., Wiebenga, A., Aguilar-Osorio, G., Amillis, S., and Uchima, C. A., et al. (2017). Comparative genomics reveals high biological diversity and specific adaptations in the industrially and medically important fungal genus *Aspergillus*. *BMC Genome Biol.* 18:28. doi: 10.1186/s13059-017-1151-0
- Emms, D. M., and Kelly, S. (2019). OrthoFinder: phylogenetic orthology inference for comparative genomics. *Genome Biol.* 20, 1–14. doi: 10.1186/s13059-019-1832-y
- Finn, R. D., Bateman, A., Clements, J., Coghill, P., Eberhardt, R. Y., Eddy, S. R., et al. (2014). Pfam: the protein families database. *Nucleic Acids Res.* 42, D222–D230. doi: 10.1093/nar/gkt1223
- Grabherr, M. G., Haas, B. J., Yassour, M., Levin, J. Z., Thompson, D. A., Amit, I., et al. (2011). Trinity: reconstructing a full-length transcriptome without a genome from RNA-Seq data. *Nat. Biotechnol.* 29:644. doi: 10.1038/nbt.1883
- Gurevich, A., Saveliev, V., Vyahhi, N., and Tesler, G. (2013). QUAST: quality assessment tool for genome assemblies. *Bioinformatics* 29, 1072–1075. doi: 10.1093/bioinformatics/btt086
- Gusakov, A. V., and Sinitsyn, A. P. (2012). Cellulases from *Penicillium* species for producing fuels from biomass. *Biofuels* 3, 463–477. doi: 10.4155/bfs.12.41

- Haas, B. J., Salzberg, S. L., Zhu, W., Pertea, M., Allen, J. E., Orvis, J., et al. (2008). Automated eukaryotic gene structure annotation using EVIDENCEModeler and the Program to Assemble Spliced Alignments. *Genome Biol.* 9:R7. doi: 10.1186/gb-2008-9-1-r7
- Haft, D. H., Selengut, J. D., Richter, R. A., Harkins, D., Basu, M. K., and Beck, E. (2012). TIGRFAMs and genome properties in 2013. *Nucleic Acids Res.* 41, D387–D395. doi: 10.1093/nar/gks1234
- Hoff, K. J., Lange, S., Lomsadze, A., Borodovsky, M., and Stanke, M. (2015). BRAKER1: unsupervised RNA-Seq-based genome annotation with GeneMark-ET and AUGUSTUS. *Bioinformatics* 32, 767–769. doi: 10.1093/bioinformatics/btv661
- Jayani, R. S., Saxena, S., and Gupta, R. (2005). Microbial pectinolytic enzymes: a review. *Process Biochem.* 40, 2931–2944. doi: 10.1016/j.procbio.2005.03.026
- Jones, P., Binns, D., Chang, H.-Y., Fraser, M., Li, W., McAnulla, C., et al. (2014). InterProScan 5: genome-scale protein function classification. *Bioinformatics* 30, 1236–1240. doi: 10.1093/bioinformatics/btu031
- Kanehisa, M., Sato, Y., and Morishima, K. (2016). BlastKOALA and GhostKOALA: KEGG tools for functional characterization of genome and metagenome sequences. *J. Mol. Biol.* 428, 726–731. doi: 10.1016/j.jmb.2015.11.006
- Kim, D., Paggi, J. M., Park, C., Bennett, C., and Salzberg, S. L. (2019). Graph-based genome alignment and genotyping with HISAT2 and HISAT-genotype. *Nat. Biotechnol.* 37, 907–915. doi: 10.1038/s41587-019-0201-4
- Kumar, S., Stecher, G., Li, M., Nkayaz, C., and Tamura, K. (2018). MEGA X: molecular evolutionary genetics analysis across computing platforms. *Mol. Biol. Evol.* 35, 1547–1549. doi: 10.1093/molbev/msy096
- Kunitake, E., Kawamura, A., Tani, S., Takenaka, S., Ogasawara, W., and Sumitani, J.-i., et al. (2015). Effects of clbR overexpression on enzyme production in *Aspergillus aculeatus* vary depending on the cellulosic biomass-degrading enzyme species. *Biosci. Biotechnol. Biochem.* 79, 488–495. doi: 10.1080/09168451.2014.982501
- Letunic, I., Doerks, T., and Bork, P. (2015). SMART: recent updates, new developments and status in 2015. *Nucleic Acids Res.* 43, D257–D260. doi: 10.1093/nar/gku949
- Lewis, T. E., Sillitoe, I., Dawson, N., Lam, S. D., Clarke, T., Lee, D., et al. (2018). Gene3D: extensive prediction of globular domains in proteins. *Nucleic Acids Res.* 46, D435–D439. doi: 10.1093/nar/gkx1069
- Lynd, L. R., Laser, M. S., Bransby, D., Dale, B. E., Davison, B., Hamilton, R., et al. (2008). How biotech can transform biofuels. *Nat. Biotechnol.* 26, 169–172. doi: 10.1038/nbt0208-169
- Miller, G. L., Blum, R., Glennon, W. E., and Burton, A. L. (1960). Measurement of carboxymethylcellulase activity. *Anal. Biochem.* 1, 127–132. doi: 10.1016/0003-2697(60)90004-X
- Mithra, M., and Padmaja, G. (2017). Strategies for enzyme saving during saccharification of pretreated lignocellulose-starch biomass: effect of enzyme dosage and detoxification chemicals. *Heliyon* 3:e00384. doi: 10.1016/j.heliyon.2017.e00384
- Murdoch, H. E., Gibb, D., André, T., Appavou, F., Brown, A., Epp, B., et al. (2019). *Renewables 2019 Global Status Report*. Paris: REN21. Available online at: https://www.ren21.net/wp-content/uploads/2019/05/gsr_2019_full_report_en.pdf
- Nogueira, K. M. V., Mendes, V., Carraro, C. B., Taveira, I. C., Oshiquiri, L. H., Gupta, V. K., et al. (2020). Sugar transporters from industrial fungi: key to improving second-generation ethanol production. *Renew. Sustain. Energy Rev.* 131:109991. doi: 10.1016/j.rser.2020.109991
- Novy, V., Nielsen, F., Seiboth, B., and Nidetzky, B. (2019). The influence of feedstock characteristics on enzyme production in *Trichoderma reesei*: a review on productivity, gene regulation and secretion profiles. *Biotechnol. Biofuels* 12:238. doi: 10.1186/s13068-019-1571-z
- Pertea, M., Kim, D., Pertea, G. M., Leek, J. T., and Salzberg, S. L. (2016). Transcript-level expression analysis of RNA-seq experiments with HISAT, StringTie and Ballgown. *Nat. Protoc.* 11, 1650–1667. doi: 10.1038/nprot.2016.095
- Poonsrisawat, A., Wanlapatit, S., Paemanee, A., Eurwilaichitr, L., Piyachomkwan, K., and Champreda, V. (2014). Viscosity reduction of cassava for very high gravity ethanol fermentation using cell wall degrading enzymes from *Aspergillus aculeatus*. *Process Biochem.* 49, 1950–1957. doi: 10.1016/j.procbio.2014.07.016
- Potter, S. C., Luciani, A., Eddy, S. R., Park, Y., Lopez, R., and Finn, R. D. (2018). HMMER web server: 2018 update. *Nucleic Acids Res.* 46, W200–W204. doi: 10.1093/nar/gky448
- Rosales-Calderon, O., and Arantes, V. (2019). A review on commercial-scale high-value products that can be produced alongside cellulosic ethanol. *Biotechnol. Biofuels* 12:240. doi: 10.1186/s13068-019-1529-1
- Saxena, A., Verma, M., Singh, B., Sangwan, P., Yadav, A. N., Dhaliwal, H. S., et al. (2019). Characteristics of an acidic phytase from *Aspergillus aculeatus* APF1 for dephytinization of biofortified wheat genotypes. *Appl. Biochem. Biotechnol.* 191, 679–694. doi: 10.1007/s12010-019-03205-9
- Sigrist, C. J., De Castro, E., Cerutti, L., Cuche, B. A., Hulo, N., Bridge, A., et al. (2012). New and continuing developments at PROSITE. *Nucleic Acids Res.* 41, D344–D347. doi: 10.1093/nar/gks1067
- Simão, F. A., Waterhouse, R. M., Ioannidis, P., Kriventseva, E. V., and Zdobnov, E. M. (2015). BUSCO: assessing genome assembly and annotation completeness with single-copy orthologs. *Bioinformatics* 31, 3210–3212.
- Stanke, M., Keller, O., Gunduz, I., Hayes, A., Waack, S., and Morgenstern, B. (2006). AUGUSTUS: *ab initio* prediction of alternative transcripts. *Nucleic Acids Res.* 34(Suppl. 2), W435–W439. doi: 10.1093/nar/gkl200
- Suwanrangsee, S., Arnthong, J., Eurwilaichitr, L., and Champreda, V. (2014). Production and characterization of multipolysaccharide degrading enzymes from *Aspergillus aculeatus* BCC199 for saccharification of agricultural residues. *J. Microbiol. Biotechnol.* 24, 1427–1437. doi: 10.4014/jmb.1406.06050
- Suwanrangsee, S., Bunternsook, B., Arnthong, J., Paemanee, A., Thamchaipenet, A., Eurwilaichitr, L., et al. (2012). Optimisation of synergistic biomass-degrading enzyme systems for efficient rice straw hydrolysis using an experimental mixture design. *Bioresour. Technol.* 119, 252–261. doi: 10.1016/j.biortech.2012.05.098
- The UniProt Consortium (2019). UniProt: a worldwide hub of protein knowledge. *Nucleic Acids Res.* 47, D506–D515. doi: 10.1093/nar/gky1049
- Wang, B., Li, J., Gao, J., Cai, P., Han, X., and Tian, C. (2017). Identification and characterization of the glucose dual-affinity transport system in *Neurospora crassa*: pleiotropic roles in nutrient transport, signaling, and carbon catabolite repression. *Biotechnol. Biofuels* 10, 1–22. doi: 10.1186/s13068-017-0705-4
- Wang, K., and Sun, R.-C. (2010). “Chapter 7.5 - biorefinery Straw for Bioethanol,” in *Cereal Straw as a Resource for Sustainable Biomaterials and Biofuels* (Amsterdam: Elsevier), 267–287. doi: 10.1016/B978-0-444-53234-3.00015-8
- Wang, M., Li, Z., Fang, X., Wang, L., and Qu, Y. (2012). “Cellulolytic enzyme production and enzymatic hydrolysis for second-generation bioethanol production,” in *Biotechnology in China III: Biofuels and Bioenergy*, eds F. W. Bai, C. G. Liu, H. Huang, G. T. Tsao (Berlin; Heidelberg: Springer), 1–24. doi: 10.1007/978-3-642-28478-6
- Webb, E. C. (1990). “Enzyme nomenclature,” in *The Terminology of Biotechnology: A Multidisciplinary Problem*, ed K. L. Loening (Berlin; Heidelberg: Springer), 51–60. doi: 10.1007/978-3-642-76011-2_6
- Wheeler, D. L., Barrett, T., Benson, D. A., Bryant, S. H., Canese, K., Chetvernin, V., et al. (2006). Database resources of the national center for biotechnology information. *Nucleic Acids Res.* 35(Suppl. 1), D5–D12. doi: 10.1093/nar/gkj158
- Zdobnov, E. M., Tegenfeldt, F., Kuznetsov, D., Waterhouse, R. M., Simão, F. A., Ioannidis, P., et al. (2017). OrthoDB v9. 1: cataloging evolutionary and functional annotations for animal, fungal, plant, archaeal, bacterial and viral orthologs. *Nucleic Acids Res.* 45, D744–D749. doi: 10.1093/nar/gkw1119
- Zhang, W., Kou, Y., Xu, J., Cao, Y., Zhao, G., Shao, J., et al. (2013). Two major facilitator superfamily sugar transporters from *Trichoderma reesei* and their roles in induction of cellulase biosynthesis. *J. Biol. Chem.* 288, 32861–32872. doi: 10.1074/jbc.M113.505826
- Zhao, L., Cheng, L., Deng, Y., Li, Z., Hong, Y., Li, C., et al. (2020). Study on rapid drying and spoilage prevention of potato pulp using solid-state fermentation with *Aspergillus aculeatus*. *Bioresour. Technol.* 296:122323. doi: 10.1016/j.biortech.2019.122323
- Zhuang, J., Marchant, M. A., Nokes, S. E., and Strobel, H. J. (2007). Economic analysis of cellulase production methods for bio-ethanol. *Appl. Eng. Agric.* 23, 679–687. doi: 10.13031/2013.23659

Zoghlami, A., and Paës, G. (2019). Lignocellulosic biomass: understanding recalcitrance and predicting hydrolysis. *Front. Chem.* 7:874. doi: 10.3389/fchem.2019.00874

Conflict of Interest: The authors declare that the research was conducted in the absence of any commercial or financial relationships that could be construed as a potential conflict of interest.

Copyright © 2021 Mhuantong, Charoensri, Poonsrisawat, Pootakham, Tangphatsornruang, Siamphan, Suwannarangsee, Eurwilaichitr, Champreda, Charoensawan and Chantasingh. This is an open-access article distributed under the terms of the Creative Commons Attribution License (CC BY). The use, distribution or reproduction in other forums is permitted, provided the original author(s) and the copyright owner(s) are credited and that the original publication in this journal is cited, in accordance with accepted academic practice. No use, distribution or reproduction is permitted which does not comply with these terms.



Toluene Dioxygenase-Catalyzed *cis*-Dihydroxylation of Quinolines: A Molecular Docking Study and Chemoenzymatic Synthesis of Quinoline Arene Oxides

Derek R. Boyd^{1*}, Narain D. Sharma¹, Pui L. Loke¹, Jonathan G. Carroll¹, Paul J. Stevenson¹, Patrick Hoering² and Christopher C. R. Allen^{2*}

¹ School of Chemistry and Chemical Engineering, Queen's University of Belfast, Belfast, United Kingdom, ² School of Biological Sciences, Queen's University of Belfast, Belfast, United Kingdom

OPEN ACCESS

Edited by:

Ligia R. Rodrigues,
University of Minho, Portugal

Reviewed by:

Jin-Song Gong,
Jiangnan University, China
Sergio F. Sousa,
University of Porto, Portugal

*Correspondence:

Derek R. Boyd
dr.boyd@qub.ac.uk
Christopher C. R. Allen
c.allen@qub.ac.uk

Specialty section:

This article was submitted to
Industrial Biotechnology,
a section of the journal
Frontiers in Bioengineering and
Biotechnology

Received: 19 October 2020

Accepted: 22 December 2020

Published: 12 February 2021

Citation:

Boyd DR, Sharma ND, Loke PL,
Carroll JG, Stevenson PJ, Hoering P
and Allen CCR (2021) Toluene
Dioxygenase-Catalyzed
cis-Dihydroxylation of Quinolines: A
Molecular Docking Study and
Chemoenzymatic Synthesis of
Quinoline Arene Oxides.
Front. Bioeng. Biotechnol. 8:619175.
doi: 10.3389/fbioe.2020.619175

Molecular docking studies of quinoline and 2-chloroquinoline substrates at the active site of toluene dioxygenase (TDO), were conducted using Autodock Vina, to identify novel edge-to-face interactions and to rationalize the observed stereoselective *cis*-dihydroxylation of carbocyclic rings and formation of isolable *cis*-dihydrodiol metabolites. These *in silico* docking results of quinoline and pyridine substrates, with TDO, also provided support for the postulated *cis*-dihydroxylation of electron-deficient pyridyl rings, to give transient *cis*-dihydrodiol intermediates and the derived hydroxyquinolines. 2-Chloroquinoline *cis*-dihydrodiol metabolites were used as precursors in the chemoenzymatic synthesis of enantiopure arene oxide and arene dioxide derivatives of quinoline, in the context of its possible mammalian metabolism and carcinogenicity.

Keywords: arene oxides, *cis*-dihydrodiols, dioxygenase, docking, biocatalysis

INTRODUCTION

Quinoline and substituted quinolines are widely distributed in the environment as urban particulates, resulting from partial combustion of fossil fuels and tobacco. Quinoline **1** is a mammalian hepatocarcinogen and a bacterial mutagen, with its metabolites binding covalently to DNA. Possible pathways responsible for these biological effects continue to be of interest (Hollstein et al., 1978; Tada et al., 1980, 1982; LaVoie et al., 1983; Agarwal et al., 1986, 1990; Willems et al., 1992; Saeki et al., 1993; Reigh et al., 1996; Suzuki et al., 2000; Dowers et al., 2004; Hakura et al., 2007; Diaz Duran et al., 2015; Matsumoto et al., 2018). Cytochrome P-450 (CYP-450) monooxygenases have been identified as responsible for catalyzing epoxidation and dearomatization of quinolines, during mammalian liver metabolism.

Bacterial cell metabolism can also involve an initial dearomatization step of quinolines, *via* arene dioxygenase-catalyzed *cis*-dihydroxylation, resulting in the isolation of stable, and postulation of transient, azaarene metabolites. This is exemplified by the metabolism of quinoline **1** (X = H), and substituted quinolines, which were studied earlier using different bacterial strains and arene dioxygenase enzyme types (Boyd et al., 1987, 1993, 1998, 2002; Bott et al., 1990; Fetzner et al., 1993; Kaiser et al., 1996; Zia et al., 2016).

Toluene dioxygenase (TDO), naphthalene dioxygenase (NDO), and biphenyl dioxygenase (BPDO) were among those bacterial enzymes found to catalyze the formation of *cis*-dihydrodiol metabolites and monohydroxylated derivatives of quinoline substrates (Boyd et al., 2002). The UV4 mutant strain of *Pseudomonas putida*, expressing TDO, was used in the biotransformation of quinoline **1** (X = H) to give *cis*-dihydrodiols **2** (33% relative yield) and the less stable *cis*-dihydrodiol **3** (1% relative yield, **Figure 1**) (Boyd et al., 1987, 1993). As the latter metabolite readily decomposed to 8-hydroxyquinoline **4** (27% relative yield), similar proportions of the *cis*-diols **2** and **3** were assumed to be initially formed from dihydroxylation of the carbocyclic ring of quinoline **1**.

No direct evidence for *cis*-dihydroxylation of the electron-poor pyridyl ring was found during analysis of the biotransformation products (Boyd et al., 1987, 1993). The combined relative yields of the isolated achiral metabolites 3-hydroxyquinoline **5** (13%) and anthranilic acid **6** (27%), were however consistent with the initial formation of the transient *cis*-dihydrodiol **7** as a further major initial metabolite (**Figure 1**). Formation of 3-hydroxyquinoline **5** could result

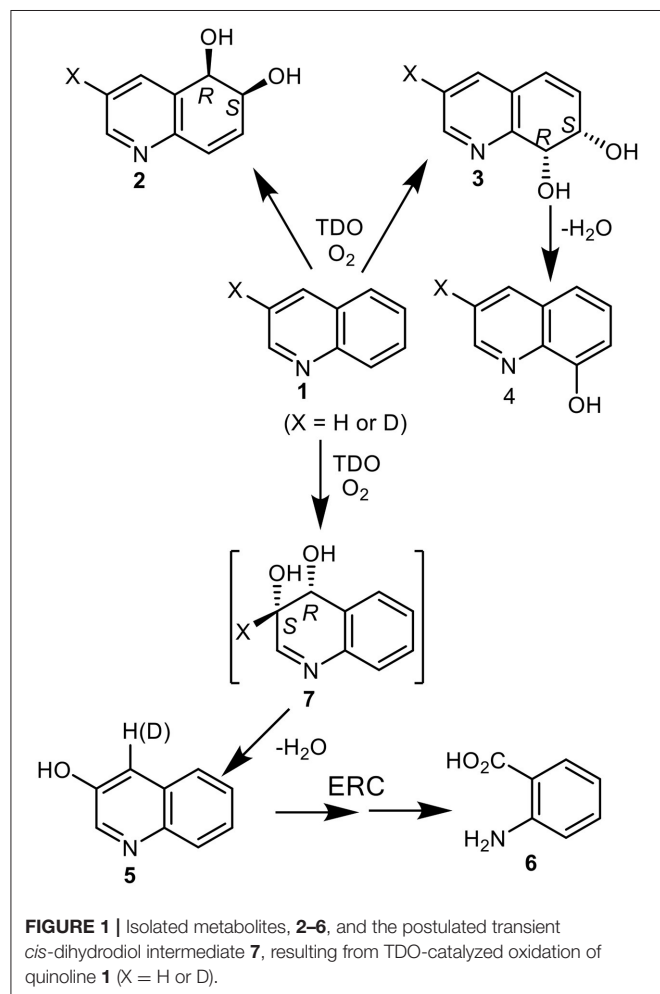
from spontaneous dehydration of intermediate **7** and of anthranilic acid **6** from enzymatic ring-cleavage (ERC) of 3-hydroxyquinoline **5**. If anthranilic acid **6** and phenol **5** were derived from intermediate *cis*-dihydrodiol **7**, the relative ratio of initially formed *cis*-dihydrodiols diols **2**, **3**, and **7** would be estimated as *ca.* 33:27:40. Further *in silico* support for the formation of transient *cis*-dihydrodiol **7** - the major metabolite of quinoline **1** (TDO as biocatalyst), was obtained from a joint study with a collaborating laboratory using the GOLD molecular docking program (unpublished data). This prompted our interest in employing the Autodock Vina program for the current study.

Indirect evidence for the undetected heterocyclic *cis*-dihydrodiol **7** was acquired from the results of an earlier biotransformation (*P. putida* UV4) of 3-deuterioquinoline **1** (X = 87% D); it yielded 4-deuterioquinolin-3-ol **5** (23% D) along with other metabolites (**Figure 1**) (Barr et al., 1998). This could be accounted for by the migration and partial retention of deuterium, from the aromatization of the intermediate *cis*-dihydrodiol **7** (X = D, **Figure 1**) via an NIH shift mechanism, as observed during aromatization of the isolated carbocyclic *cis*-dihydrodiols of naphthalene and quinoline **2** and **3**.

Pseudomonas strains are among the most common quinoline-degrading bacteria. Monohydroxylation at the C-2 position of quinoline often occurs during *Pseudomonad* biotransformations, to yield 2-hydroxyquinoline, which prefers to exist as the 2-quinolone tautomer (Kaiser et al., 1996). Substitution at the C-2 position could thus, in principle, improve the isolated yields of *cis*-dihydrodiol metabolites resulting from dioxygenase-catalyzed biotransformations of quinoline substrates. It may be a factor in: (i) the excellent isolated yield (80%) of the corresponding 7,8-*cis*-dihydrodiol obtained from NDO-catalyzed biotransformation of 2-cyanoquinoline (Zia et al., 2016) and (ii) the improved isolated yields (35–45%) of *cis*-dihydrodiol metabolites of 2-chloroquinoline (with TDO) and 2-methoxyquinoline (with BPDO) (Boyd et al., 2002), relative to the very low isolated yields of *cis*-dihydrodiols **2** and **3** obtained from quinoline **1** (X = H, <5% using TDO, **Figure 1**) (Boyd et al., 1993).

Biotransformations of 2-chloroquinoline **8**, conducted using *P. putida* UV4 whole cells resulted in the isolation of multigram quantities of *cis*-diol metabolites **9**, **10**, and **11**, possibly via intermediate **12**, and traces of 2-quinolone **13** (**Figure 2**) (Boyd et al., 1998, 2002). Since the enantiopure *cis*-dihydrodiols **9**, **10**, and **11** are more stable, and are available in much higher yields compared with quinoline *cis*-dihydrodiols **2** and **3**, they are herein used in the chemoenzymatic synthesis of enantiopure mammalian metabolites of quinoline **1**.

While the dioxygenase-catalyzed *cis*-dihydroxylation of electron-rich furan and thiophene rings has been reported, to give heterocyclic dihydrodiol metabolites (Boyd et al., 2012; Lewis, 2016), little evidence is available for the dearomatization of electron-poor pyridine rings by a similar mechanism. The possibility that TDO-catalyzed *cis*-dihydroxylation of a pyridyl ring was proposed as a result of *P. putida* UV4 biotransformations of: (i) quinoline **1**, to yield 3-hydroxyquinoline **5** via unstable intermediate **7** (**Figure 1**) (Boyd et al., 1987, 1993), (ii) 2-chloroquinoline **8**, to yield *cis*-diol **11** via transient intermediate **12** (**Figure 2**) (Boyd et al.,



1998, 2002), and (iii) 2-chloropyridine **14**, to yield 2-chloro-3-hydroxypyridine **16** via undetected intermediate **15** (Figure 3) (Garrett et al., 2006). Since none of the *cis*-dihydrodiols **7**, **12**, and **15** could be detected directly, evidence for their intermediacy is sought through the current *in silico* molecular docking studies of TDO with the corresponding substrates, quinoline **1**, 2-chloroquinoline **8** and 2-chloropyridine **14** (Results section).

Major objectives of this study were to: (i) review proposed metabolic pathways of quinoline **1** and 2-chloroquinoline **8** by *P. putida* UV 4 cells, and to compare with TDO docking results (ii) use the isolated *cis*-dihydrodiol metabolites **9** and **10** and their derivatives, in the quest for improved chemoenzymatic synthetic routes to enantiopure arene oxide and dioxide derivatives of quinoline **1**.

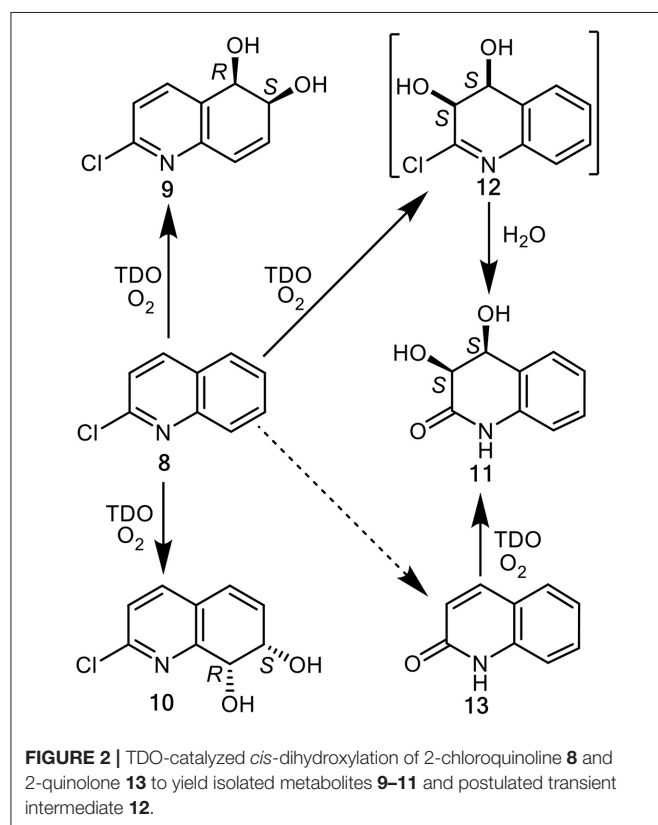


FIGURE 2 | TDO-catalyzed *cis*-dihydroxylation of 2-chloroquinoline **8** and 2-quinolone **13** to yield isolated metabolites **9–11** and postulated transient intermediate **12**.

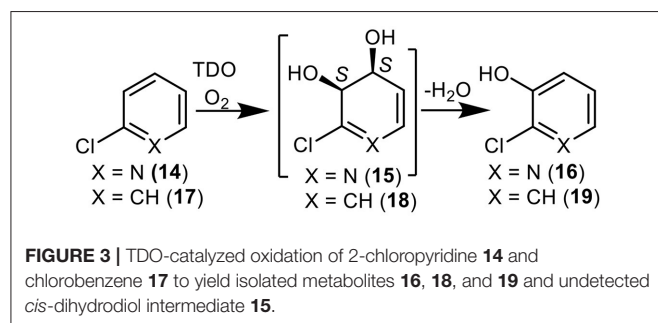


FIGURE 3 | TDO-catalyzed oxidation of 2-chloropyridine **14** and chlorobenzene **17** to yield isolated metabolites **16**, **18**, and **19** and undetected *cis*-dihydrodiol intermediate **15**.

METHODS

Laboratory Studies

¹H and ¹³C NMR spectra were recorded on Bruker Avance DPX-300 and DPX-500 instruments. Chemical shifts (δ) are reported in ppm relative to SiMe₄ and coupling constants (*J*) are given in Hertz (Hz). Mass spectra were run at 70 eV, on an AE1-MS90 mass spectrometer updated by VG Autospec, using a heated inlet system. Accurate molecular weights were determined by the peak matching method, with perfluorokerosene as the standard. Elemental microanalyses were carried out on a Perkin-Elmer 2400 CHN microanalyser and IR spectra were recorded in KBr disc or in thin film, using a Perkin-Elmer Spectrum RX1 FT-IR spectrometer. ECD spectra were obtained using a Jasco J-720 instrument and MeCN as solvent. Optical rotations ($[\alpha]_D$) measurements (10⁻¹ deg cm² g⁻¹) were carried out at ambient temperature on a Perkin-Elmer 214 polarimeter and specified solvent concentration (g/100 ml) at sodium D-line (589 nm). Melting points were recorded in degrees Celsius using a Stuart SMP10 melting point apparatus. Column chromatography and preparative layer chromatography (PLC) were performed on Merck Kieselgel type 60 (250–400 mesh) and PF_{254/366}, respectively. Merck Kieselgel type 60F₂₅₄ analytical plates were used for TLC.

The structures discussed in this section are found in Figures 8, 9, 11. Compounds **1**, **4**, **5**, **6**, **8**, **13**, **14**, **16**, **17**, **19**, **22**, **23**, **24** were purchased commercially and *cis*-dihydrodiols (+)-**9** and (+)-**10**, arene oxides (–)-**20** and (+)-**25**, were available from earlier studies (Agarwal et al., 1990; Boyd et al., 1991a, 1994, 2002).

(+)-(5*R*,6*S*)-2-Chloro-5,6-dihydroquinoline-5,6-diol **9** (Boyd et al., 1998, 2002)

mp 120–122°C (EtOAc/hexane); $[\alpha]_D$ +140 (c 0.40, MeOH); ¹H NMR δ_H (500 MHz, CDCl₃) 2.05 (1H, br s, OH), 2.71 (1H, br s, OH), 4.38 (1H, dd, *J* 5.0, *J* 5.0, H-6), 4.77 (1H, d, *J* 5.0, H-5), 6.45 (1H, dd, *J* 5.0, *J* 9.9, H-7), 6.68 (1H, d, *J* 9.9, H-8), 7.21 (1H, d, *J* 8.0, H-3), 7.85 (1H, d, *J* 8.0, H-4).

(+)-(7*S*,8*R*)-2-Chloro-7,8-dihydroquinoline-7,8-diol **10** (Boyd et al., 1998, 2002)

Colorless crystalline solid, mp 112°C (from EtOAc/hexane); $[\alpha]_D$ +148 (c 0.5, MeOH); ¹H NMR δ_H (500 MHz, CDCl₃) 2.61 (1H, br s, OH), 4.32 (1H, br s, OH), 4.46 (1H, dd, *J* 5.0, 5.0, H-7), 4.75 (1H, d, *J* 5.0, H-8), 6.30 (1H, dd, *J* 9.6, 5.0, H-6), 6.63 (1H, d, *J* 9.6, H-5), 7.25 (1H, d, *J* 8.0, H-3), 7.42 (1H, d, *J* 8.0, H-4).

(–)-(5*R*,6*S*)-5,6-Epoxy-5,6-dihydroquinoline **20** (Agarwal et al., 1990; Boyd et al., 1991a, 1994)

mp 68–71°C (pentane) [lit.rac. (Agarwal et al., 1990) 33–36°C]; $[\alpha]_D$ –23 (c 0.9, CHCl₃); ¹H NMR δ_H (300 MHz, CDCl₃) 4.16 (1H, m, H-6), 4.49 (1H, d, *J* 3.7, H-5), 6.73 (1H, dd, *J* 9.9, 3.8, H-7), 6.98 (1H, d, *J* 9.9, H-8), 7.24 (1H, m, H-3), 7.90 (1H, dd, *J* 7.6.0, 1.4 H-4), 8.62 (1H, dd, *J* 4.9.6.0, 1.4 H-2).

(+)-(7*S*,8*R*)-7,8-Epoxy-7,8-dihydroquinoline **25** (Agarwal et al., 1990; Boyd et al., 1994)

mp 54–56°C (pentane) (lit.rac. (Agarwal et al., 1990) 44–46°C); $[\alpha]_D$ +55 (c 1.1, CHCl₃); ¹H NMR δ_H (300 MHz, CDCl₃) 4.19

(1H, m, H-7), 4.66 (1H, d, *J* 3.7, H-8), 6.51 (1H, dd, *J* 9.6, 3.7, H-6), 6.72 (1H, dd, *J* 9.6, 1.7, H-5), 7.31 (1H, dd, *J* 7.7, 4.8, H-3), 7.58 (1H, dd, *J* 7.7, 0.1, H-4), 8.53 (1H, dd, *J* 4.8, 1.4, H-2).

Hydrogenation/Hydrogenolysis of *cis*-dihydrodiols (+)-9 and (+)-10 to Yield Tetrahydrodiols (–)-39 and (–)-40 (–)-(5*R*,6*S*)-5,6,7,8-Tetrahydroquinoline-5,6-diol 39 (Boyd et al., 1993)

cis-Dihydrodiol metabolite **9** (30 mg, 0.15 mmol) was dissolved in MeOH (8 cm³) and 10% Pd/C (0.5 mg) was added. The mixture was stirred under a H₂ atmosphere at atmospheric pressure for 2 h, filtered and concentrated under reduced pressure. Aqueous Na₂CO₃ solution (5%) was added to the residue, the mixture saturated with NaCl and then extracted into EtOAc (3 × 10 cm³). The combined organic layers were dried (Na₂SO₄) and the solvent evaporated to furnish (5*R*,6*S*)-diol **39** (19 mg, 81%); mp 139–140°C (EtOAc) [lit. (Boyd et al., 1993) 138–140°C]; [α]_D –7.0 (*c* 0.5, MeOH); ¹H NMR (300 MHz, CDCl₃) δ _H 1.96 (1H, m, H-7), 2.16 (1H, m, H-7'), 2.85 (1H, m, H-8), 3.09 (1H, m, H-8'), 4.1 (1H, m, H-6), 4.35 (2H, bs, 2 × OH) 4.67 (1H, d, *J* 3.4, H-5), 7.13 (1H, dd, *J* 4.8, 7.7, H-3), 7.79 (1H, dd, *J* 1.1, 7.2, H-4), 8.35 (1H, dd, *J* 1.5, 4.7, H-2).

(–)-(7*S*,8*R*)-5,6,7,8-Tetrahydroquinoline-7,8-diol 40 (Boyd et al., 1993)

Similar treatment of *cis*-dihydrodiol **10** (30 mg, 0.15 mmol) yielded (7*S*,8*R*)-diol **40** (21 mg, 81%), mp 137–139°C (EtOAc) [lit. (Boyd et al., 1993) 138–140°C]; [α]_D –72.0 (*c* 0.47, MeOH); ¹H NMR (300 MHz, CDCl₃) δ _H 1.95 (1H, m, H-6), 2.22 (1H, m, H-6'), 2.75 (1H, m, H-5), 3.20 (1H, m, H-5'), 4.32 (1H, m, H-7), 4.92 (1H, d, *J* H-8), 7.17 (1H, dd, *J* 4.7, *J* 7.7, H-3), 7.46 (1H, d, *J* 7.7, H-4), 8.40 (1H, *J* 4.7, H-2).

Synthesis of (–)-(5*R*,6*R*,7*R*,8*R*)-quinoline-5,6:7,8-dioxide **29** (Boyd et al., 1991b)

Treatment of (–)-(5*R*,6*S*)-5,6-epoxy-5,6-dihydroquinoline **20** (120 mg, 0.8 mmol) in CH₂Cl₂ with aqueous sodium hypochlorite in the presence of phase transfer reagent (t-Bu₄NHSO₄) and workup, under identical conditions used earlier in the synthesis of racemic *anti*-quinoline dioxide **29**, produced (–)-**29** (51 mg, 38%). White crystalline solid (ether-hexane); mp 85–86°C [lit. (Boyd et al., 1991b), 44–46°C]; [α]_D –100 (*c* 0.11, CHCl₃); HRMS calcd for C₉H₇NO₂, 161.0477, M⁺; found, 161.0472; ¹H NMR (300 MHz, CDCl₃) δ _H 3.73 (1H, d, *J* 3.9, H-6b), 3.91 (1H, d, *J* 4.0, H-2a), 4.05 (1H, m, H-1a), 4.08 (1H, m, H-1b), 7.28 (1H, dd, *J* 7.7, 4.8, H-5), 7.73 (1H, dd, *J* 7.5, 1.5, H-6), 8.53 (1H, dd, *J* 4.8, 1.5, H-4); ¹³C NMR (125 MHz, CDCl₃) δ _C 50.9, 53.2, 54.7, 55.5, 123.9, 127.7, 138.7, 149.8, 152.4; *m/z* 161 (M⁺, 15%), 132 (100). Electronic CD data: 269 nm ($\Delta\epsilon$ –3.299), 226 nm ($\Delta\epsilon$ –14.97), 197 nm ($\Delta\epsilon$ 11.46).

Synthesis of (+)-(5*S*,6*S*,7*R*,8*R*)-quinoline-5,6:7,8-dioxide **28** (Boyd et al., 1991b)

(+)-(7*S*,8*R*)-7,8-Epoxy-7,8-dihydroquinoline **25** (120 mg, 0.8 mmol), it was reacted with *N*-bromoacetamide (130 mg, 1.0 mmol) in THF: water (2:1), under identical reaction conditions reported for a racemic arene oxide **25** (Vila et al., 2017). After extraction (CH₂Cl₂) drying and concentration, the crude product, the correct NMR spectrum for racemic 6-bromo-5-hydroxy-7,8-epoxy-5,6,7,8-tetrahydroquinoline **41**, was then treated directly with sodium methoxide in THF to yield (+)-(5*S*,6*S*,7*R*,8*R*)-quinoline-5,6:7,8-dioxide **28**. White solid mp 153–156°C [lit. (Boyd et al., 1991b) 138–152°C]; [α]_D +25 (*c* 0.2, CHCl₃); HRMS calcd for C₉H₇NO₂, 161.0477, M⁺; found, 161.0472; ¹H NMR (500 MHz, CDCl₃) δ _H 3.95–3.99 (2H, m, H-1a and H-1b), 4.05 (1H, d, *J* 3.5, H-6b), 4.18 (1H, d, *J* 3.4, H-2a), 7.38 (1H, m, H-5), 7.95 (1H, dd, *J* 7.7, 1.6, H-6), 8.65 (1H, dd, *J* 4.9, 1.6, H-4); *m/z* 161 (M⁺, 15%), 132 (100). Electronic CD data: 274 nm ($\Delta\epsilon$ 15.93), 268 nm ($\Delta\epsilon$ 14.31), 246 nm ($\Delta\epsilon$ –3.425), 192 nm ($\Delta\epsilon$ –16.08).

Cis-dihydroxylation of (+)-*cis*-diol **9** [and **10**] and Acetylation to Yield Tetrahydroacetates, (+)-44, (–)-44 [(+)-42 and (+)-45]

To a stirred solution of (+)-*cis*-dihydrodiol **9** (200 mg, 1.02 mmol) and trimethylamine-*N*-oxide dihydrate (150 mg, 1.34 mmol) in CH₂Cl₂ (50 ml) was added a catalytic amount of OsO₄ and the mixture stirred overnight at room temperature. After the addition of a 10% solution of sodium metabisulfite (2 ml), the reaction mixture was allowed to stir for another 0.5 h and then concentrated under reduced pressure to give a crude mixture of inseparable *syn*- and *anti*-tetraols. The mixture was acetylated by heating (75–80°C), overnight, with excess of acetic anhydride (*ca.* 2 ml) in pyridine (2 ml) solution. Concentration of the reaction mixture in *vacuo*, yielded a crude mixture (3:1) of *anti*-**45** and *syn*-**44** tetraacetates. After initial purification of the mixture, using flash chromatography (silica gel, 3% MeOH in CHCl₃), followed by multiple elution PLC (20% EtOAc in hexane) separation gave major *anti*-tetraacetate (+)-**45** and minor *syn*-tetraacetate (–)-**44**.

(+)-(5*R*,6*R*,7*R*,8*R*)-5,6,7,8-Tetraacetoxy-2-chloro-5,6,7,8-tetrahydroquinoline **45**

White crystalline solid (121 mg, 30%); (*R*_f 0.3, 30% EtOAc in hexane); mp 87–88°C (from CHCl₃); [α]_D +14.6 (*c* 0.83, CHCl₃); (Found: C, 50.6; H, 4.7; N, 3.3. C₁₇H₁₈ClNO₈ requires C, 51.1; H, 4.5; N, 3.5%); ¹H NMR (500 MHz, CDCl₃) δ _H 2.07 (3H, s, OMe), 2.08 (1H, s, OMe), 2.11 (1H, s, OMe), 2.13 (1H, s, OMe), 5.63 (1H, dd, *J* 10.1, 3.9, H-6), 5.73 (1H, dd, *J* 10.1, *J* 4.1, H-7), 6.34 (1H, d, *J* 3.9, H-5), 6.39 (1H, d, *J* 4.1, H-8), 7.35 (1H, d, *J* 8.3, H-3), 7.63 (1H, d, *J* 8.3, H-4); ¹³C NMR (CDCl₃, 125 MHz) δ _C 20.5, 20.6, 20.7, 20.8, 66.7, 67.1, 67.3, 67.6, 124.9, 127.1, 139.1, 151.5, 152.3, 169.7, 169.8, 169.9, 170.2, *m/z* 339 (M⁺, 15%, ³⁵Cl), 43 (100); ν_{\max} /cm^{–1}: 1,741 (C=O).

(-)-(5R,6R,7S,8S)-5,6,7,8-Tetraacetoxy-2-chloro-5,6,7,8-tetrahydroquinoline 44

White crystalline solid (53 mg, 13%); (R_f 0.25, 30% EtOAc-hexane); mp 177–178°C (CHCl₃); [α]_D –20 (c 0.69, CHCl₃); (Found: C, 50.8; H, 4.3; N, 3.6. C₁₇H₁₈ClNO₈ requires C, 51.1; H, 4.5; N, 3.5%); HRMS calcd for C₁₇H₁₈ClNO₈, 399.0721, M⁺; found, 399.0727; ¹H NMR (500 MHz, CDCl₃) δ_H 2.07–2.17 (12 H, s, 4 × COCH₃), 5.58 (1 H, dd, J 4.5, 2.2, H-7), 5.62 (1 H, dd, J 2.2, 4.7, H-5), 6.22 (1 H, d, J 4.4, H-8), 7.34 (1 H, d, J 8.2, H-3), 7.61 (1 H, d, J 8.2, H-4); ¹³C NMR (125 MHz, CDCl₃) δ_C 19.6, 19.7, 19.8, 20.0, 65.6, 66.1, 66.3, 66.8, 124.1, 126.1, 139.3, 150.5, 151.3, 168.7, 168.8, 168.9, 169.1; m/z 399 (M⁺, 16%, ³⁵Cl), 43 (100); ν_{max}/cm^{-1} : 1,741 (C=O).

(+)-(5S,6S,7R,8R)-5,6,7,8-Tetraacetoxy-2-chloro-5,6,7,8-tetrahydroquinoline 44

Employing a similar osmylation/acetylation procedure, used for metabolite (+)-9, to *cis*-dihydrodiol (+)-10 gave a mixture (1:3) of the opposite *syn*-tetraacetate enantiomer, (+)-44, [α]_D +19.0 (c 0.74, CHCl₃) and the *anti*-tetraacetate enantiomer (+)-45.

Hydrolysis of Chlorotetraacetates (-)-44, (+)-44, and (+)-45 to Yield Chlorotetrols (-)-42, (+)-42, and (+)-43

(-)-(5R,6R,7S,8S)-2-Chloro-5,6,7,8-tetrahydro-5,6,7,8-quinoline tetraol 42

A solution of tetraacetate (-)-44 (300 mg, 0.75 mmol) in MeOH (30 ml) was saturated with NH₃ gas at 0°C and was left overnight in an ice bath. The solvent was evaporated under reduced pressure, and the ammonium acetate side product was removed by sublimation under high vacuum. Crystallization of the residue from a mixture of acetone-MeOH-CHCl₃ gave pure tetrol (-)-42 (130 mg, 75%), white needles; mp 153–154°C; [α]_D –8 (c 0.68, MeOH); (Found: C, 45.7; H, 4.3; N, 5.8. C₉H₁₀NO₄Cl requires C, 46.7; H, 4.3; N, 6.1%); ¹H NMR (500 MHz, D₂O) δ_H 4.17 (1 H, m, J 2.1, 4.4, H-7), 4.19 (1 H, m, J 2.0, 4.13, H-6), 4.68 (1 H, d, J 4.4, H-8), 4.77 (1 H, d, J 4.13, H-5), 7.45 (1 H, d, J 8.3, H-3), 7.93 (1 H, d, J 8.3, H-4).

(+)-(5S,6S,7R,8R)-2-Chloro-5,6,7,8-tetrahydro-5,6,7,8-quinoline tetrol 42

Similar treatment of tetraacetate (+)-44 gave pure tetrol (+)-42 [α]_D +7 (c 0.44, MeOH).

(+)-5R,6R,7R,8R)-2-Chloro-5,6,7,8-tetrahydro-5,6,7,8-quinoline tetrol 43

Tetraacetate (+)-45 (1.35 g, 3.41 mmol) was deprotected and crystallized in a similar manner to compound (-)-44 to yield pure tetraol (+)-43 (600 mg, 76%), white crystals; mp 189–192°C; [α]_D +14.6 (c 0.57, MeOH); (Found: C, 46.6; H, 4.1; N, 6.0. C₉H₁₀NO₄Cl requires C, 46.7; H, 4.3; N, 6.1%); Found: M⁺ 231.03090, C₉H₁₀ClNO₄ requires 231.02984; ν_{max}/cm^{-1} : 3391 (OH); ¹H NMR (500 MHz, D₂O) δ_H 4.25 (1 H, dd, J 5.6, J 3.9, H-6), 4.30 (1 H, dd, J 5.6, J 4.0, H-7), 4.91 (1 H, d, J 4.0, H-8), 5.00 (1 H, d, J 3.9, H-5), 7.57 (1 H, d, J 8.3, H-3), 7.97 (1 H, d, J 8.3, H-4); ¹³C NMR (125 MHz, D₂O) δ_C 67.9, 69.0, 69.1, 70.3, 125.6,

131.2, 142.5, 151.5, 154.6; m/z 231 (M⁺, 5%, ³⁵Cl), 213 (34%), 171 (100).

Hydrogenolysis of Chlorotetrols (-)-42, (+)-42, and (+)-43 to Yield Tetrols (-)-46, (+)-46, and (-)-48

(+)-(5R,6R,7S,8S)-5,6,7,8-Tetrahydro-5,6,7,8-quinoline tetraol 46

A solution of chlorotetraol (-)-42 (200 mg, 0.86 mmol) in MeOH (20 ml) containing 10% Pd/C (50 mg) was stirred overnight at room temperature, under H₂ atmosphere at 1 atm. pressure. The reaction mixture was basified (NH₃ solution), the catalyst was filtered off and the filtrate concentrated under reduced pressure to yield tetraol (-)-46 (120 mg, 71%), white solid (MeOH); mp 164–165°C (MeOH); [α]_D +25 (c 0.5, MeOH); (Found: C, 54.3; H, 5.3; N, 6.6. C₉H₁₁NO₄ requires C, 54.8; H, 5.6; N, 7.1%); ¹H NMR (500 MHz, D₂O) δ_H 4.28 (1 H, dd, J 4.3, 1.4, H-7), 4.34 (1 H, dd, J 4.0, 1.4, H-6), 4.88 (1 H, d, J 4.3, H-8), 4.93 (1 H, d, J 4.0, H-5), 7.56 (1 H, dd, J 7.9, 4.5, H-3), 8.10 (1 H, d, J 7.9, H-4), 8.62 (1 H, d, J 4.5, H-2).

(-)-(5S,6S,7R,8R)-5,6,7,8-Tetrahydro-5,6,7,8-quinoline tetraol 46

A similar hydrogenolysis process on compound (+)-44 yielded tetraol (-)-45, [α]_D –23 (c 0.4, MeOH).

(-)-(5R,6R,7R,8R)-5,6,7,8-Tetrahydro-5,6,7,8-quinoline tetrol 48

Hydrogenolysis of tetrol (+)-43 (0.2 g, 0.86 mmol) gave tetraol (-)-48, (0.12 g, 71%); mp 186–187°C (MeOH); [α]_D –104 (c 0.56, pyridine); (Found: C, 53.6; H, 5.8; N, 6.6. C₉H₁₁NO₄ requires C, 54.8; H, 5.6; N, 7.1%); ¹H NMR (500 MHz, D₂O) δ_H 4.33 (1 H, dd, J 6.7, J 6.8, H-7), 4.38 (1 H, dd, J 6.8, J 6.5, H-6), 5.05 (1 H, d, J 6.7, H-8), 5.09 (1 H, d, J 6.5, H-5), 7.62 (1 H, dd, J 7.8, J 4.0, H-3), 8.06 (1 H, d, J 4.0, H-2), 8.69 (1 H, d, J 7.8, H-4); m/z 197 (M⁺, 7.5%), 137 (100).

Synthesis of Dibromohydroxyacetates (-)-47, (+)-47 and Dibromodiacetate 49 From tetrols (+)-46, (-)-46, and (-)-48

(-)-(5S,6S,7R,8R)-5,8-Dibromo-6-hydroxy-5,6,7,8-tetrahydro-7-quinolinylnyl acetate 47

To a stirred solution of tetrol (+)-46 (100 mg, 0.51 mmol) in dry CH₃CN (5 ml) maintained at ice temperature, was added 1-bromocarbonyl-1-methylethyl acetate (0.15 ml, 1.04 mmol) and the stirring continued (2.5 h) at room temperature. The reaction mixture was concentrated *in vacuo*, the concentrate taken up into ether (20 ml) and washed repeatedly with 2.5% NaHCO₃ solution until the aqueous layer was basic. The combined aqueous layer was back extracted with ether and the combined ether extract dried (Na₂SO₄) and concentrated under reduced pressure. Purification of the crude product by PLC yielded compound (-)-47 (80 mg, 65%), pale yellow oil; (R_f 0.25, 55% EtOAc-hexane); [α]_D –31 (c 0.54, CHCl₃); HRMS calcd for C₁₁H₁₀NO₃Br, 282.9844, (M – HBr)⁺; found,

282.9839; ^1H NMR (500 MHz, CDCl_3) δ_{H} 2.08 (3 H, s, COCH_3), 4.90 (1 H, dd, J 8.3, 2.3, H-6), 5.30 (1 H, d, J 4.0, H-8), 5.40 (1 H, d, J 8.3, H-5), 5.75 (1 H, dd, J 4.1, J 2.3, H-7), 7.32 (1 H, dd, J 8.9, H-4), 8.00 (1 H, d, J 8.9, H-4), 8.59 (1 H, d, J 5.6, H-2); ^{13}C NMR (125 MHz, CDCl_3) δ_{C} 20.9, 46.3, 51.5, 70.3, 74.3, 123.9, 130.2, 139.6, 150.3, 151.2, 169.9; m/z 285 ($\text{M}^+\text{-HBr}$), ^{79}Br , 15%), 287 ($\text{M}^+\text{-HBr}$, ^{81}Br , 15%), 242 (100).

(+)-(5R,6R,7S,8S)-5,8-Dibromo-6-hydroxy-5,6,7,8-tetrahydro-7-quinolinyl acetate 47

A similar treatment procedure on tetrol (–)-46, yielded compound (+)-47 $[\alpha]_{\text{D}} +30$ (c 0.4, CHCl_3).

(5S,6S,7S,8S)-6,7-(Diacetoxy)-5,6-dibromo-5,6,7,8-tetrahydroquinoline 49

Similar treatment of (–)-tetraol 48 (0.15 g, 0.78 mmol) with 1-bromocarbonyl-1-methylethyl acetate gave dibromodiacetate 49 (0.21 g, 65%), pale yellow syrup; (R_f 0.7, 55% EtOAc-hexane); (Found: $\text{M}^+\text{-HBr}$, 324.996063. $\text{C}_{13}\text{H}_{12}\text{NO}_4\text{Br}$ requires M^+ , 324.994969); ^1H NMR (500 MHz, CDCl_3) δ_{H} 2.12 (3 H, s, COCH_3), 2.15 (3 H, s, COCH_3), 5.36 (1 H, d, J 6.1, H-8), 5.40 (1 H, d, J 7.5, H-5), 5.52 (1 H, m, H-6), 5.65 (1 H, m, H-7), 7.35 (1 H, dd, J 8.0, J 4.7, H-3), 7.99 (1 H, d, J 8.0, H-4), 8.65 (1 H, d, J 4.3, H-2); ^{13}C NMR (125 MHz, CDCl_3) δ_{C} 20.7, 23.9, 34.2, 46.4, 47.4, 58.8, 73.8, 124.2, 128.9, 134.1, 150.4, 150.6, 169.2, 169.3; m/z 325 ($\text{M}^+\text{-HBr}$, 50%), 79 (100).

Synthesis of Quinoline-5,6:7,8-dioxide (–)-28 and (+)-28 From 5,8-dibromo-6-hydroxy-5,6,7,8-tetrahydro-7-quinolinyl acetate (–)-47 and (+)-47

(–)-(5R,6R,7S,8S)-Quinoline-5,6:7,8-dioxide 28

A solution of bromohydrin (–)-47 (80 mg, 0.22 mmol) in THF (10 ml) was stirred at 0°C with an excess of anhydrous sodium methoxide (250 mg) for 1 h and at room temperature for another 1 h. After removal of the THF under reduced pressure ice-cold water (10 ml) was added to the residue and the aqueous mixture extracted with ether. The extract was dried (Na_2SO_4) concentrated and the crude product purified by PLC (R_f 0.2, 60% EtOAc in hexane) to give *syn*-quinoline dioxide (–)-28 (25 mg, 70%), white solid (CH_2Cl_2 -ether-hexane); mp 153–156°C (lit (Boyd et al., 1991b) rac. mp 138–152°C); $[\alpha]_{\text{D}} -26$ (c 0.2, CHCl_3); HRMS calcd for $\text{C}_9\text{H}_7\text{NO}_2$, 161.0477, M^+ ; found, 161.0472; ^1H NMR (500 MHz, CDCl_3) δ_{H} 3.95–3.99 (2 H, m, H-1a, and H-1b), 4.05 (1 H, d, J 3.5, H-6b), 4.18 (1 H, d, J 3.4, H-2a), 7.38 (1 H, m, H-5), 7.95 (1 H, dd, J 7.7, 1.6, H-6), 8.65 (1 H, dd, J 4.9, 1.6, H-4); m/z 161 (M^+ , 15%), 132 (100). Electronic CD data: 274 nm ($\Delta\epsilon$ 15.93), 268 nm ($\Delta\epsilon$ 14.31), 246 nm ($\Delta\epsilon$ –3.425), 192 nm ($\Delta\epsilon$ –16.08).

(+)-(5S,6S,7R,8R)-Quinoline-5,6:7,8-dioxide 28

Dibromoacetate (–)-46 yielded quinoline dioxide 28 $[\alpha]_{\text{D}} +25$ (c 0.2, CHCl_3).

Synthesis of (5R,6R,7R,8R)-Quinoline-5,6:7,8-dioxide 29 and (5R,6S)-8-bromoquinoline-5,6-oxide 50 From diacetoxy-5,6-dibromo-5,6,7,8-tetrahydroquinoline 49

Similar treatment of dibromodiacetate 49 (200 mg, 0.48 mmol) with sodium methoxide gave a mixture of two products. PLC separation (50% EtOAc-hexane) yielded quinoline dioxide (–)-29 (46 mg, 60%) and bromoquinoline oxide (–)-50 (16 mg, 15%).

(–)-(5R,6R,7R,8R)-Quinoline-5,6:7,8-dioxide 29

R_f 0.4 (EtOAc-hexane); white solid; mp 85–86°C (ether-hexane) [lit. Boyd et al., 1991b rac.m.p. 44–46°C]; $[\alpha]_{\text{D}} -100$ (c 0.11, CHCl_3); (Found: M^+ 161.047158. $\text{C}_9\text{H}_7\text{NO}_2$ requires 161.047679); ^1H NMR (300 MHz, CDCl_3) δ_{H} 3.73 (1 H, d, J 3.9, H-6b), 3.91 (1 H, d, J 4.0, H-2a), 4.05 (1 H, m, H-1a), 4.08 (1 H, m, H-1b), 7.28 (1 H, dd, J 7.7, J 4.8, H-5), 7.73 (1 H, dd, J 7.5, J 1.5, H-6), 8.53 (1 H, dd, J 4.8, J 1.5, H-4); ^{13}C NMR (125 MHz, CDCl_3) δ_{C} 50.9, 53.2, 54.7, 55.5, 123.9, 127.7, 138.7, 149.8, 152.4; m/z 161 (M^+ , 15%), 132 (100). Electronic CD data: 269 nm ($\Delta\epsilon$ –3.30), 226 nm ($\Delta\epsilon$ –14.97), 197 nm ($\Delta\epsilon$ 11.46).

(–)-(5R,6S)-8-Bromo quinoline-5,6-oxide 50

R_f 0.6 (50% EtOAc-hexane); white solid; mp 107–108°C (ether-pet. ether), $[\alpha]_{\text{D}} -104$ (c 0.5, CHCl_3); (Found: C, 48.9; H, 2.2; N, 6.0. $\text{C}_9\text{H}_6\text{NOBr}$ requires C, 48.3; H, 2.7; N, 6.2); ^1H NMR (500 MHz, CDCl_3) δ_{H} 4.16 (1 H, dd, J 4.3, J 3.9, H-1a), 4.53 (1 H, d, J 3.8, H-7b), 7.25 (1 H, d, J 4.3, H-2), 7.35 (1 H, dd, J 7.7, J 4.9, H-6), 7.95 (1 H, d, J 7.6, H-7), 8.78 (1 H, d, J 4.9, H-5); ^{13}C NMR (125 MHz, CDCl_3) δ_{C} 53.7, 56.6, 123.3, 128.8, 129.1, 132.1, 137.8, 149.9, 150.0; m/z 223 (M^+ , ^{79}Br , 60%), 225 (M^+ , ^{81}Br , 60%), 89 (100); Electronic CD data: 302 nm ($\Delta\epsilon$ –1.92), 276 nm ($\Delta\epsilon$ 2.48), 239 nm ($\Delta\epsilon$ –8.93), 233 nm ($\Delta\epsilon$ –8.60), 225 nm ($\Delta\epsilon$ –9.38).

Docking Process

All small molecule structures were created in.pdb format using UCSF Chimera (University of California). The crystal structures of TDO (PDB ID: 3en1) and NDO (1o7M) were obtained from the RCSB Protein Data Bank. The toluene contained in the TDO crystal structure was removed using UCSF Chimera. The dioxygen molecule was added to the iron prosthetic group of TDO (Fe, His222, His228, Asp376) from the iron prosthetic group (Fe, dioxygen, His-208, His-213, and Asp-362) of the NDO crystal structure using the “super” function of PyMol 2.4.0 to overlay the two partial structures at the position of 3en1 and copy the dioxygen atoms to the 3en1 model. All structures in.pdb format were then stripped of water molecules and converted to .pdbqt format using AutoDock Tools 1.5.6 (Scripps Research Institute).

The docking was performed using AutoDock Vina 1.1.2 (Scripps Research Institute) with the following configuration:

```
center_x = 46.46
center_y = 120.49
center_z = 201.877
size_x = 16
```



```

size_y = 16
size_z = 16
exhaustiveness = 100

```

This configuration includes the amino acids within 6 Å of the toluene present in the 3en1 crystal structure: Gln215, Phe216, Met220, His222, Ala223, His228, Leu 272, Ile276, Ile232, Val309, His311, Leu321, Ile324, Phe366, Phe372, and Asp376. Only Met220 is not shown in the docking structures as it blocked the view on the docking orientation and was considered irrelevant for catalytic purposes.

Based on earlier publications and current understanding of the binding site and catalytic mechanism, His 222 is involved in edge-to-face binding of the substrate to direct a planar orientation, presenting a face to the active site. The probability for the methyl group of the toluene substrate to be oriented toward Phe216 is reduced by this residue, thus resulting in the observed enantiomeric excess. His311 and Asn215 are considered to be essential for the catalytic mechanism, as His311 is a H-acceptor and Asn215 is considered to be part of a water channel.

The docking model was assessed by docking toluene and comparing obtained orientations to the toluene position in the crystal structure. A total of nine orientations were obtained ranging from -5.3 to -4.2 kcal/mol $^{-1}$. Three orientations emerged that present the 2,3-double bond to the dioxygen for dihydroxylation (see **Supplementary Figures S-13A–C**). These orientations showed minor differences in position compared to the orientation observed in the crystal structure (1–1.2 Å) and compared to each other. The difference in position between the docked and crystal structure was probably affected by the docking with dioxygen, as the crystal structure does not contain dioxygen, allowing the toluene to be closer to the iron prosthetic group. Two identical orientations emerged (see **Supplementary Figure S-13D**) which would result in the opposite enantiomer being formed. Given the enantiomeric excess of >98% of the dihydroxylated product of toluene, it appears unlikely that this orientation is readily dihydroxylated.

RESULTS

Molecular Docking of TDO With Quinoline 1, 2-Chloroquinoline 8, 2-Chloropyridine 14 and Chlorobenzene 17

Molecular docking studies of TDO-catalyzed *cis*-dihydroxylations of mono- and di-substituted benzene substrates were conducted in other laboratories, using the GOLD program (Vila et al., 2016a,b, 2017). AutoDock and AutoDock Vina programs have similarly been used in our laboratories, to study TDO-catalyzed *cis*-dihydroxylation of other types of monocyclic arenes, e.g., substituted phenols and anilines and tricyclic heteroarenes, e.g., dibenzofuran and dibenzothiophene (Hoering et al., 2016; Boyd et al., 2017, 2019). Relative free binding energies (kcal/mol $^{-1}$) and relative proximity of arene bonds to dioxygen, within the TDO active site (Å), were determined by applying the AutoDock Vina program to monocyclic arenes

(toluene, chlorobenzene) and mono- and bicyclic- azarenes in the current study.

Using the AutoDock Vina docking model, to indicate binding energy (kcal/mol $^{-1}$) and bond proximity (Å) values of TDO with quinoline substrate **1** (X = H), *cis*-dihydroxylation of the carbocyclic ring was predicted to occur preferentially at the 5,6- (**Figure 4A**, -6.4 kcal/mol $^{-1}$, 3.6–3.7 Å) and 7,8- bonds (**Figure 4B**, -6.0 kcal/mol $^{-1}$, 3.6 Å). This would be consistent with formation of similar quantities of the 5R,6S and 7S,8R *cis*-dihydrodiols **2** and **3**, respectively. When the isolated yields of *cis*-dihydrodiol **3** and the derived 8-hydroxyquinoline **4** are combined, the relative proportions of originally formed *cis*-dihydrodiol regioisomers **2:3** were similar and 5R,6S and 7S,8R configurations were firmly established (Boyd et al., 1987, 1993).

Alternative *in silico* orientations of quinoline **1** within the TDO active site (**Figure 4C**, -6.5 kcal/mol $^{-1}$, 3.7–4.2 Å), and (**Supplementary Figure 4D**, -5.8 kcal/mol $^{-1}$, 3.8–4.2 Å), would lead to the incorrect 5S,6R and 7R,8S absolute configurations for isolated metabolites **2** and **3**, respectively. Although these orientations had similar binding energies, compared with **Figures 4A,B** it was presumed that the larger distances between the relevant bonds and proximate dioxygen atom were the determining factors.

Support for the intermediacy of the undetected heterocyclic ring *cis*-dihydrodiol **7** was provided by the AutoDock Vina-derived prediction that TDO-catalyzed *cis*-dihydroxylation could occur at the 3,4-bond of the pyridine ring to yield transient intermediate (3S,4R)-**7** (**Figure 4C**, -6.5 kcal/mol $^{-1}$, 3.6–3.7 Å). The opposite (3R,4S) enantiomer **7** might also be expected from the orientation of quinoline **1** in **Figure 4A**. While a similar binding energy (-6.4 kcal/mol $^{-1}$) is shown in **Figure 4A**, this orientation may be less favored, due to a larger distance from the nearest dioxygen atom (3.8–4.3 Å).

In silico data collected using the Autodock Vina TDO-docking program with 2-chloroquinoline **8** as substrate, similarly led to the prediction that *cis*-dihydroxylation should occur at the 5,6-position, to give (5R,6S)-dihydrodiol **9** (**Figure 5A**, -5.8 kcal/mol $^{-1}$, 3.7–3.8 Å) and at the 7,8-bond to form (7S,8R)-dihydrodiol **10** (**Figure 5B**, -6.0 kcal/mol $^{-1}$, 3.5–3.6 Å). Alternative docking orientations could also result in *cis*-dihydroxylation at the 5,6 bond (**Figure 5C**, -5.1 kcal/mol $^{-1}$, 4.1–4.5 Å) and the 7,8 bond (**Supplementary Figure 5D**, -6.2 kcal/mol $^{-1}$, 4.1–4.5 Å), but the resulting *cis*-diol metabolites **9** and **10** would have the opposite absolute configurations to the isolated metabolites (5R,6S and 7S,8R, respectively). The orientations in **Figure 5C** and **Supplementary Figure 5D** were again assumed to be less favored, due to the larger distances between substrate and nearby dioxygen atoms. Thus, the absolute configurations of the quinoline *cis*-dihydrodiols (**2**, **3**, **9**, **10**) predicted by *in silico* results were identical to those found earlier for metabolites isolated from *P. putida* UV4 biotransformations (Boyd et al., 1987, 1993, 1998, 2002).

More evidence for the TDO-catalyzed *cis*-dihydroxylation of a pyridyl ring was sought by docking studies of 2-chloropyridine **14** and comparison with chlorobenzene **17**. Substrates **14** (**Figure 6**, -4.8 kcal/mol $^{-1}$, 3.0–3.6 Å) and **17** (**Figure 7**, -4.9 kcal/mol $^{-1}$, 3.0–3.6 Å) were found to adopt similar orientations, within the

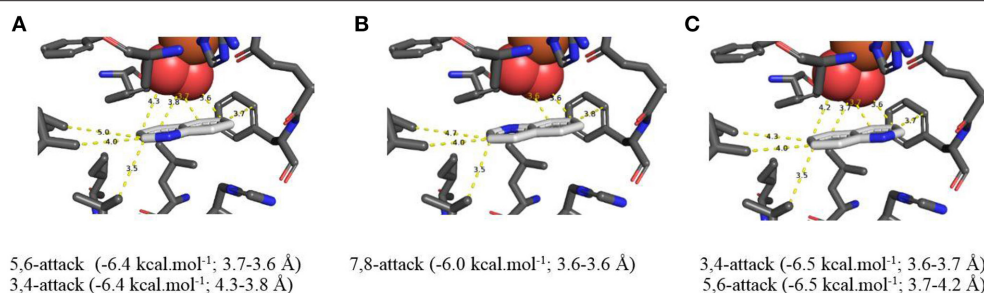


FIGURE 4 | (A–C) TDO docking orientations of quinoline **1** ($X = \text{H}$) consistent with preferential *cis*-dihydroxylation at 5,6- ($-6.4 \text{ kcal.mol}^{-1}$, **A**), 7,8- ($-6.0 \text{ kcal.mol}^{-1}$, **B**), and 3,4-bonds ($-6.5 \text{ kcal.mol}^{-1}$, **C**). Hydrophobic substrate coordinating amino acids in the active site shown include Phe 326 and Val 309. The iron atom shown is coordinated by His 222, 228, and Asp 376. The positioning of the docked substrate relative to the positioned bound oxygen is consistent with experimentally observed product regio specificity.

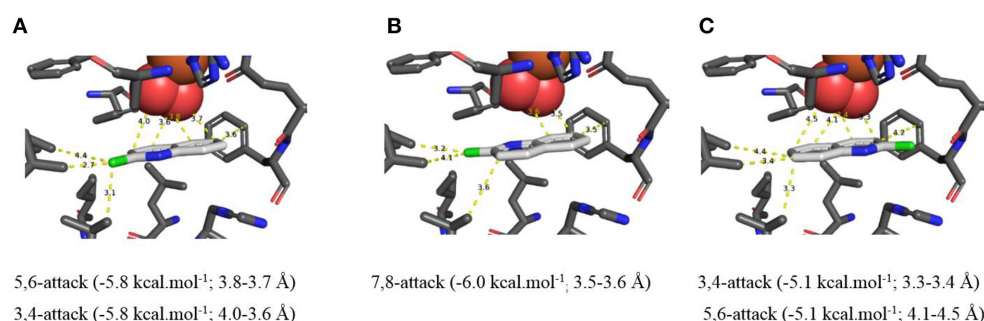


FIGURE 5 | (A–C) TDO docking of 2-chloroquinoline **8** with *cis*-dihydroxylation at a 5,6- (**A**, $-5.8 \text{ kcal.mol}^{-1}$), 7,8- (**B**, $-6.0 \text{ kcal.mol}^{-1}$), and 3,4-bond (**C**, $-5.1 \text{ kcal.mol}^{-1}$). Hydrophobic substrate coordinating amino acids in the active site shown include Phe 326 and Val 309. The iron atom shown is coordinated by His 222, 228, and Asp 376. The positioning of the docked substrate relative to the positioned bound oxygen is consistent with experimentally observed product regio specificity.

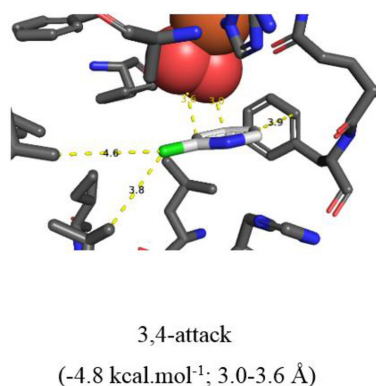


FIGURE 6 | TDO docking of 2-chloropyridine **14** with *cis*-dihydroxylation at a 3,4-bond ($-4.8 \text{ kcal.mol}^{-1}$, this figure) and of chlorobenzene **17** at a 2,3 bond ($-4.9 \text{ kcal.mol}^{-1}$, **Figure 7**). Hydrophobic substrate coordinating amino acids in the active site shown include Phe 326 and Val 309. The iron atom shown is coordinated by His 222, 228, and Asp 376. The positioning of the docked substrate relative to the positioned bound oxygen is consistent with experimentally observed product regio specificity.

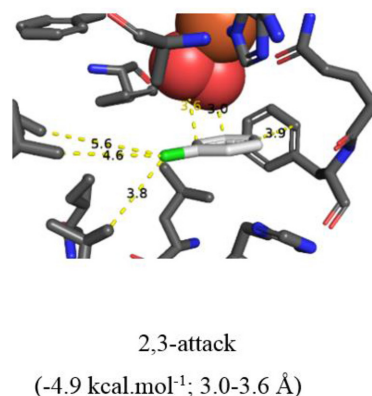


FIGURE 7 | Same as **Figure 6**.

TDO active site, leading to the prediction that the derived (*S,S*) enantiomers of *cis*-dihydrodiols **15** and **18**, would be formed preferentially. The (2*S*,3*S*) configuration for isolated metabolite

18, and its dehydration to yield phenol **16**, was already established (Ziffer et al., 1977). The undetected intermediate **15**, derived from 2-chloropyridine **14**, was assumed to dehydrate more readily to yield the isolated hydroxypyridine **16** (Garrett et al., 2006). These docking results thus support the mechanism shown in **Figure 3** (**14** → **15** → **16**).

Based on the AutoDock Vina results, the orientations within the TDO active site, favored by heterocyclic arene substrates, e.g., **1** ($X = H$), **8**, and **14**, as well as substituted benzene substrates e.g., toluene and chlorobenzene **17**, all revealed evidence of edge-to-face (T-bonding) interactions with Phe-216 and His-222. The simultaneous edge-to-face interactions, of amino acid residues Phe-216 and His-222, with both the phenyl and pyridyl rings of substrates **1**, **8**, and **14** in the present context, were noteworthy. Docking distances between the proximate T-bonding H atoms and arene faces of quinoline **1** (Supplementary Figures 4A₁-A₃) were estimated to be within the range 2.6–2.8 Å, assuming a C-H bond length of 1.08 Å. These inter-ring distances are in accord with the calculated interacting H-to-ring center perpendicular distances, of *ca.* 2.6–2.8 Å and observed distances *ca.* 2.70–2.86 Å, from X-ray crystallographic analysis, using a range of model systems (Hoering et al., 2016; Boyd et al., 2019). Keyhole pictures, looking through the rear face of the component aromatic ring, showed both edge to face-T (Supplementary Figures 4A₃,B₃,C₃), and face tilted-T dockings (Supplementary Figures 4A₂,B₂,C₂) of quinoline **1** with TDO. This was consistent with the attractive interactions between phenyl rings (Supplementary Figures 4A₁,B₁), phenyl/pyridyl rings (Supplementary Figure 4C₁), phenyl/imidazolyl rings (Supplementary Figures 4A₁,B₁), and pyridyl/imidazolyl rings (Supplementary Figure 4C₁).

It was concluded that the observed absolute configurations of the isolated carbocyclic ring *cis*-dihydrodiol metabolites **2**, **3**, **9**, and **10** were in agreement with preferred *in silico* docking orientations of the corresponding substrates (Figures 4A,B, 5A,B). The preferred orientations of quinoline **1** (Figure 4C), 2-chloroquinoline **8** (Figure 5C), and 2-chloropyridine **14** (Figure 6), would also be supportive of TDO-catalyzed *cis*-dihydroxylation occurring at the pyridine rings to give the undetected *cis*-dihydrodiol intermediates **7**, **12**, and **15**.

Chemoenzymatic Synthesis of Isolated and Potential Arene Oxide Metabolites of Quinoline

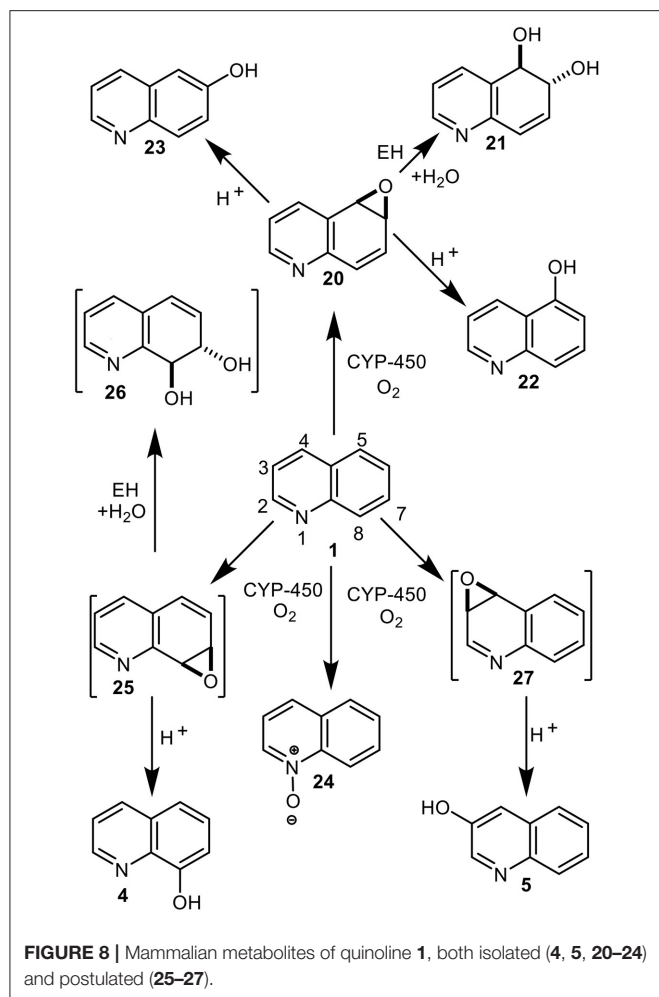
The docking studies described in Figures 4A,B, 5A,B enabled us to develop novel chemoenzymatic approaches for the preparation of different types of chiral azaarene derivatives. The availability of the *cis*-diol **10** as the major metabolite from TDO-catalyzed *cis*-dihydroxylation of 2-chloroquinoline **8**, resulted in its first use in chemoenzymatic synthesis, when chiral 2,2′-bipyridines and 2,2′-bipyridine *N*-oxides were produced (Boyd et al., 2008, 2010). These compounds were found to be useful ligands for asymmetric oxidation (→ 97% ee) (Boyd et al., 2008), cyclopropanation (→ 95% ee) (Boyd et al., 2008), aminolysis (→ 84% ee) (Boyd et al., 2010), and allylation reactions (→ 86% ee) (Boyd et al., 2010). Further possible applications of both *cis*-diol metabolites **9** and **10**, to the chemoenzymatic synthesis of detected and possible mammalian metabolites of quinolines, were also developed.

The identification of a 1,2-epoxide, a mammalian metabolite of naphthalene (Jerina et al., 1968), resulting from cytochrome P-450 (CYP-450)-catalyzed epoxidation, led to a quest for other examples of arene oxide metabolites. A similar type

of monooxygenase-catalyzed dearomatization was later found to yield epoxide metabolites of both monocyclic arenes (e.g., benzene 1,2-oxide) and polycyclic azaarenes (e.g., quinoline 5,6-oxide) (Agarwal et al., 1986). Arene dioxides, *trans*-dihydrodiols, *trans*-tetrahydrodiol epoxides, and tetrahydroarene tetrols were later identified as other mammalian metabolites of naphthalene (Stillwell et al., 1978, 1982; Horning et al., 1980). Further studies established that liver metabolism of larger (tetracyclic and pentacyclic) bay-region arene and heteroarene substrates often involved epoxide intermediates associated with their mutagenicity and tumorigenicity. The metabolic sequence: arenes → arene oxides → *trans*-dihydrodiols → *trans*-tetrahydrodiol epoxides → DNA-adducts, became known as the *Bay-region Mechanism* (Buening et al., 1978; Karle et al., 2004; Chang et al., 2013).

Identification of mammalian metabolites of quinoline **1** and their role in its mutagenicity and tumorigenicity, has been of interest for more than 40 years (Hollstein et al., 1978; Tada et al., 1980, 1982; LaVoie et al., 1983; Agarwal et al., 1986, 1990; Willems et al., 1992; Saeki et al., 1993; Reigh et al., 1996; Suzuki et al., 2000; Dowers et al., 2004; Hakura et al., 2007; Diaz Duran et al., 2015; Matsumoto et al., 2018). Several quinoline arene oxides, e.g., **20** and **27**, were initially postulated as possible liver microsomal metabolites of quinoline **1** (Hollstein et al., 1978; Tada et al., 1980, 1982; LaVoie et al., 1983), before 5,6-arene oxide **20** was finally confirmed as a major metabolite (Figure 8) (Agarwal et al., 1986). Epoxide hydrolyase-catalyzed hydrolysis of the identified 5,6-arene oxide **20** would also account for the isolated *trans*-dihydrodiol metabolite **21**, and aromatization of the undetected 3,4-arene oxide **27** could yield the isolated 3-hydroxyquinoline **5**. Transient arene oxides, including compound **27**, resulting from CYP-450-catalyzed epoxidation of quinoline **1**, were initially postulated to be responsible for its mutagenicity and carcinogenicity (Hollstein et al., 1978; Tada et al., 1980, 1982; LaVoie et al., 1983). Liver microsomal metabolism of quinoline **1** also yielded DNA adducts, which on hydrolysis, under acidic or basic conditions, gave 3-hydroxyquinoline **5**. Efforts to identify mammalian metabolic pathways responsible for the mutagenicity (and carcinogenicity) of quinoline **1** (Willems et al., 1992; Suzuki et al., 2000), required the chemical synthesis of identified, and possible, metabolites of similar structures to those derived earlier from naphthalene (e.g., phenols, arene oxides, arene dioxides, *trans*-dihydrodiols, and *trans*-tetrahydrodiol epoxides) (Jerina et al., 1968; Stillwell et al., 1978, 1982; Horning et al., 1980).

The syntheses of racemic quinoline arene oxides (**20**, **25**), *trans*-dihydrodiols (**21**, **26**), *syn*- and *anti*- arene dioxides (**28** and **29**), and *trans*-diol epoxides (**30** and **31**), were previously reported (Agarwal et al., 1986; Boyd et al., 1989, 1994; Bushman et al., 1989; Willems et al., 1992) (Figures 8, 10). These chiral compounds, along with achiral metabolites including *N*-oxide **24** and phenols **4**, **5**, **22**, and **23**, were tested for mutagenicity, using the Ames/*Salmonella* microsomes method (Willems et al., 1992; Suzuki et al., 2000). As none of these metabolites or possible metabolites, were found to be more mutagenic than quinoline **1**, it was assumed that a metabolic sequence similar to that in the *Bay-region Mechanism*, involving racemic arene oxides,



e.g., **20** → *trans*-dihydrodiols **21** → *trans*-tetrahydrodiol epoxides **31**, was unlikely to be involved in its mutagenicity. It was later established that the particular absolute configurations of polycyclic arene metabolites, associated with the *Bay-region Mechanism*, had a marked effect on their carcinogenicity (Buening et al., 1978; Karle et al., 2004; Chang et al., 2013). The mutagenicity of the enantiopure derivatives of quinoline **20**, **21**, **25**, **26**, **28**, **29**, **30**, and **31** was not investigated.

An alternative metabolic pathway for quinoline **1** in mammals was proposed involving dearomatization of the pyridyl ring and formation of the undetected quinoline hydrate **36** (Saeki et al., 1993, 1996, 1997a,b; Suzuki et al., 2000) (**Figure 9**). While relatively stable arene hydrate derivatives of quinoline were isolated earlier as metabolites of 5,6- and 7,8-dihydroquinolines (Agarwal et al., 1994), compound **36**, being both an enamine and an arene hydrate, would be expected to be less stable. The CYP-450-catalyzed epoxidation of enamine intermediate **36** was postulated to give the undetected epoxide **37** and to react with DNA to yield unstable adduct **38**, which rearomatized under both acidic and basic conditions to yield 3-hydroxyquinoline **5** (Saeki et al., 1993, 1996, 1997a,b; Suzuki et al., 2000). The metabolic pathway **1** → **36** → **37** → **38** (*Enamine Epoxide Theory*,

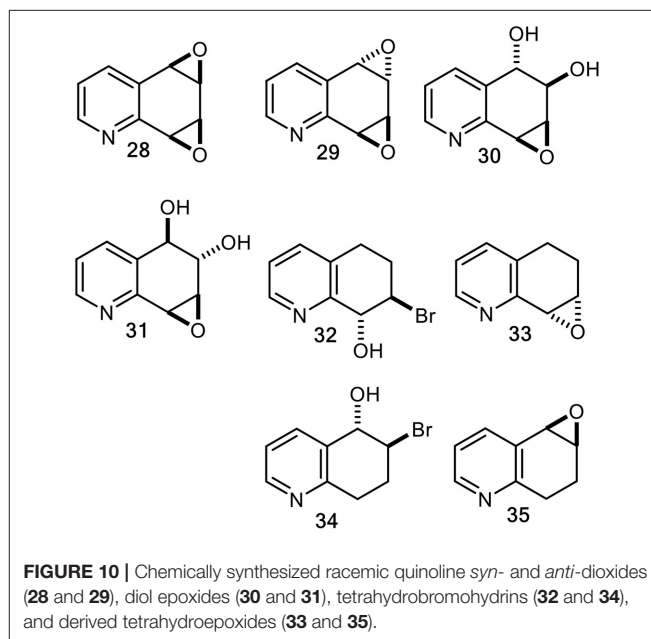
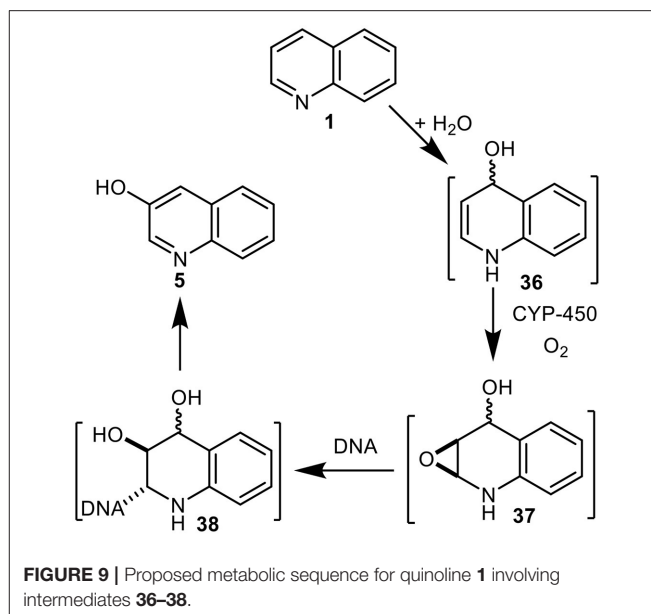


Figure 9) was thus proposed to account for the mutagenicity and carcinogenicity of quinoline **1**. It is noteworthy that while some substituted quinolines were found to be carcinogenic, 2-chloroquinoline **8** was not (Hirao et al., 1976; Hakura et al., 2007).

In the context of mutagenesis studies of known and possible mammalian metabolites of quinoline **1** (Willems et al., 1992), our multistep chemical synthesis routes to racemic quinoline oxides (**20** and **25**) and quinoline dioxides (**28** and **29**), were achieved *via* tetrahydrobromohydrins (**32**, **34**) and tetrahydroepoxides (**33**, **35**) intermediates (**Figure 10**) (Agarwal et al., 1986, 1990; Boyd et al., 1989, 1991b).

While the individual enantiomers of arene oxides **20** and **25** were separable by analytical chiral stationary phase (CSP) HPLC, this analytical scale approach was unsuitable for further chemoenzymatic synthesis studies and therefore alternative preparative methods for obtaining these enantiopure compounds were developed. The chemical resolution of bromohydrin derivatives of 1,2,3,4-polycyclic tetrahydroarenes as MTPA esters provided a generally applicable route to a range of enantiopure arene oxide derivatives, e.g., naphthalene 1,2-oxide and anthracene 1,2-oxide (Akhtar et al., 1979). Further application of this MTPA ester resolution method to racemic bromohydrin **32**, yielded enantiopure tetrahydroepoxides (7*S*,8*R*)-**33** ($[\alpha]_D^{+157}$) and (7*R*,8*S*)-**33** ($[\alpha]_D^{-157}$) intermediates and finally quinoline 7,8-oxide, (7*S*,8*R*)-**25** ($[\alpha]_D^{+55}$) and (7*R*,8*S*)-**25** ($[\alpha]_D^{-55}$, unpublished data). The racemic tetrahydroquinoline bromohydrin **34** was also resolved, but as dibenzotartarate salts to give enantiomers of quinoline 5,6-oxide (5*R*,6*S*)-**20** ($[\alpha]_D^{-23}$) and (5*S*,6*R*)-**20** ($[\alpha]_D^{+23}$) via tetrahydroepoxides (5*R*,6*S*)-**35** and (5*S*,6*R*)-**35** (Akhtar et al., 1979). The enantiopurities (>98% *ee*) of arene oxides **20** and **25** were confirmed by CSPHPLC analysis; more than ten synthetic steps from quinoline **1** were required using these chemical resolution methods.

An alternative chemoenzymatic approach to the synthesis of arene oxide enantiomers **20** and **25**, using the quinoline *cis*-dihydrodiol metabolites (5*R*,6*S*)-**2** and (7*S*,8*R*)-**3** (X = H) as precursors was then developed (Boyd et al., 1991a). This again produced the quinoline oxide enantiomers (–)-(5*R*,6*S*)-**20** and (+)-(7*S*,8*R*)-**25**, in seven steps from quinoline **1**, via tetrahydroepoxides (5*R*,6*S*)-**35** and (7*S*,8*R*)-**33**. Although this chemoenzymatic approach required fewer steps than the earlier methods involving the chemical resolution of bromohydrins **32** and **34** (Boyd et al., 1994), the very low (<5%) isolated yields of the less stable *cis*-dihydrodiol precursors **2** and **3** obtained by *P. putida* UV biotransformation (Boyd et al., 1993), was a limiting factor. As the isolated yields of the more stable *cis*-dihydrodiol metabolites **9** (9%) and **10** (21%), obtained from 2-chloroquinoline **8** were higher, under similar conditions, they were used as alternative starting compounds to yield *cis*-tetrahydrodiol intermediates (5*R*,6*S*)-**39** and (7*S*,8*R*)-**40** in the current study (Figure 11).

(5*R*,6*S*)-*cis*-Tetrahydrodiol **39** ($[\alpha]_D^{-7}$, CHCl₃) and (7*S*,8*R*)-*cis*-tetrahydrodiol **40** ($[\alpha]_D^{-72}$, CHCl₃), known precursors of arene oxides **20** and **25** (Boyd et al., 1994) were efficiently synthesized (ca. 80% yield), by catalytic hydrogenation/hydrogenolysis (H₂, Pd/C, EtOH) of the (5*R*,6*S*)-*cis*-dihydrodiol **9** ($[\alpha]_D^{+140}$, MeOH) and (7*S*,8*R*)-*cis*-dihydrodiol **10** ($[\alpha]_D^{+148}$, MeOH), respectively. This new approach avoided use of the less stable *cis*-dihydrodiol metabolites **2** and **3** and provided an improved chemoenzymatic route the corresponding arene oxides (–)-**20** and (+)-**25** (Figure 11) (Boyd et al., 1994).

Attempted epoxidation of available arene oxides **20** and **25** to yield the arene dioxide isomers **28** and **29**, using several oxidants, including *m*-chloroperoxybenzoic acid and dimethyl dioxirane, resulted in the formation of *N*-oxides. The epoxidation of arene oxides **20** and **25** in CH₂Cl₂ solution was achieved using sodium hypochlorite solution (pH 8.6) in the presence of

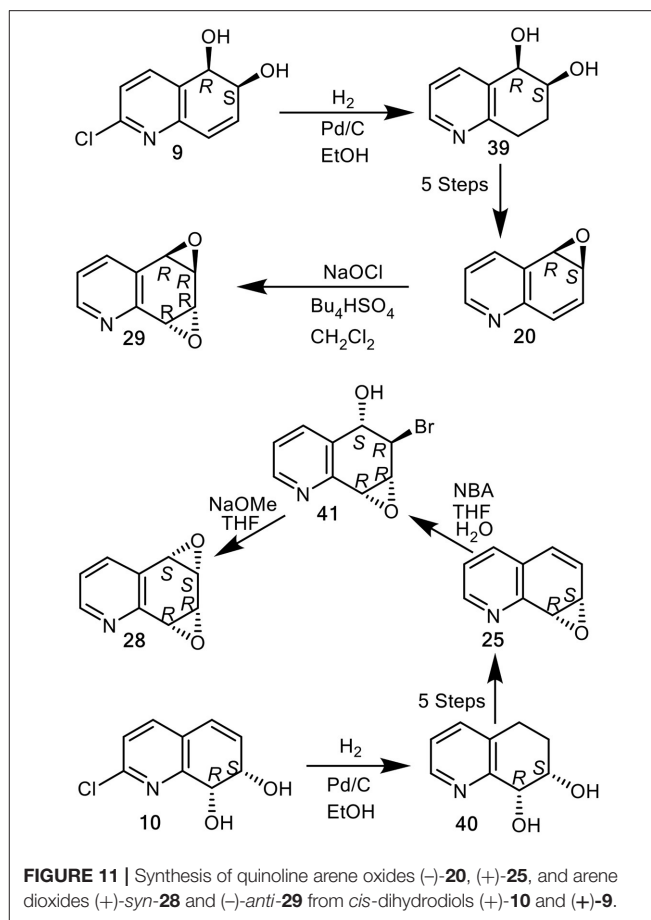


FIGURE 11 | Synthesis of quinoline arene oxides (–)-**20**, (+)-**25**, and arene dioxides (+)-*syn*-**28** and (–)-*anti*-**29** from *cis*-dihydrodiols (+)-**10** and (+)-**9**.

tetrabutylammonium hydrogen sulfate and gave *anti*-quinoline dioxide **29** exclusively. With arene oxide (–)-**20** available from earlier studies (Boyd et al., 1991a, 1994), NaOCl oxidation gave the (5*R*,6*R*,7*R*,8*R*)-arene dioxide **29** ($[\alpha]_D^{-100}$, 38% yield, Figure 11). Reaction of the (+)-(7*S*,8*R*) enantiomer of arene oxide **25** with *N*-bromoacetamide under reported conditions, yielded the crude *trans*-bromohydrin intermediate **41**, which upon treatment with sodium methoxide furnished the *syn*-quinoline dioxide (5*S*,6*S*,7*R*,8*R*)-**28** ($[\alpha]_D^{+25}$, Figure 11) (Boyd et al., 1991b).

A further approach to the synthesis of the *syn*-quinoline dioxide enantiomers (–) and (+)-**28** involved the *cis*-dihydroxylation of the 5,6-(+)-**9** and 7,8 *cis*-dihydrodiol (+)-**10**. Catalytic *cis*-hydroxylation (OsO₄, Me₃NO) of 2-chloroquinoline *cis*-dihydrodiol (+)-**9**, produced an isomeric mixture of polar tetrols **42** and **43** that could not be separated by chromatography and were converted directly to the corresponding tetraacetate derivatives **44** and **45** (1:3, Figure 12). Purification of the crude tetraacetates was achieved by flash chromatography followed by multiple elution PLC.

Hydrolysis of the minor *syn*-tetraacetate enantiomer (–)-**44**, under basic conditions (NH₃, MeOH) yielded the 2-chloroquinoline *syn*-tetrol (–)-**42** which was converted to the

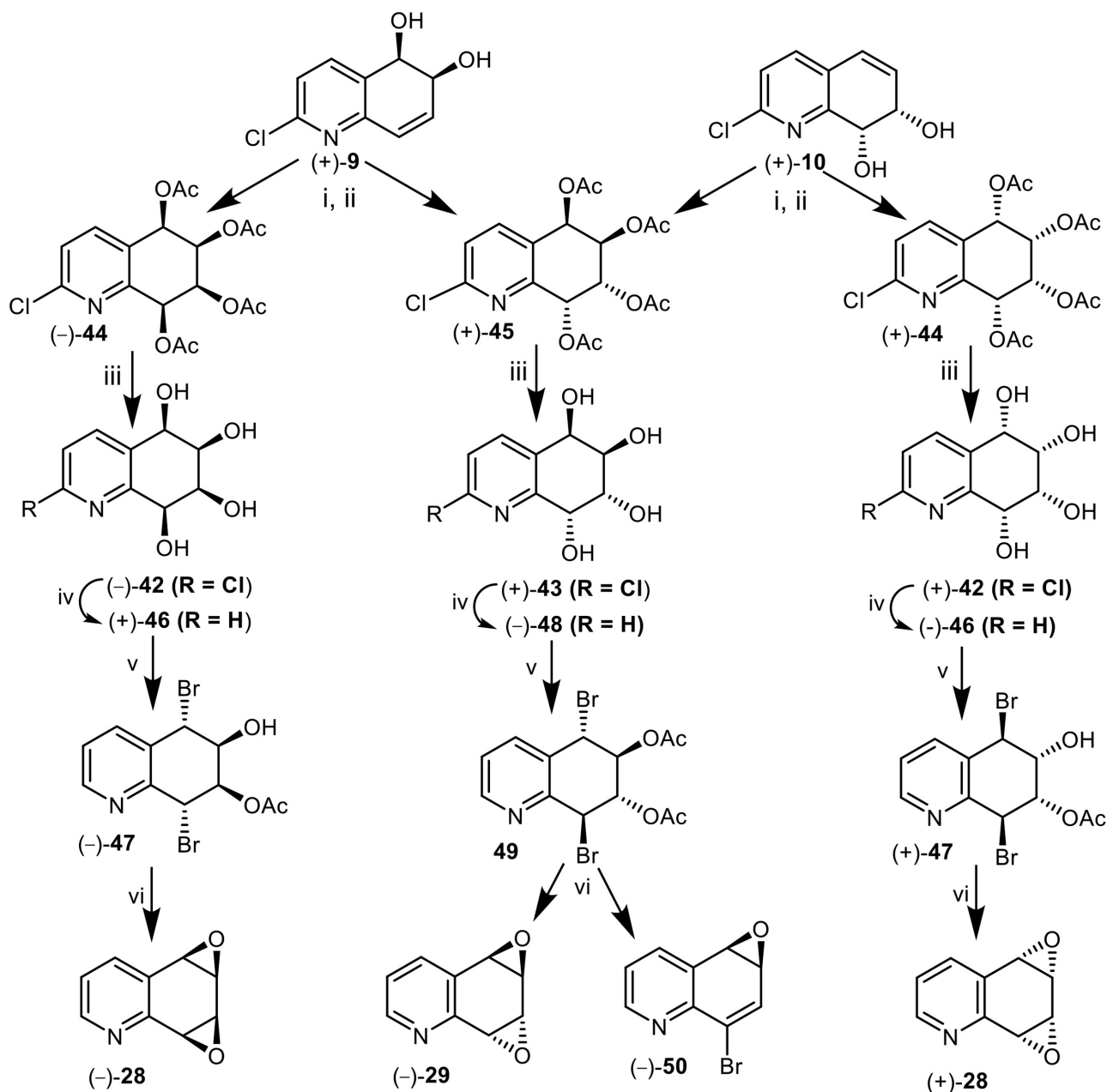


FIGURE 12 | Synthesis of *anti* (-)-**29** and *syn*-quinoline dioxides (-)-**28** and (+)-**28** from *cis*-dihydrodiols (+)-**9** and (+)-**10**. Reagents: (i) OsO₄, Me₃NO-CH₂Cl₂; (ii) Ac₂O-pyridine; (iii) NH₃, MeOH; (iv) H₂, Pd-C, MeOH; (v) AcOMe₂COBr, MeCN; (vi) NaOMe, Et₂O.

corresponding quinoline tetrol (+)-**46**, by hydrogenolysis (Pd-C). Treatment of tetrol (+)-**46** with acetoxyisobutrylbromide in MeCN solution yielded mainly a dibromoacetate, tentatively assigned as (-)-**47**; it was separated from trace amounts of the expected dibromodiacetate by PLC. Dibromoacetate **47** was formed by partial hydrolysis of the dibromodiacetate during the isolation process. Treatment of dibromomonoacetate (-)-**47** with NaOMe in THF yielded the *syn*-arene dioxide enantiomer (-)-**28** from 5,6-*cis*-dihydrodiol (+)-**9** in the sequence (+)-**9**

→ (-)-**44** → (-)-**42** → (+)-**46** → (-)-**47** → (-)-**28** (Figure 12).

In a similar manner metabolite (+)-**10** was converted into the mixture of tetraacetates **44** and **45** (1:3). The minor *syn*-tetraacetate (+)-**44**, was separated by PLC; it was assigned the opposite (5*S*,6*S*,7*R*,8*R*) absolute configuration. The *syn*-tetraacetate (+)-**44** was used in an enantiocomplementary synthetic sequence (+)-**10** → (+)-**44** → (+)-**42** → (-)-**46** → (+)-**47** → (+)-**28** (Figure 12).

anti-Tetraacetate (5*R*,6*R*,7*R*,8*R*) enantiomer (+)-**45** obtained from 5,6-(+)-**9** and 7,8-(+)-**10** *cis*-dihydrodiol metabolites, was treated in a similar manner to the *syn*-tetraacetate enantiomers (+)-**44** and (–)-**44** to yield tetrols (+)-**43**, (–)-**48**, and dibromodiacetate **49** (Figure 12). Treatment of bromoacetate **49** with sodium methoxide yields a mixture of the expected *anti*-quinoline dioxide (–)-**29** as the major product accompanied by a minor compound which was identified as 8-bromoquinoline-5,6-oxide **50**. A competing E1cB mechanism could account for the unexpected loss of acetic acid to form the minor product, arene oxide **50**. These products were thus formed *via* the synthetic sequence (+)-**9** or (+)-**10** → (+)-**45** → (+)-**43** → (–)-**48** → **49** → (–)-**29** + (–)-**50** (Figure 12).

DISCUSSION

Both Autodock and Gold programs proved to be very successful in matching the preferred *in silico* orientations of arene substrates with the experimentally confirmed regiochemistry and absolute stereochemistry of the isolated *cis*-diol metabolites. Previous docking studies of arene substrates with TDO indicated that the preferred orientations were controlled by: (i) attractive edge-to-face T shaped interactions with the orthogonal phenyl group of Phe-216 and imidazole ring of His 222 and (ii) Van der Waals interactions with the proximate hydrophobic amino acids Ile-276, Leu-272, Ile-324, Val-309, Leu-272, Phe-352 (Hoering et al., 2016; Vila et al., 2016a,b, 2017; Boyd et al., 2017, 2019). Theoretical, crystallographic and experimental support for phenyl-phenyl and phenyl-pyridyl edge-to-face bonding (T-bonding) interactions, between arene and heteroarene rings, has been reported (Jennings et al., 2001; Escudero et al., 2009; Gonzalez-Rosende et al., 2017; Aliev and Motherwell, 2019). Little evidence was available, from crystalline protein structures, for similar edge-to-face interactions between the imidazole ring of histidine with other aromatic residues, e.g., Phe, Tyr, Trp, His (Bhattacharyya et al., 2003). The possibility of further types of edge-to-face interactions between heteroarene substrates **1** (Figures 4A–C), **8** (Figures 5A–C), and **14** (Figure 6) with Phe-216 and His-222 in the active site of TDO (Figures 4–6), is also apparent.

Based on the docking orientations of 2-chloroquinoline **8** (Figures 5A,C), *cis*-dihydroxylation could also occur at the 3,4-bond of the pyridine ring. The shorter distance between this bond and dioxygen in Figure 5C (3.3–3.4 Å), would appear to favor formation of the undetected (3*R*,4*R*)-dihydrodiol **12**, over the (3*S*,4*S*) configuration resulting from the orientation of substrate **8** shown in Figure 5A (3.6–4.0 Å). Conversely, the higher binding energy, –5.8 kcal/mol^{–1}, associated with Figure 5A relative to Figure 5C (–5.1 kcal/mol^{–1}), would suggest a preference for the (3*S*,4*S*) absolute configuration, thus making a prediction of the preferred stereochemistry of *cis*-dihydrodiol **11** less reliable.

To account for the unexpected isolation of (3*S*,4*S*)-diol **11** as a product from *P. putida* UV4 biotransformations of 2-chloroquinoline **8**, the undetected *cis*-dihydrodiol **12** of

unknown absolute configuration, was originally proposed as a possible intermediate in the metabolic sequence **8** → **12** → **11** (Figure 2) (Boyd et al., 1998). Later GC-MS identification of 2-quinolone **13** as a very minor metabolite of substrate **8**, was consistent with an alternative or additional metabolic pathway (**8** → **13** → **11**, Figure 2) (Boyd et al., 2002). Stronger evidence for the latter biosynthetic route was provided when 2-quinolone **13** was used as substrate and (3*S*,4*S*)-diol **11** was found to be the only identifiable metabolite. Since 2-hydroxyquinoline is a minor tautomer of 2-quinolone **13**, the formation of *cis*-diol metabolite **11** could also be considered as a TDO-catalyzed *cis*-dihydroxylation within a substituted pyridyl ring. It is therefore possible that *cis*-diol metabolite **11** was formed from 2-chloroquinoline **8**, *via* both 2-quinolone **13** and *cis*-dihydrodiol **12** intermediates.

The previously reported regioselective and enantioselective *cis*-dihydroxylation, of the carbocyclic ring of quinoline **1**, 2-chloroquinoline **8** and 2-chloropyridine **14**, was rationalized by molecular docking (Autodock Vina) studies of these substrates. The *in silico* results revealed novel edge-to-face attractive interactions at the active site of TDO. These studies also provided support for the TDO-catalyzed *cis*-dihydroxylation of: (i) the pyridyl ring in substrates, **1**, **8**, and **14**, to yield the corresponding unstable *cis*-dihydrodiol metabolites, **7**, **12**, and **15**, and (ii) the carbocyclic ring to give stable *cis*-dihydrodiol metabolites **2**, **3**, **9**, and **10** having the correct absolute configurations. Evidence for the monooxygenase-catalyzed epoxidation and dioxygenase-catalyzed *cis*-dihydroxylation of a pyridyl ring was discussed, in the context of both bacterial and mammalian metabolism of quinoline **1**.

Our findings are consistent with the current thinking on the catalytic mechanism for these enzymes, which is not fully understood. Barry and Challis (2013) discuss an important point, i.e., whether the Fe(III)-OOH complex in the TDO catalytic cycle reacts directly with the substrate or first undergoes rearrangement to an Fe(V)-O(OH) complex. They highlight the question of which arene carbon atom first forms a bond with an oxygen atom.

In conclusion, new synthetic applications of the relatively stable *cis*-diol metabolites **9** and **10**, derived from 2-chloroquinoline **8** were successfully investigated. These *cis*-dihydrodiols were utilized in the chemoenzymatic synthesis of the corresponding *cis*-tetrahydrodiols **39** and **40**, required in the synthesis of enantiopure quinoline arene oxides, (–)-**20** and (+)-**25**. This process was greatly facilitated by molecular docking preliminary studies. The unexpected 8-bromoquinoline oxide (–)-**50** was obtained during the synthesis of *anti*-(–)-**29** and *syn*-quinoline dioxide enantiomers (–)-**28** and (+)-**28** from *cis*-dihydrodiols **9** and **10**.

DATA AVAILABILITY STATEMENT

The datasets presented in this study can be found in online repositories. The names of the repository/repositories and accession number(s) can be found in the article/Supplementary Material.

AUTHOR CONTRIBUTIONS

CA, DB, NS, and PS supervised the research, designed the research, obtained the funding, wrote the manuscript, and designed the experiments. PH conducted the modeling and docking. JC, PL, and NS conducted the laboratory synthesis/biotransformations. All authors contributed to the article and approved the submitted version.

FUNDING

Financial support for post-graduate studentships, RA funding, and academic staff funding was gratefully received from BBSRC (grant number 81/ABC09451 to DB and NS for RA and academic funding, grant number BB/E013848/1 to CA for academic funding) and the Leverhulme Trust (to CA/PH for

Ph.D. and academic funding), the European Social Fund (JC for Ph.D. funding) and Queen's University of Belfast, Oxford Glycosciences, and the Overseas Research Studentship (to PL for Ph.D. funding).

ACKNOWLEDGMENTS

We thank Professor Brian Jennings for helpful discussion and Dr. Lynne Hamilton for preliminary results.

SUPPLEMENTARY MATERIAL

The Supplementary Material for this article can be found online at: <https://www.frontiersin.org/articles/10.3389/fbioe.2020.619175/full#supplementary-material>

REFERENCES

- Agarwal, R., Boyd, D. R., Sharma, N. D., McMordie, R. A. S., Porter, H. P., van Ommen, B., et al. (1994). Chemical and enzyme-catalysed synthesis of quinoline arene hydrates. *Bioorg. Med. Chem.* 2, 439–446. doi: 10.1016/0968-0896(94)80013-8
- Agarwal, S. K., Boyd, D. R., Davies, R. J. H., Hamilton, L., Jerina, D. M., McCullough, J. J., et al. (1990). Synthesis of arene oxide and trans-dihydrodiol metabolites of quinoline. *J. Chem. Soc. Perkin Trans. 1*, 1969–1974. doi: 10.1039/p19900001969
- Agarwal, S. K., Boyd, D. R., Porter, H. P., Jennings, W. B., Grossman, S. J., and Jerina, D. M. (1986). Arene oxides and trans-dihydrodiols of quinoline. *Tetrahedron Lett.* 27, 4253–4256. doi: 10.1016/S0040-4039(00)94245-X
- Akhtar, M. N., Boyd, D. R., Hamilton, J. G., and Hamilton, J. C. (1979). Synthesis of (+)- and (–)-naphthalene and anthracene 1,2-oxides. *J. Chem. Soc. Perkin Trans. 1*, 2437–2440. doi: 10.1039/P19790002437
- Aliev, A. E., and Motherwell, W. B. (2019). Some recent advances in the design and use of molecular balances for the experimental quantification of intramolecular noncovalent interactions of pi systems. *Chem. Eur. J.* 25, 10516–10530. doi: 10.1002/chem.201900854
- Barr, S. C., Bowers, N., Boyd, D. R., Sharma, N. D., Hamilton, L., McMordie, R. A. S., et al. (1998). The potential role of cis-dihydrodiol intermediates in bacterial aromatic hydroxylation and the NIH Shift. *J. Chem. Soc. Perkin Trans. 1*, 3443–3451. doi: 10.1039/a805077e
- Barry, S. M., and Challis, G. L. (2013). Mechanism and catalytic diversity of Rieske non-heme iron-dependant oxygenases. *ACS Catal.* 3, 2363–2370. doi: 10.1021/cs400087p
- Bhattacharyya, R., Saha, R. P., Samanta, U., and Chakrabarti, P. (2003). Geometry of interaction of the histidine ring with other planar and basic residues. *J. Proteome Res.* 2, 255–263. doi: 10.1021/pr025584d
- Bott, G., Schmidt, M., Rommel, T. O., and Lingens, F. (1990). Microbial metabolism of quinoline and related compounds. V. Degradation of 1H-4-oxoquinoline by *Pseudomonas putida* 33/1. *Biol. Chem.* 371, 999–1003. doi: 10.1515/bchm3.1990.371.2.999
- Boyd, D. R., Bushman, D. R., Davies, R. J. H., Dorrity, M. R. J., Hamilton, L., Jerina, D. M., et al. (1991a). Absolute configurations of the arene oxide, trans-dihydrodiol and cis-dihydrodiol products resulting from metabolism of quinoline at the 5,6-bond. *Tetrahedron Lett.* 32, 2963–2966. doi: 10.1016/0040-4039(91)80663-Q
- Boyd, D. R., Davies, R. J. H., Dunlop, R., Porter, H. P., Hamilton, L., and McCullough, J. J. (1989). Non-enzymatic hydration, amine addition, and oxidation reactions of aza-arene oxides. *J. Chem. Soc. Chem. Commun.* 1989, 163–165. doi: 10.1039/c39890000163
- Boyd, D. R., Davies, R. J. H., Hamilton, L., McCullough, J. J., and Porter, H. P. (1991b). Arene oxides of quinoline: epoxidation, N-oxidation and N-methylation reactions. *J. Chem. Soc. Perkin Trans. 1*, 2189–2192. doi: 10.1039/p19910002189
- Boyd, D. R., McMordie, R. A. S., Porter, H. P., Dalton, H., Jenkins, R. O., and Howarth, O. W. (1987). Metabolism of bicyclic aza-arenes by *Pseudomonas putida* to yield vicinal cis-dihydrodiols and phenols. *J. Chem. Soc. Chem. Commun.* 1987, 1722–1724. doi: 10.1039/c39870001722
- Boyd, D. R., Sharma, N. D., Agarwal, R., Kerley, N. A., McMordie, R. A. S. Smith, A., et al. (1994). A new synthetic route to non-K and bay region arene oxide metabolites from cis-diols. *J. Chem. Soc. Chem. Commun.* 1994, 1693–1694. doi: 10.1039/c39940001693
- Boyd, D. R., Sharma, N. D., Brannigan, I. N., Evans, T. A., Haughey, S. A., McMurray, B. T., et al. (2012). Toluene dioxygenase-catalyzed cis-dihydroxylation of benzo[b]thiophenes and benzo[b]furans: synthesis of benzo[b]thiophene 2,3-oxide. *Org. Biomol. Chem.* 10, 7292–7304. doi: 10.1039/c2ob26120k
- Boyd, D. R., Sharma, N. D., Brannigan, I. N., McGivern, C. J., Nockemann, P., Stevenson, P., et al. (2019). Cis-dihydroxylation of tricyclic arenes and heteroarenes catalyzed by toluene dioxygenase: a molecular docking study and experimental validation. *Adv. Synth. Catal.* 361, 2526–2537. doi: 10.1002/adsc.201900147
- Boyd, D. R., Sharma, N. D., Carroll, J. G., Malone, J. F., Mackerracher, D. G., and Allen, C. C. R. (1998). Dioxygenase-catalysed cis-dihydrodiol formation in the carbo- and hetero-cyclic rings of quinolines. *Chem. Commun.* 1998, 683–684. doi: 10.1039/a709138i
- Boyd, D. R., Sharma, N. D., Dorrity, M. R. J., Hand, M. V., McMordie, R. A. S., Malone, J. F., et al. (1993). Structure and stereochemistry of cis-dihydrodiol and phenol metabolites of bicyclic azaarenes from *Pseudomonas putida* UV4. *J. Chem. Soc. Perkin Trans. 1*, 1065–1071. doi: 10.1039/p19930001065
- Boyd, D. R., Sharma, N. D., McIntyre, P. B. A., Stevenson, P. J., McRoberts, W. C., Gohil, A., et al. (2017). Enzyme-catalysed synthesis of cyclohex-2-en-1-one cis-diols from substituted phenols, anilines and derived 4-hydroxycyclohex-2-en-1-ones. *Adv. Synth. Catal.* 359, 4002–4014. doi: 10.1002/adsc.201700711
- Boyd, D. R., Sharma, N. D., Modyanova, L. V., Carroll, J. G., Malone, J. F., Allen, C. C. R., et al. (2002). Dioxygenase-catalyzed cis-dihydroxylation of pyridine-ring systems. *Can. J. Chem.* 80, 589–600. doi: 10.1139/v02-062
- Boyd, D. R., Sharma, N. D., Sbircea, L., Murphy, D., Belhocine, T., Malone, J. F., et al. (2008). Azaarene cis-dihydrodiol-derived 2,2'-bipyridine ligands for asymmetric allylic oxidation and cyclopropanation. *Chem. Commun.* 2008, 5535–5537. doi: 10.1039/b814678k
- Boyd, D. R., Sharma, N. D., Sbircea, L., Murphy, D., Malone, J. F., James, S. L., et al. (2010). Chemoenzymatic synthesis of chiral 2,2'-bipyridine ligands and their N-oxide derivatives: applications in the asymmetric aminolysis of epoxides

- and asymmetric allylation of aldehydes. *Org. Biomol. Chem.* 8, 1081–1090. doi: 10.1039/b919894f
- Buening, M. K., Wislocki, P. G., Levin, W., Yagi, H., Thakker, D. R., Akagi, H., et al. (1978). Tumorigenicity of the optical enantiomers of the diastereomeric benzo[a]pyrene 7,8-diol-9,10-epoxides in newborn mice: exceptional activity of (+)-7b,8a-dihydroxy-9a,10a epoxy-7,8,9,10-tetrahydrobenzo[a]pyrene. *Proc. Natl. Acad. Sci. U.S.A.* 75, 5358–5361. doi: 10.1073/pnas.75.11.5358
- Bushman, D. R., Sayer, J. M., Boyd, D. R., and Jerina, D. M. (1989). Solvolysis of the quinoline 5,6- and 7,8-oxides: effect of the ring nitrogen. *J. Am. Chem. Soc.* 111, 2688–2691. doi: 10.1021/ja00189a051
- Chang, R. L., Wood, A. W., Huang, M. T., Xie, J. G., Cui, X. X., Reuhl, K. R., et al. (2013). Mutagenicity and tumorigenicity of the four enantiopure bay-region 3,4-diol-1,2-epoxide isomers of dibenz[a,h]anthracene. *Carcinogenesis* 34, 2184–2191. doi: 10.1093/carcin/bgt164
- Diaz Duran, L. T., Rincon, N. O., Galvis, C. E. P., Kouznetsov, V. V., and Lorenzo, J. L. F. (2015). Genotoxicity risk assessment of diversely substituted quinolines using the SOS chromotest. *Environ. Toxicol.* 30, 278–292. doi: 10.1002/tox.21905
- Dowers, T. S., Rock, D. A., Perkins, B. N. S., and Jones, J. P. (2004). An analysis of the regioselectivity of aromatic hydroxylation and N-oxygenation by cytochrome P450 enzymes. *Drug. Metab. Dispos.* 32, 328–332. doi: 10.1124/dmd.32.3.328
- Escudero, D., Estarellas, C., Frontera, A., Quinonero, D., and Deya, P. M. (2009). Theoretical and crystallographic study of edge-to-face aromatic interactions between pyridine moieties and benzene. *Chem. Phys. Lett.* 468, 280–285. doi: 10.1016/j.cplett.2008.12.007
- Fetzner, S., Volger, B., and Lingens, F. (1993). Transformation of 2-chloroquinoline to 2-chloro-cis-7,8-dihydro-7,8-dihydroxyquinoline by quinoline-grown resting cells of *Pseudomonas putida* 86. *FEMS Microbiol. Lett.* 112:151. doi: 10.1111/j.1574-6968.1993.tb06441.x
- Garrett, M. D., Scott, R., Sheldrake, G. N., Dalton, H., and Goode, P. (2006). Biotransformation of substituted pyridines with dioxygenase-containing microorganisms. *Org. Biomol. Chem.* 4, 2710–2715. doi: 10.1039/b606113c
- Gonzalez-Rosende, M. E., Castillo, E., Jennings, W. B., and Malone, J. F. (2017). Stereodynamics and edge-to-face CH– π aromatic interactions in imino compounds containing heterocyclic rings. *Org. Biomol. Chem.* 15, 1484–1494. doi: 10.1039/C6OB02618D
- Hakura, A., Kadoi, M., Suzuki, T., and Saeki, K. I. (2007). Clastogenicity of quinoline derivatives in the liver micronucleus assay using rats and mice. *J. Health Sci.* 53, 470–474. doi: 10.1248/jhs.53.470
- Hirao, K., Shinohara, Y., Tsuda, H., Fukushima, S., Takahashi, M., and Ito, N. (1976). Carcinogenic activity of quinoline on rat liver. *Cancer Res.* 36, 329–335.
- Hoering, P., Rothschild-Mancinelli, K., Sharma, N. D., Boyd, D. R., and Allen, C. C. R. (2016). Oxidative biotransformations of phenol substrates catalysed by toluene dioxygenase: a molecular docking study. *J. Mol. Catal. B. Enzym.* 134, 396–406. doi: 10.1016/j.molcatb.2016.10.013
- Hollstein, M., Talcott, R., and Wei, E. (1978). Quinoline: conversion to a mutagen by human and rodent liver. *J. Natl. Cancer Inst.* 60, 405–410. doi: 10.1093/jnci/60.2.405
- Horning, M. G., Stillwell, W. G., Griffin, G. W., and Tsang, W. S. (1980). Epoxide intermediates in the metabolism of naphthalene by the rat. *Drug Metab. Dispos.* 8, 404–414.
- Jennings, W. B., Farrell, B. M., and Malone, J. F. (2001). Attractive intramolecular edge-to-face aromatic interactions in flexible organic molecules. *Acc. Chem. Res.* 34, 885–894. doi: 10.1021/ar0100475
- Jerina, D. M., Daly, J. W., Witkop, B., Zaltz-Nirenberg, P., and Udenfriend, S. (1968). The role of arene oxide-oxepin systems in the metabolism of aromatic substrates. III. Formation of 1,2-naphthalene oxide from naphthalene by liver microsomes. *J. Am. Chem. Soc.* 90, 6525–6527. doi: 10.1021/ja01025a058
- Kaiser, J. P., Feng, Y., and Bollag, J.-M. (1996). Microbial metabolism of pyridine, quinoline, acridine, and their derivatives under aerobic and anaerobic conditions. *Microbiol. Rev.* 60:493. doi: 10.1128/MR.60.3.483-498.1996
- Karle, I. L., Yagi, H., Sayer, J. M., and Jerina, D. M. (2004). Crystal and molecular structure of a benzo[a]pyrene 7,8-diol 9,10-epoxide N²-deoxyguanosine adduct: absolute configuration and conformation. *Proc. Natl. Acad. Sci. U.S.A.* 101, 1433–1438. doi: 10.1073/pnas.0307305101
- LaVoie, E. J., Adams, E. A., Shigematsu, A., and Hoffmann, D. (1983). On the metabolism of quinoline and isoquinoline: possible molecular basis for differences in biological activities. *Carcinogenesis* 4, 1169–1173. doi: 10.1093/carcin/4.9.1169
- Lewis, S. E. (2016). “Asymmetric dearomatization under enzymatic conditions”, in *Asymmetric Dearomatization Reactions*, ed S. L. You (Weinheim: Wiley-VCH), 279–346. doi: 10.1002/9783527698479.ch12
- Matsumoto, M., Kano, H., Suzuki, M., Noguchi, T., Umeda, Y., and Fukushima, S. (2018). Carcinogenicity of quinoline by drinking-water administration in rats and mice. *J. Toxicol. Sci.* 43, 113–127. doi: 10.2131/jts.43.113
- Reigh, G., McMahon, H., Ishizaki, M., Ohara, T., Shimane, K., Esumi, Y., et al. (1996). Cytochrome P450 species involved in the metabolism of quinoline. *Carcinogenesis* 17, 1989–1996.
- Saeki, K., Kawai, H., Kawazoe, Y., and Hakura, H. (1997b). Dual stimulatory and inhibitory effects of fluorine-substitution on mutagenicity: an extension of the enamine epoxide theory for activation of the quinoline nucleus. *Biol. Pharm. Bull.* 20, 646–650. doi: 10.1248/bpb.20.646
- Saeki, K. I., Kadoi, M., Kawazoe, Y., Futakuchi, M., Tiwawech, D., and Shirai, T. (1997a). Modification of the carcinogenic potency of quinoline, a hepatocarcinogen, by fluorine atom substitution: evaluation of carcinogenicity by a medium-term assay. *biol. Pharm. Bull.* 20, 40–43. doi: 10.1248/bpb.20.40
- Saeki, K. I., Takahashi, K., and Kawazoe, Y. (1993). Metabolism of mutagenicity-deprived 3-fluoroquinoline: comparison with mutagenic quinoline. *Biol. Pharm. Bull.* 16, 232–234. doi: 10.1248/bpb.16.232
- Saeki, K. I., Takahashi, K., and Kawazoe, Y. (1996). Potent mutagenic potential of 4-methylquinoline: metabolic and mechanistic considerations. *Biol. Pharm. Bull.* 19, 541–546. doi: 10.1248/bpb.19.541
- Stillwell, W. G., Bouwsma, O. J., Thenot, J. P., Horning, M. G., Griffin, G. W., Ishikawa, K., et al. (1978). Methylthio metabolites of naphthalene excreted by the rat. *Res. Commun. Chem. Pathol. Pharmacol.* 20, 509–530. doi: 10.1016/B978-0-08-023768-8.52191-5
- Stillwell, W. G., Horning, M. G., Griffin, G. W., and Tsang, W. S. (1982). Identification and synthesis of the isomeric tetrahydroxytetrahydronaphthalene metabolites excreted in rat urine. *Drug Metab. Dispos.* 10, 11–14.
- Suzuki, T., Wang, X., Miyata, Y., Saeki, K. I., Kohara, A., Kawazoe, Y., et al. (2000). Hepatocarcinogen quinoline induces G:C to C:G transversions in the cII gene in the liver of lambda/lacZ transgenic mice (MutaMouse). *Mutat. Res.* 456, 73–81. doi: 10.1016/S0027-5107(00)00128-7
- Tada, M., Takahashi, K., and Kawazoe, Y. (1982). Binding of quinoline to nucleic acid in a subcellular microsomal system. *Chem. Pharm. Bull.* 30, 3834–3837. doi: 10.1248/cpb.30.3834
- Tada, M., Takahashi, K., Kawazoe, Y., and Ito, N. (1980). Binding of quinoline to nucleic acid in a subcellular microsomal system. *Chem. Biol. Interact.* 29, 257–266. doi: 10.1016/0009-2797(80)90145-3
- Vila, M. A., Pazos, M., Iglesias, C., Veiga, N., Seoane, G., and Carrera, I. (2016a). Toluene dioxygenase-catalysed oxidation of benzyl azide to benzonitrile: mechanistic insights for an unprecedented enzymatic transformation. *Chem. Bio. Chem.* 17, 291–295. doi: 10.1002/cbic.201500653
- Vila, M. A., Umpierrez, D., Seoane, G., Rodriguez, S., Carrera, I., and Veiga, N. (2016b). Computational insights into the oxidation of mono- and 1,4-disubstituted arenes by the toluene dioxygenase enzymatic complex. *J. Mol. Catal. B. Enzym.* 133, S410–S419. doi: 10.1016/j.molcatb.2017.03.003
- Vila, M. A., Umpierrez, D., Veiga, N., Seoane, G., Carrera, I., and Giordano, S. R. (2017). Site-directed mutagenesis studies on the toluene dioxygenase enzymatic system: role of phenylalanine 366, threonine 365 and isoleucine 324 in the chemo-, regio-, and stereoselectivity. *Adv. Synth. Catal.* 359, 2149–2157. doi: 10.1002/adsc.201700444
- Willems, M. I., Dubois, G., Boyd, D. R., Davies, R. J. H., Hamilton, L., McCullough, J. J., et al. (1992). Comparison of the mutagenicity of

- quinoline and all monohydroxyquinolines with a series of arene oxide, trans-dihydrodiol, diol epoxide, N-oxide and arene hydrate derivatives of quinoline in the Ames/Salmonella microsome test. *Mutat. Res.* 278, 227–236. doi: 10.1016/S0165-1218(10)80002-3
- Zia, M. F., Vasko, A. G., Riedl, Z., Hametner, C., Hajos, G., Mereiter, K., et al. (2016). Biodihydroxylation of substituted quinolines and isoquinolines by recombinant whole-cell mediated biotransformations. *Tetrahedron* 72, 7348–7355. doi: 10.1016/j.tet.2016.06.077
- Ziffer, H., Kabuto, K., Gibson, D. T., Kobal, V. M., and Jerina, D. M. (1977). The absolute stereochemistry of several cis-dihydrodiols microbially produced from substituted benzenes. *Tetrahedron* 33, 2491–2496. doi: 10.1016/0040-4020(77)80070-7
- Conflict of Interest:** The authors declare that the research was conducted in the absence of any commercial or financial relationships that could be construed as a potential conflict of interest.

Copyright © 2021 Boyd, Sharma, Loke, Carroll, Stevenson, Hoering and Allen. This is an open-access article distributed under the terms of the Creative Commons Attribution License (CC BY). The use, distribution or reproduction in other forums is permitted, provided the original author(s) and the copyright owner(s) are credited and that the original publication in this journal is cited, in accordance with accepted academic practice. No use, distribution or reproduction is permitted which does not comply with these terms.



Optimization of Inulin Hydrolysis by *Penicillium lanosocoeruleum* Inulinases and Efficient Conversion Into Polyhydroxyalkanoates

Iolanda Corrado¹, Nicoletta Cascelli¹, Georgia Ntasi¹, Leila Birolo¹, Giovanni Sannia¹ and Cinzia Pezzella^{2*}

¹ Department of Chemical Sciences, University of Naples Federico II, Complesso Universitario di Monte Sant'Angelo, Naples, Italy, ² Department of Agricultural Sciences, University of Naples Federico II, Naples, Italy

OPEN ACCESS

Edited by:

Manuel Benedetti,
University of L'Aquila, Italy

Reviewed by:

Helen Treichel,
Universidade Federal da Fronteira Sul,
Brazil

Naveen Kango,
Dr. Hari Singh Gour University, India

*Correspondence:

Cinzia Pezzella
cpezzella@unina.it

Specialty section:

This article was submitted to
Industrial Biotechnology,
a section of the journal
Frontiers in Bioengineering and
Biotechnology

Received: 13 October 2020

Accepted: 29 January 2021

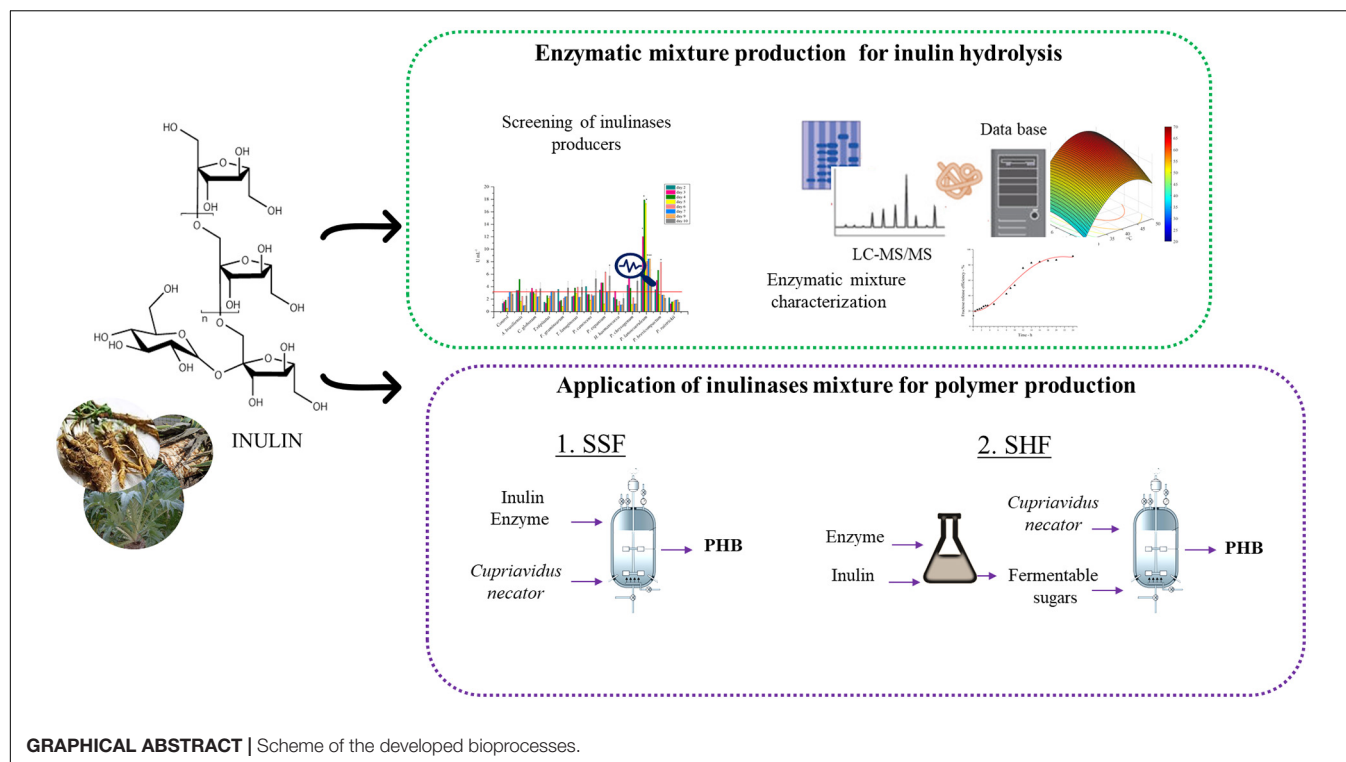
Published: 01 March 2021

Citation:

Corrado I, Cascelli N, Ntasi G,
Birolo L, Sannia G and Pezzella C
(2021) Optimization of Inulin
Hydrolysis by *Penicillium*
lanosocoeruleum Inulinases
and Efficient Conversion Into
Polyhydroxyalkanoates.
Front. Bioeng. Biotechnol. 9:616908.
doi: 10.3389/fbioe.2021.616908

Inulin, a polydisperse fructan found as a common storage polysaccharide in the roots of several plants, represents a renewable non-food biomass resource for the synthesis of bio-based products. Exploitation of inulin-containing feedstocks requires the integration of different processes, including inulinase production, saccharification of inulin, and microbial fermentation for the conversion of released sugars into added-value products. In this work paper, a new microbial source of inulinase, *Penicillium lanosocoeruleum*, was identified through the screening of a fungal library. Inulinase production using inulin as C-source was optimized, reaching up to 28 U mL⁻¹ at the 4th day of growth. The fungal inulinase mixture (*Plal*) was characterized for pH and temperature stability and activity profile, and its isoenzymes composition was investigated by proteomic strategies. Statistical optimization of inulin hydrolysis was performed using a central composite rotatable design (CCRD), by analyzing the effect of four factors. In the optimized conditions (T, 45.5°C; pH, 5.1; substrate concentration, 60 g L⁻¹; enzyme loading, 50 U g_{substrate}⁻¹), up to 96% inulin is converted in fructose within 20 h. The integration of *Plal* in a process for polyhydroxyalkanoate (PHA) production by *Cupriavidus necator* from inulin was tested in both separated hydrolysis and fermentation (SHF) and simultaneous saccharification and fermentation (SSF). A maximum of 3.2 g L⁻¹ of PHB accumulation, corresponding to 82% polymer content, was achieved in the SSF. The proved efficiency in inulin hydrolysis and its effective integration into a SSF process pave the way to a profitable exploitation of the *Plal* enzymatic mixture in inulin-based biorefineries.

Keywords: response surface methodology, simultaneous saccharification and fermentation, inulin hydrolysis, polyhydroxybutyrate, inulin, biorefinery



INTRODUCTION

The biorefinery concept focuses on the sustainable conversion of renewable biomasses into a broad range of industrial products, materials, and energy. Inulin-rich biomasses represent inexpensive, renewable, and abundant feedstock to build up a biorefinery strategy (Li et al., 2013; Hughes et al., 2017; Bedzo et al., 2020). Inulin is a linear polysaccharide (β -2,1-linked d-fructose residues terminated by a glucose residue) accumulated as a storage carbohydrate in plants such as chicory and dahlia and, more interestingly, in low-requirement crops, such as *Jerusalem artichoke* and *Cynara cardunculus* (Hughes et al., 2017). Growing well in non-fertile and harsh lands, these inulin-containing biomasses do not compete with grain crops for arable land and have received attention as renewable resource for the production of several bio-based products through microbial bioprocesses (Chi et al., 2011; Qiu et al., 2018; Singh et al., 2019, 2020a).

Among the emerging bio-based products, bioplastics derived from microbial processes, polyhydroxyalkanoates (PHA), represent promising “green” alternatives to conventional plastics. Synthesized by a wide range of bacteria from renewable sources, PHA are fully biodegradable polyesters, exhibiting a wide spectrum of properties, very close to those of fossil-derived polyolefins (Samui and Kanai, 2019; Medeiros Garcia Alcântara et al., 2020). PHA properties are dependent on their monomer chain length (ranging from the most common C4 monomer, butyrate, to $C \geq 6$ monomers) with a composition strictly influenced by the supplied carbon source and the specific metabolic pathway activated in the cell. This variability translates into a wide range of material properties allowing this polymer

to find applications in different sectors (Raza et al., 2018; Zhong et al., 2020). The use of low-cost substrates as starting feedstock for microbial fermentation therefore represents the keystone to promote a cost-effective and sustainable exploitation of this class of biopolymers (Kumar et al., 2019; Tsang et al., 2019; Vastano et al., 2019; Guzik et al., 2020; Surendran et al., 2020).

Hydrolysis into fermentable monosaccharides is a prerequisite for inulin utilization as carbon and energy source in the subsequent fermentation processes. Acid hydrolysis is a common method to achieve fast and cheap inulin conversion into fermentable sugars; however, it results in the formation of colored by-products as well as in the production of inhibitors of microbial growth. Enzymatic processes, conversely, besides representing an environmentally friendly alternative to acid hydrolysis, prevent the formation of pigments and inhibitors, paving the way to combined hydrolysis and fermentation steps, with an advantage in terms of overall time, costs, and productivity of the process (Qiu et al., 2018). The key enzymes involved in inulin hydrolysis are inulinases, which are glycosyl hydrolases, belonging to the GH32 family, that catalyze the hydrolysis of fructans. Based on their differential hydrolytic activity, they can be classified into exo-inulinases (E.C. 3.8.1.80), acting by removing fructose moieties from the non-reducing end of inulin, or endoinulinases (E.C. 3.2.1.7), which randomly break any β -2,1 glycosidic bond in the inulin molecule, thus releasing inulotrioses (F3), inulotetraoses (F4), and other IOSs oligosaccharides (Hughes et al., 2017). While exoinulinases have been shown to display a significant amount of activity toward sucrose, endoinulinases lack invertase activity (Chi et al., 2009; Singh et al., 2019, 2020b).

Inulinases have been reported to be present in plants, animals, and various microorganisms. The latter are the most preferred source of inulinases due to their easier manipulation, higher production levels, and variety of their properties (Singh and Chauhan, 2016, 2017). Numerous fungal, yeast, and bacterial strains have been isolated for their ability to produce inulinases (Rawat et al., 2017b; Singh et al., 2019); fungal inulinases are the most attractive for their production levels, low substrate requirement, and tolerance to low pH and high temperature (Singh and Singh, 2017). As a matter of fact, microbial inulinases have been widely exploited: exo-inulinases, in high-fructose syrup preparation (Rawat et al., 2017a; Singh et al., 2017) and endo-inulinases in the production of inulo-oligosaccharides (IOS) as functional probiotics (Singh and Singh, 2010; Chikkerur et al., 2020; Singh et al., 2020b, 2021).

Despite the high potential, the high price of commercial inulinases and the lack of efficient inulinase catalyzed processes still represent the main limitations to their effective exploitation (Qiu et al., 2019b). The cost-competitiveness of inulinase production can be achieved by using a cheap inulin-rich feedstock for their production, and several examples have been reported in this field (Singh et al., 2019). On the other hand, search for new, better-performing enzymes by exploring the potential of new inulinase producers represents a viable strategy to promote the exploitation of these enzymes in industrial processes as well as in the valorization of inulin-rich biomasses.

The production of different microbial products, including ethanol, butanol, citric and succinic acids, and single-cell proteins (Singh et al., 2020a), has been achieved while exploiting microbial inulinases in separate hydrolysis and fermentation (SHF) and simultaneous saccharification and fermentation (SSF) processes. Only few microbial strains are naturally endowed with the ability of both hydrolyzing inulin and converting fructose into value-added chemicals. Consolidated bioprocesses (CBP) based on biomass-derived inulin have been reported for the microbial production of lactic acid (Choi et al., 2012), ethanol (Khatun et al., 2017), poly-(γ -glutamic acid) (Qiu et al., 2019a), exopolysaccharide (Meng et al., 2021), and single-cell oils (Zhao et al., 2010). On the other hand, PHA production from inulin has been less explored. *Cupriavidus necator*, one of the most widely known PHA producers, is able to accumulate polyhydroxybutyrate (PHB) with high productivity from fructose but lacks the ability to utilize inulin as C-source (Bhatia et al., 2018). As a fact, only examples of SHF processes for PHA production from inulin extracts have been reported for this strain (Koutinas et al., 2013; Haas et al., 2015).

In the perspective of designing processes for saccharification of inulin substrate, the optimization of inulinase reaction conditions is essential for their utilization in the SHF process, while expanding the pool of available inulinases will help to address the specific process conditions imposed by the SSF process (Zheng et al., 2018b).

In this work, a collection of fungi was screened as inulinase producers. The inulinase mixture obtained from the best-performing fungus was characterized and used to optimize a protocol for inulin hydrolysis through an approach of statistical

design of experiments. The fructose-containing hydrolyzate was used as starting feedstock for the production of PHAs from *C. necator* in an SHF process. Furthermore, the exploitation of the inulinase mixture in an SSF strategy for PHA production was also tested and the performances of the two processes were compared.

MATERIALS AND METHODS

Microbial Strains and Culture Conditions

Fungal strains were obtained from the *Mycotheca Universitatis Taurinensis* (MUT) culture collection. *C. necator* DSM 428 production was used for PHB production.

All fungi were grown and maintained on Malt Extract Agar medium (MEA) (for 1 L): 20.0 g malt extract, 2.0 g peptone, 20.0 g agar, and 20.0 g glucose through periodic transfer at 28°C (40°C for *Thermomyces lanuginosus*) for 7–9 days. A minimal medium (MM) (Vries et al., 2017) supplemented with inulin at 10 g L⁻¹ was used for the screening in liquid medium and for inulinase production. Inulin from chicory root, used in the culture media, was provided by Lineavi, Germany.

Cupriavidus necator DSM 428 strain was grown aerobically at 30°C in both rich (Tryptic Soy Broth, TSB) and minimal media (MM_{CN}) according to Budde et al. (2011a,b).

Screening of the Fungal Library

For screening in liquid medium, all fungi were grown on an MEA plate for 7–9 days. A mycelium plug (1 cm diameter) was transferred on the MM + Inulin 1% w/v agar plate for an additional 7–10 days before the inoculum in liquid medium. Shake flasks, smooth conventional or baffled (250 mL), containing 50 mL of MM were inoculated with four mycelium plugs (0.5 cm diameter) and incubated at 28°C (40°C for *Thermomyces lanuginosus*) in an orbital shaker at 200 rpm.

Inulinase Production From *Penicillium lanosocoeruleum*

Penicillium lanosocoeruleum cultures were made on an agar MM medium with 1% glucose and then transferred to a liquid medium. 1% w/v of inulin, glucose, or fructose was tested as different carbon sources for the preinoculum phase. After 3 days of growth (28°C, 200 rpm), the preinoculum was milled, tenfold diluted into 1-L baffled flasks containing the MM medium plus 10 g L⁻¹ inulin, and grown for 10 days in the same conditions. Different medium/flask volume ratios were tested in the inoculum phase (1:2; 1:3; 1:5). Samples of fungal cultures were daily withdrawn and assayed for inulinase activity in the culture broth.

Different methods were tested to concentrate secreted inulinases in the crude extract: (i) precipitation by the addition of 80% (NH₄)₂SO₄ at 4°C; (ii) precipitation in cold acetone at fourfold volume with respect to the sample; and (iii) ultrafiltration in Amicon® Stirred Cell Millipore with a 10-kDa cutoff cellulose membrane.

Total protein content was determined according to the method of Bradford (1976) using bovine serum albumin (BSA)

as standard. The concentrated *P. lanosocoeruleum* enzymatic mixture recovered after the ultrafiltration step was herein defined *PlaI*.

Inulinase Activity Assay

Enzymatic activity on inulin and sucrose substrates was measured using the 3,5-dinitrosalicylic acid (DNS) reagent method in conformity with (Miller, 1959). A 0.2 mL of sample was added to 1.8 mL of 0.2 mol L⁻¹ sodium acetate buffer, pH 5.0, containing 0.5% w/v of high purity grade inulin (provided by Sigma) or 1% of sucrose. The mixture was incubated at 37°C for 15 min. Total reducing sugars were measured by adding 3 mL DNS reagent and boiling in a water bath for 5 min. Samples were allowed to cool, and their absorbance was read at 540 nm. A calibration curve was obtained using fructose as standard. One enzymatic unit (inulinase or invertase activity) was defined as the amount of the enzyme which produces 1 μmol of reducing sugars per minute. All the assays were carried out in duplicate.

The effect of pH on inulinase activity was measured at 37°C in a pH range of 3–10.5 using 0.1 mol L⁻¹ of citric acid–sodium citrate (pH 3–4), sodium acetate (pH 4.5–5.5), phosphate (pH 6–8), and sodium carbonate (pH 9.2–10.5) buffers. The effect of temperature was determined in 0.2 mol L⁻¹ M sodium acetate buffer at pH 5, incubating the mixture for 15 min in the temperature range 30–80°C. Thermal stability of the *PlaI* mixture was determined by measuring the residual inulinase activity after incubation at 40, 60, and 80°C.

Experimental Design

Inulin hydrolysis was optimized using response surface methodology (RSM) with central composite design (CCD). Four factors were selected to evaluate the response pattern and to determine the optimal combination of temperature, pH, substrate concentration, and enzyme loading. The coded values for each parameter were as follows [−1 0 1]: temperature in °C [28, 40, 50], pH [5, 6, 7], substrate concentration in g L⁻¹ [40, 50, 60], and enzyme loading in enzyme units for gram of inulin [20, 40, 60]. The experimental design was developed using JMP® 14.1.0 (SAS Institute Inc., 1989–2019, Cary, NC)¹ and resulted in 26 conditions; all conditions were tested in triplicate.

Enzymatic Hydrolysis of Inulin

Enzymatic hydrolysis was performed in 10-mL glass vials with 5 mL working volume. Different amounts of *PlaI* were added to Na-acetate (0.1 mol L⁻¹, pH 5) or Na-phosphate buffer (0.1 mol L⁻¹, pH 6, and 7) supplemented with inulin (high-grade purity) at the desired concentration. The vials were hermetically covered and incubated for 24 h while shaking at 250 rpm.

Kinetic of inulin hydrolysis was assessed in the optimal condition defined by DOE. Samples were withdrawn at different times and incubated at 100°C to inactivate the enzymatic mixture. For each reaction, a corresponding control was carried out in the absence of enzyme, to consider possible inulin spontaneous hydrolysis. The presence of free sugars into inulin powder without any incubation was taken at time 0 h. Conversion

efficiency was calculated on the basis of maximum fructose released per gram of inulin. The complete inulin hydrolysis was carried out by incubating the *Aspergillus niger* endo-exo-inulinase enzyme mixture (SIGMA CAS: 9025-67-6) for 4 h at 50°C (5 U_{gsubstrate}⁻¹). Afterward, the mixture was kept in 100°C boiling water for 1 h to assure that the complete hydrolysis and fructose released was assayed. Concentrations of fructose and glucose were determined by D-fructose and D-glucose assay kits (K-FRUGL Megazyme).

Gel Electrophoresis and Activity Staining on Polyacrylamide Gel

SDS-PAGE was performed according to Laemmli (1970). Native electrophoresis was carried out on 7% gel according to a method proposed by Chen et al. (1996). After that, PAGE gel was subjected to activity staining (Pessoni and Braga, 2007).

In situ Digestion

The two gel bands that demonstrated inulinase activity were cut, destained, and *in situ* digested. Briefly, the gel pieces were washed with three cycles of 0.1 mol L⁻¹ NH₄HCO₃ of pH 8.0 and acetonitrile, followed by reduction (10 mmol L⁻¹ DTT in 100 mmol L⁻¹ NH₄HCO₃, 45 min, and 37°C) and alkylation (55 mmol L⁻¹ IAM in 100 mmol L⁻¹ NH₄HCO₃, 30 min, and RT). The gel pieces were washed with three further cycles of 100 mmol L⁻¹ NH₄HCO₃ of pH 8.0 and acetonitrile. Finally, the gel plugs were rehydrated in 40 mL sequencing grade modified trypsin (10 ng mL⁻¹ trypsin; 10 mmol L⁻¹ NH₄HCO₃) and incubated overnight at 37°C (Lettera et al., 2010). Peptide mixtures were eluted, vacuum-dried, and resuspended in 0.1% v/v formic acid for LC-MS/MS analysis.

LC-MS/MS

LC-MS/MS analyses were carried out on a 6520 Accurate-Mass Q-TOF LC/MS System (Agilent Technologies, Palo Alto, CA, United States) equipped with a 1200 HPLC system and a chip cube (Agilent Technologies) and on an LTQ Orbitrap-XL (Thermo Scientific, Bremen, Germany) as reported in Linn et al. (2018), and raw data were analyzed as reported in Vinciguerra et al. (2015). Each LC-MS/MS analysis was preceded and followed by blank runs to avoid carryover contamination. MS/MS spectra were transformed in Mascot Generic files (.mgf) format, and the FASTA file of all the proteins from the gene expression profiling of *P. lanosocoeruleum* were used as database for protein identification. ²(10698 sequences; 5093396 residues). A licensed version of MASCOT software³ version 2.4.0 was used. Standard parameters in the searches were as follows: trypsin as the enzyme; 3 as the allowed number of missed cleavages; 10 ppm MS tolerance and 0.6 Da MS/MS tolerance; and peptide charge from 2+ to 4+. In all the database searches, carbamidomethylation of cysteine was inserted as fixed chemical modification, but possible oxidation of methionine and the transformation of N-terminal glutamate or glutamine

¹https://www.jmp.com/it_it/home.html

²https://genome.jgi.doe.gov/portal/PenlanEProfiling_FD/PenlanEProfiling_FD.info.html

³www.matrixscience.com

to pyroglutamate were considered as variable modifications. Only proteins presenting two or more peptides were considered as positively identified. Protein scores were derived from ion scores as a non-probabilistic basis for ranking protein hits. ⁴The ion score is $-10 \cdot \log(P)$, where P is the probability that the observed peptide match is a random event. The individual ion score threshold provided by MASCOT software to evaluate the quality of matches in MS/MS data was used for the confidence threshold in protein identification. Basic Local Alignment Search Tool (BLAST) was used to calculate the sequence similarity among the amino acid sequences of the *P. lanosocoeruleum*-identified proteins with fungal proteins in the NCBI database.

PHA Production and Extraction

Cupriavidus necator was grown on a rich medium (TSB) for 24 h and precultured in MM_{Cn} for an additional 48 h before the inoculum in fermentation media. PHA production was carried out in 250-mL Erlenmeyer flasks. For the SSF process, 20 g L⁻¹ inulin was supplemented to the minimal medium together with both 40 and 80 *Plal* inulinase U g_{substrate}⁻¹. For the SHF process, inulin hydrolyzed in the best conditions defined by DOE was used as a carbon source. The pH was adjusted to 6.8 using 1 mol L⁻¹ NaOH, filtered, and added to MM_{Cn} (final concentration of fructose 20 g L⁻¹). The flasks were inoculated at 0.1 OD mL⁻¹ and incubated at 30°C on shaker running at 200 rpm for 5 days. Single flasks were taken every 24 h, and the cells were recovered by centrifugation at 5,500 g for 15 min and lyophilized for determination of the cell dry weight (cdw). Analysis of fructose concentration was carried out on culture supernatants, while the PHA polymer was extracted from the lyophilized cell according to Sayyed et al. (2009).

¹H-NMR Spectroscopy

Polyhydroxyalkanoates extracts were analyzed by ¹H-NMR spectroscopy: samples (0.5–1.5 mg) were resuspended in deuterated chloroform (500 μL). ¹H-NMR spectra were recorded on Bruker DRX-400 (¹H-NMR: 400 MHz) in CDCl₃ (internal standard, for ¹H: CHCl₃ at δ 7.26 ppm) (Mostafa et al., 2020).

Statistical Analysis

The results were statistically analyzed using the JMP 14.1.0 (SAS Institute Inc., 1989–2019, Cary, NC)¹. Arithmetic means and mean square errors (SD) were calculated in all cases. Significant differences in average values of inulinase activity measured in the liquid screening were tested using the Tukey-Kramer HSD test (significance level: $P < 0.05$). ANOVA test has been applied to the experimental results of CCRD and to model validation experiments. The interaction and quadratic effect of parameters were determined based on an alpha 0.05 using the F test. The fitted models were evaluated by normal probability plots, R^2 , and adjusted R^2 .

⁴http://www.matrixscience.com/help/interpretation_help.html

TABLE 1 | Library of fungal strains constructed in this work.

Fungal strain	Note
<i>Penicillium brevicompactum</i> MUT 793	Inulinase activity detected (Abd et al., 2014) Annotated enzyme models: 4
<i>Thermomyces lanuginosus</i> MUT 2896	Inulinase activity detected (Nguyen et al., 2013) Annotated enzyme models: nd
<i>Penicillium chrysogenum</i> MUT 618	Inulinase activity detected (Gujar et al., 2018) Annotated enzyme models: 6
<i>Penicillium canescens</i> MUT 1158	Annotated enzyme models: 13
<i>Penicillium lanosocoeruleum</i> MUT 3921	Annotated enzyme models: 9
<i>Penicillium expansum</i> MUT 1164	Inulinase activity detected (Fernandes et al., 2012) Annotated enzyme models: 4
<i>Penicillium raistrickii</i> MUT 1525	Annotated enzyme models: 5
<i>Nectria haematococca</i> MUT 5670	Growth on inulin substrate (Battaglia et al., 2011) Annotated enzyme models: 6
<i>Fusarium graminearum</i> MUT 209	Inulinase activity detected (Gonçalves et al., 2016) Annotated enzyme models: 5
<i>Chaetomium globosum</i> MUT 337	Growth on inulin substrate (Battaglia et al., 2011) Annotated enzyme models: 6
<i>Talaromyces stipitatus</i> MUT 237	Annotated enzyme models: 7 (Vries et al., 2017)
<i>Aspergillus brasiliensis</i> MUT 4853	Annotated enzyme models: 7 (Vries et al., 2017)

Information reported in the table is from scientific literature available on strains belonging to the same genus and species and/or whose genome sequence was deposited on the JGI genome portal (<https://genome.jgi.doe.gov/portal/>). The number of annotated enzyme models derives from CAZY database; nd, not detected.

RESULTS AND DISCUSSION

Screening of a Library of Fungal Strains for Inulinase Production

Library Screening

A library of twelve fungi was assembled by choosing among strains with reported evidence in literature of inulinase production and/or for which the presence of genes belonging to the GH32 inulinase family was deduced from querying the CAZY database⁵ (Table 1). All the strains were purchased from MUT collection, choosing, when available, those isolated from the rhizosphere or soil environment.

The strain collection was screened for inulinase production in liquid medium. *P. brevicompactum* and *P. lanosocoeruleum* exhibited the best performances. As a fact, the highest level of inulinase activity was detected in the extracellular media of the two abovementioned strains: about 18 U mL⁻¹ at the 4th day and 9 U mL⁻¹ at the 6th day, with an I/S ratio equal to 1 and 2, respectively, with these values being indicative of the prevalence of inulinase activity over the invertase one (Singh and Singh, 2010; Figure 1). For all the other tested strains, inulinase production does not go beyond ~5 U mL⁻¹. Based on these results, *P. lanosocoeruleum* was selected for further exploitation.

⁵<http://www.cazy.org/>

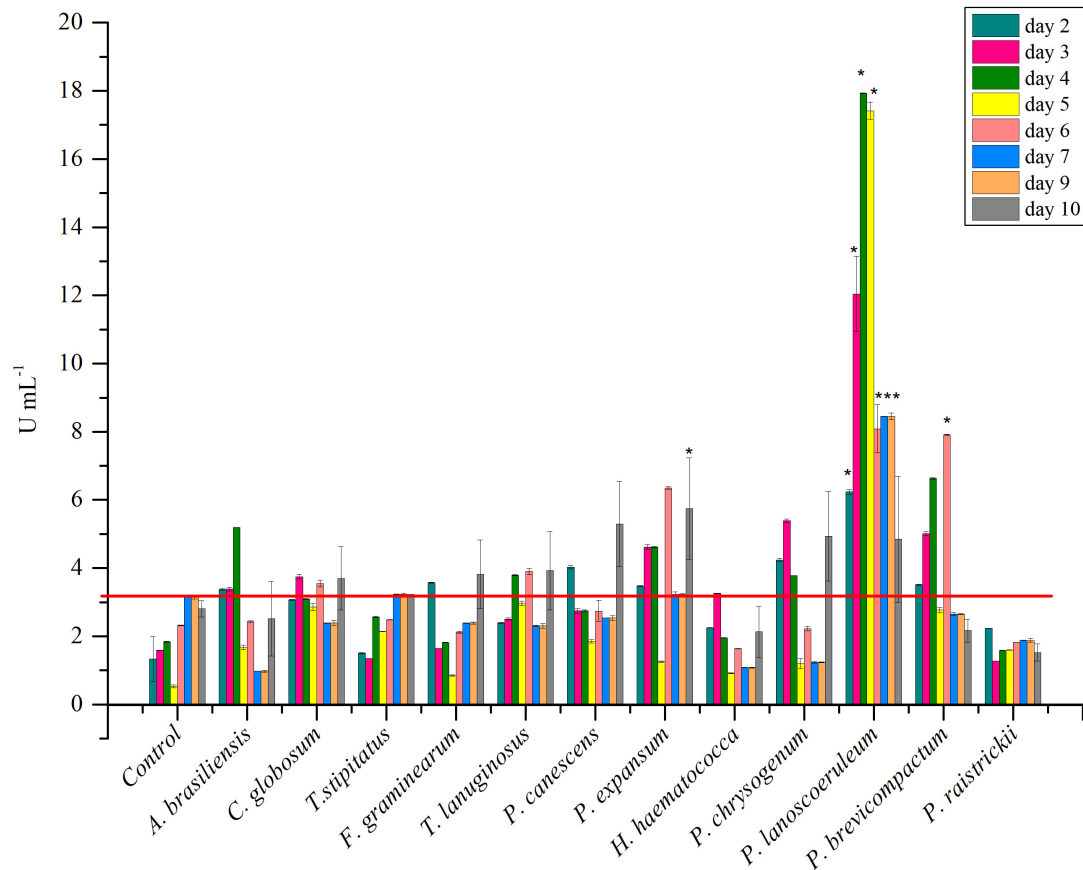


FIGURE 1 | Time-course of inulinase activity as monitored in fungal culture supernatants. Each data bar represents the mean \pm SD of two independent experiments. Significant values (*) ($P < 0.05$) were estimated respect to the uninoculated “Control” experiment, representative of spontaneous inulin hydrolysis (Tukey–Kramer HSD test, see **Supplementary Material 1**). The red line marks the maximum value of spontaneous inulin hydrolysis achieved in the same growth condition.

Inulinase Production From *P. lanosocoeruleum*

Inulinase production was carried out in liquid cultures (250 mL volume, smooth flasks) using inulin as C-source. When different medium/shake flask volume ratios were tested (1:5; 1:3; 1:2), comparable results were obtained at 1:5 and 1:3 ratios (~ 15 U mL $^{-1}$), while a significant decrease in inulinase production levels was observed at the 1:2 ratio (~ 5 U mL $^{-1}$). When the flask geometry was changed from smooth to baffled flasks, no relevant differences in terms of inulinase production levels were observed, whatever was the medium/flask volume ratio used. However, the use of baffled flasks assured more reproducible results, possibly because of a reduced formation of fungal pellets. Interestingly, when the culture was scaled up to 1 L, the use of baffled flasks yielded an almost three-fold higher inulinase production with respect to not-baffled ones (~ 15 U mL $^{-1}$ vs. 5 U mL $^{-1}$), confirming the levels obtained on the small scale.

The type of C-source used for preinoculum growth was found to strongly affect enzyme production in the following inoculum. When the preinoculum was carried out using glucose as C-source, a notable increase in inulinase production was achieved in the following culture step with respect to inulin and fructose.

Inulinase production has been reported to be induced by the presence of inulin itself (Singh and Singh, 2017) and to be sensible to catabolite repression by free sugars (Mahmoud et al., 2011; Singh and Chauhan, 2017; Garuba and Onilude, 2020). Consistently, no inulinase production was observed when the fungus was grown in the presence of fructose or glucose as unique C-sources in the inoculum phase. Moreover, the high fructose concentration in the preinoculum (released by inulin hydrolysis, or directly available in the medium) was found to inhibit further inulinase production in the inoculum phase, while the presence of glucose (the minority monomer in inulin polymer) did not interfere with the following inulinase production (data not shown).

In the optimized condition, *P. lanosocoeruleum* inulinase activity production reached a maximum of 28 U mL $^{-1}$ at the 4th day of growth. Inulinase production seems to be growth-associated: as a fact, a decline in enzyme activity was observed after the 4th day, possibly ascribable to the secretion of proteolytic enzymes. A similar profile was already reported for inulinase production in shake-flask fermentations of many fungal species, i.e., *Penicillium* sp. (Rawat et al., 2015b), *Aspergillus fumigatus* (Chikkerur et al., 2018),

Aspergillus niger (Mahmoud et al., 2011), and *Aspergillus tritici* (Singh et al., 2020b).

Inulinase activity levels achieved in this work are among the highest ever obtained from submerged fermentation of *Penicillium* strains. A novel strain of *Penicillium subrubescens* (FBCC 1632^T) isolated from soil has been found to produce up to 7.7 U/mL⁻¹ when tested on pure inulin (Mansouri et al., 2013), while a production level of 1 U/mL⁻¹ has been reported for *Penicillium* sp. NFCC 2768, and this strain is much more effective as inulinase producer (up to 3.9 U/mL⁻¹) when grown on inulin-rich vegetable infusions with respect to pure inulin (Rawat et al., 2015b). Similarly, four *Penicillium* strains, selected from a fungal library of inulinase producers on inulin-rich plant extract, displayed a production level ranging from 0.5 to 2.7 U/mL⁻¹ (Rawat et al., 2015a). A higher production level (up to 20 U mL⁻¹) has been achieved by Abdal-Aziz and coauthors (Abd Allah AbdAl-Aziz et al., 2012) with *Penicillium citrinum* grown on pure inulin, by increasing the incubation temperature to 35°C. A maximum of 46 U mL⁻¹ of inulinase production has been reported for *Penicillium* sp. XL10 in an inulin-containing medium after optimization of the supplied nitrogen source (Zheng et al., 2018b), while about 38 U/mL⁻¹ was obtained with *Penicillium oxalicum* BGPUP-4 in a growth media containing both inulin and lactose (Singh and Chauhan, 2017).

Characterization of the Inulinase Enzymatic Mixture

Several methods to concentrate proteins from the growth medium were tested to recover an extracellular enzymatic mixture endowed with high inulinase activity, i.e., acetone precipitation, ammonium sulfate precipitation, and ultrafiltration. The latter method provided the highest recovery of enzymatic activity (~90%), as well as an almost doubling of the specific activity of the extract (from 453 to 905 U mg⁻¹). Conversely, acetone and ammonium sulfate precipitation resulted in a dramatic drop of the recovered activity (~10% yield of recovered activity), probably due to the high glycosylation level typical of secreted fungal proteins. The notable specific activity of the *P. lanosocoeruleum* crude extract (*PlaI*) denotes a high inulinase production ability of the strain. As a fact, the specific activity so far reported for enzymatic extracts from *Penicillium* strains ranges from 80 to 740 U mg⁻¹ and has been achieved after at least two purification steps (Pandey et al., 2016).

The ultrafiltrated broth enriched in inulinase activity, herein defined as *PlaI*, was further characterized. The effect of temperature on the activity of the inulinase mixture was determined in the range 30–80°C. *PlaI* displays a maximum at 50°C and retains >70% of its activity in the range 30–60°C (Figure 2A). The pH activity profile displays a maximum at pH 5, along with a retention of more than 50% of the enzymatic activity in the pH range 4.5–7 (Figure 2B). The heterogeneity of the enzymatic mixture may explain the deviation from a bell-shaped behavior between pH 6 and 7 (Figure 2B). The biochemical properties exhibited by *PlaI* are in agreement with the characteristics reported for most of the purified fungal

inulinases, i.e., a pH optimum in a range 4–7 and a temperature optimum in the range 30–60°C (Rawat et al., 2017b).

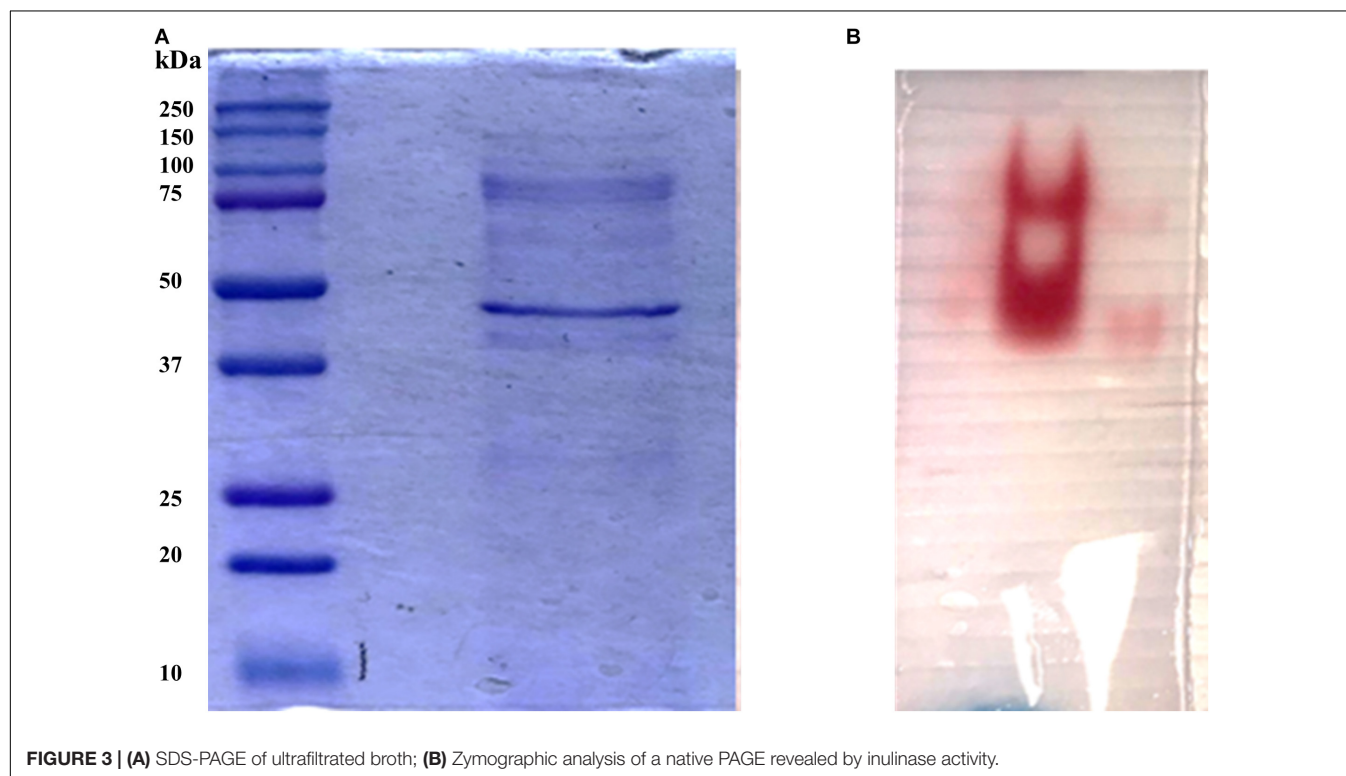
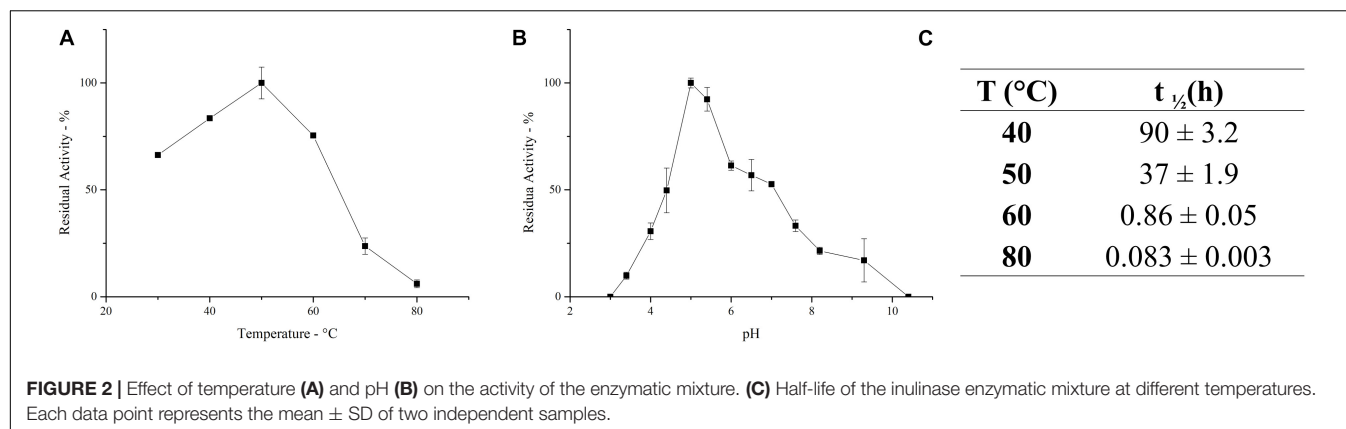
PlaI thermostability was evaluated at selected temperatures, and $t_{1/2}$ was calculated at each value (Figure 2C). The mixture shows a very good stability at 40°C, retaining its full activity up to 3 days of incubation. A reduction in thermal stability was observed at 50°C, although the enzymatic mixture still retains 50% of its activity after 37 h. The high activity of *PlaI* at 50°C, combined with the observed stability at this temperature, represents an extremely advantageous feature for inulin processing on an industrial scale, allowing the solubilization of inulin at high concentrations (Flores-Gallegos et al., 2015; Qiu et al., 2018). However, a drastic drop in enzyme stability was recorded at higher temperatures: at 60°C, the half-life of the enzymatic mixture is lower than 1 h, while at 80°C it sharply reduces to a few minutes.

Protein Characterization of the Inulinase Mixture

In order to identify the proteins endowed with inulinase activity, the *PlaI* enzymatic mixture was analyzed by zymography, by staining for inulinase activity (Figure 3). The two active protein bands were detected, excised, and analyzed by an *in situ* proteomic approach, and the proteins were identified by searching raw LC-MSMS data against the set of putative proteins encoded in the annotated *P. lanosocoeruleum* genome (see text footnote 2).

Table 2 reports the proteins identified in the two active bands (see Supplementary Material 2 for details of identified peptides). Several putative glycosyl hydrolase (GH) proteins of different families were identified in both bands. In the upper band in the gel, 10 proteins were identified; 9 proteins in the lower gel band. Three proteins (Protein ID: 323309; 417764; 371227) were found to be annotated as members of the GH32 family, with two of them present in both gel bands. When submitted to BlastP analysis, Penla1_323309 displays 74.8 and 72.7% identity with *Aspergillus fumigatus* InuD exoinulinase (Q4WDS4) and *Aspergillus lentulus* exoinulinase InuE (A0A0S7DXQ8), respectively, and is closely related to several other fungal exoinulinases. Penla1_417764 shows the highest identity (90.9%) with a putative GH32 hydrolase from *Penicillium rubens* as well as 63.4 and 62.5% identity with the exoinulinases InuE from *A. niger* (A2R0E0) and *A. awamori* (Q96TU3), respectively. From the multiple alignment with representative members of fungal exoinulinases, both Penla1_323309 and Penla1_417764 exhibit all the conserved motifs and residues characterizing this class of enzymes (Figure 4). Interestingly, the two putative *P. lanosocoeruleum* exoinulinases differ for the length of an internal sequence reported to function as an additional non-catalytic inulin-affinity region in *Penicillium* sp. TN-88 InuD, responsible for a higher affinity for the substrate (Moriyama and Ohta, 2007).

Penla1_371227, instead, resulted to be related to fungal endoinulinases, displaying 74.7 and 69.6% identities with *Penicillium subrubescens* endoinulinase Inu2 and *A. niger* InuA, respectively. Consistently, the Penla1_371227 sequence reveals the presence of all the conserved motifs and the unique aminoacidic residues described for fungal endoinulinases (Chikkerur et al., 2018; Singh et al., 2020a; Figure 4).



Inulin Hydrolysis by *Plal* Mixture Using Response Surface Methodology

An experimental design approach was applied to investigate the effect of different parameters on the *Plal*-catalyzed hydrolysis of inulin. In all the tested experimental conditions, inulin was efficiently converted into monomeric sugars (Table 3). ANOVA was used to determine the influence of independent variables on the dependent response. The *F* value, which substantiates the significance of the model, is 73.42, which is very high if compared to the critical value, thus indicating its significance (Supplementary Material 3). On the basis of a regression analysis, a second-order polynomial equation in terms of the coded value was generated:

$$\begin{aligned} \text{Fructose} = & -152.7 + 45.32 * A + 6.911 * B - 3.79 * C \\ & -0.256 * D - 0.211 * A * B - 0.140 * A * C + 0.047 * \\ & A * D + 0.031 * B * C - 0.006 * B * D + 0.007 * C * \\ & D - 2.885 * A^2 - 0.081 * B^2 + 0.038 * C^2 + 0.004 * D^2 \end{aligned}$$

where A is the pH; B, the temperature (°C); C, the substrate concentration (g L^{-1}); and D, the enzyme loading (U g^{-1}).

The significance of each parameter's coefficient was assessed by Prob > *F* value: values less than 0.05 indicate the significance of the model terms, and values greater than 0.1 depicts insignificance model terms. In the selected model, all the tested factors (A, B, C, D) have an effect on the hydrolysis process. The interaction effects between pH and temperature (*A*B*)

TABLE 2 | Protein identification in the active gel lanes by LC-MSMS.

Band gel lane	Protein ID	Score	Number of identified peptides	Protein sequence coverage (%)	Genome annotation
Lower gel band lane	323309	295	10	19	GH32 family/GH116 family
	371227	204	8	16	GH32 family
	376719	166	5	9	Multicopper oxidase
	327740	165	6	16	GH43 family
	383312	149	7	14	Glucosylglycosaccharide oxidase
	387674	122	6	10	GH64 family
	383083	120	5	16	GH17 family
	417764	111	4	7	GH32 family
	381496	62	5	11	Putative oxidoreductase
	384244	423	20	54	GMC oxidoreductase family
Upper gel band lane	315441	274	12	42	GH2 family
	400960	253	11	32	Uncharacterized protein
	371227	185	10	34	GH32 family
	385992	181	10	32	Amidase
	323309	177	12	33	GH32 family/GH116 family
	401322	99	7	18	GH20 family
	373946	147	11	28	GH3 family
	383654	145	11	31	Uncharacterized protein
	401322	99	7	18	GH20 family

Protein bands were in situ digested and analyzed by LC-MSMS, and raw data was searched on the protein database as described in details in the "Materials and Methods" section. Search details and extensive description of the identified peptides are reported in **Supplementary Material 2**. The proteins belonging to the Gh32 family are highlighted in bold.

Description of the glycosyl hydrolase (GH) families according to CAZypedia (<http://www.cazypedia.org/>): **GH2**: includes the following activities, β -galactosidases, β -glucuronidases, β -mannosidases, α - β -glucosaminidases, and a mannosylglycoprotein endo- β -mannosidase; **GH3**: groups together α -acting β -D-glucosidases, α -L-arabinofuranosidases, β -D-xylopyranosidases, N-acetyl- β -D-glucosaminidases, and N-acetyl- β -D-glucosaminide phosphorylases; **GH17**: includes two major groups of enzymes with related but distinct substrate specificities, namely, 1,3- β -D-glucan endohydrolases and 1,3;1,4- β -D-glucan endohydrolases; **GH20**: includes α -acting β -N-acetylglucosaminidases, β -N-acetylglucosaminidase β -6-SO₃-N-acetylglucosaminidases, and α -acting lacto-N-biosidases; **GH32**: includes: enzymes able to hydrolyze fructose containing polysaccharides, i.e., inulinases, invertases, levanases, and other; **GH43**: includes the following major activities, α -L-arabinofuranosidases, endo- α -L-arabinanases (or endo-processive arabinanases) and β -D-xylosidases; **GH64**: laminaripentaose-producing β (1,3)-glucanases; **GH116**: includes enzymes with diverse specificities, including β -xylosidase, β -glucosidase, and N-acetylglucosaminidase; **GMC oxidoreductase**: glucose dehydrogenase/choline dehydrogenase/mandelonitrile lyase.

and substrate concentration and temperature (B^*C) were also significant (**Supplementary Material 3**).

The quadratic terms of pH, temperature, and substrate concentration show significant contribution to the model. P -value < 0.0001 suggests that pH and temperature are the experimental variables with the greatest influence on inulin hydrolysis, and therefore a small variation in their value will strongly affect the product formation rate. Moreover, the negative sign of the coded coefficients A and B suggests that the curve is concave.

The P -value 0.008 for the quadratic substrate concentration term indicates an effect of this variable on the hydrolysis process, although less significant than that of the pH and T. The positive sign of the relative coefficient indicates that the curve is convex; thus, the uppermost is the substrate concentration, the higher is the amount of released fructose. On the contrary, the probability value of the coefficient of the quadratic effect of enzyme loading is very high (0.337), indicating that the quadratic model does not fit with the observed data. As a fact, the contribution of this parameter is better described by a linear model. The *Lack of Fit* F -value of a model is useful to describe the co-relation between response variable and independent factors. The fitness of our experimental model is proved by a non-significant *Lack of Fit* F -value (0.543). The goodness of the models is also confirmed by the determination ($R^2 = 0.98$) and adjusted determination

coefficients ($\text{Adj.}R^2 = 0.97$). Moreover, a difference < 0.2 between adjusted R^2 and predicted R^2 (0.95) values further substantiated the robustness of the model.

On the basis of this model, the optimal conditions to maximize inulin conversion (69.4 g L⁻¹ of fructose) are as follows: T, 45.4°C; pH, 5.1; substrate concentration, 60 g L⁻¹; enzyme loading, 50 U g_{substrate}⁻¹.

The three-dimensional surface plots display the interaction between two independent variables on the dependent variables (fructose), while keeping the other two independent variables at their respective optimal values (45.4°C, pH 5.1, inulin 60 g L⁻¹, and 50 U g_{substrate}⁻¹) (**Figure 5**). The 3D graph plots of the combined effect of temperature with three variables, i.e., pH, enzyme loading, and substrate concentration, suggest that there is an optimal temperature range between about 35 and 55°C in which the highest fructose concentration can be achieved (**Figures 5A,C,E**). Specifically, in this temperature range, the highest fructose release can be reached if pH is lower than 6. Consequently, a decrease in the response yield is observed out of this temperature range at pH > 6 (**Figure 5A**).

It is worth noting that, in the same optimal temperature range, the substrate concentration has a remarkable effect on the release of fructose, with the highest value was obtained at an increasing inulin amount (**Figure 5B**). Conversely, the combined effect of

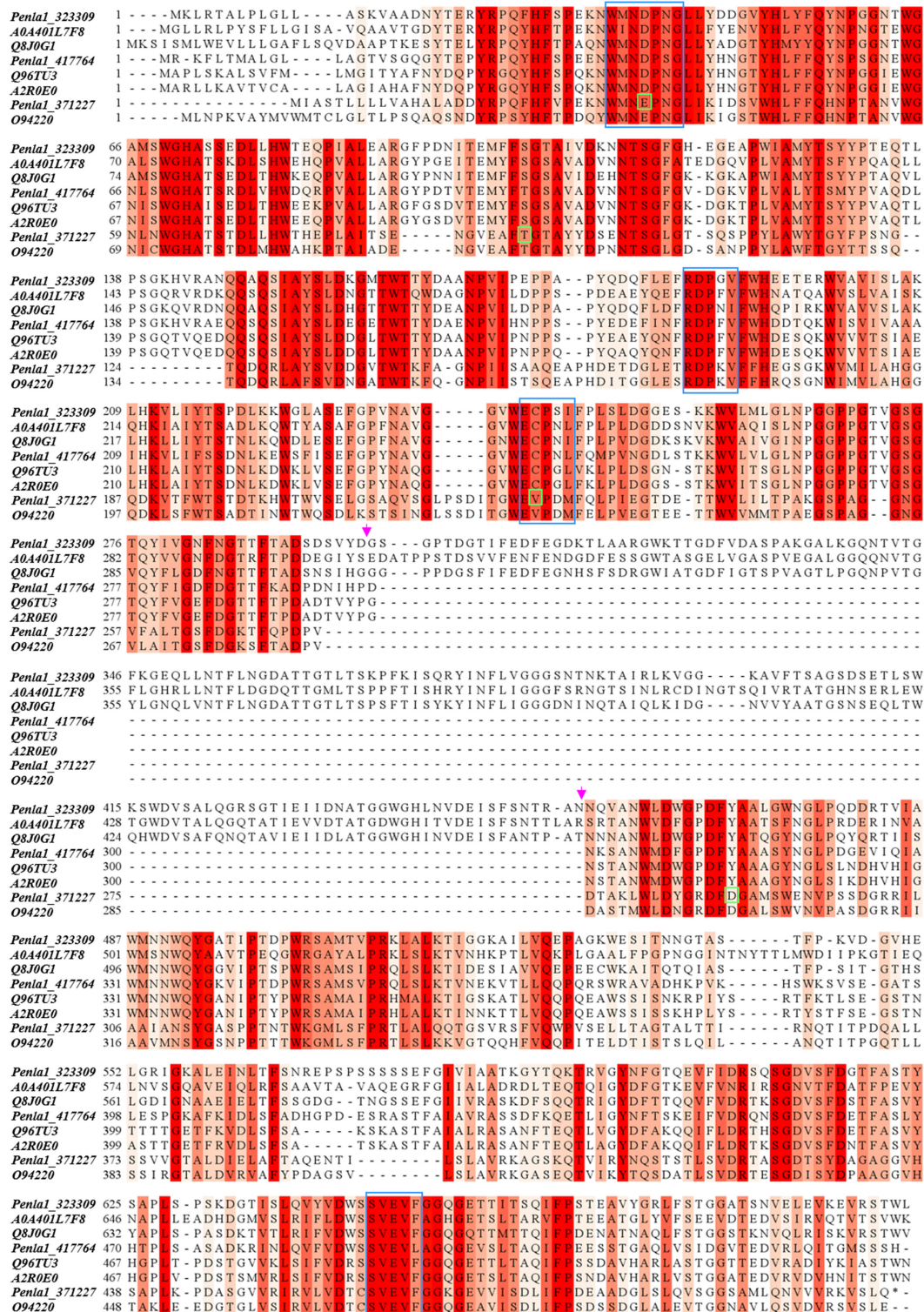


FIGURE 4 | Sequence alignment of identified *P. lanosocoeruleum* inulinases with representative members of fungal exo- and endo-inulinases. The following sequences were used in the alignment: A04401L7: exoinulinase from *Aspergillus awamori*; Q8J0G1: exoinulinase InuE from *Penicillium* sp. TN-88; Q96TU3: exoinulinase InuE from *Aspergillus awamori*; A2R0E0: exoinulinase InuE from *Aspergillus niger*; O94220: endoinulinase Inu2 from *Aspergillus ficuum*. The alignment was achieved using the CLUSTAL W program. Sequence conservation is shown in different shades of red. Conserved motifs of exoinulinases are highlighted by blue boxes; distinctive endoinulinase residues in green boxes. The pink arrows delimit the internal “inulin-affinity” region.

TABLE 3 | Enzymatic inulin conversion under the experimental conditions (pH, T, substrate concentration, and enzyme loading) explored in the CCRD.

	pH	°C	Substrate concentration (g L ⁻¹)	U g _{substrate} ⁻¹	Fructose (g L ⁻¹)	St. dev.	Conversion efficiency %
1	5	37.5	45	27.5	39.66	0.79	73.4
2	5	37.5	45	42.5	44.06	0.64	81.6
3	5	37.5	55	27.5	45.05	1.01	68.3
4	5	37.5	55	42.5	53.23	1.07	80.7
5	5	52.5	45	27.5	36.03	0.98	66.7
6	5	52.5	45	42.5	41.24	0.50	76.4
7	5	52.5	55	27.5	47.26	0.51	71.6
8	5	52.5	55	42.5	52.81	0.24	80.0
9	7	37.5	45	27.5	35.61	0.25	65.9
10	7	37.5	45	42.5	41.95	0.62	77.7
11	7	37.5	55	27.5	37.87	0.21	57.4
12	7	37.5	55	42.5	47.70	0.23	72.3
13	7	52.5	45	27.5	24.72	0.61	45.8
14	7	52.5	45	42.5	32.77	0.08	60.7
15	7	52.5	55	27.5	35.44	1.08	53.7
16	7	52.5	55	42.5	40.17	0.77	60.9
17	4	45	50	35	45.05	0.36	75.1
18	8	45	50	35	26.36	1.07	43.9
19	6	30	50	35	35.01	1.38	58.3
20	6	60	50	35	22.99	0.01	38.3
21	6	45	40	35	42.14	1.26	87.8
22	6	45	60	35	60.00	1.08	83.3
23	6	45	50	20	43.26	0.21	72.1
24	6	45	50	50	53.01	0.59	88.3
25	6	45	50	35	47.07	1.02	78.4
26	6	45	50	35	46.03	0.42	76.7

Fructose concentration has been determined after 24 h incubation. Conversion efficiency has been calculated as reported in the section "Enzymatic Hydrolysis of Inulin".

enzyme loading and temperature is not significant: at the optimal temperature, 45.4°C, more than 60 g L⁻¹ of fructose can be obtained even when lowering the enzyme amount from 50 to 30 U g_{substrate}⁻¹. Within the optimal temperature range, about 50–60 g L⁻¹ of fructose is released whatever is the amount of enzyme used (20–50 U g_{substrate}⁻¹) (**Figure 5C**).

The combined effect of pH and enzyme loading indicates that at the optimal pH (5.1) more than 60 g L⁻¹ of fructose is obtained using from 30 to 50 U g_{substrate}⁻¹. However, when moving far from the optimum, a comparable response is assured by increasing the enzyme loading (**Figure 5D**). Similarly to what was observed for temperature, a pH optimal range (4–6.5) can also be identified, within which an increasing amount of fructose can be obtained by increasing the substrate concentration (**Figure 5E**). Taking together all the observed effects, it can be assumed that within the optimal range of pH and T, fructose release can be adjusted by acting on enzyme and substrate concentrations (**Figure 5F**). Interestingly, in the investigated range of substrate concentration, from 40 to more than 60 g L⁻¹ of released fructose can be achieved by using an intermediate enzyme loading (30 U g_{substrate}⁻¹).

In order to validate the RSM model, experiments were carried out in the proximity of the estimated optimal conditions (**Table 4**). The predicted results were compared to the

experimentally obtained values, and the *T*-test at 95% confidence showed no significant differences between predicted and experimental values.

The ANOVA (*F*-test) applied to the experimental data resulted in an *F*-value of 21.64 and *R*² = 0.88. Thus, the proposed RSM model can be a useful tool to predict maximum inulin conversion.

The kinetics of inulin conversion in the optimized hydrolysis condition is reported in **Figure 6**. The release of fructose increases progressively to reach about 60% in the first 8 h. The 90% is achieved in 16 h, settling in a plateau level of 97% of conversion after 20 h. Experimental data were fitted with a third-order polynomial model. The goodness of the predictive models is confirmed by the determination coefficient (*R*² = 0.99).

Although the available literature data on inulin hydrolysis are not easily comparable because of the several variables affecting the process (source and amount of inulin, reaction conditions, determination of inulin conversion) (Sirisansaneeyakul et al., 2007; Mutanda et al., 2009; Saber and El-Nagg, 2009; Wang et al., 2013; Zheng et al., 2018a), the results obtained with *Plal* mixture are worth of notice, since an almost complete hydrolysis at high substrate concentration (60 g L⁻¹) was achieved in the optimized conditions. In a similar RSM-based approach, up to 95% fructose yield has been obtained by hydrolysis of 60 g L⁻¹ Jerusalem artichoke-derived inulin,

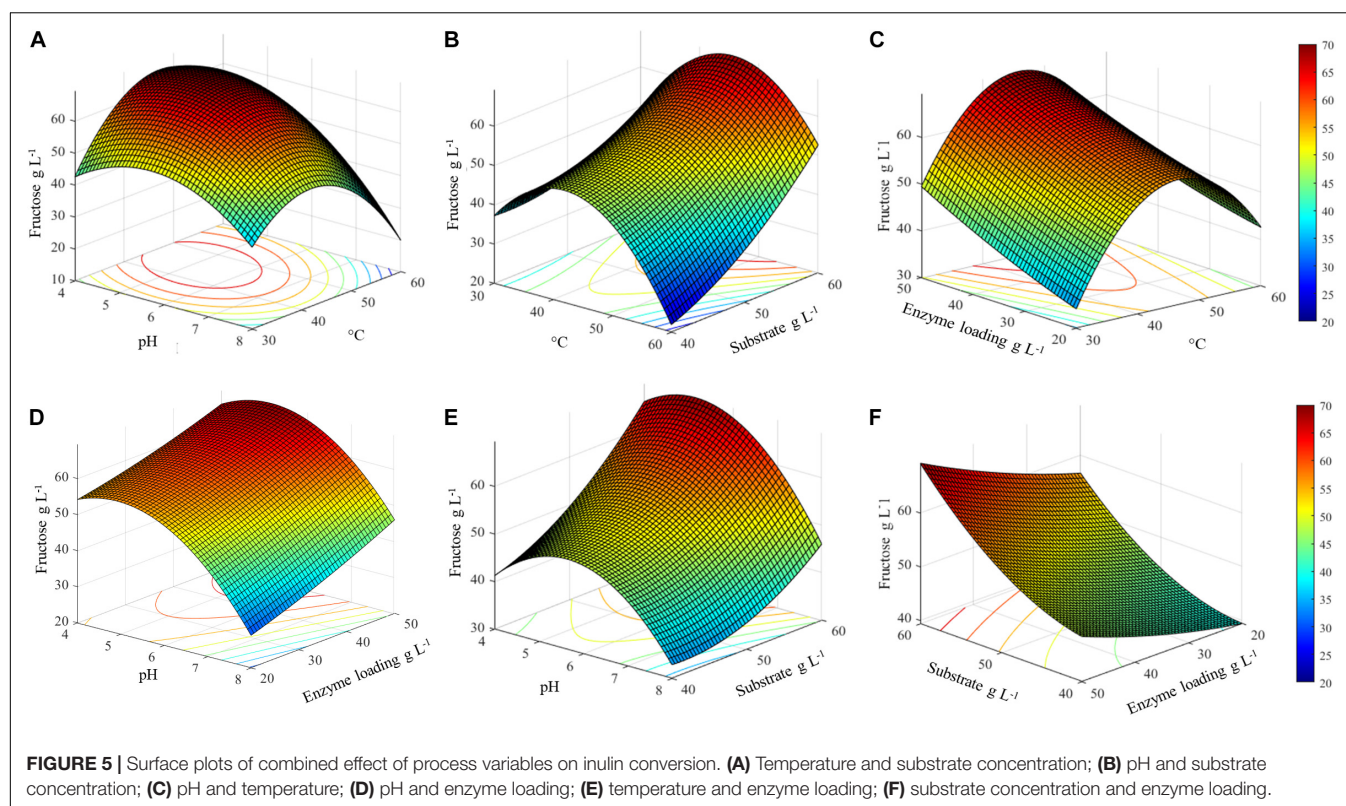


TABLE 4 | Model validation: predicted and experimental enzymatic inulin conversion around the estimated optimal conditions.

pH	Temperature°C	Substrate concentrationg L ⁻¹	Enzyme loadingU g _{substrate} ⁻¹	Fructose g L ⁻¹	
				Predicted	Experimental
5.1	45.5	60	50	69.4	69.8 ± 1.5
5.6	38.2	60	50	65.1	64.2 ± 0.8
4.3	46.6	60	50	67.1	66.4 ± 0.6

with a commercial *A. niger* inulinase (10 U/g⁻¹, 48°C, pH 4.8) (Sarchami and Rehmann, 2014). The definition of optimal T and pH for inulin hydrolysis by commercial Fructozyme (Novozyme) with an RSM approach has led to a fructose yield of 82.5% after 12 h at 35°C and pH 5.2, with 30 U/g⁻¹ of Jerusalem artichoke powder (Wang et al., 2013). Statistical optimization of inulin hydrolysis has been applied to immobilized inulinase from *A. tubingensis*, resulting, in the best conditions (60°C, 10 U/g⁻¹, 12 h), in a hydrolysis yield higher than 70 and 85% from chicory and asparagus inulin, respectively, both supplied at 17.5% (Trivedi et al., 2015). High conversion efficiency (up to 88%) in a short time (5 h) using *P. citrinum* inulinases has been also reported, by using a lower amount of inulin (10 g L⁻¹) and a very high enzyme loading (2,500 U g_{substrate}⁻¹) (El-Hersh et al., 2011). Similarly, a variable degree of hydrolysis, in the range 50–70%, has been shown by using a high amount of *A. tamarii* AR-IN9 inulinase (1,000–3,000 U/g) at 45°C, pH 5.2, after 2 h, depending on the agro-waste used as inulin source (Saber and El-Nagg, 2009).

Exploitation of *PlaI* Mixture in a Process for PHA Production From Inulin

The applicability of the *PlaI* mixture was tested in a combined process of inulin hydrolysis and PHA production by *C. necator* DSM428. Previous reports have shown that high PHB accumulation in *C. necator* has been achieved starting from an initial fructose concentration of 20 g L⁻¹ (Budde et al., 2011a; Koutinas et al., 2013). For the design of an SSF process, *PlaI* hydrolytic performances were preliminarily tested in conditions reproducing the *C. necator* culture media (MM_{Cn}, pH 6.8, 30°C) containing 20 g L⁻¹ inulin, corresponding to a maximum yield of 24 g L⁻¹ releasable fructose.

When different *PlaI* amounts (10, 20, 40, and 80 U g_{substrate}⁻¹) were tested, the amount of released fructose after 24 h of incubation increases linearly (2.4, 3.8, 7.4, and 10.3 g L⁻¹, respectively). However, all the obtained values were largely below the theoretical ones expected from a complete substrate hydrolysis. Inulinase activity measured in culture resulted to be reduced up to 42% of the initial one, indicating that both the pH

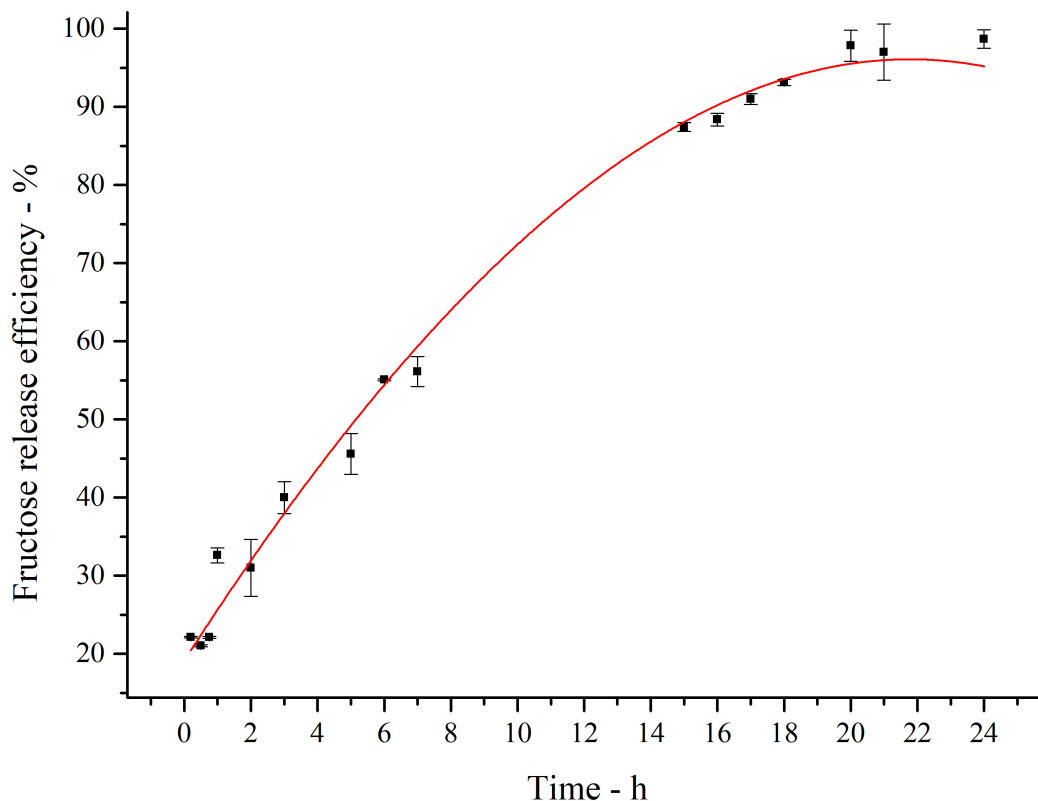


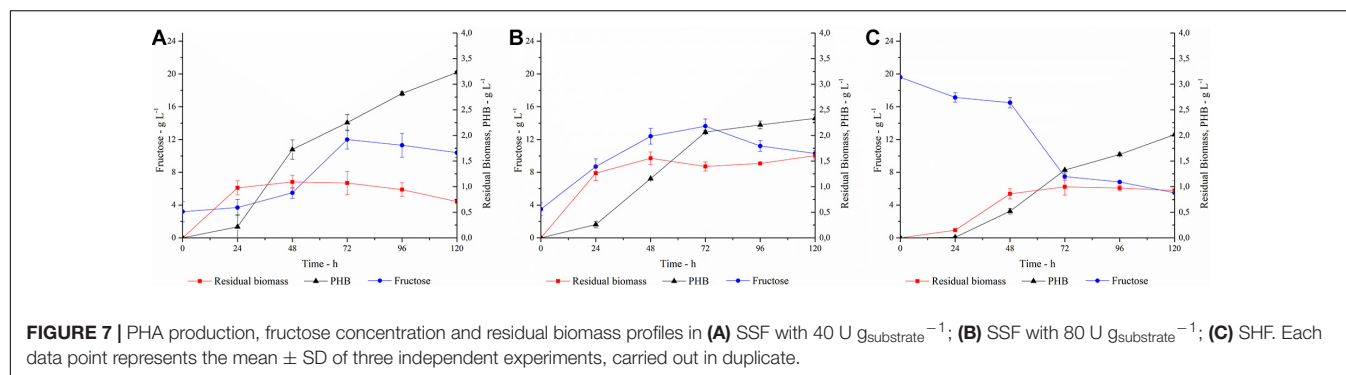
FIGURE 6 | Fitted curve plot of kinetics of inulin conversion in the optimized hydrolysis condition. Regression analysis was performed with OriginLab (OriginLab Corporation, Northampton, MA, United States). The determination coefficient for polynomial fit is $R^2 = 0.99$.

and salt concentration of the growth medium affected the *Plal* enzymatic activity.

In order to ensure an adequate amount of C-source for the microbial growth, the SSF process was carried out adding 40 $\text{U g}_{\text{substrate}}^{-1}$ (trial A) or 80 $\text{U g}_{\text{substrate}}^{-1}$ (trial B) of *Plal* to the culture medium containing 20 g L^{-1} inulin, and the process triggered with the simultaneous inoculation of *C. necator* (Figures 7A,B). About 3 g L^{-1} of fructose was measured at the zero time, the inoculum time, corresponding to the amount of free sugars present in the inulin substrate used in these trials.

In trial A, with a *Plal* concentration of 40 $\text{U g}_{\text{substrate}}^{-1}$, a slow increase in fructose concentration coupled to cellular growth was observed in the first 24 h, after which the cells entered the stationary phase. PHA accumulation started at 24 h and constantly increased during the stationary phase, reaching up to 3.2 g L^{-1} at 120 h, corresponding to 82% of polymer content. The fructose profile was monitored during the growth and reflects the simultaneity of the two processes, i.e., fructose release due to inulin hydrolysis and its consumption due to microbial growth. The rate of fructose release was higher than its consumption up to 72 h, determining an increase in fructose concentration. Conversely, after 72 h, fructose concentration slightly decreased, probably for a slowdown in the inulin hydrolysis, due to enzyme inactivation and/or inulin consumption. It is worth noting that the *Plal* mixture ensures a high level of fructose during the whole

process, supporting PHA accumulation, despite the unfavorable starting conditions of the growth media for its activity. Most likely, acidification of the culture media and salt consumption occurring during the microbial growth could help in restoring the conditions for optimal *Plal* activity. When the same process was carried out in the presence of 80 $\text{U g}_{\text{substrate}}^{-1}$ of *Plal* (Trial B), no increase in polymer accumulation was observed. As a fact, a maximum of 2.3 g L^{-1} PHA was achieved after 120 h, corresponding to a 60% polymer content. Thus, comparing the two SSF processes, a higher biomass accumulation was obtained in Trial B. The kinetic of polymer accumulation also followed a different trend in the presence of a higher *Plal* loading, displaying a rapid increase up to 72 h, reaching an almost stationary level at 120 h. Hence, a slower and more gradual release of fructose in Trial A seems to be more favorable for PHA accumulation. In both processes, the released glucose was not utilized as C-source, in agreement with data already reported for the same *C. necator* strain (Azubuike et al., 2019). In both trials, a residual fructose settled to about 10 g L^{-1} at the end of the process, probably due to the exhaustion of other medium components, such as N-source or oxygen, as already reported by Koutinas in 2013 (Koutinas et al., 2013). Further trials carried out using a higher inulin concentration in the growth medium (30 g L^{-1}) resulted in an overall inhibition of cellular growth, with about 0.8 g L^{-1} cdw at 120 h (data not shown). On the other hand, negligible



PHA production (0.032 g L⁻¹) and biomass levels (0.4 g L⁻¹) were obtained at 120 h, in a control experiment performed in the absence of *Plal*.

The SSF processes were compared to the SHF one (Trial C) where the best conditions for inulin hydrolysis, as determined by DOE, were applied and the resulting hydrolyzate was used as C-source for the PHA production process (Figure 7C). The pH of the hydrolyzate was adjusted to 6.8, and the fermentation was carried out with a C-source content of 2 g L⁻¹ and 20 g L⁻¹ for glucose and fructose, respectively. In this condition, the growth is characterized by a long lag phase, with fructose concentration decreasing slowly in the first 48 h. Polymer accumulation occurred in the stationary growth phase, reaching up to 2 g L⁻¹ after 120 h, corresponding to about 62% polymer content. As observed in Trial B, the availability of high fructose level in the first growth phase promotes a lower PHA accumulation with respect to the conditions that ensure a more gradual release of fructose (Trial A).

Only few examples have been reported so far on the use of inulin-rich biomasses as renewable feedstocks for PHA production (Koutinas et al., 2013; Haas et al., 2015). Koutinas et al. used ground Jerusalem artichoke tubers as substrate in solid-state fermentation of *Aspergillus awamori*, producing a crude enzymatic mixture that was later employed in the hydrolysis of the inulin extracted from the tubers. The crude hydrolyzate was tested as fermentation medium for PHB production from *C. necator*, achieving up to 52% of intracellular PHB content and a concentration of 4 g L⁻¹ of polymer (Koutinas et al., 2013). Similarly, Haas et al. described a process for the production of PHB from chicory root hydrolyzate using a commercially available inulinase mix of endo/exo-inulinases, comparing the performances of three different *C. necator* strains. Up to 78% PHB accumulation has been reported for the best-performing strain (Haas et al., 2015).

To our knowledge, this is the first example of SSF finalized to PHA production from inulin. Although it is well reported that the SSF strategy usually leads to superior productivity of the target product with respect to SHF, since it circumvents the inhibitory effect of high sugar concentration on cell growth (Ge et al., 2010; Li et al., 2014); it is worth noting that this process is effective only if fermentation conditions are also optimal for enzyme activity (Wang et al., 2013). The encouraging results obtained in shaken flasks represents a proof of concept of the exploitability of the

Plal mixture in the PHA production process by *C. necator*. It is expected that the implementation of the proposed SSF process in bioreactors, with fine controls of oxygen levels, will further improve its performance.

In all the conditions tested (Trials A, B, C), the polymer was extracted and analyzed by H-NMR. The spectra display the presence of three groups of characteristic signals of the homopolymer polyhydroxybutyrate (PHB) (Mostafa et al., 2020): the resonance peak at 1.2 ppm is attributed to the methyl group coupled to one proton; a doublet of quadruplet at 2.4 ppm is attributed to a methylene group adjacent to an asymmetric carbon atom bearing a single proton; and a multiplet at 5.2 ppm is characteristic of the methine group (Supplementary Material 4).

CONCLUSION

In this work, a new microbial source of inulinase, *P. lanosocoeruleum*, was identified by screening a fungal library. Three potentially active inulinases, two related to the exoinulinase and one to the endoinulinase families, were identified in the *Plal* enzymatic mixture.

The application of a statistical experimental design allowed to define the optimal conditions for inulin hydrolysis by *Plal*, leading to envisage its exploitation as effective biocatalyst mixture for inulin processing.

The optimal conditions defined for the hydrolysis could be exported and incorporated into a process for industrial fructose syrup production, since in these conditions the formation of undesired color as well as the production of unwanted by products such as fructose dianhydrides are prevented (Mutanda et al., 2009). Additionally, information on the isoenzymes composition of the *Plal* mixture represents the starting point for further characterization of the single isoenzymes, to be carried out through their purification from the culture broth or their recombinant expression in suitable hosts. The availability of each single isoenzyme will allow the formulation of inulinase mixtures with different composition in terms of endo- and exo- inulinase activities, addressing specific applications, such as the generation of fructose as well as of inulo-oligosaccharides (IOS) for applications as probiotics in food and pharmaceutical industries.

The integration of *Plal*-catalyzed hydrolysis within a fermentation process finalized to the production of added-value

bio-based products was tested, using PHA production as a case study. Two different process configurations, such as SHF and SSF, were explored, with the latter displaying the best performances in terms of biopolymer yields.

In conclusion, the results herein described let to foresee a profitable and versatile utilization of the *Plal* mixture in inulin-based biorefineries.

DATA AVAILABILITY STATEMENT

The original contributions presented in the study are included in the article/**Supplementary Material**, further inquiries can be directed to the corresponding author.

AUTHOR CONTRIBUTIONS

IC: investigation, DOE experiments, PHA production, and formal analysis. NC: investigation, screening of fungal library, and inulinase characterization. GN: proteomic analysis. CP: conceptualization and writing of original draft. LB: supervision.

REFERENCES

- Abd, A. A., Aty, E., Wehaidy, H. R., and Mostafa, F. A. (2014). Optimization of inulinase production from low cost substrates using Plackett - Burman and Taguchi methods. *Carbohydr. Polym.* 102, 261–268.
- Abd Allah AbdAl-Aziz, S., El-Metwally, M. M., and Ismail Ali Saber, W. E. (2012). Molecular identification of a novel inulinolytic fungus isolated from and grown on tubers of *Helianthus tuberosus* and statistical screening of medium components. *World J. Microbiol. Biotechnol.* 28, 3245–3254. doi: 10.1007/s11274-012-1134-y
- Azubuike, C., Edwards, M., Gatehouse, A., and Howard, T. P. (2019). Data driven modelling of a chemically defined growth medium for *Cupriavidus necator* H16. *bioRxiv* [Preprint], doi: 10.1101/548891
- Battaglia, E., Benoit, I., Brink, J., Van Den Wiebenga, A., Coutinho, P. M., Henrissat, B., et al. (2011). Carbohydrate-active enzymes from the zygomycete fungus *Rhizopus oryzae*: a highly specialized approach to carbohydrate degradation depicted at genome level. *BMC Genom.* 12:38. doi: 10.1186/1471-2164-12-38
- Bedzo, O. K. K., Mandegari, M., and Görgens, J. F. (2020). Techno-economic analysis of inuloooligosaccharides, protein, and biofuel co-production from *Jerusalem artichoke* tubers: a biorefinery approach. *Biofuels Bioprod. Bioref.* 14, 776–793. doi: 10.1002/bbb.2105
- Bhatia, S. K., Yoon, J. J., Kim, H. J., Hong, J. W., Gi Hong, Y., Song, H. S., et al. (2018). Engineering of artificial microbial consortia of *Ralstonia eutropha* and *Bacillus subtilis* for poly(3-hydroxybutyrate-co-3-hydroxyvalerate) copolymer production from sugarcane sugar without precursor feeding. *Bioresour. Technol.* 257, 92–101. doi: 10.1016/j.biortech.2018.02.056
- Bradford, M. M. (1976). A rapid and sensitive method for the quantitation of microgram quantities of protein utilizing the principle of protein-dye binding. *Anal. Biochem.* 72, 248–254.
- Budde, C. F., Riedel, S. L., Hübner, F., Risch, S., Popovici, M. K., Rha, C., et al. (2011a). Growth and polyhydroxybutyrate production by *Ralstonia eutropha* in emulsified plant oil medium. *Appl. Microbiol. Biotechnol.* 89, 1611–1619. doi: 10.1007/s00253-011-3102-0
- Budde, C. F., Riedel, S. L., Willis, L. B., Rha, C., and Sinskey, A. J. (2011b). Production of poly(3-hydroxybutyrate-co-3-hydroxyhexanoate) from plant oil by engineered *Ralstonia eutropha* strains. *Appl. Environ. Microbiol.* 77, 2847–2854. doi: 10.1128/AEM.02429-10
- Chen, J. S., Saxton, J., Hemming, F. W., and Peberdy, J. F. (1996). Purification and partial characterization of the high and low molecular weight form (S- and F-form) of invertase secreted by *Aspergillus nidulans*. *Biochim. Biophys. Acta Protein Struct. Mol. Enzymol.* 1296, 207–218. doi: 10.1016/0167-4838(96)00073-8
- Chi, Z., Chi, Z., Zhang, T., Liu, G., and Yue, L. (2009). Inulinase-expressing microorganisms and applications of inulinases. *Appl. Microbiol. Biotechnol.* 82, 211–220. doi: 10.1007/s00253-008-1827-1
- Chi, Z. M., Zhang, T., Cao, T. S., Liu, X. Y., Cui, W., and Zhao, C. H. (2011). Biotechnological potential of inulin for bioprocesses. *Bioresour. Technol.* 102, 4295–4303. doi: 10.1016/j.biortech.2010.12.086
- Chikkerur, J., Samanta, A. K., Dhali, A., Kolte, A. P., Roy, S., and Maria, P. (2018). In Silico evaluation and identification of fungi capable of producing endo-inulinase enzyme. *PLoS One* 13:e0200607. doi: 10.1371/journal.pone.0200607
- Chikkerur, J., Samanta, A. K., Kolte, A. P., Dhali, A., and Roy, S. (2020). Production of short chain fructo-oligosaccharides from inulin of chicory root using fungal Endoinulinase. *Appl. Biochem. Biotechnol.* 191, 695–715. doi: 10.1007/s12010-019-03215-7
- Choi, H. Y., Ryu, H. K., Park, K. M., Lee, E. G., Lee, H., Kim, S. W., et al. (2012). Direct lactic acid fermentation of *Jerusalem artichoke* tuber extract using *Lactobacillus paracasei* without acidic or enzymatic inulin hydrolysis. *Bioresour. Technol.* 114, 745–747. doi: 10.1016/j.biortech.2012.03.075
- El-Hersh, M. S., Saber, W. I. A., and Ali El-Nag, N. E.-A. (2011). Production strategy of inulinase by *Penicillium citrinum* AR-IN2 on some agricultural by-products. *Microbiol. J.* 1, 79–88. doi: 10.3923/mj.2011.79.88
- Fernandes, M. R. V. S., Nsabimana, C., and Jiang, B. (2012). *Penicillium expansum* SK 16 as a novel inulinase-producing strain isolated from decomposed dahlia tubers. *Res. J. Biotechnol.* 7, 102–106.
- Flores-Gallegos, A. C., Contreras-Esquivel, J. C., Morlett-Chávez, J. A., Aguilar, C. N., and Rodríguez-Herrera, R. (2015). Comparative study of fungal strains for thermostable inulinase production. *J. Biosci. Bioeng.* 119, 421–426. doi: 10.1016/j.jbiosc.2014.09.020
- Garuba, E. O., and Onilude, A. A. (2020). Exo-Inulinase Production by a catabolite repression-resistant mutant *Thermophilic Aspergillus tamarii* -U4 in solid state fermentation. *Biotechnol. J. Inter.* 24, 21–31. doi: 10.9734/BJI/2020/v24i430110
- Ge, X. Y., Qian, H., and Zhang, W. G. (2010). Enhancement of L-lactic acid production in *Lactobacillus casei* from *jerusalem artichoke* tubers by kinetic optimization and citrate metabolism. *J. Microbiol. Biotechnol.* 20, 101–109. doi: 10.4014/jmb.0905.05032
- Gonçalves, H. B., Jorge, J. A., and Guimarães, L. H. S. (2016). Production and characterization of an extracellular β -D-Fructofuranosidase from *Fusarium*

GS: supervision and funding acquisition. All authors contributed to the article and approved the submitted version.

FUNDING

This work was supported by grants from PRIN: Progetti di ricerca di Rilevante Interesse Nazionale – Bando 2017. “CARDoon valorisation by InteGrAted biorefinery (CARDIGAN).” IC acknowledges Università degli Studi di Napoli Federico II for doctoral fellowships. GN received funding from the Marie Skłodowska-Curie Grant Agreement No. 722606, TEMPERA (Teaching Emerging Methods in Palaeoproteomics for the European Research Area).

SUPPLEMENTARY MATERIAL

The Supplementary Material for this article can be found online at: <https://www.frontiersin.org/articles/10.3389/fbioe.2021.616908/full#supplementary-material>

- Graminearum* during solid-state fermentation using wheat bran as a carbon source. *J. Food Biochem.* 40, 655–663. doi: 10.1111/jfbc.12253
- Gujar, V. V., Fuke, P., Khardenavis, A. A., and Purohit, H. J. (2018). Draft genome sequence of *Penicillium chrysogenum* strain HKF2, a fungus with potential for production of prebiotic synthesizing enzymes. *3 Biotech.* 5, 5–9.
- Guzik, M., Witko, T., Steinbüchel, A., Wojnarowska, M., Sołtysik, M., and Wawak, S. (2020). What has been trending in the research of Polyhydroxyalkanoates? A systematic review. *Front. Bioeng. Biotechnol.* 8:959. doi: 10.3389/fbioe.2020.00959
- Haas, C., Steinwandter, V., De Apodaca, E. D., Madurga, B. M., Smerilli, M., Dietrich, T., et al. (2015). Production of PHB from chicory roots - comparison of three *Cupriavidus necator* STRAINS. *Chem. Biochem. Eng. Q.* 29, 99–112. doi: 10.15255/CABEQ.2014.2250
- Hughes, S. R., Qureshi, N., López-Núñez, J. C., Jones, M. A., Jarodsky, J. M., Galindo-Leva, L. A., et al. (2017). Utilization of inulin-containing waste in industrial fermentations to produce biofuels and bio-based chemicals. *World J. Microbiol. Biotechnol.* 33, 1–15. doi: 10.1007/s11274-017-2241-6
- Khatun, M. M., Liu, C. G., Zhao, X. Q., Yuan, W. J., and Bai, F. W. (2017). Consolidated ethanol production from *Jerusalem artichoke* tubers at elevated temperature by *Saccharomyces cerevisiae* engineered with inulinase expression through cell surface display. *J. Ind. Microbiol. Biotechnol.* 44, 295–301. doi: 10.1007/s10295-016-1881-0
- Koutinas, A. A., Garcia, I. L., Kopsahelis, N., Papanikolaou, S., Webb, C., Villar, M. A., et al. (2013). Production of fermentation feedstock from *jerusalem artichoke* tubers and its potential for polyhydroxybutyrate synthesis. *Waste Biomass Valoriz.* 4, 359–370. doi: 10.1007/s12649-012-9154-2
- Kumar, P., Maharjan, A., Jun, H. B., and Kim, B. S. (2019). Bioconversion of lignin and its derivatives into polyhydroxyalkanoates: challenges and opportunities. *Biotechnol. Appl. Biochem.* 66, 153–162. doi: 10.1002/bab.1720
- Laemmli, U. K. (1970). Cleavage of structural proteins during the assembly of the head of bacteriophage T4. *Nature* 227, 680–685.
- Lettera, V., Piscitelli, A., Leo, G., Birolo, L., Pezzella, C., and Sannia, G. (2010). Identification of a new member of *Pleurotus ostreatus* lacase family from mature fruiting body. *Fungal Biol.* 114, 724–730. doi: 10.1016/j.funbio.2010.06.004
- Li, L., Chen, C., Li, K., Wang, Y., Gao, C., Ma, C., et al. (2014). Efficient simultaneous saccharification and fermentation of inulin to 2,3-butanediol by thermophilic *Bacillus licheniformis* ATCC 14580. *Appl. Environ. Microbiol.* 80, 6458–6464. doi: 10.1128/AEM.01802-14
- Li, L., Li, L., Wang, Y., Du, Y., and Qin, S. (2013). Biorefinery products from the inulin-containing crop *Jerusalem artichoke*. *Biotechnol. Lett.* 35, 471–477. doi: 10.1007/s10529-012-1104-3
- Linn, R., Bonaduce, I., Ntasi, G., Birolo, L., Yasur-Landau, A., Cline, E. H., et al. (2018). Evolved gas analysis-mass spectrometry to identify the earliest organic binder in aegian style wall paintings. *Angew. Chem. Int. Edn.* 57, 13257–13260. doi: 10.1002/anie.201806520
- Mahmoud, D. A. R., Mahdy, E. S. M. E., Shousha, W. G., Refaat, H. W., and Abdel-Fattah, A. F. (2011). Raw garlic as a new substrate for inulinase production in comparison to dry garlic. *Aust. J. Basic Appl. Sci.* 5, 453–462.
- Mansouri, S., Houbraken, J., Samson, R. A., Frisvad, J. C., Christensen, M., Tuthill, D. E., et al. (2013). *Penicillium subrubescens*, a new species efficiently producing inulinase. *Antonie Leeuwenh. Int. J. Gen. Mol. Microbiol.* 103, 1343–1357. doi: 10.1007/s10482-013-9915-3
- Medeiros Garcia Alcántara, J., Distant, F., Storti, G., Moscatelli, D., Morbidelli, M., and Sponchioni, M. (2020). Current trends in the production of biodegradable bioplastics: the case of polyhydroxyalkanoates. *Biotechnol. Adv.* 42:107582. doi: 10.1016/j.biotechadv.2020.107582
- Meng, Q., Lu, C., Gao, H., Chen, G., Wu, L., Wu, J., et al. (2021). Efficient biosynthesis of exopolysaccharide from *Jerusalem artichoke* using a novel strain of *Bacillus velezensis* LT-2. *Bioresour. Technol.* 320:124346. doi: 10.1016/j.biortech.2020.124346
- Miller, G. L. (1959). Use of dinitrosalicylic acid reagent for determination of reducing sugar. *Anal. Chem.* 31, 426–428. doi: 10.1021/ac60147a030
- Moriyama, S., and Ohta, K. (2007). Functional characterization and evolutionary implication of the internal 157-amino-acid sequence of an exoinulinase from *Penicillium* sp. strain TN-88. *J. Biosci. Bioeng.* 103, 293–297. doi: 10.1263/jbb.103.293
- Mostafa, Y. S., Alrumman, S. A., Alamri, S. A., Otaif, K. A., Mostafa, M. S., and Alfaify, A. M. (2020). Bioplastic (poly-3-hydroxybutyrate) production by the marine bacterium *Pseudodonghicola xiamenensis* through date syrup valorization and structural assessment of the biopolymer. *Sci. Rep.* 10, 1–13. doi: 10.1038/s41598-020-65858-5
- Mutanda, T., Wilhelmi, B., and Whiteley, C. G. (2009). Controlled production of fructose by an exoinulinase from *Aspergillus ficuum*. *Appl. Biochem. Biotechnol.* 159, 65–77. doi: 10.1007/s12010-008-8479-6
- Nguyen, Q. D., Sujtő, N. M., Bujna, E., Hoschke, Á., and Rezessy-szabó, J. M. (2013). Effects of medium composition and process parameters on the production of extracellular inulinase by *Thermomyces lanuginosus*. *Food Technol. Biotechnol.* 51, 36–44.
- Pandey, A., Negi, S., and Soccol, C. R. (2016). *Current Developments in Biotechnology and Bioengineering: Production, Isolation and Purification of Industrial Products*. Amsterdam: Elsevier, doi: 10.1016/j.jclepro.2017.05.040
- Pessoni, R. A. B., and Braga, M. R. (2007). Purification and properties of exoinulinases from *Penicillium janczewskii* growing on distinct carbon sources purification and properties of exo-inulinases from *Penicillium janczewskii* growing on distinct carbon sources. *Mycologia* 99, 493–503. doi: 10.3852/mycologia.99.4.493
- Qiu, Y., Lei, P., Zhang, Y., Sha, Y., Zhan, Y., Xu, Z., et al. (2018). Recent advances in bio-based multi-products of agricultural *Jerusalem artichoke* resources. *Biotechnol. Biofuels* 11, 1–15. doi: 10.1186/s13068-018-1152-6
- Qiu, Y., Zhang, Y., Zhu, Y., Sha, Y., Xu, Z., Feng, X., et al. (2019a). Improving poly-(γ -glutamic acid) production from a glutamic acid-independent strain from inulin substrate by consolidated bioprocessing. *Bioproc. Biosyst. Eng.* 42, 1711–1720. doi: 10.1007/s00449-019-02167-w
- Qiu, Y., Zhu, Y., Zhan, Y., Zhang, Y., Sha, Y., Xu, Z., et al. (2019b). Systematic unravelling of the inulin hydrolase from *Bacillus amyloliquefaciens* for efficient conversion of inulin to poly-(γ -glutamic acid). *Biotechnol. Biofuels* 12, 1–14. doi: 10.1186/s13068-019-1485-9
- Rawat, H. K., Ganaie, M. A., and Kango, N. (2015a). Production of inulinase, fructosyltransferase and sucrase from fungi on low-value inulin-rich substrates and their use in generation of fructose and fructo-oligosaccharides. *Antonie Leeuwenh. Int. J. Gen. Mol. Microbiol.* 107, 799–811. doi: 10.1007/s10482-014-0373-3
- Rawat, H. K., Jain, S. C., and Kango, N. (2015b). Production and properties of inulinase from *Penicillium* sp. NFCC 2768 grown on inulin-rich vegetal infusions. *Biocatal. Biotransform.* 33, 61–68. doi: 10.3109/10242422.2015.1018188
- Rawat, H. K., Soni, H., Kango, N., and Kumar, C. G. (2017a). Continuous generation of fructose from *Taraxacum officinale* tap root extract and inulin by immobilized inulinase in a packed-bed reactor. *Biocatal. Agric. Biotechnol.* 9, 134–140. doi: 10.1016/j.bcab.2016.11.007
- Rawat, H. K., Soni, H., Treichel, H., and Kango, N. (2017b). Biotechnological potential of microbial inulinases: recent perspective. *Crit. Rev. Food Sci. Nutr.* 57, 3818–3829. doi: 10.1080/10408398.2016.1147419
- Raza, Z. A., Abid, S., and Banat, I. M. (2018). Polyhydroxyalkanoates: characteristics, production, recent developments and applications. *Int. Biodeterior. Biodegrad.* 126, 45–56. doi: 10.1016/j.ibiod.2017.10.001
- Saber, W. I. A., and El-Nagg, N. E. (2009). Optimization of fermentation conditions for the biosynthesis of inulinase by the new source; *Aspergillus tamarii* and hydrolysis of some inulin containing agro-wastes. *Biotechnology* 8, 425–433. doi: 10.3923/biotech.2009.425.433
- Samui, A. B., and Kanai, T. (2019). Polyhydroxyalkanoates based copolymers. *Int. J. Biol. Macromol.* 140, 522–537. doi: 10.1016/j.ijbiomac.2019.08.147
- Sarchami, T., and Rehmann, L. (2014). Optimizing enzymatic hydrolysis of inulin from *Jerusalem artichoke* tubers for fermentative butanol production. *Biomass Bioenergy* 69, 175–182. doi: 10.1016/j.biombioe.2014.07.018
- Sayed, R. Z., Gangurde, N. S., and Chincholkar, S. B. (2009). Hypochlorite digestion method for efficient recovery of PHB from *Alcaligenes faecalis*. *Indian J. Microbiol.* 49, 230–232. doi: 10.1007/s12088-009-0036-7
- Singh, N., Yadav, M., Khanna, S., and Sahu, O. (2017). Sustainable fragrance cum antimicrobial finishing on cotton: indigenous essential oil. *Sustain. Chem. Pharm.* 5, 22–29. doi: 10.1016/j.scp.2017.01.003

- Singh, R., and Chauhan, K. (2016). Production, purification, characterization and applications of fungal inulinases. *Curr. Biotechnol.* 7:19. doi: 10.2174/2211550105666160512142330
- Singh, R. S., and Chauhan, K. (2017). Inulinase production from a new inulinase producer, *Penicillium oxalicum* BGPUP-4. *Biocatal. Agric. Biotechnol.* 9, 1–10. doi: 10.1016/j.bcab.2016.10.012
- Singh, R. S., and Singh, R. P. (2010). Production of fructooligosaccharides from inulin by endoinulinases and their prebiotic potential. *Food Technol. Biotechnol.* 48, 435–450.
- Singh, R. S., and Singh, R. P. (2017). “18 - Inulinases,” in *Current Developments in Biotechnology and Bioengineering*, eds A. Pandey, S. Negi, and C. R. Soccol (Amsterdam: Elsevier), 423–446.
- Singh, R. S., Singh, T., Hassan, M., and Kennedy, J. F. (2020a). Updates on inulinases: structural aspects and biotechnological applications. *Int. J. Biol. Macromol.* 164, 193–210. doi: 10.1016/j.ijbiomac.2020.07.078
- Singh, R. S., Singh, T., and Pandey, A. (2020b). Fungal endoinulinase production from raw *Asparagus* inulin for the production of fructooligosaccharides. *Bioresour. Technol. Rep.* 10:100417. doi: 10.1016/j.biteb.2020.100417
- Singh, R. S., Singh, T., and Kennedy, J. F. (2021). Understanding the interactive influence of hydrolytic conditions on biocatalytic production of fructooligosaccharides from inulin. *Int. J. Biol. Macromol.* 166, 9–17. doi: 10.1016/j.ijbiomac.2020.11.171
- Singh, R. S., Singh, T., and Larroche, C. (2019). Biotechnological applications of inulin-rich feedstocks. *Bioresour. Technol.* 273, 641–653. doi: 10.1016/j.biortech.2018.11.031
- Sirisansaneeyakul, S., Worawuthiyanan, N., Vanichsriratana, W., Srinophakun, P., and Chisti, Y. (2007). Production of fructose from inulin using mixed inulinases from *Aspergillus niger* and *Candida guilliermondii*. *World J. Microbiol. Biotechnol.* 23, 543–552. doi: 10.1007/s11274-006-9258-6
- Surendran, A., Lakshmanan, M., Chee, J. Y., Sulaiman, A. M., Thuoc, D., and Van Sudesh, K. (2020). Can polyhydroxyalkanoates be produced efficiently from waste plant and animal oils? *Front. Bioeng. Biotechnol.* 8:169. doi: 10.3389/fbioe.2020.00169
- Trivedi, S., Divecha, J., Shah, T., and Shah, A. (2015). Rapid and efficient bioconversion of chicory inulin to fructose by immobilized thermostable inulinase from *Aspergillus tubingensis* CR16. *Bioresour. Bioprocess.* 2:32. doi: 10.1186/s40643-015-0060-x
- Tsang, Y. F., Kumar, V., Samadar, P., Yang, Y., Lee, J., Ok, Y. S., et al. (2019). Production of bioplastic through food waste valorization. *Environ. Int.* 127, 625–644. doi: 10.1016/j.envint.2019.03.076
- Vastano, M., Corrado, I., Sannia, G., Solaiman, D. K. Y., and Pezzella, C. (2019). Conversion of no/low value waste frying oils into biodiesel and polyhydroxyalkanoates. *Sci. Rep.* 9, 1–8. doi: 10.1038/s41598-019-50278-x
- Vinciguerra, R., Galano, E., Vallone, F., Greco, G., Vergara, A., Bonaduce, I., et al. (2015). Deglycosylation step to improve the identification of egg proteins in art samples. *Anal. Chem.* 87, 10178–10182. doi: 10.1021/acs.analchem.5b02423
- Vries, R. P., De Riley, R., Wiebenga, A., Aguilar-osorio, G., Amillis, S., Uchima, C. A., et al. (2017). Comparative genomics reveals high biological diversity and specific adaptations in the industrially and medically important fungal genus *Aspergillus*. *Genome Biol.* 18:28. doi: 10.1186/s13059-017-1151-0
- Wang, L., Xue, Z., Zhao, B., Yu, B., Xu, P., and Ma, Y. (2013). Jerusalem artichoke powder: a useful material in producing high-optical-purity L-lactate using an efficient sugar-utilizing thermophilic *Bacillus coagulans* strain. *Bioresour. Technol.* 130, 174–180. doi: 10.1016/j.biortech.2012.11.144
- Zhao, C. H., Cui, W., Liu, X. Y., Chi, Z. M., and Madzak, C. (2010). Expression of inulinase gene in the oleaginous yeast *Yarrowia lipolytica* and single cell oil production from inulin-containing materials. *Metab. Eng.* 12, 510–517. doi: 10.1016/j.ymben.2010.09.001
- Zheng, Z., Xu, Q., and Liu, P. (2018a). Enhanced inulin Saccharification by self-produced inulinase from a newly isolated *Penicillium* sp. and its application in D -Lactic acid production. *Appl. Biochem. Biotechnol.* 186, 122–131.
- Zheng, Z., Xu, Q., Liu, P., Zhou, F., and Ouyang, J. (2018b). Enhanced inulin saccharification by self-produced inulinase from a newly isolated *Penicillium* sp. and its application in d-Lactic acid production. *Appl. Biochem. Biotechnol.* 186, 122–131. doi: 10.1007/s12010-018-2730-6
- Zhong, Y., Godwin, P., Jin, Y., and Xiao, H. (2020). Biodegradable polymers and green-based antimicrobial packaging materials: a mini-review. *Adv. Ind. Eng. Polym. Res.* 3, 27–35. doi: 10.1016/j.aiepr.2019.11.002

Conflict of Interest: The authors declare that the research was conducted in the absence of any commercial or financial relationships that could be construed as a potential conflict of interest.

Copyright © 2021 Corrado, Cascelli, Ntasi, Birolo, Sannia and Pezzella. This is an open-access article distributed under the terms of the Creative Commons Attribution License (CC BY). The use, distribution or reproduction in other forums is permitted, provided the original author(s) and the copyright owner(s) are credited and that the original publication in this journal is cited, in accordance with accepted academic practice. No use, distribution or reproduction is permitted which does not comply with these terms.



Wasteful Azo Dyes as a Source of Biologically Active Building Blocks

Ana Fernandes¹, Bruna Pinto^{1,2}, Lorenzo Bonardo¹, Beatriz Royo¹, M. Paula Robalo^{2,3*} and Lígia O. Martins^{1*}

¹ Instituto de Tecnologia Química e Biológica António Xavier, Universidade Nova de Lisboa, Oeiras, Portugal, ² Área Departamental de Engenharia Química, Instituto Superior de Engenharia de Lisboa (ISEL), Instituto Politécnico de Lisboa, Lisbon, Portugal, ³ Centro de Química Estrutural, Complexo I, Instituto Superior Técnico, Universidade de Lisboa, Lisbon, Portugal

OPEN ACCESS

Edited by:

Giovanni Sanna,
University of Naples Federico II, Italy

Reviewed by:

Carla Silva,
University of Minho, Portugal
Madalina Tudorache,
University of Bucharest, Romania

*Correspondence:

Lígia O. Martins
lmartins@itqb.unl.pt
M. Paula Robalo
mprobalo@deq.isel.ipl.pt

Specialty section:

This article was submitted to
Industrial Biotechnology,
a section of the journal
Frontiers in Bioengineering and
Biotechnology

Received: 25 February 2021

Accepted: 04 May 2021

Published: 15 June 2021

Citation:

Fernandes A, Pinto B, Bonardo L,
Royo B, Robalo MP and Martins LO
(2021) Wasteful Azo Dyes as a Source
of Biologically Active Building Blocks.
Front. Bioeng. Biotechnol. 9:672436.
doi: 10.3389/fbioe.2021.672436

In this work, an environment-friendly enzymatic strategy was developed for the valorisation of dye-containing wastewaters. We set up biocatalytic processes for the conversion of azo dyes representative of the main classes used in the textile industry into valuable aromatic compounds: aromatic amines, phenoxazinones, phenazines, and naphthoquinones. First, purified preparations of PpAzoR azoreductase efficiently reduced mordant, acid, reactive, and direct azo dyes into aromatic amines, and CotA-laccase oxidised these compounds into phenazines, phenoxazinones, and naphthoquinones. Second, whole cells containing the overproduced enzymes were utilised in the two-step enzymatic conversion of the model mordant black 9 dye into sodium 2-amino-3-oxo-3*H*-phenoxazine-8-sulphonate, allowing to overcome the drawbacks associated with the use of expensive purified enzymes, co-factors, or exquisite reaction conditions. Third, cells immobilised in sodium alginate allowed recycling the biocatalysts and achieving very good to excellent final phenoxazine product yields (up to 80%) in water and with less impurities in the final reaction mixtures. Finally, one-pot systems using recycled immobilised cells co-producing both enzymes resulted in the highest phenoxazinone yields (90%) through the sequential use of static and stirring conditions, controlling the oxygenation of reaction mixtures and the successive activity of azoreductase (anaerobic) and laccase (aerobic).

Keywords: laccases, aromatic amines, whole-cell catalysis, phenazines, phenoxazinones, azoreductase

INTRODUCTION

More than 100,000 different recalcitrant synthetic dyes are currently used in the textile, food, paper, printing, leather, and cosmetics industries (Carmen and Daniela, 2012). It is estimated that around 10⁵ tonnes of dyes and dyestuff are released into the environment in the 200 billion litres of wastewaters, which result annually from the aforementioned industrial activities (Kant, 2012). Wastewaters containing dyes, from which 70% are azo dyes with one or more azo bonds (R₁-N-N-R₂), in addition to aesthetic problems, represent a liability since many azo dyes as well as their breakdown products are toxic and potentially mutagenic to living organisms (Rawat et al., 2016; Hassaan and Nemr, 2017).

The vast majority of dye-containing wastewater treatments rely on the use of physico-chemical methods, including precipitation, coagulation, and filtration (Pereira and Alves, 2012;

Vikrant et al., 2018). In spite of their recognised efficiency in decolourisation processes, they rely on the use of hazardous additives, produce large amounts of sludge, and are frequently not skilful for full wastewater detoxification. Biological treatment technologies are eco-friendly and cost-effective alternatives (Rai et al., 2005; Saratale et al., 2011; Khan et al., 2013). In particular, enzymatic processes are particularly attractive considering that biological decolourisation is assigned to the action of a limited number of enzymes: azoreductases, laccases, and peroxidases (Rodriguez-Couto, 2009; Mendes et al., 2015; Singh et al., 2015). Enzymatic processes are sustainable, eco-friendly, and particularly attractive considering their specificity for dye degradation while keeping intact valuable dyeing additives or fibres that can potentially be re-used, resulting in significant reductions in water consumption. At present, treatment of dye-containing wastewaters is mostly focused in their remediation; however, the implementation of appropriate approaches has potential to couple the degradation of dyes to their conversion into valuable chemicals. This is in line with the principles of circular economy emphasising the urgency to design out waste and pollution, keep products, and materials in use and regenerate natural systems (Geissdoerfer et al., 2017; Lange et al., 2021).

In a previous work, we showed that the coupled action of PpAzoR azoreductase from *Pseudomonas putida* MET94 and CotA-laccase from *Bacillus subtilis* resulted in the decolourisation as well as in the detoxification of a large array of structurally diverse azo dyes and model wastewaters (Mendes et al., 2011a). Herein, we report the coupled action of these enzymes in the valorisation of azo dyes commonly present in wastewaters. Azoreductases are highly effective in decolourising azo dyes yielding aromatic amines, building blocks in different industries, including agrochemical, fine chemical, and pharmaceutical. CotA-laccase oxidises a wide range of aromatic amines with different substitution patterns (*ortho*-phenylenediamines, substituted *para*-phenylenediamines, and *ortho*-amino-phenols, among others) that are precursors of dimeric and trimeric dyes as well as of substituted heterocyclic frameworks (phenazine, phenoxazinone, and carbazole derivatives), multifunctional and versatile building blocks widely distributed in a vast array of biologically active compounds (Martins et al., 2020). The five dyes used in this study, namely, mordant black 9 (MB9), mordant black 3 (MB3), acid red 266 (AR266), reactive yellow 145 (RY145), and direct red 80 (DR80), were chosen as they represent the most common classes of azo dyes used in the textile industry, for example, in cotton and wool-dyeing processes (Carmen and Daniela, 2012), and also because we had previous results showing that the sequential treatment with PpAzoR and CotA-laccase results in maximal decolourisation and detoxification levels (Mendes et al., 2011a).

In this work, we have identified, using NMR spectroscopy, the aromatic amines resulting from azo dye degradation by the PpAzoR azoreductase, and the heterocyclic products (phenazines, phenoxazinones, and naphthoquinones) that resulted from the oxidation of these aromatic amines with CotA-laccase. We have optimised using the MB9 azo dye, two-step and one-pot bioprocesses using free and immobilised *Escherichia coli* cells that have overproduced the enzymes of interest, resulting

in reactions performed in water and at mild conditions of temperature, which led to 90% phenoxazine conversion yields.

MATERIALS AND METHODS

Chemicals

All chemicals and solvents were obtained from commercial suppliers and were used without further purification. The dyes used in this study were as follows: MB9 (λ_{max} = 550 nm; purity of 48%), MB3 (λ_{max} = 550 nm; purity of 40%), AR266 (λ_{max} = 470 nm; purity of 30%), RY145 (λ_{max} = 420 nm; purity of 50%), and DR80 (λ_{max} = 530 nm; purity of 50%). MB9 was purchased from DyStar Textilfarben (Frankfurt, Germany) and MB3 from Honeywell Fluka (Bucharest, Romania); and AR266, RY145, and DR80 were purchased from Town End (Leeds, United Kingdom).

Bacterial Strains and Plasmids

Escherichia coli strain DH5 α (Novagen, Madison, WI, United States) was used for routine propagation and amplification of plasmid constructs; and *E. coli* Tuner (DE3, Novagen), *E. coli* KRX (Promega, Madison, WI, United States), and *E. coli* BL21 star (DE3, Novagen) were tested as host of plasmids for gene expression. Three plasmids were used: pLOM10, coding for CotA-laccase from *B. subtilis* (Martins et al., 2002); pVB-8, coding for the evolved variant 2A1-Y179H of *P. putida* MET94 PpAzoR (Brissos et al., 2014); and pAIF-2, a pET-Duet-1 construct, coding for both wild-type PpAzoR and CotA-laccase genes (Mendes et al., 2011a).

Preparation of Purified Enzymes and Whole-Cell Systems

Escherichia coli recombinant cells overproducing the enzymes of interest were cultivated in Luria-Bertani (LB) media supplemented with 100 $\mu\text{g ml}^{-1}$ of ampicillin following previously described procedures (Durao et al., 2008; Mendes et al., 2011b). The cells were harvested by centrifugation (8,000 \times g, 10 min, 4°C) and washed with 0.9% (w/v) NaCl.

- (i) For reactions using purified enzymes, cells were disrupted using a French press, cell debris were removed by centrifugation (18,000 \times g, 2 h, 4°C), and enzymes were purified from supernatants using well-established chromatographic methods (Bento et al., 2005; Mendes et al., 2011b). CotA-laccase activity was determined at 37°C using 0.1 mM of ABTS as substrate (ϵ_{420} = 36,000 $\text{M}^{-1} \text{cm}^{-1}$) in 0.1 M of sodium acetate buffer, pH 4.3. The activity of PpAzoR azoreductase was measured in 0.1 M of sodium phosphate buffer, pH 7, using 0.1 mM of anthraquinone-2-sulphonate (AQS) and 0.25 mM of β -nicotinamide adenine dinucleotide phosphate (NADPH; ϵ_{340} = 6,200 $\text{M}^{-1} \text{cm}^{-1}$) at 42°C. One unit (U) of enzymatic activity was defined as the amount of enzyme required to convert 1 μmol of substrate per min. Aliquots of purified enzymes were stored at -20°C prior to use. The protein concentration was determined

using the Bradford assay with bovine serum albumin as the standard.

- (ii) For reactions with free and immobilised whole cells, *E. coli* cells were suspended in distilled water, the optical density was measured at 600 nm (OD_{600}), aliquots of cell suspensions containing around 300-mg dry cell weight (DCW) were centrifuged, and pellets stored at -20°C prior to use. A calibration curve of OD_{600} versus DCW (mg ml^{-1}) after drying cell suspensions (at different OD_{600}) at 100°C until no variation in weight was previously performed. Immobilisation was performed after suspending cell pellets (300- or 600-mg DCW) in 2 ml of a 2% sodium alginate solution, followed by dropwise addition to a 0.15 M of CaCl_2 solution under continuous stirring. The spheres were left to solidify for 90 min, then were washed with distilled water, and stored at 4°C until use.

Two-Step Enzymatic Bioprocess Using Enzymes

The first step of bioconversion of dyes using purified PpAzoR azoreductase was performed in serum bottles (20 ml) containing 2 mM of β -nicotinamide adenine dinucleotide hydrogen (NADH) and 0.8–1.0 mM of azo dyes (MB9, MB3, AR266, RY145, and DR80) in 0.1 M of sodium phosphate buffer, pH 7, made anaerobic by nitrogen bubbling followed by sealing with rubber stoppers. The 10-ml mixtures were incubated at 30°C , and reactions were started by adding 5 U ml^{-1} of an anoxic preparation of purified enzyme. Decolourisation was monitored at the maximum wavelength of each dye. When decolourisation was $\geq 85\%$, reaction mixtures were transferred to a 50-ml Erlenmeyer flask, 1 U ml^{-1} of CotA-laccase was added, and these were shaken at 180 rpm at 37°C for 24 h.

Two-Step Enzymatic Bioprocess Using Free and Immobilised Whole Cells

The first PpAzoR catalysed step was performed in 5 ml of water or 20 mM of sodium phosphate buffer (pH 7) at 30°C in the presence of free or immobilised cells (60 or 120 mg DCW ml^{-1}). Reactions were started by the addition of MB9 to a final concentration of 0.96 mM. Decolourisation was monitored at 550 nm (λ_{max} for MB9). After decolourisation levels reached values higher than 85% (~ 24 h of reaction), mixtures were shaken at 180 rpm, at 37°C , for an additional period of 24 h. Recycled biocatalysts were tested for the first enzymatic step, as follows: after 24 h of reaction, 5 ml of 0.96 mM of MB9 was added to the reaction mixture. This procedure was repeated four times in 24-h periods up to a maximum of 96 h. After this time, the second step with CotA-laccase was performed as described above. The products of reactions after the first and second enzymatic steps were quantified by high-performance liquid chromatography (HPLC) using a calibration curve performed with an isolated final compound (please see below). Each experience was performed at least five times, and standard deviations were lower than 15%.

Product Characterisation

UV-visible spectra of substrates and reaction mixtures were obtained on a Nicolet Evolution 300 spectrophotometer (Thermo Fisher Scientific, Waltham, MA, United States). Decolourisation was assessed by measuring the absorbance of reaction mixtures at the wavelength of maximal absorbance for each dye tested [decolourisation (%) = $(\text{Abs initial} - \text{Abs final}) / \text{Abs final} \times 100$]. For the identification of products, reaction mixtures were lyophilised, suspended in appropriate deuterated solvent, and analysed by NMR. ^1H - and ^{13}C -NMR spectra were obtained at room temperature with an Advance Bruker 400 MHz spectrometer (Billerica, MA, United States) in $\text{CD}_3\text{OD}-d_4$ or D_2O solvents (see **Supplementary Table 1**). The chemical shifts are reported in part per million (ppm) using the solvent signal as internal reference. The final product of MB9 conversion, after the sequential action of PpAzoR and CotA-laccase, was separated and collected by HPLC, and its molecular extinction coefficient was determined in the concentration range of 0.05–0.8 mM at 430 nm using a Synergy 2, BioTek (Winooski, VT, United States) microplate reader. For the quantification of products of reactions using MB9, samples of reaction were centrifuged and analysed by HPLC on a Waters Alliance 2695 equipped with a Waters photodiode array detector. The separations were performed in a Purospher STAR RP-18e column (250 mm \times 4 mm), 5- μm particle size (Merck, KGaA, Gernsheim, Germany). The injection volume was 60 μl , and the flow rate was 0.8 ml min^{-1} at a column oven temperature of 40°C . Eluent A was 0.1 M of ammonium acetate pH 6.7, and eluent B was a mixture of methanol:acetonitrile (70:30, v/v). The following gradient was used for products separation: 0–2 min, isocratic elution of 100% eluent A; 2–16 min, linear gradient from 100 to 60% of eluent A; 16–24 min, linear gradient from 60 to 45% of eluent A; 24–28 min, linear gradient from 45 to 20% of eluent A; 28–32 min, isocratic elution of 20% eluent A; 32–30 min, linear gradient from 20 to 100% of eluent A; and 33–43 min, equilibrium to the initial conditions of the following injection.

RESULTS AND DISCUSSION

Two-Step Bioconversion of Dyes Using Purified Enzymes

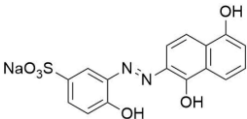
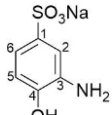
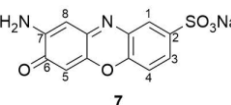
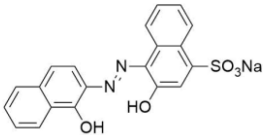
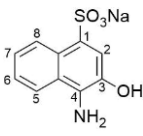
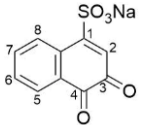
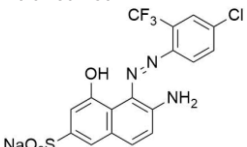
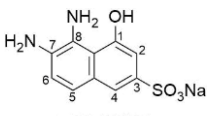
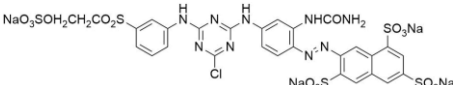
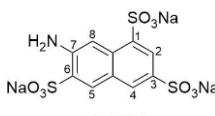
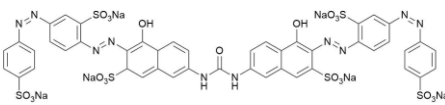
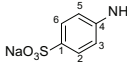
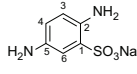
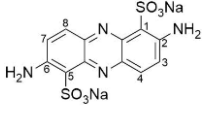
The reactions of PpAzoR azoreductase, with the five azo dyes, were performed under anaerobic conditions and yielded decolourisation levels above 85% after 24 h of reaction as assessed by UV-Vis at the λ_{max} of each dye (**Table 1**). The final reaction mixtures were analysed by ^1H -NMR spectroscopy (in $\text{CD}_3\text{OD}-d_4$; **Figure 1** and **Supplementary Figures 1–4**), which indicated the complete disappearance of the initial dyes and the presence of aromatic amines as well as NAD^+ , the oxidation product of NADH and other compounds derived from the NADH/ NAD^+ degradation. In the reduction of the MB9 by the PpAzoR one aromatic amine, SAHBS was detected in the ^1H -NMR spectrum (**Figure 1C,b**), similarly to the other dyes where only one of the two expected amines was identified (**Supplementary Table 2**), except in the case of DR80 dye, where two of the three expected

amines were identified (Table 1). SAHNS, 2 (Supplementary Figure 1C), SDAHNS, 3 (Supplementary Figure 2C), and SANTS, 4 (Supplementary Figure 3C) are products of the reaction with MB3, AR266, and RY145, respectively; and SABS, 5, and SDBS, 6 (Supplementary Figure 4C) are from the reaction with DR80. The absence of some expected amines in the reaction mixtures is attributed to their autooxidation, upon exposure to oxygen, leading to the production of unstable forms and further involvement in oligomeric or polymeric reactions, as previously reported (Kudlich et al., 1999; Pinheiro et al., 2004; Carvalho et al., 2008).

The second step of the biotransformation was initiated upon addition of CotA-laccase and set-up of aerobic conditions (Martins et al., 2002). The oxidation of SAHBS (1), the PpAzoR product from the MB9 dye, resulted in the formation of the coloured sodium 2-amino-3-oxo-3H-phenoxazine-8-sulphonate

(7) (Forte et al., 2010). The oxidation of compound 2, the PpAzoR product from MB3, led to the formation of *ortho*-naphthoquinone (8) (Sousa, 2015). Considering the enzymatic pathway proposed for the oxidation of *ortho*-aminophenol derivatives mediated by CotA-laccase, the *ortho*-quinone core can be obtained through a hydrolysis process of the *ortho*-quinoneimine intermediate formed during CotA-laccase oxidation (Sousa et al., 2014). The CotA-laccase oxidation of the SDAHNS (3), obtained from AR266, originates a complex mixture of products, resulting from putative reoxidation, polymerisation, or hydrolysis processes, which impaired their full characterisation. For RY145, the analysis of the mixture after the second enzymatic oxidative step showed that amine (4) is not a substrate of CotA-laccase probably due to the presence of the three electron-withdrawing sulphonate groups, thereby decreasing the electron density in the naphthalenic structure

TABLE 1 | Dyes used in this study and products obtained after reaction with the PpAzoR azoreductase (1st step) and CotA-laccase (2nd step), as identified by NMR spectroscopy.

Azo dye	Decolourisation after 1 st step (%)	Products		
		1 st step	2 nd step	
Mordant black 9 	90 ± 2	 1 (SAHBS)	 7	
Mordant black 3 	85 ± 4	 2 (SAHNS)	 8	
Acid red 266 	87 ± 1	 3 (SDAHNS)	ND	
Reactive yellow 145 	90 ± 3	 4 (SANT)	nd	
Direct red 80 	96 ± 2	 5 (SABS)	 6 (SDBS)	 9

SAHBS, sodium 3-amino-4-hydroxybenzene-1-sulphonate; SAHNS, sodium 4-amino-3-hydroxynaphthalene-1-sulphonate; SDAHNS, sodium 5,6-diamino-4-hydroxynaphthalene-2-sulphonate; SANTS, sodium 7-aminonaphthalene-1,3,6-trisulphonate; SABS, sodium 4-aminobenzene-1-sulphonate; SDBS, sodium 2,5-diaminobenzene sulphonate; ND, not determined; nd, not detected.

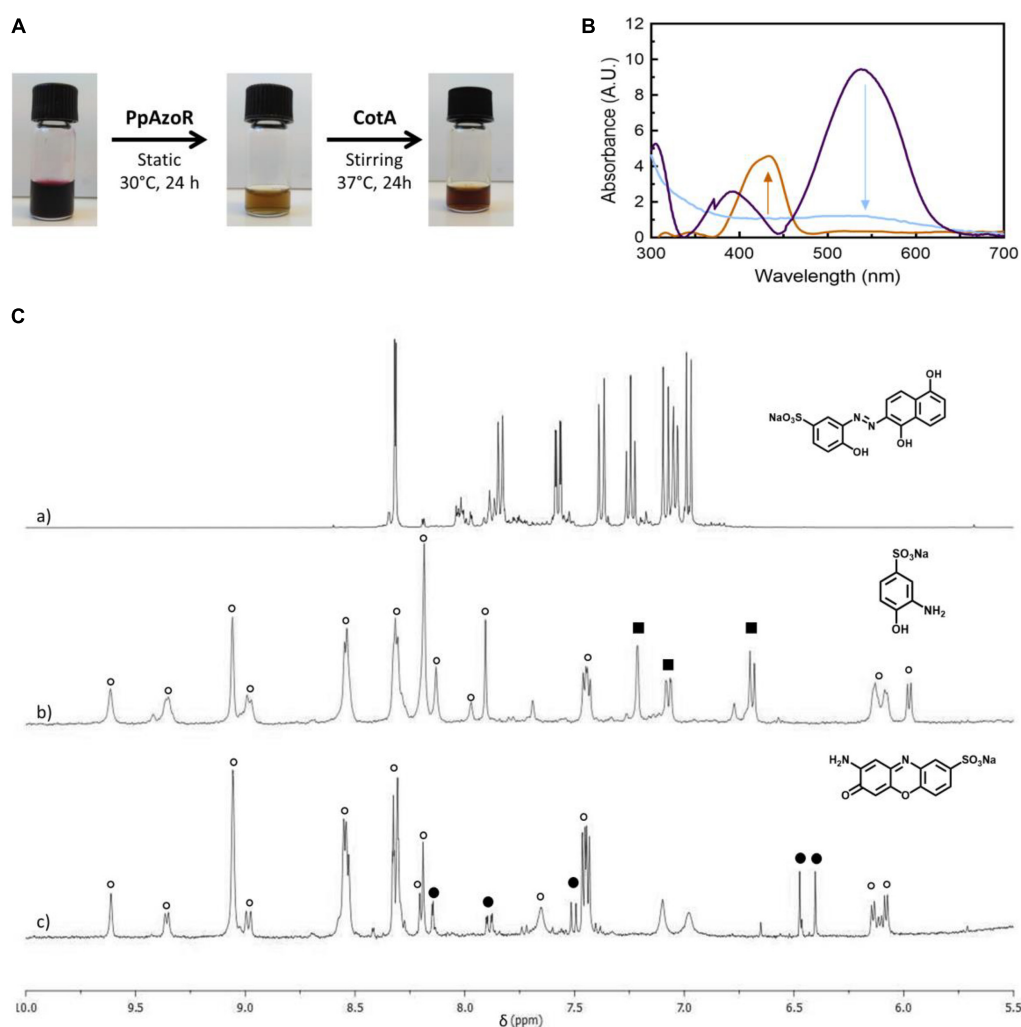


FIGURE 1 | (A) Products of the MB9 bioconversion upon the sequential reaction with purified PpAzoR azoreductase and CotA-laccase, under anaerobic and aerobic conditions, respectively. **(B)** UV-Vis spectra of the initial reaction mixture (purple) and after reaction with PpAzoR azoreductase (light blue) and CotA-laccase (light brown). **(C)** ¹H-NMR spectra (aromatic region) of MB9 **(a)** and of the products of reaction after addition of PpAzoR azoreductase **(b)** and CotA-laccase **(c)**. Resonances due to NAD⁺ and other intermediates resulting from NADH/NAD⁺ degradation (open circles), SAHBS (filled squares), and compound 7 (filled circles) are labelled.

and making the amine group less favourable to oxidation (Sousa et al., 2013). The mixture obtained by CotA-laccase oxidation of amines SABS (5) and SDBS (6) reveals the presence of a coloured phenazine (9), obtained from the self-coupling reaction of SDBS (Sousa et al., 2014), while SABS (5) due to the presence of the electron-deficient sulphonate group in the *para* position is not a CotA-laccase substrate (Sousa et al., 2013). Overall, our results show that the sequential use of PpAzoR and CotA results in the conversion of all azo dyes into structurally different building blocks, aromatic amines, naphthoquinones, phenoxazinones, and phenazines. These are biological active motifs of antibiotics (McDonald et al., 1999), antitumor agents (Corona et al., 2009; Vairavelu et al., 2014), and pesticides (Piro et al., 2013). They are also useful precursors for the manufacturing of pharmaceuticals (Cholo et al., 2012), fine chemicals (Forte et al., 2010; Morel and Christie, 2011), and

biosensors (Piro et al., 2013). Furthermore, synthetic chemical approaches for the synthesis of these heteroaromatic compounds use stoichiometric amounts of chemicals, strong acids, and high temperatures and result in low production yields (Shruti et al., 2018). In order to set up not only environment-friendly but also cost-effective processes, we performed dye conversion assays using free and immobilised whole-cell systems that overproduced the enzymes of interest.

Set-Up of Free and Immobilised Whole-Cell Systems

Whole-cell bioprocesses are very advantageous since they reduce operational costs associated with enzyme purification and the supply of expensive co-factors such as NAD(P)H, which is recycled by the metabolism of resting cells (Carvalho, 2016;

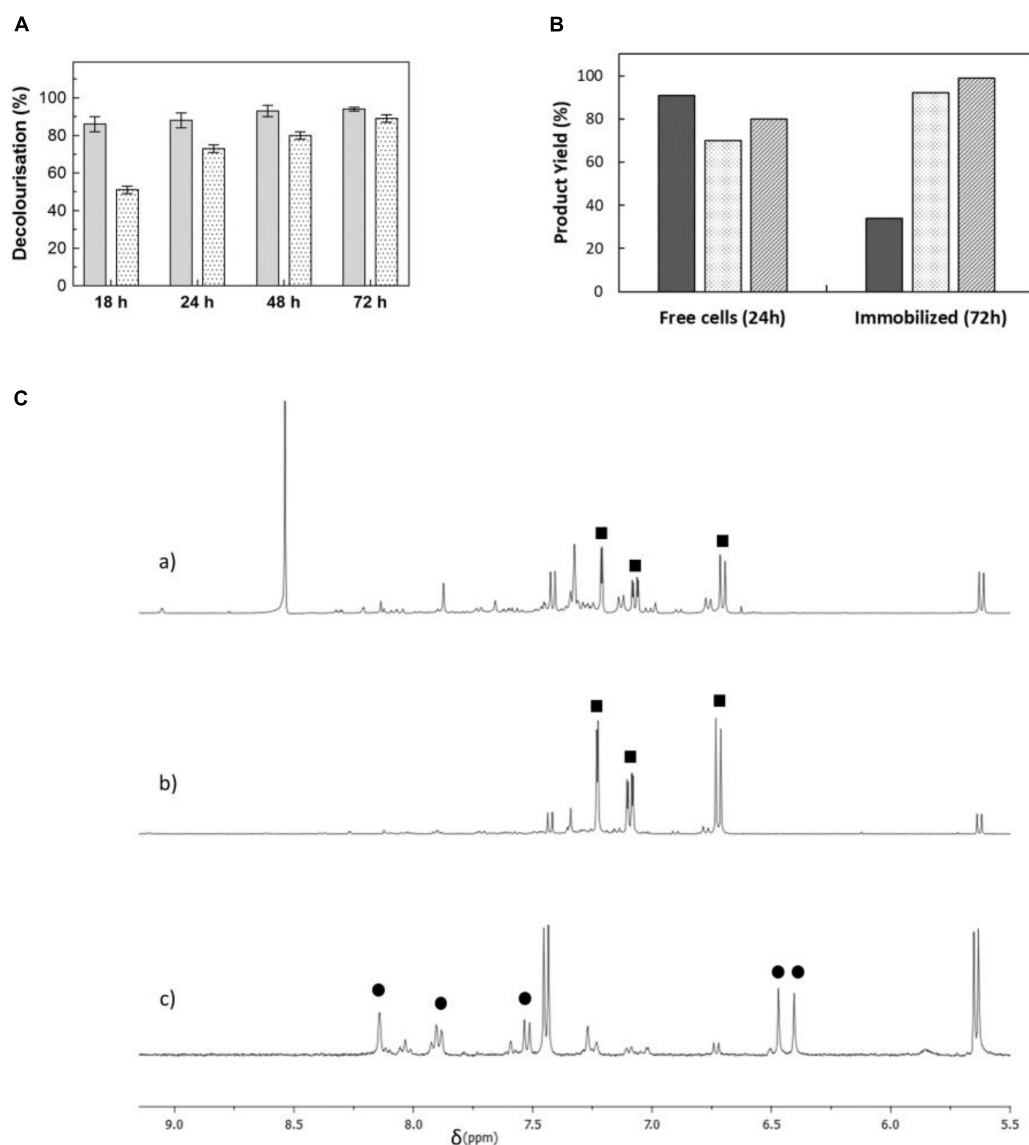


FIGURE 2 | (A) Time-course decolourisation of MB9 using free (light grey bars) and immobilised (dotted bars) cells containing PpAzoR azoreductase (60 mg DCW ml^{-1}) at 30°C in static conditions. **(B)** Yields of SAHBS in processes using free and immobilised cells of *Escherichia coli* Tuner (light black), BL21 star (light grey), and KRX cells (dark grey). **(C)** ¹H-NMR spectra (aromatic region) of reaction mixtures containing MB9 with **(a)** free or **(b)** immobilised *E. coli* KRX cells overproducing PpAzoR in static conditions at 30°C and **(c)** after addition of immobilised *E. coli* KRX cells overproducing CotA-laccase under stirring conditions at 37°C. Resonances due to SAHBS (filled squares) and compound 7 (filled circles) are labelled.

Lin and Tao, 2017). Moreover, processes with whole cells (i.e., resting cells) are very advantageous since cells efficiently take out oxygen from the media and allow the anaerobic PpAzoR to decolourise azo dyes while avoiding the need of using flasks sealed with rubber stoppers and made anaerobic by argon bubbling. Therefore, time-course decolourisation assays of the model dye MB9 were performed using different *E. coli* strains overproducing PpAzoR variant 2A1-Y179H, which shows fourfold higher activity than the wild-type enzyme (Brissos et al., 2014). Whole-cell reactions resulted in decolourisation levels close to 95% with 70–91% product yields (0.66–0.87 mM of SAHBS; **Figures 2A,B**) after 24 h of reaction. In general, it

was observed that the levels of decolourisation were higher than product yields most likely related to adsorption of dyes to cell surfaces (Prigione et al., 2008). The ¹H-NMR analysis of the reaction mixtures showed only resonances attributed to SAHBS (**Figures 2C,a**), in contrast to the reactions using purified enzymes where NADPH was added to the reaction mixtures (see **Figures 1C,b**), but also the presence of other signals, which are due to intracellular metabolites derived from cells. Next, we have performed reactions in alginate-immobilised cells, considering that immobilisation eases the recycling of biocatalysts, which is critical for the implementation of cost-effective processes (Devi et al., 2017). Decolourisation with immobilised cells was

TABLE 2 | Bioconversion of MB9 using immobilised *Escherichia coli* KRX whole cells (120 mg DCW ml⁻¹) overproducing each enzyme separately (two-step) and overproducing both enzymes simultaneously (one-pot).

Reaction	SAHBS (mM)	Yield step 1 (%)	Compound 7 (mM)	Yield step 2 (%)	Overall yield (%)
Two-step	0.71	74	0.36	99	74
	0.76	80	0.37	97	78
One-pot	–	–	0.24	–	50
	–	–	0.44	–	91

The first step was performed in static conditions at 30°C upon addition of MB9 dye (1 cycle) or four 24-h sequential additions of MB9 dye (4 cycles). The second step was performed in stirring conditions, at 37°C, for 24 h. Reactions were performed in water.

slower (~90% decolourisation only after 72 h; **Figure 2B**), most likely due to the presence of the alginate matrix that restricts diffusion of substrate through the beads. However, reactions with immobilised cells displayed a cleaner ¹H-NMR spectrum indicating that cell encapsulation prevented leakage of undesirable intracellular metabolites (**Figures 2C,b**). *E. coli* KRX cells were selected for further studies considering their superior performance (**Figure 2B** and **Supplementary Figure 5**). The amount of cells in alginate beads was increased from 60 to 120 mg DCW ml⁻¹, and buffer was replaced by water to increase the cost-effectiveness and sustainability of the bioprocess, and after 24 h, a significant increase in decolourisation of MB9 (89%) was achieved (**Supplementary Figure 6**). In these conditions, the conversion yields of MB9 to SAHBS reached 74% (**Table 2**). The addition of CotA-laccase resulted in the full conversion (99%) of the amine to the phenoxazinone (7) (**Figures 2C,c** and **Table 2**). Next, we tested a recycling system by using a 24-h stepwise addition of a 0.96 mM MB9 dye to immobilised cells containing the PpAzoR azoreductase under static conditions, which resulted in a slight increase in the final product yields (**Table 2**). Finally, one-pot reactions were set up using immobilised *E. coli* cells that have co-produced both the PpAzoR and the CotA enzymes, reducing twofold the time and cost associated with cell production (**Table 2**). One-pot bioprocesses show obvious advantages such as low costs, higher yields, and environmental benefits (Sydnes, 2014). The sequential activity of the two enzymes was controlled by the aeration conditions: first, static conditions during 24 h to promote PpAzoR activity, followed by stirring at 180 rpm for 24 h reaction, where CotA that couples the oxidation of substrates to the reduction of oxygen to water is active. This approach resulted in lower phenoxazinone yields (50%) as compared when using *E. coli* cells harbouring separately the target enzymes (**Table 2**). However, when the first step was performed in a recycled manner, i.e., through 24-h stepwise addition of dye solution, the overall performance improved significantly, affording 91% product yields. The activity recovery was measured in both the two-step and the one-pot reactions, and we found that after the first, second, and third cycles, the activity measured is around 100, 75, and 60% of the initial activity, respectively; it takes four cycles to observe a drop in the biocatalyst activity to values around 40% of the initial activity. The high yields of products achieved give confidence

for their ease purification using preparative HPLC techniques. This enzymatic system resulted in 80–100% decolourisation of model acid, reactive, and direct dye baths (Mendes et al., 2011a). The toxicity after the sequential treatment was also significantly reduced, giving good indications that valuable compounds can be extracted from these model dye baths. Further studies to substantiate the biocatalytic efficiency of the system proposed using model and real wastewaters need to be performed in order to fully exploit the enzymatic bioprocesses described that respect principles of circularity, sustainability, and planetary boundaries.

CONCLUSION

Azo dyes are xenobiotic molecules whose structures were designed to resist decolourisation and degradation, which in turn challenge its sustainable and efficient eradication from the environment. We had proven that the sequential use of PpAzoR azoreductase and CotA-laccase enzymes resulted in the decolourisation, degradation, and conversion into valuable compounds of a set of azo dyes, mordant, acid, reactive and direct, and low-cost feedstock, commonly found in dye-containing wastewaters of textile-related industries. For the set-up of the biocatalytic bioprocess, we took advantage of the previously known complementary catalytic properties of azoreductases and laccases; i.e., azoreductases reduce azo dyes to aromatic amines and laccases promote their oxidative coupling into valuable aromatic compounds, precursors of biologically active molecules. Free and immobilised whole cells of *E. coli* containing these enzymes allowed developing an economically feasible bioprocess resulting in less contaminated reaction mixtures with final product yields that go up to ~90%. The optimised biocatalytic systems offer a sustainable and promising approach for cleaning up dye-containing wastewaters while producing valuable chemicals with a range of applications in chemical industries.

DATA AVAILABILITY STATEMENT

The raw data supporting the conclusions of this article will be made available by the authors, without undue reservation.

AUTHOR CONTRIBUTIONS

AF conducted most of the experiments. BP developed the two-step biotransformation system using purified enzymes. LB helped in developing whole-cell systems. MR made the NMR analysis. BR discussed the results and participated in the writing. LM proposed and supervised the whole project. All authors contributed to the article and approved the submitted version.

FUNDING

This work was supported by the project grant PTDC/BBB-EBB/0122/2014, PTDC/BII-BBF/29564/2017, UID/Multi/045 51/2013, and Project LISBOA-01-0145-FEDER-007660 funded

by FEDER funds through COMPETE2020—Programa Operacional Competitividade e Internacionalização (POCI) and Fundação para a Ciência e a Tecnologia (FCT), Portugal.

ACKNOWLEDGMENTS

The authors thank João Carita, Isabel Pacheco, and Cristina Leitão (Research Facilities, ITQB-NOVA) for the technical assistance. The NMR spectrometer used is part of the National

NMR Facility (RECI/BBB-BQB/0230/2012). AF thank the Sustainable Chemistry Ph.D. program for the doctoral grant PD/BD/109637/2015.

SUPPLEMENTARY MATERIAL

The Supplementary Material for this article can be found online at: <https://www.frontiersin.org/articles/10.3389/fbioe.2021.672436/full#supplementary-material>

REFERENCES

- Bento, I., Martins, L. O., Lopes, G. G., Carrondo, M. A., and Lindley, P. F. (2005). Dioxygen reduction by multi-copper oxidases; a structural perspective. *Dalton Trans.* 7, 3507–3513. doi: 10.1039/b504806k
- Brissos, V., Gonçalves, N., Melo, E. P., and Martins, L. O. (2014). Improving kinetic or thermodynamic stability of an azoreductase by directed evolution. *PLoS One* 9:e87209. doi: 10.1371/journal.pone.0087209
- Carmen, Z., and Daniela, S. (2012). *Textile Organic Dyes – Characteristics, Polluting Effects and Separation/Elimination Procedures from Industrial Effluents – A Critical Overview*. London: IntechOpen.
- Carvalho, C. C. C. R. (2016). Whole-cell biocatalysts: essential workers from nature to industry. *Microb. Biotechnol.* 10, 250–263. doi: 10.1111/1751-7915.12363
- Carvalho, M. C., Pereira, C., Gonçalves, I. C., Pinheiro, H. M., Santos, A. R., Lopes, A., et al. (2008). Assessment of the biodegradability of a monosulfonated azo dye and aromatic amines. *Int. Biodeterior. Biodegradation* 62, 96–103. doi: 10.1016/j.ibiod.2007.12.008
- Cholo, M. C., Steel, H. C., Fourie, P. B., Germishuizen, W. A., and Anderson, R. (2012). Clofazimine: current status and future prospects. *J. Antimicrob. Chemother.* 67, 290–298. doi: 10.1093/jac/dkr444
- Corona, P., Carta, A., Loriga, M., Vitale, G., and Paglietti, G. (2009). Synthesis and in vitro antitumor activity of new quinoxaline derivatives. *Eur. J. Med. Chem.* 44, 1579–1591. doi: 10.1016/j.ejmech.2008.07.025
- Devi, P., Wahidullah, S., Sheikh, F., Pereira, R., Narkhede, N., Amonkar, D., et al. (2017). Biotransformation and detoxification of xyldine orange dye using immobilized cells of marine-derived *Lysinibacillus sphaericus* D3. *Mar. Drugs* 15:30. doi: 10.3390/md15020030
- Durao, P., Chen, Z., Fernandes, A. T., Hildebrandt, P., Murgida, D. H., Todorovic, S., et al. (2008). Copper incorporation into recombinant CotA laccase from *Bacillus subtilis*: characterization of fully copper loaded enzymes. *J. Biol. Inorg. Chem.* 13, 183–193. doi: 10.1007/s00775-007-0312-0
- Forte, S., Polak, J., Valensin, D., Taddei, M., Basosi, R., Vanhulle, S., et al. (2010). Synthesis and structural characterization of a novel phenoxazinone dye by use of a fungal laccase. *J. Mol. Catal. B Enz.* 63, 116–120. doi: 10.1016/j.molcatb.2009.12.018
- Geissdoerfer, M., Savaget, P., Bocken, N. M. P., and Hultink, E. J. (2017). The Circular economy a new sustainability paradigm? *J. Clean. Prod.* 143, 757–768. doi: 10.1016/j.jclepro.2016.12.048
- Hassaan, M. A., and Nemr, A. E. (2017). Health and environmental impacts of dyes: mini review. *Am. J. Environ. Sci. Eng.* 1, 64–67.
- Kant, R. (2012). Textile dyeing industry an environmental hazard. *Nat. Sci.* 4, 22–26. doi: 10.4236/ns.2012.41004
- Khan, R., Bhawana, P., and Fulekar, M. H. (2013). Microbial decolorization and degradation of synthetic dyes: a review. *Rev. Environ. Sci. Biotechnol.* 12, 75–97. doi: 10.1007/s11157-012-9287-6
- Kudlich, M., Hetheridge, M. J., Knackmuss, H. J., and Stolz, A. (1999). Autoxidation reactions of different aromatic o-aminohydroxynaphthalenes that are formed during the anaerobic reduction of sulfonated azo dyes. *Environ. Sci. Technol.* 33, 896–901. doi: 10.1021/es9808346
- Lange, L., Connor, K. O., Arason, S., Bundgaard-Jorgensen, U., Canalis, A., Carrez, D., et al. (2021). Developing a sustainable and circular bio-based economy in EU: by partnering across sectors, upscaling and using new knowledge faster, and for the benefit of climate, environment & biodiversity, and people & business. *Front. Bioeng. Biotechnol.* 8:619066. doi: 10.3389/fbioe.2020.619066
- Lin, B. X., and Tao, Y. (2017). Whole-cell biocatalysts by design. *Microb. Cell Fact.* 16:106.
- Martins, L. O., Melo, E. P., Sanchez-Amat, A., and Robalo, M. P. (2020). “Bacterial laccases: some recent advances and applications,” in *Laccases in Bioremediation and Waste Valorisation*, ed. D. Schlosser (Cham: Springer), 27–55. doi: 10.1007/978-3-030-47906-0_2
- Martins, L. O., Soares, C. M., Pereira, M. M., Teixeira, M., Costa, T., Jones, G. H., et al. (2002). Molecular and biochemical characterization of a highly stable bacterial laccase that occurs as a structural component of the *Bacillus subtilis* endospore coat. *J. Biol. Chem.* 277, 18849–18859. doi: 10.1074/jbc.m200827200
- McDonald, M., Wilkinson, B., Van’t Land, C. W., Mocek, U., Lee, S., and Floss, H. G. (1999). Biosynthesis of phenazine antibiotics in *Streptomyces antibioticus*: stereochemistry of methyl transfer from carbon-2 of acetate. *J. Am. Chem. Soc.* 121, 5619–5624. doi: 10.1021/ja991159i
- Mendes, S., Farinha, A., Ramos, C. G., Leitao, J. H., Viegas, C. A., and Martins, L. O. (2011a). Synergistic action of azoreductase and laccase leads to maximal decolorization and detoxification of model dye-containing wastewaters. *Bioresour. Technol.* 102, 9852–9859. doi: 10.1016/j.biortech.2011.07.108
- Mendes, S., Pereira, L., Batista, C., and Martins, L. O. (2011b). Molecular determinants of azo reduction activity in the strain *Pseudomonas putida* MET94. *Appl. Microbiol. Biotechnol.* 92, 393–405. doi: 10.1007/s00253-011-3366-4
- Mendes, S., Robalo, M. P., and Martins, L. O. (2015). “Bacterial enzymes and multi-enzymatic systems for cleaning-up dyes from the Environment,” in *Microbial Degradation of Synthetic Dyes in Waste Waters*, ed. S. N. Singh (Cham: Springer), 27–55. doi: 10.1007/978-3-319-10942-8_2
- Morel, O. J. X., and Christie, R. M. (2011). Current trends in the chemistry of permanent hair dyeing. *Chem. Rev.* 111, 2537–2561. doi: 10.1021/cr1000145
- Pereira, L., and Alves, M. S. (2012). “Dyes - environmental impact and remediation,” in *Environmental Protection Strategies for Sustainable Development, Strategies for Sustainability*, eds A. Malik, and E. Grohmann (Dordrecht: Springer).
- Pinheiro, H. M., Touraud, E., and Thomas, O. (2004). Aromatic amines from azo dye reduction: status review with emphasis on direct UV spectrophotometric detection in textile industry wastewaters. *Dyes Pigm.* 61, 121–139. doi: 10.1016/j.dyepig.2003.10.009
- Piro, B., Reisberg, S., Anquentin, G., Duc, H.-T., and Pham, M.-C. (2013). Quinone-based polymers for label-free and reagentless electrochemical immunosensors: application to proteins, antibodies and pesticides detection. *Biosensors* 3, 58–76. doi: 10.3390/bios3010058
- Prigione, V., Tigini, V., Pezzella, C., Anastasi, A., Sannia, G., and Varese, G. C. (2008). Decolourisation and detoxification of textile effluents by fungal biosorption. *Water Res.* 42, 2911–2920. doi: 10.1016/j.watres.2008.03.003
- Rai, H. S., Bhattacharyya, M. S., Singh, J., Bansal, T. K., Vats, P., and Banerjee, U. C. (2005). Removal of dyes from the effluent of textile and dyestuff manufacturing industry: a review of emerging techniques with reference to biological treatment. *Crit. Rev. Environ. Sci. Technol.* 35, 219–238. doi: 10.1080/10643380509017932
- Rawat, D., Mishra, V., and Sharma, R. S. (2016). Detoxification of azo dyes in the context of environmental processes. *Chemosphere* 155, 591–605. doi: 10.1016/j.chemosphere.2016.04.068

- Rodriguez-Couto, S. (2009). Enzymatic biotransformation of synthetic dyes. *Curr. Drug Metab.* 10, 1048–1054. doi: 10.2174/13892000979071850
- Saratale, R. G., Saratale, G. D., Chang, J. S., and Govindwar, S. P. (2011). Bacterial decolorization and degradation of azo dyes: a review. *J. Taiwan Inst. Chem. Eng.* 42, 138–157.
- Shruti, J. D., Kishore, D., and Sain, S. (2018). Recent advancement in the synthesis of phenoxazine derivatives and their analogues. *Synth. Commun.* 48, 1377–1402. doi: 10.1080/00397911.2018.1448090
- Singh, R. L., Singh, P. K., and Singh, R. P. (2015). Enzymatic decolorization and degradation of azo dyes – a review. *Int. Biodeterior. Biodegradation* 104, 21–31. doi: 10.1016/j.ibiod.2015.04.027
- Sousa, A. C. (2015). *Biotransformação de Aminas Aromáticas Catalisada por Laccases*. Lisboa: Universidade Técnica de Lisboa.
- Sousa, A. C., Martins, L. O., and Robalo, M. P. (2013). Laccase-catalysed homocoupling of primary amines towards the biosynthesis of dyes. *Adv. Synth. Catal.* 355, 1857–1865.
- Sousa, A. C., Oliveira, M. C., Martins, L. O., and Robalo, M. P. (2014). Towards the rational biosynthesis of substituted phenazines and phenoxazinones by laccases. *Green Chem.* 16, 4127–4136. doi: 10.1039/c4gc00901k
- Sydnés, M. O. (2014). One-pot reactions: a step towards greener chemistry. *Curr. Green Chem.* 1, 216–226. doi: 10.2174/2213346101666140221225404
- Vairavelu, L., Zeller, M., and Prasad, K. J. R. (2014). Solvent-free synthesis of heteroannulated carbazoles: a novel class of anti-tumor agents. *Bioorg. Chem.* 54, 12–20. doi: 10.1016/j.bioorg.2014.03.003
- Vikrant, K., Giri, B. S., Raza, N., Roy, K., Kim, K. H., Rai, B. N., et al. (2018). Recent advancements in bioremediation of dye: current status and challenges. *Bioresour. Technol.* 253, 355–367. doi: 10.1016/j.biortech.2018.01.029

Conflict of Interest: The authors declare that the research was conducted in the absence of any commercial or financial relationships that could be construed as a potential conflict of interest.

Copyright © 2021 Fernandes, Pinto, Bonardo, Royo, Robalo and Martins. This is an open-access article distributed under the terms of the Creative Commons Attribution License (CC BY). The use, distribution or reproduction in other forums is permitted, provided the original author(s) and the copyright owner(s) are credited and that the original publication in this journal is cited, in accordance with accepted academic practice. No use, distribution or reproduction is permitted which does not comply with these terms.

Advantages of publishing in Frontiers



OPEN ACCESS

Articles are free to read
for greatest visibility
and readership



FAST PUBLICATION

Around 90 days
from submission
to decision



HIGH QUALITY PEER-REVIEW

Rigorous, collaborative,
and constructive
peer-review



TRANSPARENT PEER-REVIEW

Editors and reviewers
acknowledged by name
on published articles

Frontiers

Avenue du Tribunal-Fédéral 34
1005 Lausanne | Switzerland

Visit us: www.frontiersin.org

Contact us: frontiersin.org/about/contact



REPRODUCIBILITY OF RESEARCH

Support open data
and methods to enhance
research reproducibility



DIGITAL PUBLISHING

Articles designed
for optimal readership
across devices



FOLLOW US

@frontiersin



IMPACT METRICS

Advanced article metrics
track visibility across
digital media



EXTENSIVE PROMOTION

Marketing
and promotion
of impactful research



LOOP RESEARCH NETWORK

Our network
increases your
article's readership